EFFECT OF FLOW INTENSITY AND COLLARS ON SCOUR DEPTHS AROUND BRIDGE ABUTMENTS

A THESIS SUBMITTED TO
THE GRADUATE SCHOOL OF NATURAL AND APPLIED SCIENCES
OF
MIDDLE EAST TECHNICAL UNIVERSITY

BY

SERKAN GÖKMENER

IN PARTIAL FULFILLMENT OF THE REQUIREMENTS
FOR
THE DEGREE OF DOCTOR OF PHILOSOPHY
IN
CIVIL ENGINEERING

MAY 2023

Approval of the thesis:

EFFECT OF FLOW INTENSITY AND COLLARS ON SCOUR DEPTHS AROUND BRIDGE ABUTMENTS

submitted by **SERKAN GÖKMENER** in partial fulfillment of the requirements for the degree of **Doctor of Philosophy** i**n Civil Engineering, Middle East Technical University** by,

Prof. Dr. Halil Kalıpçılar
Dean, Graduate School of **Natural and Applied Sciences** ________________

Prof. Dr. Erdem Canbay
Head of the Department, **Civil Engineering** ________________

Prof. Dr. Ayşe Burcu Altan-Sakarya
Supervisor, **Civil Engineering, METU** ________________

Prof. Dr. Mustafa Göğüş
Co-Supervisor, **Civil Engineering, Çankaya University** ________________

Examining Committee Members:

Prof. Dr. Mehmet Ali Kökpınar
Civil Engineering, TED University ________________

Prof. Dr. Ayşe Burcu Altan-Sakarya
Civil Engineering, METU ________________

Assoc. Prof. Dr. Elif Oğuz
Civil Engineering, METU ________________

Assoc. Prof. Dr. Ali Ercan
Civil Engineering, METU ________________

Assoc. Prof. Dr. Aslı Numanoğlu Genç
Civil Engineering, TED University ________________

Date: 05.05.2023

I hereby declare that all information in this document has been obtained and presented in accordance with academic rules and ethical conduct. I also declare that, as required by these rules and conduct, I have fully cited and referenced all material and results that are not original to this work.

Name Last name : Serkan, Gökmener

Signature :

ABSTRACT

EFFECT OF FLOW INTENSITY AND COLLARS ON SCOUR DEPTHS AROUND BRIDGE ABUTMENTS

Gökmener, Serkan
Doctor of Philosophy, Civil Engineering
Supervisor : Prof. Dr. Ayşe Burcu Altan-Sakarya
Co-Supervisor: Prof. Dr. Mustafa Göğüş

May 2023, 315 pages

In this experimental study, the temporal development of the local scour was studied around semi-circular end and rectangular bridge abutments under unsteady-state clear-water flow conditions in a rectangular sediment channel. Six different abutment lengths having constant width with uniform sand as bed material were tested for 3 different successive flow intensities each applied continuously for 2 hours. Effects of the abutment length, flow intensity and temporal variation on the scour depths around semi-circular end and rectangular bridge abutments were investigated. According to the results, it was shown that flow intensity is the most important parameter in scour development and the maximum scour depth always occurs at the front noses of the abutments. Then, the performance of collars on reducing local scour depth around semi-circular end and rectangular bridge abutments under unsteady-state clear-water flow conditions was examined. Three different abutment lengths having constant widths were tested with varying sizes of collars that are located at different elevations relative to the bed level. The effect of abutment length, collar width, collar elevation, flow intensity and temporal variation on local scour reduction performances of collars were tested. According to the experimental results, it can be stated that the application of collars around semi-circular end and rectangular bridge abutments decreases the local scour depth by up to 72%. Best collar performances were generally achieved for the largest collar width located around bed level. Also, semi-circular end collars gave more efficient results in reducing the scour depths than rectangular collars. Finally, additional experiments were carried out in order to understand the effect of flow depth on scour reduction efficiencies of the collars and it was observed that the flow depth had no significant effect in reducing the scour depth for longer abutments but had a significant effect for shorter ones.

Keywords: Collar, Rectangular abutments, Scour, Scour Countermeasures, Semi-circular end abutments, Unsteady-state flow conditions

ÖZ

AKIM ŞİDDETİ VE YATAY PLAKALARIN KÖPRÜ YAN AYAKLARI ETRAFINDA OLUŞAN OYULMA DERİNLİKLERİNE ETKİSİ

Gökmener, Serkan
Doktora, İnşaat Mühendisliği
Tez Yöneticisi: Prof. Dr. Ayşe Burcu Altan-Sakarya
Ortak Tez Yöneticisi: Prof. Dr. Mustafa Göğüş

Mayıs 2023, 315 sayfa

Bu deneysel çalışmada; dikdörtgen kesitli bir sediman kanalında, düzensiz akış ve temiz su oyulması koşullarında yarı dairesel ve dikdörtgen köprü yan ayakları etrafındaki yerel oyulmaların zamansal gelişimi incelenmiştir. Sabit genişliğe sahip 6 farklı yan ayak uzunluğu, üniform kum yatak malzemesinde, 2 saat boyunca sürekli olarak uygulanan 3 farklı ardışık akım şiddeti için test edilmiştir. Yan ayak uzunluğunun, akım şiddetinin ve zamansal değişimin, yarı dairesel ve dikdörtgen köprü yan ayakları etrafındaki yerel oyulmaların derinliğine olan etkisi incelenmiştir. Sonuçlara göre, akım şiddetinin oyulma derinliğinin gelişiminde en önemli parametre olduğu görülmüş ve maksimum oyulma derinliği her daim yan ayakların ön uçlarında oluşmuştur. Ardından, düzensiz akış ve temiz su oyulması koşullarında yarı dairesel ve dikdörtgen köprü yan ayakları etrafındaki yerel oyulma derinliğini azaltmak için yan ayakların etrafına yatay plakalar monte edilmiş ve etkileri incelenmiştir. Sabit genişliğe sahip üç farklı yan ayak uzunluğu, yatak seviyesine göre farklı yüksekliklerde bulunan farklı plaka boyutları kullanılarak test edilmiştir. Yan ayak uzunluğunun, plaka genişliğinin ve konumunun, akım şiddetinin ve deney süresinin, plakaların yerel oyulma derinliğini azaltmasına olan etkisi ortaya konmuştur. Deneysel bulgulara göre, plakaların, yerel oyulma derinliğini %72 mertebesine kadar azalttığı görülmüştür. En iyi plaka performansları genellikle yatak seviyesine yerleştirilen en büyük plaka genişliği için elde edilmiştir. Ayrıca, yarı dairesel yatay plakaların, dikdörtgen yatay plakalara göre oyulma derinliğini azaltmada daha etkili olduğu ortaya konmuştur. Son olarak, akım derinliğinin, plakaların oyulma derinliğini azaltma verimliliği üzerindeki etkisini anlamak için ek deneyler yapılmış ve akış derinliğinin daha uzun yan ayaklarda, plakaların oyulma derinliğini azaltma performansına önemli bir etkisinin olmadığı, kısa yan ayaklarda ise önemli bir etkisinin olduğu görülmüştür.

Anahtar Kelimeler: Dikdörtgen Yan Ayaklar, Düzensiz Akım Koşulları, Oyulma, Oyulma Tedbirleri, Yarı Dairesel Yan Ayaklar, Yatay Plakalar

Herkes ve hiç kimse için,

ACKNOWLEDGMENTS

The author wishes to express his deepest gratitude to his supervisors Prof. Dr. Mustafa Göğüş and Prof. Dr. Ayşe Burcu Altan-Sakarya for their guidance, advice, criticism, encouragement and insight throughout the research.

The author is so grateful to Assoc. Prof. Dr. Elif Oğuz for her inspiration, advice and encouragement throughout his study period in METU Hydraulics Laboratory.

The author would also like to thank Prof. Dr. Mehmet Ali Kökpınar, Prof. Dr. Elçin Kentel, Assoc. Prof. Dr. Aslı Numanoğlu Genç and Assoc. Prof. Dr. Ali Ercan for their suggestions and comments.

The author would like to express his appreciation to Erkan Koyuncuoğlu, Gülçin Melek, Mehmet Vahit Aşık, Mehmet Sedat Gözlet, Kaan Göllü, Cemre Çağlar, Orçin Akgönül, Ege Cem Saltık, Beyhan İpekyüz and Diğdem Angın for their support and friendship.

The author would also thank his lifelong friends and colleagues; Abiddin Berhan Melek, Emre Haspolat, Kutay Yılmaz, Gökalp Doğukan Demirbaş, Melih Uğur Kondakçı, Ezgi Budak Çötel, Doğa Derman Çiçek and Erhan Tarık Karayama for their advice, helpfulness and friendship during the study period.

Within the scope of this study, many experiments were conducted in the METU Hydraulics Laboratory. Those experiments could not have been completed without the help of technical assistance. The author would like to thank Hüseyin Gündoğdu and Eyüp Uğur for their technical efforts during the experiments. However, the author especially expresses his gratitude to Emre Kavak, the wonderkid of Hydraulics Laboratory, for his technical advice, effort and friendship during the experiments.

The author is also so grateful to the mother of the Hydraulics Laboratory, Necla Çankaya Lostar for her kindliness and helpfulness throughout his study period in METU Hydraulics Laboratory.

The author finally would like to express his gratitude to his mother Tuna Gökmener and his father Emin Bülent Gökmener for their endless love, patience and confidence during his life.

TABLE OF CONTENTS

APPENDICES

LIST OF TABLES

TABLES

LIST OF FIGURES

FIGURES

LIST OF ABBREVIATIONS

CFD	Computational Fluid Dynamics
FHWA	Federal Highway Administration
FPE	First Phase Experiments
RC	Rectangular Abutment
SC	Semi-circular End Abutment
SPE	Second Phase Experiment
SSIIM	Sediment Simulation in Intakes with Multiblock

LIST OF SYMBOLS

$A_{abutment}$ abutment area on the horizontal plane (m^2)

A_{collar} area of the abutment with a collar on the horizontal plane (m^2)

a_0 regression coefficient

a_1 regression coefficient

a_2 regression coefficient

a_3 regression coefficient

a_4 regression coefficient

B channel width

B_a abutment width

B_c collar width around the abutment

C cohesiveness

C_u uniformity coefficient, $C_u = \frac{d_{60}}{d_{10}}$

d_{10} sediment size for which 10% of the sediment is finer

d_{16} sediment size for which 16% of the sediment is finer

d_{50} median size diameter

d_{60} sediment size for which 60% of the sediment is finer

d_{84} sediment size for which 84% of the sediment is finer

d_s scour depth

$(d_s)_{max}$ maximum scour depth at the abutment at the end of the given time duration

$(d_s)_{max,c}$ maximum scour depth at the abutment with collar

$(d_s)_u$ scour depth at the upstream nose of the abutment

$(d_s)_f$ scour depth at the front nose of the abutment

$(d_s)_d$ scour depth at the downstream nose of the abutment

F_d densimetric Froude number, $F_d = U/(g'd_{50})^{0.5}$

F_t threshold Froude number, $F_t = U/U_t$

F_r Froude number, $F_r = U/\sqrt{gy}$

g gravitational acceleration

g' reduced gravitational acceleration

K_a abutment shape factor

K_d sediment size effect factor

K_G geometry of channel factor

K_H flow factor

L_a abutment length

L_R reference length

N shape factor

P unsteady flow parameter

R^2 correlation coefficient

R_e^* particle Reynolds number

R_h hydraulic radius

Q discharge of the flow

S_0 slope of the channel

S_e energy slope of the flow

S_g specific gravity

S_p particle shape factor

t generic time

t_p time period of the experiment for a given flow intensity starting from the beginning as 2 hours, 4 hours and 6 hours

T dimensionless time

t_{max} total time period of the experiment (=6 hours)

U mean approach flow velocity

U_c value of the U at the threshold of grain motion

U_* shear velocity of the approach flow

U_{*c} value of the U_* at the threshold of grain motion

U_t threshold approach velocity

w fall velocity of the particle

x axial distance along the flow direction

y flow depth

$y_{0.7}$ flow depth operated during U/U_c=0.7

y_c critical flow depth at the threshold of grain motion

Z_c is the collar level on the abutment with reference to the bed level

α regression coefficient

α_a skewness

α_c dimensionless critical shear stress

σ_g standard deviation of the particle size distribution, $\sigma_g = \sqrt{\frac{d_{84}}{d_{16}}}$

ρ	density of the fluid
ρ_s	density of the sediment
μ	dynamic viscosity of the fluid
ξ	perpendicular distance to the flow direction
φ	angle of response
Θ	$(A_{abutment} + A_{collar})/A_{abutment}$

CHAPTER 1

INTRODUCTION

1.1 General Remarks

Humankind has struggled with difficult natural conditions to supply necessities such as water, nutrition, and shelter since ancient times. The increasing population has brought increasing demands, so humans started to travel, migrate and trade to find new resources to supply their needs. In order to achieve these challenges and especially provide easy transportation across the water, bridges have been constructed on the waterways. Most of the bridges consist of vertical columns and piers to reduce the effect of shear forces and bending moments to increase the structural capacity of the bridges. However, these elements create another severe problem due to the relation between flow structure and erodible material while solving structural issues. This problem is called "scour."

The "scour" phenomenon is basically the removal of sediments such as sand and gravel from the river bed when the flow faces an obstacle such as piers and abutments. In other words, the separation of flow because of the interaction of bridge elements (e.g., piers, abutments) and water causes scour around bridge foundations. Scour failure of bridges occurs suddenly, so monitoring these failures is almost impossible during flood events. These failures cause not only substantial economic loss and also loss of lives.

The statistical studies that have been conducted in the last decades indicate that the most common reason for bridge failures is the degradation of the bed material around bridge foundations (Kayatürk, 2005). According to the Federal Highway Administration of the USA, 17 bridges in New York and New England were damaged or collapsed by scouring due to the spring floods in 1987. Over 50 bridges in Georgia sustained damage from storm-related flooding in 1994, costing about $130 million (Federal Highway Administration, 2001). Wardhana and Hadipriono (2003) analyzed 500 bridge failures in the United States between 1989 and 2000 and revealed that 53% of the bridge failures were caused by flood events. Imhof (2004) stated that the main causes of bridge failures are natural hazards such as flood/scouring events (Figure 1.1 and Figure 1.2).

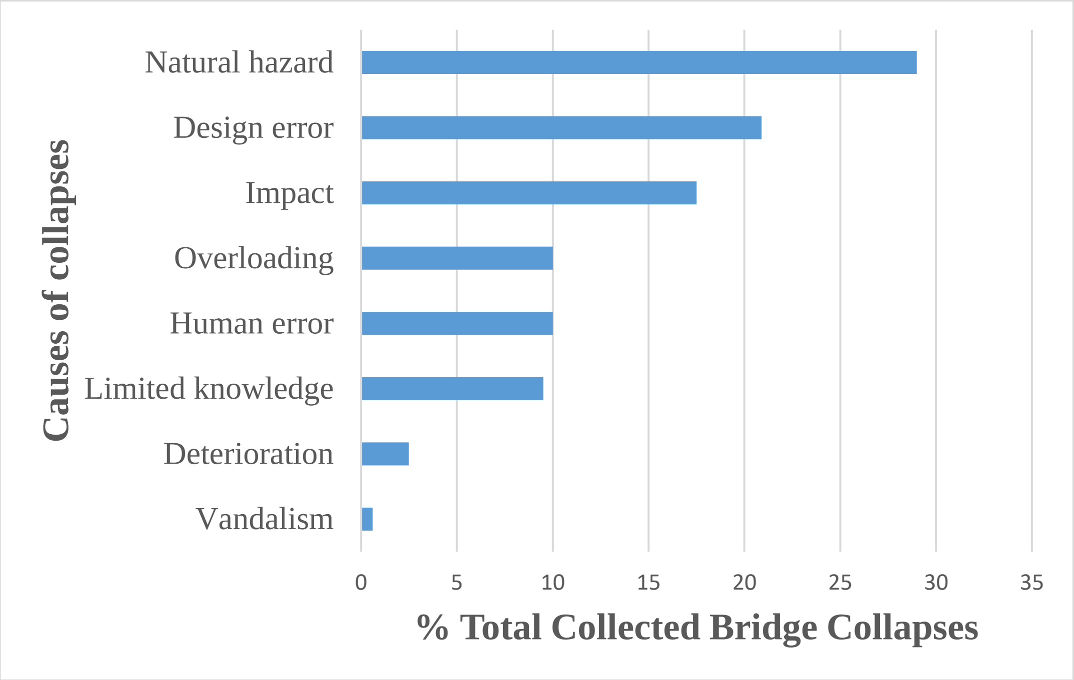

Figure 1.1. Main causes of bridge failures (Imhof, 2004)

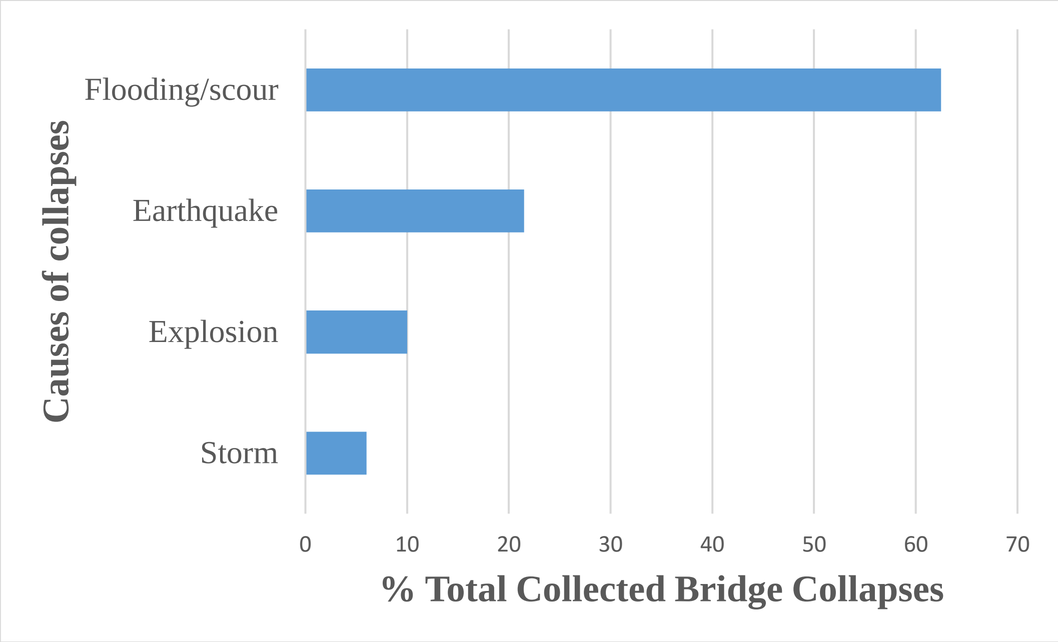

Figure 1.2 Different natural hazards cause bridge failures (Imhof, 2004)

Considering the statistical studies that have been conducted, it is obvious that the hydraulic design of the bridges against flood/scouring events is critical, as well as the structural design of the bridges.

1.2 The Motivation of the Study

According to previous studies, the abutment scour during flood events is one of the most common reasons for bridge failures (Melville, 1992; Richardson and Richardson; 1993). Based on an analysis of the 383 bridge failures in the United States caused by flood/scouring events in 1973, 75% of failures were attributed to abutment scour, while 25% were caused by pier scour (Federal Highway Administration, 2001). Moreover, Kandasamy and Melville (1998) stated that the abutment and approach scour were the main reason for 6 out of 10 bridge failures in New Zealand during Cyclone Bola. Despite the studies mentioned above, abutment scour get still less attention than pier scour. Hence, abutment scour and its countermeasures should be focused on more to understand its mechanism and to prevent possible bridge failures due to the abutment scour.

Furthermore, increased uncertainty of runoff and precipitation prediction due to climate change increases the importance of the hydraulic design of bridges. According to Barkdoll (2012) and Nasr et al. (2020), flooding risk starts to grow with the increase in precipitation due to climate change in most regions. So, scour formation around the bridge elements under flood or unsteady approach flow conditions is more important nowadays. However, there are few studies on the scour mechanism under flood waves due to the complexity of the experimental procedure related to the fast variation of the flow parameters and the difficulty of obtaining a generalized formula to predict scour depth (Oliveto and Hager, 2005a). For that reason, the effect of flow variation on scour development and the behavior of scour countermeasures against scour formation must be studied in more detail by considering both experimental and numerical approaches to understand scour formation under flood waves.

In this study, investigations had been conducted by using experimental approaches rather than numerical approaches, since in the literature, there is not any experimental study considering the effect of collars as a scour countermeasure around bridge abutments under unsteady-state approach flow conditions. In addition, the facilities of the METU Hydraulic Laboratory provide vast experimental opportunities to carry out an experimental study on scour formation around bridge elements. However, the existing computing capacity of the laboratory is limited to carrying out long-continued scour formation studies by using numerical approaches. Hence, it was decided to investigate the subject experimentally.

The scope of this experimental study is to investigate the effect of collars as scour countermeasures and the impact of flow intensity on local scour formation around bridge abutments under unsteady-state clear-water approach flow conditions. For this reason, semi-circular end and rectangular abutments of various sizes were tested using uniform cohesionless sand of d_{50}=1.50 mm at the Middle East Technical University Hydraulics Laboratory under unsteady-state clear-water approach flow conditions with and without collars. To get unsteady-state approach flow conditions, a step-wise hydrograph having a 6-hour duration was applied in the experiments.

Firstly, abutments were tested without collars to examine the effect of flow intensity, abutment length and time on local scour development around the abutments. Then, collars of varying sizes at various elevations with respect to the bed level attached to the abutments were tested to investigate the scour reduction efficiencies of collars. Results of the experiments were compared with the studies of Kayatürk (2005), Doğan (2008), Daşkın (2011) and Tekin (2012), which were conducted with different abutment shapes, flow depths and the grain sizes of the uniform cohesionless bed material under steady-state clear-water approach flow conditions in order to indicate the effect of unsteadiness on the temporal development of scour and scour reduction efficiencies of the collars.

1.3 Synopsis of Thesis

In Chapter 2, scour and bridge abutment scour mechanism is explained by referring to the literature. Experimental setup, materials, measurement techniques, and devices are mentioned in Chapter 3. The temporal development of the scour around bridge abutments and the application of collars around bridge abutments as a countermeasure is discussed based on the experimental results of this study in Chapters 4 and 5, respectively. Relevant studies in the literature are also presented in those chapters. Finally, Chapter 6 includes the conclusions and recommendations for future studies.

CHAPTER 2

BRIDGE ABUTMENT SCOUR

As mentioned in Chapter 1, one of the primary reasons for bridge failures is the scour at the foundations of bridges that consist of piers and abutments (Barbhuiya and Dey, 2004). For this reason, the abutment scour mechanism and the parameters that affect it should be discussed in detail at the beginning. Accordingly, this chapter will represent fundamental issues on bridge abutment scour before considering this study's methodology and findings.

2.1 Definition of Scour

Scour is a natural phenomenon that occurs in streams and rivers caused by the erosive action of flowing water (Breusers et al., 1977). In other words, scour is the result of the degradation and transportation of sediment from the bed, banks of streams, and from around the piers and abutments of the bridges by the erosive action of flowing water (Arneson et al., 2012). The amount of degradation in the river bed according to the natural bed level after the scour formation starts is called the scour depth (Alabi, 2006). Bridge elements that are constructed in rivers cause contraction and separation of the flow. Thus, a significant amount of scour occurs around these bridge elements and the continuity of that scour formation around the bridge foundation can cause the bridge's failure.

2.2 Types of Scour

According to Melville and Coleman (2000), there are three types of scour that affect the safety of bridges: general scour, contraction scour and local scour (Figure 2.1.).

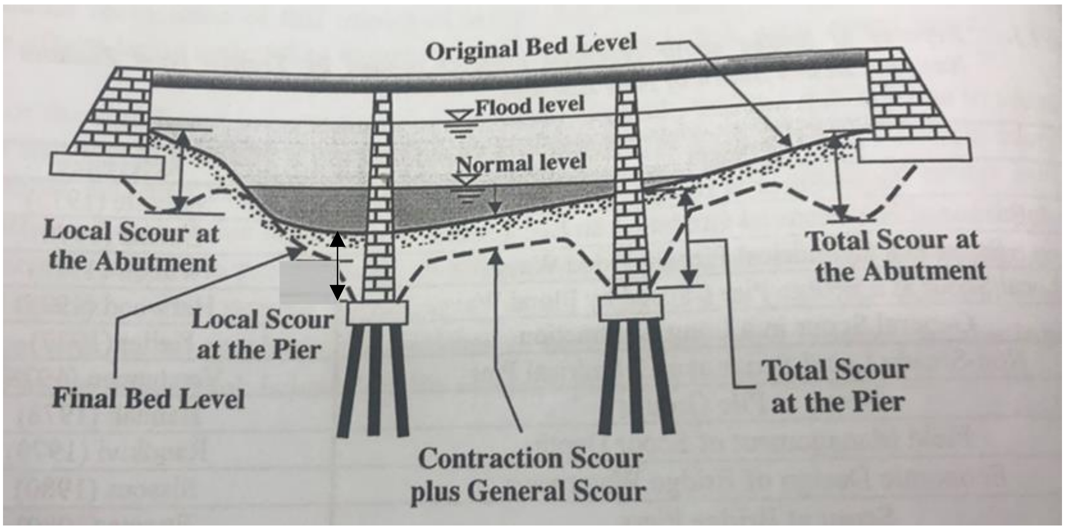

Figure 2.1 Scour types that can occur at bridges (Melville and Coleman, 2000)

The development of General Scour is independent of the existence of the bridge on the riverbed. The lowering of the riverbed and erosion process can be attributed to geomorphological changes, hydrometeorological changes, or human activities. It can develop either long-term or short-term general scour. Short-term general scour is related to single or several closely-spaced flood events. On the other hand, long-term general scour can develop on a longer time scale, even longer than the service life of a bridge.

Contrary to General Scour, Contraction Scour and Local Scour occur due to the artificial structures on the riverbed. Constriction of the flow due to the bridge or its road approaches encroaching onto the floodplain causes the development of Contraction Scour. When flow faces into the bridge elements, the flow accelerates to the narrowest section and this accelerated flow induces scour at the contracted section where contraction scour occurs. In cases of abutments, contraction scour is only critical when the abutment length is notably high relative to river width (Hoffmans et al., 2022).

Local Scour is directly developed through the interaction between bridge elements and the flow. The occurrence of scour holes around the bridge elements can be observed immediately. Local scour can occur as either clear-water or live-bed scour

(Melville and Coleman, 2000). When no sediment is provided by approaching flow into the scour hole while scour formation is in progress, the condition is referred to as clear-water scour. In clear-water scour conditions, the possible maximum local scour depth, or equilibrium scour depth, is obtained when the removal of the bed material from the scour hole slowdowns almost to stop. On the hand, live-bed scour occurs when scour hole is filled with bed material due to continuous sediment transport by the approaching flow. The equilibrium scour depth for the live-bed scour is obtained when the time-averaged movement of bed material into the scour hole equals that removed from it (Melville and Coleman, 2000). The equilibrium live-bed scour depth was observed to be almost 10% lesser than the clear-bed scour depth (Barbhuiya and Dey, 2004).

2.3 Bridge Abutment Scour Mechanism

Bridge elements in the waterway cause highly complex flow-boundary interactions (Arneson et al., 2012). In a river, disturbed flow by bridge abutments starts to accelerate and separate at the upstream face of the abutment while passing the bridge abutment (Abou Seida et al., 2009). This separation at the flow causes degradation and transportation of the bed material around the abutments. As the scour hole around the abutments increases, the complexity of the flow field increases and the separation of the flow induces a 3D vortex flow system around the abutment (Barbhuiya and Dey, 2004). This 3D vortex system involves downflow vortex, primary vortex, secondary vortices and wake vortices (Kwan, 1984), as illustrated in Figure 2.2.

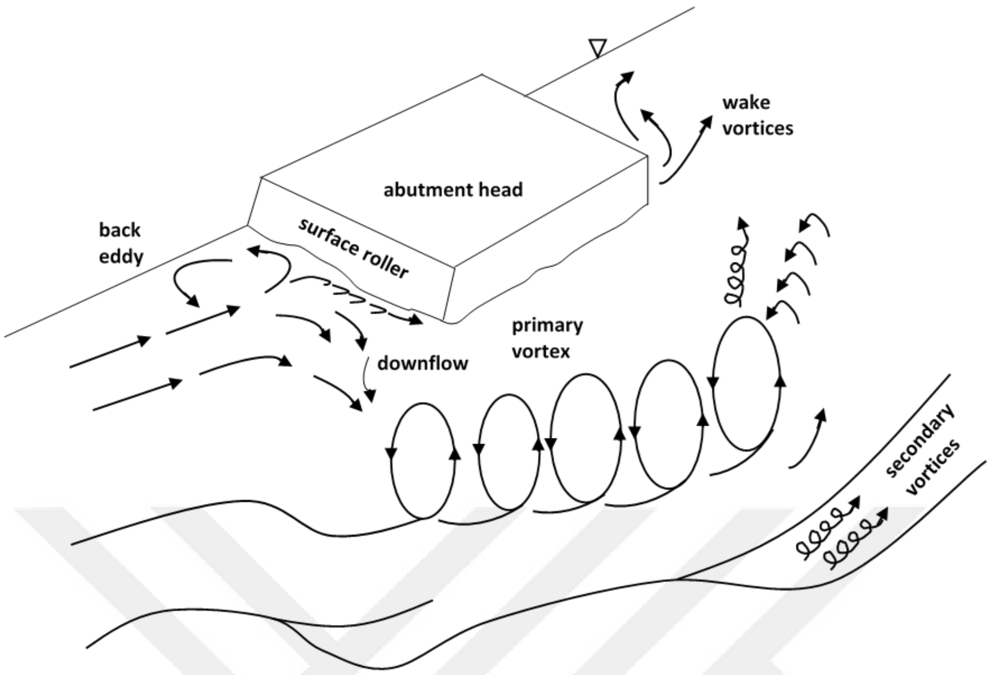

Figure 2.2 General view of the abutment scour (Kwan, 1984)

When flow interacts with the upstream face of the abutment, it accelerates downward toward the sediment bed in a jet motion. Therefore, local shear stresses around the abutment increase with flow acceleration. When the shear stress of the flow exceeds the critical shear stress for the bed material, incipient motion on the bed material starts at the upstream corner of the abutment. Then, the flow tends downward due to the flow separation and initiation of scour at the upstream side of the abutment starts. This downflow motion causes the formation of primary vortex that occurs parallel to the bottom surface of the abutment. This primary vortex or principal vortex was identified by Kwan (1988) and Kwan and Melville (1994), similar to the horseshoe vortex at piers along with the downflow that is the main reason for local scour at bridge abutments (Barbhuiya and Dey, 2004). Since the abutment causes flow constriction, the downflow vortex and the primary vortex are combined with the secondary vortices. Then wake vortices start to occur at the downstream end of the abutment due to the flow separation at the abutment side (Papanicolaou and Hilldale, 2002). The secondary and wake vortices define the boundaries of the stagnant wake region (Papanicolaou et al., 2004). Secondary vortices occur next to the primary vortex with a counter-rotational direction to the primary vortex (Kwan and Melville, 1994). On the other side, Barbhuiya and Dey (2004) define wake vortices as unstable shear layers that roll up to form eddy structures due to flow separation. The wake vortices move downstream due to the flow, act like small tornadoes and lift sediments from the bed. The strength of wake vortices is very small compared to the primary vortex (Barbhuiya and Dey, 2004).

The size and depth of the scour hole increase as the strength of the primary vortex and downward flow increase because of erosion and the removal of more sediment particles from the scour hole (Daşkın, 2011). The scour hole deepens and enlarges because the sediment particles are removed from the scour hole due to the flow field and bottom shear stress until the equilibrium condition is reached. In the equilibrium condition, there is almost no change in the scour pattern with time for clear-water scour conditions; in other words, the development of the scour pattern comes to an end when the equilibrium condition is reached. On the contrary, for live-bed scour conditions, sediment supply into the scour hole continues so that the scour pattern may change over time. However, the scour shape around the abutments can generally be described as an inverted cone with some secondary groove formations in the river bed brought on by secondary vortices. (Abou Seida et al., 2009).

The three-dimensional turbulent flow field in a scour hole at a semi-circular end and vertical-wall end abutments under clear-water scour conditions was investigated by Dey and Barbhuiya (2005a, 2006). Based on experimental results, Dey and Barbhuiya (2005a, 2006) stated that the main characteristic features of the flow at a semi-circular end and vertical-wall abutments are attributed mainly to the primary vortex and skewed velocity distribution. The scour hole's upstream border operates as a line of separation where the approaching flow divides, creating a vortex flow inside the scour hole that behaves as a separation zone. The vortex pushes up the downflow, which was created by the downward negative stagnation pressure gradient of the approaching flow velocity along the upstream face of the abutment.

Additionally, a primary vortex flow, which migrates downstream by the side of the abutment, was shown to form as the oncoming flow curves down into the scour hole and rolls. In the downstream, the flow characteristics become turbulent, erratic, and reversed. This situation occurs because of the shedding of wakes downstream of the abutment generated by the flow separation at the abutment side.

2.4 Parameters Influencing Local Scour At Abutments

According to Arneson et al. (2012), the parameters that affect the magnitude of the local scour depth around the abutments can be given as; the flow depth, approach flow velocity, length of the abutment that is perpendicular to the flow, shape of the abutment, angle of attack of the approach flow to the abutment, bed configuration, size and gradation of bed material, and ice formation or jams and debris flow.

On the other hand, Barbhuiya and Dey (2004) classified the parameters related to the scour depth around the abutments into 6 basic groups. These parameters are related to the channel geometry (1), the fluid (2), the approaching flow conditions (3), the abutment (4), the bed material (5), and time (6). These parameters are listed in more detail below;

1. Channel geometry parameters: Cross-section shape, slope and width.

2. Fluid parameters: Density, temperature and viscosity.

3. Approaching flow parameters: flow depth, gravitational acceleration, mean flow velocity, shear velocity, and roughness.

4. Abutment parameters: Shape, size, surface condition and the position of the abutment relative to the flow.

5. Bed material parameters: Angle of response, cohesiveness, grain size distribution and mass density.

6. Scouring time can be considered an additional parameter for the scour hole development.

Moreover, related parameters with the scour depth around the abutments, according to Li et al. (2006), are shown as a function of the local scour depth, d_s, below and listed in Table 2.1:

$$d_s = f[\rho, \mu, y, U, S_e, g, B, S_0, K_G, d_{50}, S_g, \sigma_g, w, S_p, \varphi, C, \alpha_c, R_e^*, L_a, \alpha_a, K_a, t] \qquad (2.1)$$

Table 2.1 Parameters that affect the local scour around the abutments (retrieved from Daşkın, 2011)

Parameter Name	Symbols	Attribution
Density	ρ	FLUID
Dynamic Viscosity	μ	
Gravitational Acceleration	g	FLOW
Normal Flow Depth	y	
Mean Approach Velocity	U	
Energy Slope of Flow	S_e	
Width of Channel	B	CHANNEL
Slope of Channel	S_0	
Geometry of Channel	K_G	
Median Size	d_{50}	BED MATERIAL
Specific Gravity	S_g	
Standard Deviation	σ_g	
Fall Velocity	w	
Particle Shape Factor	S_p	
Angle of Repose	φ	
Cohesiveness	C	
Dimensionless Critical Shear Stress	α_c	
Particle Reynolds Number	Re^*	
Length of Abutment	L_a	ABUTMENT
Skewness	α_a	
Shape of Abutment	K_a	
Time	t	TIME

These parameters that are given above can be simplified by neglecting some of them for specific conditions. Thus, the remaining parameters that are given below in a nondimensionalized form can be accepted as the most critical parameters affecting the scour development around the abutments (Li et al., 2006):

$$\frac{d_s}{L} = f\left(t, \frac{U}{U_c}, \frac{L_a}{d_{50}}, \frac{L_a}{y}, \sigma_g, K_a, K_g, \alpha_a\right) \tag{2.2}$$

where U_c is the critical mean velocity at which the sediment particles start to move at the channel bed and U/U_c is the flow intensity.

Each parameter that is underlined above has significant effects on the scour formation around the bridge abutments, so considering these parameters during the design process is a critical issue. Therefore, some of these parameters are explained detailed in the following sections.

2.4.1 Effect of Time

Development of local scour around the bridge elements is a time-dependent process. As it is expected, scour hole enlarges with increasing time. Therefore, the temporal development of scour and the required time to reach its equilibrium state should be investigated carefully to make a proper bridge foundation design

Equilibrium scour depth is the maximum scour depth in a scour hole when the scour formation stops and the size and shape of the scour hole become constant. In other words, the scouring rate becomes insignificant as the asymptotic state of the scour is attained (Tekin, 2012).

A schematic diagram of the temporal variation of clear-water and live-bed scour at a cylindrical pier is shown in Figure 2.3 (Chabert and Engeldinger, 1956). It can be seen that from Figure 2.3, the necessary time to reach an equilibrium state is longer for the clear-water scour than for the live-bed scour.

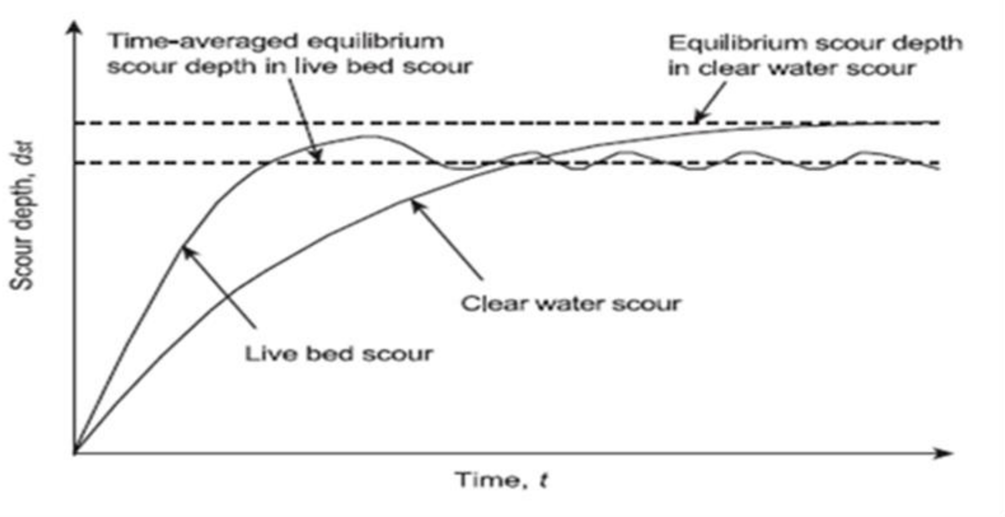

Figure 2.3 Temporal variation of clear-water and live-bed scour (Chabert and Engeldinger, 1956)

According to Melville and Chiew (1999), the necessary time to reach the equilibrium state of the scour hole increases rapidly with the increasing approach flow velocity for clear-water scour; on the other hand, a rapid decrease occurs for the live-bed scour. They also mentioned that for a given approach flow velocity and flow depth, the necessary time to reach equilibrium scour depth increases as the pier diameter increases. Although it takes a very long time to get the equilibrium scour depth, Melville and Chiew (1999) observed that between 50% and 80% of the equilibrium scour depth is developed after 10% of the time to reach equilibrium scour depth. Moreover, several experimental studies showed that 70% and 90% of the equilibrium scour depths are achieved during the first 30 and 150 minutes of the experiments, respectively (Borghei et al., 2012).

Barbhuiya and Dey (2004) stated that "Rouse (1965), Gill (1972), Rajaratnam and Nwachukwu (1983), Dargahi (1990), Ettema (1980), Kohli and Hager (2001), Oliveto and Hager (2002) and Coleman et al. (2003) think that the variation of the scour depth with time is logarithmic. Ahmad (1953), Franzetti et al. (1982), Kandasamy (1989), Whitehouse (1997), Cardoso and Bettess (1999), and Ballio and

Orsi (2000) propose an exponential time-variation of the scour; while Breusers (1967) and Cunha (1975) give a power law distribution".

In addition, most studies stated that the equilibrium scour depth developed under laboratory conditions does not show consistency with the real-time scour development under flood events. Also, predicting the maximum scour depth with its time is very difficult for flood events. This issue will be discussed in detail in Chapter 4.

2.4.2 Effect of Flow Velocity and Intensity

Flow intensity can be defined as the ratio of the shear velocity (U_*) to the critical shear velocity (U_{*c}). According to Melville and Chiew (1999), the ratio of the approach mean velocity (U) to the critical mean velocity (U_c) can also be accepted as the flow intensity because of the measuring problems of the shear velocity. The maximum scour depth occurs when the ratio of $U_*/U_{*c}=1$ that is identified as the threshold peak. However, scour depth around the abutment starts to decrease and then increases again to its maximum value while increasing flow intensity at higher flow intensities than the threshold peak (Melville, 1992). Therefore, it is obvious that the maximum scour depth occurs at the threshold condition under clear-water scour conditions.

Flow intensity is directly related to the Froude Number, F_r. So, researchers such as Garde et al. (1961), Zaghloul and McCorquodale (1975), Zaghloul (1983), Rajaratnam and Nwachkwu (1983) and Froehlich (1989) considered the Froude number in their studies (Barbhuiya and Dey, 2004). Garde et al. (1961) stated that the approach flow velocity could be expressed as the Froude number while predicting the maximum scour depth. Kandasamy (1989) demonstrated that the depth of scouring increases as the depth of flow increases, which is caused by the inclusion of the Froude number.

Dongol (1994) observed that increasing the shear velocity and flow velocity until the threshold condition leads to increased local scour depth. Laursen and Toch (1956), Chabert and Engeldinger (1956), Gill (1972), Breusers et al. (1977), Ettema (1980), Raudkivi and Ettema (1983), Chiew (1984), and Melville and Chiew (1999) also indicated the same trend. In recent years, Tabarestani and Zarrati (2017) stated that the scour depth increases approximately 4.6 times when the flow intensity is increased from 0.55 to 0.95.

2.4.3 Effect of Flow Depth

The relationship between scour depth and flow depth has been studied by many researchers such as Chabert and Engeldinger (1956), Laursen and Toch (1956), Gill (1972), Breusers et al. (1977), Ettema (1980), Wong (1982), Tey (1984), Kwan (1988), Kandasamy (1989), Breusers and Raudkivi (1991), Dongol (1994), Hoffmans and Verheij (1997), Melville and Coleman (2000). Experimental data from Gill (1972), Wong (1982), Tey (1984) and Kandasamy (1989) showed that an increase in approaching flow depth leads to an increase in the maximum scour depth for a given flow intensity. According to Richardson and Davis (2001), an increase in flow depth can increase the scour depth with a ratio of 1.1- 2.15 depending on the abutment shape. Moreover, the maximum scour depth might increase 2 times or more with increasing flow depth for the pier, whereas the increasing rate of the maximum scour depth is smaller for the abutments depending on the abutment shape (Arneson et al., 2012).

Experimental results of Wong (1982), Tey (1984), Kwan (1988), Kandasamy (1989) and Dongol (1994) indicated that the scour depth around the abutment increases at a decreasing rate with flow depth until normalized flow depth, L_a/y, reaches a limit value (Li et al., 2006). When the limit value exceeds, the scour depth becomes independent of flow depth. In other words, the effect of flow depth on the equilibrium scour depth was investigated by considering the impact of the abutment length on the equilibrium scour depth. Dey and Barbhuiya (2004) stated that the equilibrium scour depth increases with increasing flow depth for shallower flow depths; on the other hand, the equilibrium scour depth is not affected by a change in flow depth for higher flow depths.

2.4.4 Effect of Sediment Size

The median size diameter of sediment particles, d_{50}, is an important factor in evaluating the effect of bed material on the scour formation.

According to Ahmad (1953), Izzard and Bradley (1958) and Garde et al. (1961), the rate of scour is faster for fine sediments than for coarse sediments. Gill (1972) stated that although coarse sediments cause more scour than fine sediments under clear-water scour, scour depth for fine sediments is greater than coarse sediment for a given absolute approaching bed shear stress.

Dongol (1994) presented the sediment coarseness as the ratio of abutment length, L_a, and median sediment size, d_{50}, to show the effect of sediment size on scour depth. He classified sediment coarseness into four groups: fine ($L_a/d_{50}>100$), intermediate ($40<L_a/d_{50}<100$), coarse ($10<L_a/d_{50}<40$) and very coarse sediment ($L_a/d_{50}<10$). It was also stated that the equilibrium scour depth increases with increasing median sediment size for a given abutment length, where $L_a/d_{50}<40$. However, with larger values of L_a/d_{50}, the sediment size does not affect scour depth (Li et al., 2006).

Ettema (1980) and Chiew (1984) found when the median sediment size is smaller than 50 times of a bridge pier, the effect of sediment size is insignificant on scour depth (Melville, 1992). Later, Melville (1997) and Coleman et al. (2003) tested this condition (i.e., $L_a/d_{50}\geq50$) for the abutments. For $L_a/d_{50}<50$, scour depth increases with increasing L_a/d_{50} and has a peak value at $L_a/d_{50}=50$; however, for larger values of L_a/d_{50}, scour depth does not depend on sediment size (Coleman et al., 2003).

On the other hand, Laursen (1960) indicated that the sediment size significantly influences the maximum scour depth under clear-water conditions but not under live-bed conditions (Barbhuiya and Dey, 2004). As Laursen (1960) did, some early pier scour studies discussed that sediment size has no noticeable impact on local scour under live-bed conditions. In contrast, others proposed that as sediment size increases, the scour depth decreases. The vast majority of studies have demonstrated that particle size affects local scour when clear-water flow conditions are considered (Li et al., 2006).

2.4.5 Effect of Sediment Gradation

Since river bed materials are generally nonuniform, the uniformity degree of the sediment particles also affects the scour formation. Hence, the geometric standard deviation of the particle size distribution, σ_g, and coefficient of uniformity, C_u, which are represented below, are used to measure the uniformity of sediment particles.

$$\sigma_g = \sqrt{\frac{d_{84}}{d_{16}}} \tag{2.3}$$

$$C_u = \frac{d_{60}}{d_{10}} \tag{2.4}$$

Ettema (1980) and Raudkivi and Ettema (1983) indicated a relationship between the maximum scour depth at piers and the geometric standard deviation of particle size distribution. The limit value of σ_g is obtained at 1.35, where the bed materials having σ_g bigger than the limit value are nonuniform sediments and smaller ones are uniform sediments (Breusers and Raudkvi, 1991). Nonuniform sediments induce smaller scour depths than uniform sediments. In nonuniform sediments, a process of armoring in the scour hole starts, exposing the coarser fraction as the finer fraction is washed out. The armor layer gradually raises the critical bed shear stress, which inhibits the scour hole evolution (Dey and Barbhuiya, 2005b). Li et al. (2006), along with Ettema (1980), Wong (1982), Melville (1992), and Dongol (1994), stated that the scour depth gradually increases with decreasing σ_g value.

The parameter as the coefficient of uniformity, $C_{u,}$ is also used to determine the uniformity of the sediments (Doğan, 2008). Sediment particles having C_u values less than 3.0 are classified as uniform sediments, otherwise nonuniform sediments.

According to Dongol (1994), the effect of sediment grading on scour development has more influence at lower flow velocities (Li et al., 2006).

2.4.6 Effect of Abutment Length

The effect of abutment length and contraction ratio on scour depth around abutments has extensively been discussed in the literature. Researchers like Garde et al. (1961), Gill (1972), Neill (1973), Zaghloul and McCorquodale (1975), and Rajaratnam and Nwachukwu (1983) focused on the contraction ratio in their studies. However, Neill (1973) stated that the contraction ratio becomes a secondary influence for short abutment cases because the short abutments lead to a very wide channel; therefore, the contraction ratio as a scaling parameter can not be considered for short abutment cases (Barbhuiya and Dey, 2004). Moreover, Laursen (1963), Cunha (1975), Wong (1982), Tey (1984), Kandasamy (1989), and Melville (1992) stated the local scour formation is independent of the contraction ratio. Consequently, in abutment scour studies, the abutment length has been considered an influential factor.

Kandasamy (1989) stated that the decreased opening ratio due to the increased abutment length leads to a larger scour depth. Melville (1992) indicated the scour depth increases with increased abutment length at a decreasing rate. He also classified the abutment lengths as short ($L_a/y \leq 1$), intermediate ($1 < L_a/y < 25$) and long ($L_a/y \geq 25$) based on the ratio of abutment length to flow depth. Kayatürk (2005) also remarked that based on her experimental investigation, the maximum scour depth increases with increasing the abutment length for a given Froude number. According to Koken and Gogus (2015), the size and coherence of the primary horseshoe vortex are much smaller for short spur dikes than for long spur dikes, and a larger bed shear stress region occurs around the long spur dikes. Consequently, this situation explains the less scour formation around smaller obstacles since the primary vortex and bed shear stress region are closely attributed to the size of the scour hole.

2.4.7 Effect of Abutment Shape

The abutment shape is a decisive parameter for the magnitude of the local scour depth. Since streamlined obstacles, such as semi-circular, spill-through and wing-wall abutments, produce weaker downflow and secondary vortices than blunt obstructions, such as vertical-wall abutments, the magnitude of the local scour depth for blunt obstacles is observed to be relatively larger (Barbhuiya and Dey, 2004). According to the experimental studies conducted by Laursen and Toch (1956), Liu et al. (1961), Garde et al. (1961) and Wong (1982), the observed scour depth value is greater for the vertical-wall abutments than for the spill-through and wing-wall abutments. Furthermore, Laursen and Toch (1956) stated that the local scour depth is 15% smaller for streamlined abutments. Li (2005) reported that the deepest scour depth occurs at the vertical-wall abutments and the smallest scour depth is produced on the most gentle sloped spill-through abutment based on experimental data from Dongol (1994). Based on the experimental study conducted for the short abutments, Hosseinjanzadeh et al. (2021) indicated that the greatest scour hole magnitudes are obtained for the vertical-wall abutments, then semi-circular and wing-wall abutments, respectively. Although the semi-circular abutments produce greater scour depths than wing-wall abutments, the differences can be considered insignificant.

Melville (1992) proposed the shape factor, K_s, to present the impact of the abutment shape on equilibrium scour depth. The shape factors of the commonly used bridge abutment shapes, according to Melville (1992), such as vertical-wall, semi-circular, wing-wall and various types of spill-through, are presented in Figure 2.4. Data from the experimental studies conducted by Gill (1972), Wong (1982), Tey (1984), Kwan (1984, 1988) and Dongol (1994) were used to generate the values in Figure 2.4.

Abutment model	Abutment shape	Shape factor, K_s
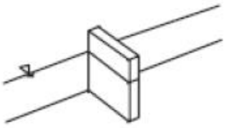	Vertical-wall	1·00
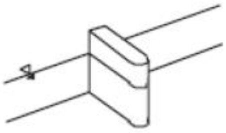	Semicircular ended	0·75
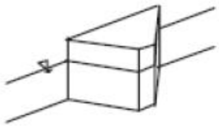	45° wing-wall	0·75
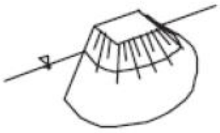	Spill-through with slope horizontal : vertical	
	0·5 : 1	0·60
	1 : 1	0·50
	1·5 : 1	0·45

Figure 2.4 Abutment shape factors (Barbhuiya and Dey, 2004)

Melville (1992) also indicated that the effect of abutment shape on scour depth reduces as the abutment becomes longer. Therefore, for the $L_a/y \geq 10$, where L_a is the abutment length and y is the flow depth, K_s^* was proposed as an adjusted shape factor. K_s^* varies linearly between the value of K_s at L_a/y = 10 and 25, then becomes unity.

2.4.8 Effect of Abutment Skewness

In general, bridges are built at a straight zone of the river channel and perpendicular to the flow in order to provide the shortest span and eliminate skewness. However, inclined abutments can be constructed because of the road layout limitations and the river channel's geometry. The inclination of the abutment relative to the mean flow direction is known as abutment skewness (Li et al., 2006). A scheme of abutment skewness angle, α_a, is illustrated in Figure 2.5.

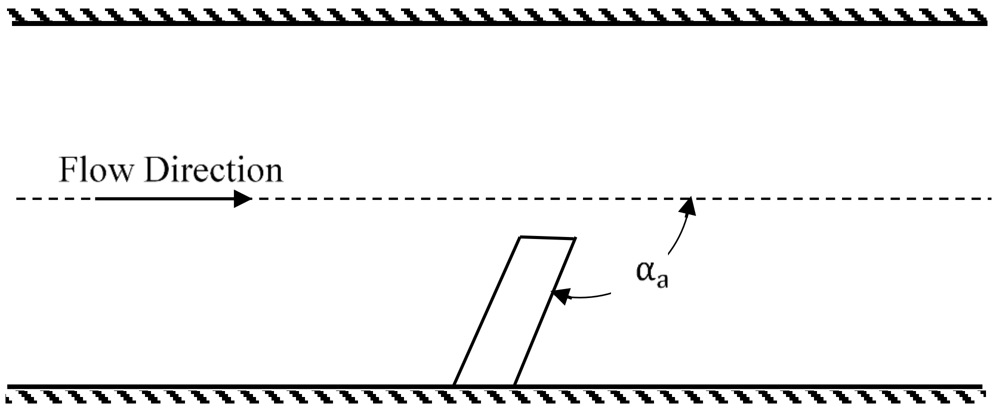

Figure 2.5 Abutment skewness angle

The effect of abutment skewness on local scour has been investigated by Ahmad (1953), Laursen and Toch (1956), Laursen (1958), Garde et al. (1961), Sastry (1962), Zaghloul (1983), Kwan (1984), Kandasamy (1985), Melville (1992) and Koken (2011).

According to the experimental studies of Garde et al. (1961) and Kwan (1984), the greatest scour depths are observed at the spur dikes with an inclination of 90° for the same abutment, flow and sediment conditions. On the other hand, Zaghloul (1983) revealed that the maximum equilibrium scour depth occurs in the case of an upstream spur dike inclination, while the smallest equilibrium scour depth occurs at the spur dike inclined downstream (Barbhuiya and Dey, 2004). Melville (1992) proposed an alignment factor, K_θ, which can be implemented for the longer abutments ($L_a/y > 3$), whereas the skewness effect for the abutment lengths smaller than the limit value is obtained as negligible. Koken (2011) stated that the magnitude of the primary vortex is the largest when the spur is perpendicular to the flow direction ($\alpha_a = 90^\circ$). The potential scour area is approximately 2% and 15% smaller for the cases of $\alpha_a = 60^\circ$ and 120°, respectively, compared to the case of $\alpha_a = 90^\circ$.

CHAPTER 3

EXPERIMENTAL SETUP

The experiments were carried out in a laboratory flume having a deep recess box filled with sediment in the Hydraulics Laboratory of the Civil Engineering Department of Middle East Technical University, Ankara, Turkey. Detailed information about the experimental setup, flow characteristics, measurement techniques and devices that were used during the experiments are mentioned in this chapter.

3.1 Flume

Experiments were carried out in a rectangular sediment channel with plexiglass walls, 28.5 m in length and 1.5 m in width with a slope of S_0= 0.001. The length of the sand layer was 5.8 m in the flow direction having a depth of 0.48 m and located at a distance of 13.5 m from the entrance section of the channel (Figures 3.1- 3.3). By measuring the flow velocity distributions from upstream of the abutments along the channel length, it was observed that the approach flow was fully-developed and uniform during the experiments. The necessary discharge was supplied by a pump from a constant-head water tank to the experimental setup. A control gate was set at the end of the channel to regulate the flow depth and intensity. A sharp-crested rectangular weir having a width of 1.5 m and a height of 0.30 m is mounted at the upstream section of the flume. The crest of this weir is located about 1 m above the channel bottom. Therefore, the flow coming over the weir first falls into an energy-dissipating pool where the energy of the flow is dissipated. Then it passes through bricks and a sheet-iron filter set at the entrance of the channel to reduce turbulence of the flow and to provide stable, uniform flow conditions.

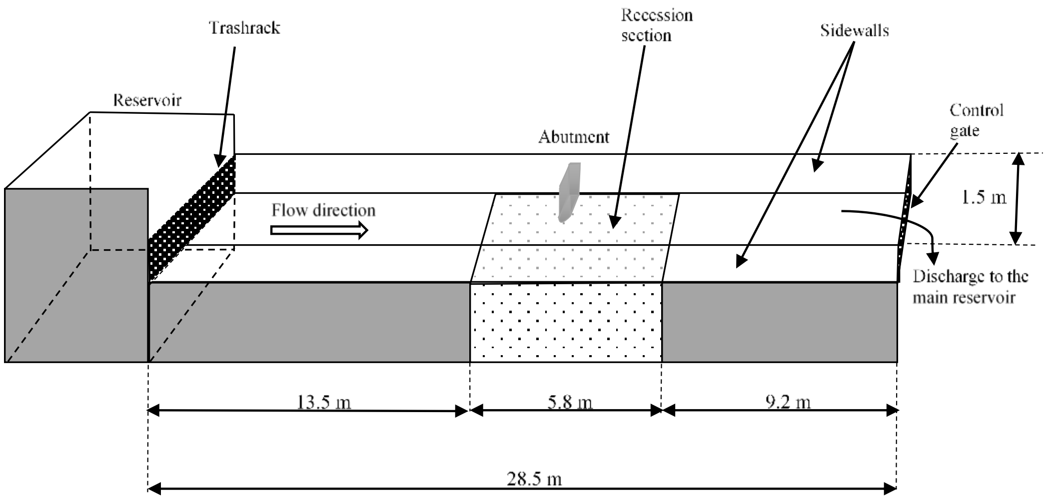

Figure 3.1 Sketch of the experimental setup (Gogus et al., 2023)

Figure 3.2 View of the experimental setup from upstream

Figure 3.3 View of the experimental setup from downstream

3.2 Abutment and Collar Models

Abutments of 6 different lengths, L_a = 15 cm, 20 cm, 25 cm, 30 cm, 35 cm and 40 cm, made of plexiglass, were tested during the experiments. Since the effect of abutment width, B_a, on the scour hole development is small and negligible (Oliveto and Hager, 2002; Kumcu et al., 2007), the widths of the abutments within the scope of this study were kept constant at 10 cm. As scour countermeasure, collars with variable widths of B_c = 5 cm, 7.5 cm, and 10 cm, which were made of 3 mm-thick plexiglass, were tested during the experiments. The collars were located around the abutment at sections $Z_c/y_{0.7}$= -0.50, -0.25, ±0.00, where Z_c is the collar elevation relative to the bed level. A sketch of the abutment model with the attachment of a collar is given in Figure 3.4. Moreover, various abutment-collar arrangements from the experiments are shown in Figures 3.5-3.7.

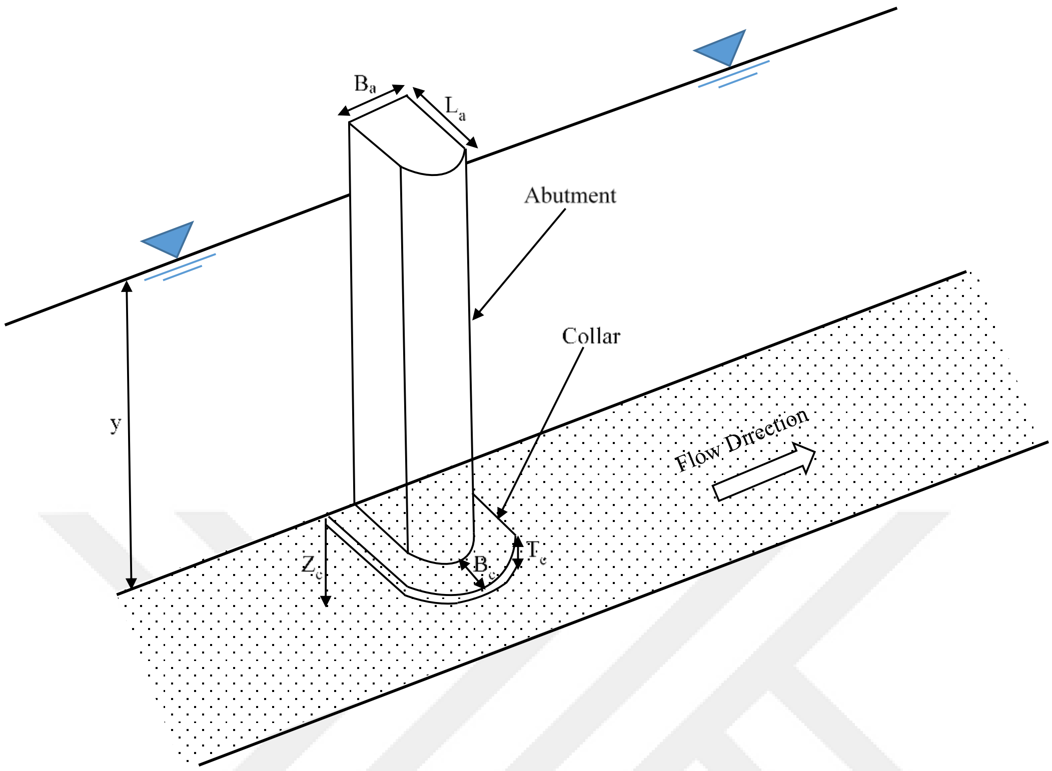

Figure 3.4 Sketch of the abutment-collar arrangement for semi-circular end abutment (Gogus et al., 2023)

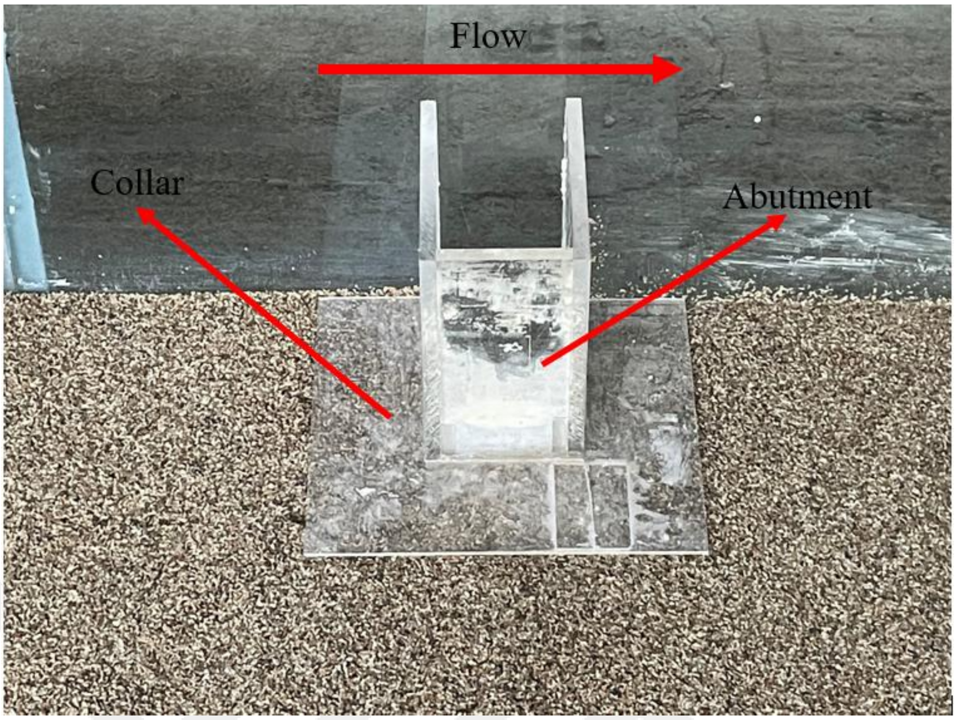

Figure 3.5 View of abutment-collar arrangement

Figure 3.6 Semi-circular end abutment of L_a=35 cm with a collar of B_c=7.5 cm at Z_c/y=-0.25

Figure 3.7 Rectangular abutment of L_a=40 cm with a collar of B_c=10 cm at Z_c/y=±0.00

3.3 Sand Material

Uniform sand having a median size diameter of d_{50}=1.5 mm, the standard deviation of the particle size distribution of σ_g=1.29, and a uniformity coefficient of $C_u = d_{60}/d_{10}$ =1.7 was used in the experiments as an erodible material.

3.4 Flow Characteristics

In scouring problems, the flow intensity is defined as either the ratio of shear velocities, U_*/U_{*c}, or the ratio of mean velocities U/U_c (Li et al., 2006). In this study, the flow depth required to have clear-water flow conditions was determined by using the ratio of U/U_c, where U is the average velocity of the approach flow and U_c is the value of U at the threshold of grain motion (Li et al., 2006; Kumcu et al., 2007, 2014; Khosravinia et al., 2018). Before starting the experiments, a series of preliminary experiments were conducted in the channel without an abutment by observing the initiation of grain motion in order to determine the critical water depth and discharge. From these experiments, the critical water depth and the mean approach flow velocity were observed as y_c= 12.1 cm and U_c= 0.3736 m/s, respectively, when the discharge was Q=0.0678 m^3/s. Critical shear velocity was also calculated theoretically from Shield's diagram by using the equation proposed by Melville and Coleman (2000), in which the units of the parameters U_{*c} and d_{50} are (m/s) and (mm), respectively:

$$U_{*c} = 0.0305\sqrt{d_{50}} - \frac{0.0065}{d_{50}} \tag{3.1}$$

The critical shear velocity was calculated as 0.032 and 0.033 m/s from the experimental and theoretical approaches, respectively.

3.5 Devices Used in the Measurements

An electromagnetic flowmeter was attached to the intake pipe of the flume to measure the flow discharge with an accuracy of ± 2% (Figure 3.8).

In order to investigate the temporal development of scour around abutments without collars, the bathymetry of the bed was scanned at certain time intervals around the abutments by an acoustic device with an accuracy of ± 1mm (Sea Tek 5 MHz Ultrasonic Ranging System) (Figure 3.9).

However, for the experiments conducted with the attachment of the collar to the abutment, the acoustic device could not give consistent results due to the reflection problem caused by the collar. Therefore, for those cases, the maximum scour depths around the abutments were measured with a point gauge with an accuracy of ±1 mm (Figure 3.10) after the experiments were completed.

Figure 3.8 View of the electromagnetic flowmeter attached to the intake pipe

Figure 3.9 Sea Tek 5 MHz Ultrasonic Ranging System (Tekin et al., 2012)

Figure 3.10 View of the point-gauge

CHAPTER 4

TEMPORAL DEVELOPMENT OF LOCAL SCOUR AROUND BRIDGE ABUTMENTS

In this chapter of this study, experimental results of the temporal evolution of local scour depth around semi-circular end and rectangular bridge abutments under unsteady-state clear-water approach flow conditions are presented and discussed. However, before referring to the experimental results, previous studies conducted on this subject will be presented, and then the methodology and procedure of the experiments are explained in detail.

4.1 Literature Review

In the past, several studies were conducted to estimate the maximum scour depths around bridge elements such as piers and abutments (Yanmaz and Altinbilek, 1991; Melville, 1992; Kandasamy and Melville, 1998; Melville and Chiew, 1999; Cardoso and Bettess, 1999; Francesco and Enrico, 2001; Oliveto and Hager, 2002; Coleman et al., 2003, Kumcu et al., 2007). However, these studies mainly focused on predicting equilibrium scour depth for steady-state flow conditions. Contrary to laboratory studies conducted under steady-state flow conditions, bridge failures generally occur during flood events under unsteady-state flow conditions. Furthermore, it is revealed that the maximum scour depths under flood events are much smaller than predictions for equilibrium scour- depths under steady-state flow conditions (Chang et al., 2004; Lai et al., 2009; Borghei et al., 2012, Link et al., 2017). According to Hager and Unger (2010), steady-state approaches overestimate the maximum scour depth by approximately 30%. Nevertheless, several studies have been conducted over the last decades to predict the scour depth around bridge elements under unsteady-state approach flow conditions.

Kothyari et al. (1992) investigated the temporal variation of scour around circular bridge piers under unsteady and steady-state clear-water approach flow conditions by considering sediment uniformity. Experimental results showed that scour depth increases with time for all cases. An algorithm was proposed to obtain the temporal variation of scour depth for uniform sediments. Based on experimental data, a dimensionless empirical formula related to flow, fluid, sediment properties and pier geometry was derived to predict the maximum scour depth. Comparison of the observed and computed data showed that the generated empirical formula reasonably predicts the temporal development of the scour depth around bridge piers for both uniform and nonuniform sediments.

Melville and Chiew (1999) conducted experiments on the temporal development of local scour depth at cylindrical bridge piers in uniform sand beds. An equilibrium time scale parameter was prepared and an empirical formula was developed to calculate this parameter. Moreover, another empirical formula was provided to estimate the necessary time taken to reach the equilibrium scour depth. In conclusion, it was indicated that approximately 50%- 80% of the equilibrium scour depth is developed in a period of 10% of the time to reach the equilibrium scour depth.

Oliveto and Hager (2002) investigated the temporal development of scour depth for bridge piers and abutments. 6 rectangular abutment lengths and 8 circular pier diameters with various uniform and nonuniform sediment sizes were tested during the experiments. Experimental data were used to derive an empirical equation to predict the maximum scour depth. The presented empirical equation will be discussed in the next subsections in detail.

Chang et al. (2004) conducted several experiments under steady and unsteady clear-water flow conditions with uniform and nonuniform-sized sediment particles to observe the scour development around circular bridge piers. Different stepwise hydrographs were tested for unsteady flow conditions with varying peak discharge and time (Figure 4.1).

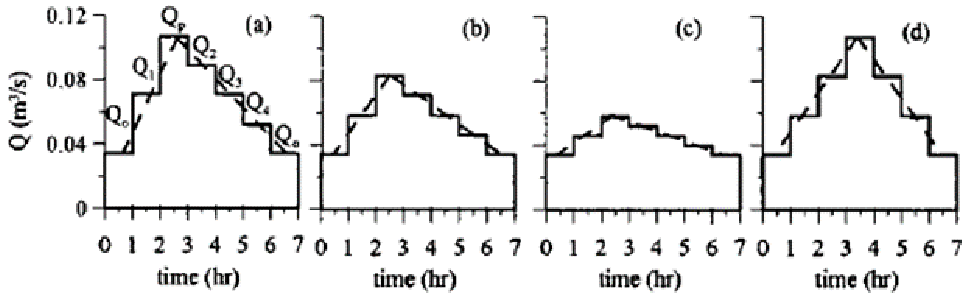

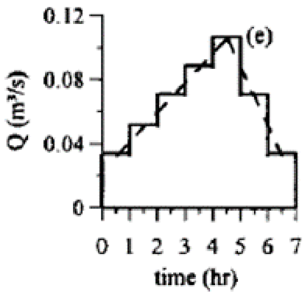

Graph	Run	V_o	V_1	V_2	V_3	V_4	V_p
(a)	U1,U6,U10	22.7	31.3	33.8	31.3	27.9	35.5
(b)	U2,U7,U11	22.7	29.2	31.3	29.2	26.4	33.1
(c)	U3,U8,U12	22.7	26.4	27.9	26.4	24.7	29.2
(d)	U4	22.7	29.2	33.1	33.1	29.2	35.5
(e)	U5,U9,U13	22.7	27.9	31.3	33.8	31.3	35.5

unit : cm / s

Figure 4.1 Stepwise hydrographs used in the experiments (Chang et al., 2004)

Results of the experiments under unsteady-state clear-water approach flow conditions showed that scour depth and rate increase with increasing flow intensity, but the falling limb has no significant effect on scour evolution. Although the time to reach peak discharge affects instant scour depth, it does not affect final scour depth. Finally, a numerical method based on the mixing layer concept was developed to determine equilibrium scour depth for nonuniform-sized sediment particles condition.

Oliveto and Hager (2005a) presented another study that follow up on the previous study stated above. 4 different problems were examined about local scour at bridge elements and specified limitations to use the presented equation in Oliveto and Hager (2002); experiments were conducted to determine minimum laboratory dimensions to apply Froude similitude, the effect of sloping abutments on scour formation, an empirical equation to apply spur dikes and scour formation under unsteady clear-water flow conditions. Both single and double-peaked hydrographs were applied during the experiments. It was mentioned that although the experimental data were fitted to the presented equation in Oliveto and Hager (2002) with a reducing coefficient of the equation, knowledge about the effect of threshold Froude number, $F_d = U/U_t$ where U is the approach flow velocity and U_t is the threshold approach velocity, $U_t = 1.65(g'd_{50})^{1/2}\sigma^{1/3}(R_h/d_{50})^{1/6}$, under unsteady flow conditions is not enough yet.

Lai et al. (2009) discussed the effect of flow intensity, peak time and uniformity of sediment on the maximum local scour depth around bridge piers under unsteady clear-water flow conditions with uniform and nonuniform sized sediment particles. An empirical formula was formed in order to calculate the maximum scour depth for uniform-sized sediment, $(d_s)_{max}$, by using the experimental data of the previous studies, as given below;

$$\frac{(d_s)_{max}}{D} = \alpha K_d K_h P \qquad 4.1$$

where α is the regression coefficient calibrated as 3.9, D is the pier diameter, K_d and K_h presented by Melville (1992) are the factors for sediment size effect and flow, and P is the unsteady flow parameter depending on flow intensity and properties of the hydrograph. On the other hand, Equation 4.1 also shows good agreement for predicting maximum scour depth for nonuniform-sized sediments in the case of adapting d_{84} as the effective sediment size.

Hager and Unger (2010) applied a previously proposed equation (Oliveto and Hager, 2002) to estimate the scour depth on single-peaked flood waves. It was indicated that time-dependent scour formation and the end scour depth were mainly associated with the densimetric Froude number and median sediment size. The impact of the peak approach flow velocity, sediment and fluid properties, geometry and size of the pier on scour formation was also emphasized.

Lu et al. (2011) investigated the temporal development of scour depth around nonuniform cylindrical bridge piers with unexposed foundations (Figure 4.2). The experiments were done in a rectangular channel under steady and unsteady-state clear-water flow conditions using uniform sand particle size (d_{50}= 0.52 mm). A semi-empirical model was developed using the primary vortex and volumetric rate of sediment transport for both steady and unsteady-state flow conditions. In order to achieve flood conditions, three different hydrographs in terms of flow intensity and peak time values were used in the experiments. It was observed that scour formation occurred at Zone 1 above the foundation level for small piers and low flow depths during the experiments. In contrast, for larger piers and higher flow depths, scour formation was observed at Zone 3 with a larger scour hole and the scour formation reached below the foundation level.

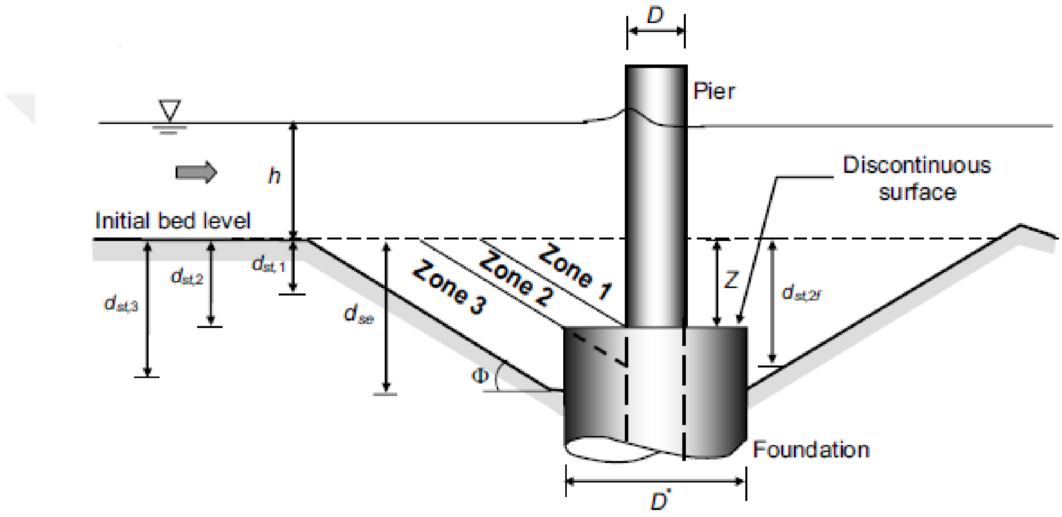

Figure 4.2 Scheme of the pier and pier foundation (Lu et al., 2012)

Finally, a superposition method using an effective pier diameter was applied to model the scouring process for Zone 3. According to the comparison of the experimental and calculated data, the generated model reasonably estimates the scour depth at nonuniform piers under unsteady flow conditions with a maximum error of 7%.

Borghei et al. (2012) studied the effects of unsteady flow hydrograph shape on scour depth around bridge piers. Tests were carried out in a rectangular channel under steady and unsteady-state clear-water approach flow conditions. Various types of hydrographs were tested with varying peak flow discharges and time.

As the study's main purpose, another empirical formula was created to calculate the scour depth under unsteady flow conditions based on data from 60 experiments as given below;

$$\frac{d_s(T)}{d_{s(UT)}} = [1 - e^{-0.6931(\frac{T}{t_{50}})^{0.333}}] \qquad 4.2$$

where $d_s(T)$, $d_{s(UT)}$, T and t_{50} are total scour depth because of repetitions of the hydrograph, equilibrium scour depth due to the hydrograph, time and base time of hydrograph, respectively. Moreover, it was revealed that 70% of the total scour develops in the first 30 minutes of the flow and 90% of the total scour depth occurs in the first 150 minutes. Also, it was mentioned that total scour depth is related to the peak discharge of the flow rather than the peak time of the maximum flow discharge. The effect of the number of peak discharges on local scour depth was found as insignificant.

Salamatian et al. (2014) investigated the temporal development of scour at cylindrical bridge piers during a flood under clear-water approach flow conditions with uniform-sized sediments. Flood conditions were generated by testing 8 different hydrographs having different peak discharge, flow intensity, duration and time to peak discharge. Experimental results indicated that scour depth increases during the rising limb of the hydrograph. On the contrary, the falling limb of the hydrograph has no significant effect on scour depth. Furthermore, the final scour depth is not affected by the time occurrence of the peak discharge. It was also stated that when flow intensity is increased by 25%, scour depth at the pier increases by approximately 48%, so flow intensity was considered the most critical parameter affecting temporal scour development.

Tabarestani and Zarrati (2017) studied local scour evolution around bridge piers under various flood hydrographs. Authors stated that since longer peak flow intensity or discharge durations had commonly been studied on scouring under flood conditions, the rising duration of hydrograph in the experiments was limited to 30 minutes to predict the effect of sudden floods on scour formation around bridge piers.

Experiments were performed in a horizontal flume that 14 m long, 0.75 m wide and 0.6 m deep with uniform sediment size. Thirty-six experiments were carried out with different flow intensities and time to peak discharge. Based on experimental results, scour depth increases 4.6 times by increasing flow intensity from 0.50 to 0.95 while the width and length of the scour hole increase 5.8 times. Thus, it was concluded that flow intensity is more influential on scour dimensions than scour depth. Accordingly, as the rising limb duration of the hydrograph is increased, scour hole dimensions as well as increase. Although the duration to peak flow discharge directly affects scour hole development, it has no significant effect on the final scour hole geometry.

Link et al. (2017) and Pizzaro et al. (2017) proposed a mathematical model to predict time-dependent scour depth around bridge piers under steady and unsteady-state clear-water flow conditions. The model was developed based on dimensionless effective work that includes the effect of the hydrograph shape, rising and falling limbs of the hydrograph, peak flow discharge, duration, and its relationship with the dimensionless scour depth. In this model, the hydrograph duration was discretized to compute the dimensionless work for each interval of unsteady discharge. In order to calibrate and test the model, a series of experiments were performed with varying flood conditions having different hydrograph properties and peak flow discharges. The developed model gives good results with the experimental results of this study and previous studies in the literature.

Bombar (2020) carried out an experimental study on scour formation around bridge piers under different asymmetrical hydrographs in terms of rising duration with high unsteadiness. A five-step method that reasonably agrees with the experimental data of several studies was developed by using the experimental data of this and previous studies in the literature to predict the final scour depth for unsteady flood hydrographs of short durations. It was stated that the scour formation started 25% earlier at the front nose pier than at the side. The final scour depth and rate of the scour development at the sides are higher than at the front nose, especially for higher unsteadiness. Since the higher unsteadiness during the rising limb of the hydrograph leads to increased turbulence intensity, the mobility of the erodible bed around piers accelerates. Hence, the rising limb of the hydrographs is dominantly responsible for scour formation compared with the falling limb of the hydrographs.

Gumgum and Guney (2020) performed experiments by using 16 different triangular hydrographs having different characteristics to investigate temporal scour evolution around circular piers under unsteady-state live-bed water conditions. It was noticed that the flow properties are the most significant parameter on scour depth evolution during the rising limb. Also, the duration of the hydrograph significantly affects the scour depth evolution. Likewise, either increasing the flow velocity or duration of the hydrographs leads to an increase in scour depth. Contrary to clear-water flow conditions, sediment movement into the scour hole was observed during the falling limb of the hydrograph. Yet it was concluded that the scour depth magnitude decreases during the falling limb.

Gjunsburgs et al. (2021) proposed a semi-analytical model based on the bed sediment movement equation to predict the scour depth around vertical-wall abutments located on floodplains under unsteady-state clear-water flow conditions. In order to prove the reasonability of the model, more than 50 experiments were conducted with varying flow depths, discharges, Froude numbers and contraction rates. According to the comparison of experimental and calculated data, the model reasonably predicts the scour depth and scour volume around vertical wall abutments.

Solati et al. (2021) investigated the effect of flood, peak flow duration, and hydrograph pattern on the scouring process around cylindrical piers in sharp bend channels under clear-water and live-bed scour conditions. Based on the experimental results, for single-peaked hydrographs, the maximum scour depth increased by 25% while increasing the hydrograph duration from 25 minutes to 100 minutes. Besides that length of the scour pattern increases by 150% towards the downstream. Moreover, the maximum local scour depth, scour hole area and volume were observed by 35%, 80%, and 425%, respectively, greater for the unsteady-state flow conditions when compared with the steady-state flow conditions. On the other hand, experiments with double-peaked hydrographs having the same total duration as the single-peaked ones showed that despite the duration to reach the peak time and the number of the peak of the hydrograph affects the temporal evolution of scour depth, it is insignificant on the final scour depth.

Abolfathi et al. (2022) conducted a series of experiments to investigate the temporal evolution of scour around pile groups that consists of 3 piles with the same distance to each other under unsteady-state clear-water flow conditions. Twenty-seven different single-peaked hydrographs with different shapes, durations and flow intensities were tested to observe the effect of the unsteadiness parameter on scour development. Based on experimental results, it was indicated that increasing the peak flow discharge by 15% and 26% leads to an increase in the final scour depth around the first pile by 17% and 37%, respectively. On the other hand, increasing the duration of the hydrograph by 50% and 75% causes an 11-14% and 20-26% increase in final scour depths around the first pile. Also, as the duration to reach the peak discharge is increased by 33%, the final scour depth value occurs 44% faster.

Farshad et al. (2022) investigated the effect of spur dike permeability and orientation, base and peak discharge, and duration of hydrograph on the evolution of scour depth around spur dikes under steady and unsteady-state clear-water flow conditions. It was indicated that the maximum scour depth for similar flow conditions and duration is greater for steady-state flow conditions than for unsteady-state flow conditions, as expected. Since the maximum flow discharge is given from the beginning of the experiment during steady flow, the scour depth evolution will be faster. Moreover, it was noticed that the base time of the hydrograph strongly influences the maximum scour depth. As the base time was increased from 15 to 60 min, the maximum scour depth increased by 18% to 37% for various cases. Furthermore, 70% to 90% of the maximum scour depth developed until half of the hydrograph. For such cases, the maximum scour depth was observed even during the hydrograph's falling limb, but those differences were marked as insignificant.

Raikar et al. (2022) studied the temporal evolution of scour around wing-wall, vertical-wall and semi-circular end abutments under steady and unsteady-state clear-water flow conditions. During the experiments, 3 different stepwise hydrographs having the same peak flow intensity and duration but various shapes based on time to reach peak flow intensity values were tested. It was concluded that the maximum scour depth is greater for the vertical-wall abutments than the other tested shapes of abutments. Besides, the finer sediments lead to larger scour depths than coarser sediments. It was also claimed that the time to reach peak flow intensity is increased, and scour depth increases. Accordingly, an abutment-scour model related to flow intensity, flow shallowness, time and sediment coarseness was generated to predict the scour depth around abutments under steady flow conditions.

$$\frac{d_s}{L_a} = a_0 \left(\frac{y}{L_a}\right)^{a_1} \left(\frac{L_a}{d_{50}}\right)^{a_2} (F_d)^{a_3} (\log_{10} T_R)^{a_4} \quad 4.3$$

where d_s is the scour depth, L_a is the abutment length, y is the flow depth, d_{50} is the median sediment size, F_d is the densimetric Froude number, T_R is the reference time and a_1, a_2, a_3, a_4 are regression coefficients. The regression coefficients were determined for different ranges of flow shallowness. In order to implement the generated empirical formula for unsteady flow conditions, a six-step superposition method was recommended. Based on the comparison of experimental and calculated data, the presented model reasonably estimates the scour depth for any time during the rising limb of hydrographs.

Hydrograph, flow and sediment properties of the studies under unsteady-state flow conditions mentioned above are listed in Table 4.1.

Table 4.1 Summary of previous studies conducted on the temporal scour development around obstacles under unsteady-state flow conditions

Study	Obstacle	Type of Hydrograph	Duration (hr)	Ranges of Flow Intensity	Sediment Uniformity	Median Sediment Size, d_{50} (mm)	Approaching Flow Condition
Kothyari et al. (1992)	Pier	Triangular	7	0.82-0.98	Uniform Nonuniform	0.41, 0.50, 0.71, 0.88, 1.00, 3.00, 4.00 (uniform) 0.41 and 0.50 (nonuniform)	Clear-water scour
Chang et al. (2004)	Pier	Stepwise	7	0.6-0.9	Uniform Nonuniform	0.71 & 1.00	Clear-water scour
Oliveto and Hager (2005a)	Pier	Single & Double Peaked	0.67- 2		Uniform Nonuniform	3.10, 4.30 (nonuniform)	Clear-water scour
Hager and Unger (2010)	Pier	Single Peaked Stepwise	0.083-6		Uniform Nonuniform	1.10 (uniform) 3.10 and 3.90 (nonuniform)	Clear-water scour
Lu et al. (2011)	Pier	Stepwise	7	0.65-0.9	Uniform	0.52	Clear-water scour
Borghei et al. (2012)	Pier	Triangular	0.5-2.5	0.83	Uniform	0.98	Clear-water scour
Salamatian et al. (2014)	Pier	Stepwise		0.75-0.95	Uniform	0.67	Clear-water scour
Tabarestani and Zarrati (2017)	Pier	Stepwise	0.03-4	0.5-0.96	Uniform	0.67	Clear-water scour
Link et al. (2017)	Pier	Stepwise, Triangular	0.3-107	0.87-1	Uniform	0.36	Clear-water scour
Pizzaro et al. (2017)	Pier	Stepwise	0.25-150	0.66-0.97	Uniform	0.36	Clear-water scour
Bombar (2020)	Pier	Continuous	0.083-0.183	0.58-0.78	Uniform	0.43	Clear-water scour
Gumgum and Guney (2020)	Pier	Triangular	0.1-0.67		Uniform	1.63	Live-bed scour
Solati et al. (2021)	Pier	Single & Double Peaked	0.417-1.667		Uniform	1.5	Clear-water scour Live-bed scour
Gjunsburgs et al. (2021)	Abutment	Stepwise	14		Uniform	0.24 and 0.67	Clear-water scour
Abolfathi et al. (2022)	Pile	Single-Peaked	0.25-1	0.60-0.87	Uniform	0.7	Clear-water scour
Farshad et al. (2022)	Spur Dike	Single-Peaked	0.25-1	0.48-0.95	Uniform	0.8	Clear-water scour
Raikar et al. (2022)	Abutment	Stepwise	7	0.7- 0.85	Uniform	0.52 and 0.712	Clear-water scour

4.2 Dimensional Analysis

The dimensional analysis of the scour depth, d_s, at an abutment presented in this study is similar to the one given in Kayatürk's (2005) study. For clear-water scour conditions; the scour depth at an abutment is related to the following parameters:

$$d_s = f\{L_a, B_a, U, y, S_0, g, \rho_s, \rho, \mu, d_{50}, \sigma_g, t, t_p, t_{max}, B\} \qquad 4.4$$

where L_a= abutment length, B_a= abutment width, U= mean approach flow velocity, y= flow depth, S_0= slope of the channel, g= gravitational acceleration, ρ_s= density of the sediment, ρ= density of the fluid, μ= dynamic viscosity of the fluid, d_{50}= median particle grain size, $\sigma_g=(d_{84}/d_{16})^{0.5}$= geometric standard deviation of sediment size distribution, d_{84}= sediment size for which 84% of the sediment is finer, d_{16}= sediment size for which 16% of the sediment is finer, t= generic time, t_p= time period of the experiment for a given flow intensity starting from the beginning as 2 hours, 4 hours and 6 hours, t_{max}= total period of the experiment (=6 hours) and represents the entire duration of a flood, B=channel width. Here t_{max} represents, in real cases, the total duration of a flood.

Parameters that are given in Equation 4.4 can be transformed into the dimensionless parameters as:

$$\frac{d_s}{y} = f\left\{\frac{L_a}{y}, \frac{B_a}{y}, \frac{\rho_s}{p}, \frac{U}{\sqrt{gy}}, \frac{B}{y}, \frac{\mu}{U\rho y}, \frac{Ut}{y}, \frac{t_p}{t_{max}}, S_0, \sigma_g, \frac{d_{50}}{y}\right\} \qquad 4.5$$

Since the experiments were carried out with one sediment size and constant channel width, abutment width and bed slope, the related dimensionless terms given in Equation 4.5 can be removed along with ignored viscous effects due to the turbulent nature of the flows in open channels. The channel is wide enough to avoid sidewall effects. The Froude number, $U/\sqrt{gy}$ can be replaced by the flow intensity, U/U_c. Thus, Equation 4.5 can be simplified as:

$$\frac{d_s}{y} = f\left\{\frac{L_a}{y}, \frac{U}{U_c}, \frac{Ut}{y}, \frac{t_p}{t_{max}}\right\} \qquad 4.6$$

where the scour depth normalized with the flow depth appears to be dependent on dimensionless abutment length, dimensionless time, and flow intensity.

4.3 Experimental Procedure

In this experimental study, 12 different experiments were performed on abutments of lengths L_a=15 cm, 20 cm, 25 cm, 30 cm, 35 cm and 40 cm, having a constant width of B_a=10 cm under unsteady-state clear-water approach flow conditions to investigate the local scour development around the semi-circular end and rectangular bridge abutments. A stepwise hydrograph based on flow intensity was applied with a constant flow discharge (Q=0.0678 m^3/s) for 6 hours by increasing flow intensity every 2 hours from 0.7 to 0.8 and then 0.9, respectively (Figure 4.3). Based on previous studies in the literature related to equilibrium scour, the necessary time to reach the equilibrium conditions is approximately 50 hours (Farshad et al., 2022). However, in real flood cases, the magnitude of the scour depth could not reach the equilibrium conditions due to the duration of the flood that lasts before reaching the equilibrium conditions (Cao and Gu, 2015; Gu et al., 2020; Hasegawa et al., 2020). Hence, the experiments conducted under steady-state approach flow conditions to achieve the equilibrium scour depth might mostly overestimate the scour depth for flood conditions. Furthermore, researchers such as Tekin (2012), Khosravinia et al. (2018) and Pandey et al. (2020) showed that approximately 70-75% of the equilibrium scour depth is developed in less than 2 hours. Also, Melville and Chiew (1999) stated that 50-80% of the maximum scour depth occurs at around 10% of the equilibrium time. Therefore, considering the studies mentioned above, 6 hours which consists of 2 hours for each successive flow intensity value is found sufficient to conduct the experiments.

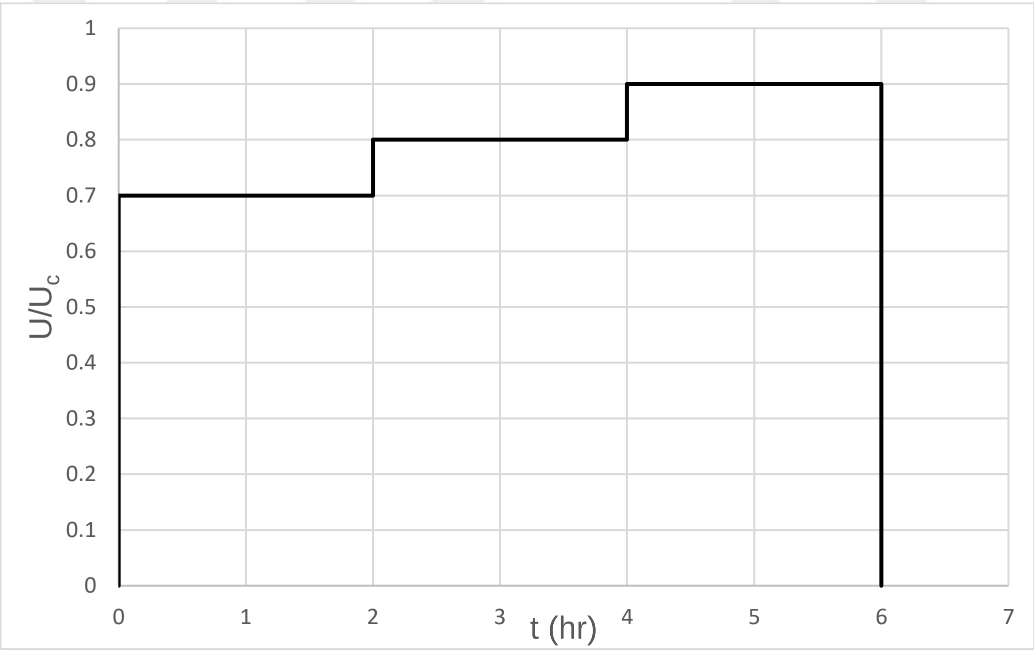

Figure 4.3 Stepwise hydrograph used in the experiments (Gokmener and Gogus, 2022)

Flow intensity was increased by decreasing the flow depth with the help of the tailwater gate located downstream of the flume. Flow depth was measured with a ruler having an accuracy of ± 1mm that is glued to the wall of the sand layer of the flume. Before starting the experiments with an abutment, a series of experiments were conducted without an abutment to obtain flow discharge and the velocity value at the grain motion threshold. Detailed information about those experiments was given in Section 3.4. The experimental conditions of each experiment are summarized in Table 4.2.

Table 4.2 Summary of the experimental conditions of this study (SC= Semi-circular end abutment, RC= Rectangular abutment)

Experiment No	L_a (cm)	Q (l/s)	t (hrs)	y (cm)	U (m/s)	F_r	F_t	U_c (m/s)	U/U_c
SC1 RC1	40	67.8	0-2	17.4	0.262	0.2	0.494	0.3736	0.7
			2-4	15.2	0.299	0.24	0.575	0.3736	0.8
			4-6	13.5	0.336	0.29	0.658	0.3736	0.9
SC2 RC2	35	67.8	0-2	17.4	0.262	0.2	0.494	0.3736	0.7
			2-4	15.2	0.299	0.24	0.575	0.3736	0.8
			4-6	13.5	0.336	0.29	0.658	0.3736	0.9
SC3 RC3	30	67.8	0-2	17.4	0.262	0.2	0.494	0.3736	0.7
			2-4	15.2	0.299	0.24	0.575	0.3736	0.8
			4-6	13.5	0.336	0.29	0.658	0.3736	0.9
SC4 RC4	25	67.8	0-2	17.4	0.262	0.2	0.494	0.3736	0.7
			2-4	15.2	0.299	0.24	0.575	0.3736	0.8
			4-6	13.5	0.336	0.29	0.658	0.3736	0.9
SC5 RC5	20	67.8	0-2	17.4	0.262	0.2	0.494	0.3736	0.7
			2-4	15.2	0.299	0.24	0.575	0.3736	0.8
			4-6	13.5	0.336	0.29	0.658	0.3736	0.9
SC6 RC6	15	67.8	0-2	17.4	0.262	0.2	0.494	0.3736	0.7
			2-4	15.2	0.299	0.24	0.575	0.3736	0.8
			4-6	13.5	0.336	0.29	0.658	0.3736	0.9

Before each experiment, the sand layer was compressed and flattened carefully to have a smooth and homogenous surface. A small discharge was supplied to the flume so that the surface of the sediment bed was not disturbed. After the flow reached the tailgate of the channel, the discharge was slowly increased until it came to the target value (Q=0.0678 m^3/s), and the tailwater gate at downstream was adjusted until getting desired flow depth (y=17.4 cm) and flow intensity (U/U_c=0.7). When the flow depth was stabilized, the acoustic measuring device was activated to measure the bathymetry of the erodible bed around the abutment. Temporal local scour development around the abutment was measured at 24 different points by 24 inducers of the measuring device (Figures 4.4 and 4.5). Scour development around the abutment was recorded every 15 minutes by the device. 2 and 4 hours later, the tailwater gate was again adjusted to obtain the flow depths, y=15.2 cm and 13.5 cm, and flow intensities, U/U_c=0.8 and 0.9, respectively. Then the same procedure was repeated. Totally 6 hours later, the final scour depths were obtained, and the experiment was ended. Since the effect of the falling limb of the hydrograph is not significant for the local scouring under clear-water scour conditions (Chang et al., 2004; Oliveto and Hager, 2005a; Lu et al., 2011; Borghei et al., 2012), the local scouring during the falling limb was not considered in this study.

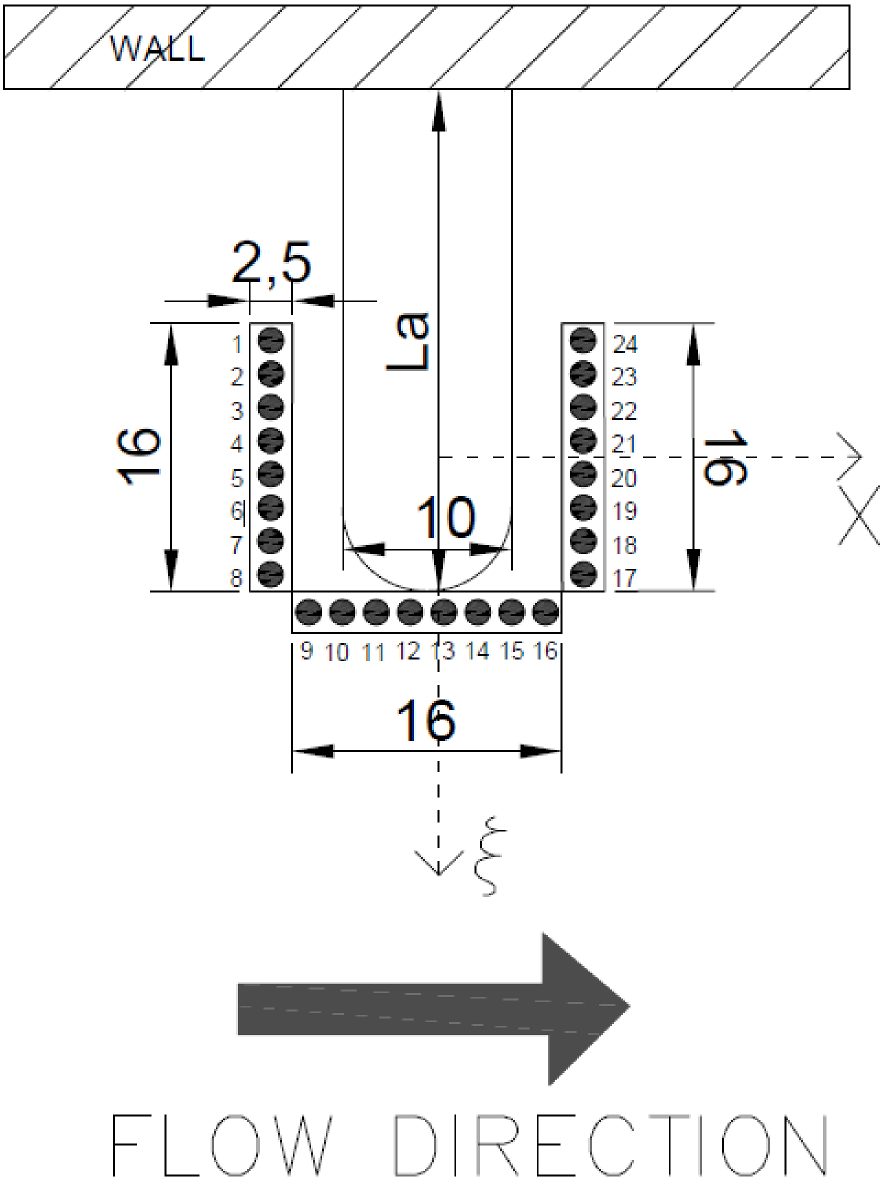

Figure 4.4 Schematic illustration of the semi-circular end abutment and the location of the inducers belonging to the acoustic measuring device to measure the scour depths (dimensions are in cm)

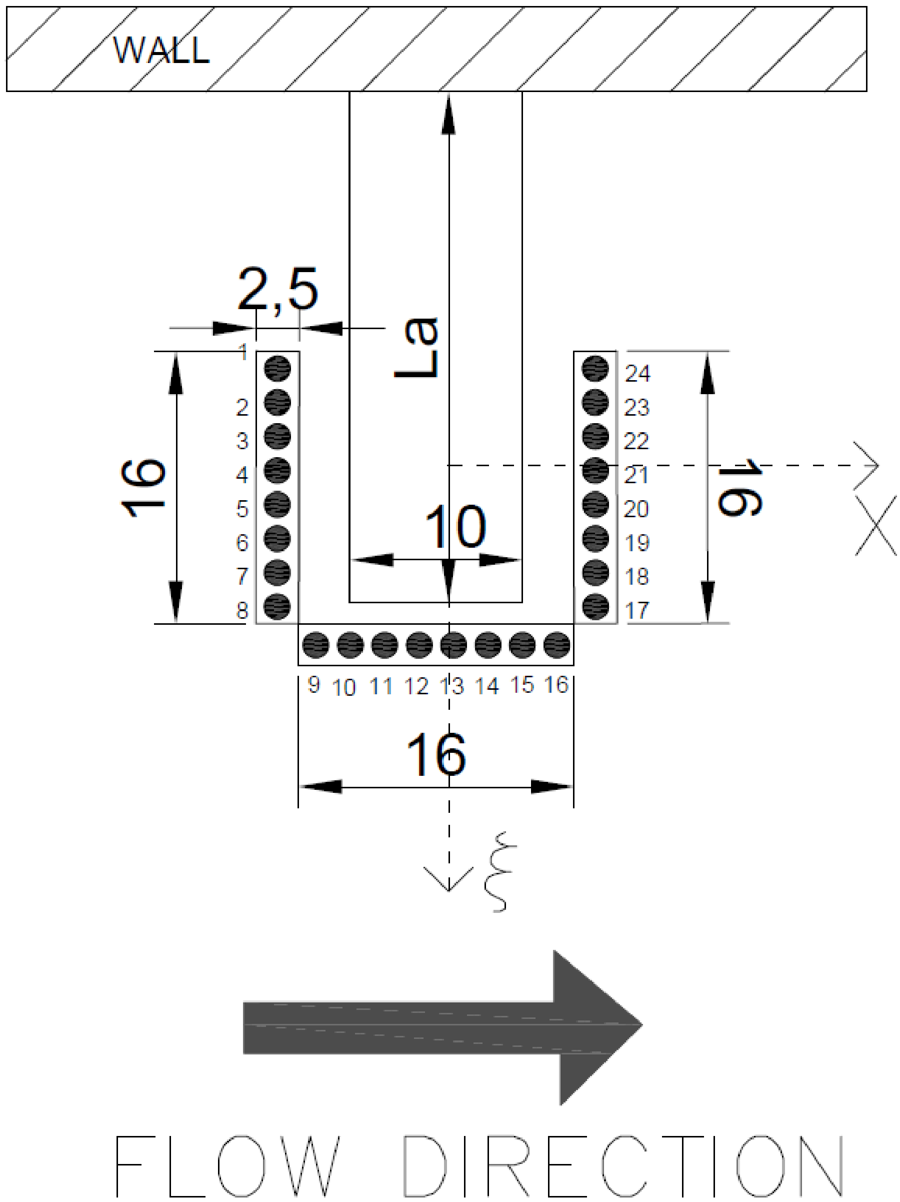

Figure 4.5 Schematic illustration of the rectangular abutment and the location of the inducers belonging to the acoustic measuring device to measure the scour depths (dimensions are in cm)

4.4 Analysis and Discussion of Experimental Results

This section analyzes and discusses experimental results of the temporal development of local scour around semi-circular end and rectangular bridge abutments with varying lengths and flow intensities under unsteady-state clear-water flow conditions. A sample of the related data is provided in Appendix A.

4.4.1 Scour Profiles Around The Abutments

Temporal development of the scour holes around semi-circular end and rectangular bridge abutments having abutment lengths of 15 cm, 20 cm, 25 cm, 30 cm, 35 cm and 40 cm under a stepwise hydrograph that is illustrated in Figure 4.3 are presented and discussed in the following subsections. 24 inducers were used during the experiments to measure the scour depths around the abutments (Figures 4.4- 4.5). Inducers 1- 8, 9-16- 17-24 were located on the abutment's upstream, front and downstream sides, respectively. Scour profiles were non-dimensionalized according to the flow depth at the first 2 hours of the experiment with the flow intensity value of 0.7 ($y_{0.7}$= 17.4 cm).

4.4.1.1 Semi-Circular End Bridge Abutments

4.4.1.1.1 The Abutment of Length L_a= 40 cm

The temporal development of the scour hole around the abutment of length L_a= 40 cm is presented in Figures 4.6- 4.14. During the first 2 hours, with the flow intensity value of 0.7, the scour hole development was rapid in the first hour of the experiment. Then, the increasing rate of the scour hole development decreased gradually at the following time intervals. Especially the development of the scour hole was relatively small between the 105th and 120th minutes. At the upstream side of the abutment, scour hole development was greater for the locations of $-0.2<\xi/y_{0.7}<0.3$ during the first two hours, where ξ is the perpendicular distance to the flow direction and $y_{0.7}$ is the flow depth during the first 2 hours of the experiment with the flow intensity value of 0.7. On the other hand, the development of the deposition of the sediment particles was observed rather than scour formation for the location of $-0.05<\xi/y_{0.7}<0.4$ at the downstream side of the abutment. However, these zones were later covered by the scour hole with increasing time and flow intensity. Maximum scour depths were observed between Inducers; 4 and 7 along the upstream side, 12 and 13 along the front side and 17 and 18 along the downstream side of the abutment. In other words, the maximum scour depths were observed at the upstream, front and downstream sides of the abutment for the locations of $-0.05<\xi/y_{0.7}<0.3$, $-0.05<y/y_{0.7}<0.05$ and $\xi/y_{0.7}=-0.4$, respectively.

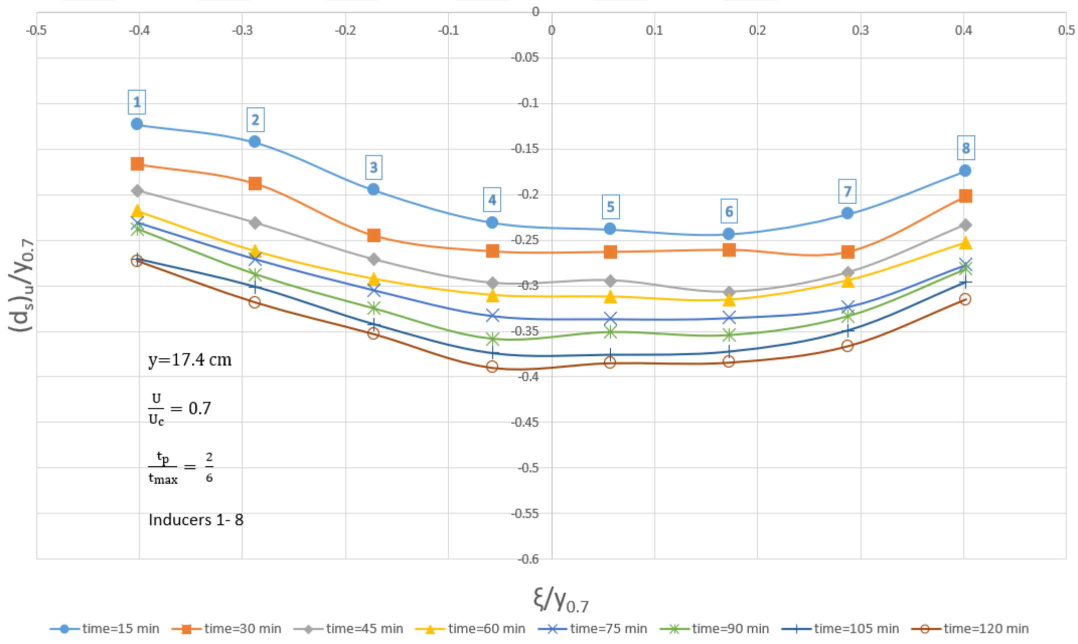

Figure 4.6 Temporal development of scour hole around the semi-circular end abutment of length L_a=40 cm for U/U_c = 0.70 along Inducers 1 - 8

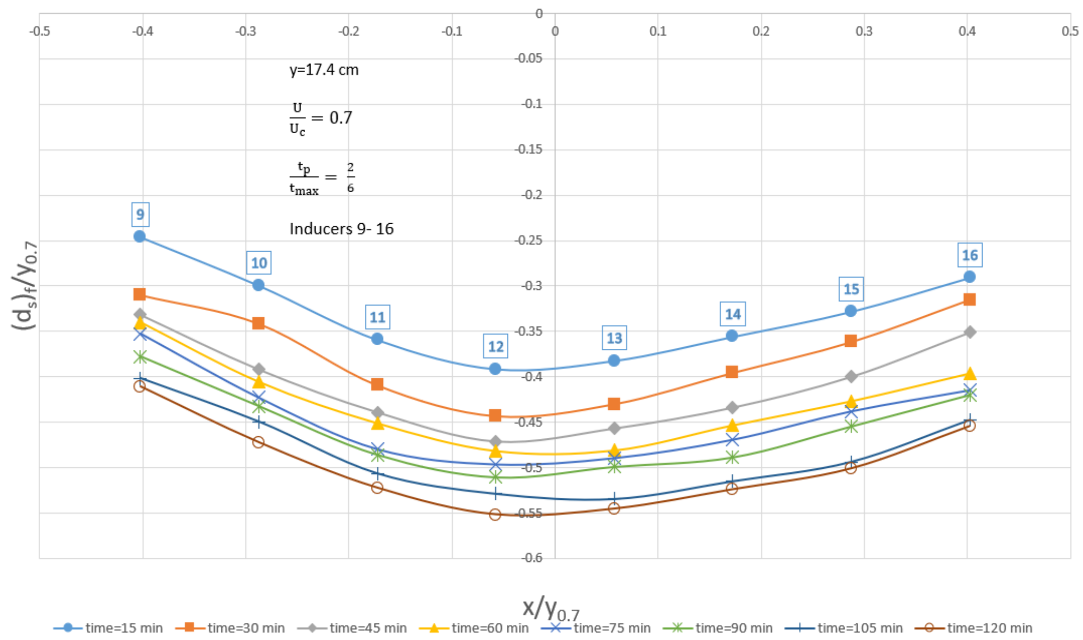

Figure 4.7 Temporal development of scour hole around the semi-circular end abutment of length L_a=40 cm for U/U_c = 0.70 along Inducers 9 - 16

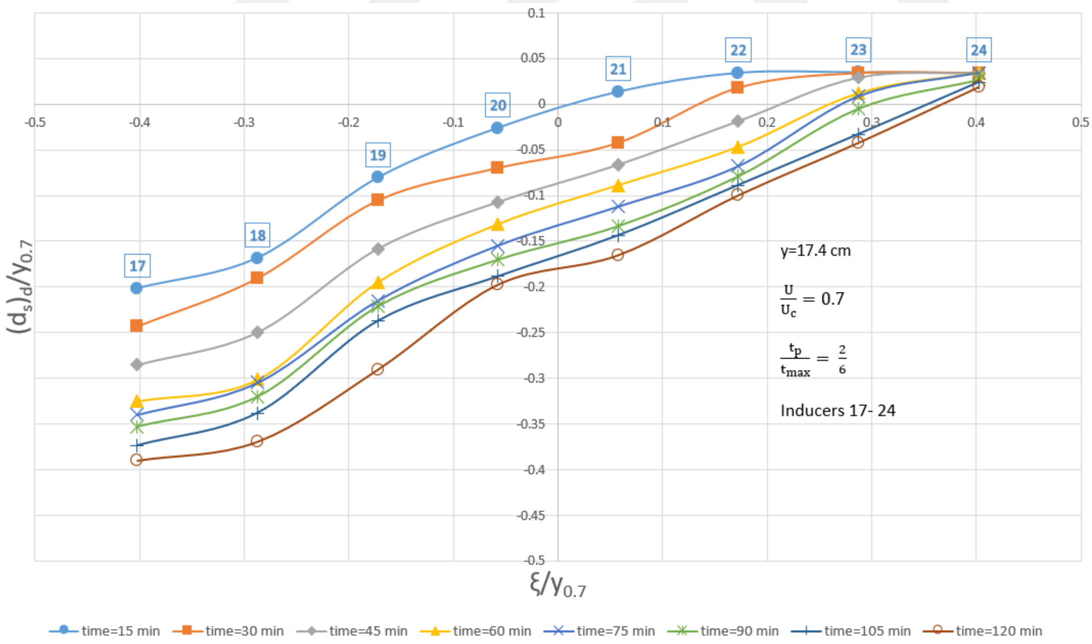

Figure 4.8 Temporal development of scour hole around the semi-circular end abutment of length L_a=40 cm for U/U_c = 0.70 along Inducers 17 - 24

When the first 2 hours were completed with the flow intensity of 0.7, the flow intensity was increased to the value of 0.8 and a rapid development on the scour hole was observed between 120th and 135th minutes. Then, scour hole development continued gradually with a decreasing rate between 135th and 240th minutes. Maximum scour depths were observed between Inducers; 4 and 7 along the upstream side, 12 and 13 along the front side, and 17 and 18 along the downstream side of the abutment. In other words, the locations of the maximum scour depths measured around all sides of the abutment were similar to those measured at the end of the 2nd hour.

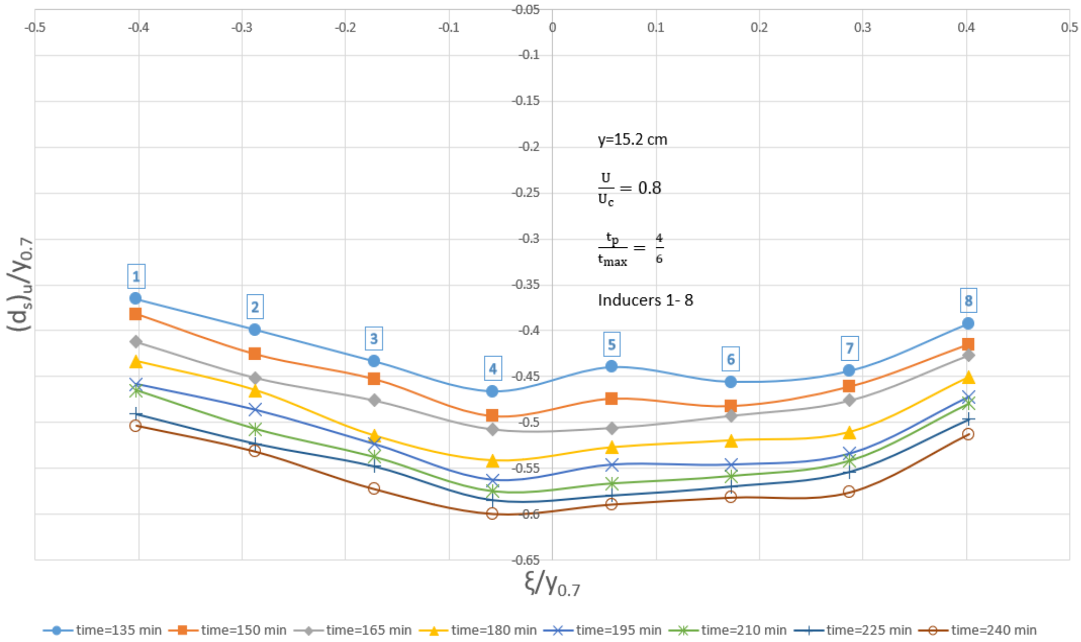

Figure 4.9 Temporal development of scour hole around the semi-circular end abutment of length L_a=40 cm for U/U_c = 0.80 along Inducers 1 - 8

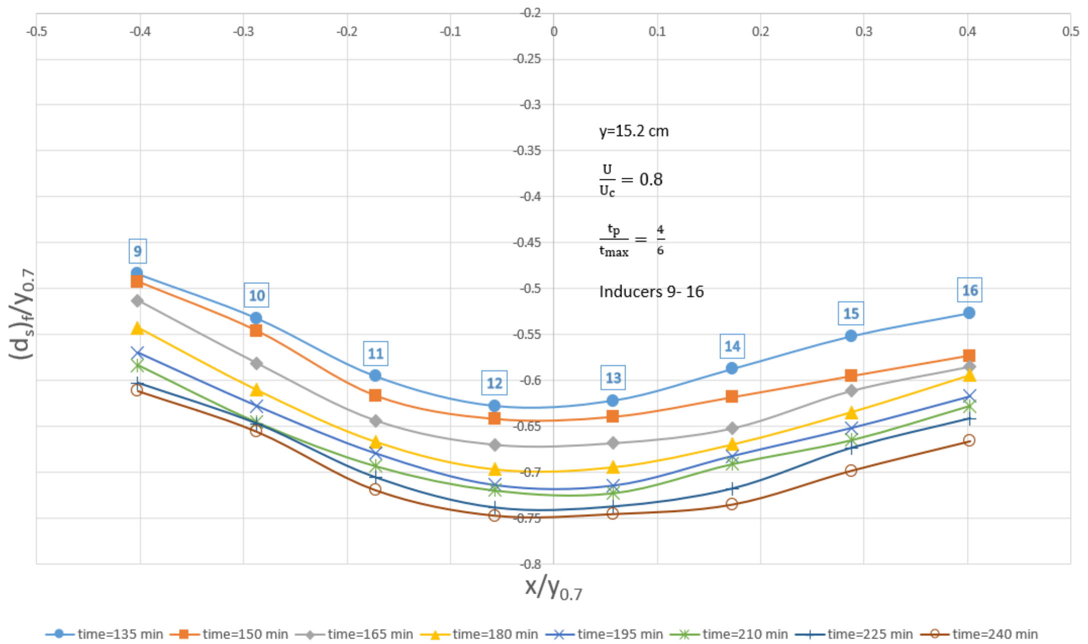

Figure 4.10 Temporal development of scour hole around the semi-circular end abutment of length L_a=40 cm for U/U_c = 0.80 along Inducers 9 - 16

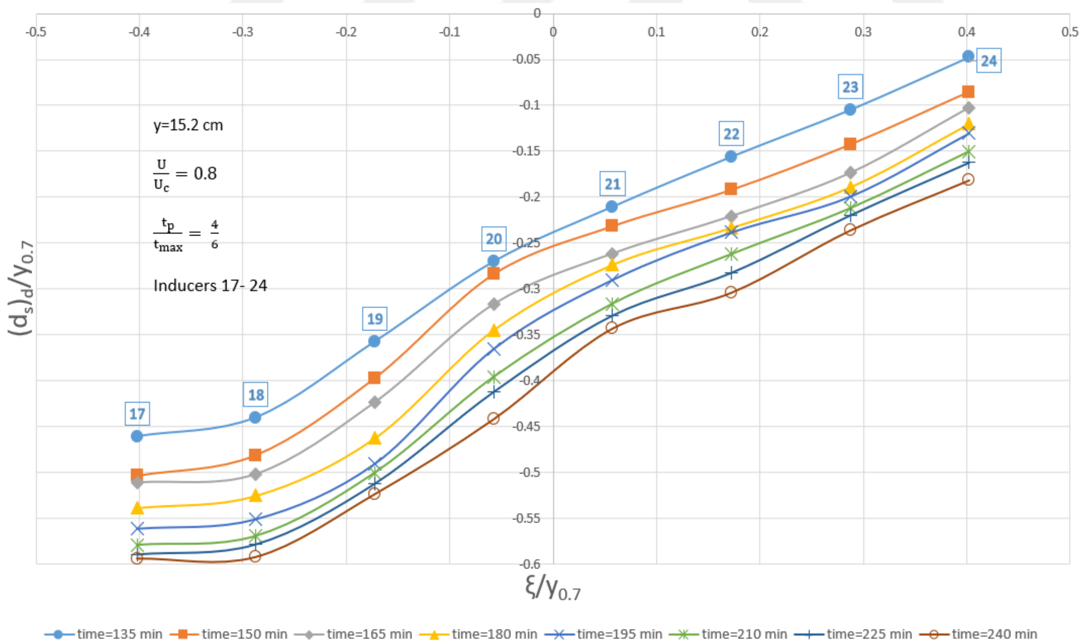

Figure 4.11 Temporal development of scour hole around the semi-circular end abutment of length L_a=40 cm for U/U_c = 0.80 along Inducers 17 - 24

After that, the increasing rate of the scour depth was slow until the flow intensity was increased to 0.9. Scour hole development increased rapidly between 240th and 255th minutes at the upstream and downstream sides of the abutment due to the increased flow intensity. Then, the scour hole development decreased gradually with increasing time except for the location of $-0.2<\xi/y_{0.7}<0.1$ at the front side of the abutment. In this zone, the development of the scour hole was more than the others. On the contrary, at the downstream side for locations of $-0.2<\xi/y_{0.7}<0.4$, scour depth decreased between the 240th and 255th minutes due to the rapid accumulation of sediment particles from upstream and increment was started after 255th minutes in those zones. The development rate of scour hole was small around the abutment after the 300th minute. The maximum or final dimensionless scour depths were recorded as $d_s/y_{0.7}$=-0.79, -0.93 and -0.75 at the abutment's upstream, front and downstream sides, respectively. Approximately 81% of the maximum final scour depth value was observed at the 4th hour of the experiment.

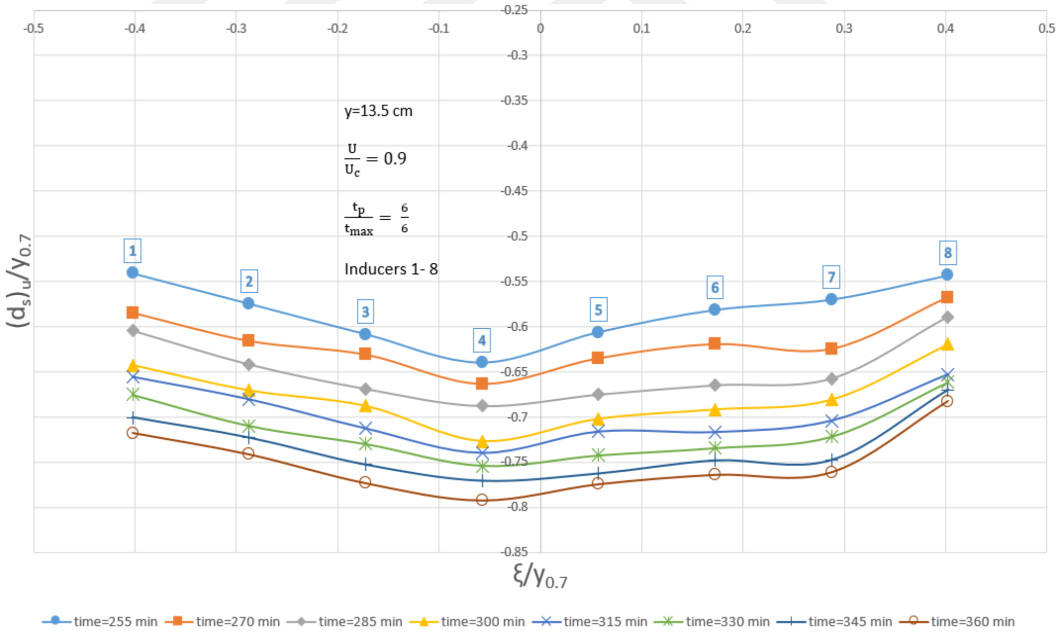

Figure 4.12 Temporal development of scour hole around the semi-circular end abutment of length L_a=40 cm for U/U_c = 0.90 along Inducers 1 - 8

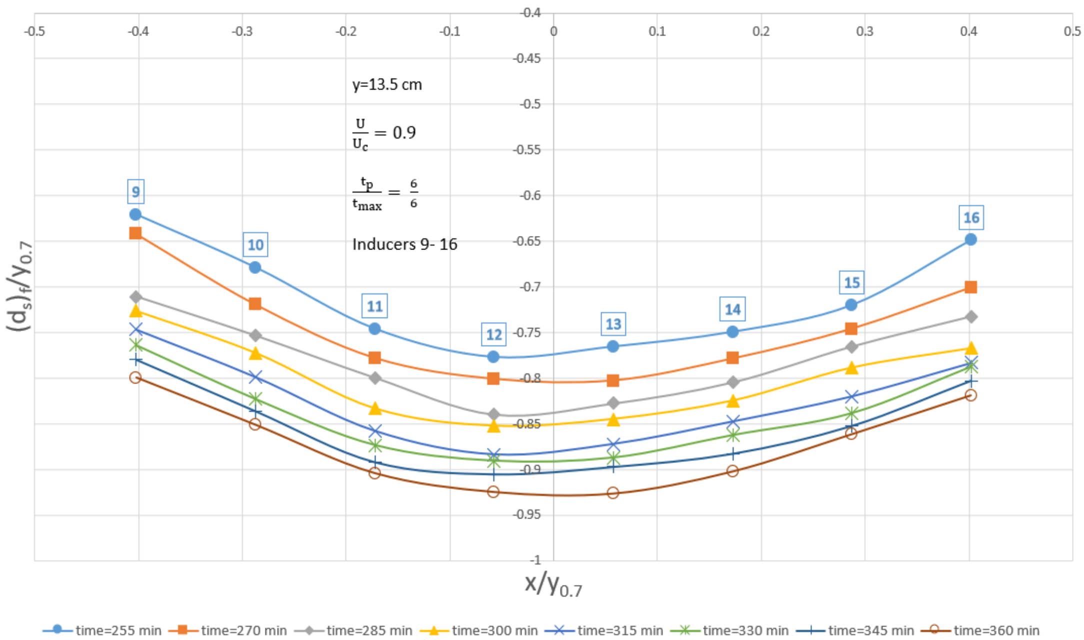

Figure 4.13 Temporal development of scour hole around the semi-circular end abutment of length L_a=40 cm for U/U_c = 0.90 along Inducers 9 - 16

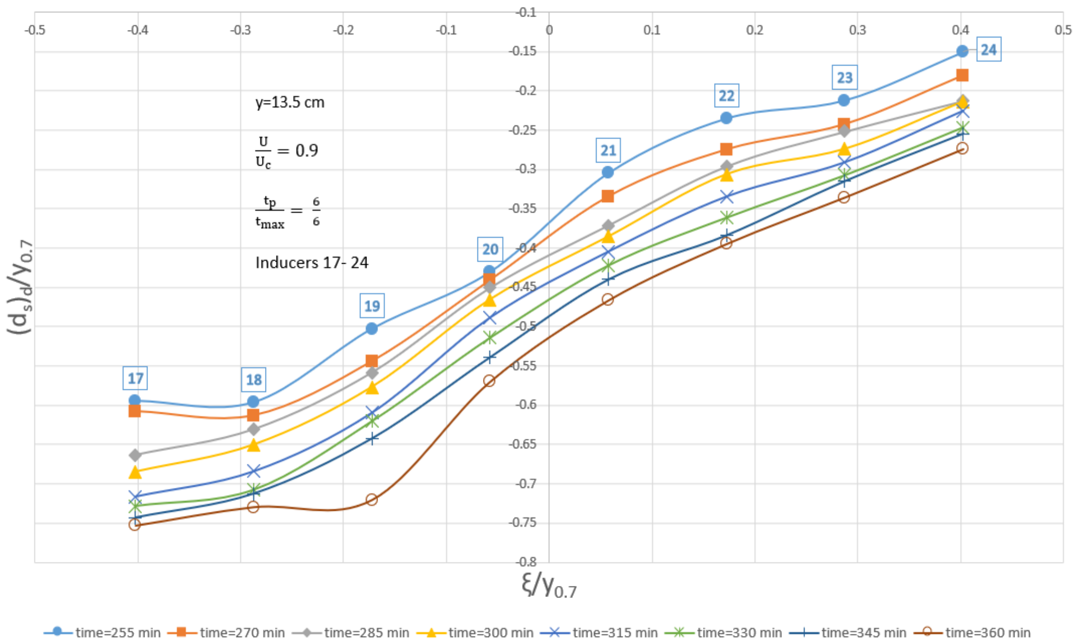

Figure 4.14 Temporal development of scour hole around the semi-circular end abutment of length L_a=40 cm for U/U_c = 0.90 along Inducers 17 - 24

4.4.1.1.2 The Abutment of Length L_a= 35 cm

Figures 4.15- 4.23 show the temporal development of the scour hole around the abutment with a length of L_a= 35 cm. During the first 2 hours of the experiment, with the flow intensity value of 0.7, the scour hole rapidly enlarged and deepened within the first hour of the experiment. In the eventual one hour, the scour hole's development continued, but the increasing rate of the development gradually decreased. In particular, the development of the scour hole was relatively small between the 90th and 120th minutes. At the upstream side of the abutment, the scour depth value was greater for the location of $-0.2<\xi/y_{0.7}<0.3$ during the first 2 hours of the experiment. On the other hand, deposition of the sand particles was observed at the downstream side of the abutment for the location of $-0.1<\xi/y_{0.7}<0.4$. However, with increasing time and flow intensity, significant scour formations were observed in these zones after the 30th minute of the experiment. Maximum scour depths were measured between Inducers 4 and 7 along the upstream side, Inducers 12 and 13 along the front side, and Inducers 17 and 18 along the downstream side of the abutment.

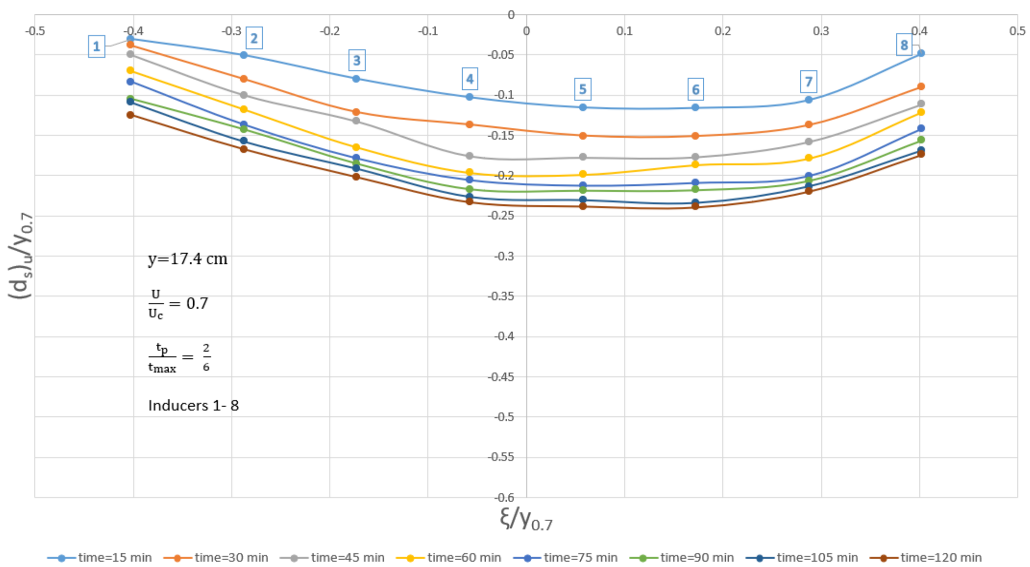

Figure 4.15 Temporal development of scour hole around the semi-circular end abutment of length L_a=35 cm for U/U_c = 0.70 along Inducers 1 - 8

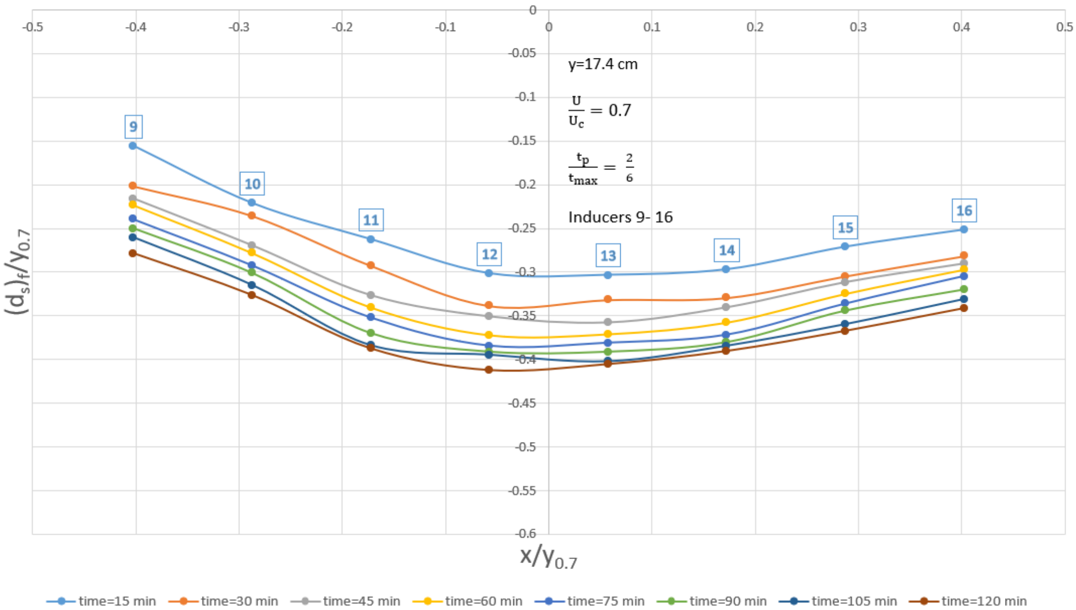

Figure 4.16 Temporal development of scour hole around the semi-circular end abutment of length L_a=35 cm for U/U_c = 0.70 along Inducers 9 - 16

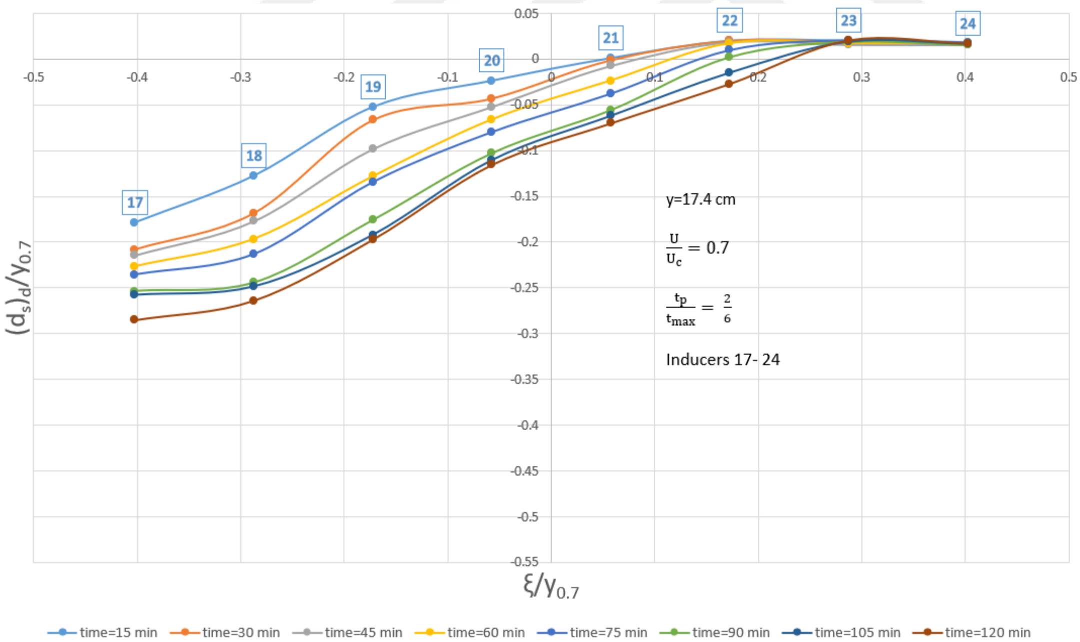

Figure 4.17 Temporal development of scour hole around the semi-circular end abutment of length L_a=35 cm for U/U_c = 0.70 along Inducers 17 - 24

After completing the first 2 hours of the experiment with the flow intensity of 0.7, the flow intensity value was increased to the value of 0.8, and it was obtained that the scouring rate was high between the 120th and 150th minutes. Then, the scour development gradually continued at the subsequent time intervals. However, the increasing rate of the scour development decreased at the 180th minute and scouring proceeded quite slowly between the 180th and 240th minutes. The maximum scour depths at the upstream and downstream sides of the abutment were observed for the locations of $-0.05<\xi/y_{0.7}<0.3$ and $-0.4<\xi/y_{0.7}<0.3$, respectively. The maximum scour depth around the abutment was observed at the front side, $-0.05<x/y_{0.7}<0.05$, as expected. At the end of the 4 hours of the experiment, deposition zones at the downstream side of the abutment completely degraded with the removal of the sediment due to the increased time and flow intensity.

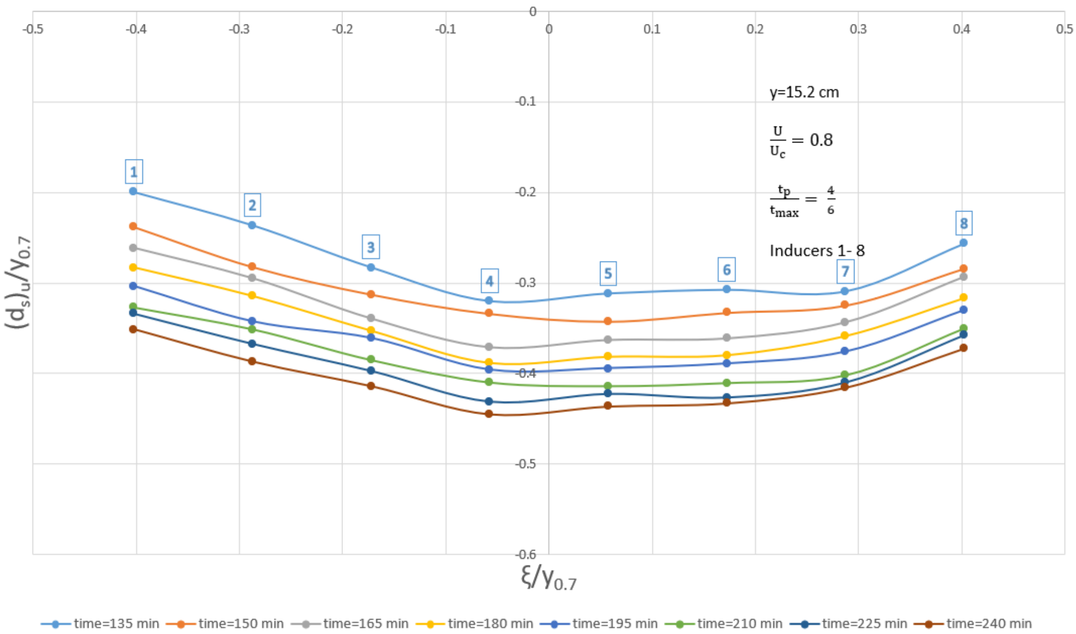

Figure 4.18 Temporal development of scour hole around the semi-circular end abutment of length L_a=35 cm for U/U_c = 0.80 along Inducers 1 - 8

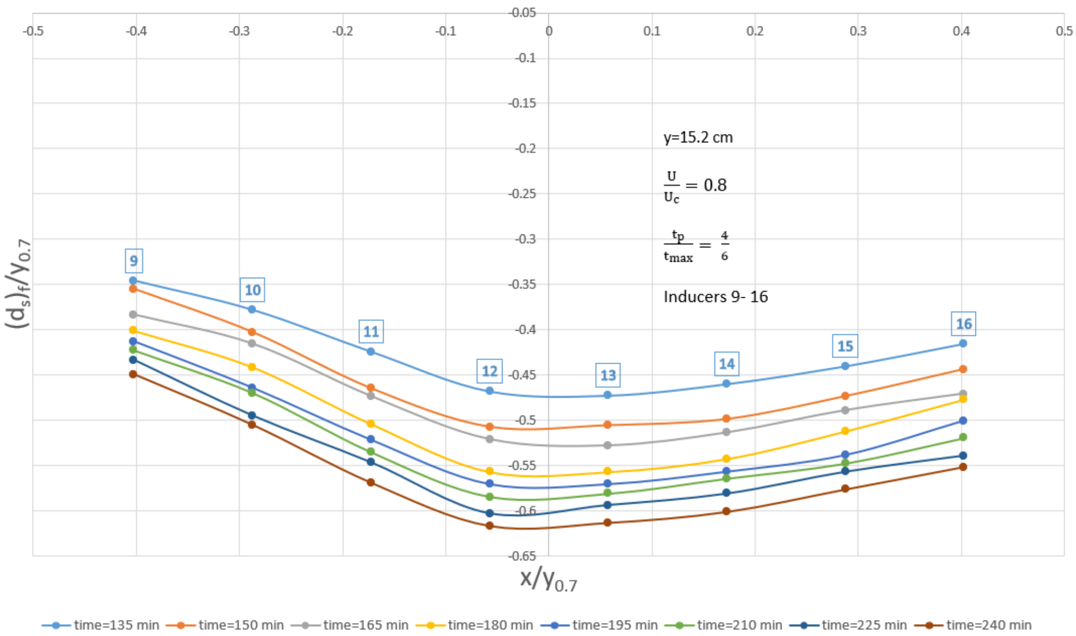

Figure 4.19 Temporal development of scour hole around the semi-circular end abutment of length L_a=35 cm for U/U_c = 0.80 along Inducers 9 - 16

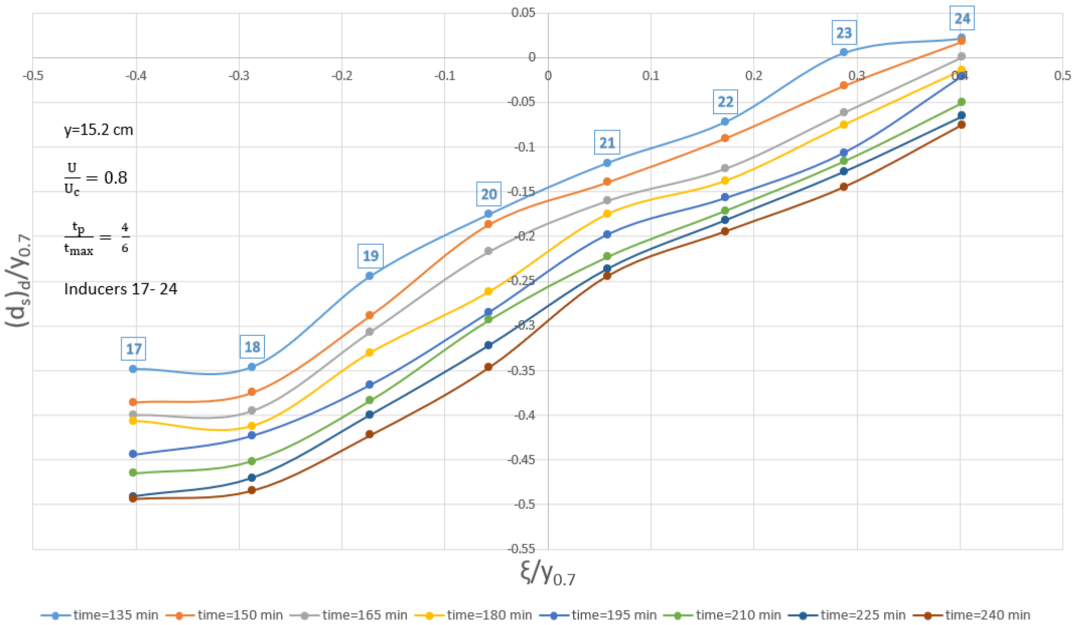

Figure 4.20 Temporal development of scour hole around the semi-circular end abutment of length L_a=35 cm for U/U_c = 0.80 along Inducers 17 - 24

Finally, for the last 2 hours, the flow intensity value was increased to 0.9 and scour hole quickly enlarged and deepened between the 240th and 270th minutes. However, at the downstream side for the locations of $-0.3<\xi/y_{0.7}<0.4$, small instantaneous decreases in the scour depths were measured between the 240th and 255th minutes. This situation might occur due to the movement of the sediment particles with increased flow intensity. Afterward, scour development gradually proceeded with a decreasing rate like the previous flow intensity values of 0.7 and 0.8. The locations of the maximum scour depths at the front and downstream sides of the abutment did not change for the case of U/U_c= 0.9; however, enlargement of the scour hole was clearly observed at the upstream side of the abutment leads to similar scour depth values all along the upstream side. The maximum or final dimensionless scour depths were recorded as $d_s/y_{0.7}$=-0.73, -0.83 and -0.67 at the abutment's upstream, front and downstream sides, respectively. The 73% of the maximum final scour depth value was observed at the 4th hour of the experiment, end of the case of U/U_c= 0.8 for the abutment of length L_a= 35 cm.

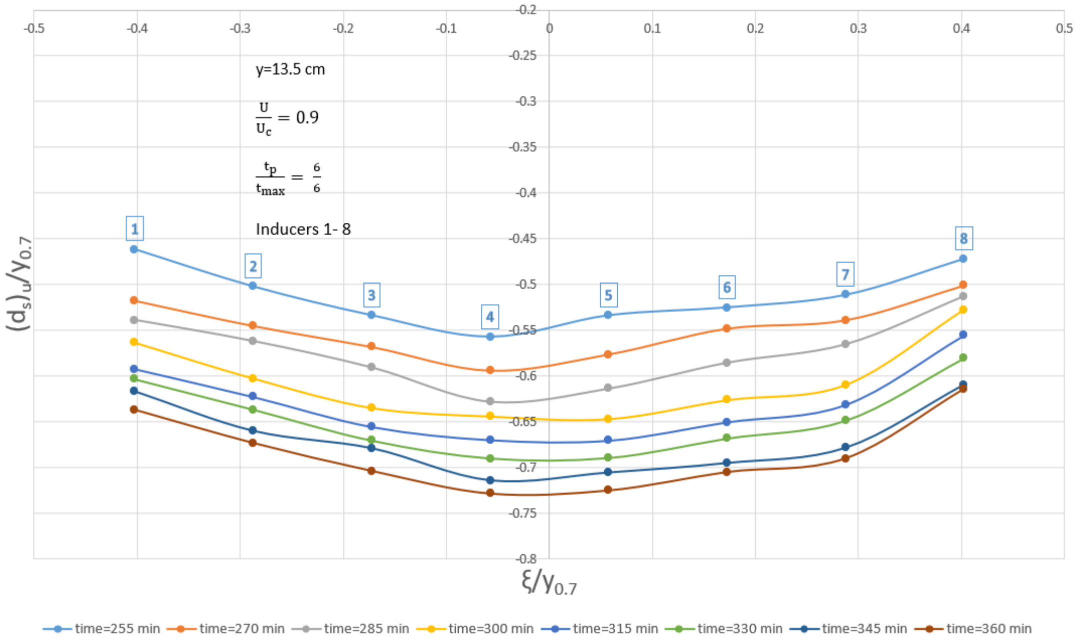

Figure 4.21 Temporal development of scour hole around the semi-circular end abutment of length L_a=35 cm for U/U_c = 0.90 along Inducers 1 - 8

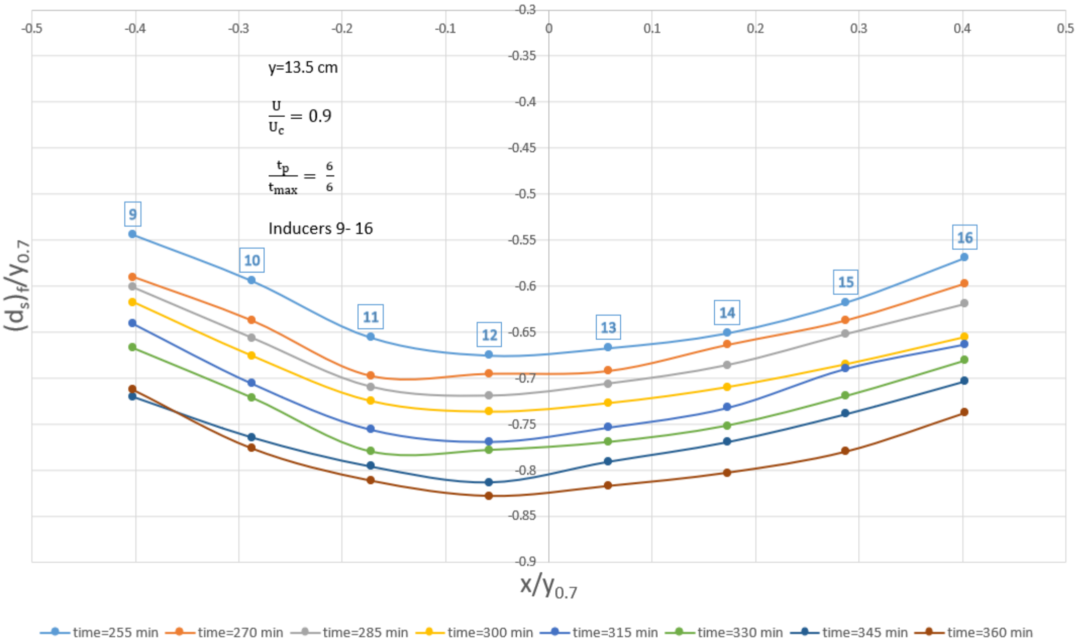

Figure 4.22 Temporal development of scour hole around the semi-circular end abutment of length L_a=35 cm for U/U_c = 0.90 along Inducers 9 - 16

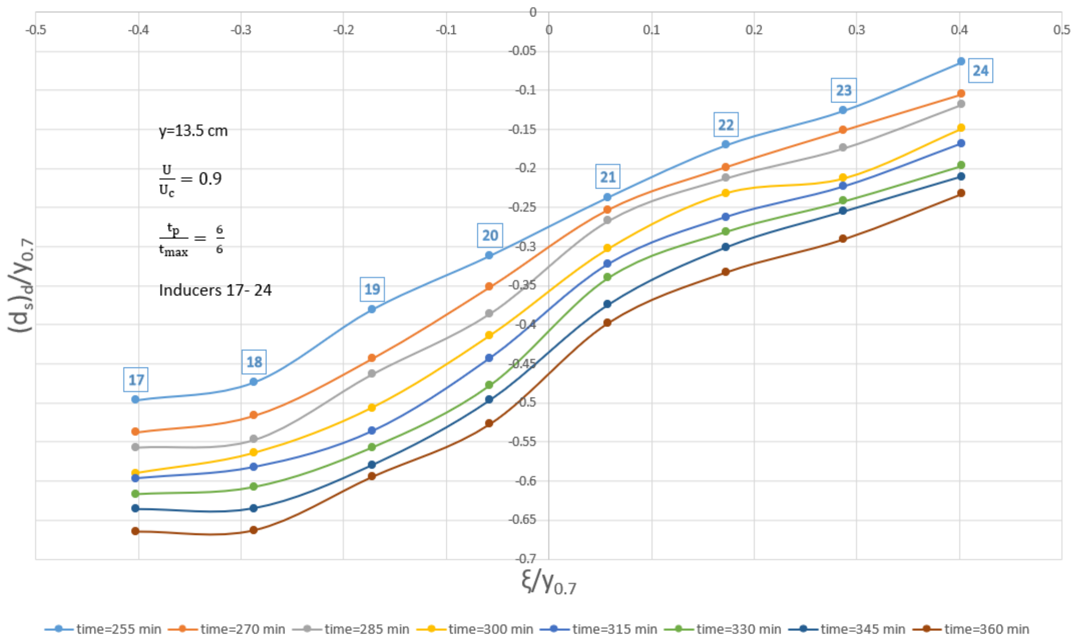

Figure 4.23 Temporal development of scour hole around the semi-circular end abutment of length L_a=35 cm for U/U_c = 0.90 along Inducers 17 - 24

4.4.1.1.3 The Abutment of Length L_a= 30 cm

For the abutment of length L_a=30 cm, the temporal development of scour hole is presented in Figures 4.24- 4.32. In this case, during the first 2 hours with the flow intensity of 0.7, the scour hole gradually developed until the 105th minute. After that, the scour hole development nearly stopped at the upstream and front sides of the abutment. On the other hand, the increasing rate of scour development slowed down after the 60th minute at the downstream side of the abutment. The maximum scour depths were observed for the zone of $-0.05<\xi/y_{0.7}<0.3$ at the upstream side of the abutment. The maximum scour depth at the front side of the abutment was recorded at the x/y= 0.05 where Inducer 13 was placed. At the downstream side of the abutment, deposition of the sediment particles was observed rather than scour at the initial stages of the experiment, except for the location of $-0.40<\xi/y_{0.7}<-0.10$. Development of scour hole was apparently observed after the 60th minute at the location of $-0.40<\xi/y_{0.7}<0$. At the location of $0.00<\xi/y_{0.7}<0.40$, deposition of sediment particles still occurred even though it reduced at the 75th minute.

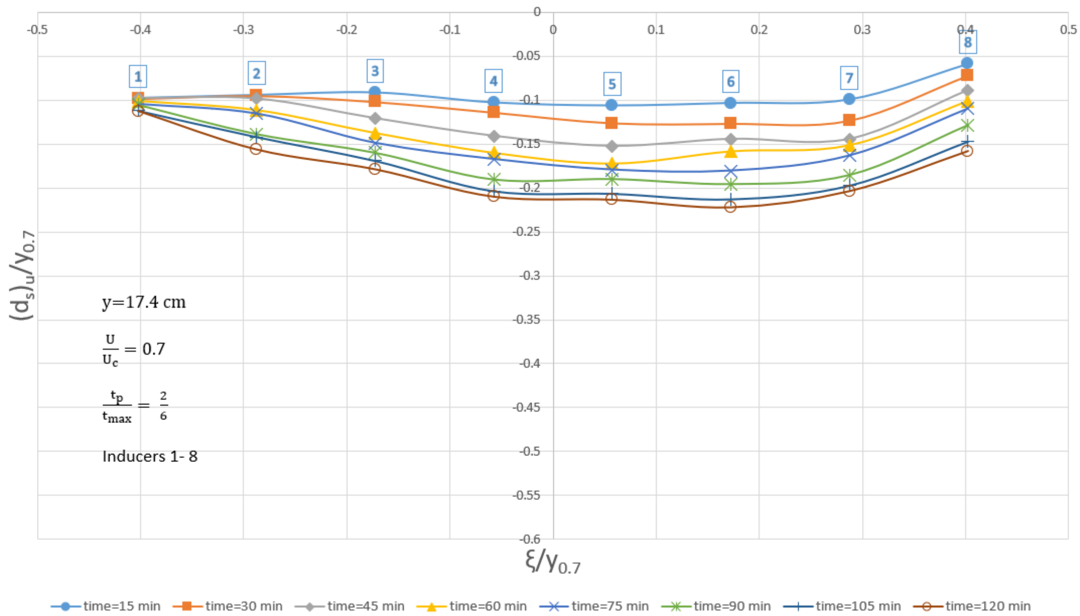

Figure 4.24 Temporal development of scour hole around the semi-circular end abutment of length L_a=30 cm for U/U_c = 0.70 along Inducers 1 - 8

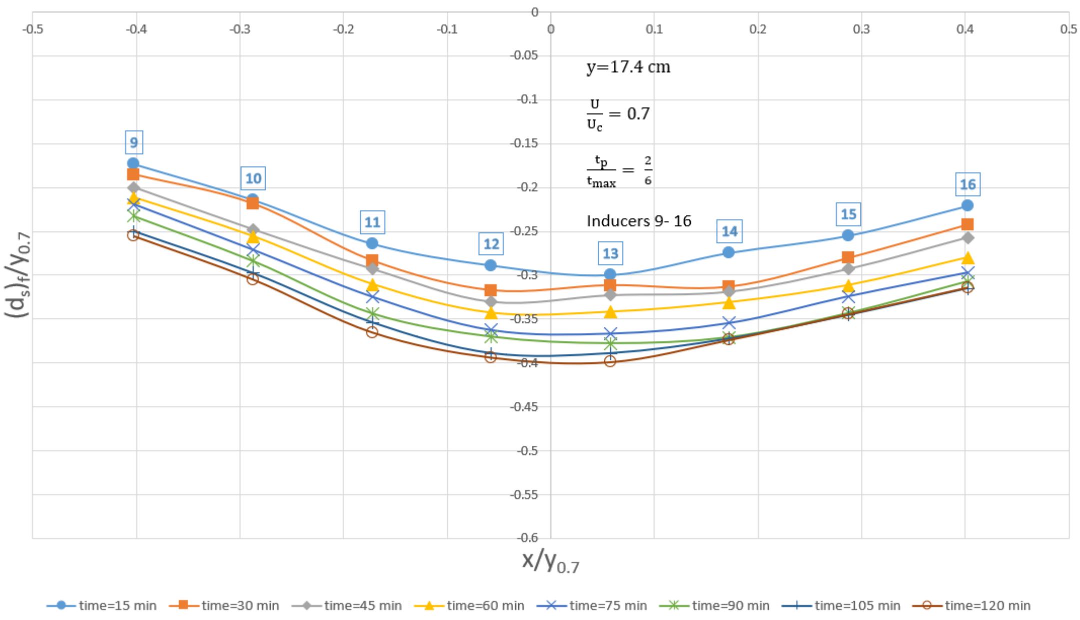

Figure 4.25 Temporal development of scour hole around the semi-circular end abutment of length L_a=30 cm for U/U_c = 0.70 along Inducers 9 - 16

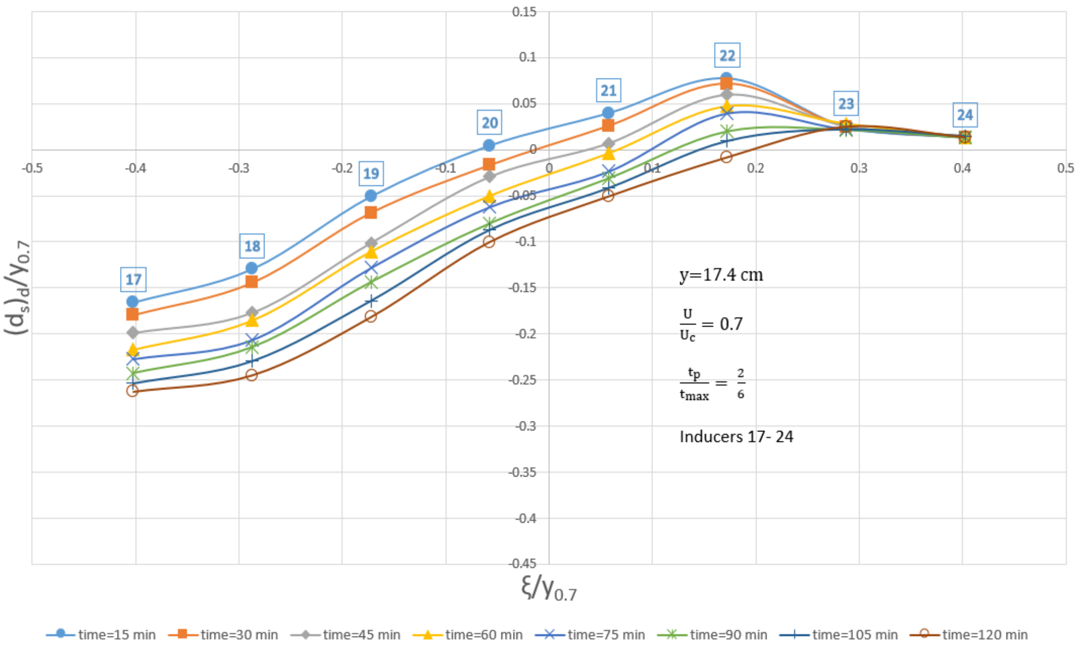

Figure 4.26 Temporal development of scour hole around the semi-circular end abutment of length L_a=30 cm for U/U_c = 0.70 along Inducers 17 - 24

When flow intensity was increased to 0.8, a rapid development in the scour hole was observed between the 120th and 150th minutes, as expected. After that, size of the scour hole gradually increased at a decreasing rate and there was almost no change between the 225th and 240th minutes. At the end of the 4th hour, the maximum scour depths were recorded at the upstream side of the abutment for the region of -0.05<$\xi/y_{0.7}$<0.15. At the front side of the abutment, the maximum scour depths were observed for the region of -0.05<$x/y_{0.7}$<0.15, where Inducers between 12 and 14 were placed. At the downstream side of the abutment, the maximum scour depths were observed for the location of -0.4<$\xi/y_{0.7}$<0.3.

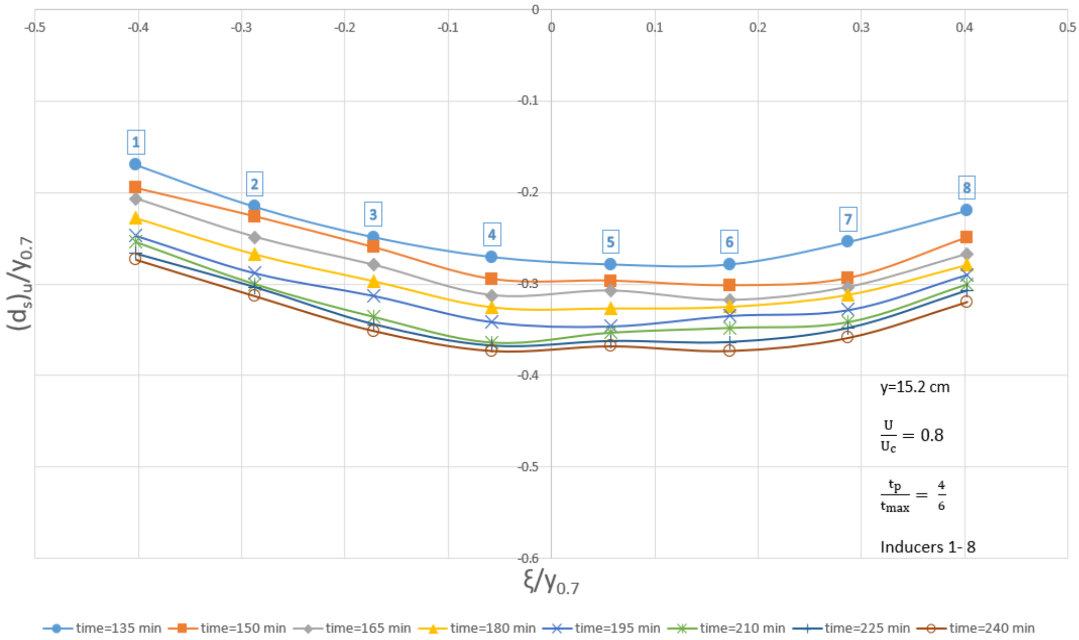

Figure 4.27 Temporal development of scour hole around the semi-circular end abutment of length L_a=30 cm for U/U_c = 0.80 along Inducers 1 - 8

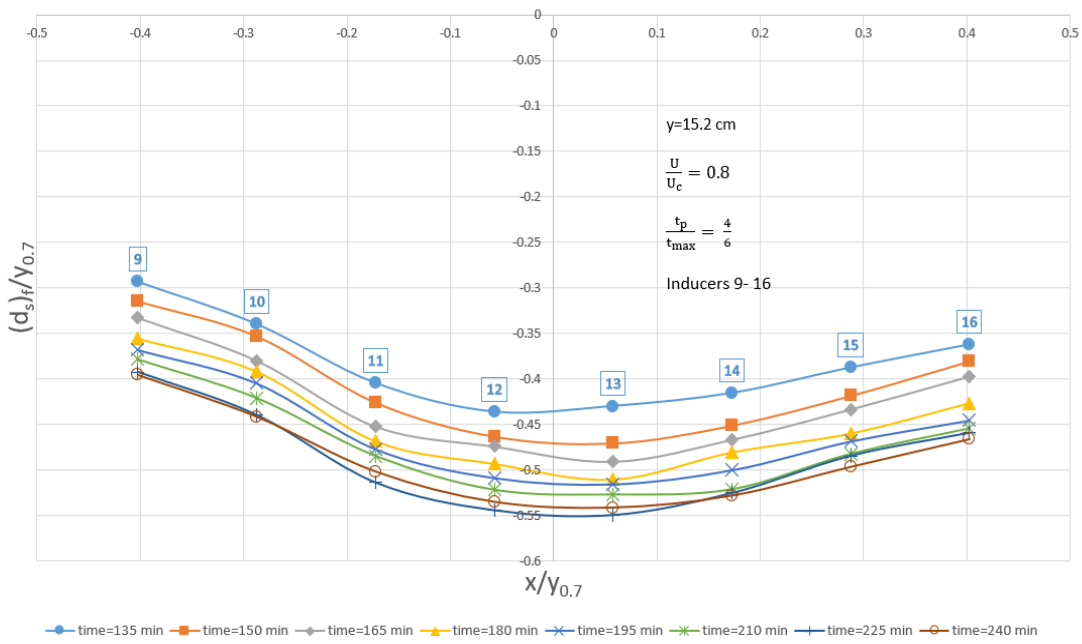

Figure 4.28 Temporal development of scour hole around the semi-circular end abutment of length L_a=30 cm for U/U_c = 0.80 along Inducers 9 - 16

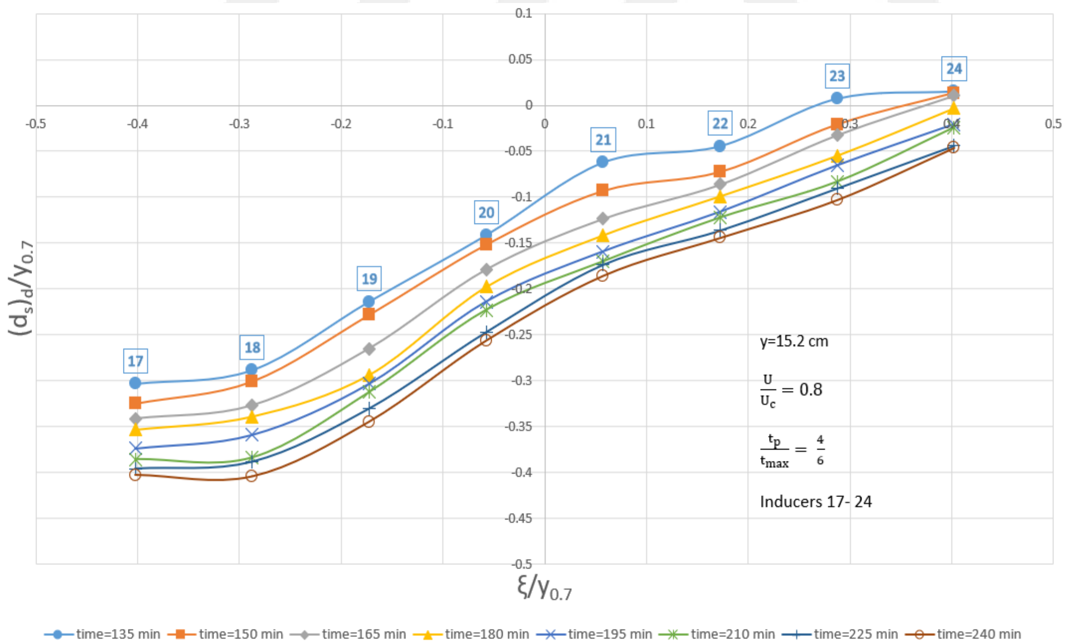

Figure 4.29 Temporal development of scour hole around the semi-circular end abutment of length L_a=30 cm for U/U_c = 0.80 along Inducers 17 - 24

Finally, for the last 2 hours, the flow intensity was increased to 0.9 from 0.8. Similar to the previous cases, the increased flow intensity leads to a rapid increase in scour development at the initial stages. Afterward, the scour hole development slowed, especially after the 315th minute. At the upstream and front sides of the abutment, the maximum scour depths were relatively observed at $\xi/y_{0.7}$= -0.05 and $x/y_{0.7}$= -0.05, respectively. Moreover, at the downstream side of the abutment, the location of -0.4<$\xi/y_{0.7}$<-0.3 was recorded as the maximum scour depth region. The maximum or final dimensionless scour depths were recorded as $d_s/y_{0.7}$=-0.63, -0.71 and -0.55 at the abutment's upstream, front and downstream sides, respectively. The 74% of the maximum final scour depth value was observed at the 4th hour of the experiment, end of the case of U/U_c= 0.8 for the abutment of length L_a= 30 cm.

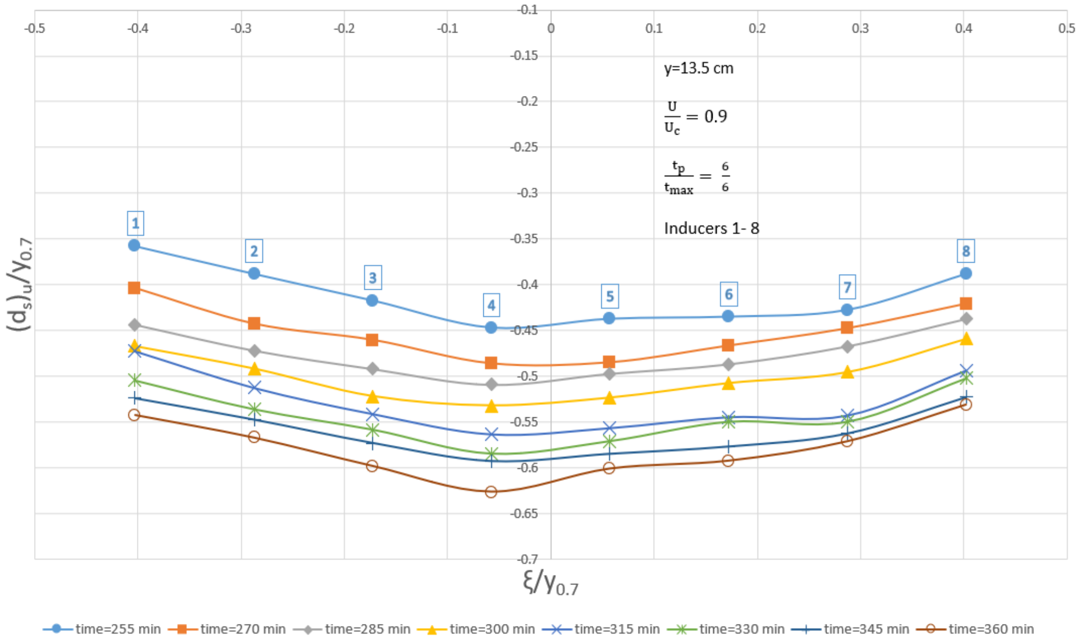

Figure 4.30 Temporal development of scour hole around the semi-circular end abutment of length L_a=30 cm for U/U_c = 0.90 along Inducers 1 - 8

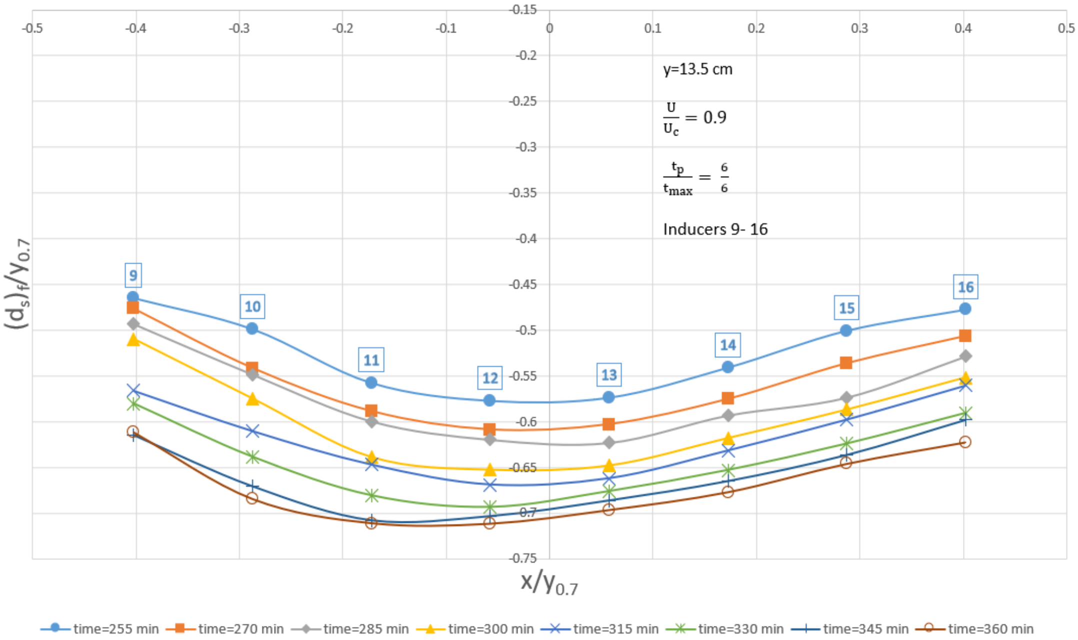

Figure 4.31 Temporal development of scour hole around the semi-circular end abutment of length L_a=30 cm for U/U_c = 0.90 along Inducers 9 - 16

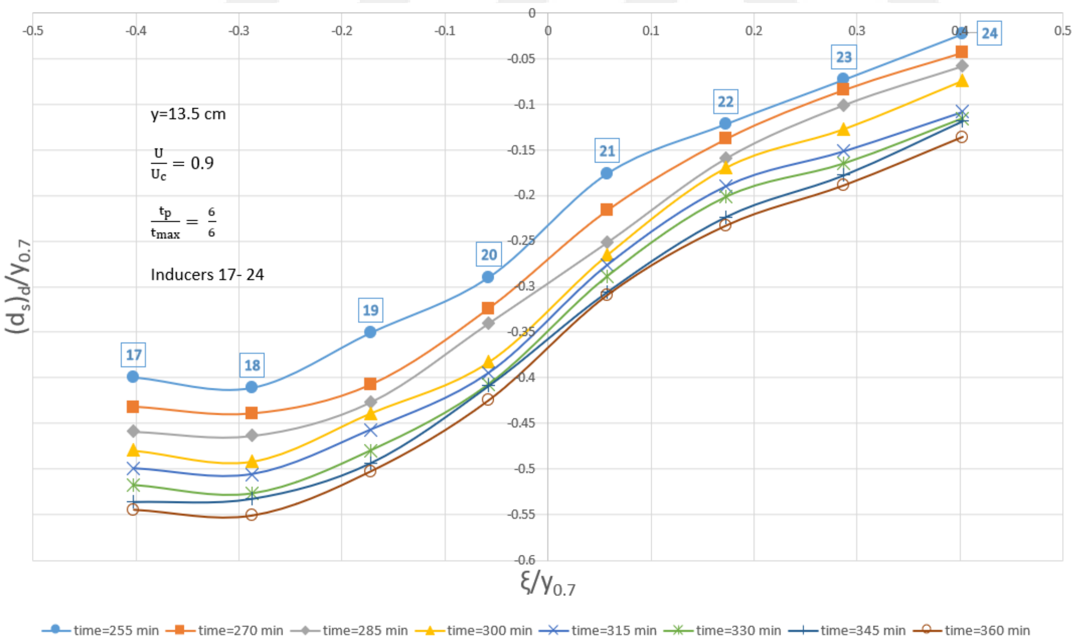

Figure 4.32 Temporal development of scour hole around the semi-circular end abutment of length L_a=30 cm for U/U_c = 0.90 along Inducers 17 - 24

4.4.1.1.4 The Abutment of Length L_a= 25 cm

The temporal development of scour holes around the abutment of length L_a= 25 cm is presented in Figures 4.33- 4.41. During the first 2 hours of the experiment, with the flow intensity of 0.7, scour hole development was very slow relative to the abutments of lengths L_a= 30, 35 and 40 cm. In this period, deposition occurred rather than scouring at the abutment's downstream side. Since the size and development speed of scour hole decrease as the abutment length decreases, the deposition of the sand particles during the first 2 hours of the experiment can be expected for this and smaller abutment lengths. Although scour formations can be considered negligible at the upstream site, scour hole development was observed at the upstream side of the abutment. On the contrary, the scour hole development was relatively rapid in the first 15 minutes at the front side of the abutment. Afterward, the development of scour hole gradually continued until the end of the first 2 hours. However, it should be noticed that the maximum scour depths were measured within the range of 3- 3.5 cm.

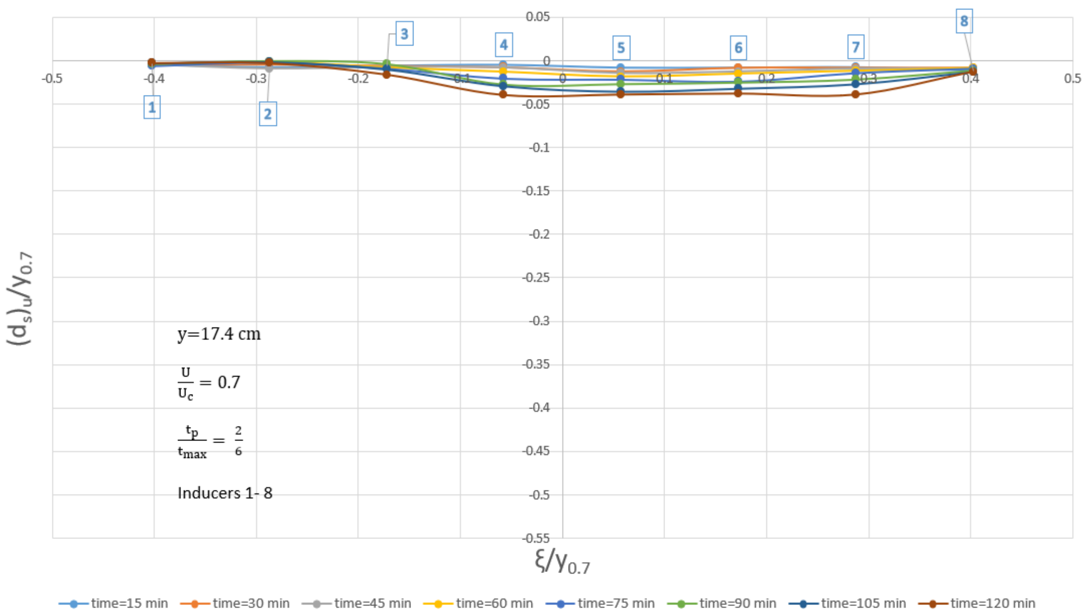

Figure 4.33 Temporal development of scour hole around the semi-circular end abutment of length L_a=25 cm for U/U_c = 0.70 along Inducers 1 - 8

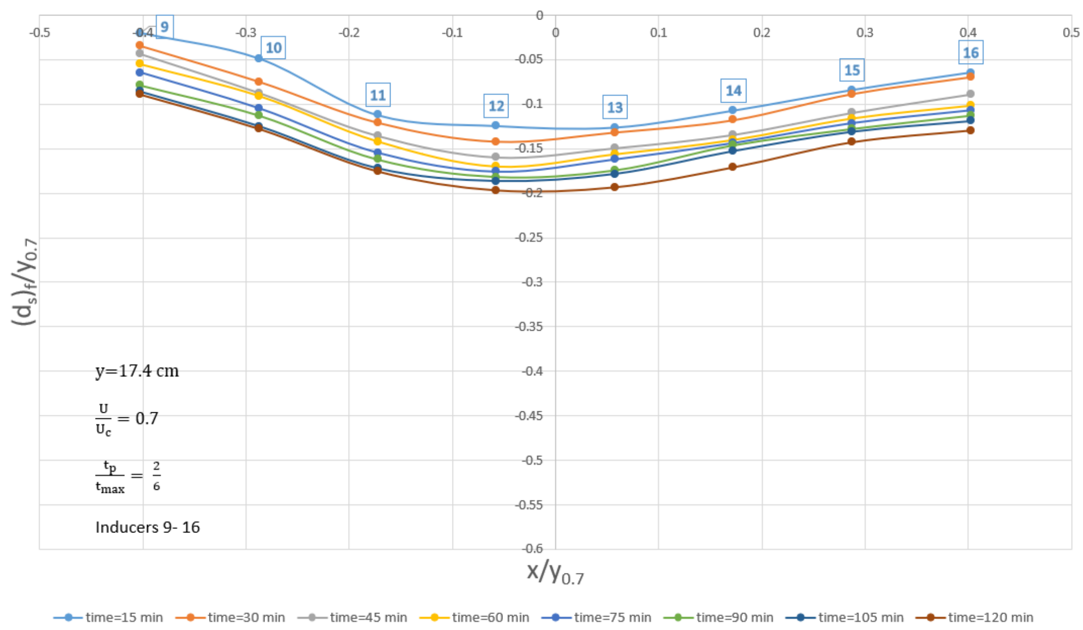

Figure 4.34 Temporal development of scour hole around the semi-circular end abutment of length L_a=25 cm for U/U_c = 0.70 along Inducers 9 - 16

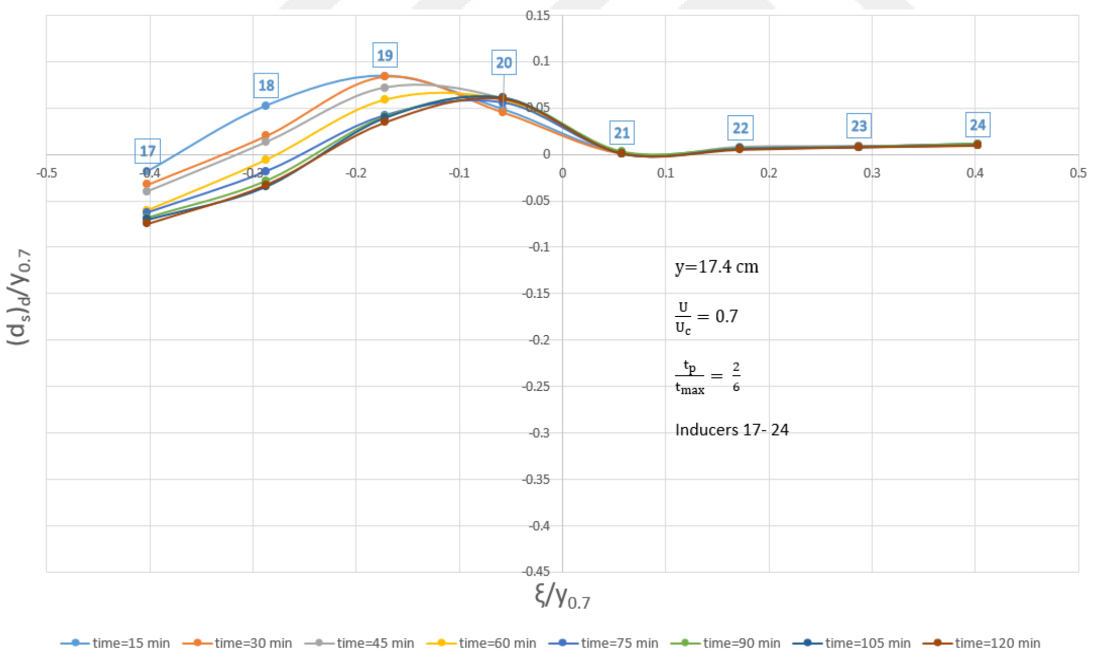

Figure 4.35 Temporal development of scour hole around the semi-circular end abutment of length L_a=25 cm for U/U_c = 0.70 along Inducers 17 - 24

During the second 2 hours, with the flow intensity of 0.8, scour hole rapidly enlarged and deepened due to the increased flow intensity at the abutment's upstream side between the 120th and 135th minutes. Then scour hole development continues gradually with a decreasing rate to the end of the 240th minute. The maximum scour depths were observed at $-0.15<\xi/y_{0.7}<0.20$ on this side. At the downstream side of the abutment, the deposition of sand particles still occurred for the location of $0.00<\xi/y_{0.7}<0.40$ during this period; however, the scouring process was started and gradually developed for the location of $-0.40<\xi/y_{0.7}<0.00$. At the end of the second 2 hours, the whole region was scoured and the maximum scour depths were observed in this region ($-0.40<\xi/y_{0.7}<0.30$). Contrary to the abutments' upstream and downstream sides, deposition was not observed at the front side of the abutment. After the rapid development of the scour hole between the 120th and 135th minutes, scour hole development continued until the 225th minute. Between the 225th and 240th minute, there was almost no change in the scour hole geometry. On this side, the maximum scour depths were measured at the $-0.05<\xi/y_{0.7}<0.05$, where Inducers 12 and 13 were located.

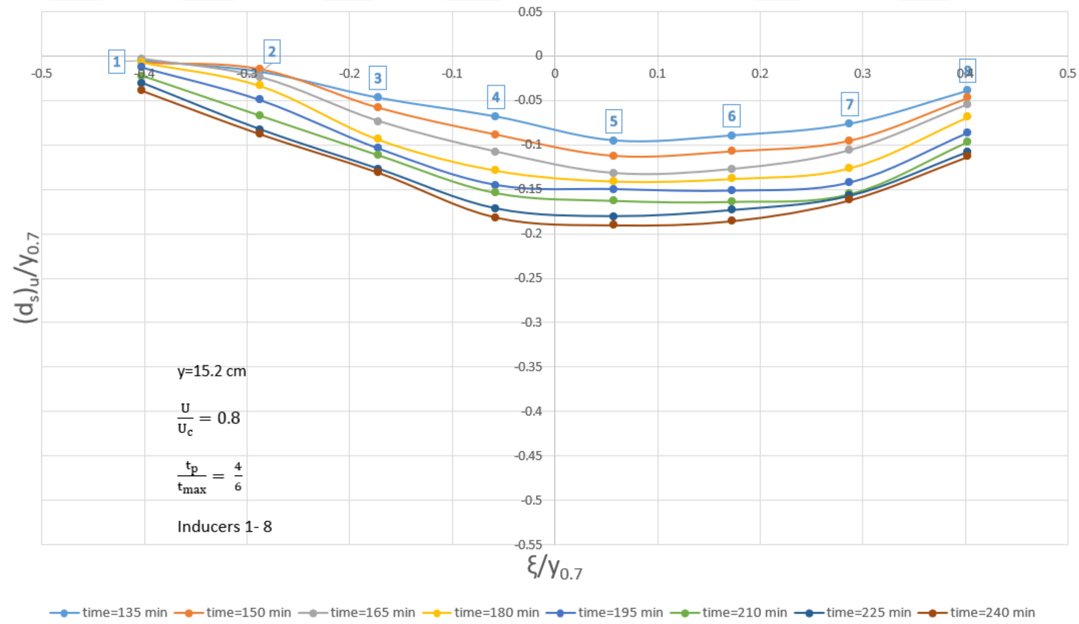

Figure 4.36 Temporal development of scour hole around the semi-circular end abutment of length L_a=25 cm for U/U_c = 0.80 along Inducers 1 - 8

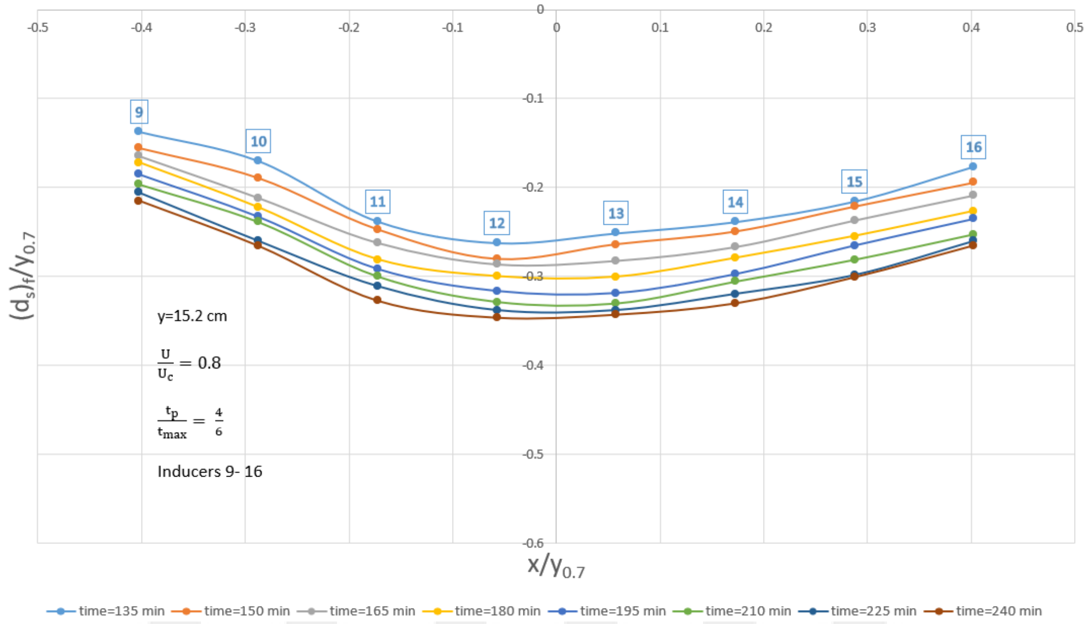

Figure 4.37 Temporal development of scour hole around the semi-circular end abutment of length L_a=25 cm for U/U_c = 0.80 along Inducers 9 - 16

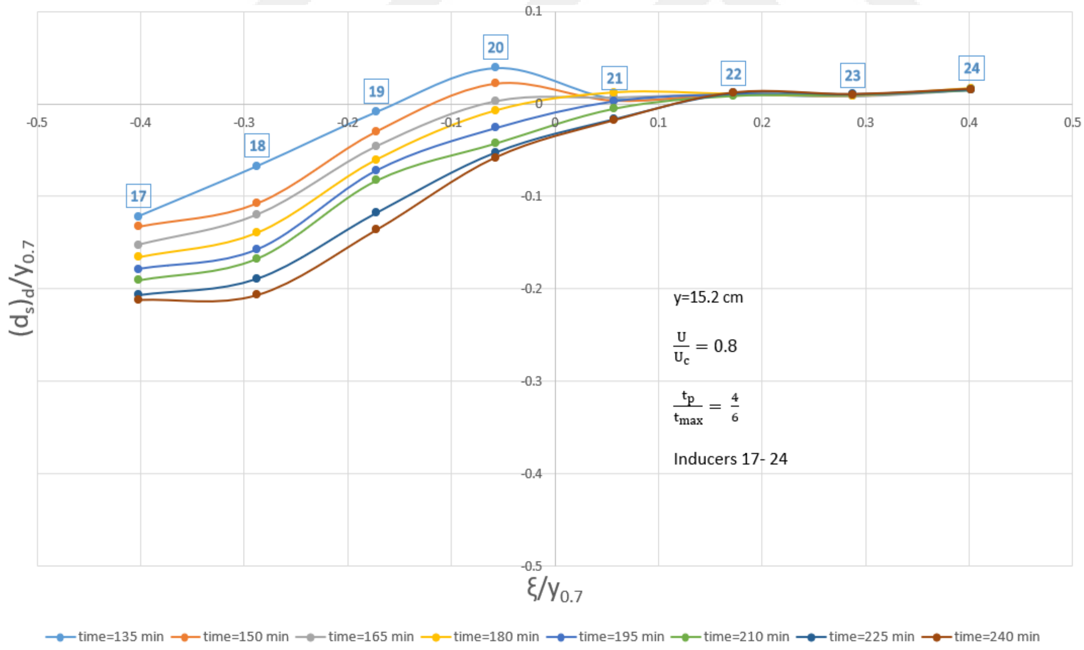

Figure 4.38 Temporal development of scour hole around the semi-circular end abutment of length L_a=25 cm for U/U_c = 0.80 along Inducers 17 - 24

After the flow intensity was increased to 0.9, a rapid scour development was observed between the 240th and 285th minutes of the experiment around all sides of the abutment. Then, scour hole gradually grew with increasing time. At the upstream and front sides of the abutment, the increasing rate of the scour hole development decreased after the 285th minute. Between the 345th and 360th minutes, the development of scour hole was recorded as negligible for all sides of the abutment. Maximum scour depths at the abutment's upstream, front and downstream sides were observed for the locations of $0.10<\xi/y_{0.7}<0.30$, $-0.20<x/y_{0.7}<0.20$, $-0.40<\xi/y_{0.7}<-0.30$, respectively. The location of the maximum scour depths at the upstream side was oppositely shifted relative to the abutment compared to the first 4 hours of the experiment. Also, the deposition of sand particles was observed at $0.30<\xi/y_{0.7}<0.40$ for the downstream side of the abutment. In this location, scouring proceeded after the 345th minute. The maximum or final dimensionless scour depths were recorded as $d_s/y_{0.7}$=-0.39, -0.54 and -0.40 at the abutment's upstream, front and downstream sides, respectively. The 62% of the maximum final scour depth value was recorded at the 4th hour of the experiment.

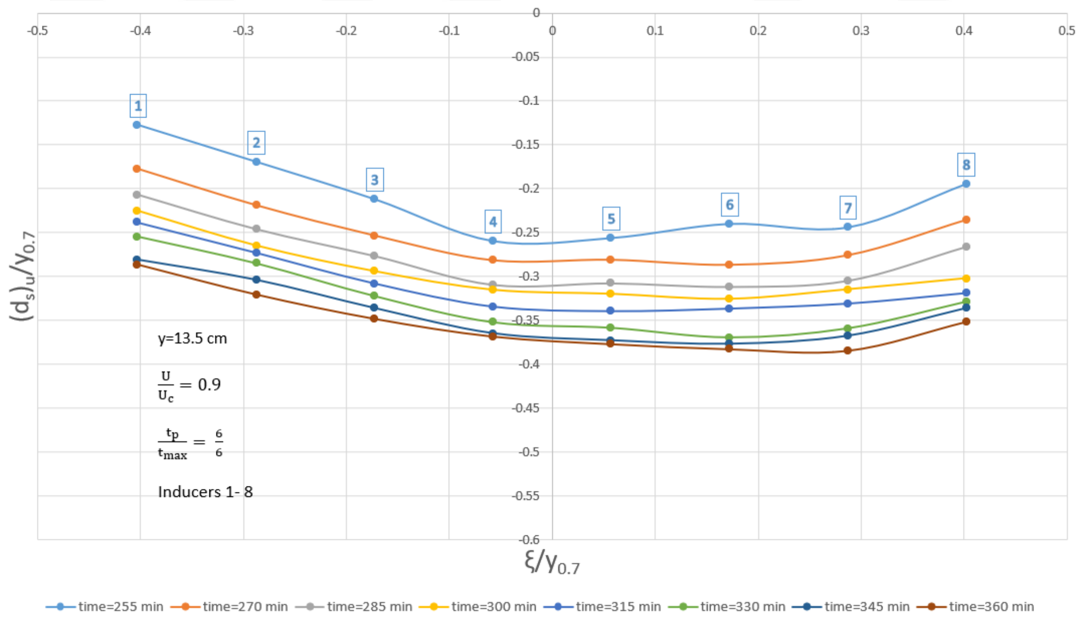

Figure 4.39 Temporal development of scour hole around the semi-circular end abutment of length L_a=25 cm for U/U_c = 0.90 along Inducers 1 - 8

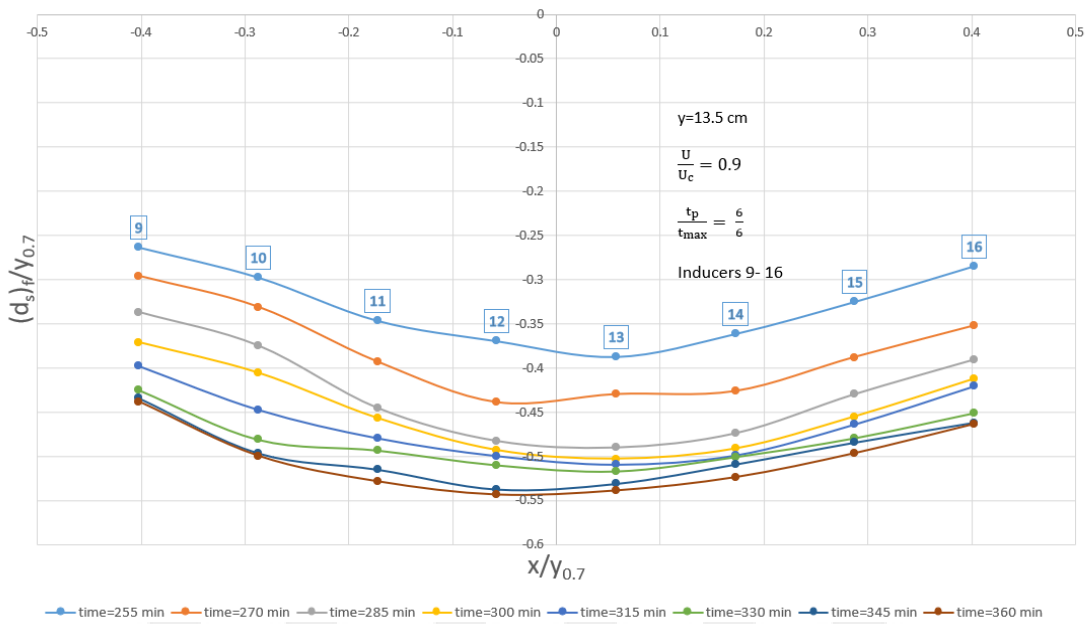

Figure 4.40 Temporal development of scour hole around the semi-circular end abutment of length L_a=25 cm for U/U_c = 0.90 along Inducers 9 - 16

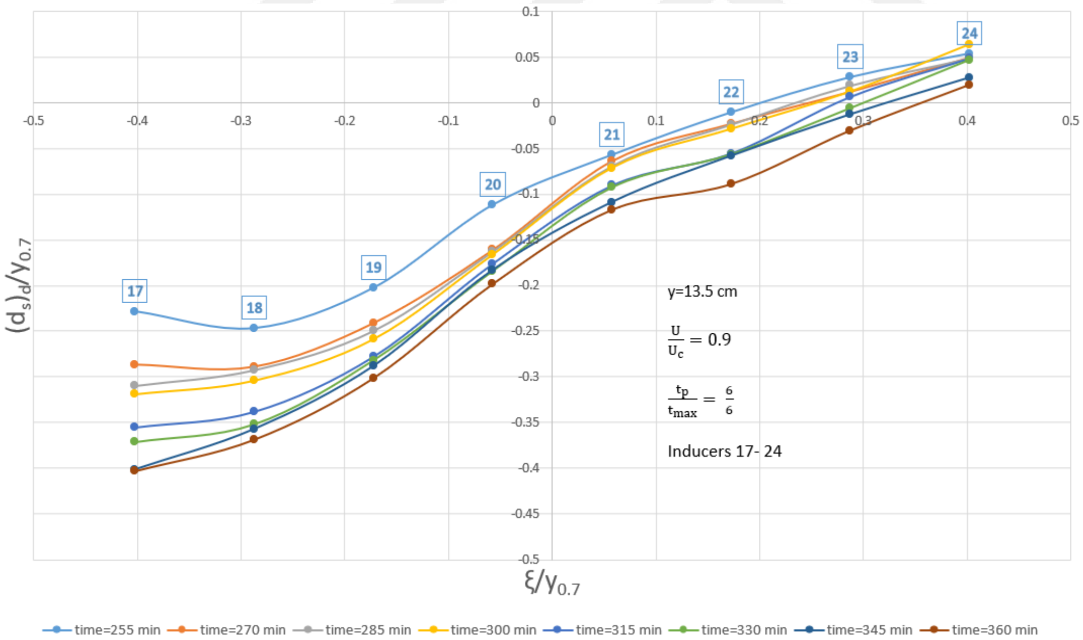

Figure 4.41 Temporal development of scour hole around the semi-circular end abutment of length L_a=25 cm for U/U_c = 0.90 along Inducers 17 - 24

4.4.1.1.5 The Abutment of Length L_a= 20 cm

The temporal development of the scour hole around the abutment with a length of L_a= 20 cm is presented in Figures 4.42-4.50. During the first 2 hours of the experiment, with the flow intensity of 0.7, there were almost no scour formations at the upstream and downstream sides of the abutment. Furthermore, sediment particles mainly accumulated around the downstream side of the abutment. On the other hand, scour hole had already started to gradually develop at the front side of the abutment during the first 15 minutes of the experiment. However, the maximum scour depth end of the 180th minute was in the range of 1.5- 2.0 cm at $-0.05<x/y_{0.7}<0.05$, and there were almost no changes in the scour hole after the 60th minute. Therefore, these formations may be accepted as insignificant.

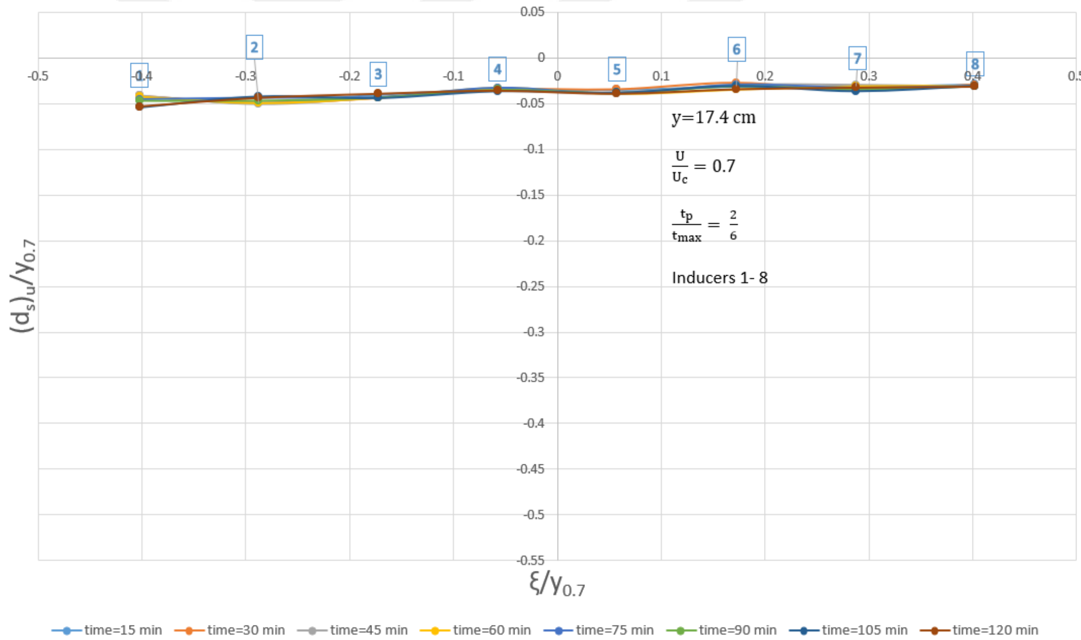

Figure 4.42 Temporal development of scour hole around the semi-circular end abutment of length L_a=20 cm for U/U_c = 0.70 along Inducers 1 - 8

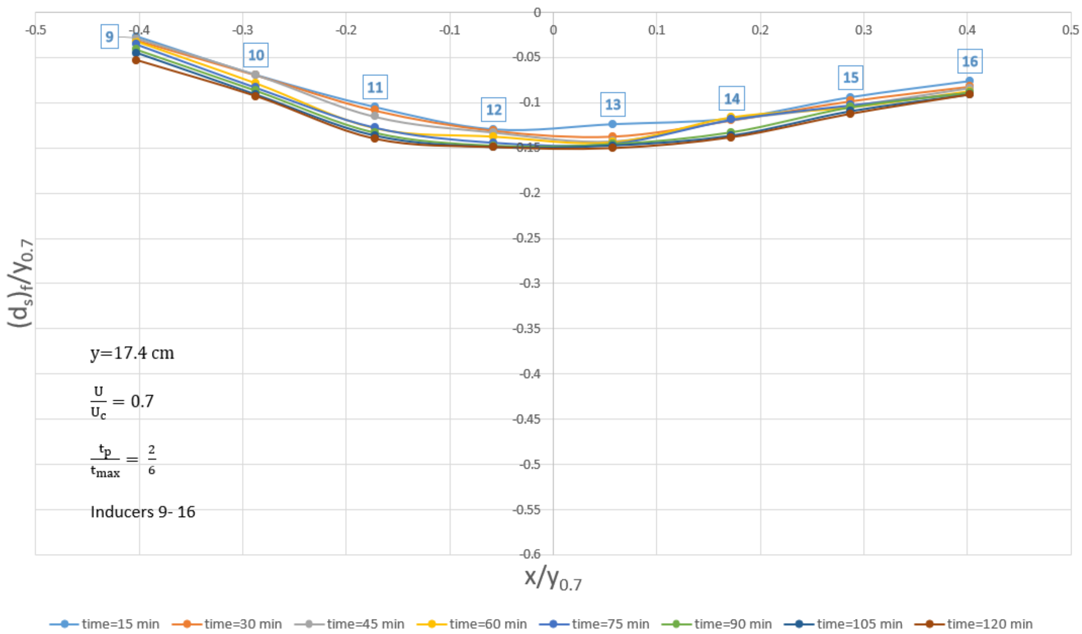

Figure 4.43 Temporal development of scour hole around the semi-circular end abutment of length L_a=20 cm for U/U_c = 0.70 along Inducers 9 - 16

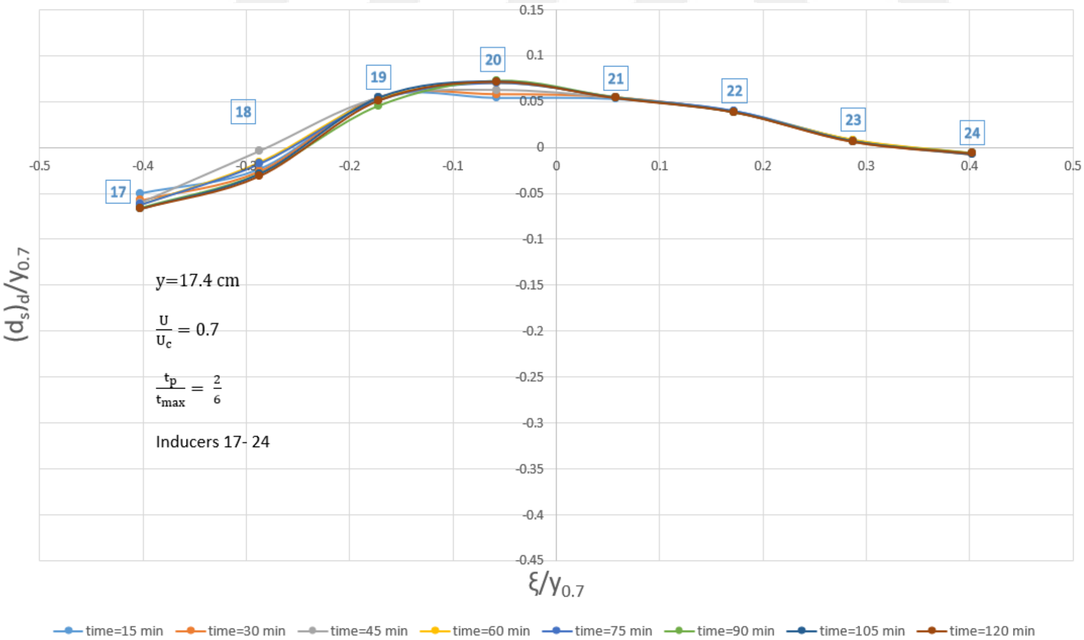

Figure 4.44 Temporal development of scour hole around the semi-circular end abutment of length L_a=20 cm for U/U_c = 0.70 along Inducers 17 - 24

During the second 2 hours, with the flow intensity of 0.8, scour hole rapidly developed between the 120th and 150th minutes at the front side of the abutment. Then, scour holes gradually developed in this region. The maximum scour depth at the front side of the abutment was obtained for the location of $x/y_{0.7}$= -0.05. On the other hand, scour hole formation was observed at the upstream side, but the magnitude of the scour hole can be accepted as insignificant. Moreover, in this time interval, scour holes also started to develop at the downstream side of the abutment. In particular, small scour depths were recorded after the 120th minute for the location of -0.4<$\xi/y_{0.7}$<-0.3 at the downstream side. In the other zones that are close to the sidewall at the downstream side, deposition of sand particles was observed.

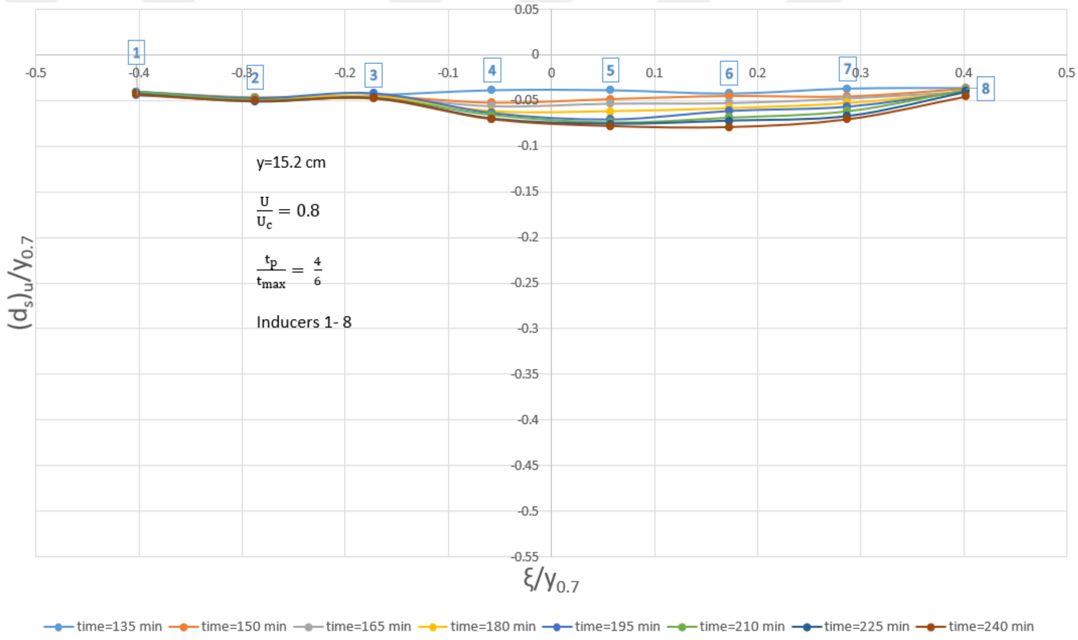

Figure 4.45 Temporal development of scour hole around the semi-circular end abutment of length L_a=20 cm for U/U_c = 0.80 along Inducers 1 - 8

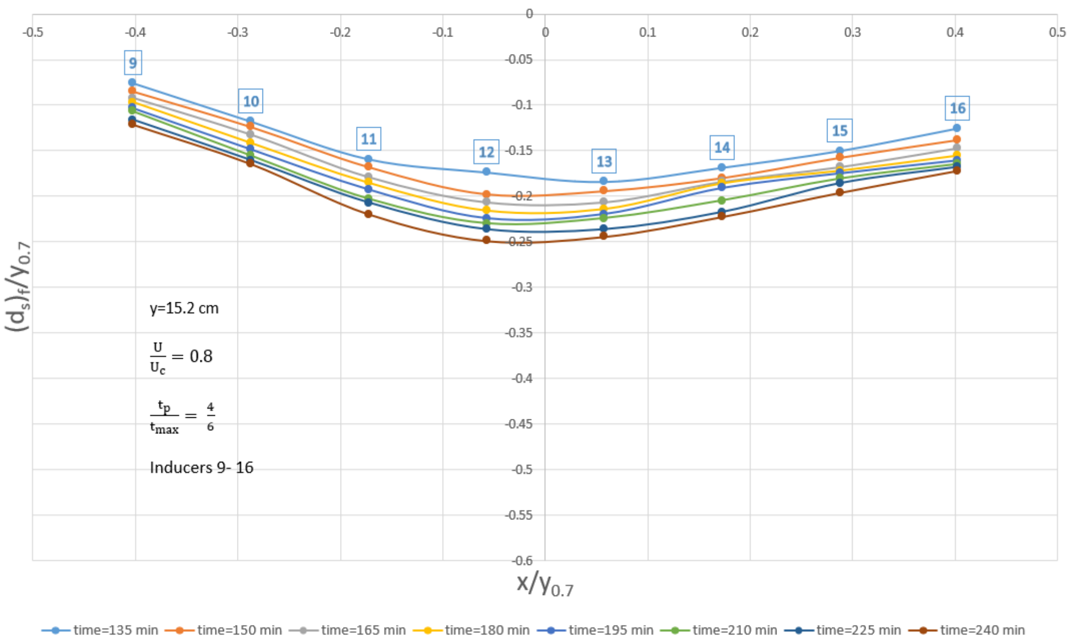

Figure 4.46 Temporal development of scour hole around the semi-circular end abutment of length L_a=20 cm for U/U_c = 0.80 along Inducers 9 - 16

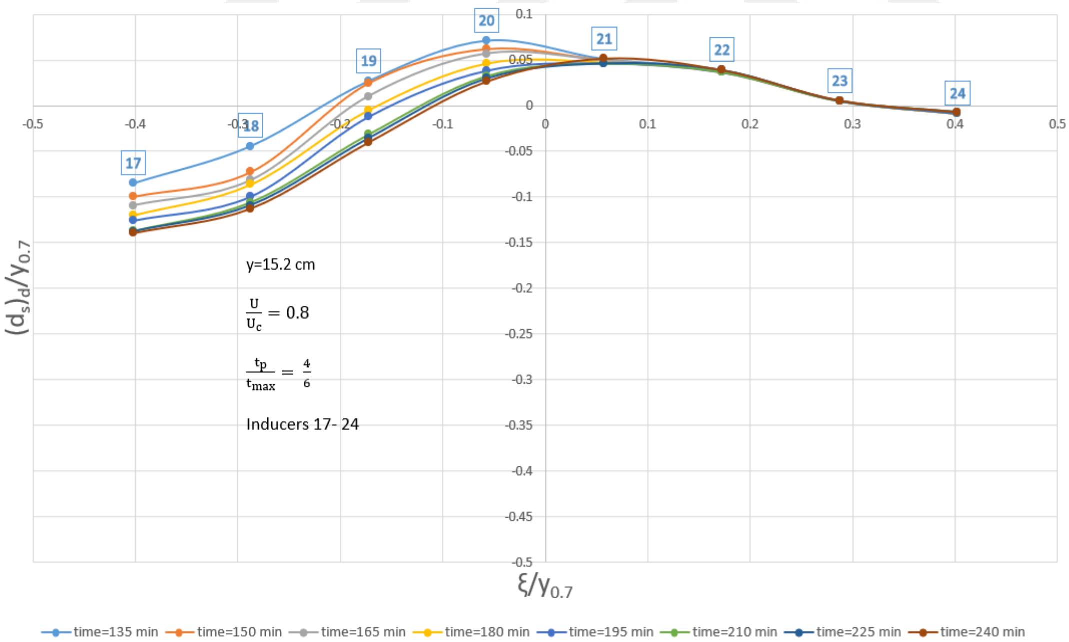

Figure 4.47 Temporal development of scour hole around the semi-circular end abutment of length L_a=20 cm for U/U_c = 0.80 along Inducers 17 - 24

After the flow intensity was increased to 0.9 from 0.8, scour hole around the abutment rapidly enlarged and deepened. At the upstream side of the abutment, deposited sand particles disappeared and noteworthy scour depths were observed, especially after the 270th minute. On this side, the maximum scour depths were observed for the locations of $0.00<\xi/y_{0.7}<0.30$. At the front side of the abutment, the scour hole development stepped down after the 300th minute and small alterations were observed during the last hour of the experiment. The maximum scour depth was absolutely recorded at the $x/y_{0.7}$= -0.05 on this side. On the other hand, in this subsequent with the flow intensity of 0.9, notable scour depths started to occur at the downstream side. Furthermore, sand particles at the deposited zones of $0.0<\xi/y_{0.7}<0.4$ were gradually degraded and scour hole development was started. The maximum or final dimensionless scour depths were measured as $d_s/y_{0.7}$=-0.29, -0.42 and -0.26 at the abutment's upstream, front and downstream sides, respectively. The 56% of the maximum final scour depth value was recorded at the 4th hour of the experiment.

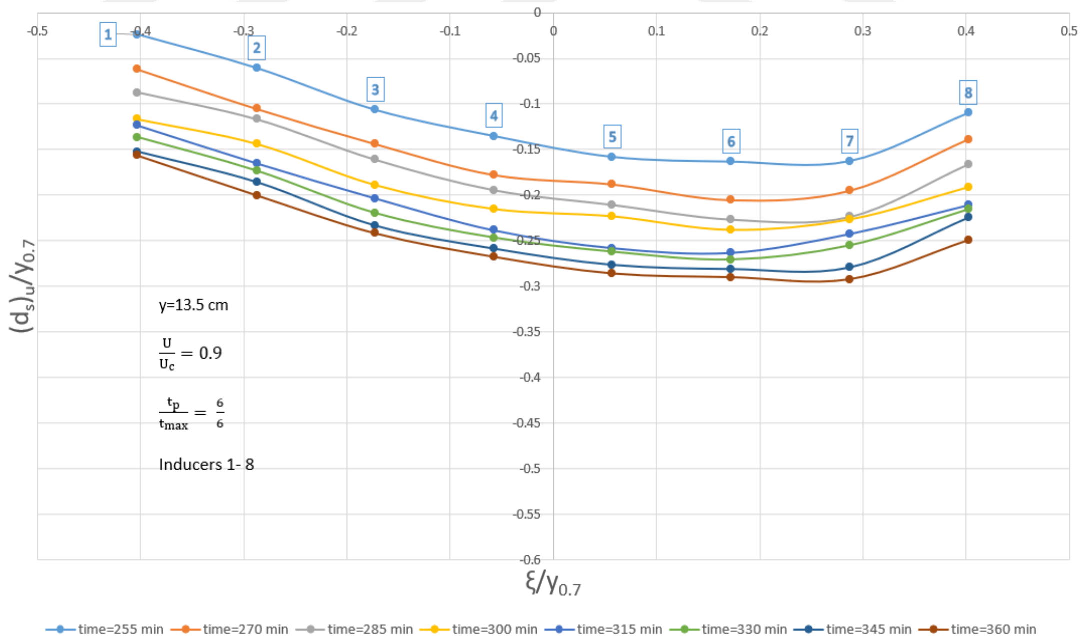

Figure 4.48 Temporal development of scour hole around the semi-circular end abutment of length L_a=20 cm for U/U_c = 0.90 along Inducers 1 - 8

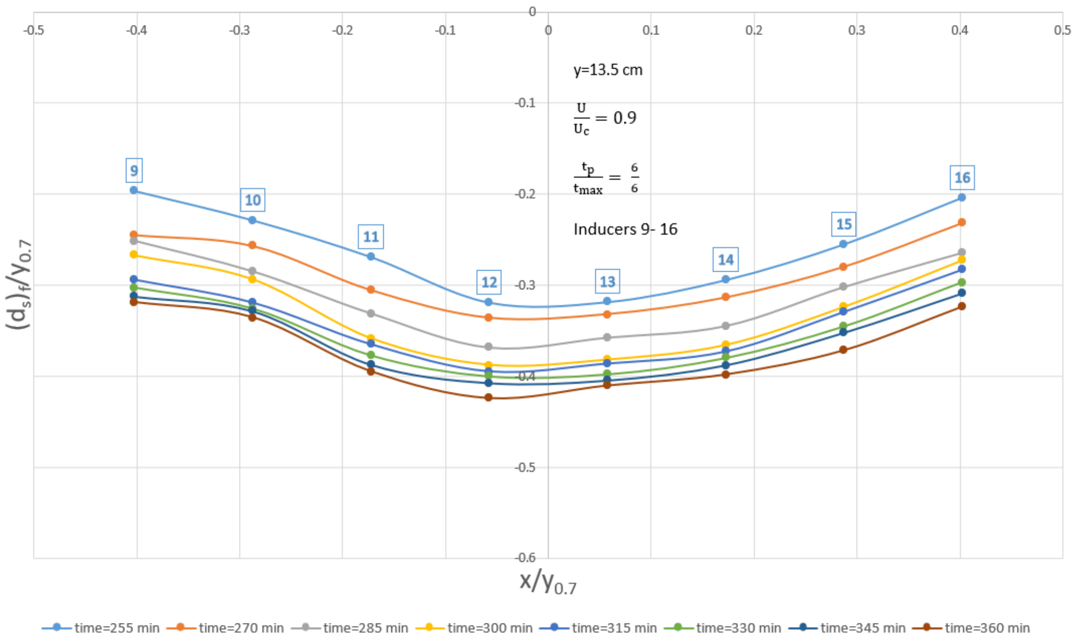

Figure 4.49 Temporal development of scour hole around the semi-circular end abutment of length L_a=20 cm for U/U_c = 0.90 along Inducers 9 - 16

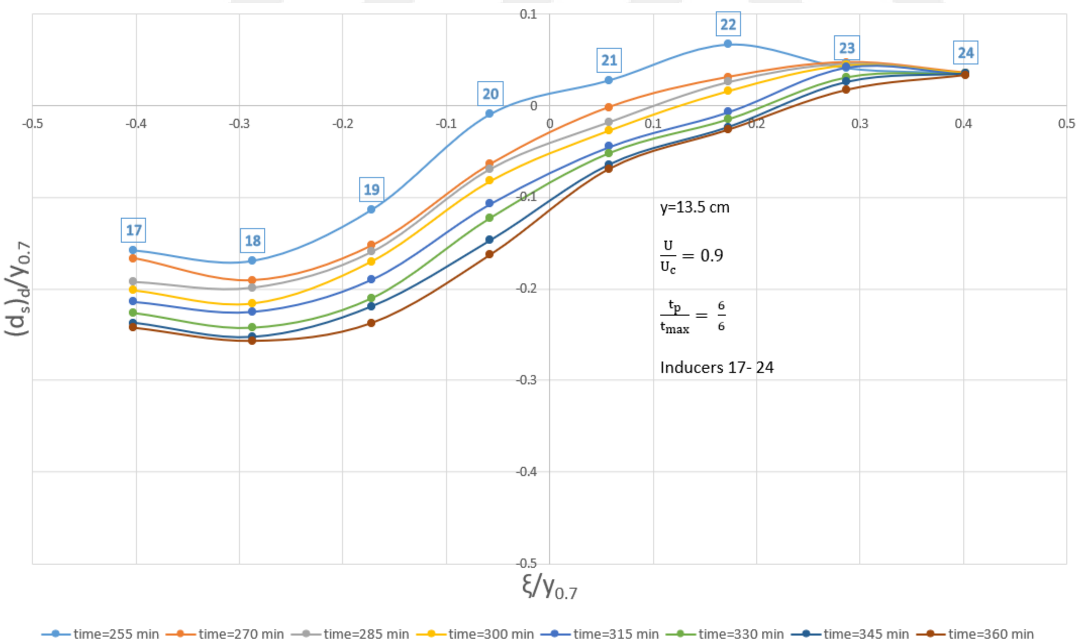

Figure 4.50 Temporal development of scour hole around the semi-circular end abutment of length L_a=20 cm for U/U_c = 0.90 along Inducers 17 - 24

4.4.1.1.6 The Abutment of Length L_a= 15 cm

Figures 4.51- 4.59 shows the temporal development of scour hole around the abutment with a length of L_a= 15 cm, which was the shortest abutment length tested during the experiments. During the first 4 hours of the experiment, with the flow intensities of 0.7 and 0.8, there was almost no activity of sediment particles at the upstream side of the abutment. Also, it was observed that the sediment particles slightly accumulated and created small ripples at the downstream side of the abutment. Nevertheless, scouring proceeded at the front side for the location of -0.2<$x/y_{0.7}$<0.2 during the first 2 hours of the experiment. Then, during the next 2 hours with the flow intensity of 0.8, scour hole was enlarged toward the location of $x/y_{0.7}$=0.3. However, it should be underlined that scour development was almost negligible for those time intervals.

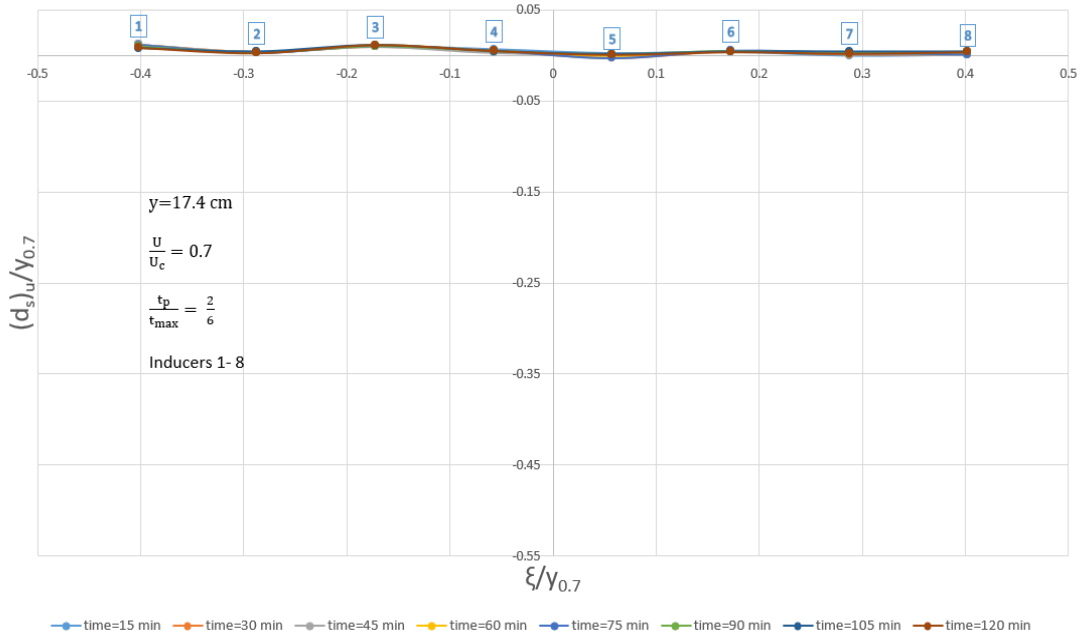

Figure 4.51 Temporal development of scour hole around the semi-circular end abutment of length L_a=15 cm for U/U_c = 0.70 along Inducers 1 - 8

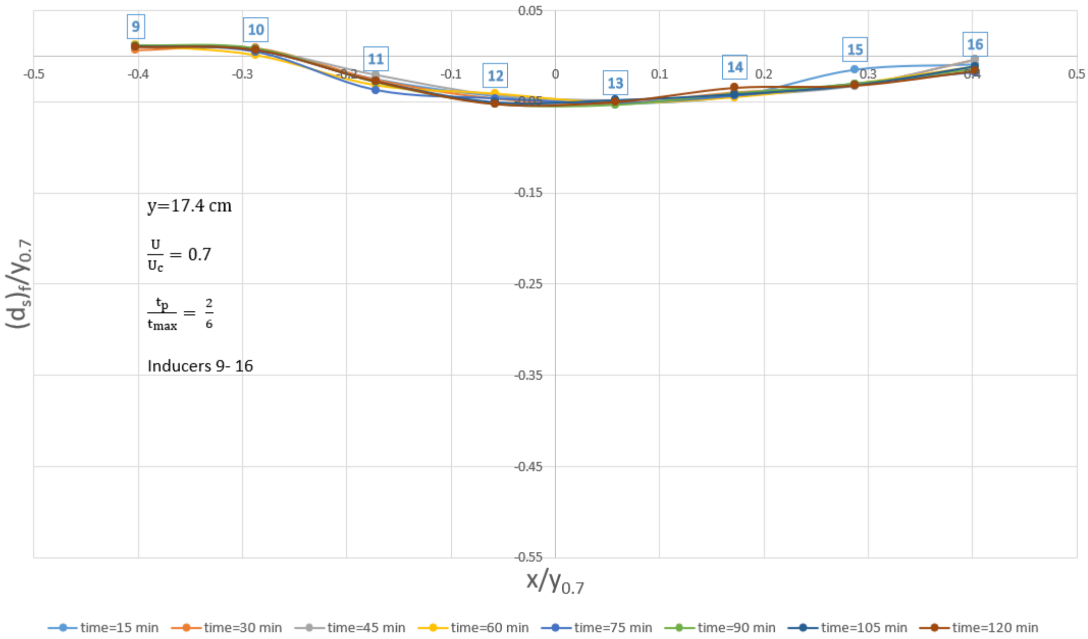

Figure 4.52 Temporal development of scour hole around the semi-circular end abutment of length L_a=15 cm for U/U_c = 0.70 along Inducers 9 - 16

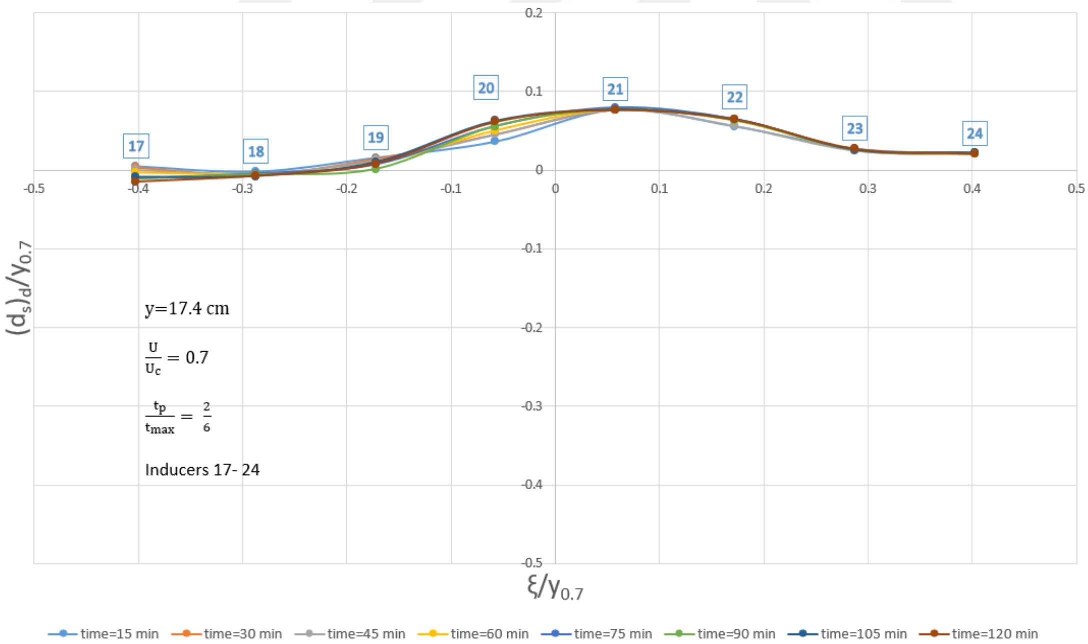

Figure 4.53 Temporal development of scour hole around the semi-circular end abutment of length L_a=15 cm for U/U_c = 0.70 along Inducers 17 - 24

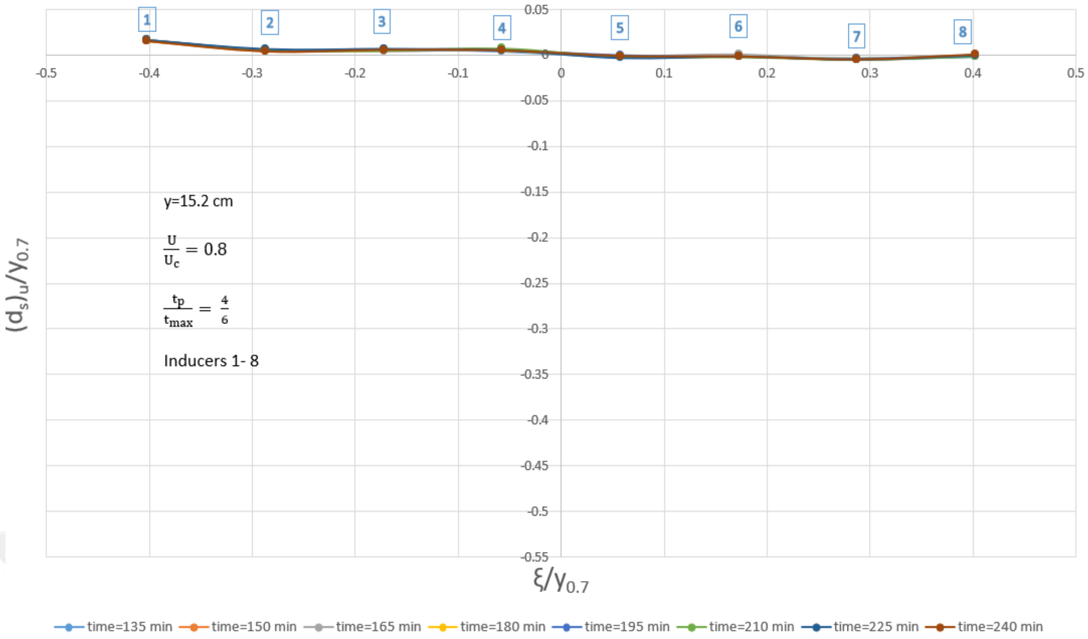

Figure 4.54 Temporal development of scour hole around the semi-circular end abutment of length L_a=15 cm for U/U_c = 0.80 along Inducers 1 - 8

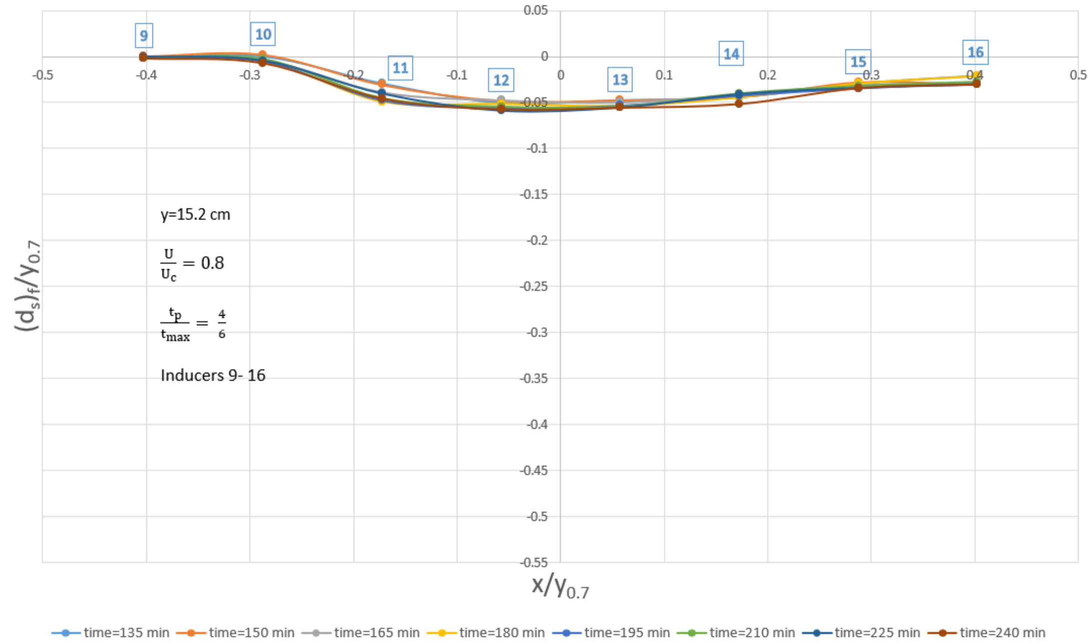

Figure 4.55 Temporal development of scour hole around the semi-circular end abutment of length L_a=15 cm for U/U_c = 0.80 along Inducers 9 - 16

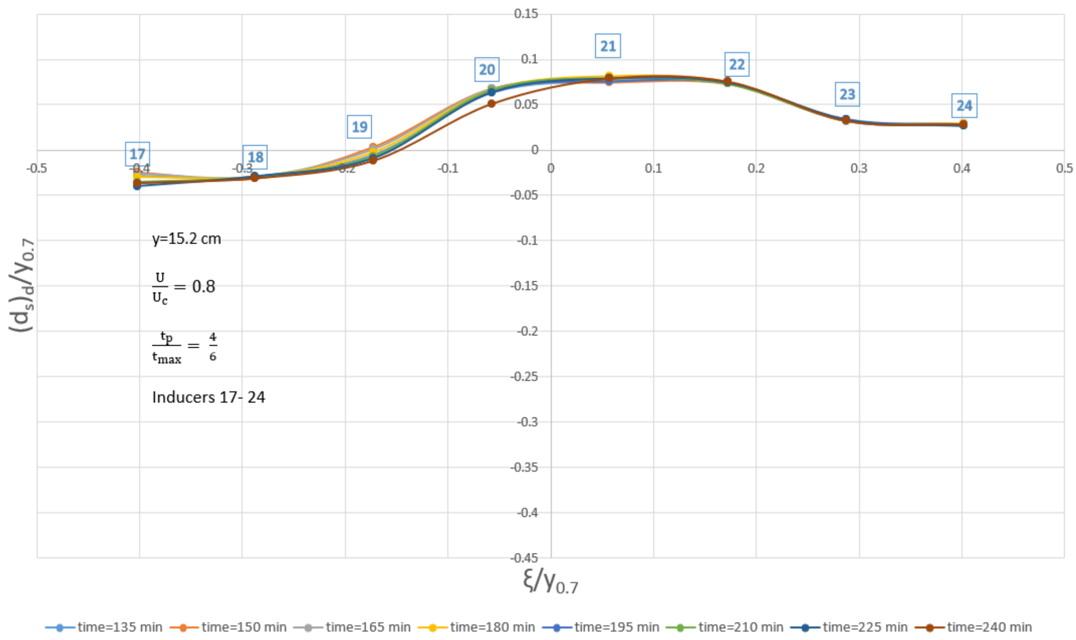

Figure 4.56 Temporal development of scour hole around the semi-circular end abutment of length L_a=15 cm for U/U_c = 0.80 along Inducers 17 - 24

When the flow intensity increased to 0.9 at the 4th hour of the experiment, scour development around the abutment was finally started. At the front side of the abutment, scour hole development gradually continued until the 330th minute and then scour development slowed down to the end of the experiment. On this side, maximum scour depths were observed at $-0.2<x/y_{0.7}<0.2$. However, observed scour depths around the upstream and downstream sides of the abutment were still less. Nevertheless, at the downstream side, considerable scour depths were observed at $-0.4<\xi/y_{0.7}<-0.20$ after the 285th minute of the experiment. The maximum or final dimensionless scour depths were measured as $d_s/y_{0.7}$=-0.08, -0.15 and -0.15 at the abutment's upstream, front and downstream sides, respectively. Only 23% of the maximum or final scour depth value was recorded at the 4th hour of the experiment due to the immotility of the bed during the first 4th hour of the experiment. However, a rapid scour hole development was observed after increasing the flow intensity value to 0.9. Hence, 76% of the maximum scour depth was recorded at the 5th hour of the experiment.

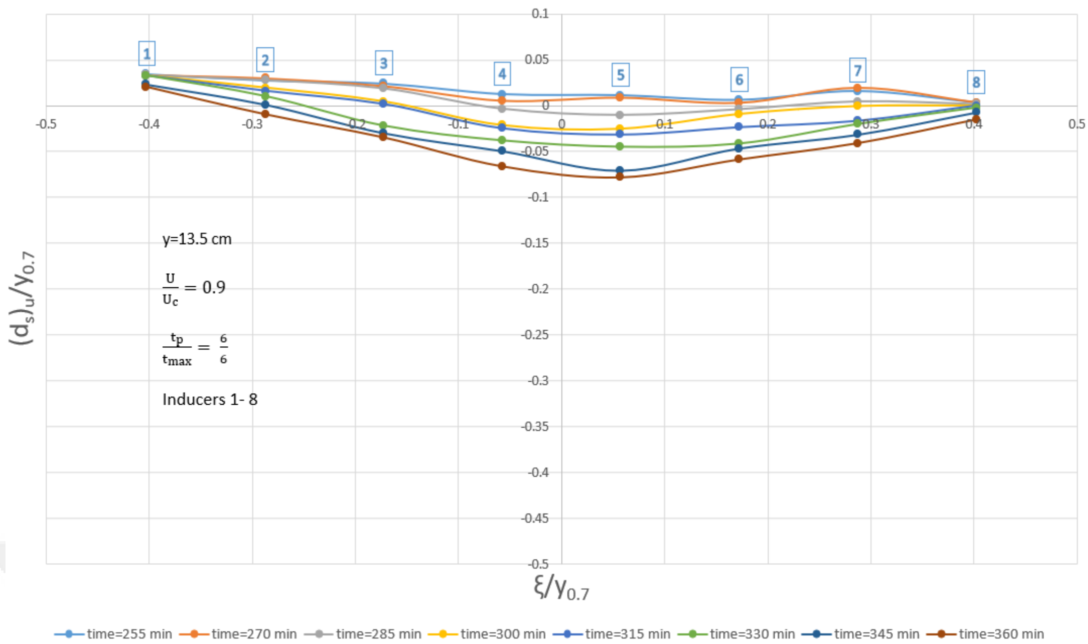

Figure 4.57 Temporal development of scour hole around the semi-circular end abutment of length L_a=15 cm for U/U_c = 0.90 along Inducers 1 - 8

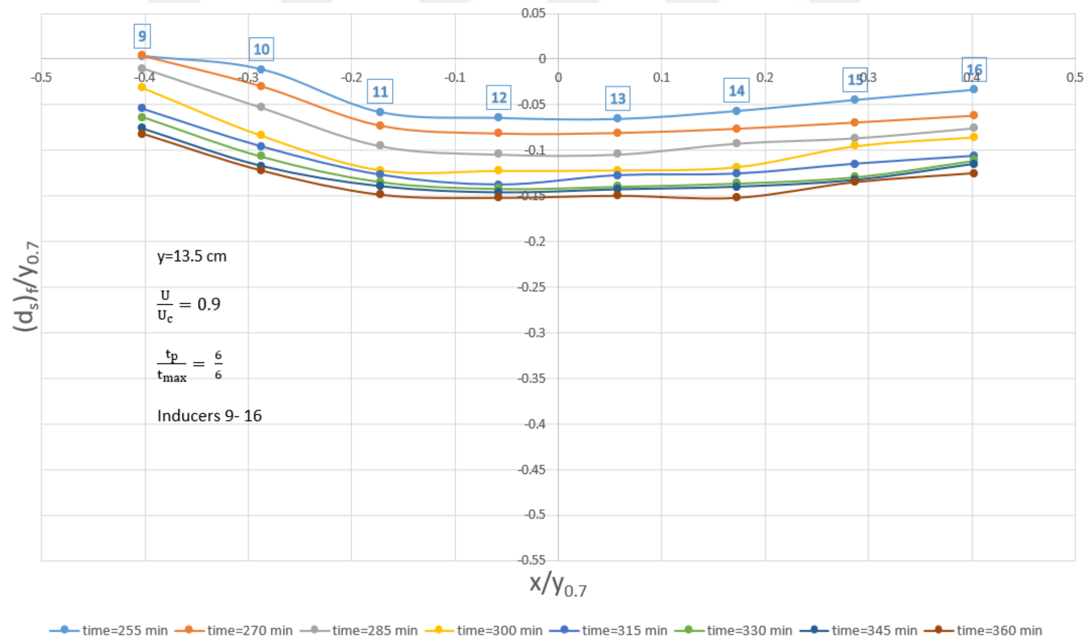

Figure 4.58 Temporal development of scour hole around the semi-circular end abutment of length L_a=15 cm for U/U_c = 0.90 along Inducers 9 - 16

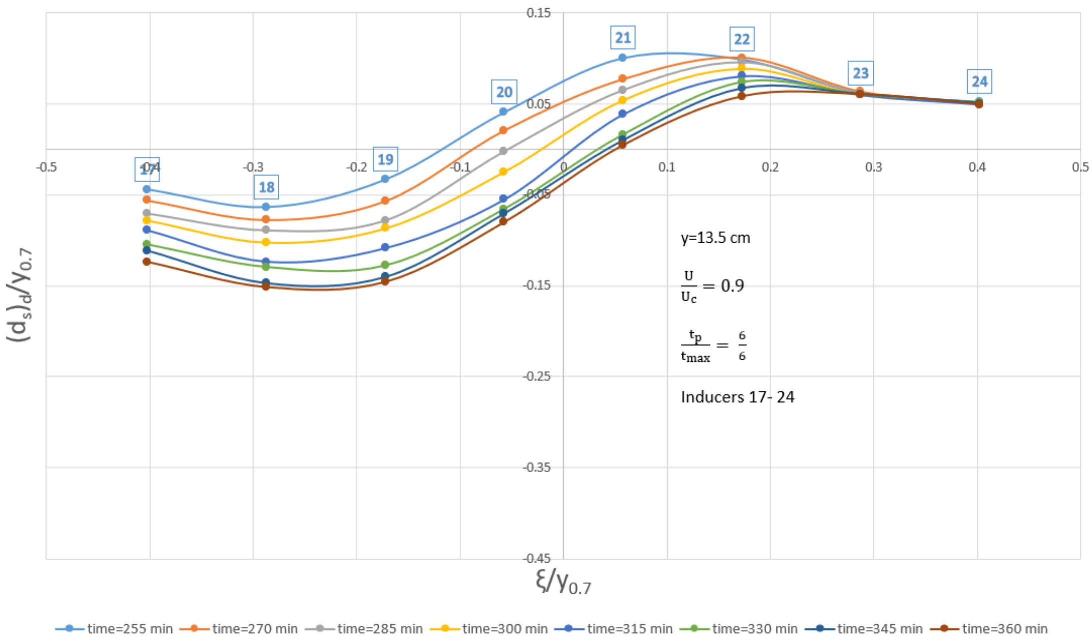

Figure 4.59 Temporal development of scour hole around the semi-circular end abutment of length L_a=15 cm for U/U_c = 0.90 along Inducers 17 - 24

4.4.1.2 Rectangular Abutments

4.4.1.2.1 The Abutment of Length L_a= 40 cm

In Figures 4.60-4.68, the temporal development of scour hole around the abutment with a length of L_a= 40 is presented. During the first 2 hours of the experiments with the flow intensity of 0.7, a rapid scour hole development was observed at the upstream and front sides of the abutment. Especially the scour development was very fast until the 15th minute. Then, scour holes gradually developed at a decreasing rate with increasing time. Furthermore, on the upstream side, there is almost no change in the scour depth between the 105th and 120th minutes. In this period, the maximum scour depths were recorded at $-0.05<\xi/y_{0.7}<0.30$ and $-0.2<x/y_{0.7}<0.05$ for the upstream and front sides, respectively. On the contrary, on the downstream side, scouring started to proceed after the 15th minute and significant scour depths were measured after the 60th minute, particularly for the locations of $-0.4<\xi/y_{0.7}<-0.10$.

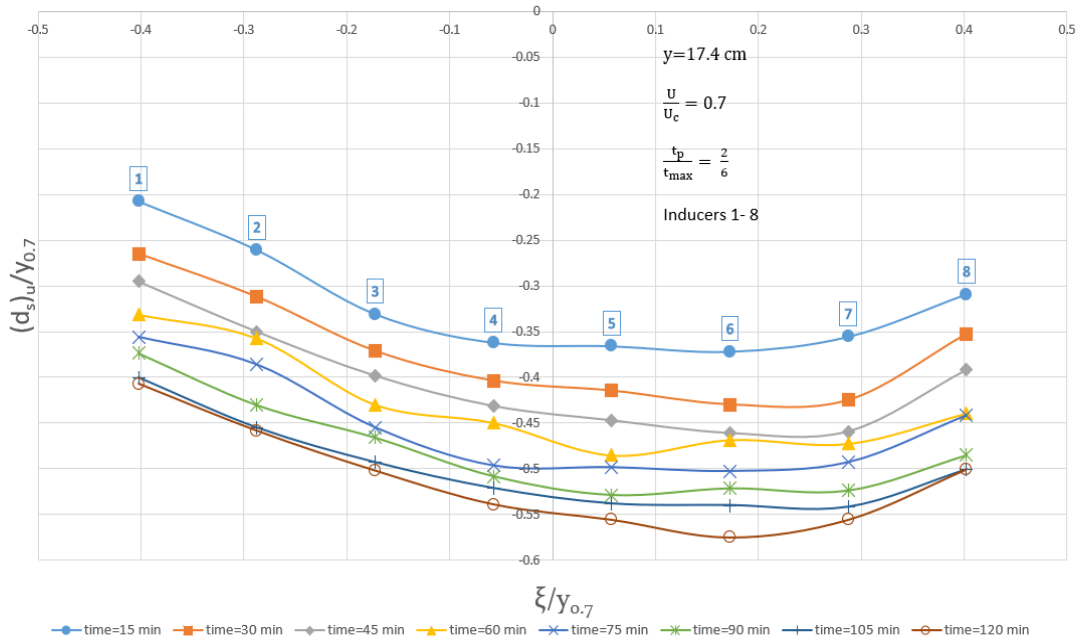

Figure 4.60 Temporal development of scour hole around the rectangular abutment of length L_a=40 cm for U/U_c = 0.70 along Inducers 1 - 8

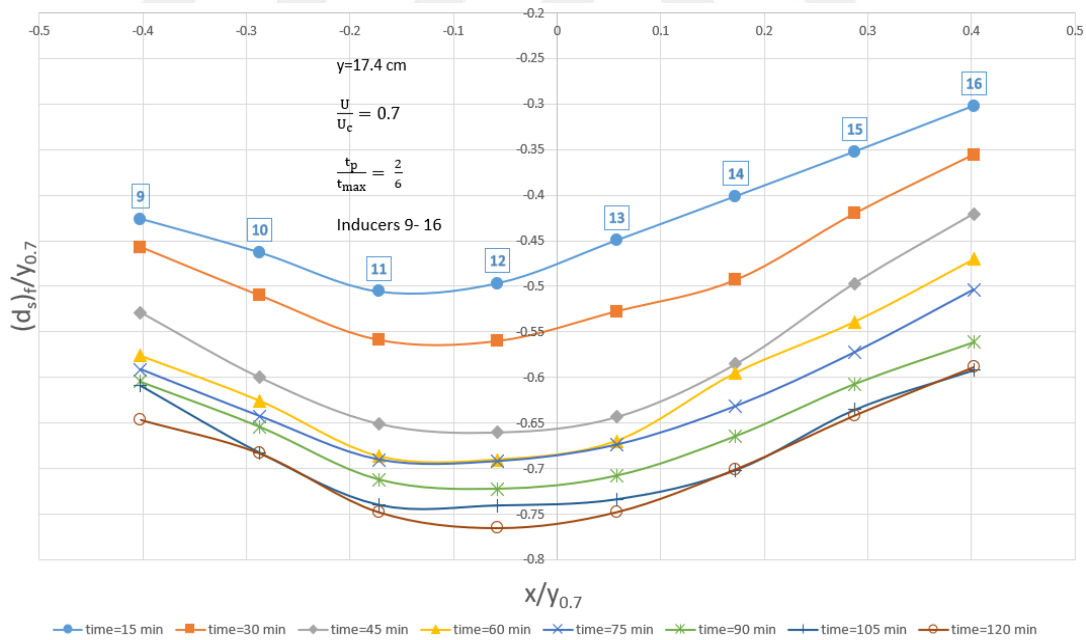

Figure 4.61 Temporal development of scour hole around the rectangular abutment of length L_a=40 cm for U/U_c = 0.70 along Inducers 9 - 16

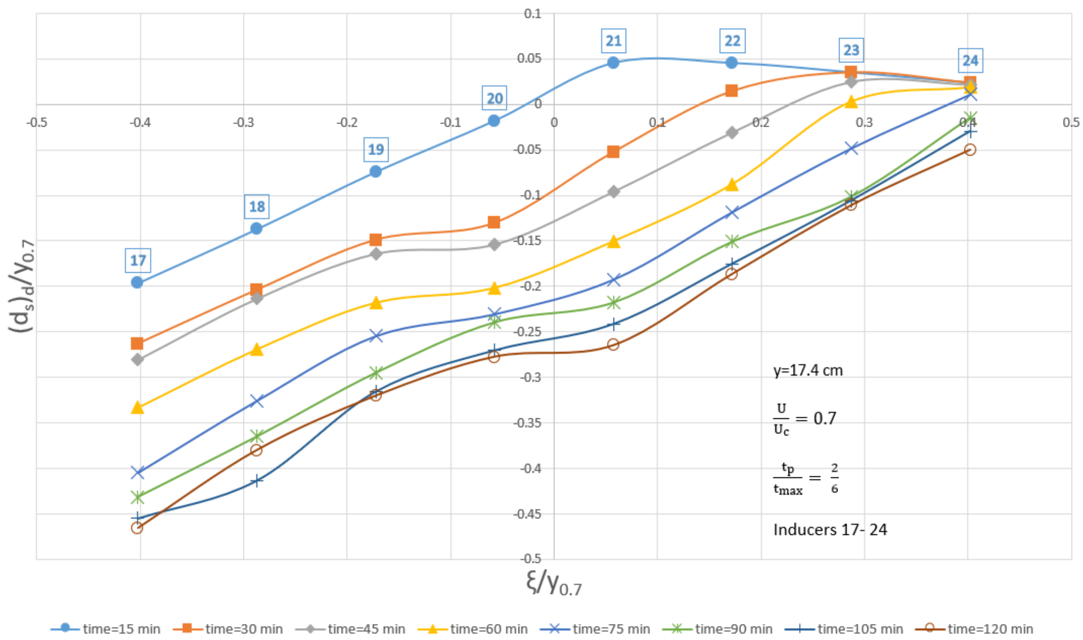

Figure 4.62 Temporal development of scour hole around the rectangular abutment of length L_a=40 cm for U/U_c = 0.70 along Inducers 17 - 24

After the flow intensity was increased to 0.8, the rate of the scour hole development accelerated, especially between the 120th and 150th and minutes at the upstream and front sides of the abutment. Moreover, a rapid increment continued for the downstream side even at the 180th minute. Afterward, the scour development continued gradually with a decreasing rate until the end of this phase of the experiment. In this stage of the experiment, the maximum scour depths at the upstream, front and downstream sides of the abutment were recorded for the locations of $\xi/y_{0.7}$= -0.05, $-0.2<x/y_{0.7}<0.05$ and at $-0.40<\xi/y_{0.7}<-0.30$, respectively.

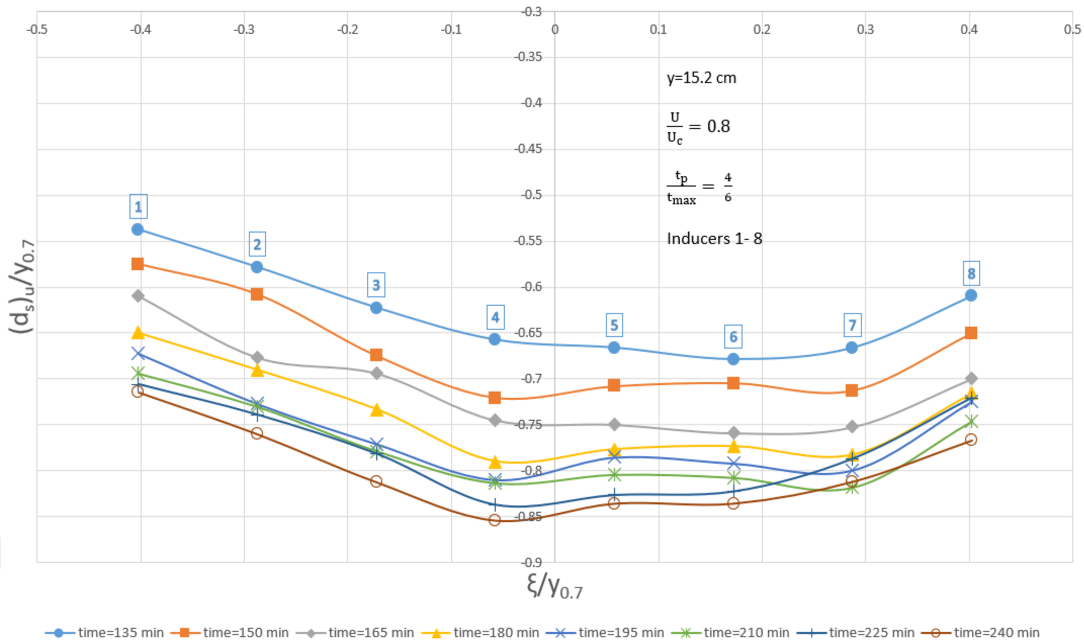

Figure 4.63 Temporal development of scour hole around the rectangular abutment of length L_a=40 cm for U/U_c = 0.80 along Inducers 1 - 8

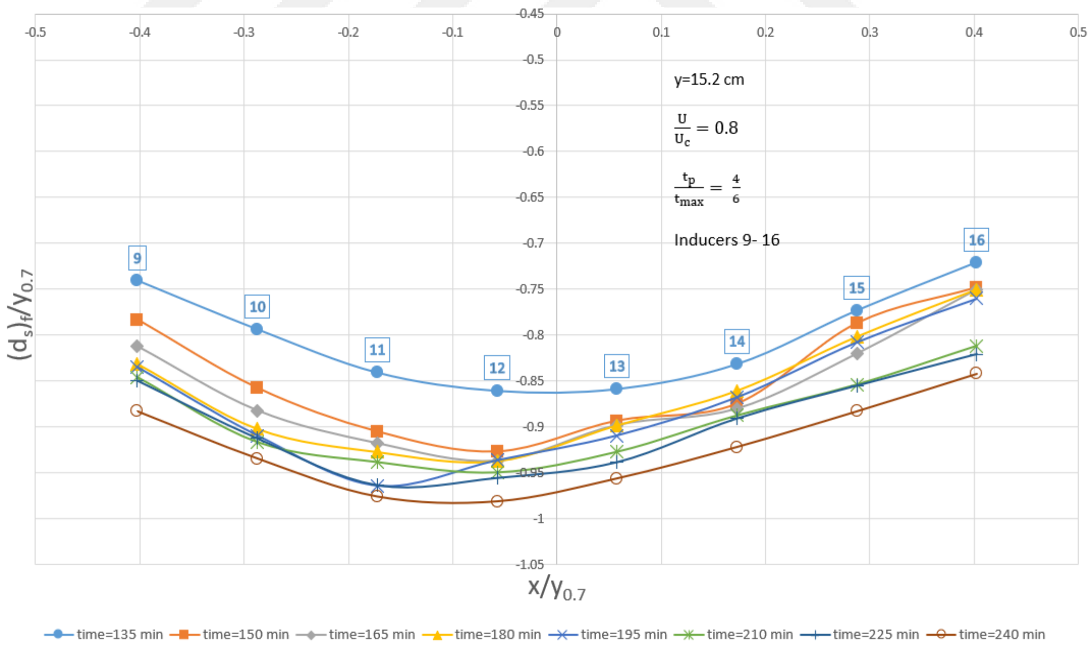

Figure 4.64 Temporal development of scour hole around the rectangular abutment of length L_a=40 cm for U/U_c = 0.80 along Inducers 9 - 16

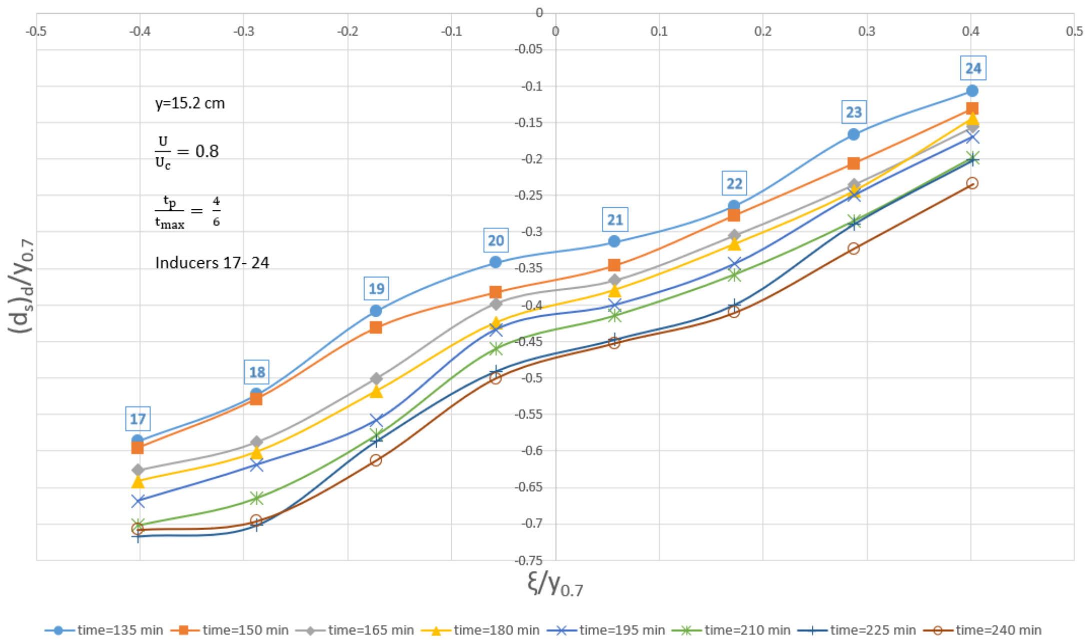

Figure 4.65 Temporal development of scour hole around the rectangular abutment of length L_a=40 cm for U/U_c = 0.80 along Inducers 17 - 24

During the last 2 hours of the experiment, with the flow intensity of 0.9, scour hole development was quite fast between the 240th and 270th minute. Then, scour hole development was gradually slow until the end of the experiment. Especially between the 345th and 360th minutes of the experiment, the alteration of the scour depth around the abutment was almost negligible. Moreover, a small decrease in scour depths was observed at the downstream side of the abutment between the 240th and 255th minutes because of the movement of the sediment particles from the upstream and front sides of the abutment along with increased flow intensity. The locations of the maximum scour depths were measured for the upstream, front and downstream sides of the abutment at $-0.05<\xi/y_{0.7}<0.30$, $-0.20<x/y_{0.7}<-0.10$, $\xi/y_{0.7}=-0.40$, respectively. The maximum or final dimensionless scour depths were recorded as $d_s/y_{0.7}$=-1.03, -1.21 and -0.92 at the abutment's upstream, front and downstream sides, respectively. For this case, 81% of the final scour depth was obtained at the 4th hour of the experiment.

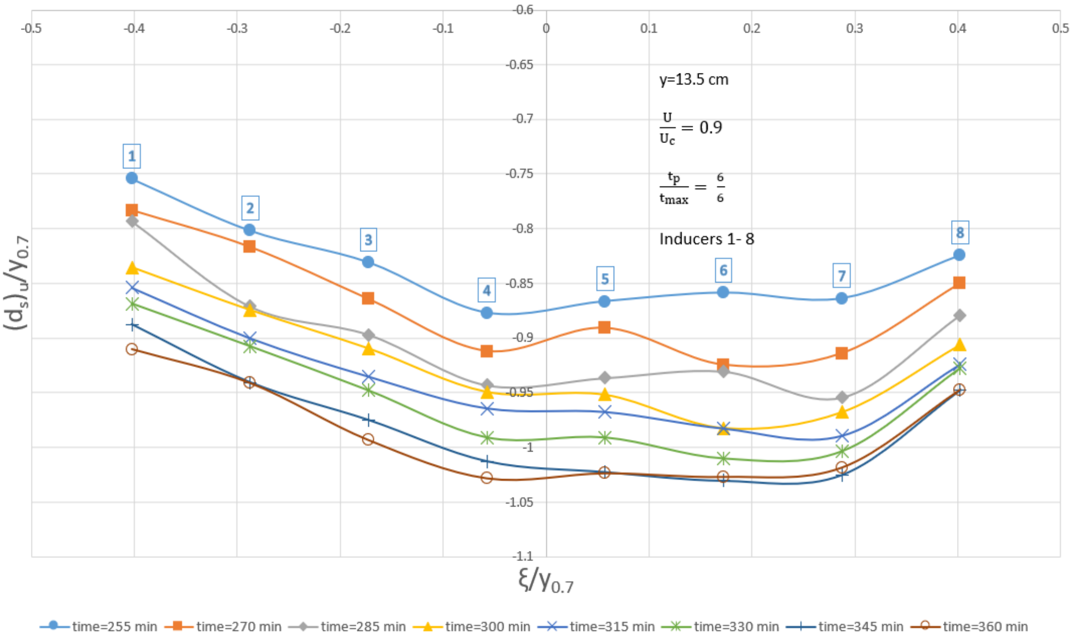

Figure 4.66 Temporal development of scour hole around the rectangular abutment of length L_a=40 cm for U/U_c = 0.90 along Inducers 1 - 8

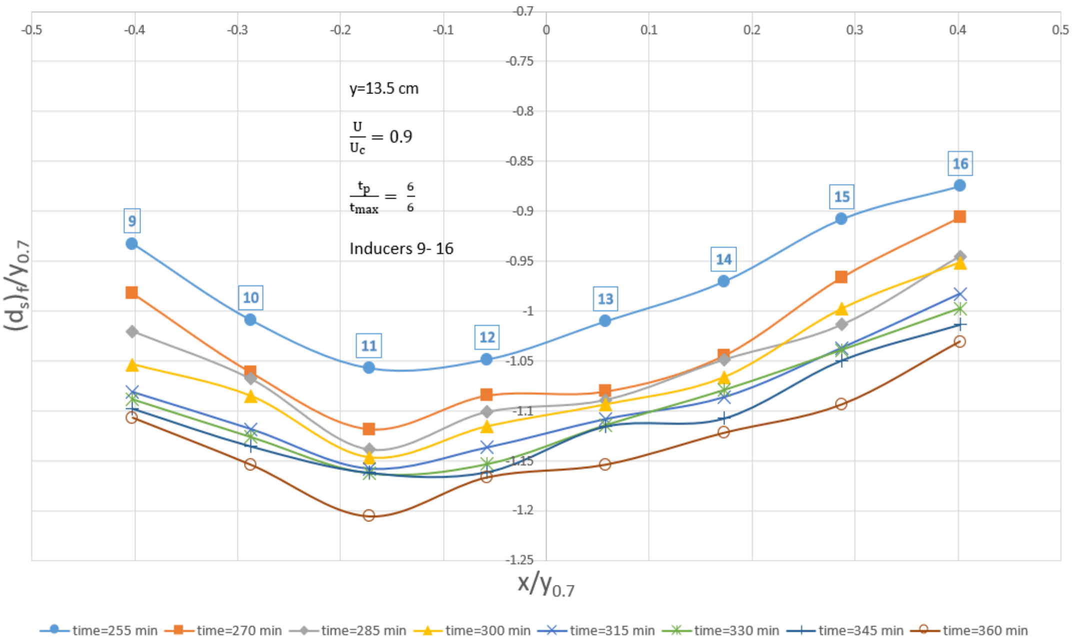

Figure 4.67 Temporal development of scour hole around the rectangular abutment of length L_a=40 cm for U/U_c = 0.90 along Inducers 9 - 16

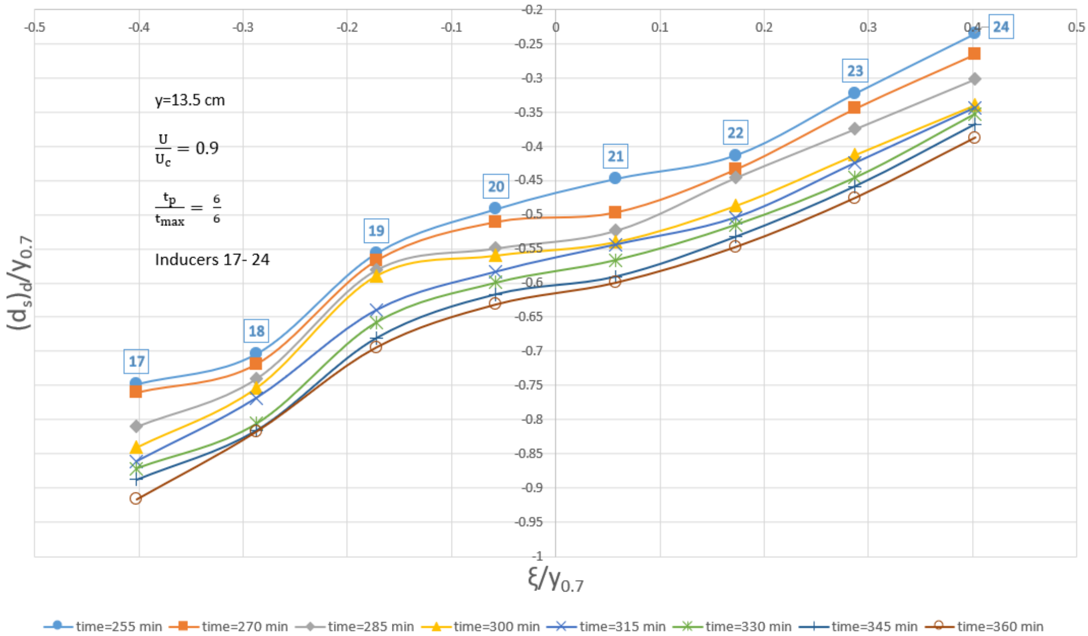

Figure 4.68 Temporal development of scour hole around the rectangular abutment of length L_a=40 cm for U/U_c = 0.90 along Inducers 17 - 24

4.4.1.2.2 The Abutment of Length L_a= 35 cm

The temporal development of the scour hole around the abutment of length L_a=35 cm are presented in Figures 4.69- 4.77. At the initial stage of the experiment, with the flow intensity value of 0.7, a rapid scour hole development was observed around the abutment. At the upstream side of the abutment, scour hole development slowed down after the 60th minute and then small increments were recorded until the end of the first 2 hours. In this region, the maximum scour depths were recorded for the locations of $0.20<\xi/y_{0.7}<0.30$. At the front side of the abutment, scour depths gradually increased between the 15th and 90th minutes. However, a significant increase in scour depths was observed between the 90th and 105th minutes. Afterward, during the last 15 minutes of this stage, any alterations were not seen in the depth and shape of the scour hole. The maximum scour depths at the front side of the abutment were recorded for the locations of $-0.15<x/y_{0.7}<-0.05$. At the downstream side of the abutment for the locations of $0.00<\xi/y_{0.7}<0.40$, deposition of sediment particles was observed rather than scour formation. Nevertheless, scouring started to proceed after the 60th minute in this region. In the regions apart from that range, scour hole enlarged and deepened gradually until the end of the first 2 hours. The maximum scour depth at the downstream side of the abutment was measured at the $\xi/y_{0.7}$=-0.40.

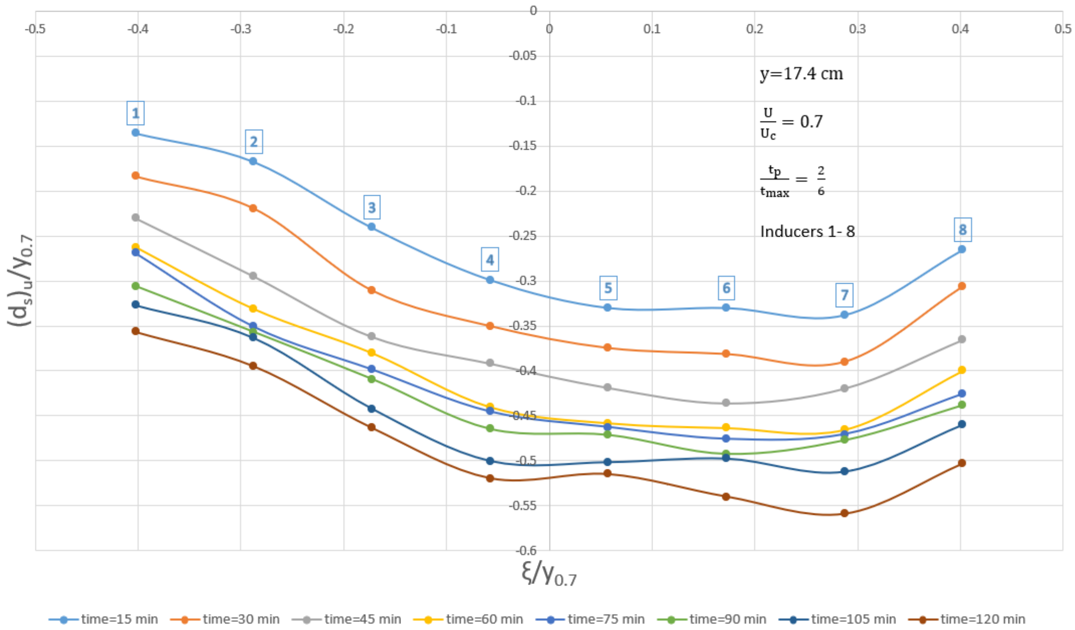

Figure 4.69 Temporal development of scour hole around the rectangular abutment of length L_a=35 cm for U/U_c = 0.70 along Inducers 1 - 8

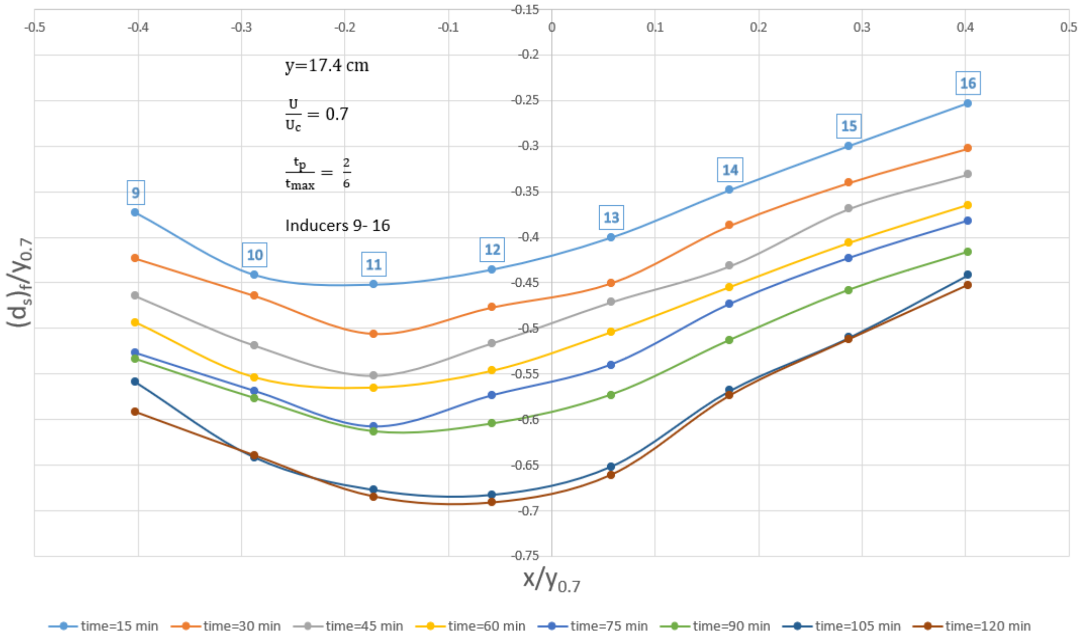

Figure 4.70 Temporal development of scour hole around the rectangular abutment of length L_a=35 cm for U/U_c = 0.70 along Inducers 9 - 16

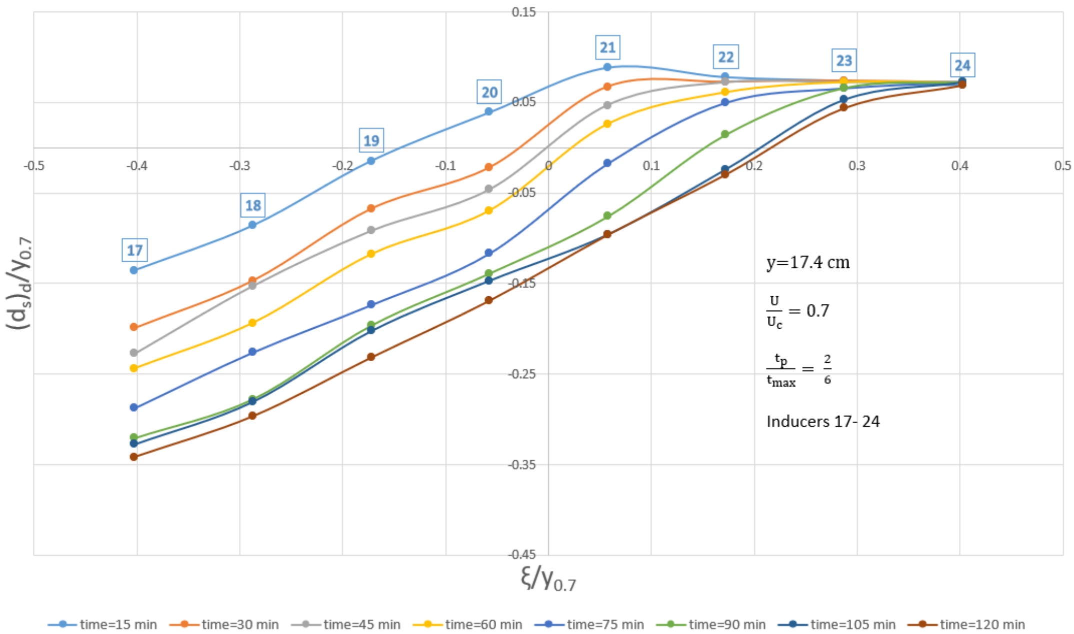

Figure 4.71 Temporal development of scour hole around the rectangular abutment of length L_a=35 cm for U/U_c = 0.70 along Inducers 17 - 24

During the second 2 hours of the experiment, scour hole rapidly enlarged by increasing the flow intensity from 0.7 to 0.8. Development of the scour hole was particularly significant between the 120th and 135th minutes at the upstream and downstream sides of the abutment. Development of the scour at the upstream was small relative to the front and downstream sides and scour depth magnitudes were approximately the same along all measurement points. Nevertheless, the scour depth is a little bit larger for the locations of $-0.05<\xi/y_{0.7}<0.30$. On the other hand, the scouring process was gradual on the downstream side of the abutment and the maximum scour depth was recorded at $\xi/y_{0.7}=-0.40$. At the front side, a significant enlargement on scour hole was measured between the 150th and 180th minutes. Afterward, alternations of the scour depth magnitude were relatively small and the maximum scour depths were recorded for the locations of $-0.20<x/y_{0.7}<-0.05$.

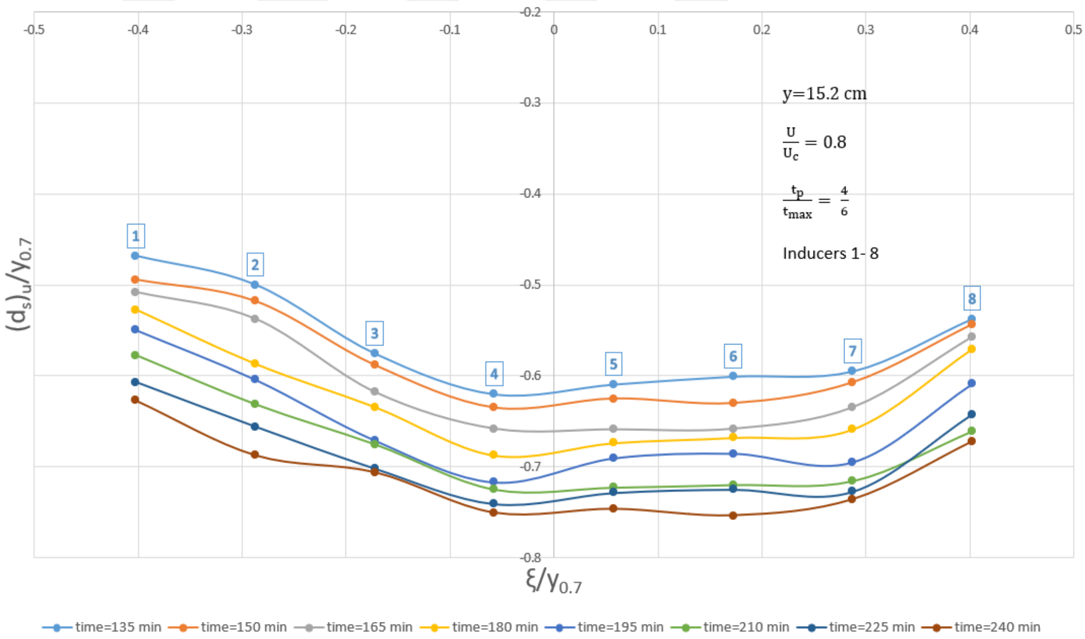

Figure 4.72 Temporal development of scour hole around the rectangular abutment of length L_a=35 cm for U/U_c = 0.80 along Inducers 1 - 8

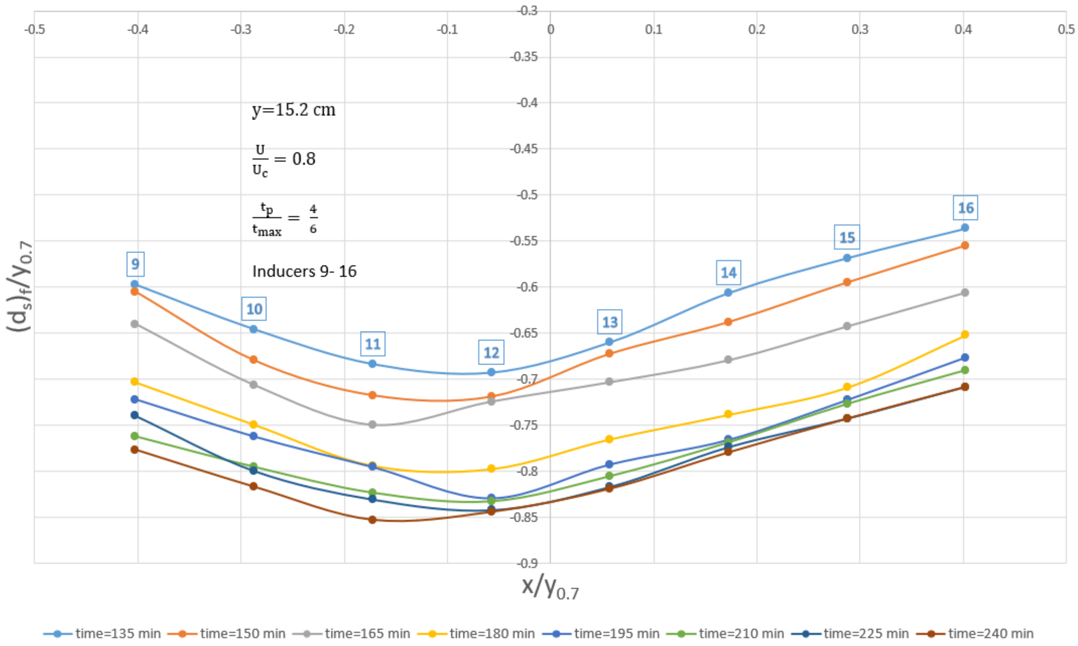

Figure 4.73 Temporal development of scour hole around the rectangular abutment of length L_a=35 cm for U/U_c = 0.80 along Inducers 9 - 16

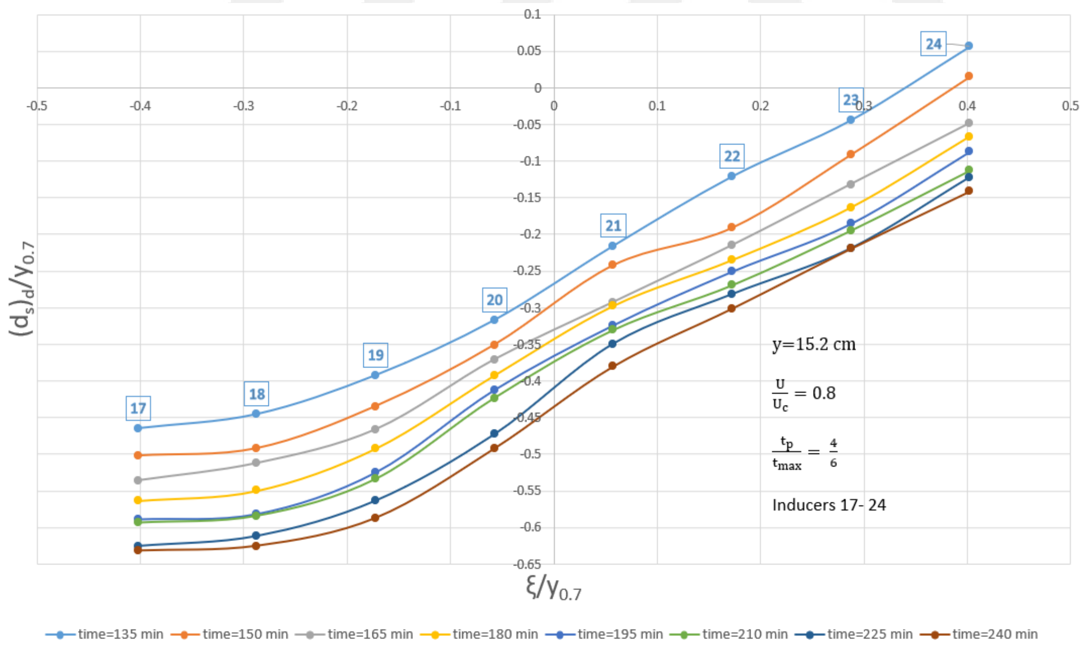

Figure 4.74 Temporal development of scour hole around the rectangular abutment of length L_a=35 cm for U/U_c = 0.80 along Inducers 17 - 24

In the final stage of the experiment, with the flow intensity of 0.9, scour depths at the upstream and front sides of the abutment rapidly enlarged and deepened between the 240th and 255th minutes due to the increased flow intensity. On the contrary, the scour depths were decreased at the downstream side of the abutment due to the transportation of the sediment particles here from the upstream in this period. However, after the 255th minute, scour depths gradually increased with a decreasing rate at all sides of the abutment until the end of the experiment. In this stage, the locations of the maximum scour depths along all sides of the abutment were similar to the previous stages having smaller flow intensities. The final or maximum scour depths around the abutment's upstream, front and downstream sides are $d_s/y_{0.7}$=-0.89, -1.03 and -0.70, respectively. Approximately %83 of the final scour depth was recorded at the 4th hour of the experiment.

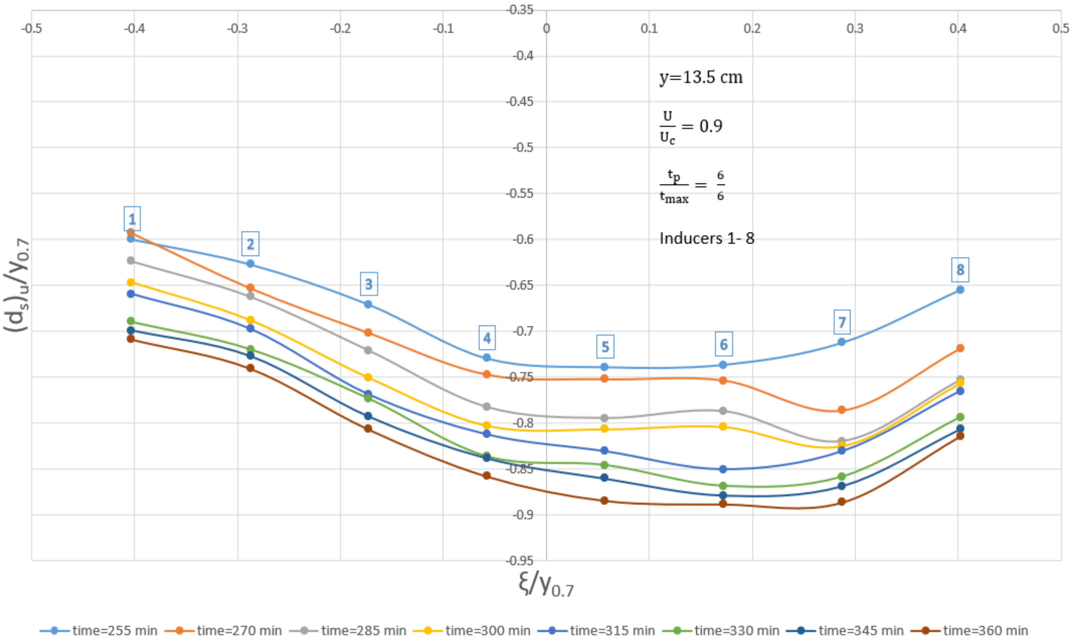

Figure 4.75 Temporal development of scour hole around the rectangular abutment of length L_a=35 cm for U/U_c = 0.90 along Inducers 1 - 8

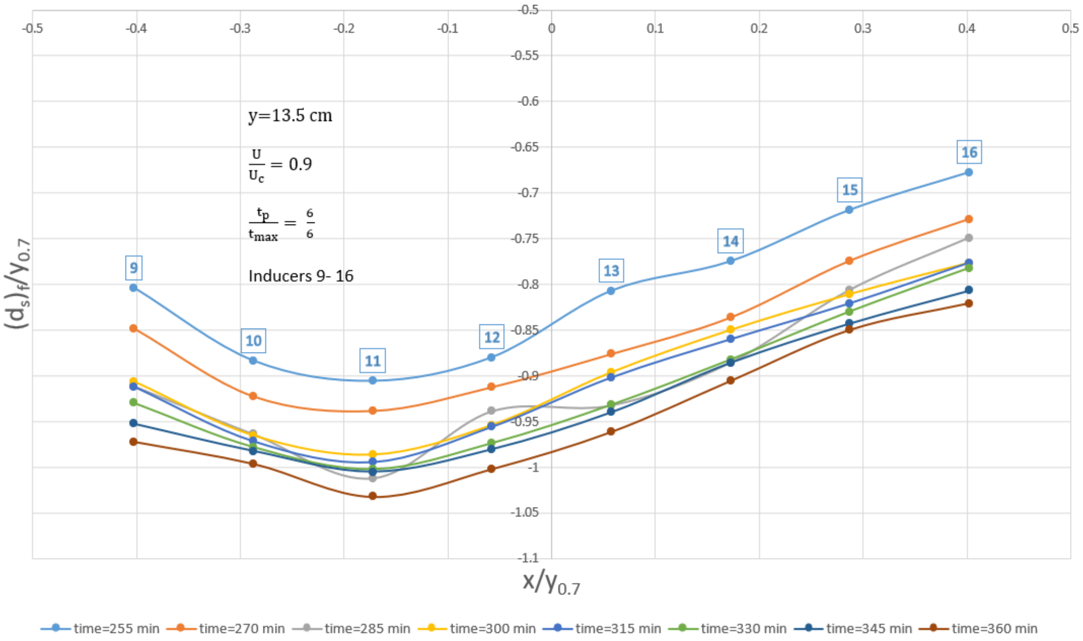

Figure 4.76 Temporal development of scour hole around the rectangular abutment of length L_a=35 cm for U/U_c = 0.90 along Inducers 9 - 16

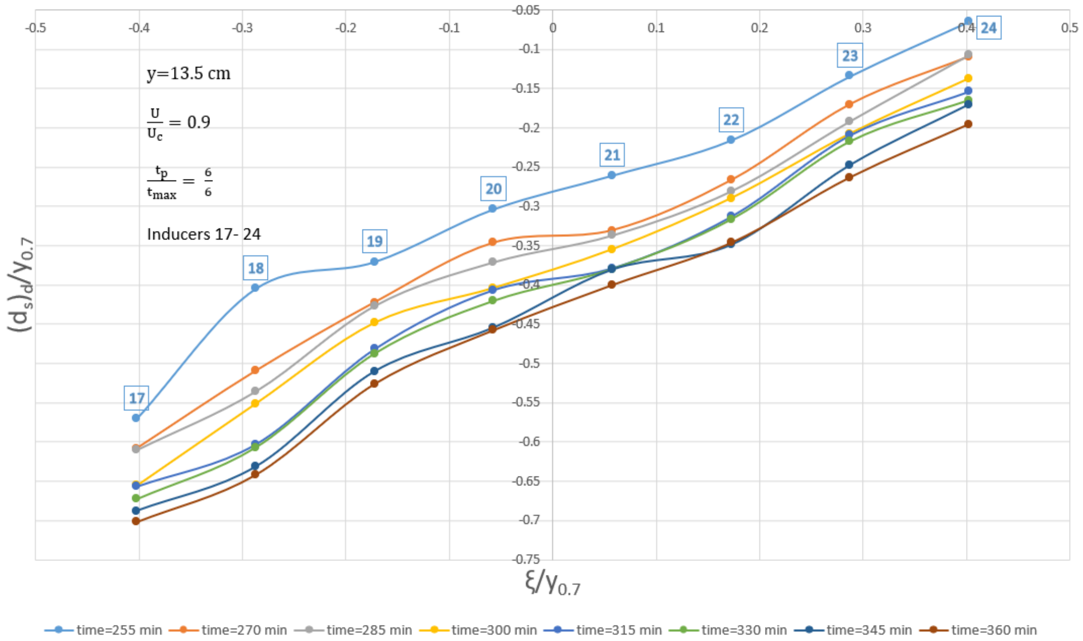

Figure 4.77 Temporal development of scour hole around the rectangular abutment of length L_a=35 cm for U/U_c = 0.90 along Inducers 17 - 24

4.4.1.2.3 The Abutment of Length L_a= 30 cm

In Figures 4.78-4.86, the temporal development of the scour hole around the abutment of length L_a=30 cm is given. During the first 2 hours of the experiment, with the flow intensity of 0.70, a rapid scour hole development was observed around the upstream and front sides of the abutment at the initial stages. On the other hand, the deposition of sediment particles was seen at the downstream side of the abutment until the 30th minute of the experiment. Then, scouring proceeded for the locations of $-0.40<\xi/y_{0.7}<0.00$ and maximum scour depth was recorded at $\xi/y_{0.7}=-0.40$. However, it should be indicated that the scour depth magnitudes on the downstream side are quite smaller compared to the upstream and front sides. At the upstream and front sides of the abutment, scour hole gradually developed until the end of 2 hours. Nonetheless, after the 60th minute, scour hole development decelerated and small alternations were observed between the 105th and 120th minutes. The maximum scour depths at the upstream and front sides of the abutment were observed for the locations of $0.20<\xi/y_{0.7}<0.30$ and $-0.30<x/y_{0.7}<-0.05$.

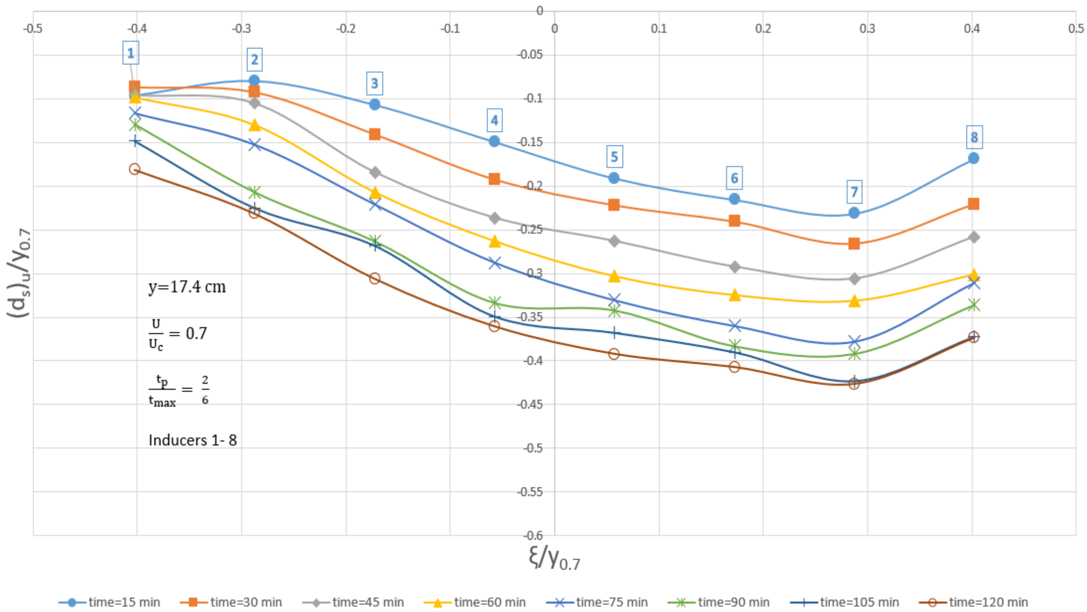

Figure 4.78 Temporal development of scour hole around the rectangular abutment of length L_a=30 cm for U/U_c = 0.70 along Inducers 1 - 8

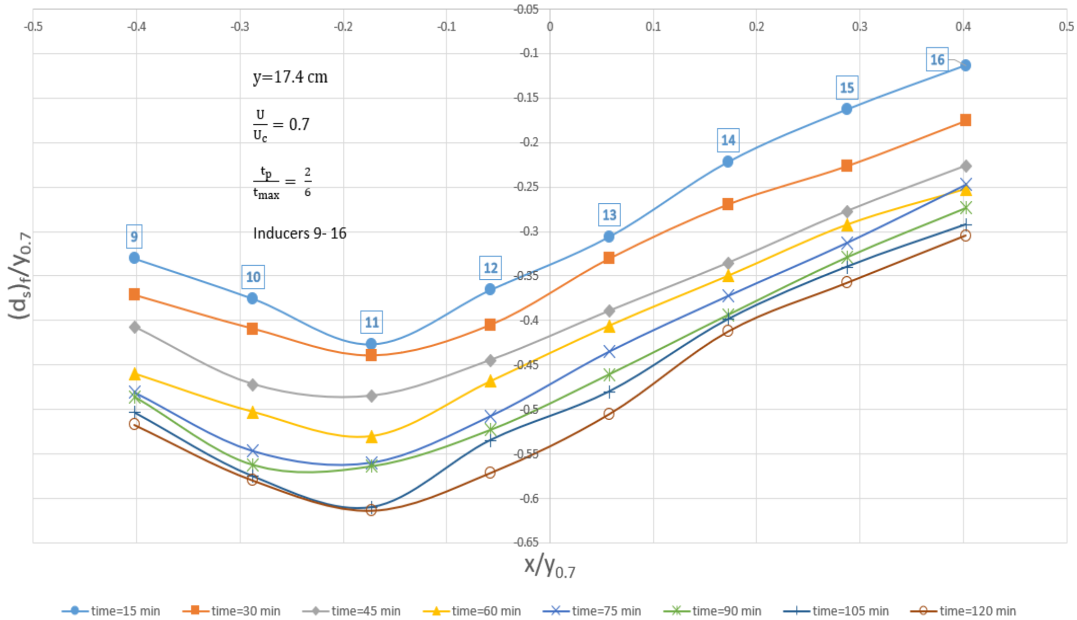

Figure 4.79 Temporal development of scour hole around the rectangular abutment of length L_a=30 cm for U/U_c = 0.70 along Inducers 9 - 16

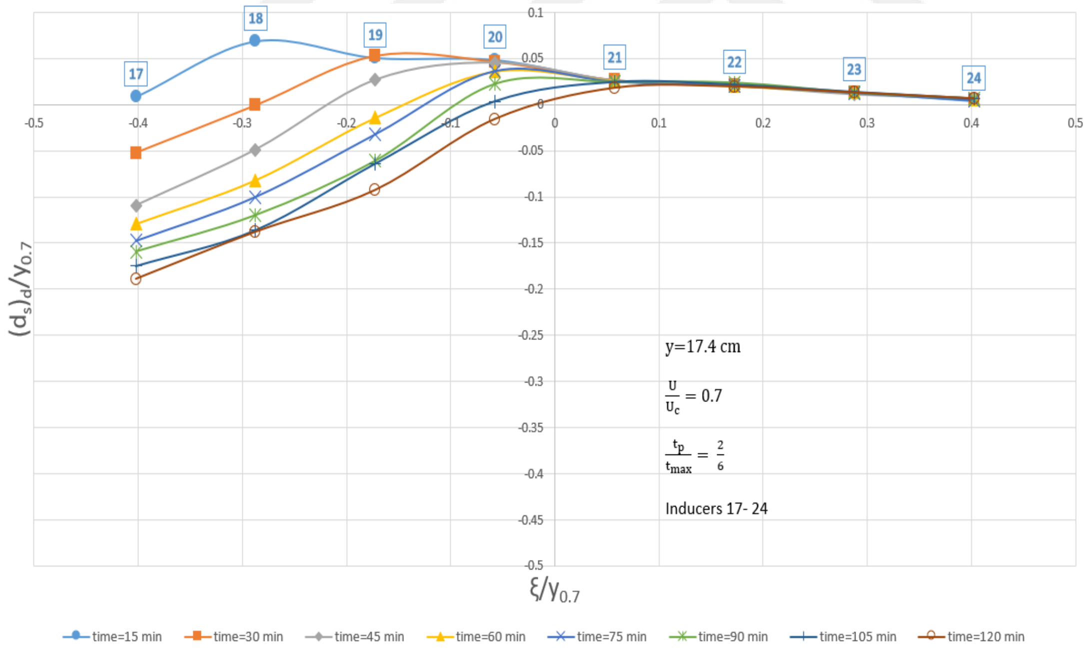

Figure 4.80 Temporal development of scour hole around the rectangular abutment of length L_a=30 cm for U/U_c = 0.70 along Inducers 17 - 24

After the flow intensity was increased to 0.8, scour depths rapidly increased at the upstream and front sides of the abutment between the 120th and 135th minutes. On the other side, small alterations were observed on the downstream side because of the accumulation of sediment particles from the upstream. But, for the deposited zones of $0.00<\xi/y_{0.7}<0.40$ at the downstream side, scour formation started to occur during the second 2 hours of the experiment. In this stage of the experiment, the scour hole gradually deepened around the abutment at a decreasing rate. Furthermore, scour depths were almost the same between the 225th and 240th minutes. The locations of the maximum scour depths in this stage were approximately the same as in the previous stage, with a flow intensity of 0.7.

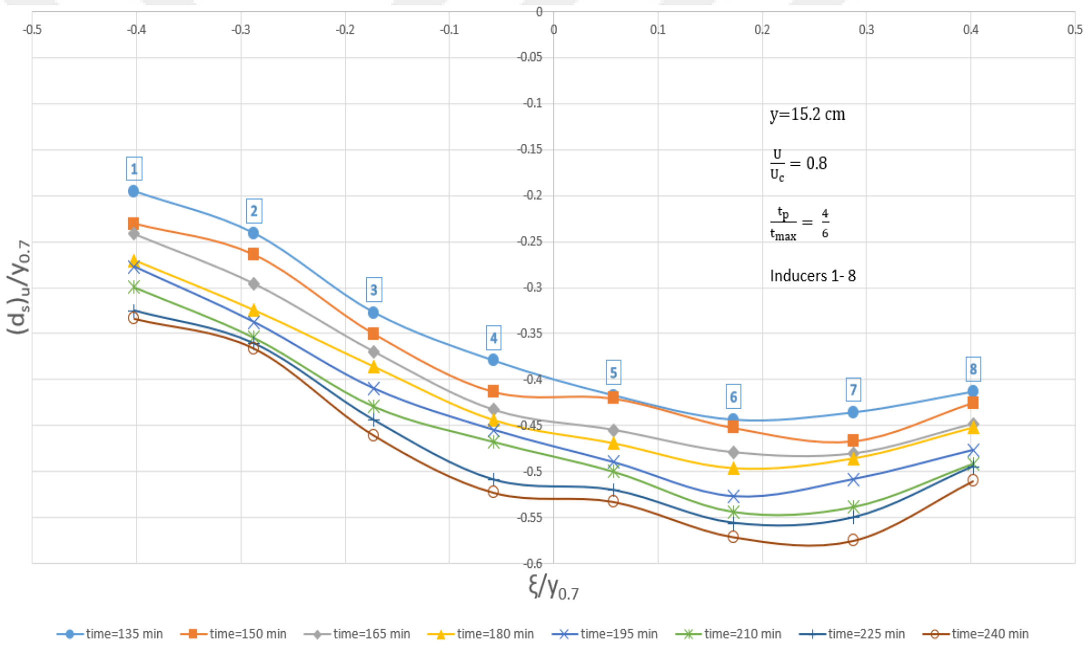

Figure 4.81 Temporal development of scour hole around the rectangular abutment of length L_a=30 cm for U/U_c = 0.80 along Inducers 1 - 8

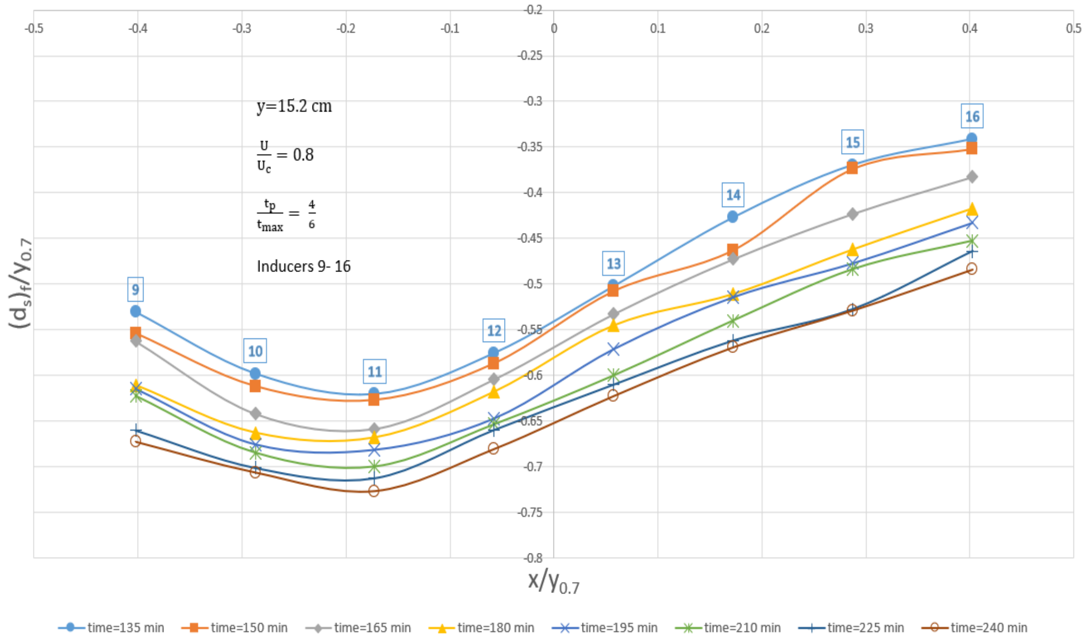

Figure 4.82 Temporal development of scour hole around the rectangular abutment of length L_a=30 cm for U/U_c = 0.80 along Inducers 9 - 16

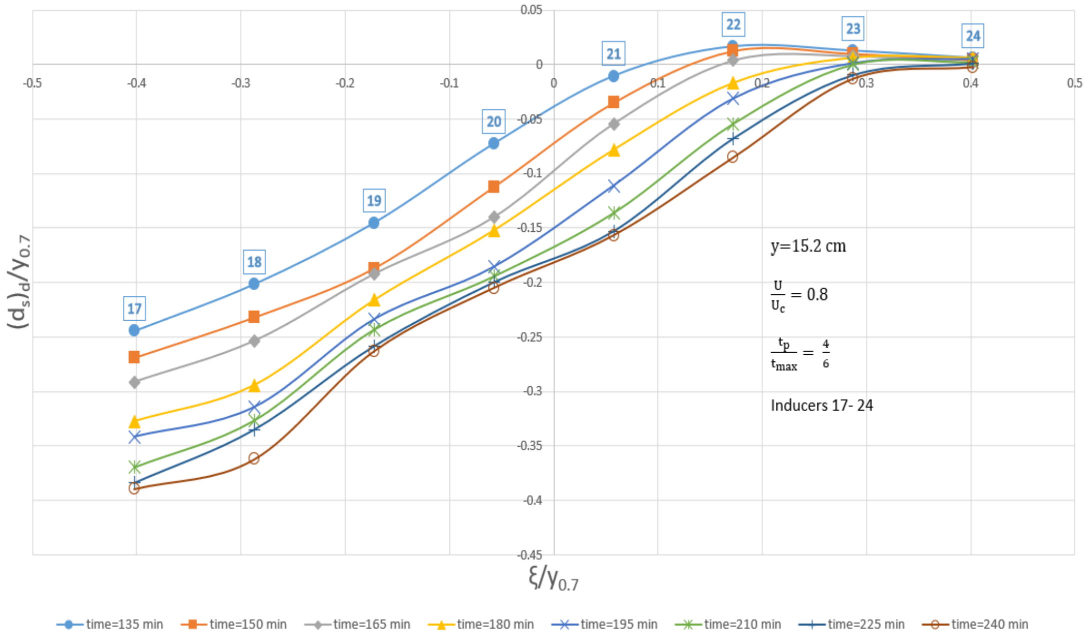

Figure 4.83 Temporal development of scour hole around the rectangular abutment of length L_a=30 cm for U/U_c = 0.80 along Inducers 17 - 24

When the flow intensity was increased to 0.9 for the last 2 hours of the experiment, the development rate of the scour hole rapidly increased between the 240th and 255th minutes. At the upstream side of the abutment, the rapid development of the scour hole continued until the 315th minute and then the development rate of the scour hole decreased. On this side, the maximum scour depths were recorded for the locations of $-0.05<\xi/y_{0.7}<0.30$. Moreover, scour hole development was very fast at the front side between the 255th and 270th minutes and then the development process slowed down until the 345th minutes. However, during the last 15 minutes of the experiment, between the 345th and 360th minutes, scouring proceeded very fast once again. At the front side of the abutment, the maximum scour depths were recorded for the locations of $-0.20<x/y_{0.7}<-0.10$. At the downstream side of the abutment, alterations of the scour depths were small between the 240th and 255th minutes. Afterward, the development of scour hole was gradual until the 345th minute. However, between the 345th and 360th minute, a reduction in the scour depths was observed. In other words, the maximum scours on the downstream side for this case were obtained at the 345th minute rather than the end of the experiment. This situation might be caused by the accumulation of sediment particles from the front side because of the rapid development of the scour hole between the 345th and 360th minutes, as it was mentioned above. On the downstream side, the maximum scour depths were measured at $-0.40<\xi/y_{0.7}<-0.30$. The final or maximum scour depths around the abutment's upstream, front and downstream sides are $d_s/y_{0.7}$=-0.80, -0.93 and -0.60, respectively. Approximately 77% of the final scour depth was recorded at the 4th hour of the experiment.

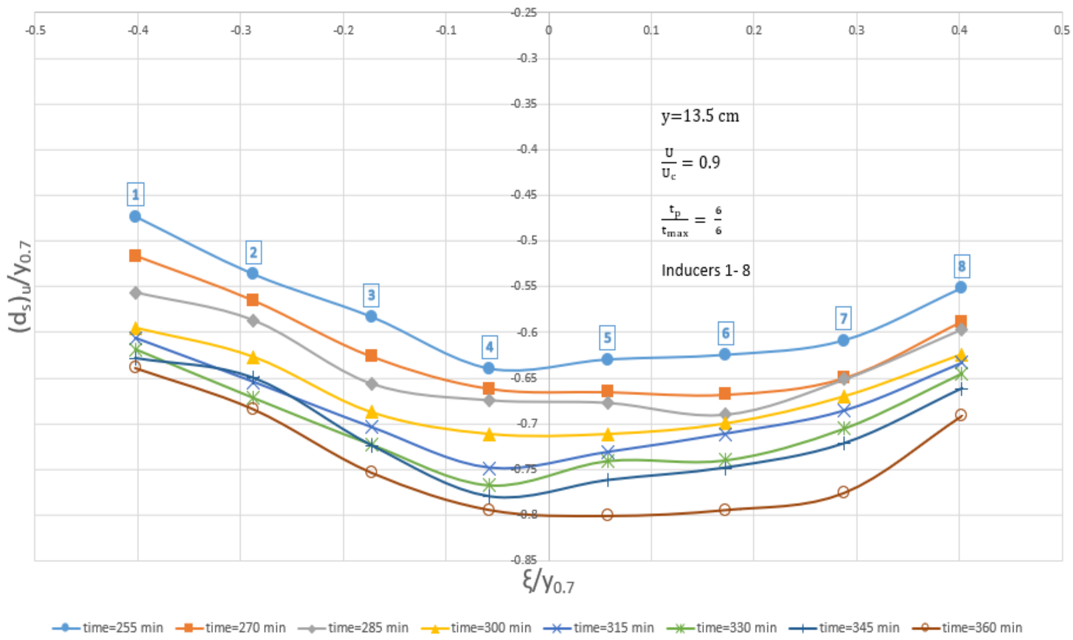

Figure 4.84 Temporal development of scour hole around the rectangular abutment of length L_a=30 cm for U/U_c = 0.90 along Inducers 1 - 8

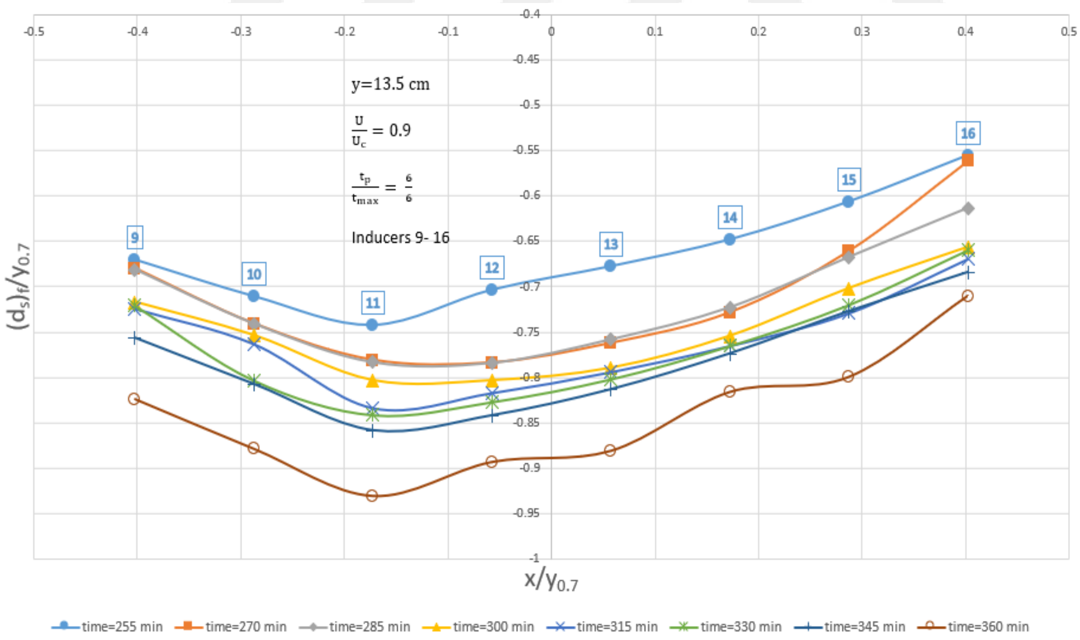

Figure 4.85 Temporal development of scour hole around the rectangular abutment of length L_a=30 cm for U/U_c = 0.90 along Inducers 9 - 16

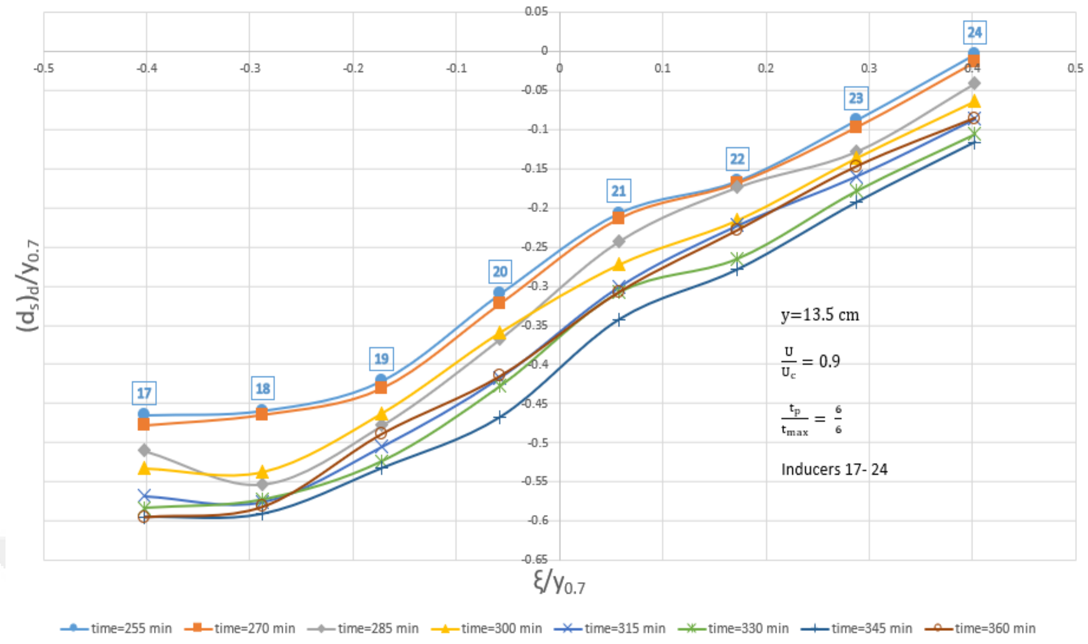

Figure 4.86 Temporal development of scour hole around the rectangular abutment of length L_a=30 cm for U/U_c = 0.90 along Inducers 17 - 24

4.4.1.2.4 The Abutment of Length L_a= 25 cm

The temporal variation of the scour hole around the abutment of length L_a=25 cm is given in Figures 4.87-4.95. During the first 2 hours of the experiment with the flow intensity of 0.7, scour hole development was fast until the 15th minute at the front side of the abutment. Then, scour hole gradually developed and after the 90th minute, there were almost no alterations on the eroded bed. At this side, the maximum scour depths were observed for the locations of $-0.20<x/y_{0.7}<-0.10$. On the other hand, the scour hole development at the upstream side of the abutment was small relative to the front side of the abutment. Nevertheless, for the locations of $-0.05<\xi/y_{0.7}<0.40$, significant scour depths were obtained. Contrary to the upstream and front sides, scour hole development was relatively slow on the downstream side of the abutment. In particular, despite scour hole development was started for the locations of $-0.40<\xi/y_{0.7}<-0.20$, after the 45th minute, the magnitude of the scour depths was almost insignificant.

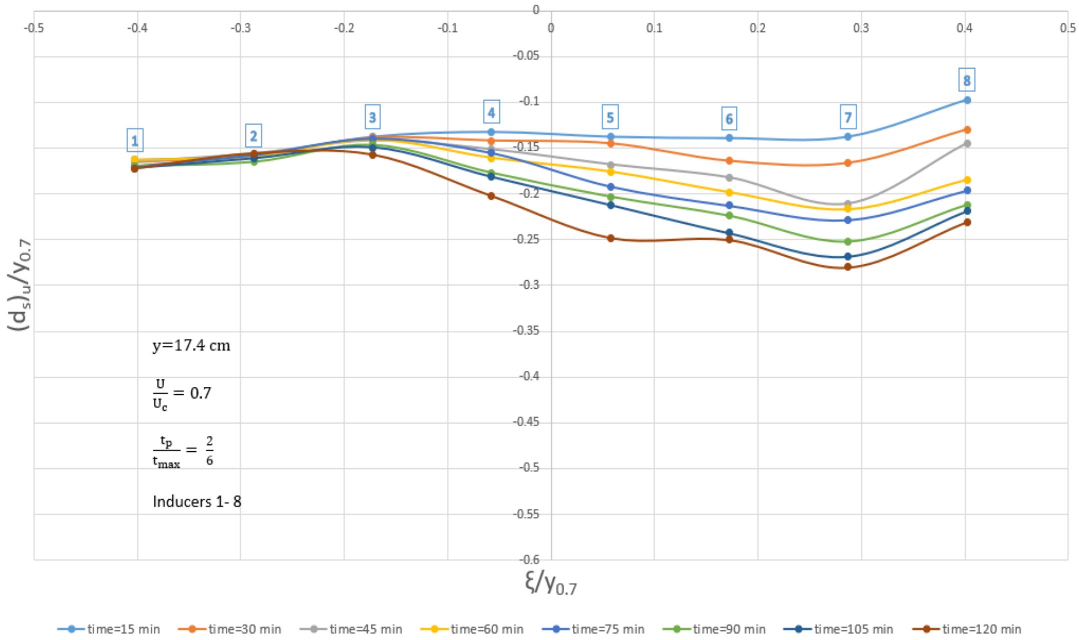

Figure 4.87 Temporal development of scour hole around the rectangular abutment of length L_a=25 cm for U/U_c = 0.70 along Inducers 1 - 8

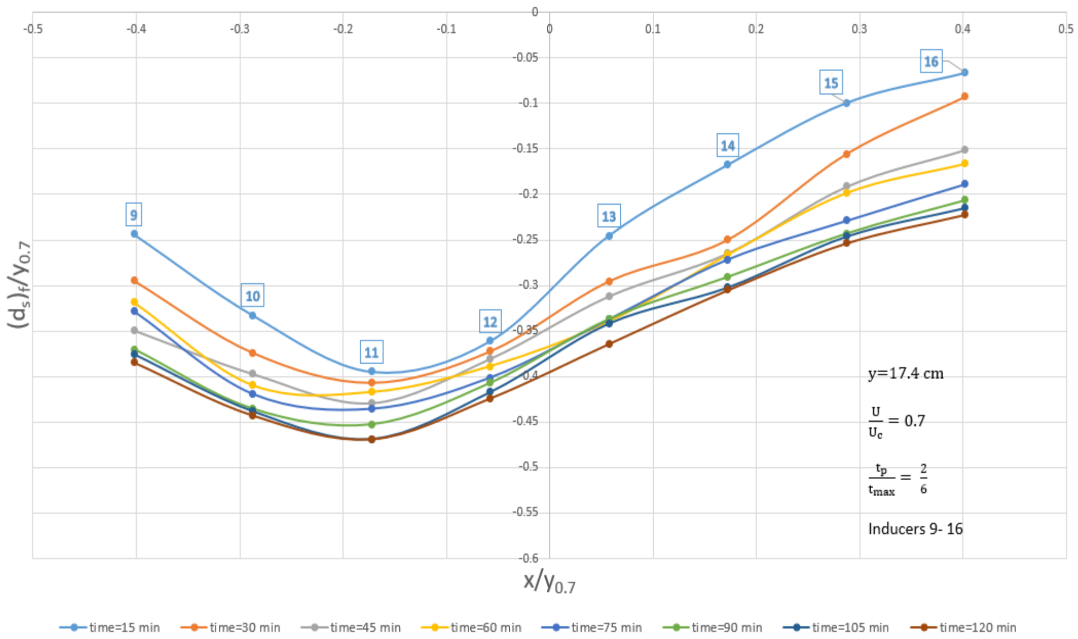

Figure 4.88 Temporal development of scour hole around the rectangular abutment of length L_a=25 cm for U/U_c = 0.70 along Inducers 9 - 16

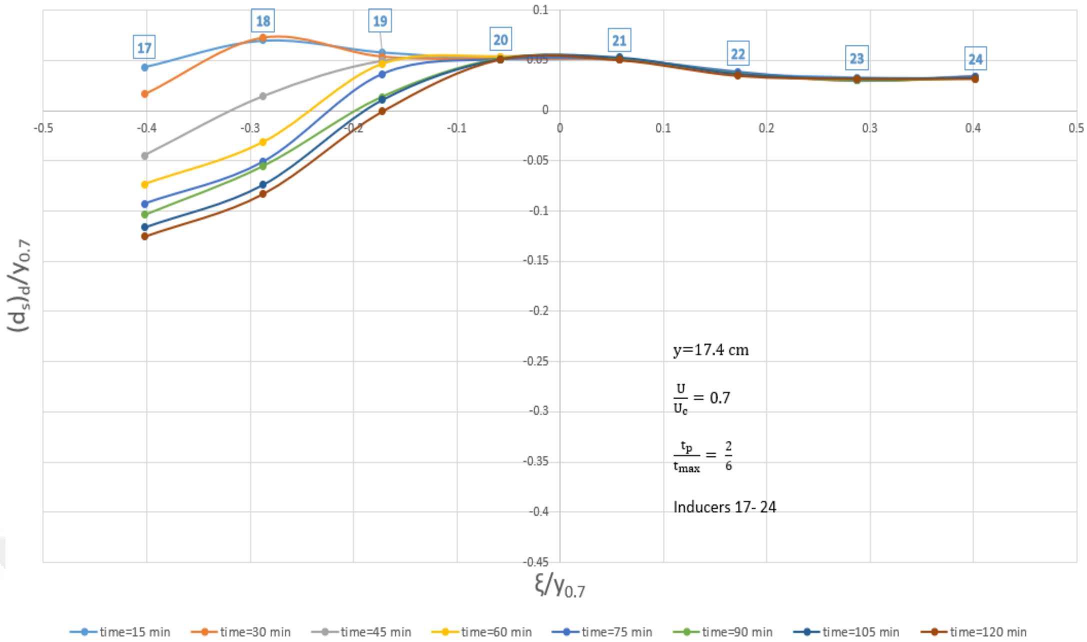

Figure 4.89 Temporal development of scour hole around the rectangular abutment of length L_a=25 cm for U/U_c = 0.70 along Inducers 17 - 24

After the flow intensity was increased to 0.8, the scour hole around the abutment rapidly evolved between the 120th and 135th minutes. Afterward, development continued with a decreasing rate until the end of the 240th minute, which means the end of this stage of the experiment. Furthermore, the magnitude of the scour depths at the upstream and front sides of the abutment was almost recorded the same between the 225th and 240th minutes. At these sides, the maximum scour depths were observed for the locations of $-0.05<\xi/y_{0.7}<0.30$ and $-0.30<x/y_{0.7}<-0.05$, respectively. Moreover, at the downstream side of the abutment, the degradation of the sediment particles eventually started for the locations of $-0.40<\xi/y_{0.7}<0.00$. For those locations, the temporal development of the scour hole was similar to the upstream and front sides. Especially after the 150th minute, remarkable scour holes were observed and the maximum scour depth on the downstream side was recorded at $\xi/y_{0.7}$=-0.40. On the other hand, for the locations of $0.10<\xi/y_{0.7}<0.40$, movement on the bed material was insignificant, similar to the first 2 hours of the experiment.

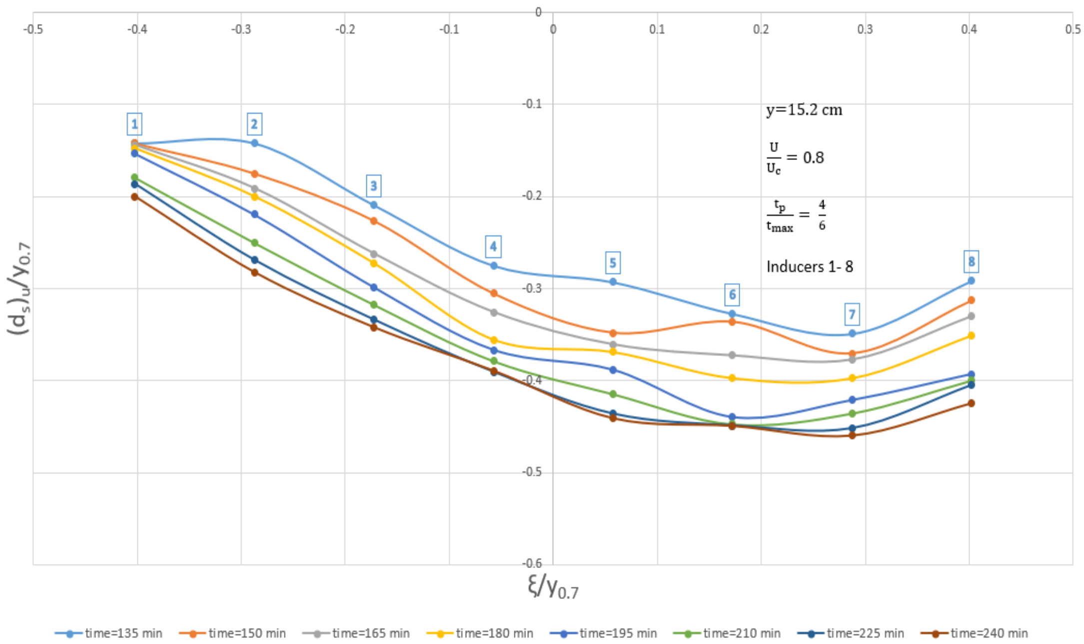

Figure 4.90 Temporal development of scour hole around the rectangular abutment of length L_a=25 cm for U/U_c = 0.80 along Inducers 1 - 8

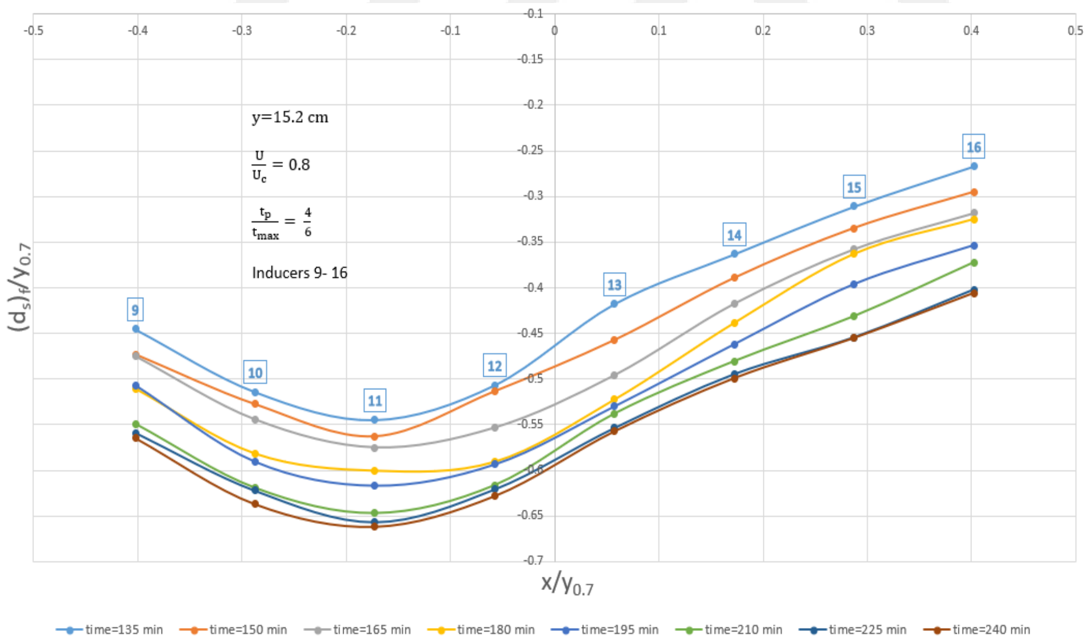

Figure 4.91 Temporal development of scour hole around the rectangular abutment of length L_a=25 cm for U/U_c = 0.80 along Inducers 9 - 16

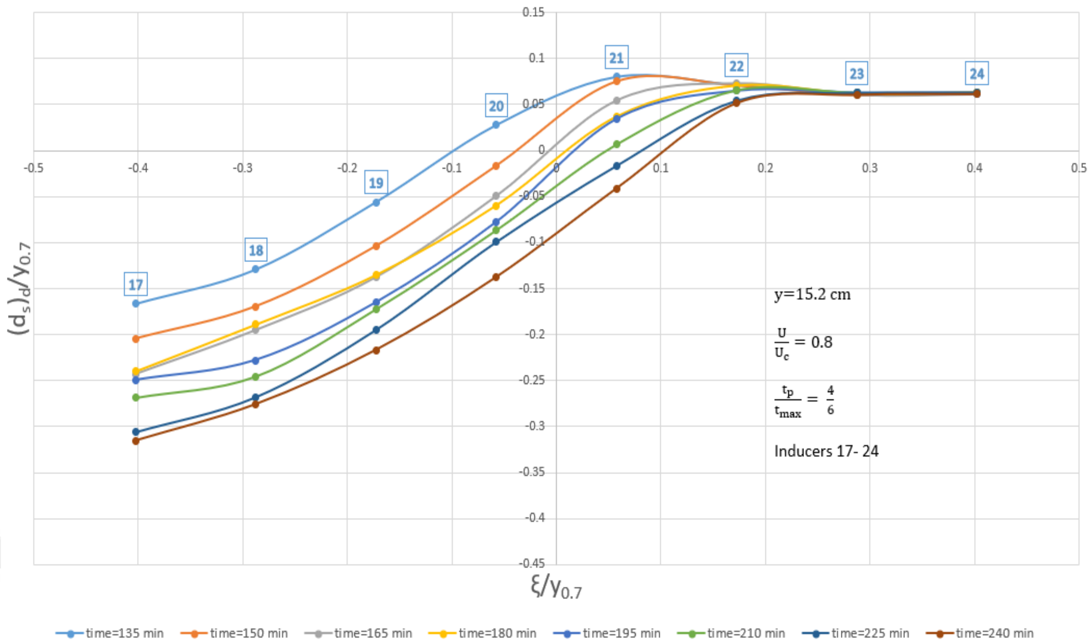

Figure 4.92 Temporal development of scour hole around the rectangular abutment of length L_a=25 cm for U/U_c = 0.80 along Inducers 17 - 24

During the last 2 hours of the experiment, with the flow intensity of 0.9, the development of the scour hole gradually continued around the abutment at a decreasing rate. Especially the magnitude of the scour depths was not changing too much between the 345th and 360th minutes at the upstream and front sides of the abutment. Furthermore, the development of the scour hole almost stopped after the 315th minute at the downstream side. In this stage of the experiment, the locations of the maximum scour depths for all sides of the abutment were similar to the previous stage mentioned above. The final or maximum scour depths around the abutment's upstream, front and downstream sides are $d_s/y_{0.7}$=-0.63, -0.78 and -0.44, respectively. Approximately 84% of the final scour depth was recorded at the 4th hour of the experiment.

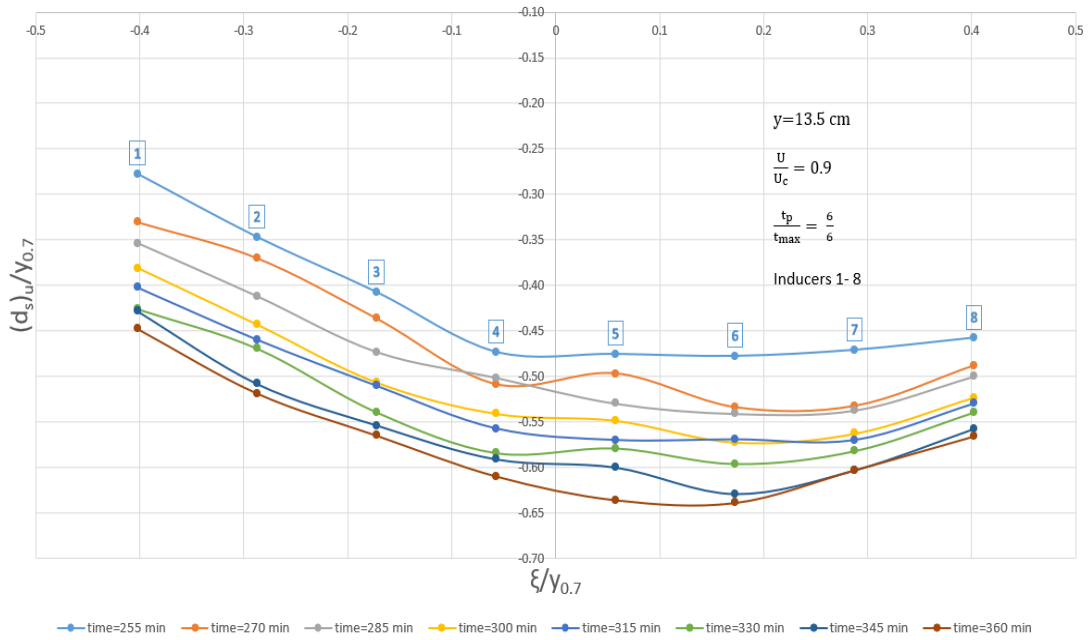

Figure 4.93 Temporal development of scour hole around the rectangular abutment of length L_a=25 cm for U/U_c = 0.90 along Inducers 1 - 8

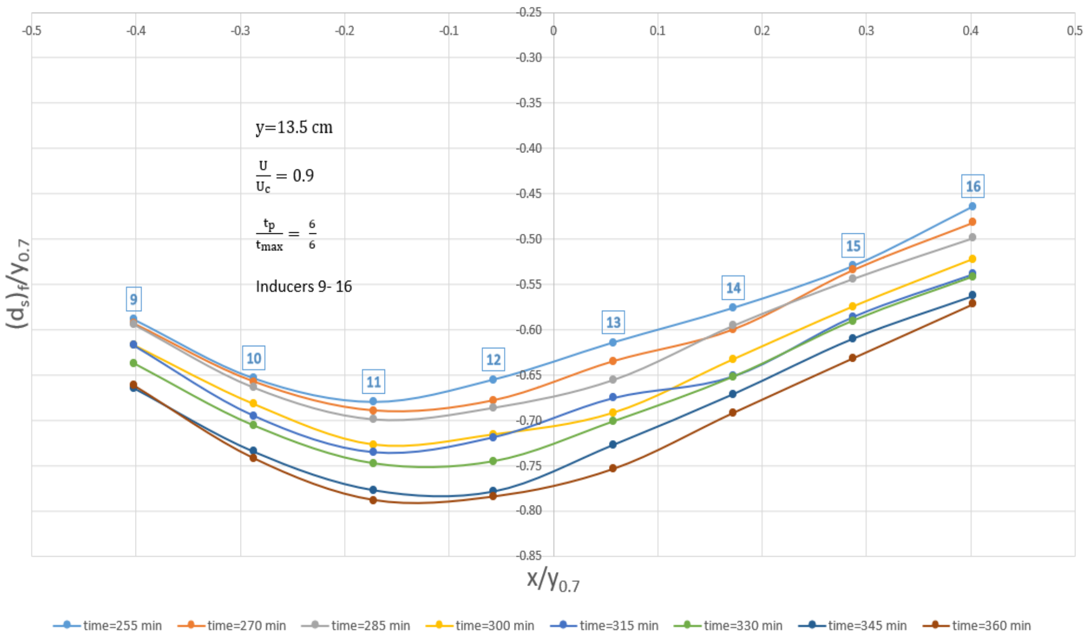

Figure 4.94 Temporal development of scour hole around the rectangular abutment of length L_a=25 cm for U/U_c = 0.90 along Inducers 9- 16

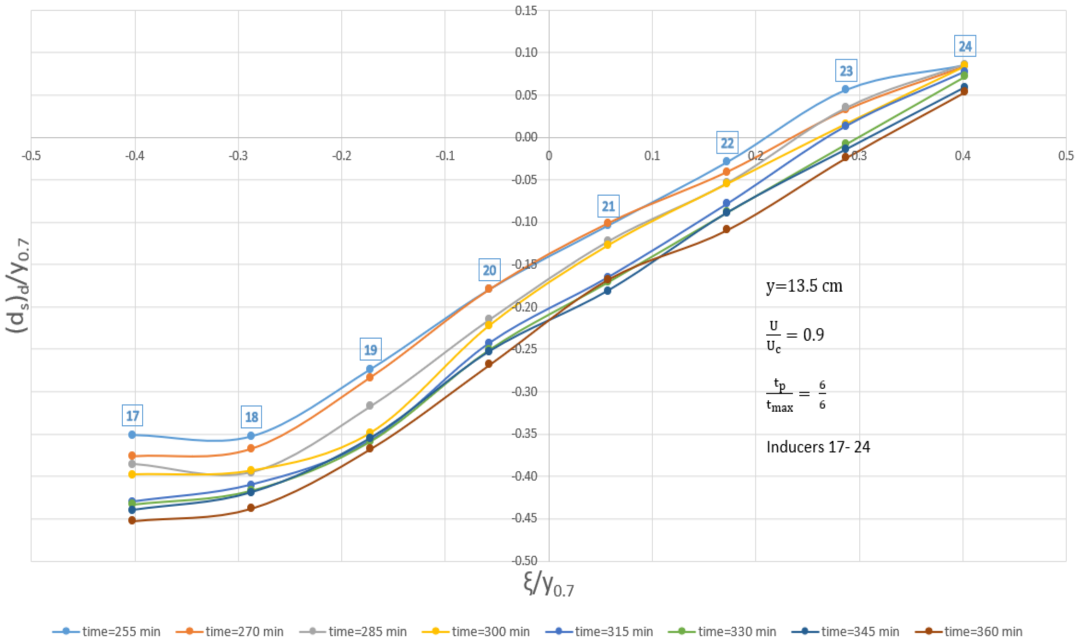

Figure 4.95 Temporal development of scour hole around the rectangular abutment of length L_a=25 cm for U/U_c = 0.90 along Inducers 17 - 24

4.4.1.2.5 The Abutment of Length L_a= 20 cm

The temporal development of the scour hole around the abutment of length L_a=20 cm is presented in Figures 4.96-104. During the first 2 hours of the experiment with the flow intensity of 0.7, scour hole development was pretty slow. At the upstream side of the abutment, despite the scouring process started for the locations of $0.00<\xi/y_{0.7}<0.40$ after the 45th minute, development was observed as irregular and the magnitude of the scour depths was relatively small. Also, on the downstream side of the abutment, there was almost no movement on the bed material. Nonetheless, a significant deposition region which decreased with increasing time was observed for the locations of $-0.40<\xi/y_{0.7}<0.20$. In this stage of the experiment, significant scour development was only obtained at the front side of the abutment. Especially the scour hole development was rapid until the 60th minute and then, scour hole development continued gradually. On the front side of the abutment, the maximum scour depths were recorded for the locations of $-0.20<x/y_{0.7}<0.10$.

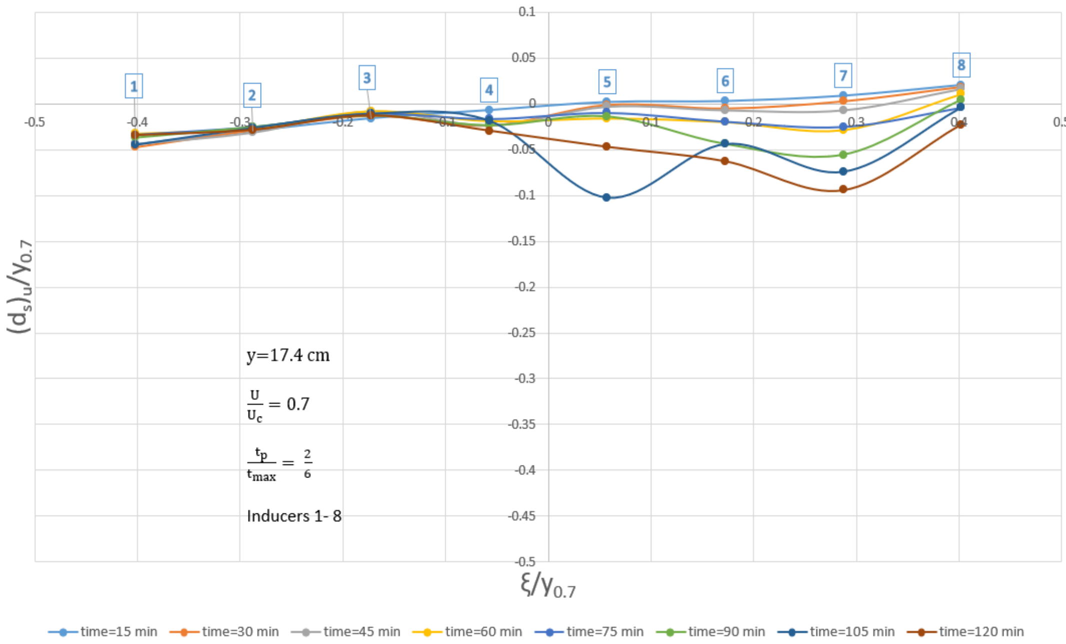

Figure 4.96 Temporal development of scour hole around the rectangular abutment of length L_a=20 cm for U/U_c = 0.70 along Inducers 1 - 8

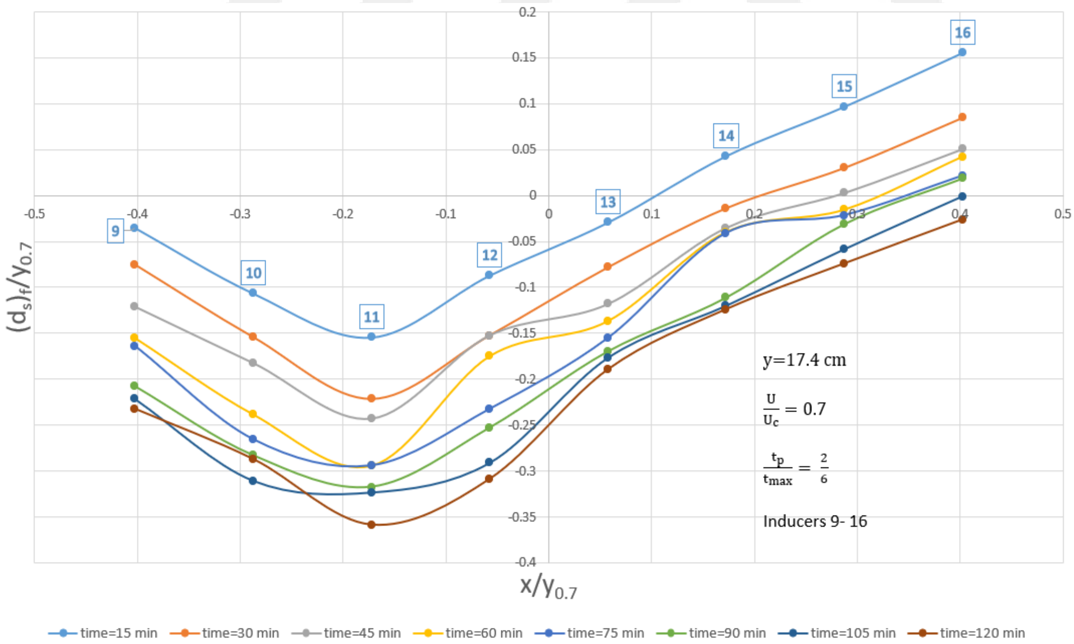

Figure 4.97 Temporal development of scour hole around the rectangular abutment of length L_a=20 cm for U/U_c = 0.70 along Inducers 9 - 16

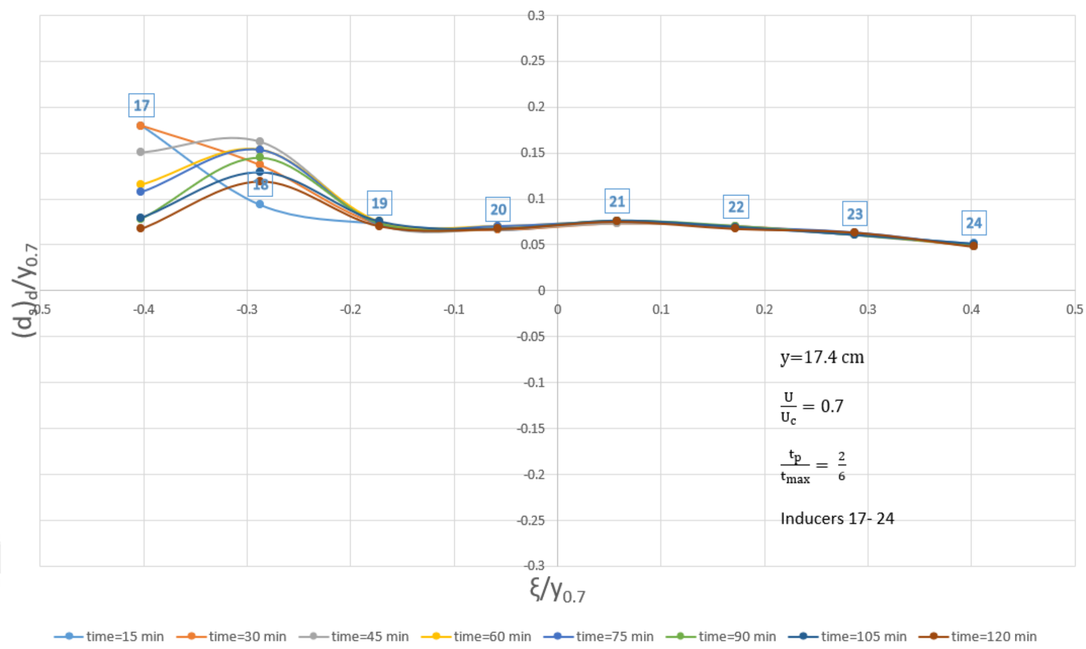

Figure 4.98 Temporal development of scour hole around the rectangular abutment of length L_a=20 cm for U/U_c = 0.70 along Inducers 17 - 24

After the flow intensity was increased to 0.8 for the next 2 hours of the experiment, significant scour formations eventually started to occur for the locations of $-0.40<\xi/y_{0.7}<-0.10$ at the upstream side of the abutment. However, it should not be forgotten that the magnitude of the scour depths was still small compared to the front side of the abutment. On the other hand, for the locations of $-0.10<\xi/y_{0.7}<0.40$, minor sediment vertexes were observed rather than scour formation. On the upstream side, the maximum scour depth was recorded at approximately $\xi/y_{0.7}$=0.30. Moreover, at the front side, the gradual development of the scour hole with a decreasing rate continued in this stage of the experiment. The maximum scour depths on the front side were recorded for the locations of $-0.20<\xi/y_{0.7}<-0.10$. Contrary to the upstream and front sides, there was still no significant movement of the sediment particles on the downstream side, even with the increased flow intensity. Nevertheless, after the 150th minute, small scour holes were observed at the downstream side of the abutment.

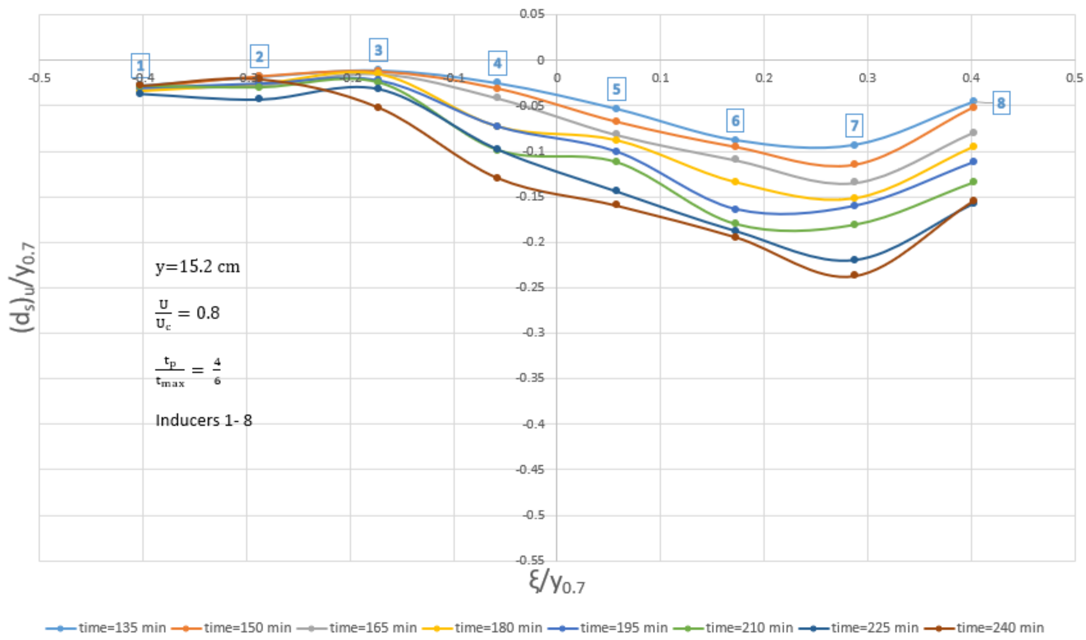

Figure 4.99 Temporal development of scour hole around the rectangular abutment of length L_a=20 cm for U/U_c = 0.80 along Inducers 1 - 8

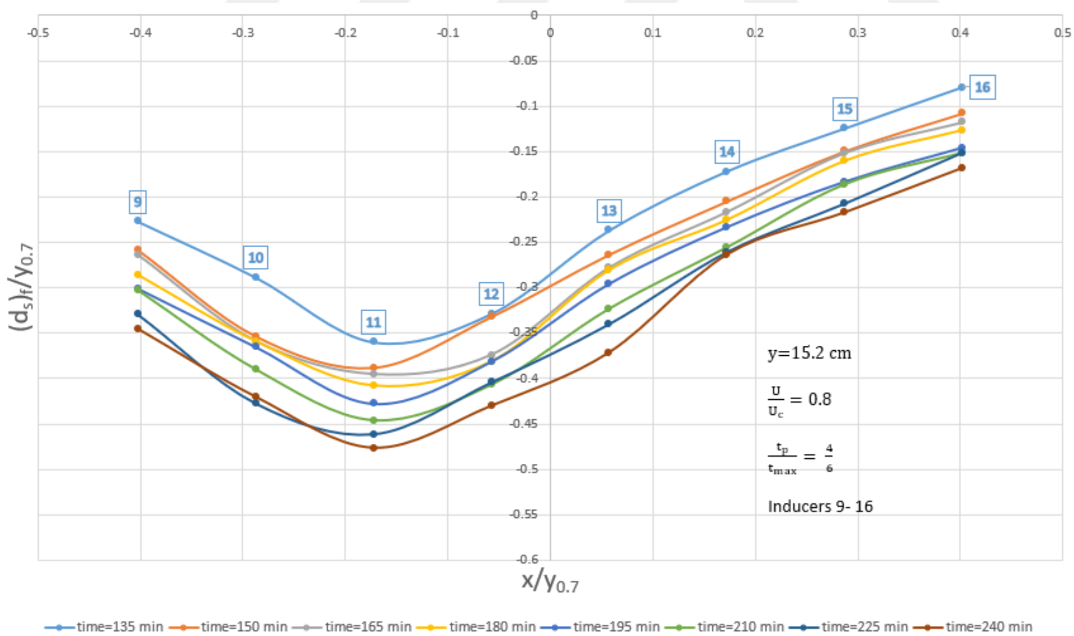

Figure 4.100 Temporal development of scour hole around the rectangular abutment of length L_a=20 cm for U/U_c = 0.80 along Inducers 9 - 16

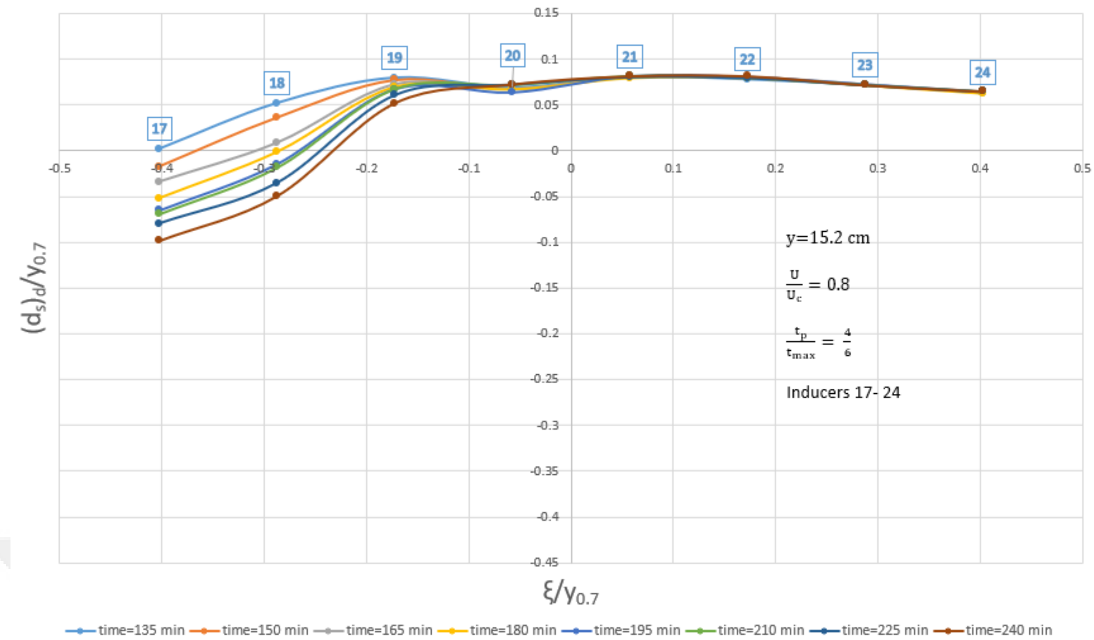

Figure 4.101 Temporal development of scour hole around the rectangular abutment of length L_a=20 cm for U/U_c = 0.80 along Inducers 17 - 24

During the last 2 hours of the experiment, with the flow intensity of 0.9, the increasing rate of the scour development at the upstream and front sides of the abutment increased and gradually continued. At the upstream and front sides, significant increases were observed in scour depths, even at the last 15 minutes of the experiment. On these sides, the maximum scour depths were obtained for the locations of $0.20<\xi/y_{0.7}<0.30$ and $-0.20<y/y_{0.7}<-0.15$. Moreover, scour formations finally started to occur on the downstream side for the locations for $-0.40<\xi/y_{0.7}<-0.00$ and gradually increased after the 240th minute. Nevertheless, it should be indicated that the magnitude of the scour depths was small relative to those on the upstream and front sides. The maximum scour depth on the downstream side was recorded at $\xi/y_{0.7}$=-0.40. The final or maximum scour depths around the abutment's upstream, front and downstream sides are $d_s/y_{0.7}$=-0.48, -0.70 and -0.29, respectively. Approximately 69% of the final scour depth was recorded at the 4th hour of the experiment.

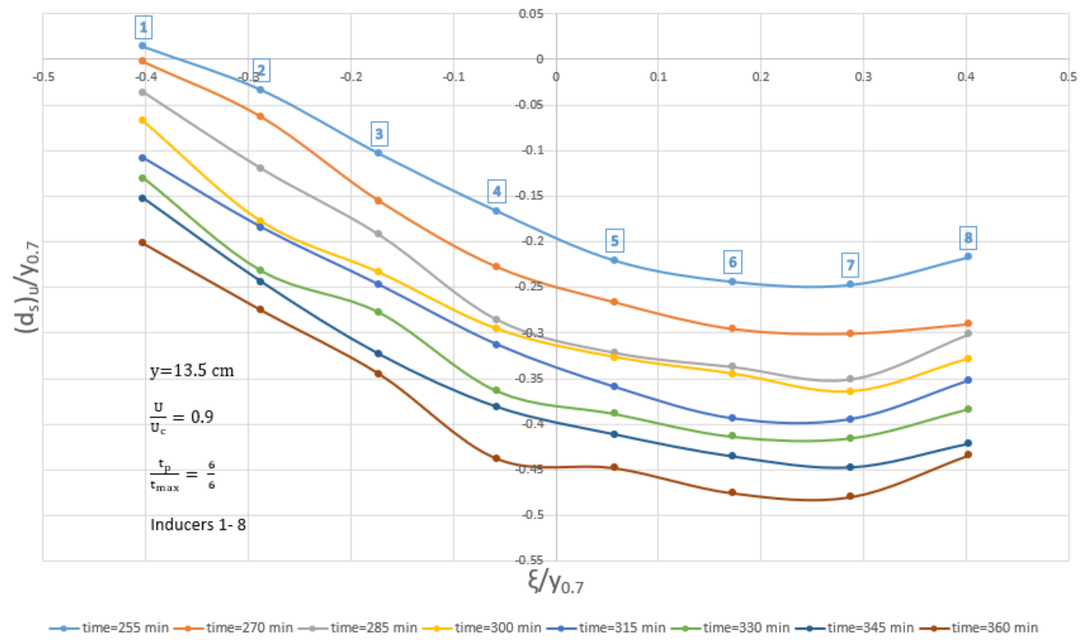

Figure 4.102 Temporal development of scour hole around the rectangular abutment of length L_a=20 cm for U/U_c = 0.90 along Inducers 1 - 8

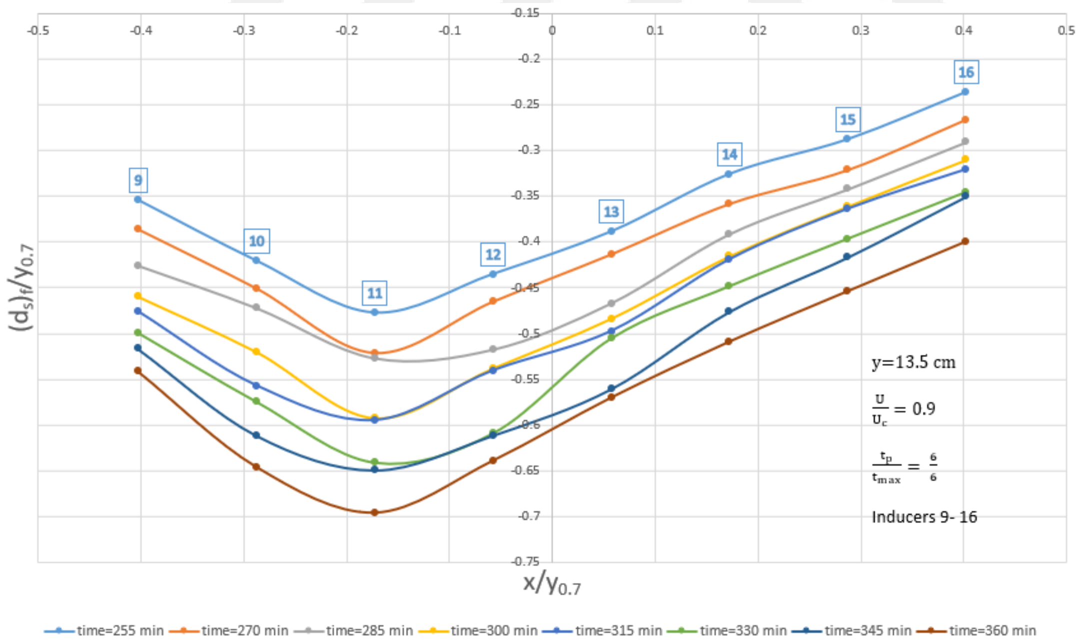

Figure 4.103 Temporal development of scour hole around the rectangular abutment of length L_a=20 cm for U/U_c = 0.90 along Inducers 9 - 16

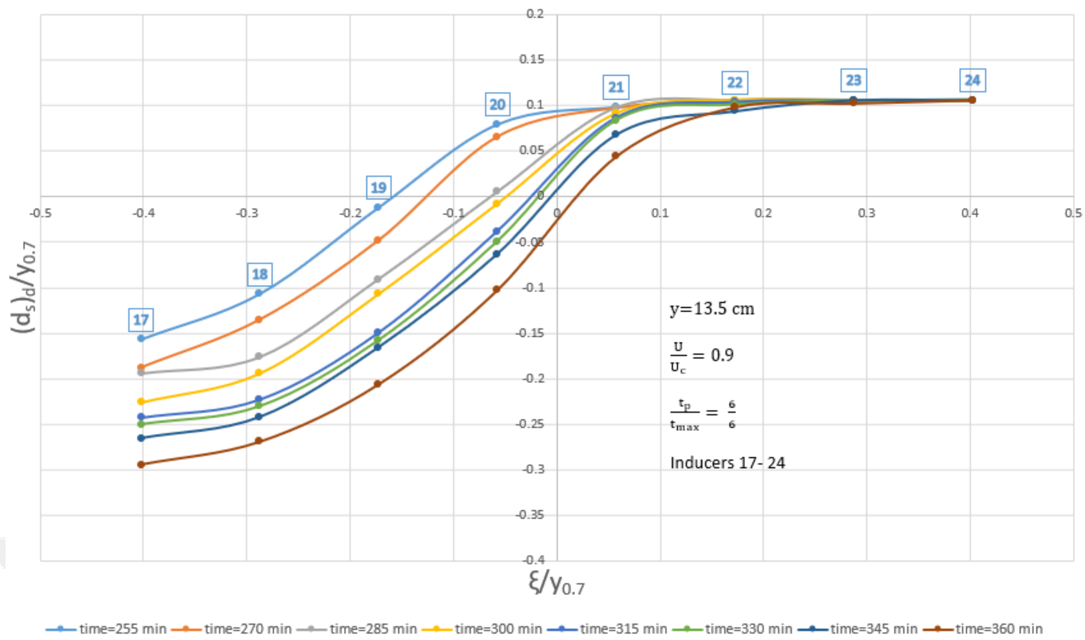

Figure 4.104 Temporal development of scour hole around the rectangular abutment of length L_a=20 cm for U/U_c = 0.90 along Inducers 17 - 24

4.4.1.2.6 The Abutment of Length L_a= 15 cm

The temporal development of the scour hole around the abutment of length L_a=15 cm is given in Figures 4.105-113. During the first 4 hours of the experiment, with the flow intensities of 0.7 and 0.8, scour hole development was pretty slow around the abutment. Since the abutment length that was tested in this case is relatively short, minor, or negligible, scour depths were accepted as reasonable at this stage of the experiment. Especially at the upstream and downstream sides of the abutment, the magnitude of the scour depths was insignificant. Nevertheless, on the upstream side, for the locations of $-0.40<\xi/y_{0.7}<0.00$, scour depths observed within the ranges of 1.5- 2 cm. However, on the downstream side, deposition of the sediment particles was observed for the locations of $-0.40<\xi/y_{0.7}<-0.20$ rather than scour. Moreover, on the front side, scour hole development was relatively rapid during the initial stages of the experiment. But after the 15th minute, scour hole development continued slowly until the 240th minute. The maximum scour depth on the front side was recorded at approximately $x/y_{0.7}$=-0.20.

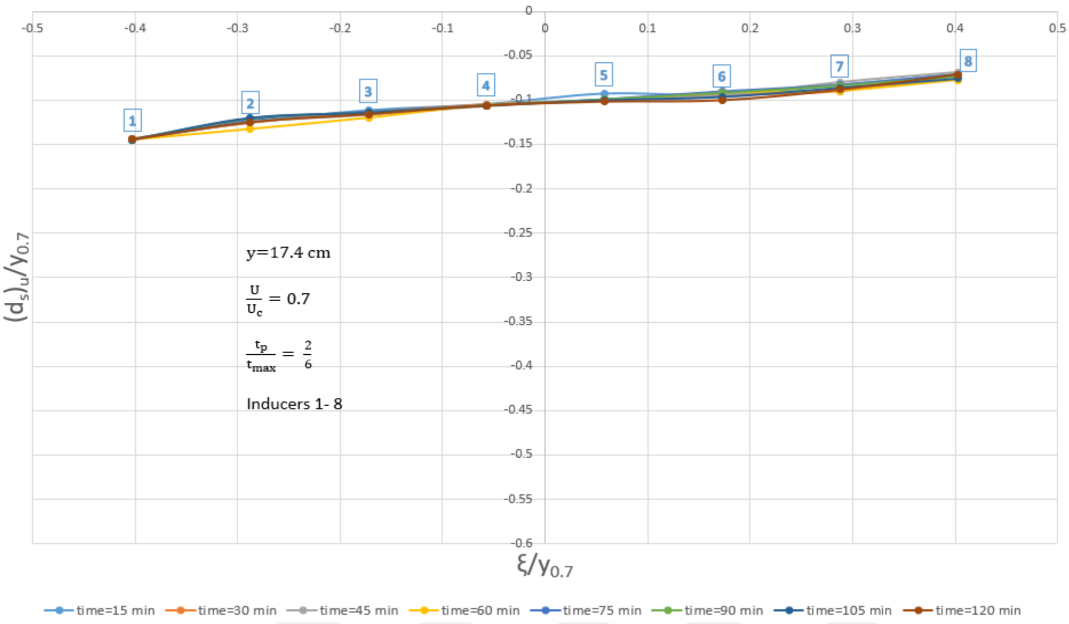

Figure 4.105 Temporal development of scour hole around the rectangular abutment of length L_a=15 cm for U/U_c = 0.70 along Inducers 1 - 8

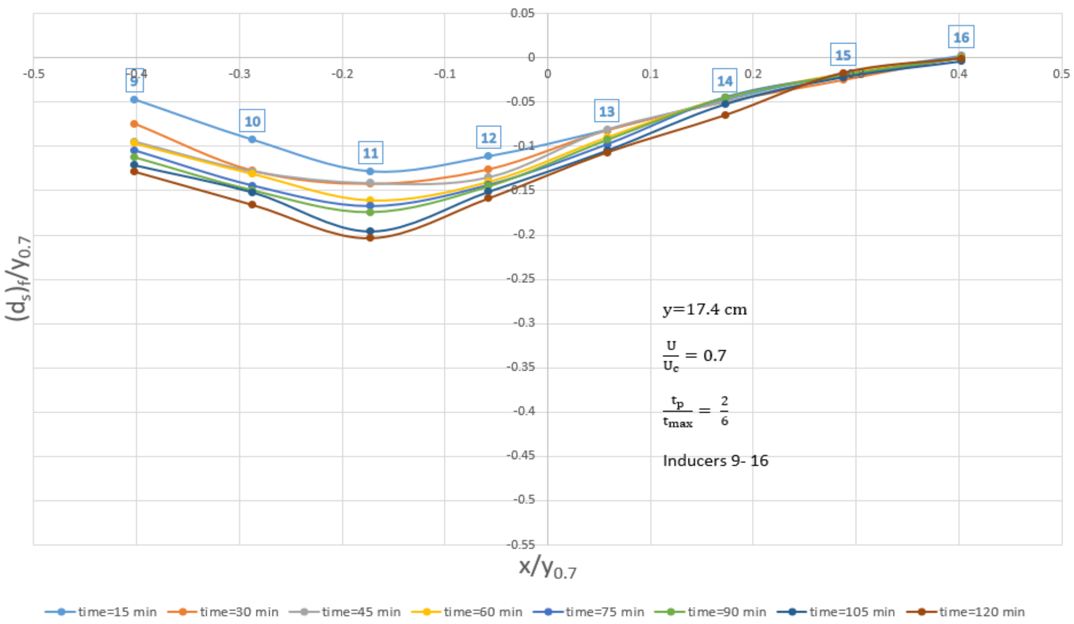

Figure 4.106 Temporal development of scour hole around the rectangular abutment of length L_a=15 cm for U/U_c = 0.70 along Inducers 9 - 16

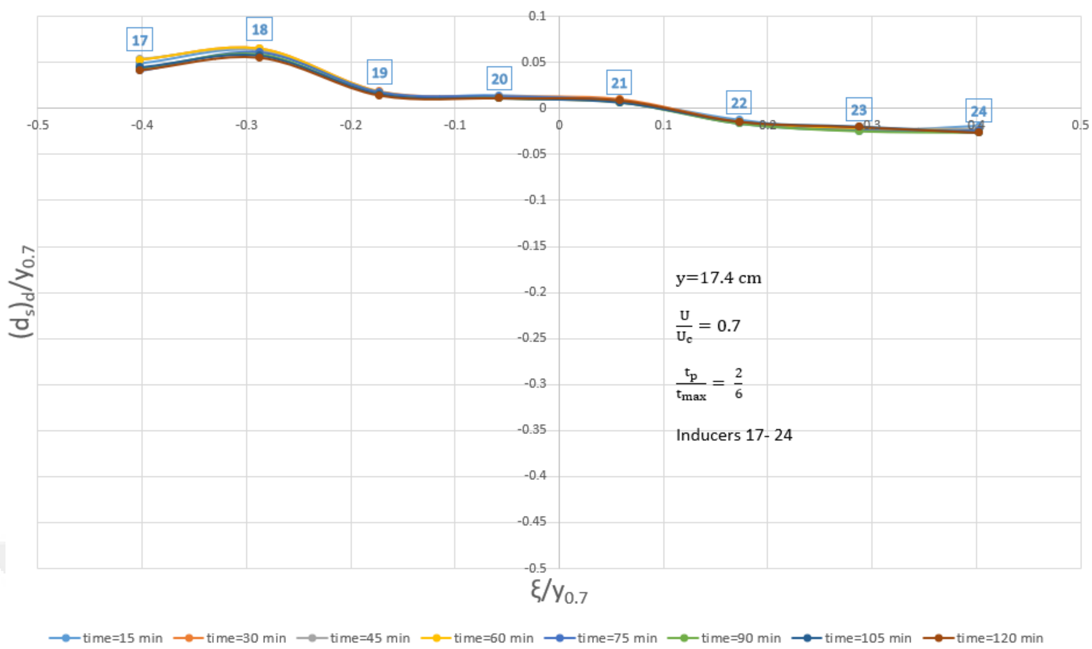

Figure 4.107 Temporal development of scour hole around the rectangular abutment of length L_a=15 cm for U/U_c = 0.70 along Inducers 17 - 24

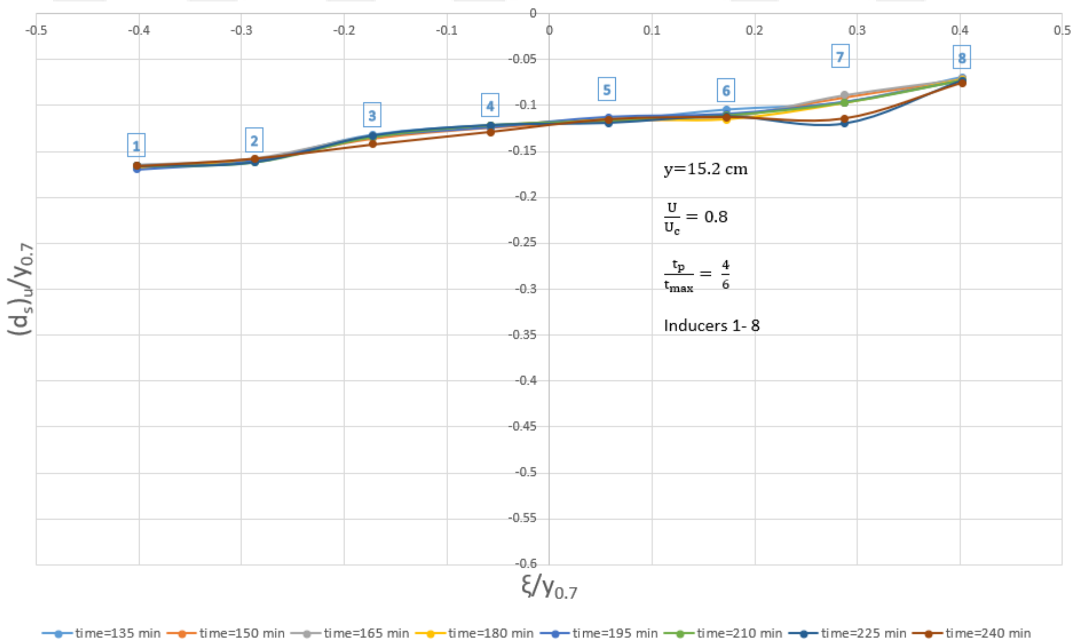

Figure 4.108 Temporal development of scour hole around the rectangular abutment of length L_a=15 cm for U/U_c = 0.80 along Inducers 1 - 8

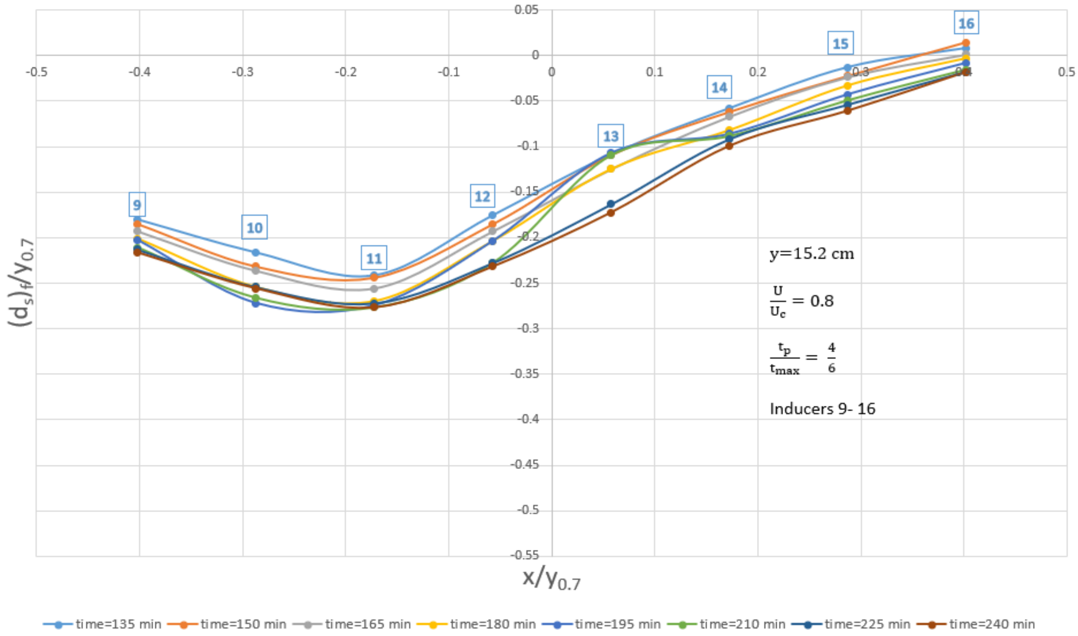

Figure 4.109 Temporal development of scour hole around the rectangular abutment of length L_a=15 cm for U/U_c = 0.80 along Inducers 9 - 16

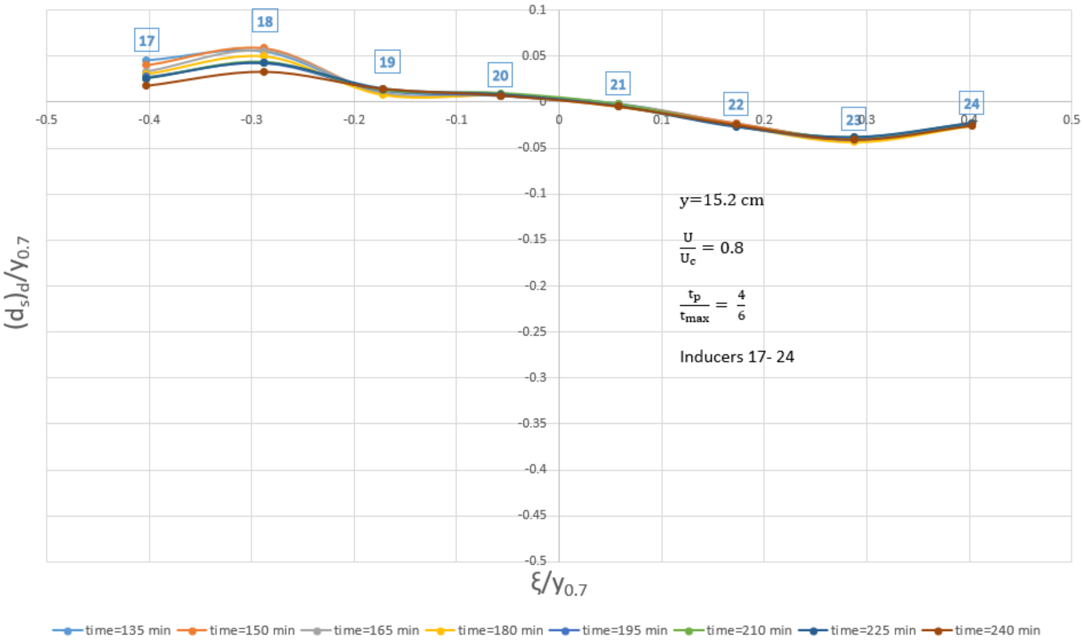

Figure 4.110 Temporal development of scour hole around the rectangular abutment of length L_a=15 cm for U/U_c = 0.80 along Inducers 17 - 24

After the flow intensity was increased to 0.9 at the 240th minute, scour hole development gradually continued at the front side of the abutment like the previous stages of the experiment having flow intensities of 0.7 and 0.8. Also, the location of the maximum scour depth on the front side of the abutment did not change with the increased flow intensity. On the other hand, increased flow intensity led to significant scours at the upstream side of the abutment. Especially for the locations of $0.00<\xi/y_{0.7}<0.30$, where the maximum scour depths were observed, the magnitude of the scour depths at the end of the experiment was approximately two times greater than those at the end of the 4th hour. Moreover, the scouring process started at the downstream side of the abutment after the 270th minute and the magnitude of the scour depths was still small, even at the end of the experiment. The maximum scour depths on the downstream side of the abutment were recorded for the locations of $-0.40<\xi/y_{0.7}<-0.30$, within the range of 1.5 and 1.8 cm.

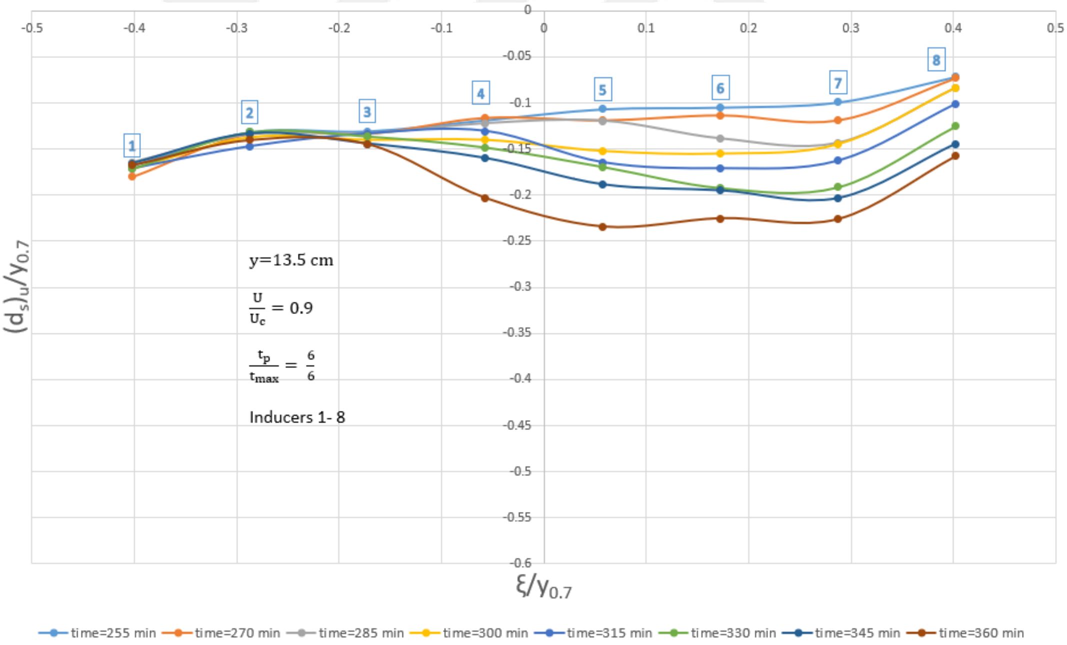

Figure 4.111 Temporal development of scour hole around the rectangular abutment of length L_a=15 cm for U/U_c = 0.90 along Inducers 1 - 8

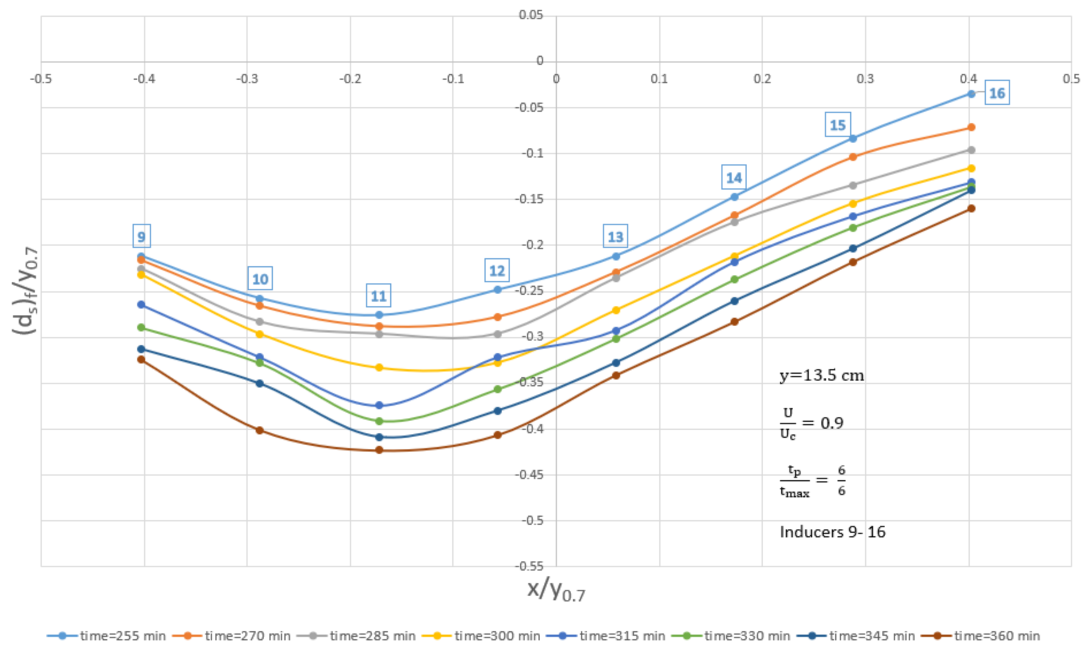

Figure 4.112 Temporal development of scour hole around the rectangular abutment of length L_a=15 cm for U/U_c = 0.90 along Inducers 9 - 16

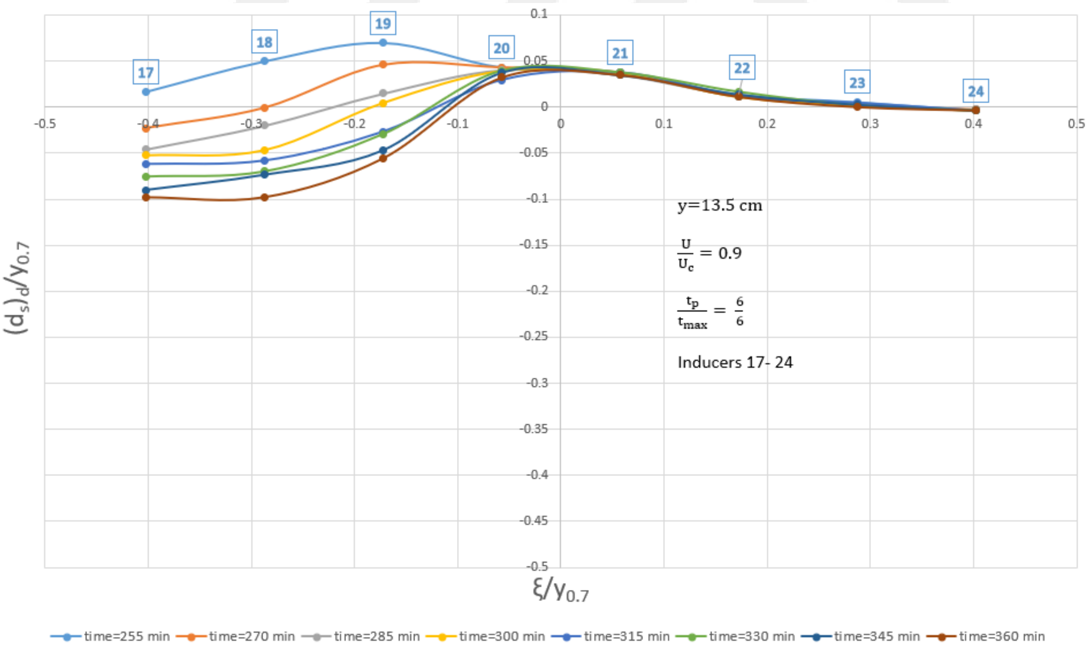

Figure 4.113 Temporal development of scour hole around the rectangular abutment of length L_a=15 cm for U/U_c = 0.90 along Inducers 17 - 24

4.4.1.3 Summary of the Scour Hole Development Around the Abutments

From the figures presented in the previous subsections, it can be clearly claimed that the greatest scour holes were observed at the front side or upstream toe of the abutment for both semi-circular and rectangular abutments, as stated in related references (Ballio and Orsi, 2000; Oliveto and Hager, 2002; Kumcu et al., 2007). In other words, the maximum scour depths at the front side were obtained along the Inducers 11-13. Although the measured maximum dimensionless scour depths were not much different for the upstream and downstream sides of the abutment, scour depths decreased dramatically at locations close to the wall on the downstream side of the abutment due to the deposition of the sediment particles caused by the downflow and primary vortices. At the upstream side of the abutment, the maximum scour depths were generally obtained along the Inducers 4-8, which means the magnitude of the scour depths increases while moving away from the sidewall and being closer to the abutment toe. On the other hand, for all cases, the maximum scour depth at the downstream side of the abutment was obtained from Inducer 17.

According to the experimental results, it can be revealed that the development of scour holes around the abutments decreases as the abutment length decreases. Likewise, the largest scour hole dimensions were obtained for the abutment of length L_a= 40 cm and the smallest for the abutment of length L_a= 15 cm. Since shorter abutment lengths led to smaller horseshoe vortex and decreased bed shear stress regions compared to longer ones (Koken and Gogus, 2015), the magnitude of the scour depths around the shorter abutments will always be smaller than the longer abutments for similar flow and sediment properties. Hence, in this study, the immotility of the sediment particles for the abutments of lengths L_a=15 cm and 20 cm during the first 4 hours of the experiments with the flow intensities of 0.7 and 0.8 can be accepted as reasonable.

Moreover, it can also be underlined that the dimensions of the scour holes around the rectangular abutments are greater than those around the semi-circular end abutments for a given abutment length and duration. Because the streamlined shape of the semi-circular end abutments causes weaker downflow and secondary vortices that are mainly responsible for scour formation than the rectangular abutment having a blunt body (Barbhuiya and Dey, 2004). Hence, the obtained results show consistency with the previous related studies in the literature, such as Laursen and Toch (1956), Melville (1992), Hosseinjanzadeh et al. (2021), and Raikar et al. (2022).

4.4.2 Scour Depths at the Downstream, Upstream and Front Sides of the Abutments

In this subsection, the maximum scour depth values at the upstream, front and downstream sides of the abutments and their relationship with each other were examined. In this study, the results of Inducer 5 (upstream side), Inducer 12 (front side), and Inducer 17 (downstream side), which are generally observed as the most critical points for each side in terms of scour depth values, were presented. Although, for some cases, the maximum scour depth values for each side were recorded on the different inducers (e.g., Inducer 6, Inducer 13), the discrepancies were detected as pretty small. Hence, in order to provide consistency on the location of scour depths, the scour depths obtained from the inducers mentioned above were used in the analysis.

Figures 4.114-116 show the variation of dimensionless scour depth, $d_s/y_{0.7}$, around the semi-circular end abutments with the dimensionless time, Ut/y, as a function of flow intensity, U/U_c. In general, the trends of the data points given in these figures for each abutment tested are very similar; the scour depths increased almost linearly with time for an abutment of a given length, especially for those of L_a=25 cm, 30 cm, 35 cm and 40 cm. For relatively short abutments investigated within the scope of this study having the lengths of L_a=15 cm and 20 cm, the rate of increase of scour depth around the above-mentioned measurement points was almost negligible for the smallest flow intensity of 0.7, slowly increased when the flow intensity of the flow became 0.8 and finally, at U/U_c=0.9 a noticeable increase in the scour depth was observed. It can be stated that the maximum scour depths occur at the front sides of the abutments compared to the other points where measurements were taken. On the other hand, at the upstream side of the abutment having the length of L_a=15 cm, the measured data of $d_s/y_{0.7}$ show that at this particular point, instead of scouring, deposition of sediment was observed where most of the $d_s/y_{0.7}$values were less than zero for the tested range of flow intensity. At longer abutment lengths than L_a=15 cm, which can be assumed as a “short abutment ($L_a/y \leq 1$)” according to Melville (1992), increasing scour depths were obtained with increasing abutment lengths. It can also be stated that within the flow intensity zones tested, as the length of the abutment increases, $d_s/y_{0.7}$ values increased for a given dimensionless time term and the maximum scour depths were observed at the upstream, downstream and front sides of the abutment of length L_a=40 cm within the tested abutments. Especially, $d_s/y_{0.7}$ values of the abutments of lengths L_a=30 cm, 35 cm and 40 cm during the first 4 hours of the experiments with the flow intensities of 0.7 and 0.8 were extremely high compared to those of L_a=15 cm, 20 cm and 25 cm. However, the differences in the scour depth values due to the abutment length decreased in the last 2 hours of the experiment with the flown intensity value of 0.9. So, it can be said that for the shorter abutment lengths as L_a=15 cm, 20 cm and 25 cm, tested in this study, the high flow intensity values triggered the occurrence of significant scour depths.

Figures 4.117-119 are plotted to show the variation of dimensionless scour depth, $d_s/y_{0.7}$, around the rectangular abutments with the dimensionless time, Ut/y, as a function of flow intensity, U/U_c. Similar to the temporal development of scour around the semi-circular end abutments, the magnitude of the scour depths linearly increased with time around the rectangular abutments. Again, the maximum scour depths were obtained on the front side of the abutment regardless of the abutment length. Also, the maximum scour depths at the upstream, front and downstream sides of the abutment were recorded for the longest abutment of length L_a=40 cm. However, the magnitude of the scour depths around the rectangular abutments for a given abutment length and time was obtained greater than those with semi-circular end abutments. As it was mentioned in the previous subsection, the blunt nature of the rectangular abutments caused greater scour depths than semi-circular end abutments. The magnitude of the maximum scour depth around the rectangular abutments at the end of the experiment was approximately obtained 30% greater than the semi-circular ones for the abutments of lengths L_a=30, 35 and 40 cm. This finding coincides with the results of Melville's (1992) study that obtained the shape factor values for the maximum scour depth around the semi-circular end and rectangular abutments as 0.75 and 1, respectively. However, for the abutments of lengths L_a=15, 20 and 25 cm, it was observed that the magnitudes of the maximum scour depth around the rectangular abutments are much greater than 30% compared to semi-circular ones. The difference was obtained by approximately 44% for the abutment of length L_a=25 cm while 67% for the abutment of length L_a=20 cm. Contrary to the semi-circular end abutments, scour development around the rectangular abutments of lengths L_a= 15 cm and 20 cm occurred even with the smallest flow intensity of 0.7 at the beginning of the experiments, especially at the front side of the abutment. However, for those relatively small abutment lengths, deposition was observed at the downstream side of the abutment with the smallest flow intensity of 0.7 and scouring proceeded with the flow intensity of 0.8 at the 4th hour of the experiments.

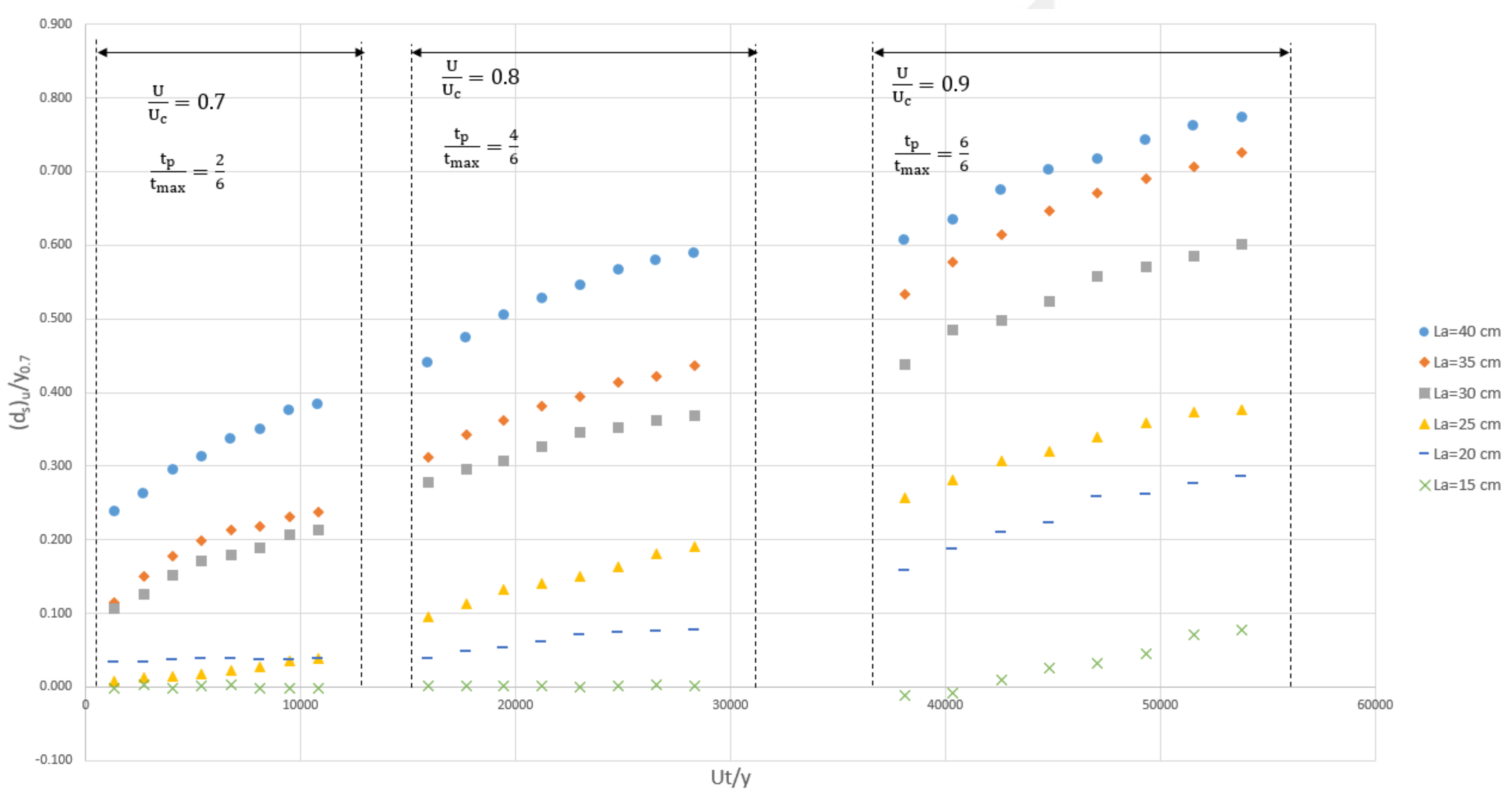

Figure 4.114 Variation of dimensionless scour depth with dimensionless time for various semi-circular end abutment lengths at Inducer 5 (upstream side)

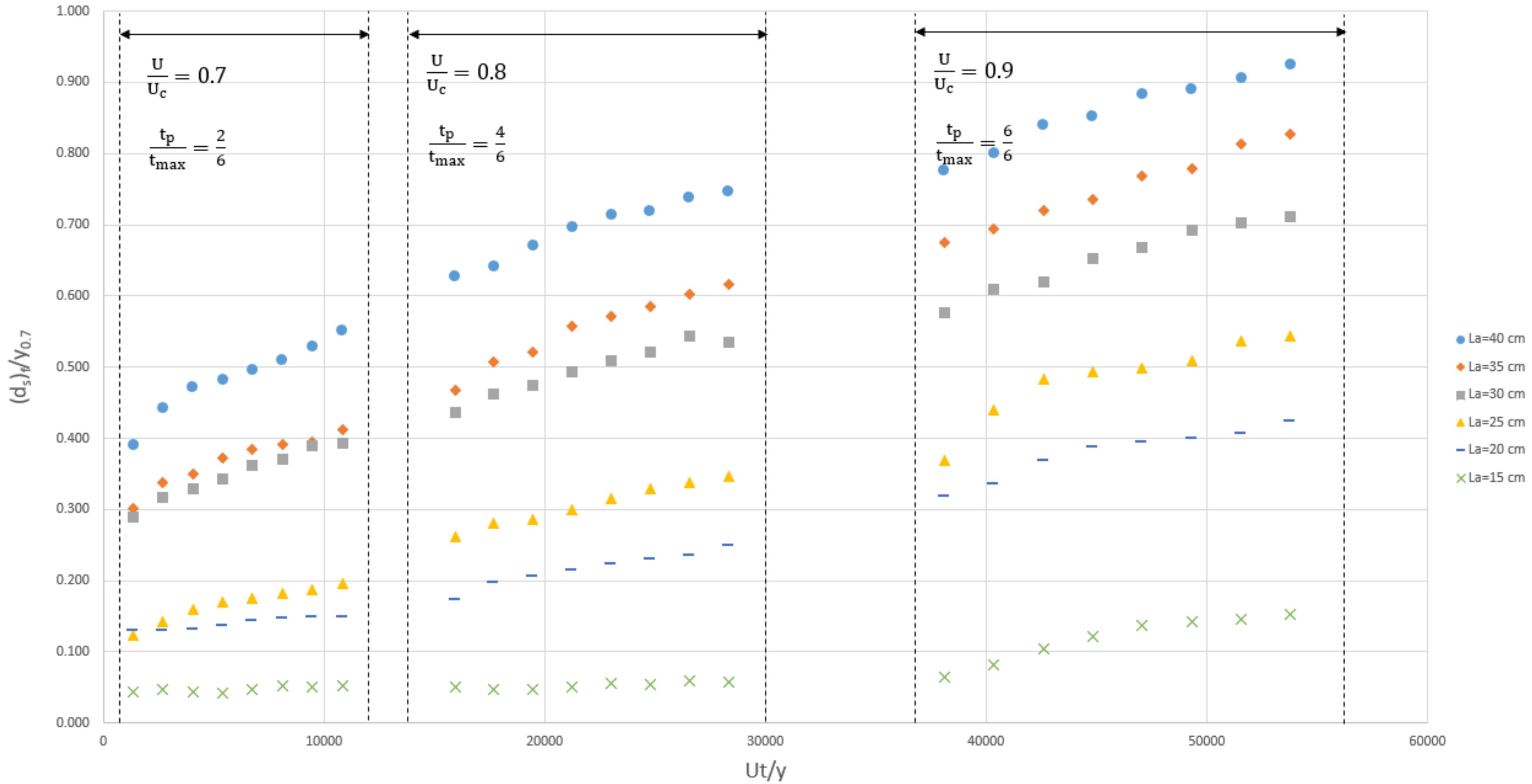

Figure 4.115 Variation of dimensionless scour depth with dimensionless time for various semi-circular end abutment lengths at Inducer 12 (front side)

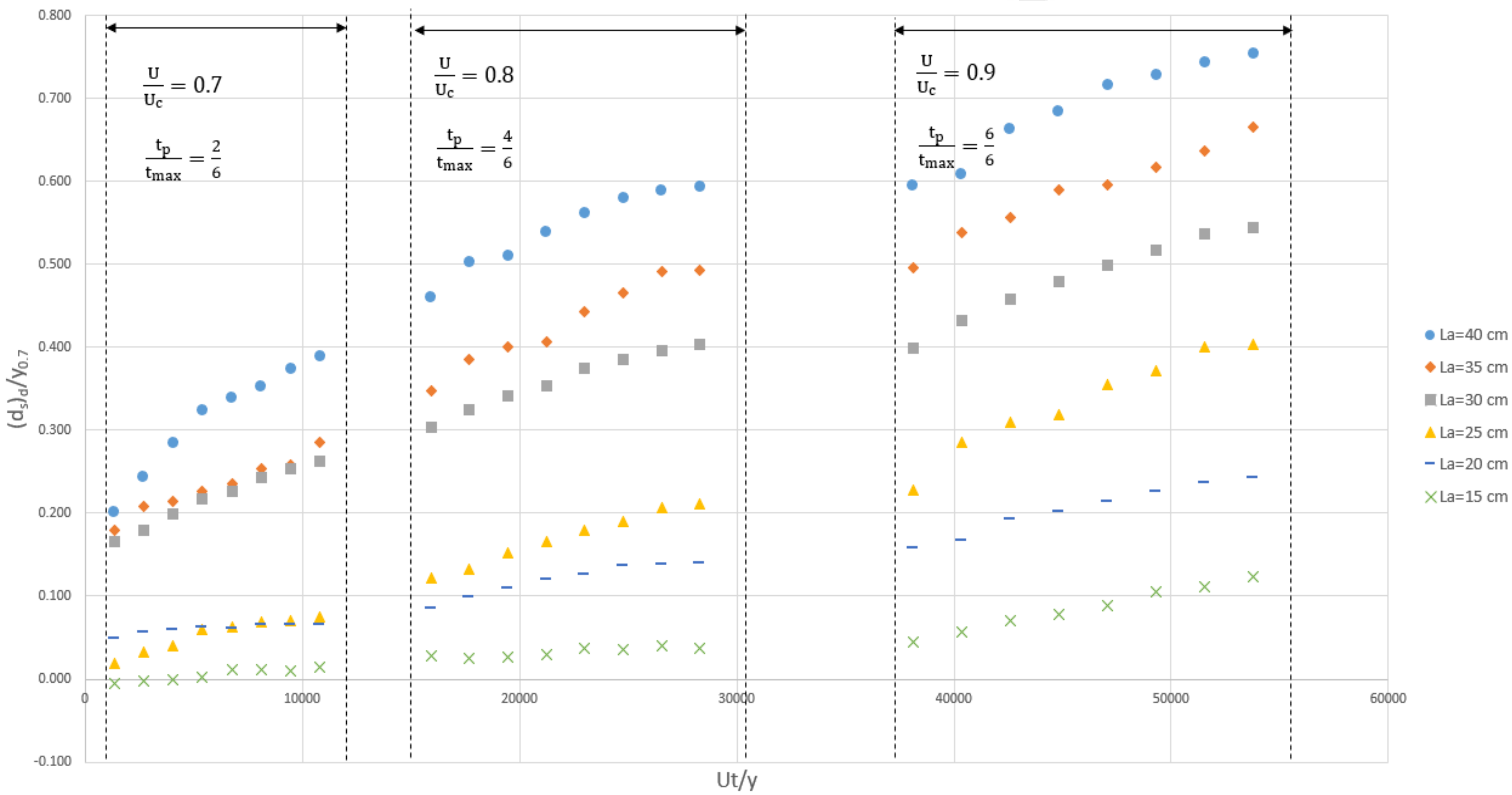

Figure 4.116 Variation of dimensionless scour depth with dimensionless time for various semi-circular end abutment lengths at Inducer 17 (downstream side)

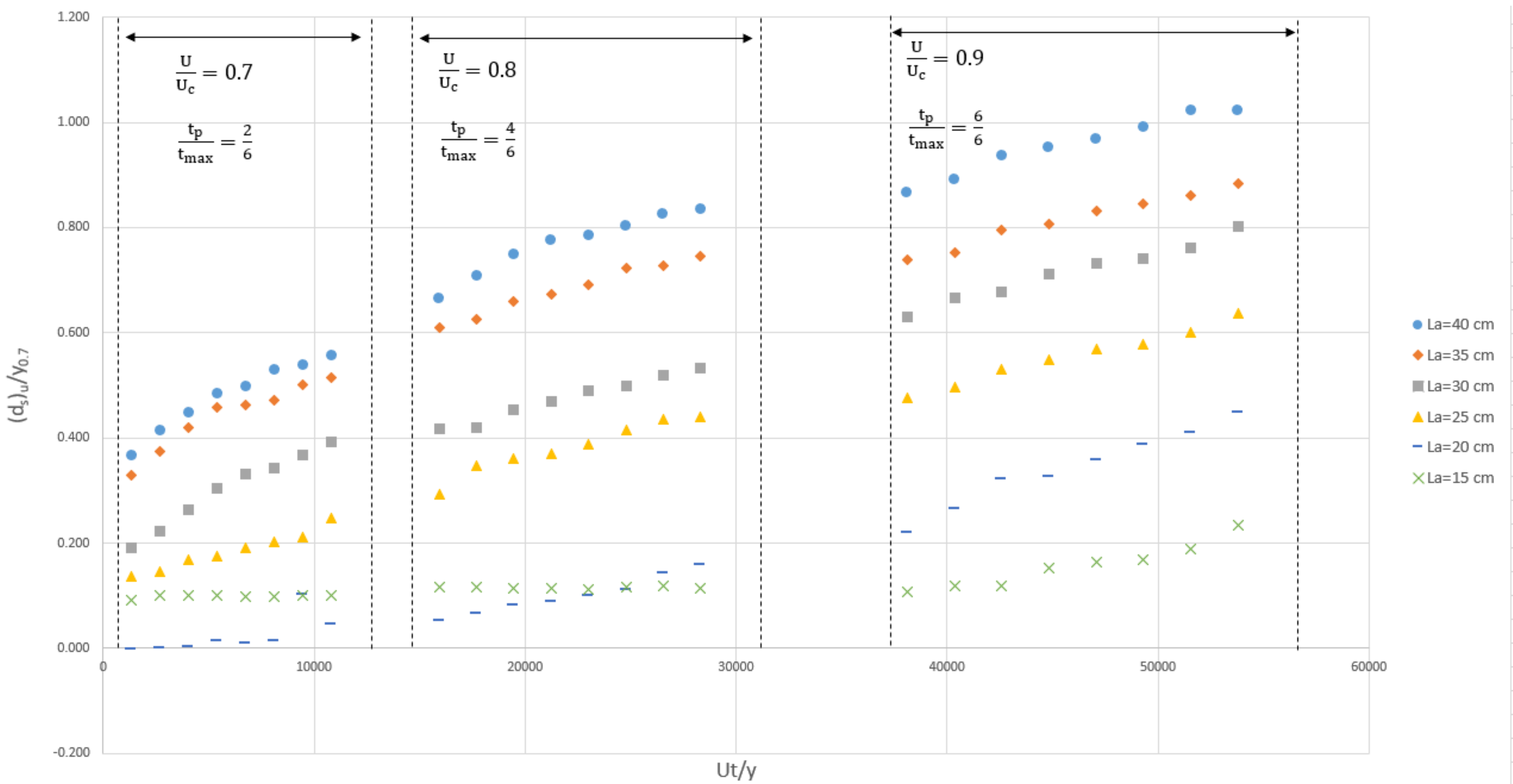

Figure 4.117 Variation of dimensionless scour depth with dimensionless time for various rectangular abutment lengths at Inducer 5 (upstream side)

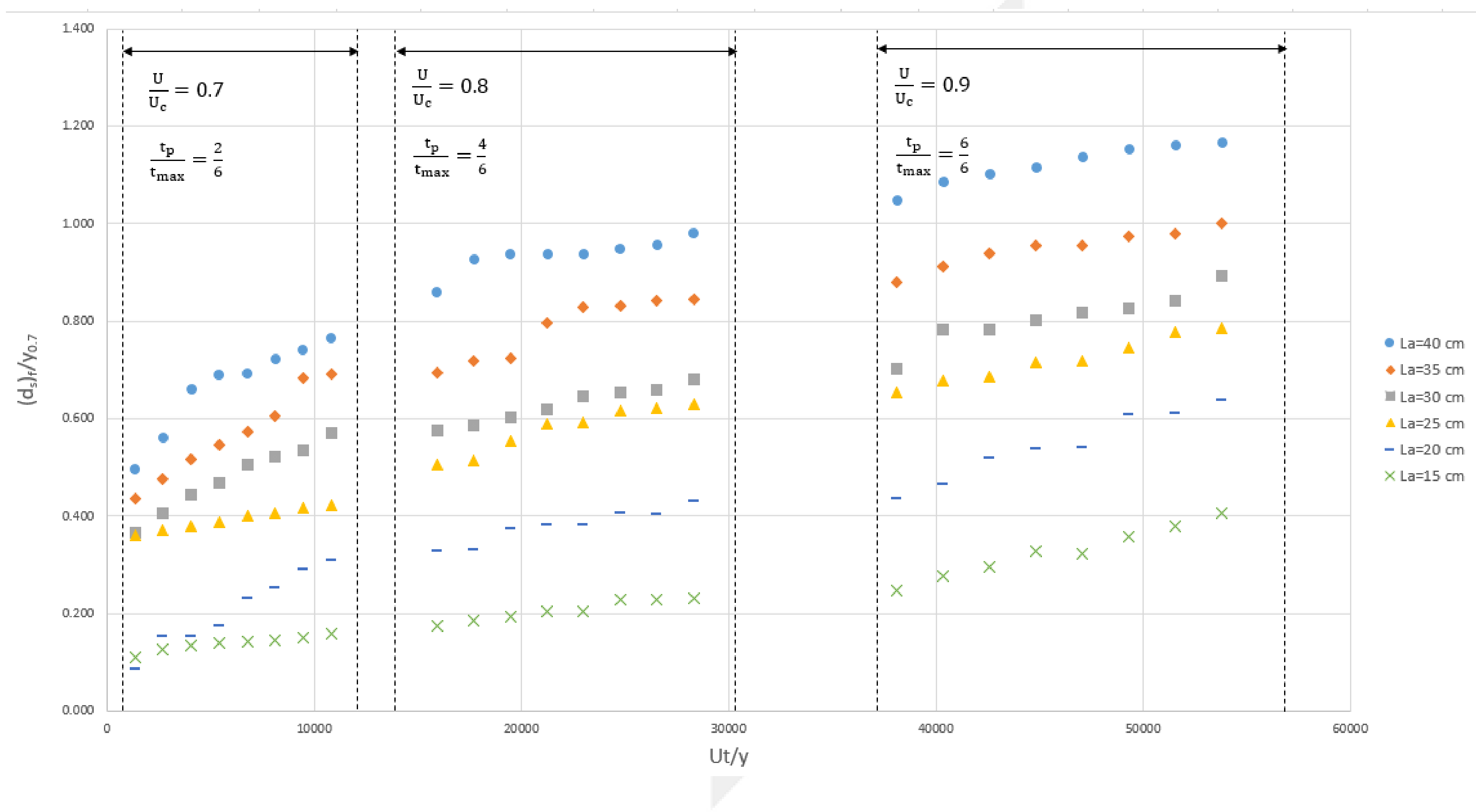

Figure 4.118 Variation of dimensionless scour depth with dimensionless time for various rectangular abutment lengths at Inducer 12 (front side)

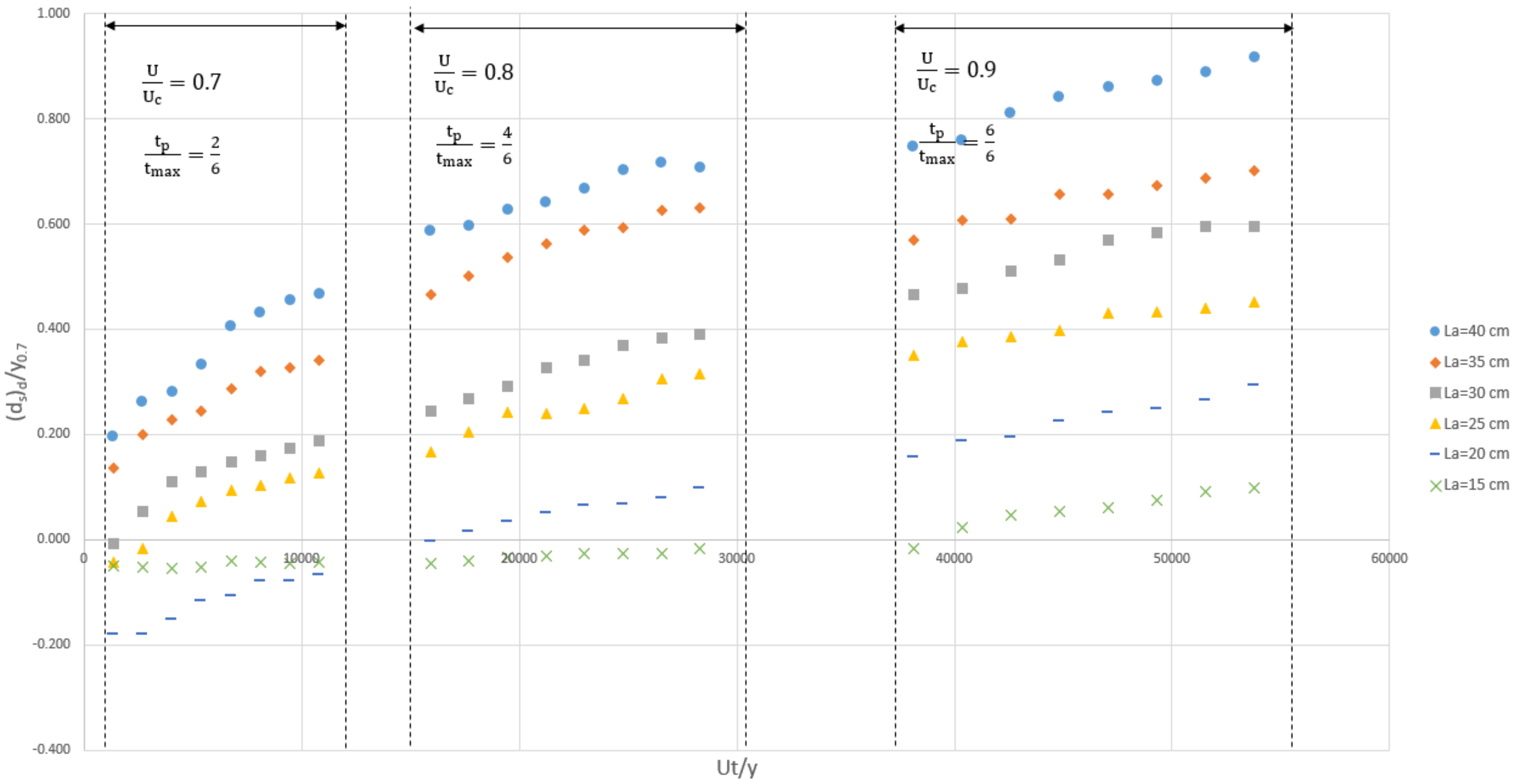

Figure 4.119 Variation of dimensionless scour depth with dimensionless time for various rectangular abutment lengths at Inducer 17 (downstream side)

Variation of the dimensionless scour depths at the downstream and upstream sides of the abutments with each other as a function of abutment length was plotted in Figure 4.120. From this figure, it can be clearly seen that the scour depths at the upstream nose are larger than those of the downstream nose for all the rectangular abutment lengths. On the other hand, for the semi-circular abutment lengths, the magnitude of the scour depths at the downstream and upstream sides of the abutment were close to each other. On the contrary, the scour depths at the downstream nose for the semi-circular abutments of lengths L_a=15 cm and 20 cm were a little bit larger than those of the upstream nose. Likewise, this situation was also observed during the first 4 hours of the experiments for the semi-circular abutments of lengths L_a=25 cm and 30 cm. So, it can be said that as the scouring rate increased due to the increased flow intensity or abutment lengths, the magnitude of the scour depths become greater on the upstream side compared to the downstream side. The presence of downflows and horseshoe vortex systems along the upstream face and wake vortices along the downstream face of an abutment play an important role in the development of the scour holes. As a function of the abutment length the effects of the aforementioned systems including flow intensity, the intensity of vortices and turbulence on the formation, location and depth of the scour holes show differences (Coleman et al., 2003). The abutments having the lengths of L_a = 15 cm and 20 cm tested in this study can be considered as short abutments and in the classification of between short and intermediate abutments. Since these abutments are in a transition zone between short and intermediate abutments, it was observed that maximum scour shifted from upstream to downstream. In both cases, the effect of the abutment length (L_a/y) on the value of $(d_s)_u$/y may be considered as negligible. To compare the numerical values of the dimensionless scour depths at the downstream and upstream noses of the abutments an empirical relationship, Equation 4.7, between these parameters was derived with R^2=0.924.

$$\frac{d_{s(d)}}{y} = -0.016 + 0.866\,\frac{d_{s(u)}}{y} \tag{4.7}$$

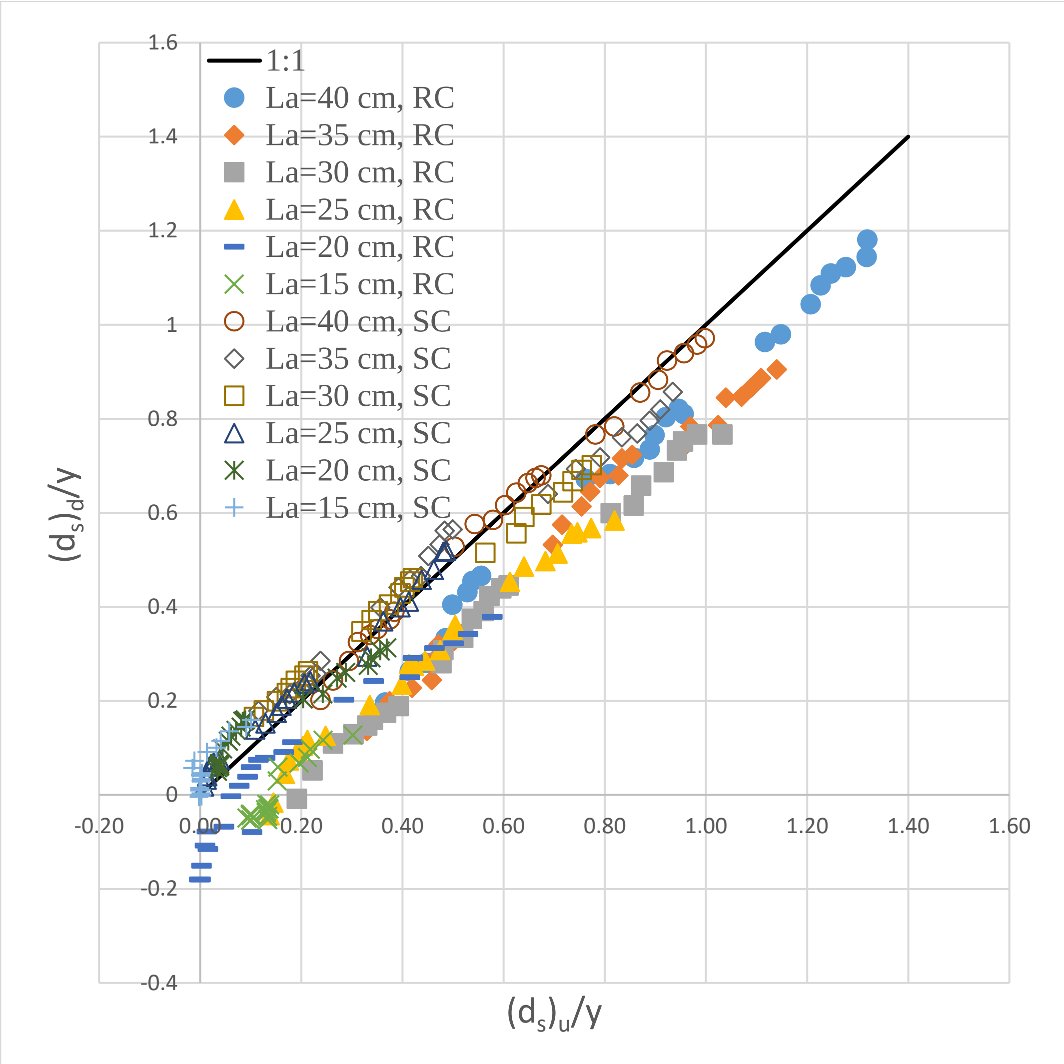

Figure 4.120 Variation of $(d_s)_d/y$ with $(d_s)_u/y$

Variation of the dimensionless scour depths at the downstream nose of the abutment with those of the front nose of the abutment is shown in Figure 4.121. This figure clearly presents that scour depths are larger at the front nose of the abutments than those of the upstream nose for all the abutments tested. Meanwhile, it can also be pointed out that the front nose of the abutments is more critical than the downstream nose in terms of scour development. The effectiveness of the abutment front nose in causing deeper scour depths than those of the abutment downstream nose becomes obvious as the abutment length and sharpness increase. The equation of the best-fit curve of the data presented in Figure 4.121 is given below in Equation 4.8 with R^2=0.903.

$$\frac{d_{s(d)}}{y} = -0.132 + 0.815\frac{d_{s(f)}}{y} \tag{4.8}$$

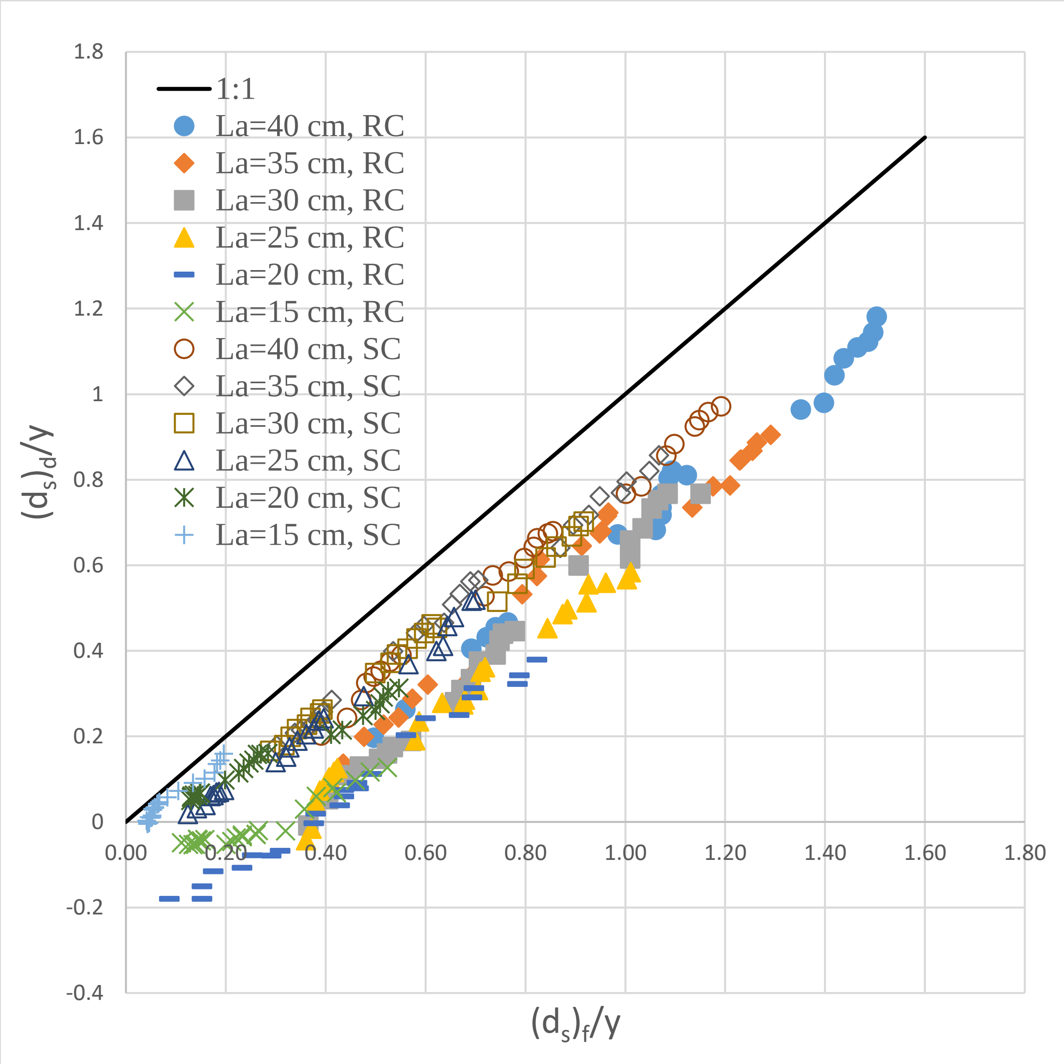

Figure 4.121 Variation of $(d_s)_f/y$ with $(d_s)_d/y$

Figure 4.122 shows that the scour depths obtained at the front nose of the abutments are always much larger than those of the upstream nose and almost the data points of all the abutments tested collapse with each other on a straight line. From this figure, it can be concluded that regardless of the abutment length the front noses of the abutments are the locations where maximum scour depths are observed. A dimensionless relationship between the scour depths at the downstream and front nose of the abutments is given in Equation 4.9 with R^2=0.973.

$$\frac{d_{s(u)}}{y} = -0.133 + 0.939\frac{d_{s(f)}}{y} \tag{4.9}$$

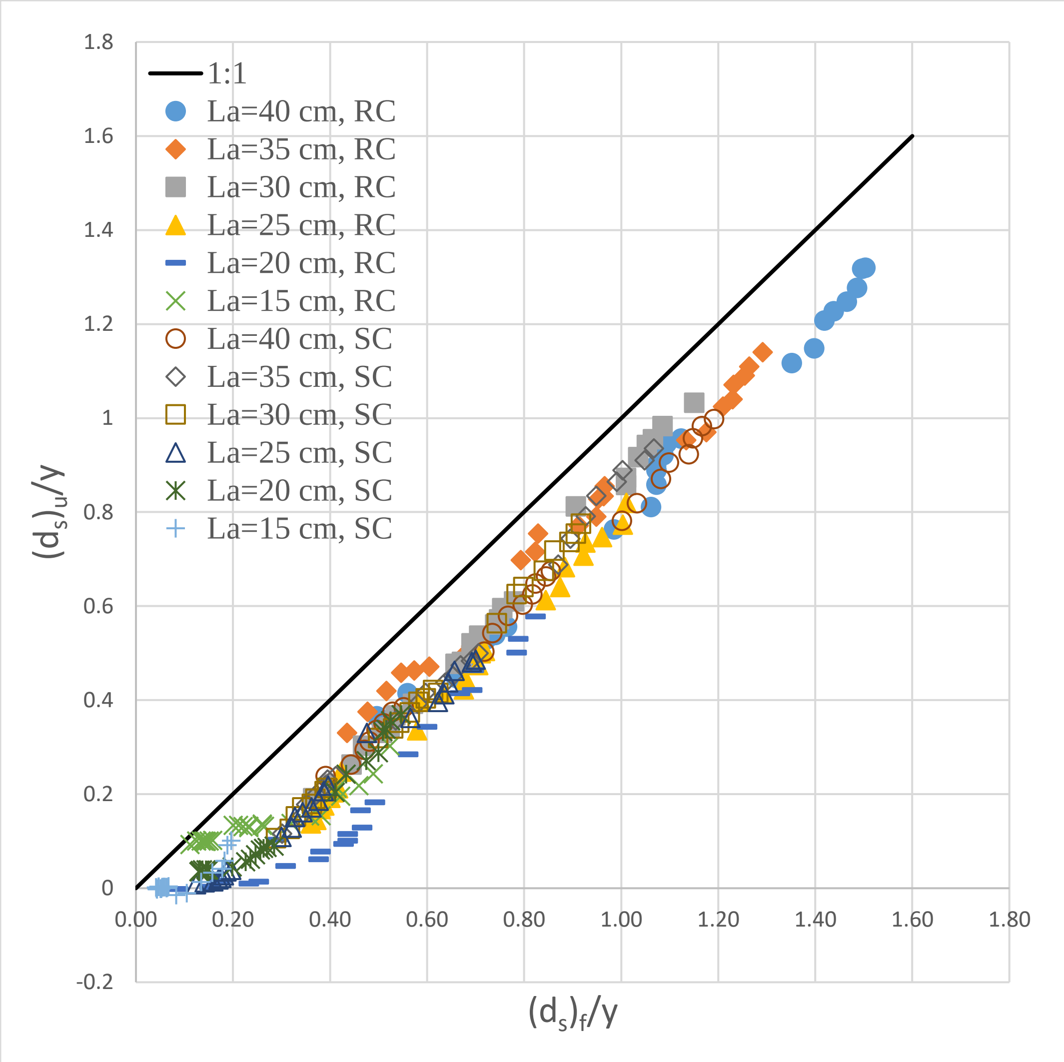

Figure 4.122 Variation of $(d_s)_f/y$ with $(d_s)_u/y$

4.4.3 Comparison of Experimental Results with the Relationship Proposed by Oliveto and Hager (2002, 2005a)

Oliveto and Hager (2002, 2005a) presented Equation 4.10 by using the data of a series of experiments to predict time-dependent local scour depth around circular piers and bridge abutments for steady-state clear water approach flow conditions.

$$Z = 0.068N\sigma^{-1/2}{F_d}^{1.5}\log(T) \tag{4.10}$$

where Z=dimensionless scour depth, N=shape number and equal to 1 for circular piers and 1.25 for rectangular abutments, F_d=densimetric Froude number ($= V/(g'd_{50})^{0.5}$ with $g' = [\{(\rho_s - \rho)/\rho\}g]$, ρ_s= density of sediment, ρ=density of fluid, g=acceleration of gravity and T=dimensionless time $[= \{(g'd_{50})^{0.5}/L_R\}t\,]$ with reference length, $L_R = {L_a}^{2/3}y^{1/3}$).

Afterward, Oliveto and Hager (2005a) proposed a superposition method by imposing their predictor, which was proposed in Oliveto and Hager (2002) to predict local scour development at bridge elements for unsteady-state approach flow conditions. It was stated that when the constant coefficient of Equation 4.11 is taken as 0.048 instead of 0.068, more accurate results could be obtained for unsteady approach flow conditions for the threshold Froude number, F_t, values of close to or lower than 0.6 (Oliveto and Hager, 2005b). Thus, their predictor changes in Equation 4.11:

$$Z = 0.048N\sigma^{-1/2}{F_d}^{1.5}\log(T) \tag{4.11}$$

The procedure stated by Oliveto and Hager (2005a) was applied to predict the scour depths. In this process, the shape factor N=1 was used due to the similarity between the shapes of piers and semi-circular end abutments for the present study's data belong to the semi-circular end abutments. However, it should not be forgotten that the scour depth around semi-circular end bridge abutments will be less than the scour depth around bridge piers due to the boundary layer effects despite the mirror image of the abutment can be considered equivalent to pier shape (Kothyari and Ranga Raju, 2001). On the other hand, the shape factor N=1.25 was used for the present study's data belonging to the rectangular abutments as it was indicated in Oliveto and Hager (2002, 2005a). The present study's experimental data at the front side of the abutment with those calculated from Equation 4.11 were compared with each other in Figures 4.123 and 4.124.

Figure 4.123 shows the calculated and experimental results of the semi-circular end abutments having lengths of L_a=30 cm, 35 cm and 40 cm that reasonably agree with each other for long abutments tested especially with increasing flow intensity in ± 30% error range. On the contrary, Equation 4.11 over-predicts scour depths for the semi-circular end abutments of lengths L_a=15 cm, 20 cm and 25 cm. On the other hand, Figure 4.124 shows that the data of this study belonging to the rectangular abutments do not show consistency with the proposed equation of Oliveto and Hager (2002, 2005a), contrary to the data of this study belonging to the semi-circular end abutments. Nevertheless, the obtained data with the highest flow intensity of 0.9 belonging to the rectangular abutments of lengths L_a=30 cm, 35 cm and 40 cm stayed in the ±30-40% error range. However, as the flow intensity decreases, the proposed equation over-predicts the scour depths. For the shorter rectangular abutment lengths of L_a=15 cm, 20 cm and 25 cm over-predictions were also observed. It should be underlined that as the abutment length decreases, the magnitude of the velocity field around the abutment length becomes smaller than the mean approach velocity since a large part of the abutment length remains in the sidewall boundary layer (Oliveto and Hager, 2005a). Hence, the over-predictions for the smaller semi-circular end and rectangular abutment lengths might occur due to this situation.

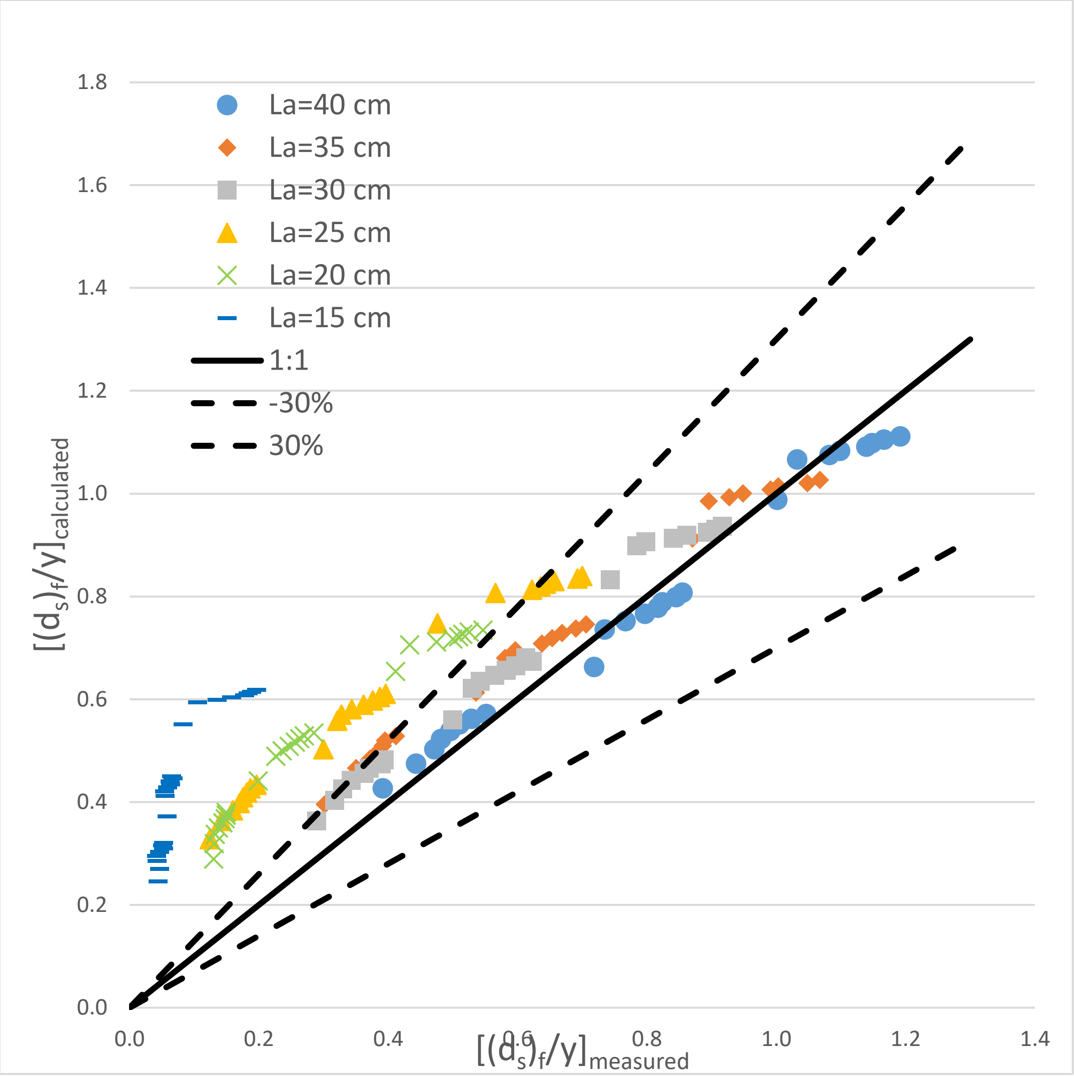

Figure 4.123 Comparison of the dimensionless scour depth data of this study belonging to semi-circular end abutments with those calculated by the equation proposed by Oliveto and Hager (2002, 2005a)

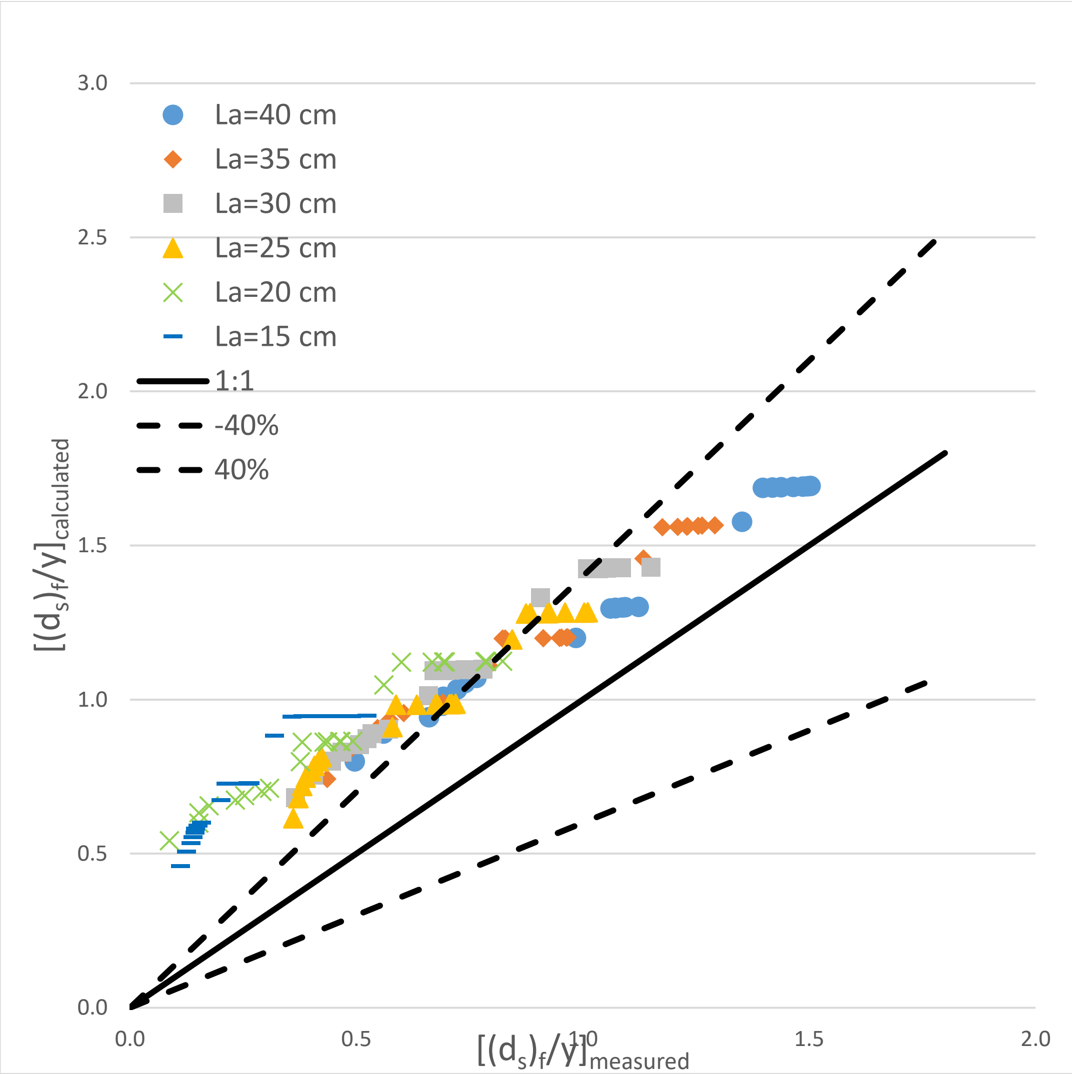

Figure 4.124 Comparison of the dimensionless scour depth data of this study belonging to rectangular abutments with those calculated by the equation proposed by Oliveto and Hager (2002, 2005a)

CHAPTER 5

APPLICATION OF COLLARS AS A SCOUR COUNTERMEASURE AROUND BRIDGE ABUTMENTS

In this chapter of this study, the countermeasure concept and common countermeasure techniques are explained in detail. In addition, the advantages and disadvantages of various countermeasure techniques are presented. Then, previous related studies found in the literature are mentioned. Finally, the results of the conducted experiments with collars in order to reduce the local scour depth around semi-circular end and rectangular bridge abutments under unsteady clear-water flow conditions are presented and the scour reduction efficiencies of the collars are discussed.

5.1 General Remarks

As mentioned in previous chapters, scour formation around bridge abutments during flood events can cause the collapse of bridges and even loss of lives. As a result of the increasing number of failure events of bridges due to abutment scour, studies have been more focused on scour countermeasures to prevent or reduce the scour formation around the bridge abutments. The main goal of studies on countermeasures for bridge scour is to establish design standards for countermeasures that are efficient in preventing or reducing local scour at the abutments to protect and restore the existing bridges from scour failures and bridges that will be constructed in the future (Li et al., 2006).

Several studies have been conducted to examine and offer recommendations for the application of scour countermeasures around bridge abutments. Notably, the FHWA Hydraulic Engineering Circular No. 23 (HEC 23) "Bridge Scour And Stream

Instability Countermeasures Experience, Selection, and Design Guidance" (2001) and NCHRP, Report 587 "Countermeasures to Protect Bridge Abutments from Scour" discuss a variety of countermeasures. Additionally, a countermeasure by HEC-23 was defined as "a measure incorporated at a stream/bridge crossing system to monitor, control, inhibit, change, delay, or minimize stream and bridge stability problems and scour by Agrawal et al. (2007) in FHWA NJ's "Handbook of Scour Countermeasures Designs" Final Report. This definition makes it clear that the choice of a countermeasure is directly related to the severity of the issue.

When choosing the appropriate countermeasures, it is critical to evaluate the environmental regulations, economic situations, availability, serviceability, applicability and design constraints in addition to assessing the current status of the problem (Daşkın, 2011). The parameters that are listed below are generally the main criteria for selecting countermeasures (NCHRP, Report 587, 2007):

- Cost,
- Technical effectiveness,
- Constructability,
- Durability and maintainability,
- Aestechich and environmental issues.

5.2 Countermeasure Concept and Applications on Abutment Scour

Scour countermeasures have been classified into two groups; armoring and flow-altering countermeasures. The armoring countermeasures such as riprap, grout-filled bags, cable-tied blocks, geo- bags, mainly focus on protecting the bridge element by keeping the scour away from the critical zones of the bridge element in terms of scour (Li et al., 2006). On the other hand, flow-altering countermeasures such as collars, vanes, slots, etc. aim to reduce the strength of the downflow and primary or horseshoe vortices in order to decrease the scour depth and deaccelerate the scour development (Tafarojnoruz et al., 2012a). Flow-altering countermeasures have been accepted as more economical than armoring countermeasures because of the required amount of stone that may not be provided around the bridge site (Zarrati et al., 2004).

Scour countermeasures against the abutment scour and their advantages and disadvantages are presented in Table 5.1.

Table 5.1 Abutment scour countermeasures and their advantages and disadvantages (Agrawal et al., 2007) (retrieved from Daşkın, 2011)

Countermeasure	Advantages	Disadvantages
Local Scour at Abutment		
Peak Flood Closure	Low initial cost	Limits access, constant monitoring
Monitoring	Low initial cost	Does not prevent scour
Riprap	Familiarity, relatively low cost and maintenance, easy to construct, ability to adjust to minor scour	Can wash out, and disturbs the channel ecosystem until vegetation reestablished
Gabions	Relatively low cost, ability to adjust to minor scour	Can be undermined, stones can wash out of wire mesh and disturb the channel ecosystem
Cable-tied Blocks	Will not wash out as easily	More difficult to construct, higher maintenance
Tile Mats	Will not wash out as easily	More difficult to construct, higher maintenance, easier for water to lift
Alarm Systems	Low initial cost	Provides no scour protection, and must be checked periodically
Articulated Mattress	Coherent structure, the individual block will not wash out	More difficult to construct, easier for water to lift
Concrete-filled Mattress	Rocks will not wash out, and relative ease of construction	Can be undermined, easy for water to lift

Table 5.1 (continued)

Locking Blocks	Coherent structure, the individual block will not wash out	More difficult to construct, easier for water to lift
Pavement	Conceptually appealing	High cost and maintenance, can be undermined, easy for water to lift
Rock Bolting	Strong, low maintenance	Costly, only for abutments on bedrock
Grouted Riprap	Rocks will not wash out, and relative ease of construction	Can be undermined, easy for water to lift
Sacrificial Piles	Conceptually appealing	Not effective, high cost
Grout Bags	Ease of construction, low cost	Bags can wash out
Sheet Piling	Stops flow, helpful in dewatering	Scour can occur near sheet piling, construction difficulty, rust
Hinged-Slab/Tethered Block System	Will not erode under extreme velocities	Could be subject to edge undermining
River Control		
Spur Dikes / Guide Banks	Proven effective	Can wash out, need to protect guide bank walls, obstructs navigation
Submerged Vanes	Elegant approach, not too expensive, effective	Obstructs navigation, possible debris snags, construction difficult
Collars	Low cost and maintenance, effective	Does not eliminate scour, does not have much experience
Attached Vanes	Low cost and maintenance, effective	Does not eliminate scour, does not have much experience

When considering the safety of hydraulic structures, scour appears to be the main threat. Despite several studies that have been conducted, the scour problem has not yet been entirely and successfully solved. After reviewing these studies, it is possible to conclude that various countermeasures could be used to reduce scour depths (Daşkın, 2011). The usage of collars is one of the most common flow-altering techniques to reduce and delay scour formation around bridge elements. The flow pattern around the bridge element is manipulated by the installation of the collar. Thus, the occurrence of the large bed shear stresses and pressure fluctuations, which causes scour formation, due to the primary vortex and the vortex tubes at the upstream side of the bridge elements being decreased (Kumcu et al., 2014). At the zones above the collar, it deaccelerates downflow movement into regions below the collar while reducing the downflow and primary vortices at the zones below the collar. Therefore, scour reduction performance of a collar mostly depend on its size and location relative to the bed level (Kumar et al., 1999). Although the efficiencies of collars in reducing the scour formation around the bridge elements have been a popular research area in the last decades, the studies have generally been focused on the pier or abutment scour under steady-state approach flow conditions. However, studies about the influence of collars on abutment scour under unsteady-state approach flow conditions have not been investigated yet. In the scope of this study, experiments were carried out to investigate scour reduction efficiencies of collars under unsteady-state clear-water approach flow conditions. The methodology, procedure and results of the experiments are given in the following subsections.

5.3 Literature Review

In the past years, several studies were conducted by researchers under steady-state approach flow conditions (Melville, 1992; Kandasamy and Melville, 1998; Kothyari and Ranga Raju, 2001; Oliveto and Hager, 2002; Coleman et al., 2003; Dey and Barbhuiya, 2005b) and quasi-unsteady or unsteady- state approach flow conditions (Oliveto and Hager 2005a; Hager and Unger 2010; Borghei et al., 2012; Tabarestani and Zarrati, 2017; Bombar, 2020; Gokmener and Gogus, 2022; Raikar et al., 2022) to understand scour mechanism and predict the temporal variation of maximum scour depth around bridge elements. Despite these extensive studies in the literature; investigating the temporal development of maximum scour depth around bridge elements is not enough to solve the issues related to the scouring process, scour countermeasures and their applications on bridge elements should also be investigated (Kumcu et al., 2014). In this subsection, a summary of extensive studies found in the literature related to the application of collars on bridge elements to reduce or eliminate the scour depth is presented.

Chiew (1992) tested the efficiencies of the collar and slot as scour countermeasures for circular piers under steady-state clear-water approach flow conditions. It was stated that the scour depth can be decreased by 20-30% by increasing collar width and lowering the collar elevation. Likewise, as the slot length and width are increased, the scour depths can also be decreased by 20-30%. The combination of collar and slot was also tested and gave successful results to eliminate the scour depth. Yet, the combination of collar and slot was presented as a cheaper alternative to riprap protection.

Kumar et. al (1999) conducted experiments on scour reduction efficiencies of rectangular slots and circular collars on local scour around bridge piers under steady-state clear-water approach flow conditions. It was mentioned that the effect of slots and collars on the flow is different from each other. If a slot is located near the bed level, it can change the direction of downflow away from the bed and also break the horseshoe vortex. If a slot is located near the water surface, downflow and horseshoe vortex can be reduced efficiently; on the other hand, a collar can divide the flow into two regions those regions above the collar downflow loses their strength and the region below the collar, downflow and horseshoe vortex are reduced. Five different collar sizes with two different pier diameters were tested during the experiments under steady-state clear-water approach flow conditions. In addition, three different uniform size grains of sand were tested. In conclusion, it was stated that the greatest scour depth was observed for the thinnest collar placed at higher elevations.

However, the smallest scour depth was observed for the thickest collar placed at lower elevations.

Zarrati et al. (2004) tested the scour reduction efficiencies of collars around rectangular bridge piers under steady-state clear-water approach flow conditions. The performance of collars was not only tested for aligned piers but also skewed piers at 5° and 10° were tested. Based on experimental results, it was indicated that the most efficient collar performance is observed when the collar was located on the bed level, having a width of 3 times of pier diameter. It was also stated that the scour reduction efficiencies of collars decreases as the skewness of the pier increases for a given pier and collar width.

Li et al. (2005) performed experiments using flat, horizontal and steel collars around a wing-wall abutment to test the performance of collars as a scour countermeasure under steady-state clear-water approach flow conditions. It was revealed that the collars show successful results in reducing scour depth around abutments by preventing secondary vortices that can lead to local scour. Moreover, the best collar performance was obtained at the elevation of 0.08y below the bed level where y is the flow depth.

Alabi (2006) conducted an experimental study to investigate the effect of collars on delaying the temporal development of scour around circular bridge piers under steady clear-water flow conditions. Three series of experiments were performed to understand the effect of flow intensity, collar width and pier diameter on the temporal development of scour. The experiments were carried out for up to 200 hours to observe the efficiencies of collars under equilibrium scour conditions. Based on experimental results, it was concluded that collars are very effective countermeasures to slow down the scouring rate and reduce scour depth around bridge piers, but it was also stated that for long durations equilibrium scour depth can be reached even usage of collars.

Kumcu et al. (2007) investigated the efficiencies of collars in reducing the temporal variation of scour around rectangular bridge abutments. Collars with varying widths and elevations were tested on varying lengths of abutments by using uniform erodible sand, d_{50}= 1.48 mm, for a 6-hour duration. It was concluded that the maximum scour depth can be decreased around the abutment between 20-80% approximately related to the size and location of the collar.

Moncada et al. (2009) studied the efficiencies of collars and slots as scour countermeasures for circular bridge piers. The experiments were carried out under steady-state clear-water approach flow conditions using uniform sand, d_{50}=1.4 mm. According to the experimental results, it was stated that the collars having width 2 times of pier diameter located at bed level, around circular piers reduce the maximum scour depth by around 55-96%. The collars located below the bed level showed also significant performances on scour reduction. Moreover, the efficiencies of collars increase with increasing collar size. It was also underlined that for the smaller approach flow depths, better collar performances were observed independent of collar size. On the other hand, it was indicated that the slots can reduce the maximum scour depth by around 48-88% based on the slot length and location.

Gogus and Dogan (2010) carried out experiments to investigate the effect of grain size on the performance of the collars in reducing scour depth around rectangular abutments. Experimental conditions were nearly the same as Kumcu et al. (2007, 2014) except for using different grain sizes of the bed material, d_{50}=0.9 mm. 97 experiments were conducted with different lengths of abutments with constant widths and the different sizes of collars with different elevations related to bed level. 6 hours continuous runs performed under steady-state clear- water approach flow conditions. Based on experimental results, it was mentioned that the efficiencies of collars increase with increasing collar width, but it is decreasing with increasing abutment length. Also, it was indicated that the collars which are located below the bed level provide optimal collar efficiency. Finally, it was mentioned that the grain size of the bed material has not any significant effect on the optimum location based on the comparison of the results with Kayatürk (2005) and Kumcu et al. (2007).

Daşkın (2011) tested the scour reduction efficiencies of collars having various widths located at different elevations around the semi-circular end abutments under steady-state clear-water approach flow conditions with constant flow intensity, U/U_c=0.9. Six different abutment lengths were tested with an almost uniform cohesionless bed material (d_{50}= 1.50 mm) for 3 h with and without collars. Based on the experimental results of the study, it was concluded that the performance of collars in reducing scour increases with increasing collar width and placing the collar below the bed level for a given abutment length. On the other hand, it was indicated that the effect of collars on the maximum scour depth reduction decreases as the abutment length increases. The maximum scour depth was reduced within a range of 9-65% depending on abutment length, collar width and collar elevation.

Tafarojnoruz et al. (2012a) evaluated scour reduction performance of six different flow-altering countermeasures around circular bridge piers under steady-state clear-water approach flow conditions. It was concluded that the collar, pier slot and transverse sacrificial piles can reduce the maximum scour depth by up to 35%, whereas the efficiencies of bed sill, submerged vanes and threading reduce by up to 20%. Based on the low efficiencies of flow-altering countermeasures on scour reduction performance observed in Tafarojnoruz et al. (2012a)'s study, Gauido et al. (2012) recommended using a combination of flow-altering countermeasures to reduce maximum scour depth around the circular piers. Therefore, the combination of bed-sill and collar together which reduce the maximum scour depth by approximately 76%, was recommended as the best combination for scour countermeasure.

Tafarojnoruz et al. (2012b) presented another study in order to investigate the combined effect of the collar and bed sill as a scour countermeasure for circular and rectangular piers. A series of experiments were conducted under steady and unsteady-state for both clear-water and live-bed scour conditions. Experimental results showed that the combination of collar and bed sill reduced the maximum scour depth by around 63% for circular piers under all different flow conditions; on the other hand, the scour reduction rate was measured by around 75% for rectangular piers under unsteady-state clear-water approach flow conditions.

Tekin (2012) conducted experiments to observe scour mechanism around semi-circular end bridge abutments under steady-state clear-water approach flow conditions with a uniform grain size of d_{50}= 1.5 mm. 34 experiments were continuously performed for 3 hours with and without collars to obtain the scour reduction efficiencies of collars for semi-circular end bridge abutments. Two different abutment lengths were tested with collar widths that were placed at various elevations relative to bed level. In order to understand the effect of flow characteristics on collar efficiency, two different flow intensity values U/U_c= 0.7 and 0.8, were also tested during the experiments. According to the experimental results, it was mentioned that collars located near the bed level give the most efficient scour depth reduction for the smaller flow intensity value of U/U_c= 0.7, on the other hand, for the bigger flow intensity value of U/U_c= 0.8, collars located below the bed level give the most efficient scour depth reduction. Finally, it was concluded that as the collar width increased, the scour reduction performance of the collars increased.

Kumcu et. al (2014) performed experiments to research collar efficiency to reduce scour depth at rectangular bridge abutments. Experiments were carried out under steady-state clear-water approach flow conditions. To achieve near-threshold flow conditions, the flow intensity value of U/U_c= 0.9 were tested. 105 different experiments were conducted for 4 different collar widths and 5 different abutment lengths having constant widths and also collars were located at various elevations relative to the bed level. Based on experimental results, it was indicated that the maximum scour depth around the abutment decreases by the attachment of a collar within a range of 70-100%. The higher collar efficiency was observed for the smaller abutment lengths while having larger collar widths that are generally placed below the bed level. Finally, the application of collars as a scour countermeasure was suggested as a cheaper alternative for riprap protection to reduce or eliminate the scouring around the abutments.

Yılmaz (2014) investigated the efficiencies collars as a scour countermeasure for spill-through abutments. Various widths of collars at different elevations with respect to the bed level under steady-state clear-water approach flow conditions were tested during the experiments. Scour reduction performances of the collars were also tested against the contraction scour by using the multiple abutment configurations. Based on experimental results, it was concluded that the collars not only reduce the maximum scour depth by around 52% for both single and multiple abutment configurations and shift the maximum scours location away from the abutment. Finally, it was stated that for the single abutment configurations, collars are more successful to reduce the scour depth for the abutment lengths, which are two times longer than the flow depth.

Karami et al. (2018) studied the effect of the collar on flow pattern and scour formation around the short rectangular abutments under steady-state clear-water approach flow conditions. It was concluded that the attachment of the collar on the abutment reduces the turbulent intensity and shear stress around the abutment, thus, scour formation is delayed because of weaker vortices. The maximum scour depth reduction was observed for the collar having a width 2 times of abutment length below the bed level by 88.2%.

Khosravinia et al. (2018) investigated the scour reduction performances of trapezoidal collars around wing-wall abutments experimentally under steady-state clear-water approach flow conditions. It was stated that increased collar width not only reduces the maximum scour depth but also delays the occurrence of scour formation. Experimental results reveal that the installation of a collar around the wing-wall abutment reduces the maximum scour depth within a range of 9%- 37% based on collar width.

Tabarestani and Zarrati (2019) performed experiments on the local scour development around a circular pier protected by a collar under steady and unsteady-state clear-water approach flow conditions. In their study, the time for reaching the scour below the collar level was considered rather than scour reduction amounts of collars to evaluate scour reduction efficiencies of collars. The results indicated that decreasing flow intensity, U/U_c from 0.99 to 0.8 delayed the onset of degradation of the bed material below the collar by 26 times. Hereby, it was stated that flow intensity is the most dominant parameter for scour development around piers either without or with a collar.

Atarodi et al. (2021) applied Taguchi Method to understand the influence of parameters such as collar elevation, size and shape on the scour formation around spur dikes to obtain optimal collar performances. According to the results, the most influential parameters affecting the collar performance were given as collar elevation, skewness, collar area and collar shape, respectively. Moreover, it was emphasized that the influence of collars on scour reduction decreases with increasing flow intensity.

Hosseinjanzadeh et al. (2021) carried out experiments to obtain the collar performance on reducing the maximum scour depth around short abutments having various shapes as the rectangular, wing-wall and semi-circular end. Four different flow intensities were tested under steady-state clear-water approach flow conditions. It was concluded that the optimal collar location is the bed level for wing-wall and semi-circular abutments while below the bed level for a rectangular abutment. Moreover, it was also underlined that the scour reduction performance of a collar increases as collar width is increased for a given collar location relative to the bed level.

Osroush et al. (2021) investigated the scour reduction efficiencies of collars and slots around rectangular bridge abutments under steady-state clear-water approach flow conditions. Experiments were conducted with either a collar or slot and combinations of them. Based on experimental results, it was stated that collar width is the significant parameter in reducing the scour depth when the collar is attached to the abutment as a scour countermeasure. In other words, as the dimensionless collar width increased from 1.6 to 2 for a given Froude number, the maximum scour around the abutment increased from 44% to 88%. On the other hand, the usage of a slot on the abutment as a scour countermeasure also gave successful results in reducing the maximum scour depth within the range of 34-59%. However, the best results for scour reduction were obtained for the attachment of the collar and slot together by reducing the scour depth by around 48-100%. Finally, it was indicated that the scour reduction efficiencies of collars and slots decreases as the Froude number increases independent of either collar or slot properties.

Valela et al. (2021) and Valela et al. (2022) designed a three-dimensional collar shape instead of widely- used flat plate collars for circular piers considering the flow pattern around the pier. The design phase was achieved by using the OpenFOAM (CFD) software and the outputs of the numerical model were studied experimentally under steady-state clear-water approach flow conditions. Based on experimental results, the optimally designed collar shape provided a remarkable decrease in both maximum scour depth and scour volume for smaller Froude numbers than 0.3 when compared with the flat plate collars. However, for larger Froude numbers, on the contrary, flat plate collars had better results on scour reduction efficiency.

Kumcu et al. (2022) performed a series of experiments to predict the downstream shift location of the maximum scour depth while a collar is attached to the abutment and pier. Experimental results showed that the attachment of a collar around a pier or abutment leads to the movement of the location of maximum scour depth to the downstream direction. Furthermore, it was underlined that as the flow intensity increased the distance of shift location of maximum scour depth to the collar or abutment decreased as well as the scour reduction efficiency of a collar. During the study, it was also obtained that the maximum average scour depths decreased by around 25-38% by the application of the collars as a scour countermeasure.

Khajavi et al. (2022) studied the efficiencies of spur dikes, which are placed at the upstream side of the abutment, as a scour countermeasure for rectangular abutments under unsteady-state clear-water flow conditions. Nine hydrographs that differ from each other in terms of duration (15, 30 and 60 minutes) and skewness were tested during the experiments. Based on experimental results, impermeable spur dikes provided a complete elimination of scour around the abutment; on the other hand, maximum scour depths around the abutment were reduced by an average of 40%. However, the duration and skewness of the hydrographs had not any significant influence on scour reduction performances of spur dike whether it is permeable or impermeable.

Flow, sediment, abutment and collar properties of the studies mentioned above related to the abutment-collar arrangement are summarized in Table 5.2.

Table 5.2 Summary of previous studies related to the abutment-collar arrangement

Study	Abutment Shape	Collar Type	Grain Size, d_{50} (mm)	Duration (h)	Ranges of Flow Intensity	Approaching Flow Condition
Li et al. (2006)	Vertical-face wing wall	Rectangular	0.8	80	0.9	Clear-water scour
Kumcu et al. (2007 and 2014)	Vertical-wall rectangular	Rectangular	1.48	6	0.9 - 1	Clear-water scour
Gogus and Dogan (2010)	Vertical-wall rectangular	Rectangular	0.9	6	0.9	Clear-water scour
Yılmaz (2014)	Spill-through	Rectangular	1.50	4	0.9	Clear-water scour
Khosravinia et al. (2018)	Wing- wall	Trapezoidal	0.40	10	0.9	Clear-water scour
Hosseinjanzadeh et al. (2021)	Vertical-wall Wing-wall Semi-circular	Rectangular Trapezoidal Semi-circular	0.91	40	0.65- 0.95	Clear-water scour
Osroush et al. (2021)	Vertical-wall rectangular	Rectangular	1.37	13	0.69, 0.79, 0.91	Clear-water scour
Kumcu et al. (2022)	Vertical-wall rectangular	Rectangular	1.48	12	0.9 - 1	Clear-water scour

5.4 Methodology of the Experiments

The maximum scour depth around an abutment with a collar, $(d_s)_{max,c}$, under unsteady-state clear-water approach flow conditions are presented as a function of parameters given below:

$$(d_s)_{max,c} = f\{L_a, B_a, B_c, Z_c, T_c, U, y, S_0, g, \rho_s, \rho, \mu, d_{50}, \sigma_g, t_p, t_{max}, B\} \tag{5.1}$$

where L_a is the length of the abutment perpendicular to the flow direction, B_a is the width of the abutment; B_c is the collar width; Z_c is the elevation of the collar with respect to the sand level; T_c is the collar thickness; U is the average flow velocity; y is the flow depth; S_0 is the bed slope of the channel; g is the acceleration of gravity; ρ_s is the density of bed material; μ is the dynamic viscosity of water; d_{50} is the median diameter of bed material; σ_g is the geometric standard deviation of bed material and σ_g is the d_{84}/d_{16}) where d_{84} is the particle diameter for which 84% of the sediment is finer; and d_{16} is the particle diameter for which 16% of the sediment is finer; t_p is the time period of the experiment for a given flow intensity starting from the beginning as 2 hours, 4 hours and 6 hours duration of the experiment; t_{max}, which equals to 6 hours in this study, is the total duration of the experiment that represents the total duration of flood and B=width of the channel.

The parameters that are given in Equation 5.1 are transformed into dimensionless parameters by applying Buckingham's π theorem as;

$$\frac{(d_s)_{max,c}}{y} = f\left\{\frac{L_a}{y}, \frac{B_a}{y}, \frac{B_c}{y}, \frac{Z_c}{y}, \frac{T_c}{y}, \frac{\rho_s}{p}, \frac{U}{\sqrt{gy}}, \frac{B}{y}, \frac{\mu}{U\rho y}, \frac{Ut_p}{y}, \frac{t_p}{t_{max}}, S_0, \sigma_g, \frac{d_{50}}{y}\right\} \tag{5.2}$$

Since the experiments were conducted with one sediment size, constant parameters of bed slope, channel width, collar thickness and abutment width, related parameters can be excluded from Equation 5.2. Considering the turbulence nature of the open channel flows viscous effects can also be neglected. Moreover, the flow intensity term, U/U_c can be written instead of the Froude number, $U/\sqrt{gy}$. Therefore, Equation 5.2 can be simplified as;

$$\frac{(d_s)_{max,c}}{y} = f\left\{\frac{L_a}{y}, \frac{L_a}{B_c}, \frac{Z_c}{y}, \frac{U}{U_c}, \frac{Ut_p}{y}, \frac{t_p}{t_{max}}\right\} \tag{5.3}$$

The performances of collars on scour reduction were calculated by comparing scour depths of a given abutment with and without collar cases using the expression given in Equation 5.4.

$$\frac{(d_s)_{max} - (d_s)_{max,c}}{(d_s)_{max}} = f\left\{\frac{L_a}{y}, \frac{L_a}{B_c}, \frac{Z_c}{y}, \frac{U}{U_c}, \frac{Ut_p}{y}, \frac{t_p}{t_{max}}\right\} \tag{5.4}$$

where $(d_s)_{max}$ is the maximum scour depth around the abutment without a collar.

5.5 Experimental Procedure

The procedure of the experiments conducted with collars is similar to the experiments conducted without collars already mentioned in Section 4.3. Also, the experimental conditions presented in Table 4.2 is valid for the experiments with collars. Three different semi-circular and rectangular abutments of lengths L_a= 20 cm, 30 cm and 40 cm made of plexiglass were tested experimentally under unsteady-state clear-water approach flow conditions. Collars having widths of 5 cm, 7.5 cm and 10 cm with a thickness of 3 mm were attached to the abutments in order to reduce the maximum scour depth. Two different collar shapes were tested during the experiments relative to the abutment shape: semi-circular end collars were attached to the semi-circular end abutments and rectangular collars were attached to the rectangular abutments. Collars were tested for three different elevations relative to the bed level; on the bed level, 0.25 and 0.5 times the flow depth, which was operated for the first 2 hours ($y_{0.7} = 17.4$ cm, $U/U_c = 0.7$) of the experiments, below the bed level.

Unsteady-state approach flow conditions were obtained by applying a step-wise hydrograph based on flow intensity (Figure 4.3). Step-wise hydrograph consists of three flow intensity values, U/U_c= 0.7, 0.8 and 0.9 each one applied continuously for 2 hours, respectively, was run for 6 hours. In addition to the justifications provided in Section 4.3 for the selected duration of the experiments, it should not be forgotten that the main aim of the present study is to investigate the scour reduction efficiencies of collars with varying size and elevation configurations rather than investigate the maximum scour depth at equilibrium conditions, so, 6 hours was found sufficient to evaluate the scour reduction performances of collars (Johnson et al., 2001; Kumcu et al., 2007, 2014 and Valela et al., 2022). The step-wise hydrograph was applied with a constant discharge (Q=0.0678 lt/s). Flow intensity was increased every 2 hours by decreasing the flow depth with adjustment of the tailwater gate at the downstream of the channel. A ruler, which was glued to the wall of the sand layer of the flume, with an accuracy of ±1 mm was used to measure the flow depth. At the beginning of the experiments, the tailwater gate at the downstream of the channel was adjusted to the flow depth, y=17.4 cm and flow intensity, U/U_c=0.7. 2 and 4 hours later, flow depth was decreased to y=15.2 and 13.5 cm, respectively in order to obtain flow intensities, U/U_c=0.8 and 0.9. Abutment lengths, collar sizes and locations during the experiments are summarized with a sketch of a semi-circular end bridge abutment-collar arrangement in Table 5.3.

Table 5.3 Abutment lengths, collar sizes and locations tested during the experiments

Abutment	Type	L_a (cm)	B_c (cm)	Z_c (cm) with respect to the bed level	$Z_c/y_{0.7}$ with respect to the bed level
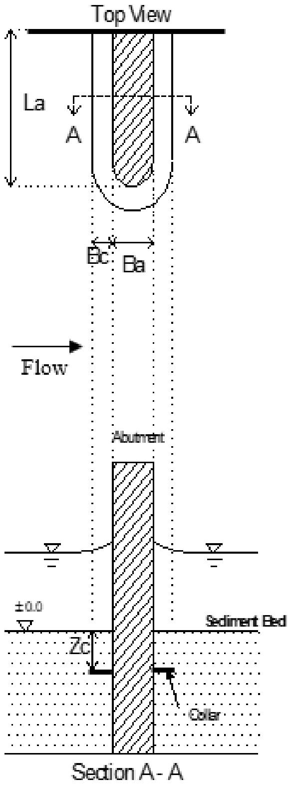	1	20	10.0	-8.70	-0.50
			7.5	-4.35	-0.25
			5.0	±0.00	±0.00
	2	30	10.0	-8.70	-0.50
			7.5	-4.35	-0.25
			5.0	±0.00	±0.00
	3	40	10.0	-8.70	-0.50
			7.5	-4.35	-0.25
			5.0	±0.00	±0.00

In order not to disturb the flow pattern and scour hole during experiments, scour depth measurements could not be done during the experiments. Moreover, it was not possible to measure the scour depths below the collar level without detaching it. Consequently, each experiment was divided into three stages (Figure 5.1). In the first stage, the flow intensity of U/U_c=0.7 was tested only for 2 hours, then the experiment was ended and scour measurements were done after the drain of water from the channel. In the second stage, U/U_c=0.7 were tested for 2 hours, then the flow intensity was gradually increased to U/U_c=0.8 and the experiment was continued for another 2 hours and then was ended. So, scour depth measurements were done at the end of the 4th hour. The same procedure was repeated in the third stage with the flow intensity of U/U_c=0.9 for another 2 hours. So, after three stages, final scour depths for the end of each stage; the 2nd, 4th and 6th hours were obtained.

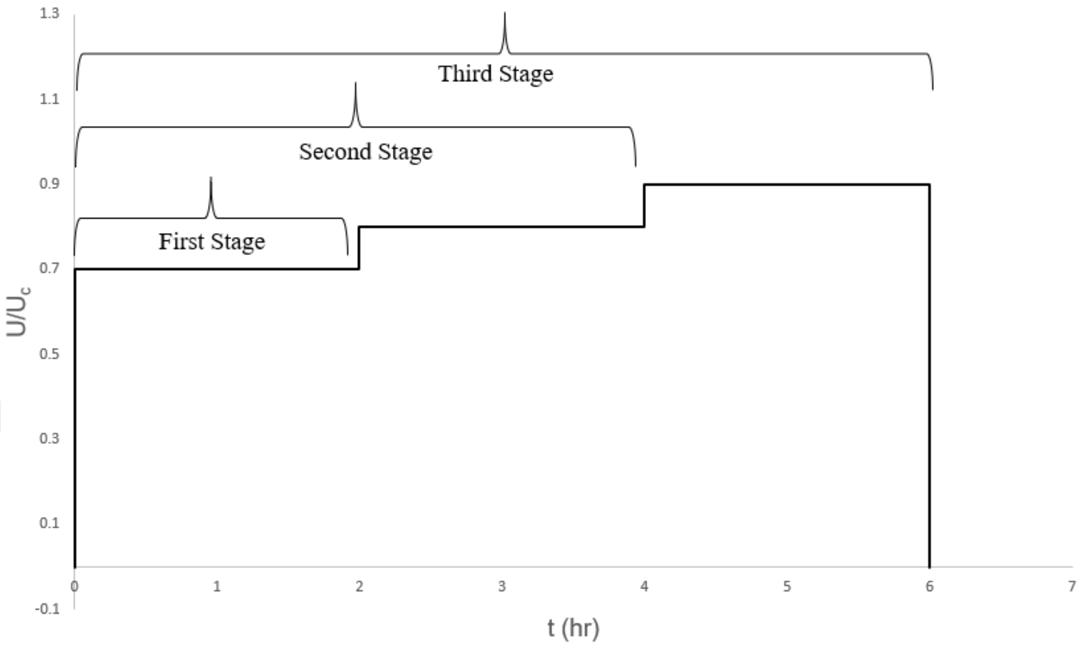

Figure 5.1 Stepwise hydrograph used in the experiments with the divided stages

5.6 Analysis and Discussion of the Experimental Results

This section analyzes and discusses the scour reduction performances of collars around semi-circular end and rectangular bridge abutments with varying lengths and flow intensities under unsteady-state clear-water flow conditions. A sample of the related data is provided in Appendix B.

As it was mentioned in the previous section, 3 different semi-circular end and rectangular bridge abutments of lengths L_a=20 cm, 30 cm and 40 cm were tested with 3 different collar widths of B_c=5 cm, 7.5 cm and 10 cm that were placed at 3 different elevations on the abutments, $Z_c/y_{0.7}$= -0.50, 0.25, ±0.00, relative to the bed level. However, the collars placed at the elevation of $Z_c/y_{0.7}$= -0.50 for the abutment of length, L_a=20 cm was not tested along the experiments since the obtained dimensionless maximum scour depths for the abutment of length L_a=20 cm were smaller than the elevation of $Z_c/y_{0.7}$= -0.50, which is obtained as ineffective for scour reduction. Within the scope of the study, 162 experiments, 18 of them without collars, were conducted with constant discharge and decreasing flow depth (increasing flow velocity and intensity) by applying a step-wise hydrograph for 6 hours with collars to investigate the performances of collars as a scour countermeasure for various flow intensities, abutment lengths, collar widths and locations.

5.6.1 Semi-Circular End Bridge Abutments

5.6.1.1 The Abutment of Length L_a= 40 cm

At the end of the first stage of the experiments with the flow intensity of 0.7, it can be clearly seen in Figure 5.2 that the maximum scour reductions were observed when the collar was located at an elevation of $Z_c/y_{0.7} = \pm 0.00$ for all the collar widths tested. At an elevation of $Z_c/y_{0.7} = \pm 0.00$, the best collar performance was observed for the collar of B_c=10 cm. On the other hand, it was also observed that as the collar width is decreased to B_c=5 cm and 7.5 cm, scour reduction efficiencies of the collars decreases. Although the performances of the collars of B_c=5 cm and 7.5 cm were similar to each other, the collar of B_c=7.5 cm gave more successful results on shifting the maximum scour depth towards the downstream side of the abutment. Moreover, when the collars were located below the bed level at an elevation of $Z_c/y_{0.7}$ =-0.25, the efficiency of the collar decreased by around 30% when compared to the collar located at an elevation of $Z_c/y_{0.7} = \pm 0.00$. At this elevation, the scour reduction efficiencies of all the collar widths were approximately obtained the same. For the first stage of the experiments, the worst collar performances were obtained when the collar was located at an elevation of $Z_c/y_{0.7}$ = -0.50. Since the scour formation did not penetrate into that level, the attachment of a collar only reduced the maximum scour depth by around 10%.

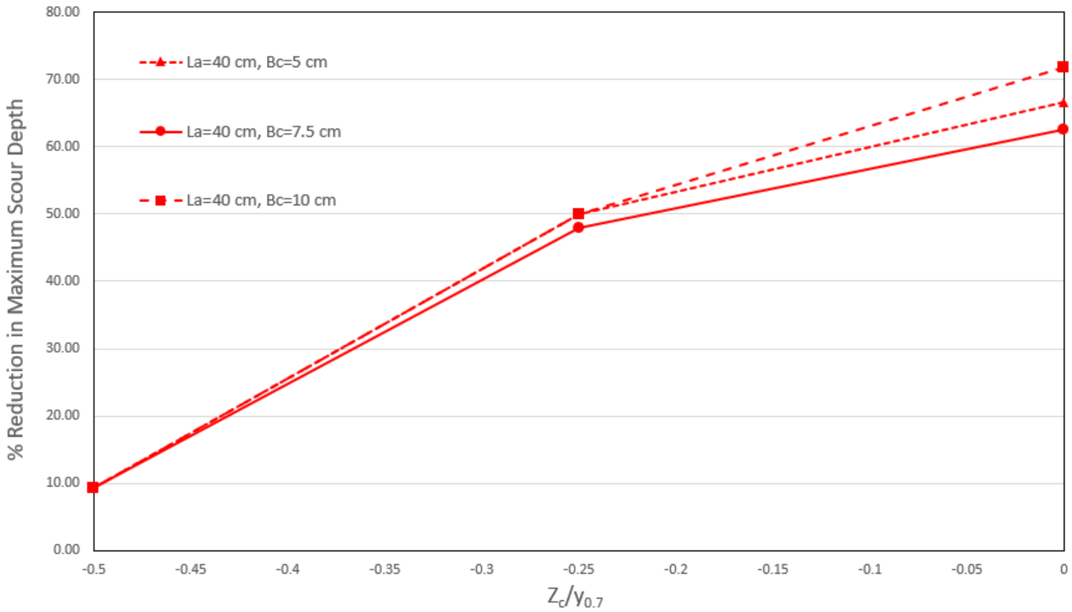

Figure 5.2 Effect of collar size and elevation on the maximum scour depth around the semi-circular end abutment of length L_a=40 cm (t= 2 hours)

At the end of the second stage of the experiments, the best collar performance was obtained at the elevation of $Z_c/y_{0.7} = \pm 0.00$ for the collar of B_c=10 cm which can be seen in Figure 5.3. On the other hand, the scour reduction efficiency of the collar of B_c=10 cm gradually decreased as the collar was placed below the bed level. Furthermore, the efficiency of the collar of B_c=10 cm at the elevation of $Z_c/y_{0.7} = -0.50$ reduced in half when compared to the $Z_c/y_{0.7} = \pm 0.00$. As it can be seen in Figure 5.3, the scour reduction performance of the collar of B_c=7.5 cm had similar trends with the collar of B_c=10 cm, however, the scour reduction performance of the collar of B_c=7.5 cm was smaller than the collar of B_c=10 cm. Despite the worst collar performance was obtained for the collar of B_c=5 cm at the elevation of $Z_c/y_{0.7} = 0.00$, the scour reduction efficiency of the collar of B_c=5 cm was approximately the same at the collar elevations of $Z_c/y_{0.7} = -0.5$ and $Z_c/y_{0.7} = \pm 0.00$ along with the performance of the collar of B_c=7.5 cm.

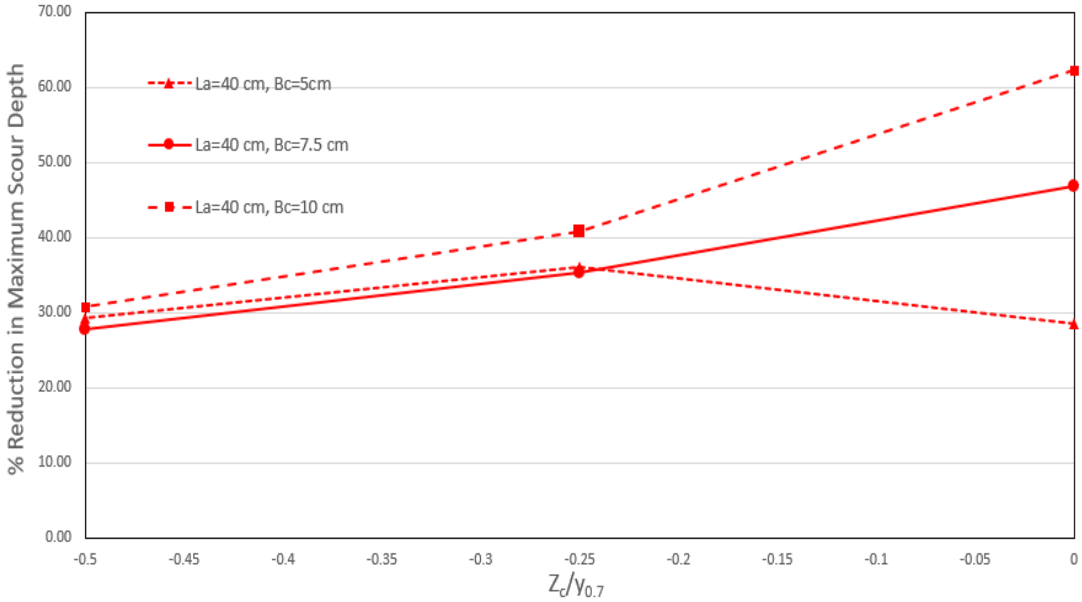

Figure 5.3 Effect of collar size and elevation on the maximum scour depth around the semi-circular end abutment of length L_a=40 cm (t= 4 hours)

Finally, at the end of the third stage of the experiments, the maximum scour reduction was observed for the collar of B_c=10 cm at the elevation of $Z_c/y_{0.7} = \pm 0.00$, on the other hand, the worst collar performance was obtained for the collar of B_c=5 cm at the elevations of $Z_c/y_{0.7} = -0.25$ and $Z_c/y_{0.7} = \pm 0.00$ (Figure 5.4). In addition, the biggest collar width, B_c=10 cm had better efficiency in reducing the maximum scour depth at all the collar elevations when compared to the collars of B_c= 5 cm and 7.5 cm. At the elevations of $Z_c/y_{0.7} = -0.25$ and $Z_c/y_{0.7} = \pm 0.00$, it was observed that the performances of collars dramatically decrease as the collar width decreases to 5 and 7.5 cm. Nevertheless, it was also observed that the scour reduction efficiencies of all collar widths did not show significant differences at the elevation of $Z_c/y_{0.7} = -0.50$.

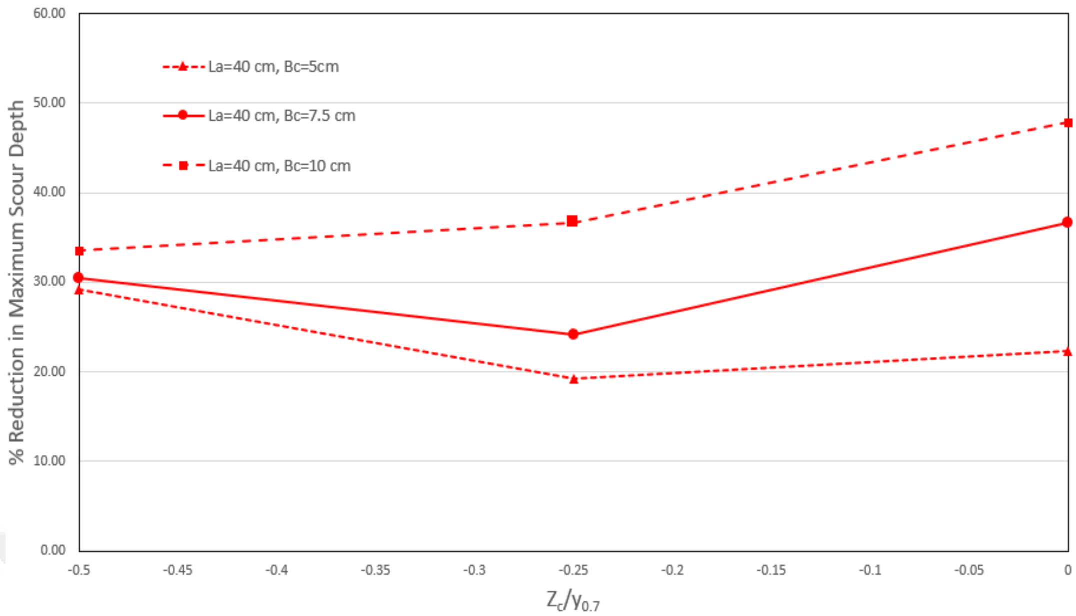

Figure 5.4 Effect of collar size and elevation on the maximum scour depth around the semi-circular end abutment of length L_a=40 cm (t= 6 hours)

Figures 5.5- 5.7 show the effect of collar size and flow intensity on the maximum scour depth around the semi-circular end abutments. At the elevations of $Z_c/y_{0.7}$= -0.25 and ±0.00, the scour reduction performances of the collars dramatically decreased as the flow intensity and the test duration increased. On the other hand, at the elevation of $Z_c/y_{0.7}$= -0.50, the scour reduction performances of the collars increased with increasing time and flow intensity. During the first and second stages of the experiments with the flow intensities of 0.7 and 0.8, the degradation of the bed material around the abutment did not reach the elevation of $Z_c/y_{0.7}$= -0.50. Hence, during these stages, the collars were placed at $Z_c/y_{0.7}$= -0.50 did not show a significant effect in reducing the maximum scour depths while the collars at the elevations of $Z_c/y_{0.7}$= -0.25 and ±0.00 were effective to reduce the maximum scour depth during the first and second stages of the experiment due to the smaller scour depths obtained during these stages.

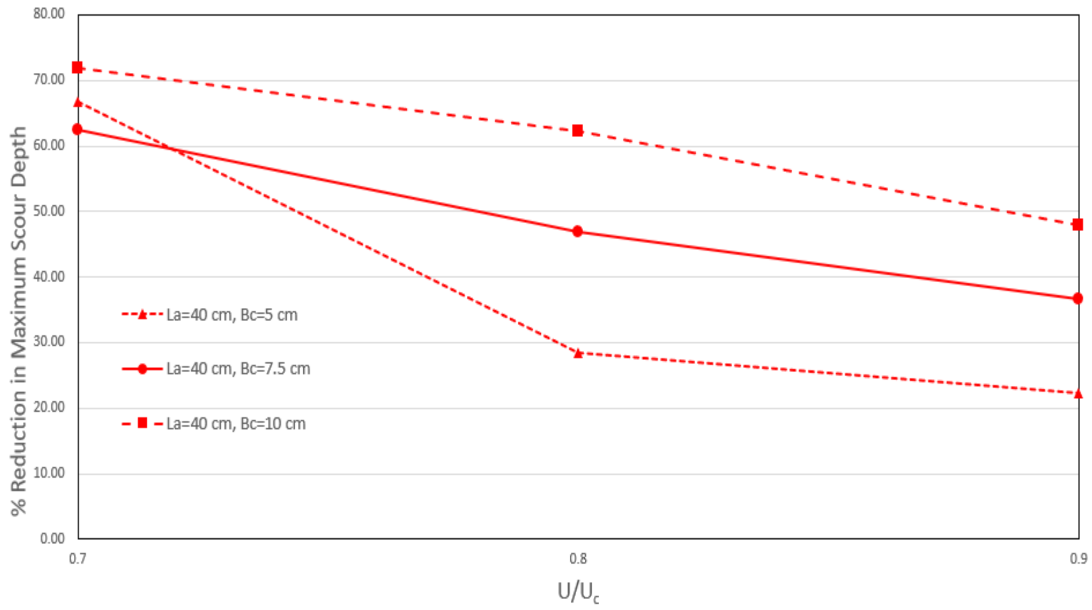

Figure 5.5 Effect of collar size and flow intensity on the maximum scour depth around the semi-circular end abutment of length L_a=40 cm for $Z_c/y_{0.7}$= ±0.00

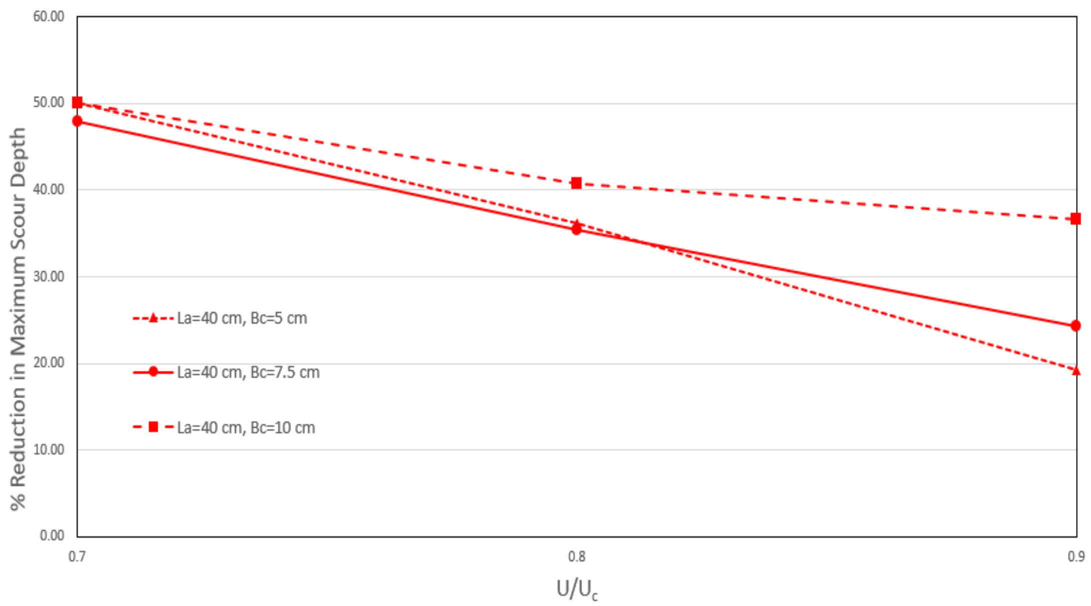

Figure 5.6 Effect of collar size and flow intensity on the maximum scour depth around the semi-circular end abutment of length L_a=40 cm for $Z_c/y_{0.7}$= -0.25

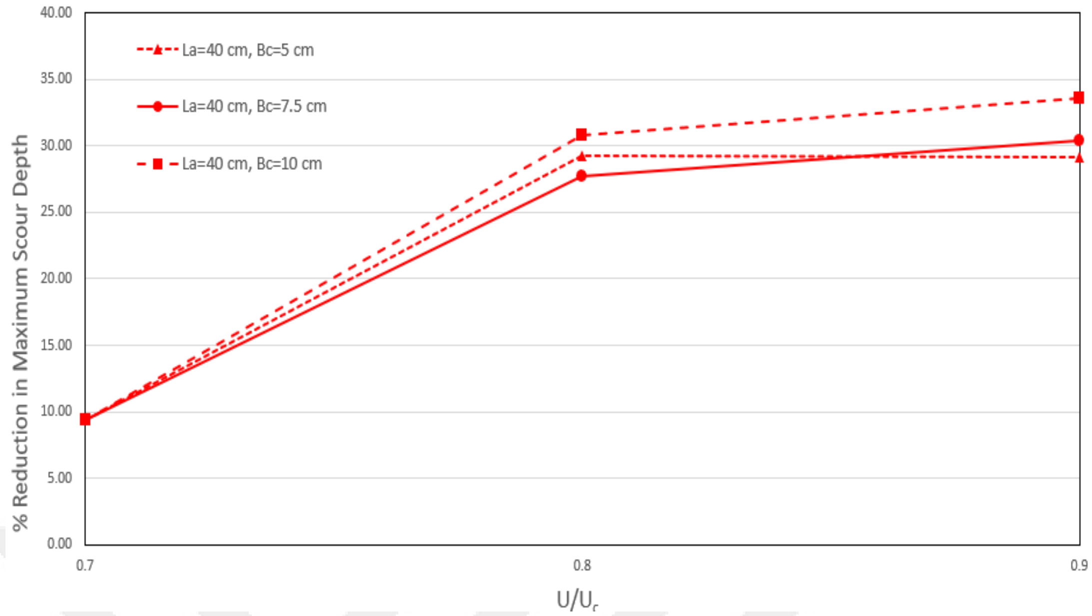

Figure 5.7 Effect of collar size and flow intensity on the maximum scour depth around the semi-circular end abutment of length L_a=40 cm for $Z_c/y_{0.7}$= -0.50

In addition, the variation of the dimensionless maximum scour depths with dimensionless time without and with collars around the abutment is shown in Figure 5.8. Based on the experimental results, the minimum scour depths were obtained for the abutment of length L_a=40 cm when the collar of B_c=10 cm was placed at the elevation of $Z_c/y_{0.7}$= ±0.00 through the experiments. On the other hand, the maximum scour depths were obtained for the collar of B_c=5 cm at the elevation of $Z_c/y_{0.7}$= -0.50, B_c=5 cm at the elevation of $Z_c/y_{0.7}$= ±0.00 and $Z_c/y_{0.7}$= -0.25 at the end of the first, second and third stages of the experiments, respectively.

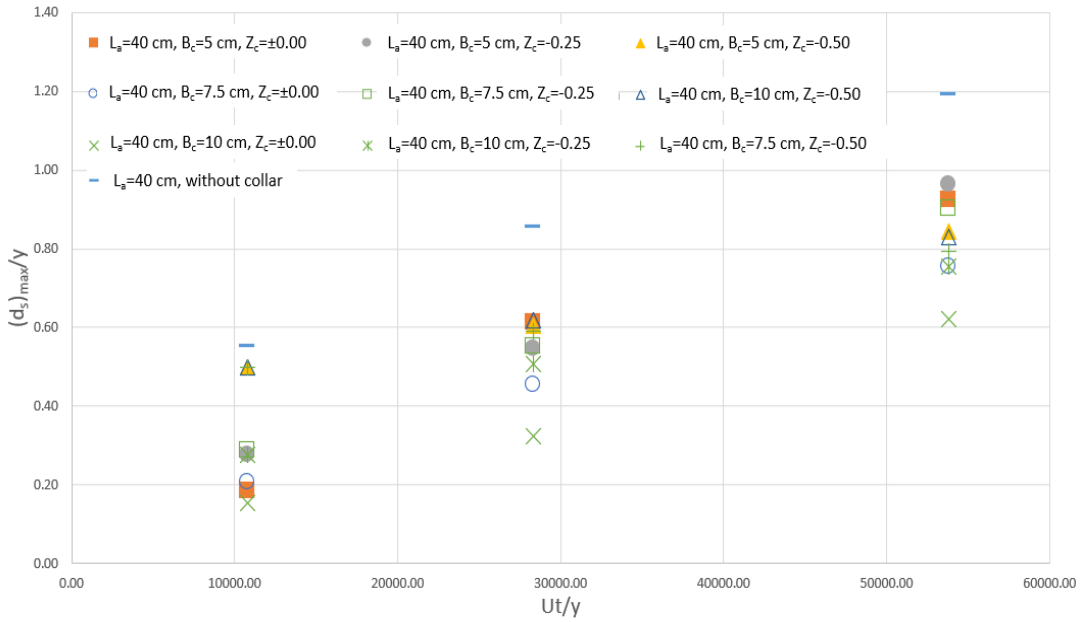

Figure 5.8 Variation of the dimensionless maximum scour depth with dimensionless time as a function of collar size and elevation for semi-circular end abutment of length L_a=40 cm

5.6.1.2 The Abutment of Length L_a=30 cm

At the end of the first stage of the experiments, scour reduction efficiencies of the collars with varying widths and locations for the abutment of length L_a=30 cm are shown in Figure 5.9. The best collar performance was observed for the collar of B_c=10 cm at the elevation of $Z_c/y_{0.7}$= ±0.00. At this elevation, the scour reduction performances of the collars of B_c=5 and 7.5 cm are approximately similar to each other and smaller than the collar of B_c= 10 cm by around 35%. As the collar was placed below the bed level, the scour reduction efficiency of the collar decreased regardless of collar width. However, for the collar of B_c=10 cm, the decrease was obtained greater than the collars of B_c=5 cm and 7.5 cm. At the elevation of $Z_c/y_{0.7}$= -0.25, the scour reduction performances of the collars of B_c=7.5 and 10 cm were observed as equal to each other and the collar of B_c=5 cm was smaller. On the other hand, at the elevation of $Z_c/y_{0.7}$= -0.50, the collars almost did not show a significant effect in reducing the maximum scour depth. However, it should also be indicated that all the maximum scour depths were obtained above the collar level of $Z_c/y_{0.7}$= -0.50 and the scour formation did not penetrate below the collar. This situation explains the low efficiencies of the collars at the elevation of $Z_c/y_{0.7}$= -0.50 regardless of the collar width.

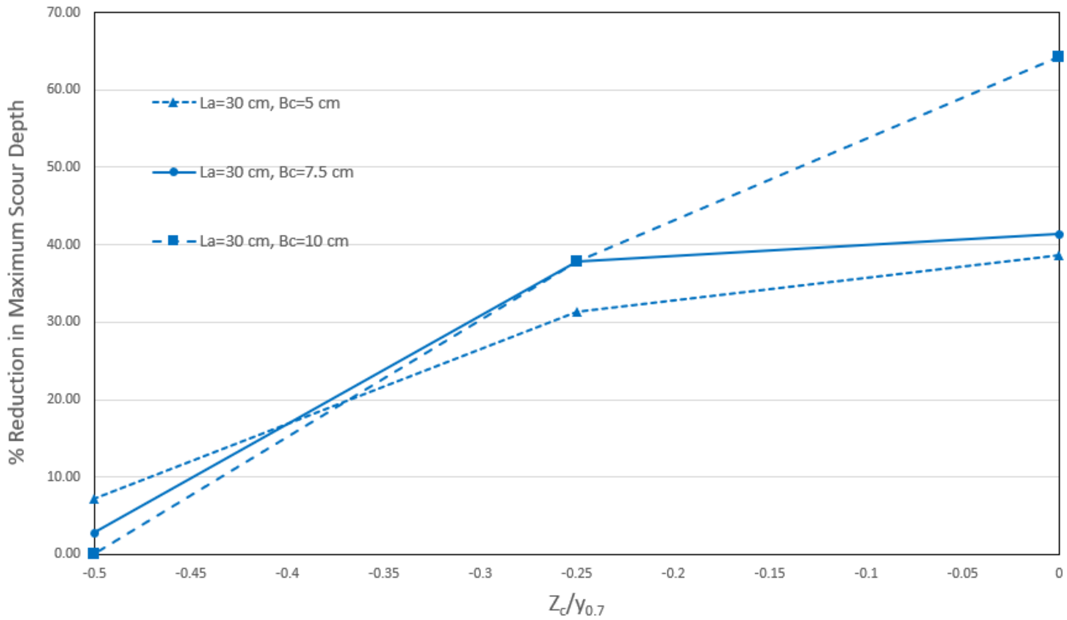

Figure 5.9 Effect of collar size and elevation on the maximum scour depth around the semi-circular end abutment of length L_a=30 cm (t= 2 hours)

At the end of the second stage, the maximum scour reduction was obtained for the collar of B_c= 10 cm at the elevation of $Z_c/y_{0.7}$= ±0.00 (Figure 5.10). The scour reduction efficiencies of the collars decreased as the collar width decreased and smaller scour reduction efficiencies were observed for the collars of B_c=5 and 7.5 cm. When the collar was placed at the elevation of $Z_c/y_{0.7}$= -0.25, the performances of the collars were decreased, but the scour reduction efficiencies of the collars were similar to each other regardless of collar width. Nevertheless, at this elevation, the maximum scour reduction was obtained for the collar of B_c=7.5 cm. Finally, the collars were tested at the elevation of $Z_c/y_{0.7}$= -0.50 and similar results were obtained as well as the first stage. At this time, the maximum scour depths were obtained for the collars of B_c=5 cm and 7.5 cm and the scour reduction efficiencies of these collars were almost insignificant. On the other hand, the best collar performance seemed for the collar of B_c=10 cm at the elevation of $Z_c/y_{0.7}$= -0.50.

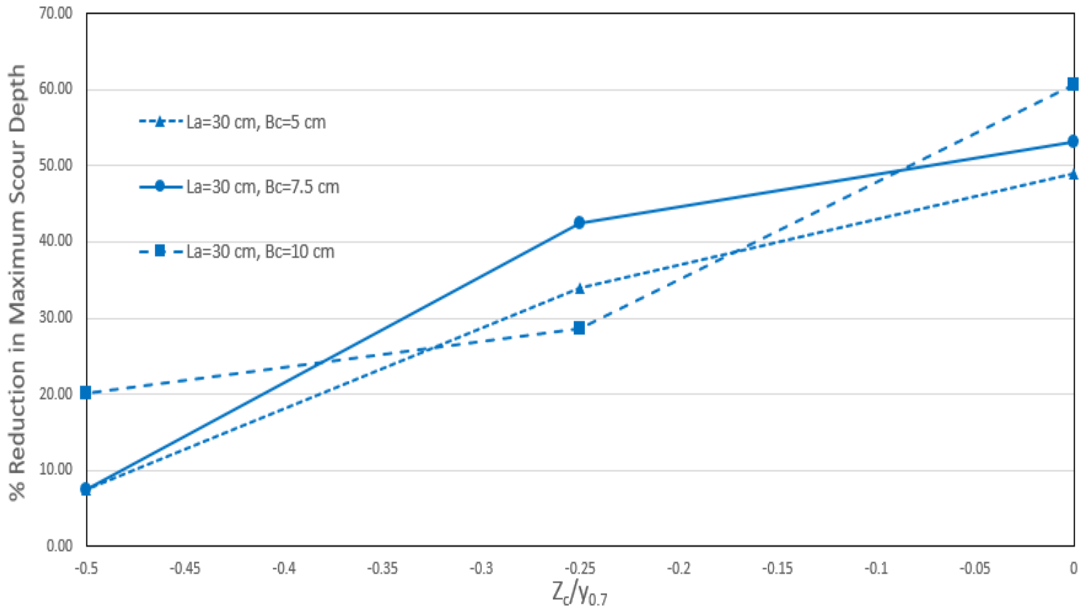

Figure 5.10 Effect of collar size and elevation on the maximum scour depth around the semi-circular end abutment of length L_a=30 cm (t=4 hours)

As it can be seen in Figure 5.11, the best collar performance in reducing the maximum scour depth was obtained for the collar of B_c=10 cm at the elevation of $Z_c/y_{0.7}$= ±0.00. The scour reduction efficiencies of the collars of B_c=5 and 7.5 cm were obtained smaller than that of B_c=10 cm at this elevation. However, the performance of the collar of B_c=10 cm dramatically decreased when the collar was placed at elevations below the bed level. The scour reduction efficiency of the collar of B_c=10 cm decreased by about half at the elevation of $Z_c/y_{0.7}$= -0.50 when compared to $Z_c/y_{0.7}$= ±0.00. Although, the performances of the collars in terms of reduction of the maximum scour depth were similar regardless of collar width when the collars were placed at the elevations of $Z_c/y_{0.7}$= -0.50 and -0.25, the increased collar width led to the occurrence of the maximum scour depth away from the abutment toe. In other words, as the collar width increased, the maximum scour depth shifted downstream of the abutment.

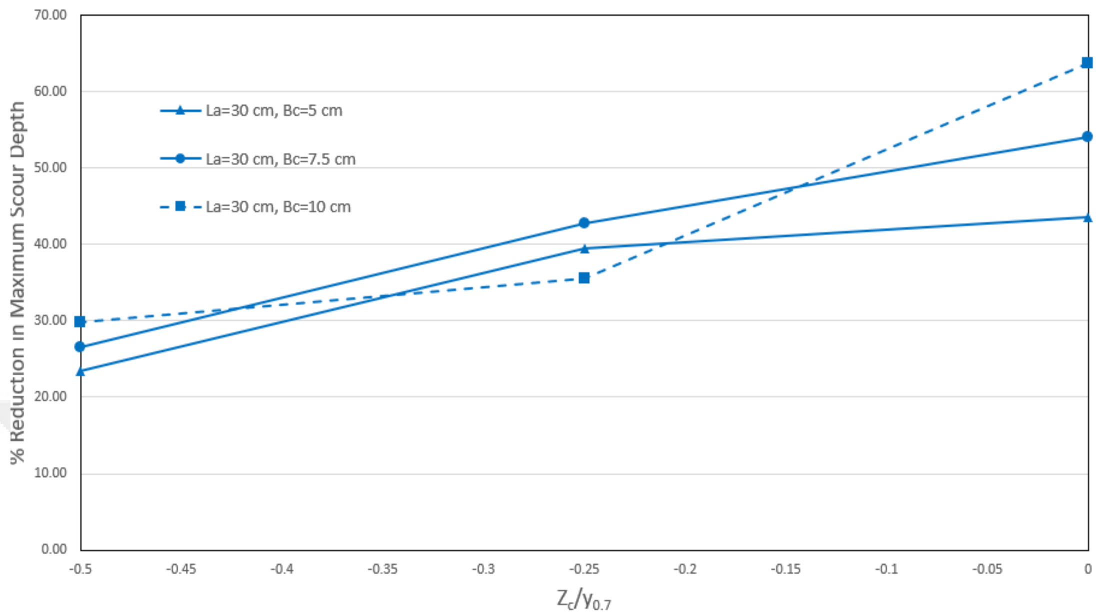

Figure 5.11 Effect of collar size and elevation on the maximum scour depth around the semi-circular end abutment of length L_a=30 cm (t=6 hours)

Figures 5.12- 5.14 show the effect of collar size and flow intensity on the maximum scour depth around the semi-circular end abutments. When collars were placed at the elevation of $Z_c/y_{0.7}$=±0.00, the scour reduction performance of the collar of B_c=10 cm was approximately the same until the end of the experiments regardless of the flow intensity. Moreover, the performances of the collars of B_c=5 and 7.5 cm slightly increased with increased flow intensity from 0.7 to 0.8, and then while the data of B_c=7.5 cm was having the same trend for the zone of U/U_c between 0.8 and 0.9, the data of B_c=5 cm showed a slightly decreasing trend. On the other hand, at the elevation of $Z_c/y_{0.7}$= -0.25, the scour reduction performances of the collars did not show significant alterations with increasing flow intensity. Finally, the worst scour reduction efficiencies of the collars were observed when the collars were placed at the elevation of $Z_c/y_{0.7}$= -0.50. At this elevation, during the first stage of the experiments, the maximum scour reductions were almost insignificant. At the end of the second stage, only the collar of B_c=10 cm showed efficiency in reducing the maximum scour depth. Nonetheless, all collar widths showed successful results in terms of maximum scour reduction at the end of the third stage due to the greater scour depths caused by increasing flow intensity and time. In other words, the collars were placed at the elevation of $Z_c/y_{0.7}$= -0.50 starts to interact with the flow and manipulate it as the degradation run out deeper around the abutment. So, collars that were located below the bed level were found as effective for the greater scour depths.

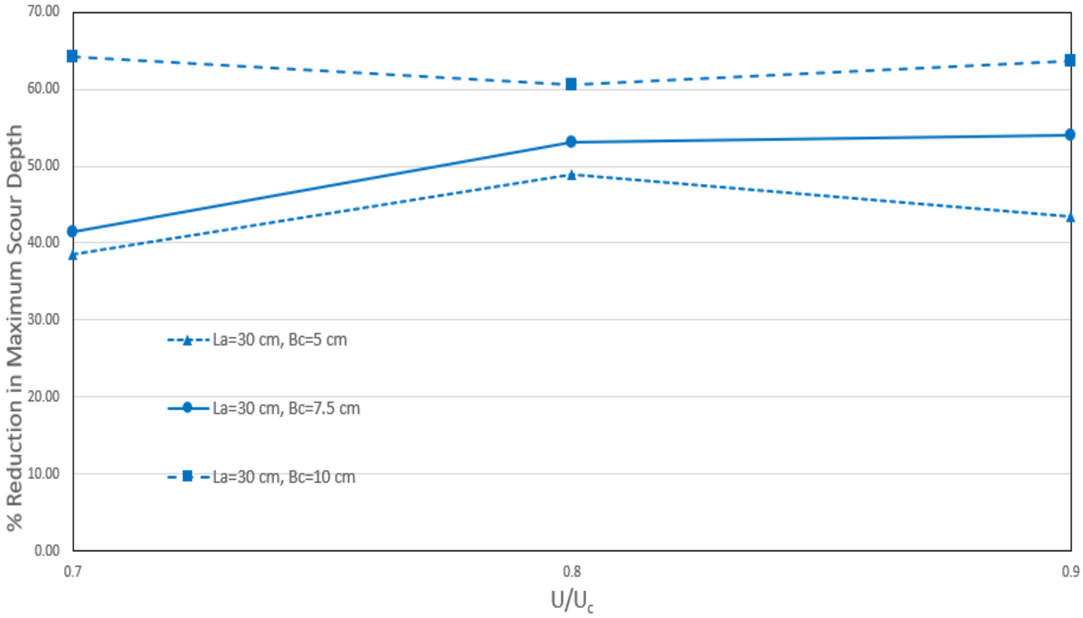

Figure 5.12 Effect of collar size and flow intensity on the maximum scour depth around the semi-circular end abutment of length L_a=30 cm for $Z_c/y_{0.7}$= ±0.00

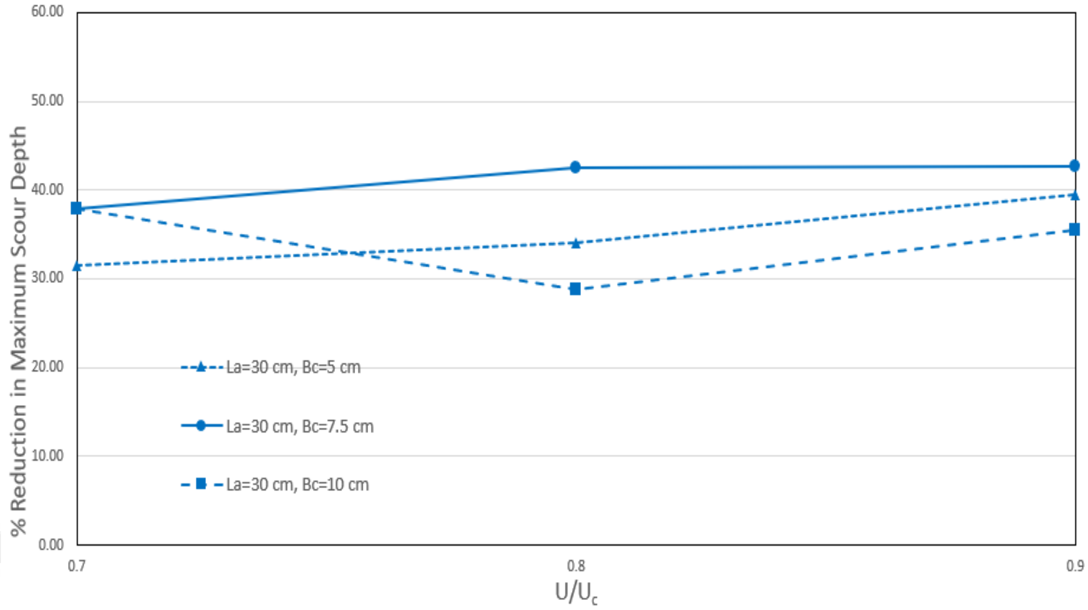

Figure 5.13 Effect of collar size and flow intensity on the maximum scour depth around the semi-circular end abutment of length L_a=30 cm for $Z_c/y_{0.7}$= -0.25

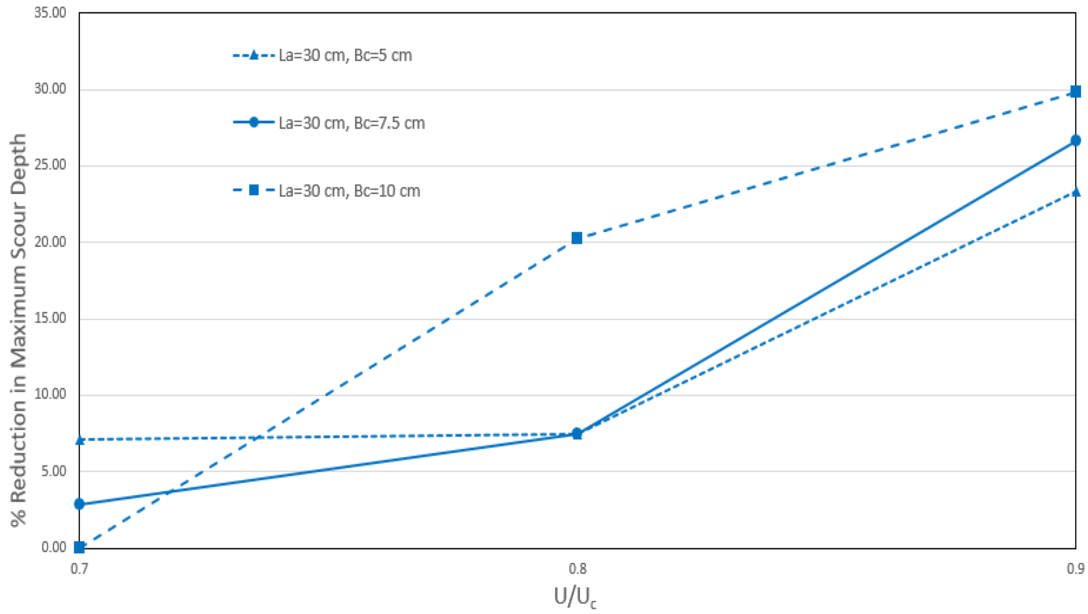

Figure 5.14 Effect of collar size and flow intensity on the maximum scour depth around the semi-circular end abutment of length L_a=30 cm for $Z_c/y_{0.7}$= -0.50

Also, the variation of the dimensionless maximum scour depths with dimensionless time without and with collars around the abutment is shown in Figure 5.15. For the abutment of length L_a=30 cm, the minimum scour depth was generally recorded when the collars of B_c=10 cm were placed at the elevation of $Z_c/y_{0.7}$= ±0.00 through the experiments. On the other hand, the maximum scour depths were obtained when the collars were placed at the elevation of $Z_c/y_{0.7}$= -0.50 regardless of the collar width.

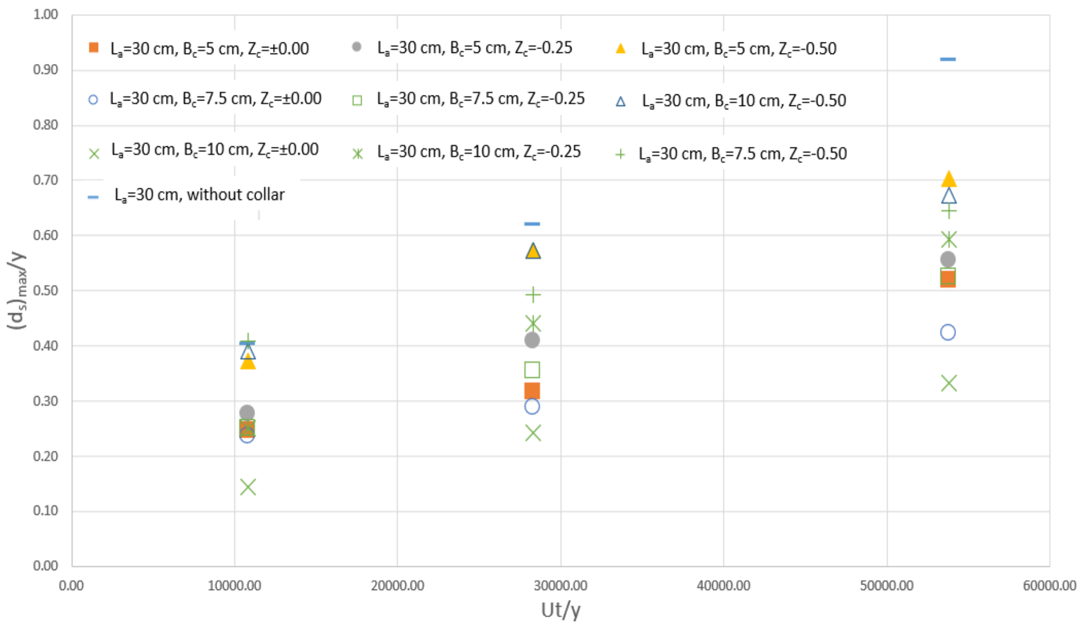

Figure 5.15 Variation of the dimensionless maximum scour depth with dimensionless time as a function of collar size and elevation for semi-circular end abutment of length L_a=30 cm

5.6.1.3 The Abutment of Length L_a=20 cm

The effect of collar size and elevation on the maximum scour depth around the semi-circular end abutment of length L_a=20 cm is shown in Figures 5.16-5.18. At the end of the first stage of the experiments, the best collar performances were observed for the collar of B_c=10 cm at the elevation of $Z_c/y_{0.7}$= ±0.00. Then, the collars of B_c=7.5 and 5 cm at the elevation of $Z_c/y_{0.7}$= ±0.00 followed it, respectively. In other words, as the collar width increased the scour reduction efficiencies of the collars were increased. On the other hand, collars were placed at the elevation of $Z_c/y_{0.7}$= -0.25

were ineffective to reduce the maximum scour depth during the first stage of the experiments. Since the shorter abutment lengths cause smaller scour depths around the abutment, the scour formation around the abutment of length L_a=20 cm at the end of 2 hours, did not reach the level of collar elevation of $Z_c/y_{0.7}$= -0.25. At the end of the second stage of the experiments, the maximum scour reductions were obtained for the collars of B_c=5, 7.5 and 10 cm at the elevation of $Z_c/y_{0.7}$= ±0.00. At this time, collars of B_c= 7.5 and 10 cm at the elevation of $Z_c/y_{0.7}$= -0.25 showed significant efficiencies in reducing the maximum scour depth. However, the collar of B_c=5 cm at the elevation of $Z_c/y_{0.7}$= -0.25 was ineffective in reducing the scour depth. Finally, at the end of the third stage, the best collar performances were obtained for the collars of B_c=7.5 and 10 cm at the elevation of $Z_c/y_{0.7}$= ±0.00. When the collars were placed at the elevation of $Z_c/y_{0.7}$= -0.25, the scour reduction performances of the collars slightly decreased compared to those placed at the elevation of $Z_c/y_{0.7}$= ±0.00. Nevertheless, the collars were still effective at this level. Although the performances of the collars of B_c=5 cm, 7.5 cm and 10 cm were similar to each other at $Z_c/y_{0.7}$= -0.25, the largest collar of B_c=10 cm gave the most successful results once again.

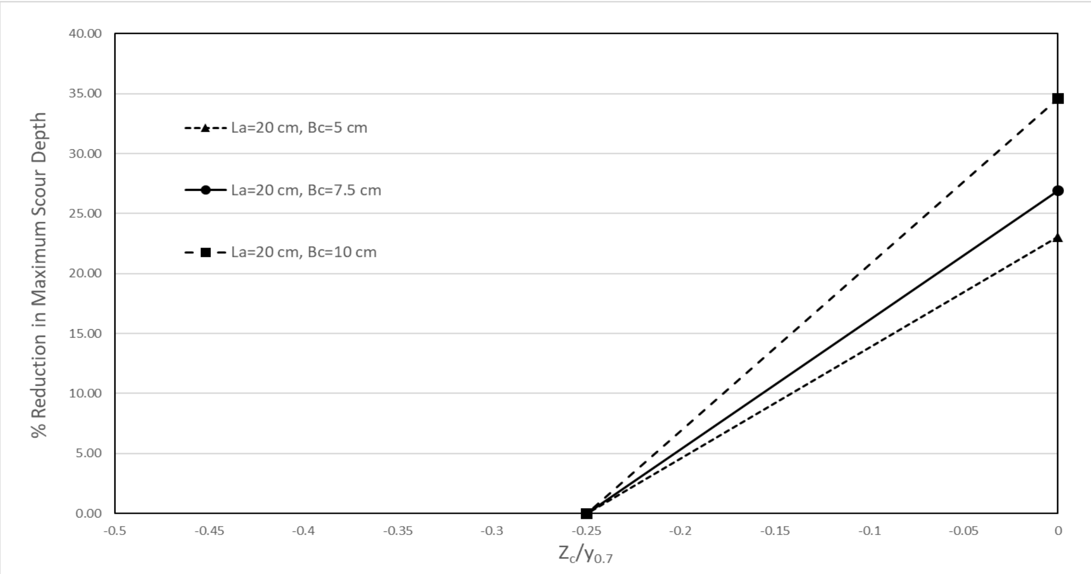

Figure 5.16 Effect of collar size and elevation on the maximum scour depth around the semi-circular abutment end of length L_a=20 cm (t=2 hours)

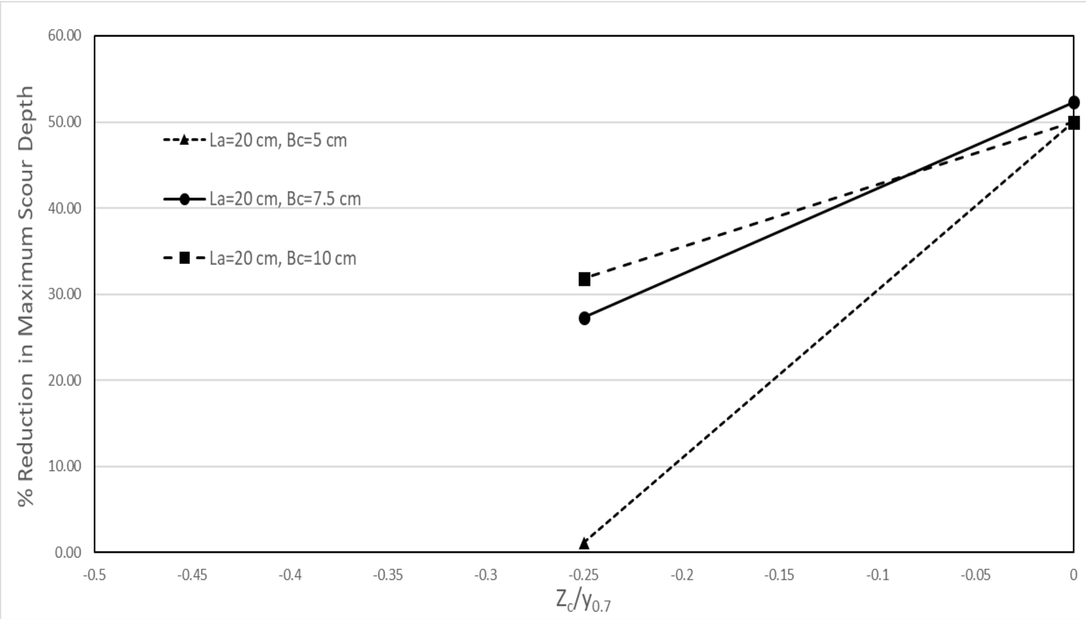

Figure 5.17 Effect of collar size and elevation on the maximum scour depth around the semi-circular end abutment of length L_a=20 cm (t=4 hours)

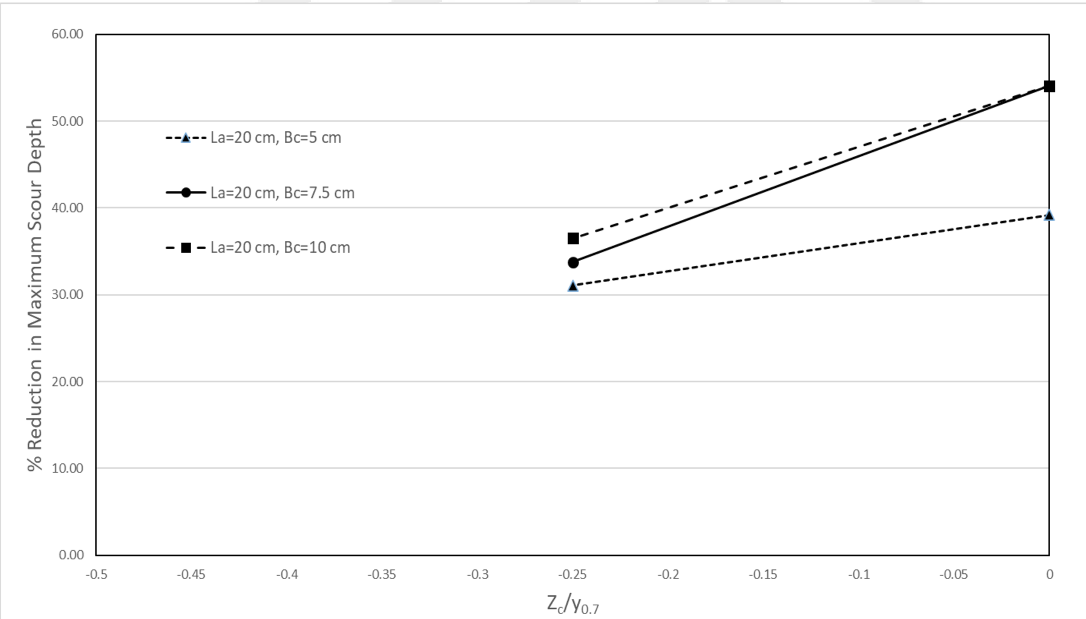

Figure 5.18 Effect of collar size and elevation on the maximum scour depth around the semi-circular end abutment of length L_a=20 cm (t=6 hours)

The effect of collar size and flow intensity on the maximum scour depth around the semi-circular end abutment of length L_a=20 cm is shown in Figures 5.19 and 5.20.

When collars were placed at the elevation of $Z_c/y_{0.7}$=±0.00, the scour reduction performances of the collars generally increased with increasing flow intensity. However, at the end of the third stage, the scour reduction performance of the collar of B_c=5 cm decreased a little bit. On the other hand, at the elevation of $Z_c/y_{0.7}$= -0.25, the scour reduction performances of the collars increased with increasing flow intensity as well as the collars were placed at the elevation of $Z_c/y_{0.7}$= -0.25. However, at this elevation, the collar of B_c=5 cm was ineffective in reducing the maximum scour depth during the first and second stages of the experiments. The scour reduction performance of the collar of B_c=5 cm dramatically increased during the third stage of the experiment and performances of the collars were observed as similar to each other at the end of the third stage regardless of collar width.

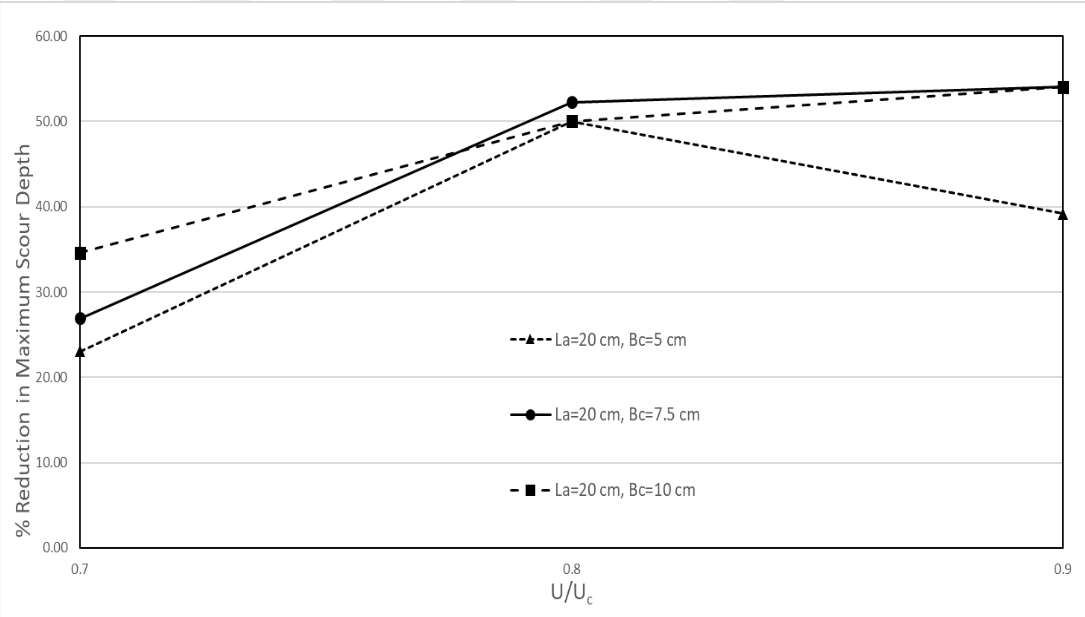

Figure 5.19 Effect of collar size and flow intensity on the maximum scour depth around the semi-circular end abutment of length L_a=20 cm for $Z_c/y_{0.7}$= ±0.00

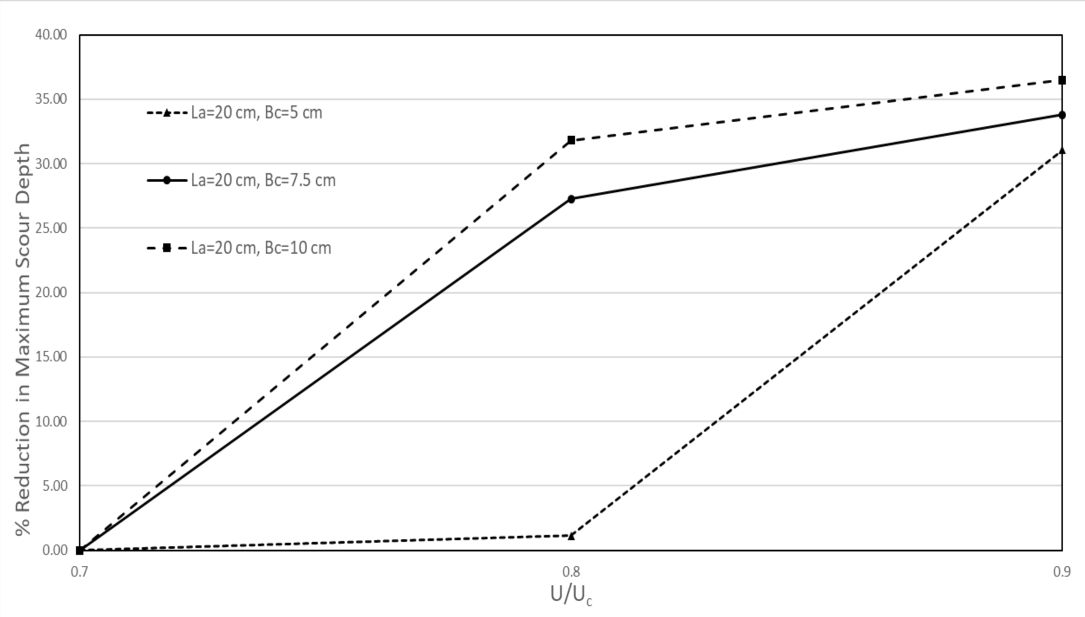

Figure 5.20 Effect of collar size and flow intensity on the maximum scour depth around the semi-circular end abutment of length L_a=20 cm for $Z_c/y_{0.7}$= -0.25

In addition, the variation of the dimensionless maximum scour depth with dimensionless time without and with collars around the abutment is shown in Figure 5.21. Based on the experimental results, the minimum scour depths were obtained for the abutment of length L_a=20 cm when the collars were placed at the elevation of $Z_c/y_{0.7}$= ±0.00 through the experiments. At this elevation, the dimensionless scour depth values of all collar widths were almost recorded close to each other at each stage of the experiments. On the contrary, the maximum scour depths were obtained for the collar of B_c=5 cm at the elevation of $Z_c/y_{0.7}$= -0.25 through the experiment. Furthermore, at the end of the first and second stages of the experiments, the measured maximum scour depths for the collar of B_c=5 cm that was tested at the elevation of $Z_c/y_{0.7}$= -0.25 were almost the same as the maximum scour depths obtained from the experiments that were conducted without a collar.

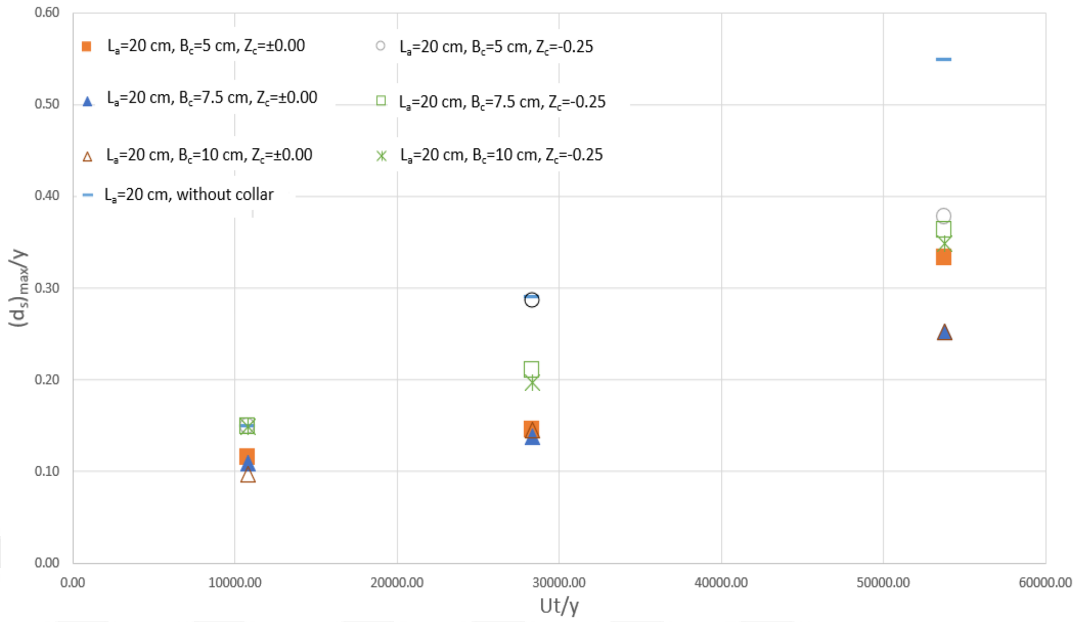

Figure 5.21 Variation of the dimensionless maximum scour depth with dimensionless time as a function of collar size and elevation for semi-circular end abutment of length L_a=20 cm

5.6.1.4 Summary

In summary, the efficiencies of the collars generally increased with increased collar size regardless of the abutment length, since the larger collars provide stronger protection to vortices and obtain smaller scour holes than those of smaller collars, it is more difficult to access strong vortices to deeper elevations. During the initial stages of the experiments, scour formation did not penetrate into the level of $Z_c/y_{0.7}$= -0.5 and -0.25, so those collars could not show significant effects in reducing the scour depth. Moreover, the scour reduction performances of the collars located at $Z_c/y_{0.7}$= -0.5 and -0.25 increased with increasing flow intensity and time due to the penetration of vortices to deeper locations that cause larger scour depths. Hence, the collars placed below the bed level would be efficient for circumstances having larger scour depth potentials such as higher flow intensity, time and abutment length.

In Figure 5.22-5.24, the effect of abutment length, collar size and elevation on the maximum scour depth around all the semi-circular end abutment lengths tested in this study is given. During the first stage of the experiments, the maximum scour reductions were obtained for the abutment of length L_a=40 cm at any collar elevation tested. Also, it can be said that the scour reduction efficiencies of the collars decreased as the abutment length decreased, especially for the collars placed at the elevations of $Z_c/y_{0.7}$= -0.25 and ±0.00. On the other hand, the scour reduction efficiencies of the collars placed at the elevation of $Z_c/y_{0.7}$= -0.50, around the abutments of lengths L_a=30 and 40 cm were close to each other and almost insignificant.

At the end of the second stage of the experiments, it can be stated that the collars started to be more efficient for the abutments of lengths L_a=20 and 30 cm when compared to the first stage of the experiments. When collars were placed at the elevation of $Z_c/y_{0.7}$= ±0.00, the best collar performances were obtained for the collar of B_c=10 cm that is attached to the abutments of lengths L_a=30 and 40 cm. At the elevation of $Z_c/y_{0.7}$= -0.25, it is hard to make any comments on the effect of abutment length and collar size on the scour reduction performances of the collars, because the related data points are quite close to each other. Finally, at the elevation of $Z_c/y_{0.7}$= -0.50, the collar performance increased as the abutment length increased as well as the first stage of the experiments. The abutment of length L_a=40 cm gave the best scour reduction efficiencies with almost all the collar sizes, except the collar of B_c=5 cm at the elevation of $Z_c/y_{0.7}$= ±0.00, tested among the other abutment lengths at any collar elevations.

At the end of the third stage of the experiments, the best collar performances in reducing the scour depths were obtained for the abutment of length L_a=30 cm regardless of the collar size and the worst ones were obtained for the abutment of length L_a=40 cm. However, when the collars were placed at the elevation of $Z_c/y_{0.7}$= -0.50, the performances of the collars were better for the abutment of length L_a=40 cm than the L_a=30 cm as well as the first and second stages of the experiments.

In conclusion, it can be stated that at low flow intensity cases (t=2 hours) the longest abutment, L_a=40 cm, with the largest collar size, B_c=10 cm, gives the maximum scour reduction as 72% at the collar elevation of $Z_c/y_{0.7}$= ±0.00. As the value of $Z_c/y_{0.7}$ gets smaller, -0.25 and then -0.50, the corresponding maximum scour reductions decrease. The best collar location regarding the maximum scour reduction is still the bed level, $Z_c/y_{0.7}$= ±0.00, when the flow intensity increased (t=4 hours and t= 6 hours). However, the long abutments are subject to more scour than the short ones, and therefore, the scour reduction efficiencies of the collars around the abutment of L_a=40 cm decreases compared to other abutment lengths tested as the flow intensity increases.

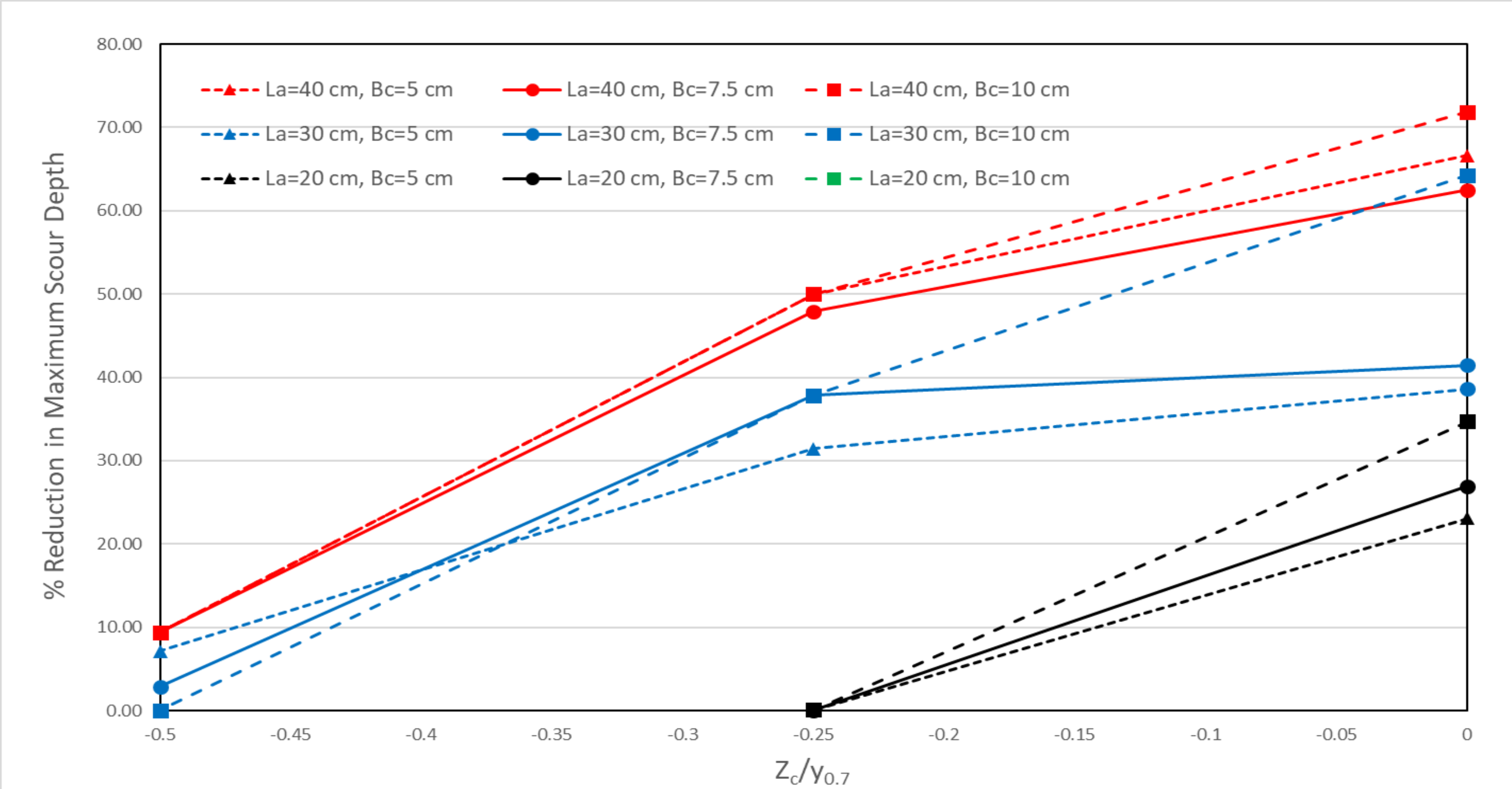

Figure 5.22 Effect of collar size and elevation on the maximum scour depth around the semi-circular end abutments (t=2 hours)

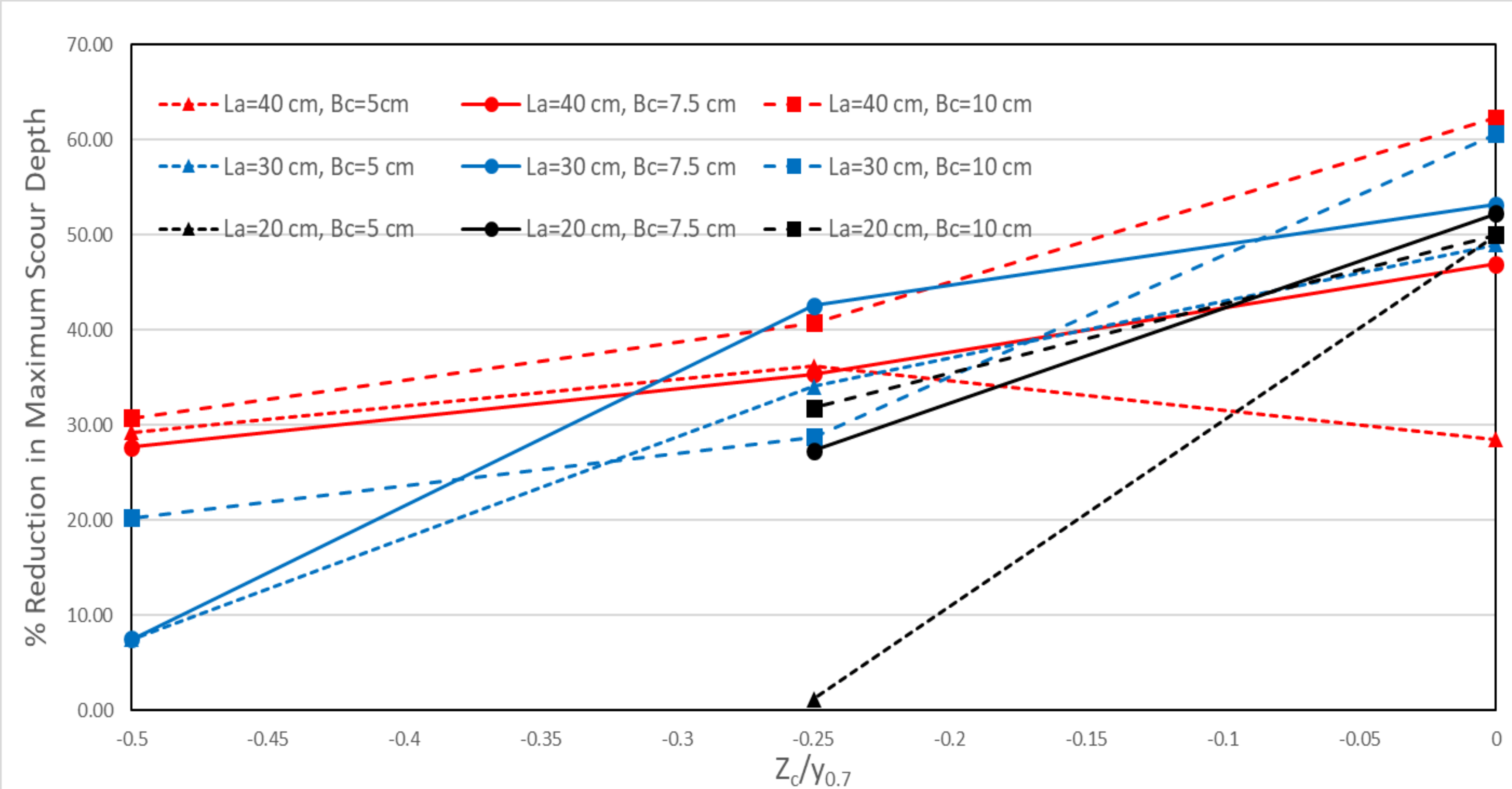

Figure 5.23 Effect of collar size and elevation on the maximum scour depth around the semi-circular end abutments (t=4 hours)

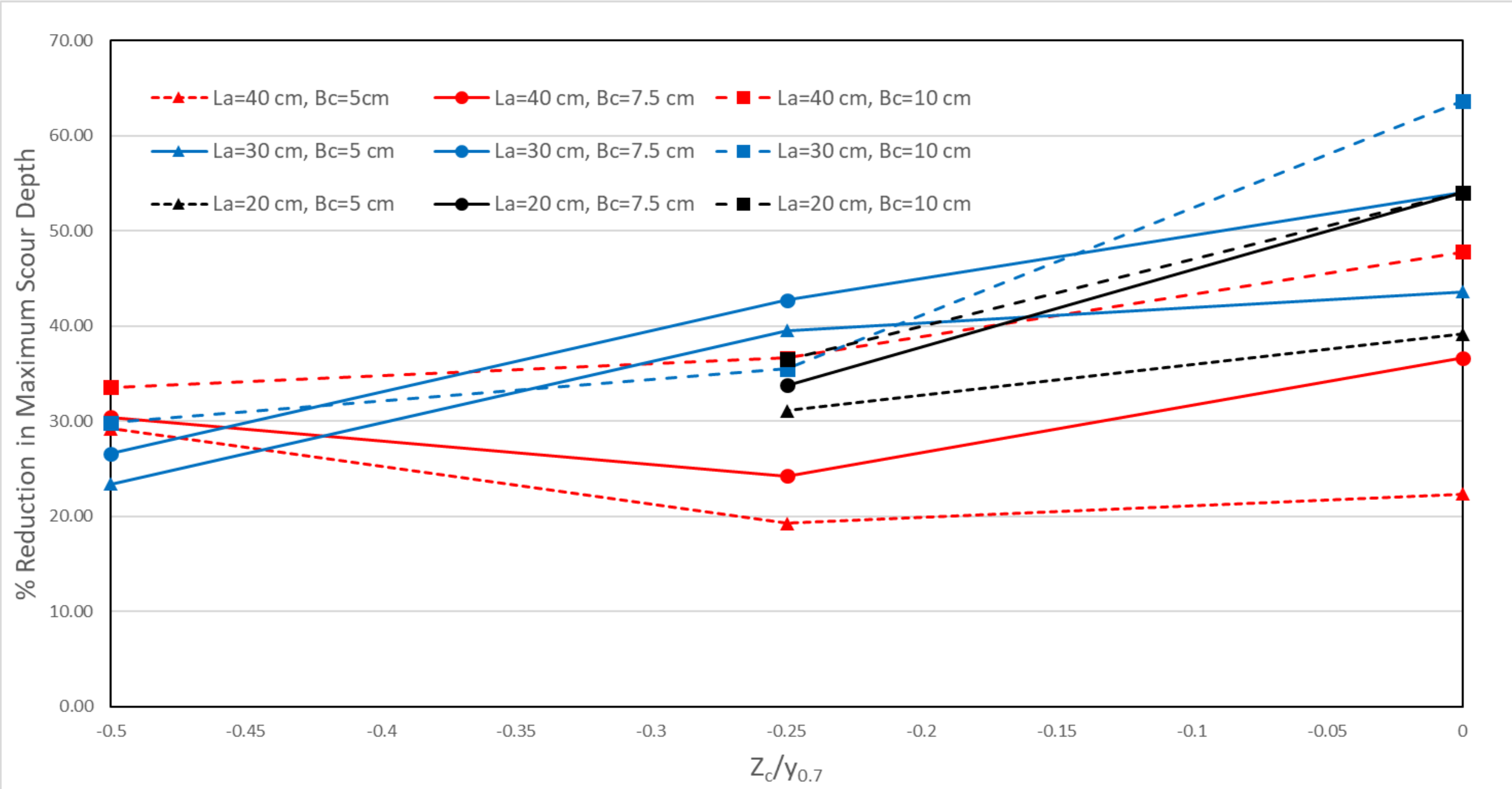

Figure 5.24 Effect of collar size and elevation on the maximum scour depth around the semi-circular end abutments (t=6 hours)

The effect of collar size and flow intensity on the maximum scour depth around all the semi-circular end abutment lengths tested in this study is presented in Figures 5.25-27. When collars were placed at the elevation of $Z_c/y_{0.7}$= ±0.00 except the zone of U/U_c between 0.7 and 0.8 for abutments of lengths L_a=20 cm and 30 cm the scour reduction performances of the collars for a given abutment length decrease with increasing U/U_c. At the end of the first stage of the experiment with the flow intensity of 0.7, the maximum scour reductions between 62.50-71.88% were observed for the abutment of length L_a=40 cm; on the other hand, at the end of the third stage of the experiment with the flow intensity of 0.9, much lower scour reductions between 22.36-47.83% were observed around the abutment of length L_a=40 cm for the collar sizes tested.

At the elevation of $Z_c/y_{0.7}$= -0.25, the scour reduction performances of the collars decreased for the abutment of length L_a=40 cm with increasing flow intensity. For the other abutment lengths tested it was observed that, in general, the scour reduction performances of the collars increased with increasing flow intensity. At the end of the first stage, the best collar performances were obtained for the abutment of length L_a=40 cm. However, at the end of the third stage, much lower collar performances were obtained for the abutment of length L_a=40 cm for a given collar size. Especially for the shortest abutment of length L_a=20 cm tested in this study, a dramatic increase was obtained in the collar performances, during the second and third stages of the experiments. Furthermore, the collar efficiency was better for the abutment of length L_a=20 cm when compared to L_a=40 cm during this period. The maximum scour reductions between 35.48-42.74% were observed at the end of the third stage for the abutment of length L_a=30 cm

When collars were tested at the elevation of $Z_c/y_{0.7}$= -0.50, the scour reduction performances of the collars attached to the abutment of length L_a=40 cm was better than the abutment of length L_a=30 cm for a given collar size during the experiments. However, as the scour depths increased with increasing flow intensity and time, the scour reduction performances of the collars attached to the abutment lengths of

L_a=30 and 40 cm started to converge to each other. In other words, as the scouring rate increased, collars started to be more effective as the abutment length decreased. The ranges of the % reductions in maximum scour depths around the semi-circular end abutments tested in this study is given in Table 5.4 as a function of collar location, flow intensity and L_a/B_c values.

Table 5.4 The ranges of minimum and maximum % reductions in maximum scour depths around the semi-circular end abutments tested

$2.0 \leq L_a/B_c \leq 8.0$			
$Z_c/y_{0.7}$	t (hour)	U/U_c	The range of % reduction in maximum scour depth
±0.00	2	0.7	23.08 - 71.88
	4	0.8	28.46 - 62.31
	6	0.9	22.36 - 63.71
-0.25	2	0.7	0.00 - 50.00
	4	0.8	1.14 - 42.55
	6	0.9	19.25 - 42.74
-0.50	2	0.7	0.00 - 9.38
	4	0.8	7.45 - 30.77
	6	0.9	23.39 - 33.54

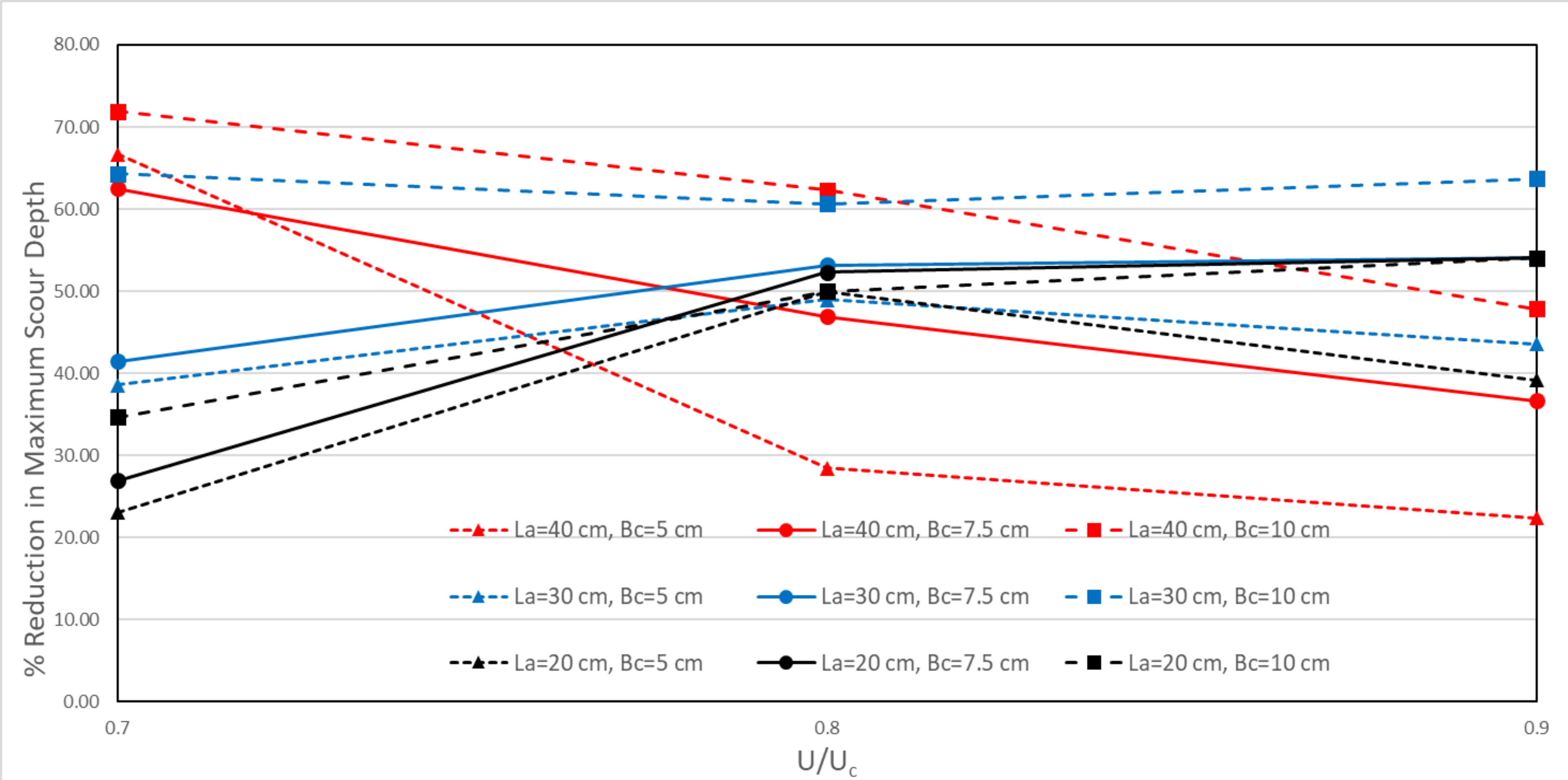

Figure 5.25 Effect of collar size and flow intensity on the maximum scour depth around the semi-circular end abutments for $Z_c/y_{0.7} = \pm 0.00$

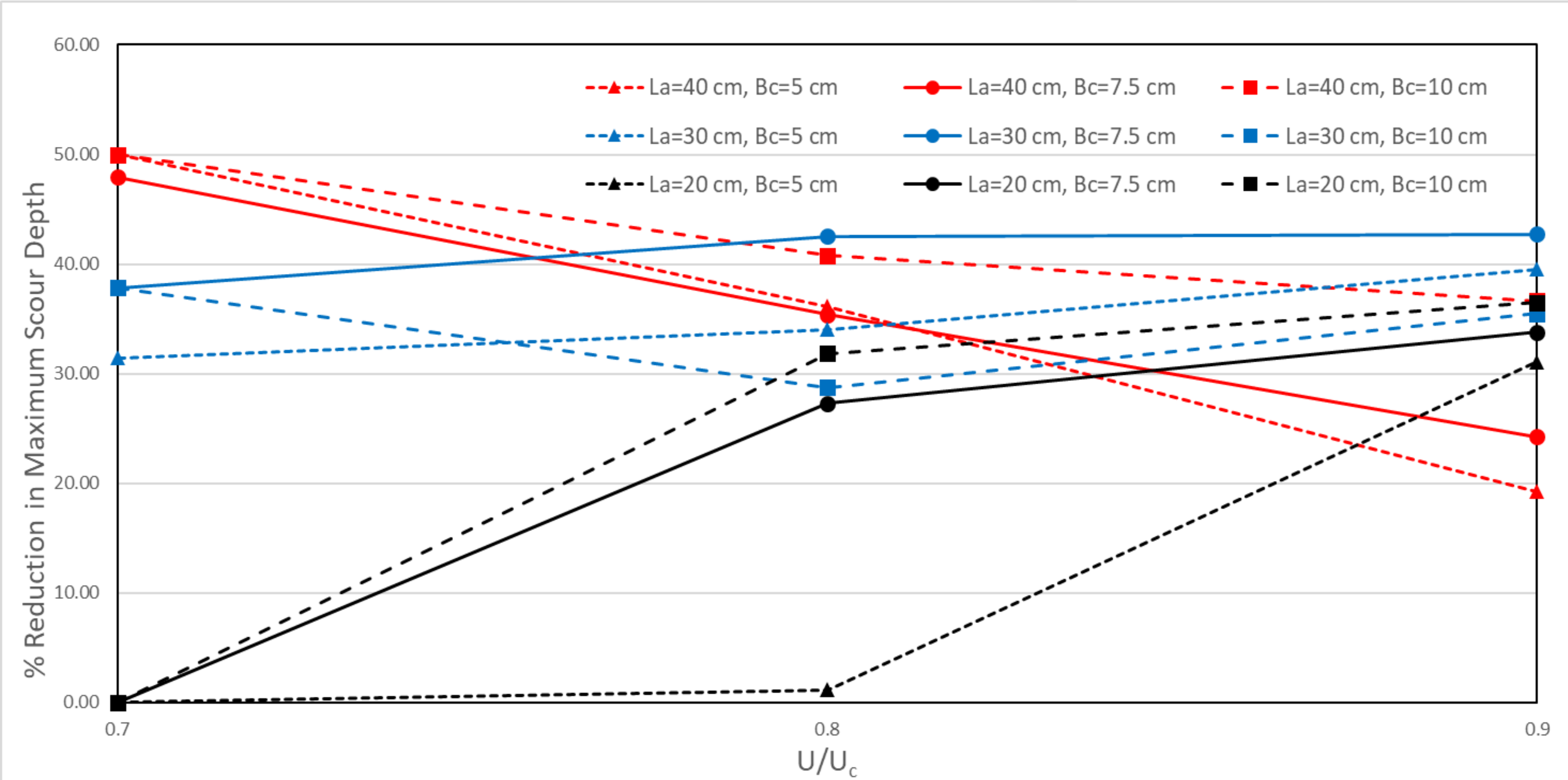

Figure 5.26 Effect of collar size and flow intensity on the maximum scour depth around the semi-circular end abutments for $Z_c/y_{0.7}$= -0.25

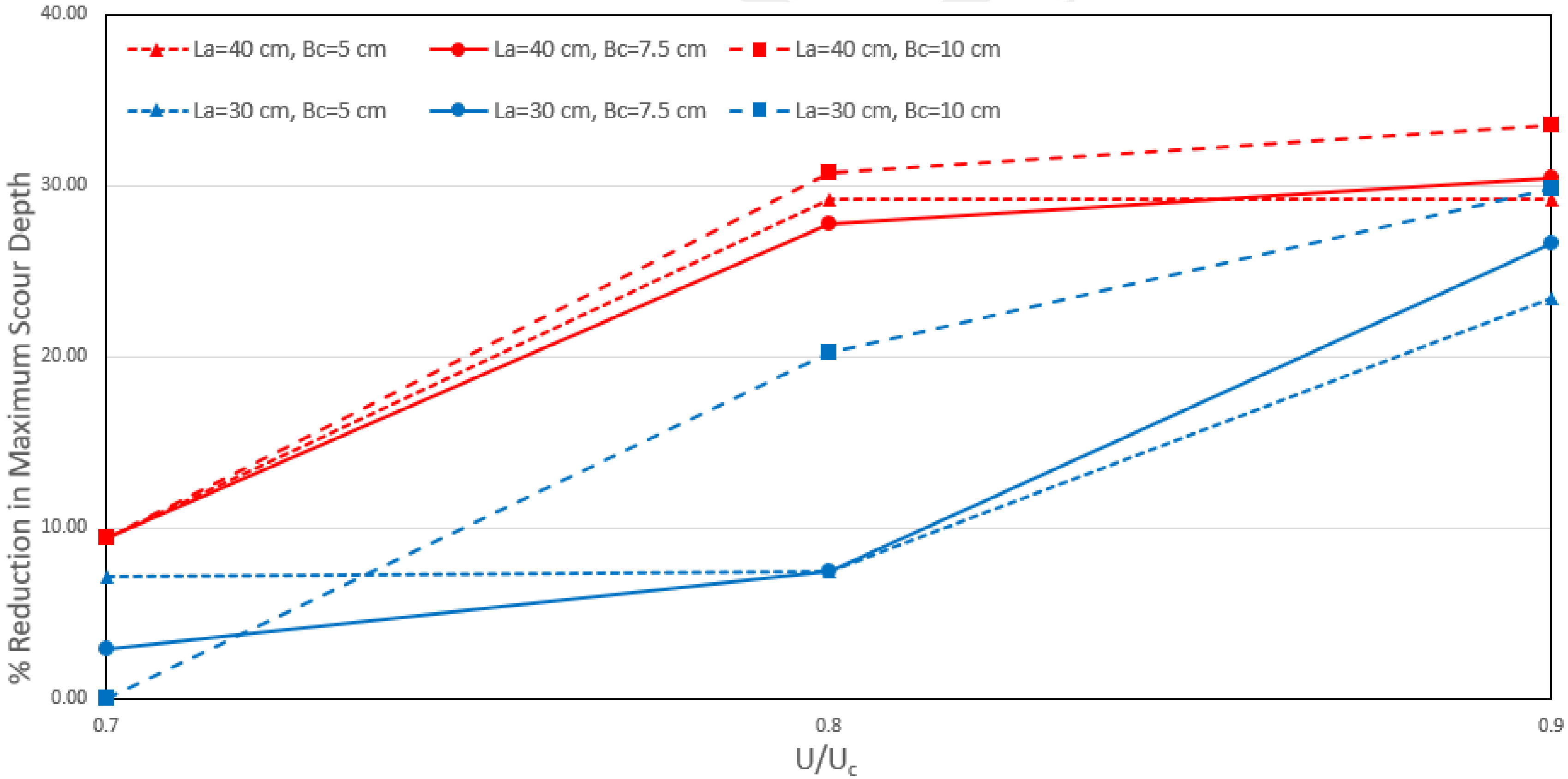

Figure 5.27 Effect of collar size and flow intensity on the maximum scour depth around the semi-circular end abutments for $Z_c/y_{0.7}$= -0.50

5.6.2 Rectangular Abutments

5.6.2.1 The Abutment of Length L_a=40 cm

As it can be seen in Figure 5.28, at the end of the first stage of the experiments with the flow intensity value of 0.7, the maximum scour reduction was obtained when the collar of B_c=10 cm is located at the elevation of $Z_c/y_{0.7}$= -±0.00. Also, the best collar performances were observed for the collar of B_c=10 cm at all collar elevations even the scour reduction performance of the collar of B_c=10 cm decreased while the collar was placed at the elevations below the bed level. On the other hand, the scour reduction performance of the collar of B_c=7.5 cm did not show significant changes when the location of the collar was changed whether on the bed level or below the bed level, yet, it should be underlined that the scour formation shifted away along the downstream of the abutment when the collar was placed below the bed level contrary to when the collar was placed at the elevation $Z_c/y_{0.7}$= -±0.00 where the scour formation penetrated below the collar level and was observed at the upstream toe of the abutment. At the elevation of $Z_c/y_{0.7}$= -±0.00, the scour reduction efficiency of the collar of B_a=5 cm was low and the maximum scour depth was observed below the collar level. The efficiency of the collar of B_c=5 cm was also low when the collar was placed at the elevation of $Z_c/y_{0.7}$= -0.50, but this time location of the maximum scour depth was shifted away downstream of the abutment. The optimal collar efficiency for the collar of B_c=5 cm was obtained when the collar was placed at the elevation of $Z_c/y_{0.7}$= -0.25. Finally, it can be stated that the scour reduction efficiency of the collars increased as the collar size increased for a given $Z_c/y_{0.7}$ except in the case of $Z_c/y_{0.7}$= -0.25. At this elevation, the scour reductions were approximately the same for the collars of B_c=5 cm and 7.5 cm.

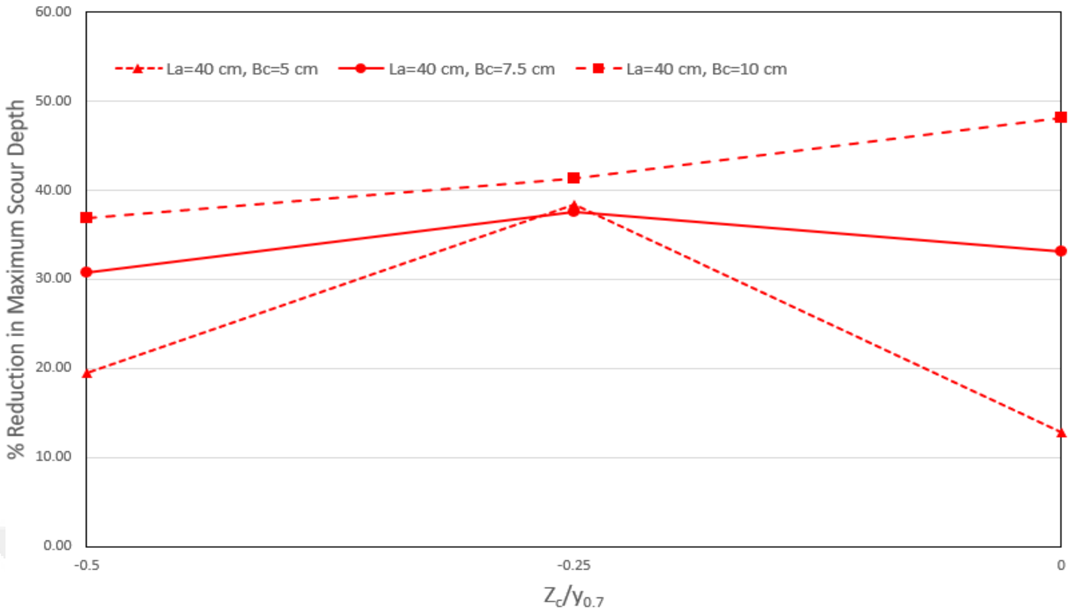

Figure 5.28 Effect of collar size and elevation on the maximum scour depth around the rectangular abutment of length L_a=40 cm (t= 2 hours)

At the end of the second stage of the experiments, the effect of collar size and elevation on the maximum scour depth is presented in Figure 5.29. From the figure, it can be stated that the scour reduction performances of the collars increases with increasing collar size for a given $Z_c/y_{0.7}$. The maximum scour reduction was observed for the collar of B_c=10 cm when the collar was placed at the elevation of $Z_c/y_{0.7}$= -0.25. At the elevation of $Z_c/y_{0.7}$= ±0.00, the scour reduction efficiencies of the collars dramatically decreased when the collar size decreased to 5 and 7.5 cm from 10 cm. When the collars were located at the elevation of $Z_c/y_{0.7}$= -0.25, the scour reduction efficiencies of the collars increased for all the collar widths tested and attained the maximum scour reductions. Afterward, when the collars were placed at the elevation of $Z_c/y_{0.7}$= -0.50, the scour reduction performances of the collars of B_c=7.5 cm and 10 cm decreased while the collar of B_c=5 cm did not show any significant difference.

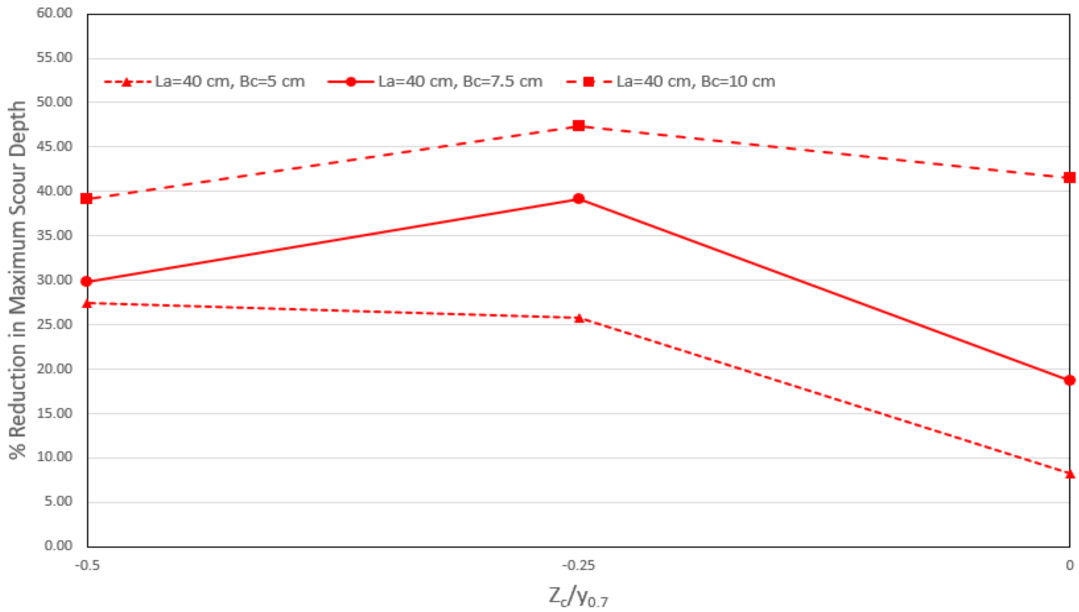

Figure 5.29 Effect of collar size and elevation on the maximum scour depth around the rectangular abutment of length L_a=40 cm (t= 4 hours)

The effect of collars with varying collar sizes and elevations in reducing the maximum scour depth at the end of the third stage of the experiments is shown in Figure 5.30. Similar to the end of the second stage of the experiments, the scour reduction efficiencies of the collars increased with increasing collar width for any $Z_c/y_{0.7}$ value tested. When the collars were placed at the elevation of $Z_c/y_{0.7}$= ±0.00, the collars of B_c=5 cm and 7.5 cm did not affect the magnitude of maximum scour depth and its location. On the other hand, the collar of B_c=10 cm reduced the maximum scour depth. When the collars were placed below the bed level, $Z_c/y_{0.7}$= -0.25 and -0.50, the collars of B_c=7.5 cm and 10 cm showed significant improvements in reducing the maximum scour depth and shifting away its location. Furthermore, the efficiencies of the collars increased with increasing the collar elevation below the bed level independent of the collar size. At the end of the experiments, the maximum scour reduction was observed for the collar of B_a=10 cm at the elevation of $Z_c/y_{0.7}$= -0.50 by around 24%.

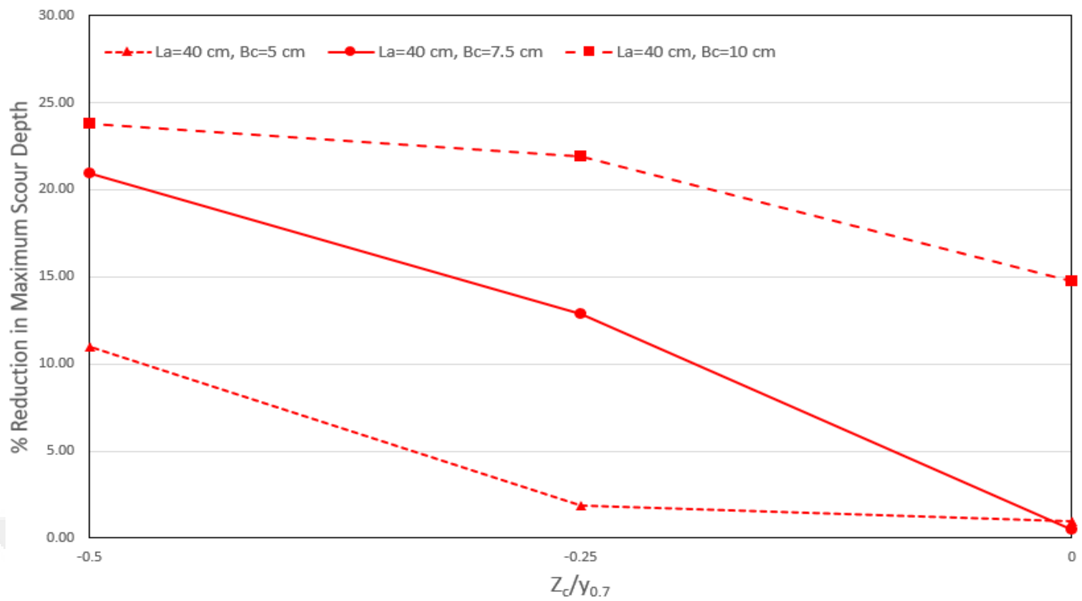

Figure 5.30 Effect of collar size and elevation on the maximum scour depth around the rectangular abutment of length L_a=40 cm (t= 6 hours)

Figures 5.31- 5.33 show the effect of collar size and flow intensity on the maximum scour depth around the rectangular end abutment of length L_a=40 cm at different $Z_c/y_{0.7}$ values. When collars were placed at the elevation of $Z_c/y_{0.7}$=±0.00, the scour reduction performances of the collars gradually decreased with increasing flow intensity and time. Furthermore, at the end of the third stage of the experiments, the collars of B_c=5 cm and 7.5 cm have no significant effect in reducing the maximum scour depth. Since the maximum scour depth was greater during the higher flow intensity values, the collars were placed at the elevation of $Z_c/y_{0.7}$= ±0.00 was inadequate in manipulating the flow and reducing the maximum scour depth. On the other hand, at the elevation of $Z_c/y_{0.7}$= -0.25, the optimal scour reduction performances were obtained at the end of the second stage of the experiments for the collars of B_c=7.5 cm and 10 cm. For these collar widths, the scour reduction efficiencies of the collars increased between the 2nd and 4th hours of the experiments with increasing flow intensity and time. However, between the 4th and 6th hours, the efficiencies of these collars dramatically decreased. Moreover, the scour reduction efficiency of the collar of B_c=5 cm gradually decreased with increasing flow intensity and time. Furthermore, at the end of the third stage, the collar of B_c=5 cm has almost no effect in reducing the maximum scour depth. Finally, when the collars were placed at the elevation of $Z_c/y_{0.7}$= -0.50, the scour reduction efficiencies of the collars for a given collar size did not show significant differences at the end of the first and second stages of the experiments. Nevertheless, the efficiencies of the collars of B_c=5 cm and 10 cm were a little bit higher at the end of the second stage of the experiments. At this elevation, the worst scour reduction performances were observed at the end of the third stage of the experiments regardless of collar size due to the greater scour depths caused by higher flow intensity and increasing time.

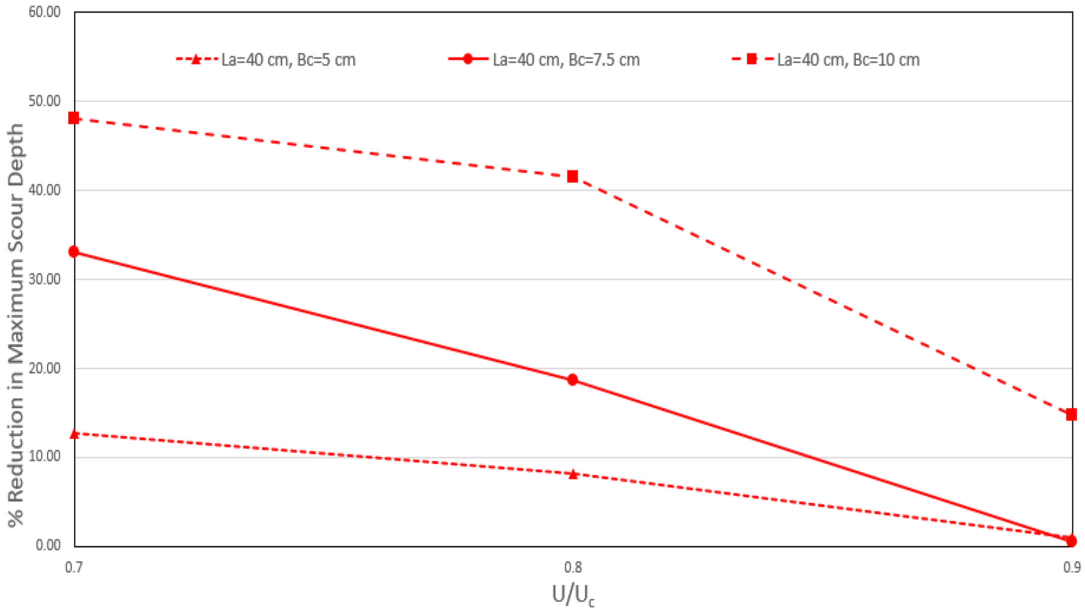

Figure 5.31 Effect of collar size and flow intensity on the maximum scour depth around the rectangular abutment of length L_a=40 cm for $Z_c/y_{0.7}$= ±0.00

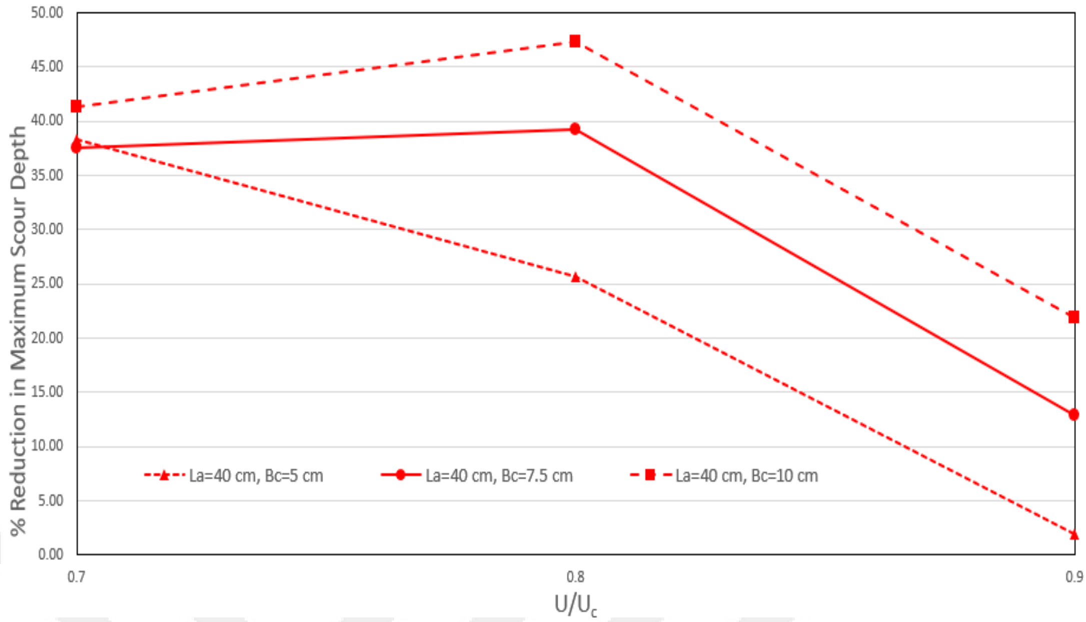

Figure 5.32 Effect of collar size and flow intensity on the maximum scour depth around the rectangular abutment of length L_a=40 cm for $Z_c/y_{0.7}$= -0.25

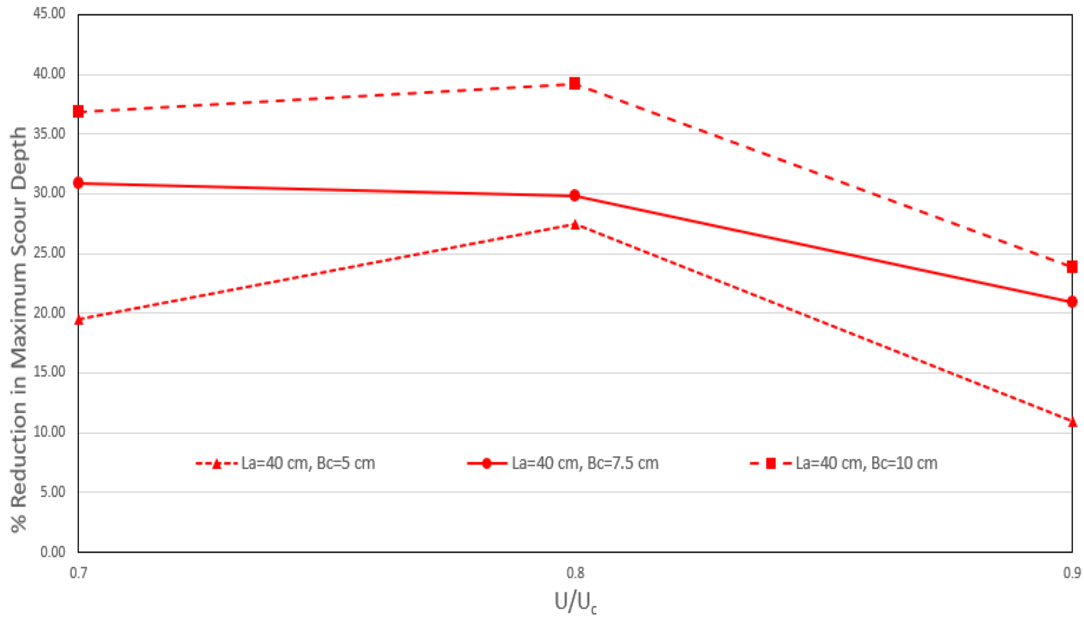

Figure 5.33 Effect of collar size and flow intensity on the maximum scour depth around the rectangular abutment of length L_a=40 cm for $Z_c/y_{0.7}$= -0.50

In Figure 5.34, the variation of the dimensionless maximum scour depths with dimensionless time for various collar size-elevation arrangements is presented.

According to the experimental results, the minimum scour depths were observed for the abutment of length L_a=40 cm when the collar of B_c=10 cm was placed at the elevation of $Z_c/y_{0.7}$= -0.25 at the end of the first and second stages of the experiments. Meanwhile, at the end of the third stage of the experiments, the minimum scour depths were obtained when the collar of B_c=10 cm was placed at the elevation of $Z_c/y_{0.7}$= -0.50. On the other hand, the maximum scour depths were generally recorded for the collar of B_c=5 cm at the elevation of $Z_c/y_{0.7}$= ±0.00 through the experiments. Furthermore, at the end of the third stage of the experiments, the measured maximum scour depths at the elevations of $Z_c/y_{0.7}$= -0.25 and ±0.00 for the collar of B_c=5 cm and at the elevation of $Z_c/y_{0.7}$= ±0.00 for the collar of B_c=7.5 cm were almost the same as those measured from the experiments conducted without a collar.

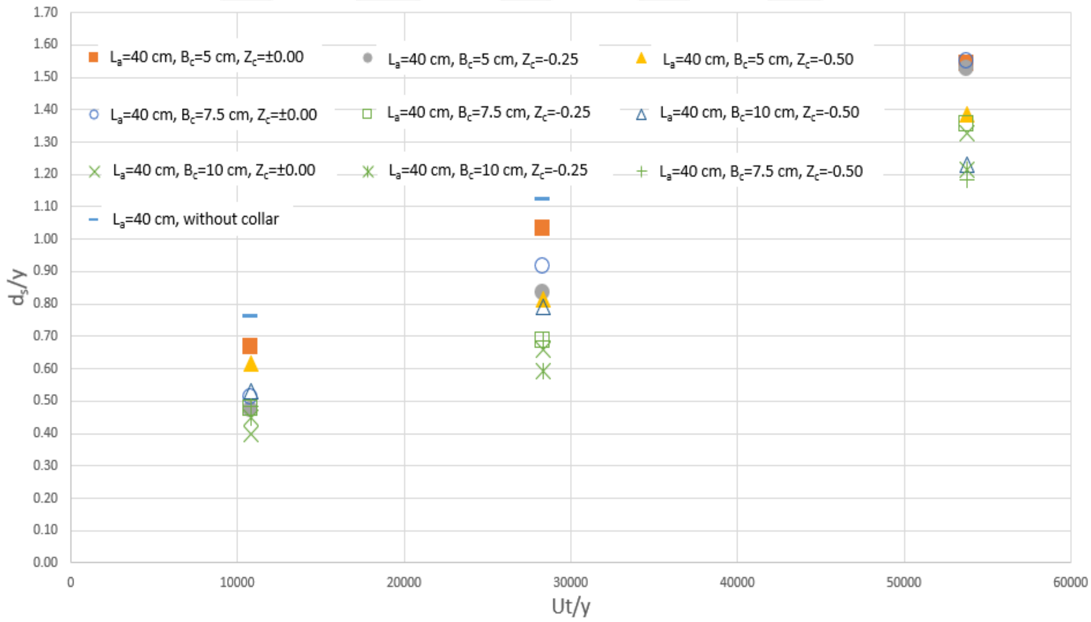

Figure 5.34 Variation of the dimensionless maximum scour depth with dimensionless time as a function of collar size and elevation for rectangular abutment of length L_a=40 cm

5.6.2.2 The Abutment of Length L_a=30 cm

The scour reduction efficiencies of the collars with varying sizes and elevations at the end of the first stage of the experiments are presented in Figure 5.35. Based on the experimental results, the optimal collar efficiencies were obtained when the collar was placed at the elevation of $Z_c/y_{0.7}$= -0.25 for a given collar size. The maximum scour reduction was observed for the collar of B_c=10 cm at the elevation of $Z_c/y_{0.7}$= -0.25. Although the scour reduction performances of the collars increased with increasing collar size, the efficiencies of the collars of B_c=7.5 and 10 cm were obtained as quite close to each other. Furthermore, at the elevation of $Z_c/y_{0.7}$= -0.50, the scour reduction efficiencies of the collars of B_c=5, 7.5 and 10 cm were approximately the same and the minimum scour reduction performances were obtained at this collar elevation.

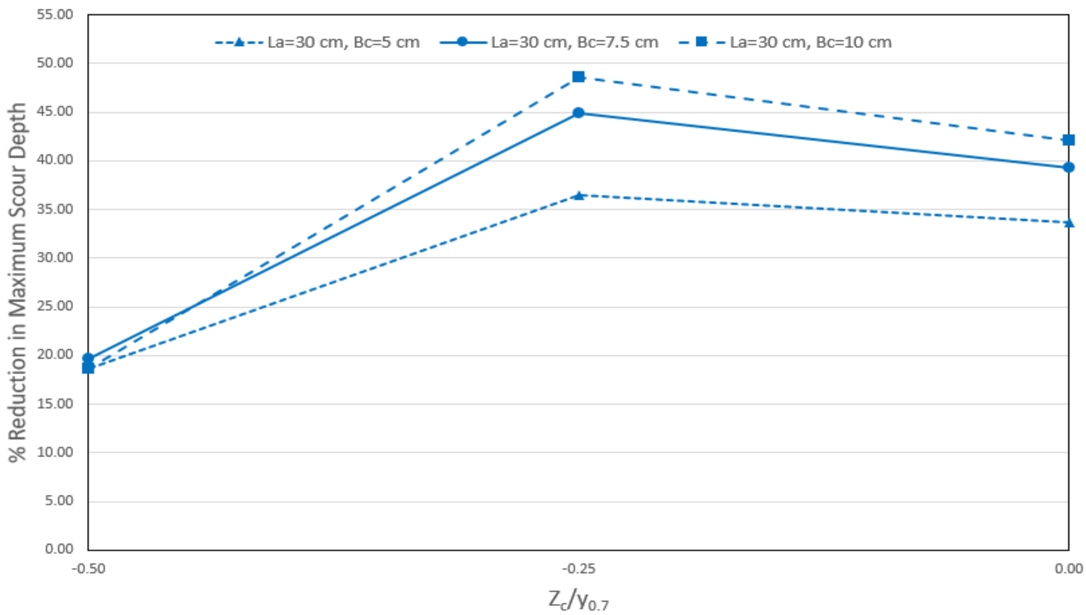

Figure 5.35 Effect of collar size and elevation on the maximum scour depth around the rectangular abutment of length L_a=30 cm (t= 2 hours)

At the end of the second stage of the experiments, it is clearly seen in Figure 5.36 that the scour reduction efficiencies of the collars increases with increasing collar size for a given $Z_c/y_{0.7}$ as well as at the end of the first stage of the experiments. At the end of the 4th hour, the maximum scour reductions were obtained for the collar of B_c=10 cm at the elevations of $Z_c/y_{0.7}$= -0.50 and -0.25. At the elevation of $Z_c/y_{0.7}$= ±0.00, the performances of the collars of B_c=7.5 and 10 cm were similar to each other. In addition, at this elevation, the scour reduction performance of the collar of B_c=5 cm was absolutely low relative to the collars of B_c=7.5 and 10 cm. However, when the collars were placed below the bed level, the efficiencies of the collars of B_c=7.5 and 10 cm gradually decreased, on the contrary, the efficiency of the collar of B_c=5 cm gradually increased. At the elevation of $Z_c/y_{0.7}$= -0.50, the efficiencies of the collars of B_c=5, 7.5 and 10 cm were close to each other since the maximum scour depth was recorded as the same as the collar level.

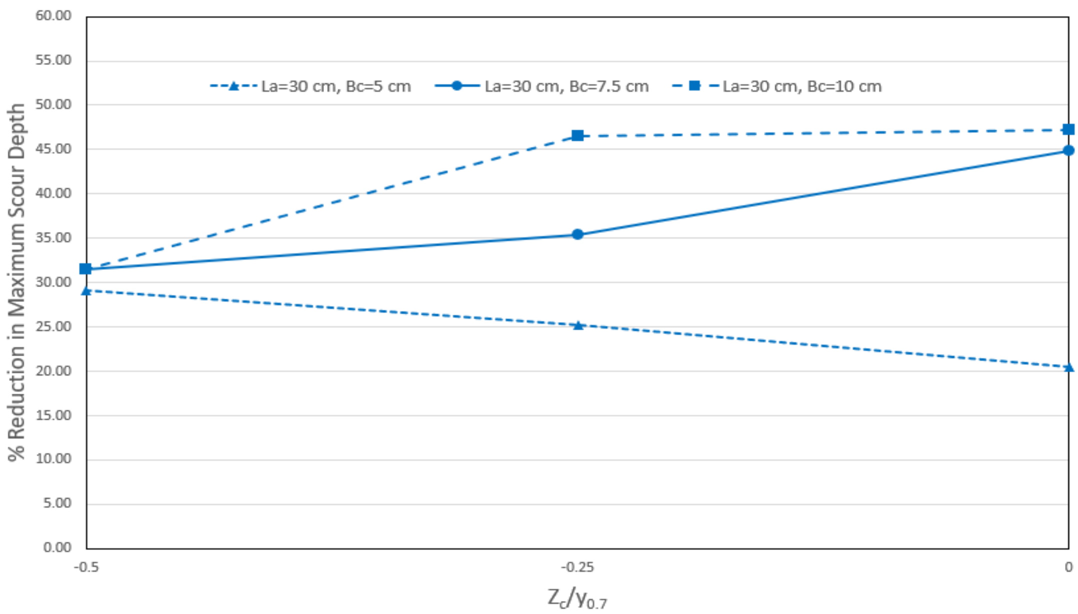

Figure 5.36 Effect of collar size and elevation on the maximum scour depth around the rectangular abutment of length L_a=30 cm (t= 4 hours)

Figure 5.37 demonstrates that at the end of the third stage of the experiments, similar trends were observed in the previous stages. However, at this time, the efficiency of the collar of B_c=5 cm was low when the collar was placed at the elevations of $Z_c/y_{0.7}$= -0.25 and ±0.00. Nevertheless, at the elevation of $Z_c/y_{0.7}$= -0.50, the collar of B_c=5 cm showed significant efficiency in reducing the maximum scour depth. The maximum scour reductions for the collars of B_a=7.5 and 10 cm were observed when collars were placed at the elevation of $Z_c/y_{0.7}$= -0.25. When the collars were placed at the elevations of $Z_c/y_{0.7}$= -0.50 and ±0.00, the scour reduction performances of the collars of B_a=7.5 and 10 cm did not have significant differences. Yet, at the elevation of $Z_c/y_{0.7}$= ±0.00, the maximum scour depth was reduced but it still occurred at the abutment toe, below the collar. On the other hand, at the elevation of $Z_c/y_{0.7}$= -0.50, the maximum scour depth shifted downstream of the abutment from the abutment toe.

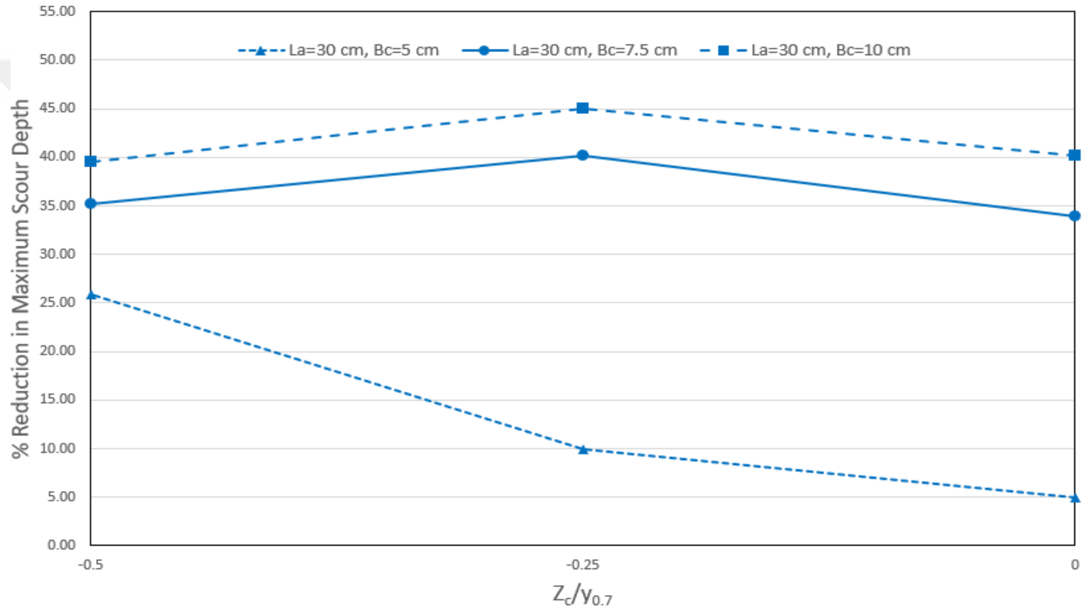

Figure 5.37 Effect of collar size and elevation on the maximum scour depth around the rectangular abutment of length L_a=30 cm (t= 6 hours)

Figures 5.38- 5.40 show the effect of collar size and flow intensity on the maximum scour depth around the rectangular end abutment of length L_a=30 cm. When collars were placed at the elevation of $Z_c/y_{0.7}$=±0.00, the scour reduction performances of the collars of B_c=7.5 and 10 cm did not show significant differences through the 6 hours of the experiments. Nevertheless, the maximum scour reductions were observed at the end of the second stage of the experiments and the minimum scour reductions were observed at the end of the third stage of the experiments. At the elevation of $Z_c/y_{0.7}$= -0.25, the scour reduction performance of the collar of B_a=10 cm was approximately the same through the 6 hours of experiments. Moreover, the optimal scour reduction performance of the collar of B_c=7.5 cm was obtained at the end of the first stage of the experiments. Yet it should be also indicated that the scour reduction efficiency of the collar of B_c=7.5 cm at the end of the third stage of the experiments was close to the obtained efficiency at the end of the first stage of the experiments. Thereby, in this elevation, the minimum scour reduction performance for the collar of B_c=7.5 cm was obtained at the end of the second stage of the experiments. On the other hand, at this elevation, the scour reduction performance of the collar of B_c=5 cm gradually decreased with increasing flow intensity and time. Furthermore, at the end of the third stage of the experiments, the collar of B_c=5 cm reduced the maximum scour depth by around 10%. Finally, when the collars were placed at the elevation of $Z_c/y_{0.7}$= -0.50, at the end of the first stage and second stages of the experiments, the performances of all the collars were almost the same. The maximum scour depths for all sizes of collars were measured as the same as the collar level during the first 4 hours of the experiments. In other words, the bed material degraded down to the collar elevation of $Z_c/y_{0.7}$= -0.50 and the scour formation did not penetrate below the collar level. Hence, the performances of the collars in reducing the scour depth increased with increasing flow intensity and time. At the end of the third stage of the experiments, the increment in the efficiencies of the collars of B_c=7.5 and 10 cm continued, but the efficiency of the collar of B_c=5 cm did not show any significant difference between the 4th and 6th hours of the experiments with the flow intensity of 0.9.

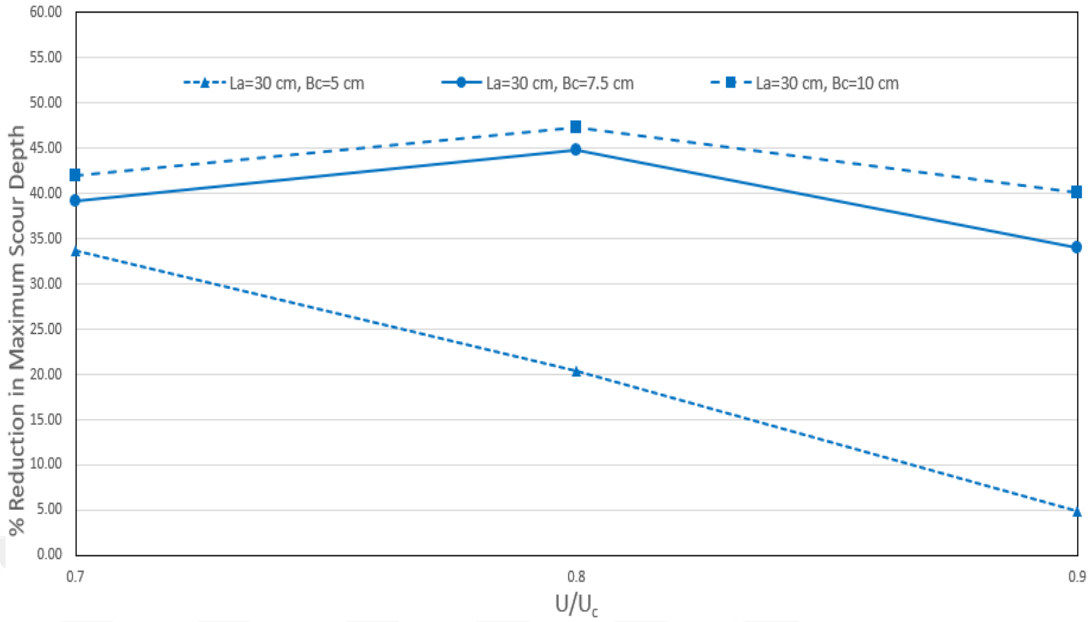

Figure 5.38 Effect of collar size and flow intensity on the maximum scour depth around the rectangular abutment of length L_a=30 cm for $Z_c/y_{0.7}$= ±0.00

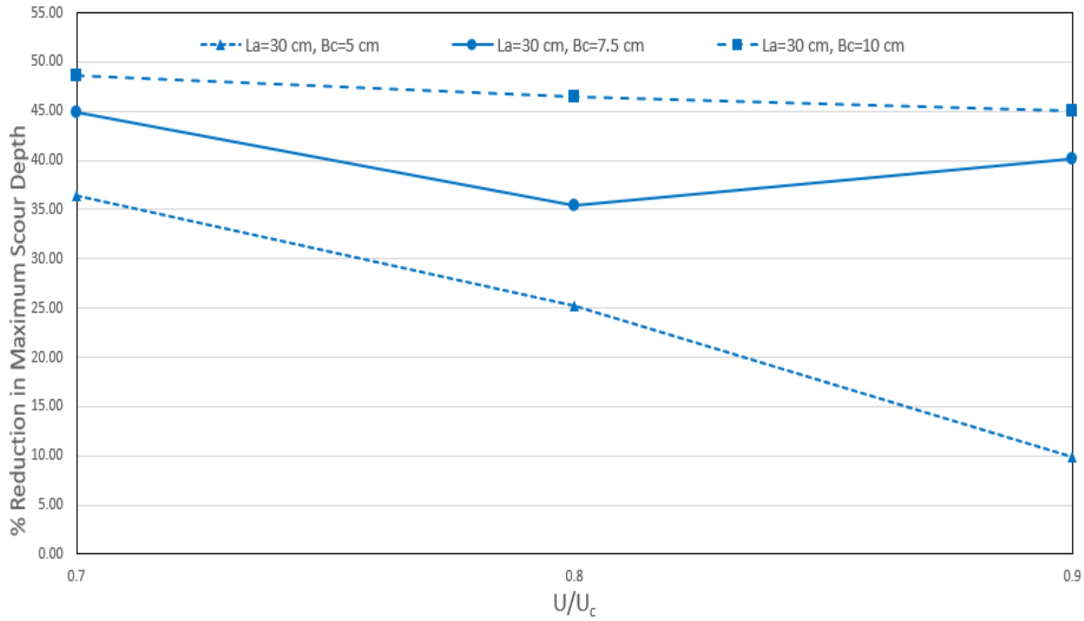

Figure 5.39 Effect of collar size and flow intensity on the maximum scour depth around the rectangular abutment of length of L_a=30 cm for $Z_c/y_{0.7}$= -0.25

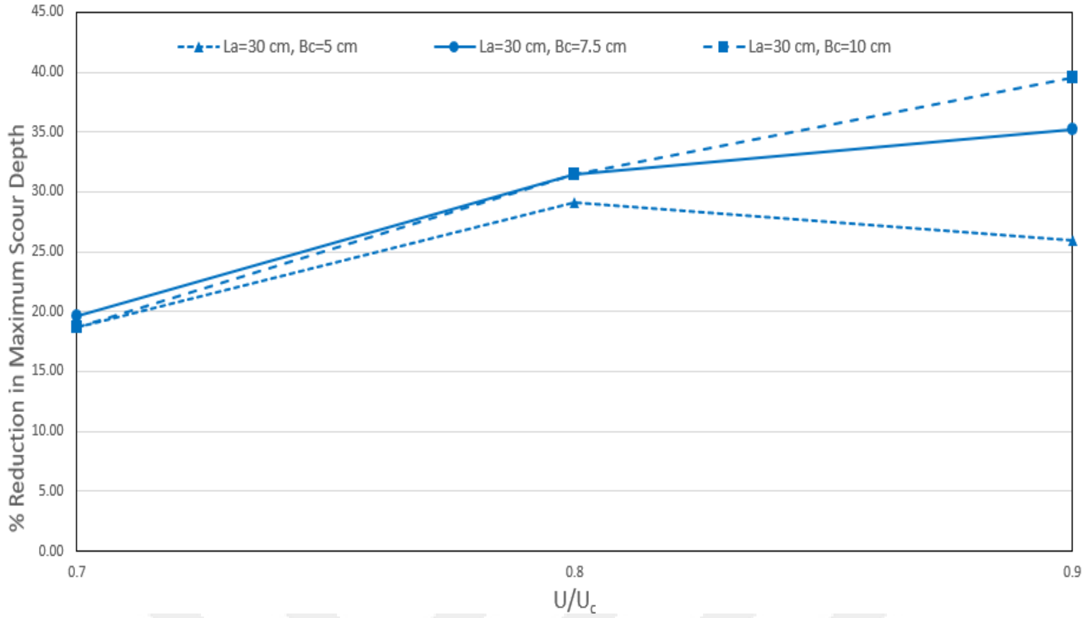

Figure 5.40 Effect of collar size and flow intensity on the maximum scour depth around the rectangular abutment of length L_a=30 cm for $Z_c/y_{0.7}$= -0.50

In Figure 5.41, the variation of the dimensionless maximum scour depths with dimensionless time for various collar size-elevation arrangements is presented. According to the experimental results, the minimum scour depths were observed for the abutment of length L_a=30 cm when the collar of B_c=10 cm was placed at the elevation of $Z_c/y_{0.7}$= -0.25 through the experiments. On the contrary, the maximum scour depths were generally recorded for the collar of B_c=5 cm at the elevation of $Z_c/y_{0.7}$= ±0.00 through the experiments.

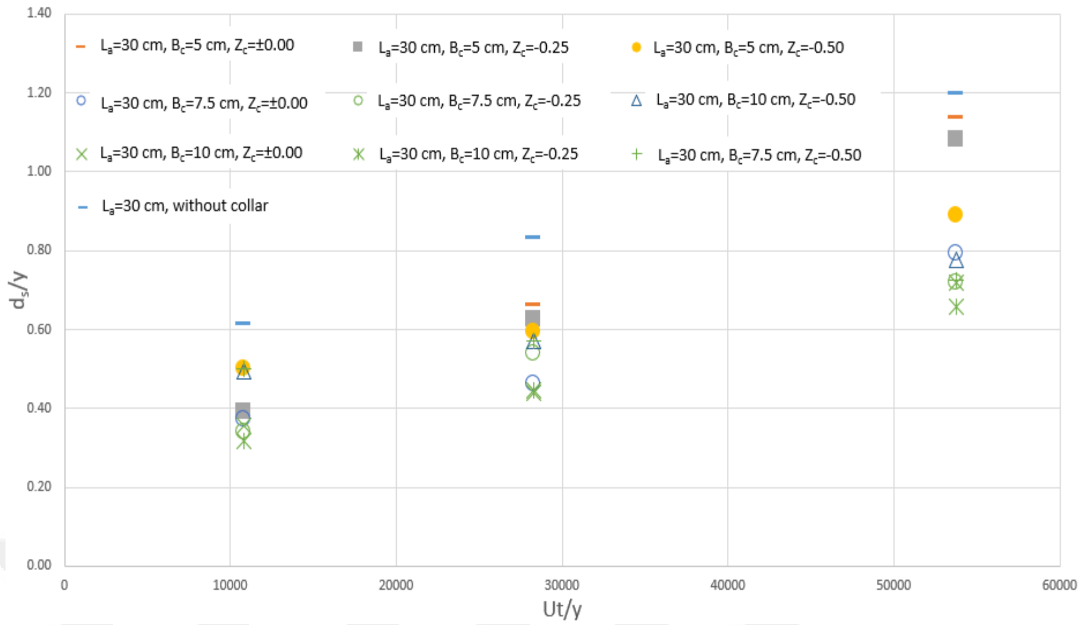

Figure 5.41 Variation of the dimensionless maximum scour depth with dimensionless time as a function of collar size and elevation for rectangular end abutment of length L_a=30 cm

5.6.2.3 The Abutment of Length L_a=20 cm

The effect of collar size and elevation on the maximum scour depth around the rectangular abutment of length L_a=20 cm is shown in Figures 5.42-5.44. At the end of the first stage of the experiments, the best collar performance was observed for the collar of B_c=10 cm at the elevation of $Z_c/y_{0.7}$= ±0.00. Also, the collar of B_c=7.5 cm was found effective in reducing the scour depth. However, the scour reduction performance of the collar of B_c=5 cm at the elevation of $Z_c/y_{0.7}$= ±0.00 did not show high efficiency. Thus it can be said that as the collar width increased the scour reduction efficiencies of the collars increased. On the other hand, when the collars were placed at the elevation of $Z_c/y_{0.7}$= -0.25, the scour reduction performances of the collars of B_c=7.5 and 10 cm decreased. Furthermore, the scour reduction efficiency of the collar of B_c=10 cm decreased at the elevation of $Z_c/y_{0.7}$= -0.25 in half when compared to the case of the elevation of $Z_c/y_{0.7}$= ±0.00. Contrary to the collars of B_c=7.5 and 10, the scour reduction performance of the collar of B_c=5 cm dramatically increased at the elevation of $Z_c/y_{0.7}$= -0.25 and gave the best result in reducing the maximum scour depth. Nevertheless, it can be also stated that the efficiencies of all the collar sizes were found close to each other at the elevation of $Z_c/y_{0.7}$= -0.25. At the end of the second stage of the experiments, the general trends of the curves given in Figure 5.43 are very similar to those in Figure 5.42. In other words, the relationship between the collar size and the reduction in the maximum scour depths did not show significant differences between the 2nd and 4th hour of the experiments. However, when the collars were located at the elevation of $Z_c/y_{0.7}$= -0.25, the scour reduction performances of the collars of B_c=5 and 7.5 cm significantly increased while the collar of B_c=10 cm a little bit decreased. In addition, at the end of the 4th hour, the scour reduction performances of the collars of B_c=7.5 cm and 10 cm were almost the same and the collar of B_c=5 cm gave the minimum scour reduction at the elevation of $Z_c/y_{0.7}$= -0.25. Finally, at the end of the third stage of the experiments, it was observed that the scour reduction performances of the collars increased regardless of the collar width when the collars were placed deeper at the bed, $Z_c/y_{0.7}$= -0.25. However, for a given collar elevation, the efficiencies of the collars of B_c=7.5 and 10 cm were found to be almost the same and much larger than those of B_c=5 cm. Since the maximum scour depth increased with increasing time and flow intensity, the collar that was placed at the bed level became insufficient to manipulate the flow and reduce or swept away the maximum scour depth. Therefore, the best collar performances were obtained for the collars of B_c=7.5 cm and 10 cm at the elevation of $Z_c/y_{0.7}$= -0.25 and the minimum one was obtained for the collar of B_c=5 cm at the elevation of $Z_c/y_{0.7}$= ±0.00.

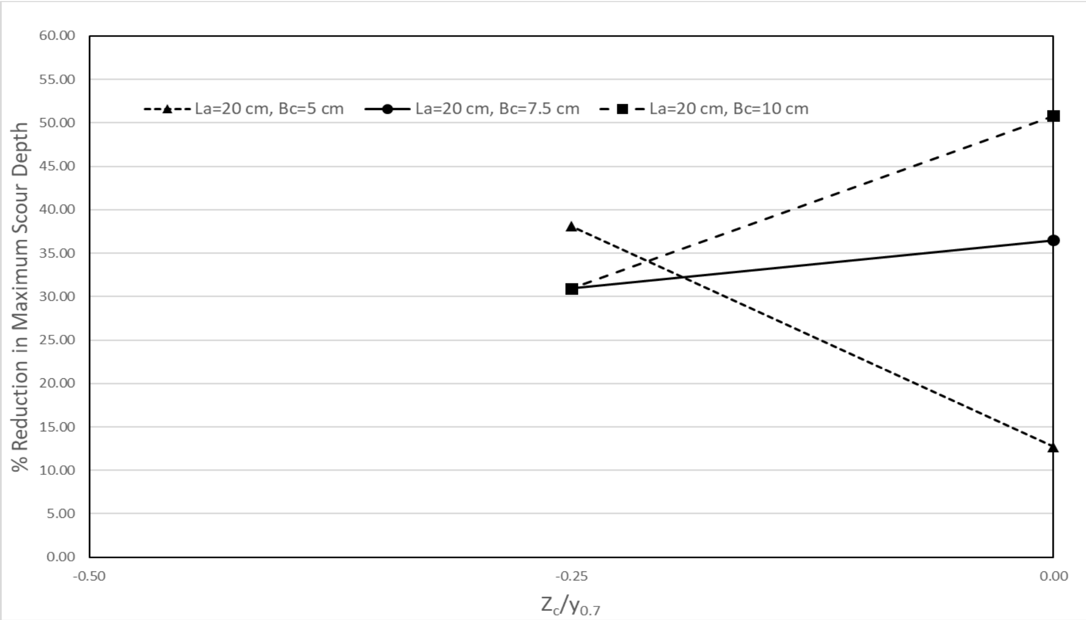

Figure 5.42 Effect of collar size and elevation on the maximum scour depth around the rectangular abutment of length L_a=20 cm (t= 2 hours)

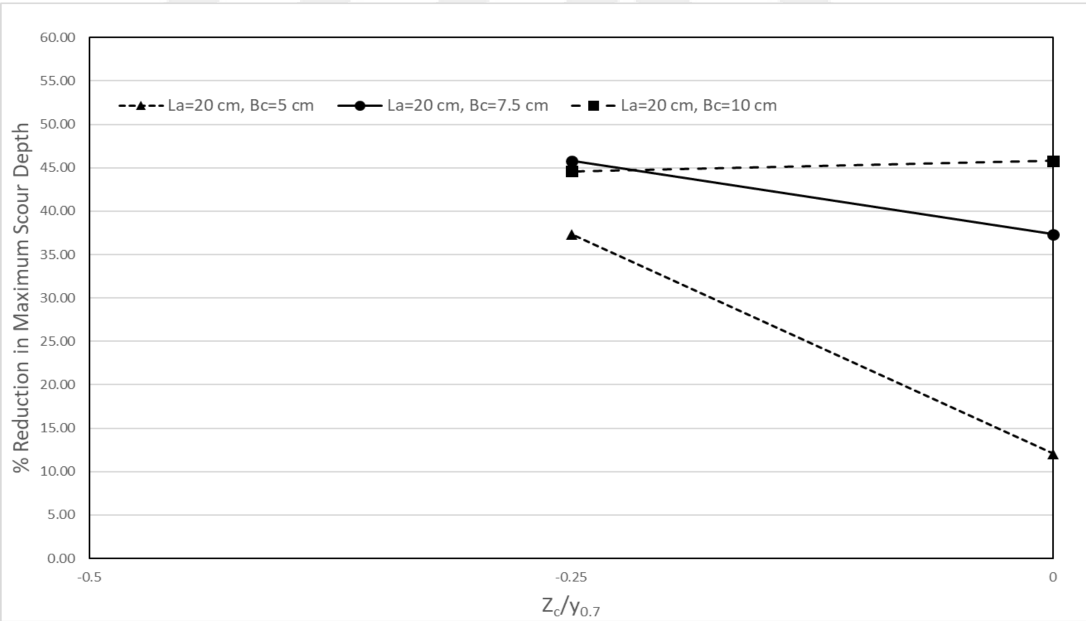

Figure 5.43 Effect of collar size and elevation on the maximum scour depth around the rectangular abutment of length L_a=20 cm (t= 4 hours)

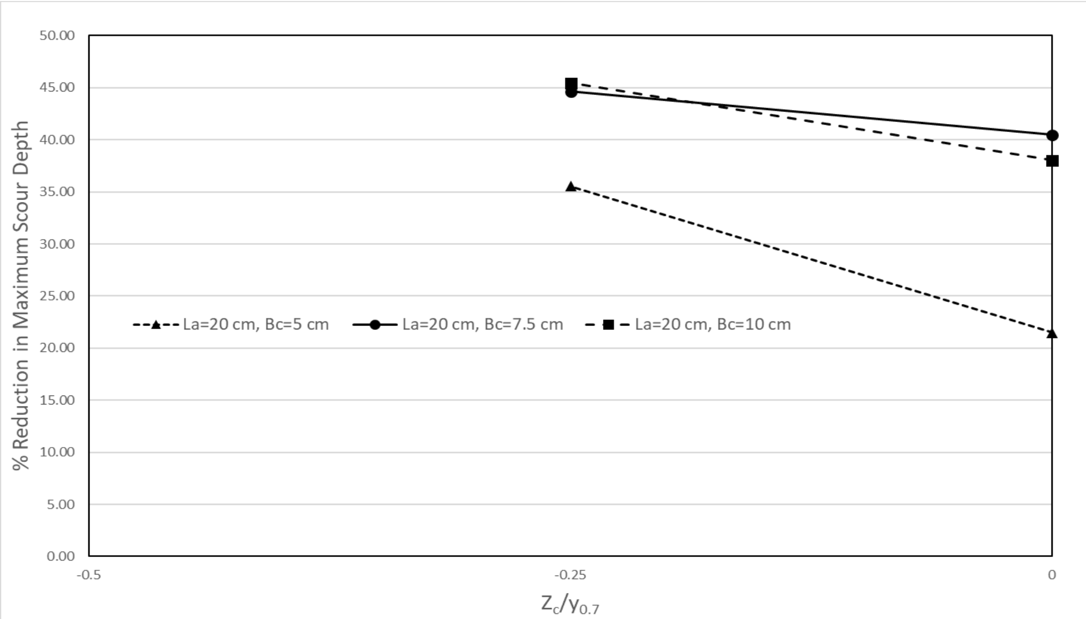

Figure 5.44 Effect of collar size and elevation on the maximum scour depth around the rectangular abutment of length L_a=20 cm (t= 6 hours)

The effect of collar size and flow intensity on the maximum scour depth around the rectangular abutment of length L_a=20 cm is presented in Figures 5.45 and 5.46. When collars were placed at the elevation of $Z_c/y_{0.7}$=±0.00, the scour reduction performances of the collars of B_c=5 and 7.5 cm did not show significant differences through the 4 hours of experiments with the flow intensities of 0.7 and 0.8. However, between the 4th and 6th hours with the flow intensity of 0.9, the performances of these collars increased and the best scour reduction performances were obtained at the end of the third stage. On the other hand, the performance of the collar of B_c=10 cm gradually decreased with increasing flow intensity and time. Furthermore, at the end of the third stage, the performances of the collars of B_c=7.5 and 10 cm were nearly the same. At the elevation of $Z_c/y_{0.7}$= -0.25, the performances of the collars of B_a=7.5 and 10 cm were similar to each other through the 6 hours of experiments. For these collar widths, the maximum scour reductions were observed at the end of the second and third stages while the minimum performances were obtained at the end of the first stage. In other words, the efficiencies of these collar widths increased between the 2nd and 4th hour of the experiments with increased flow intensity, but when the flow intensity value was increased once again at the end of the 4th hour, any significant differences were not observed in the scour reduction performances of these collar widths at the end of the 6th hour. Moreover, the scour reduction efficiency of the collar of B_c=5 cm slightly decreased with increasing flow intensity and time.

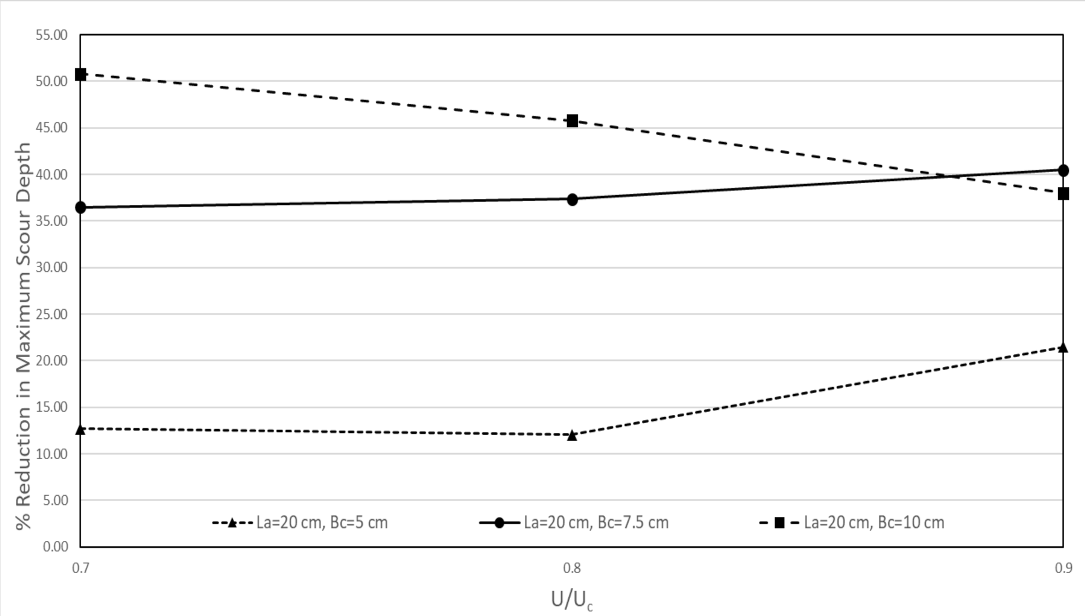

Figure 5.45 Effect of collar size and flow intensity on the maximum scour depth around the rectangular abutment of length L_a=20 cm for $Z_c/y_{0.7}$= ±0.00

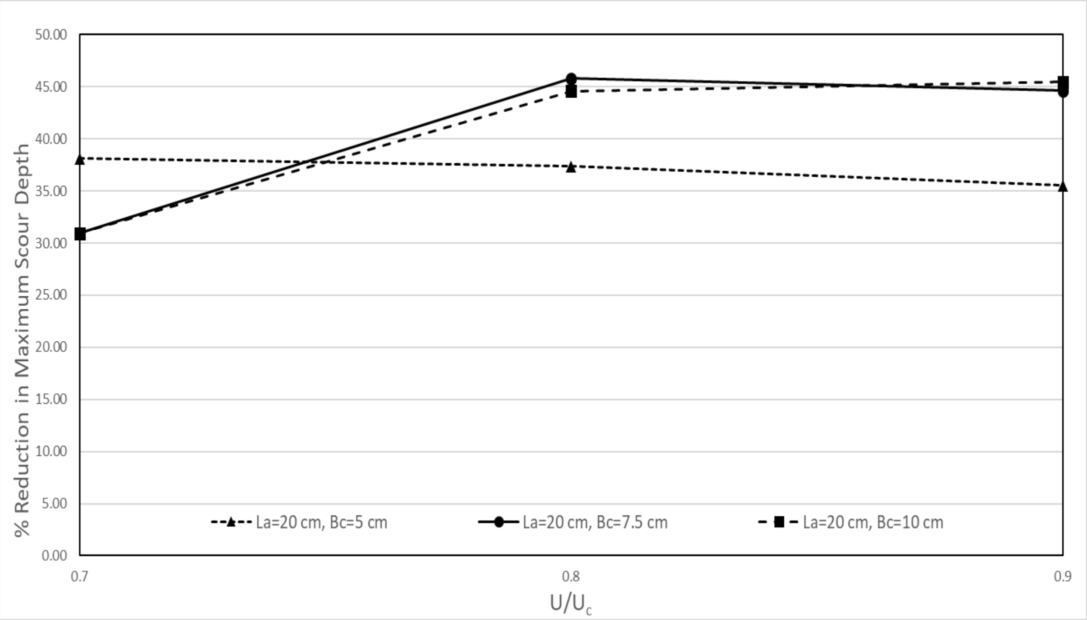

Figure 5.46 Effect of collar size and flow intensity on the maximum scour depth around the rectangular abutment of length L_a=20 cm for $Z_c/y_{0.7}$= -0.25

In addition, the variation of the dimensionless maximum scour depths with dimensionless time for various collar size-elevation arrangements is shown in Figure 5.47. Based on the experimental results, the minimum scour depths were observed for the abutment of length L_a=20 cm when the collar of B_c=10 cm was placed at the elevation of $Z_c/y_{0.7}$= ±0.00 at the end of the first and second stages of the experiments. However, at the end of the third stage, the minimum scour depths were recorded for the collars of B_c=7.5 and 10 cm that were placed at the elevation of $Z_c/y_{0.7}$= ±-0.25. On the contrary, the maximum scour depths were measured for the collar of B_c=5 cm at the elevation of $Z_c/y_{0.7}$= ±0.00 through the experiments.

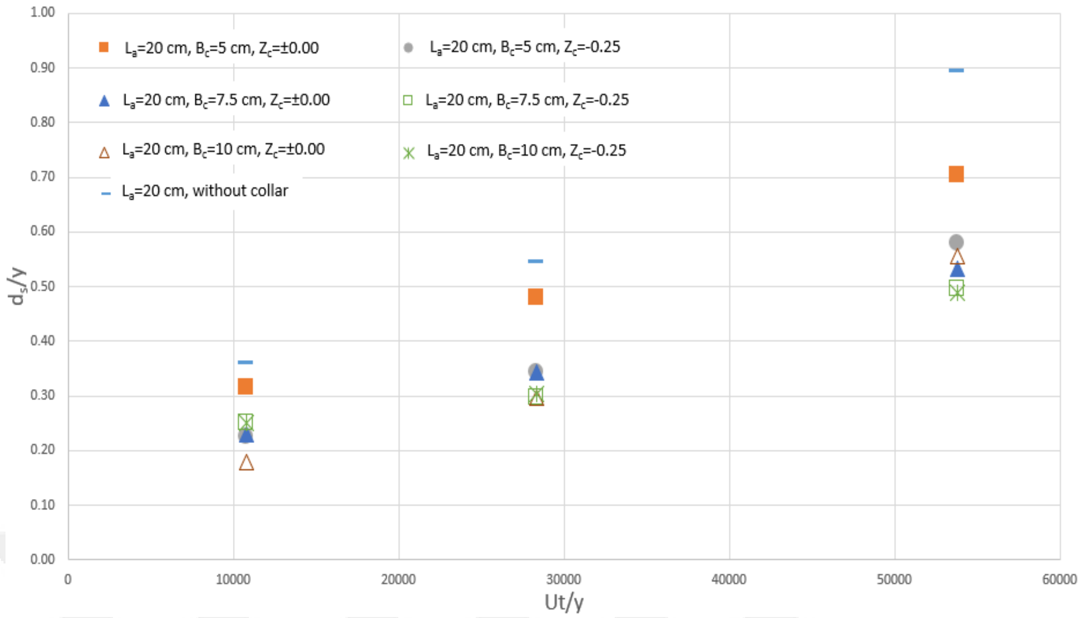

Figure 5.47 Variation of the dimensionless maximum scour depth with dimensionless time as a function of collar size and elevation for rectangular abutment of length L_a=20 cm

5.6.2.4 Summary

In summary, the collars having larger widths were generally more effective in reducing the maximum scour depth around the abutments regardless of the abutment length, since the larger collars provide stronger protection to vortices and create smaller scour holes than those of smaller collars. In all the experiments conducted, the maximum scour reductions were generally obtained when the collars were placed at the elevation of $Z_c/y_{0.7}$= -0.25. However, during the initial stages of the experiments with the flow intensity of 0.7, for the abutment of length L_a=20 cm the maximum scour reductions were obtained at the elevation of $Z_c/y_{0.7}$= ±0.00 and at the end of the third stage of the experiments, for the abutment of length L_a=40 cm, the maximum scour reductions were obtained at the elevation of $Z_c/y_{0.7}$= -0.50. Since the scour formation was greater around the abutment of length L_a=40 cm than those of L_a=20 cm, the scour formation penetrated into the deeper locations below the bed level and the maximum scour depth increased with increasing flow intensity and time. Hence, the collars that were placed at the elevation of $Z_c/y_{0.7}$= -0.50 was more efficient to reduce the maximum scour depth around longer abutment lengths such as L_a=40 cm having higher flow intensity value and duration, U/U_c=0.9 and t=6 hours, while the collars at the elevation of $Z_c/y_{0.7}$= ±0.00, was obtained as more efficient around shorter abutment lengths such as L_a=20 cm having smaller flow intensity and test duration, U/U_c=0.7, t=2 hours.

In Figure 5.48-5.50, the effect of collar size and elevation on the maximum scour depth around all the rectangular abutment lengths tested in this study is given. At the end of the first stage of the experiments, at the elevation of $Z_c/y_{0.7}$= ±0.00, the maximum scour reductions were obtained for the abutments of lengths L_a=20 and 40 cm having collars of B_c=10 cm and the worst ones were obtained for the abutments of lengths L_a=20 and 40 cm having collars of B_c=5 cm. When collars were placed at the elevation of $Z_c/y_{0.7}$= -0.25, the collar efficiency decreased for the abutment length of L_a=20 cm having collars of B_c=7.5 and 10 cm while the collar efficiency increased for the abutment of length L_a=20 cm having a collar of B_c=5 cm and abutments of lengths L_a=30 and 40 cm. In this elevation, the maximum scour reduction was observed for the abutment of length L_a=30 cm having a collar of B_c=10 cm and the worst ones were obtained for the abutment of length L_a=20 cm having collar widths of B_c=7.5 and 10 cm. For this stage of the experiments, when collars were placed at the elevations of $Z_c/y_{0.7}$= -0.25, ±0.00, it is hard to make any comments on the effect of the abutment length on scour reduction performances of the collars. However, when the collars were attached to the elevation of $Z_c/y_{0.7}$= -0.50, it can be stated that the collar efficiency increases with increasing abutment length because the scour formation around the larger abutments penetrates deeper into the bed material and the collars located deeper into the bed material can be more adequate in reducing the maximum scour depth.

At the end of the second stage, at the elevation of $Z_c/y_{0.7}$= ±0.00, the maximum scour reduction was obtained for the abutment of length L_a=30 cm and the worst ones were obtained for L_a=40 cm for a given collar size. For this collar elevation, the scour reduction performances of the collars decreased for the longer abutment of length L_a=40 cm when compared to the first stage of the experiments. Moreover, when the collars were placed at the elevation of $Z_c/y_{0.7}$= -0.25, the scour reduction efficiencies of the collars attached to the abutment of length L_a=40 cm dramatically increased and the collars were found more efficient for the abutment of length L_a=40 cm than L_a=30 cm for a given collar size. Nevertheless, it should be also underlined that the efficiency of the collar of B_c=10 cm was observed as close to each other regardless of the abutment length. At this elevation, the maximum scour reductions were obtained for the abutments of lengths L_a=30 and 40 cm having collars of B_c=10 cm and the worst ones for the abutments of lengths L_a=30 and 40 cm having collars of B_c=5 cm. Finally, at the elevation of $Z_c/y_{0.7}$= -0.50, the collars of B_c=10 cm showed more successful results in reducing the maximum scour depth for the abutment of length L_a=40 cm than L_a=30 cm as well as the first stage of the experiments. However, the efficiencies of the collars of B_c=5 and 7.5 cm attached to the abutments of lengths L_a=30 and 40 cm were close to each other. At this elevation, the optimal collar performance was obtained for the abutment of length L_a=40 cm having a collar of B_c=10 cm.

At the end of the third stage of the experiments, it can be stated that the collar efficiency decreased with increasing abutment length for a given collar elevation. At the elevation of $Z_c/y_{0.7}$= -0.25, ±0.00, the efficiency of the collar of B_c=10 cm that attached to the abutments of lengths L_a=20 and 30 cm were almost the same while the efficiencies of the collars of B_c=5 and 7.5 cm gave more successful results in reducing the maximum scour depth around the abutment of length L_a=20 cm than L_a=30 cm. At the end of the 6 hours, the best collar performances were obtained for the abutment of length L_a=30 cm having a collar size of B_c=10 cm and the worst ones were obtained for the abutment of length L_a=40 cm with B_c=5 cm.

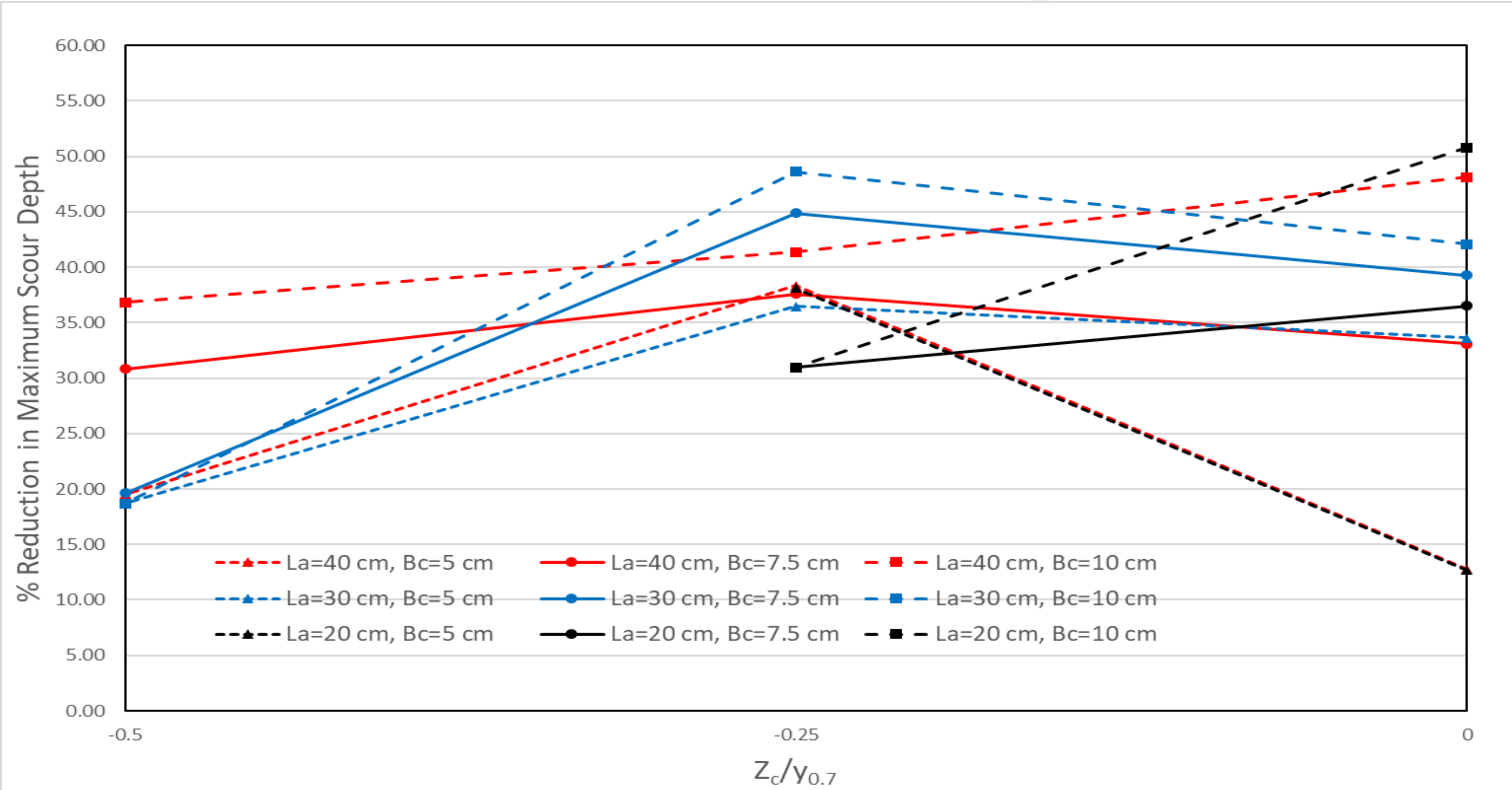

Figure 5.48 Effect of collar size and elevation on the maximum scour depth around the rectangular abutments (t=2 hours)

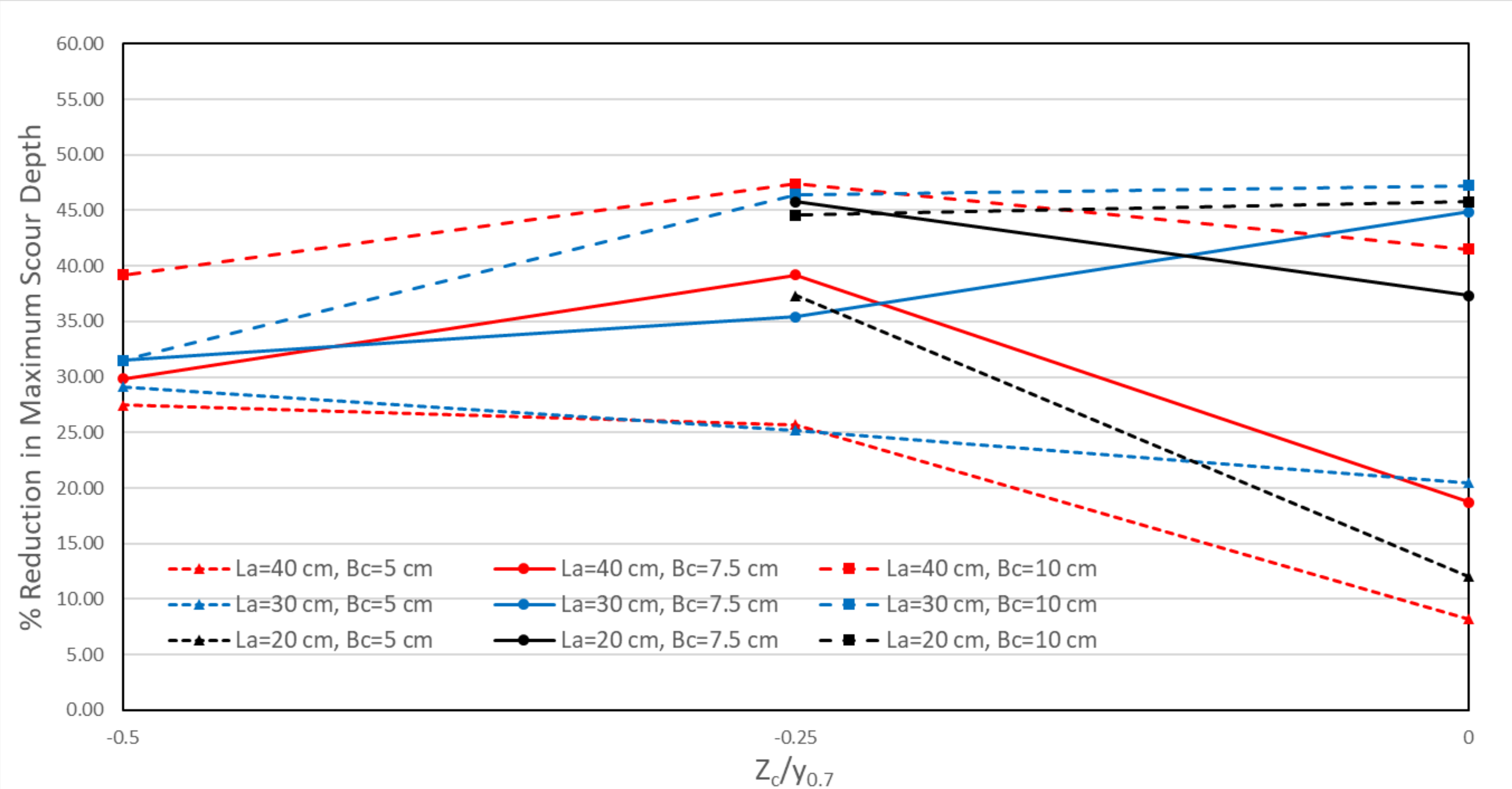

Figure 5.49 Effect of collar size and elevation on the maximum scour depth around the rectangular abutments (t=4 hours)

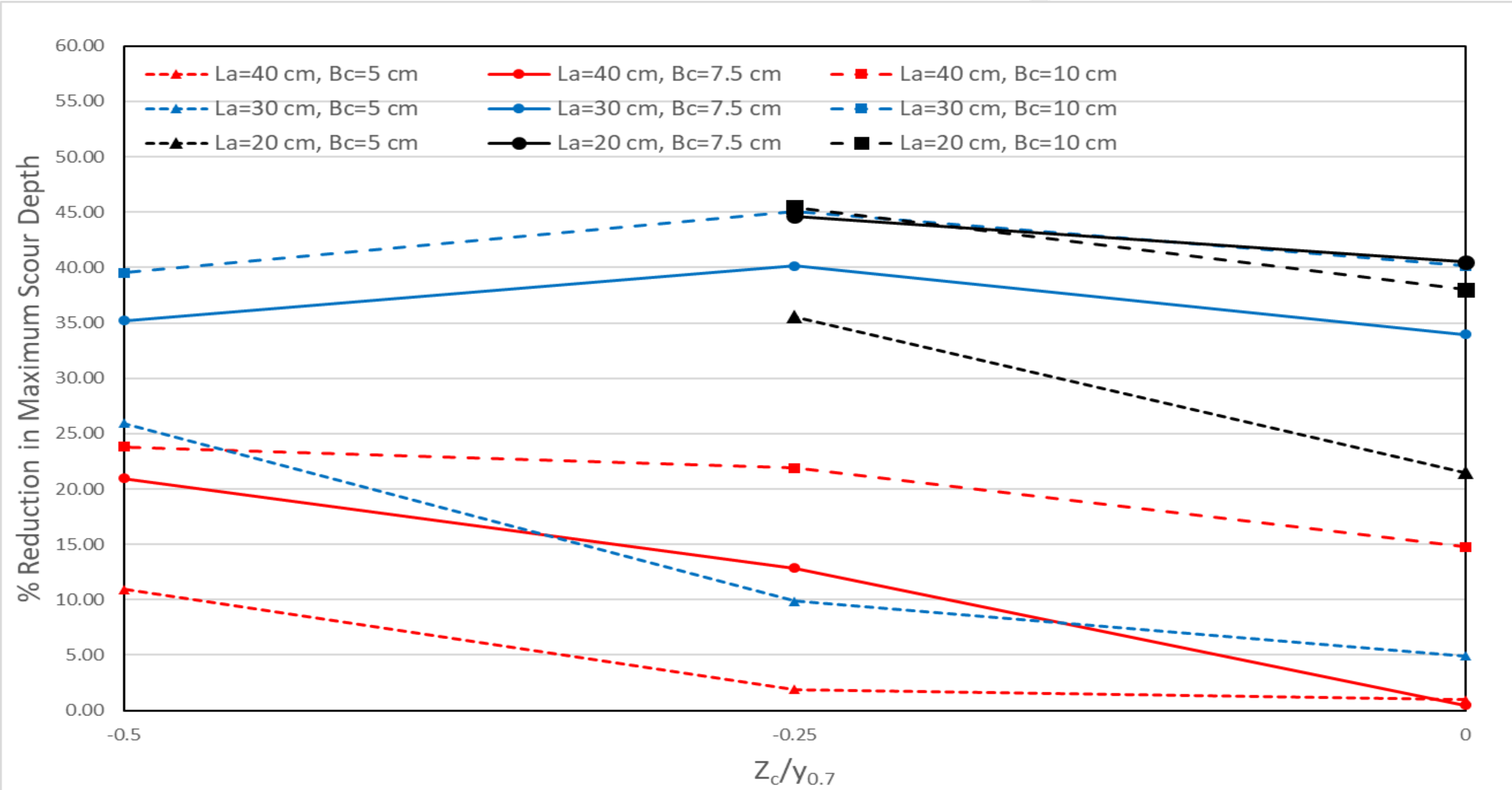

Figure 5.50 Effect of collar size and elevation on the maximum scour depth around the rectangular abutments (t=6 hours)

The effect of collar size and flow intensity on the maximum scour depth around all the rectangular abutment lengths tested in this study is presented in Figures 5.51-53. Except some abutment-collar arrangements; L_a=30 cm with B_c=7.5 cm and 10 cm, and L_a=20 cm with B_c= 5 cm and 7.5 cm in the zone of U/U_c between 0.7 and 0.8, for the rest of the cases tested, scour reduction performances decreased as U/U_c increased for a given abutment length and collar size when collars were placed at the elevation of $Z_c/y_{0.7}$= ±0.00. The effect of collars decreased as the abutment length increased with increasing flow intensity and time. At the end of the first and second stages of the experiments with the flow intensities of 0.7 and 0.8 respectively, the efficiencies of the collars did not show significant differences for the abutment lengths of L_a= 20 and 30 cm; however, for the abutment of length L_a=40 cm, the efficiencies of the collars dramatically decreased. Between the 4th and 6th hours of the experiment with the flow intensity of 0.9, the efficiencies of the collars for the longer abutments of lengths L_a=30 and 40 cm decreased while for the shorter abutment of length, L_a=20 cm increased.

At the elevation of $Z_c/y_{0.7}$= -0.25, at the end of the first and second stages of the experiments, it is hard to make any comments about the effect of abutment length on the scour reduction performances of the collars. At these periods, the maximum scour reductions were obtained for the abutments of lengths L_a=30 and 40 cm having a collar of B_c=10 cm respectively. However, between the 4th and 6th hour of the experiments, the efficiencies of the collars attached to the abutment of length L_a=40 cm dramatically decreased with the increasing flow intensity and the worst scour reductions were observed for this abutment length for a given collar size. Furthermore, the maximum scour reductions for a given collar size were observed for the shortest abutment of length L_a=20 cm except the case of U/U_c=0.7. Hence, it can be said that the efficiencies of the collars decreased as the abutment length increased during the high flow intensities.

When collars were tested at the elevation of $Z_c/y_{0.7}$= -0.50, the scour reduction performances of the collars attached to the abutment of length L_a=40 cm was generally better than the abutment of length L_a=30 cm for a given collar size. However, after the 4th hour of the experiments, when the flow intensity value increased to 0.9, the collars became more efficient for the abutment of length L_a=30 cm. Between the 4th and 6th hours, the efficiencies of the collars attached to the abutment of length L_a=40 cm dramatically decreased while L_a=30 cm increased. So, based on experimental results, it can be revealed that as the scouring rate increased, collars started to be more effective as the abutment length decreased.

The ranges of the % reductions in maximum scour depths around the rectangular abutments tested in this study is given in Table 5.5 as a function of collar location, flow intensity and L_a/B_c values.

Table 5.5 The ranges of minimum and maximum % reductions in maximum scour depths around the rectangular abutments tested

$2.0 \leq L_a/B_c \leq 8.0$			
$Z_c/y_{0.7}$	t (hour)	U/U_c	The range of % reduction in maximum scour depth
±0.00	2	0.7	12.70 - 50.79
	4	0.8	8.19 - 47.24
	6	0.9	0.48 - 40.50
-0.25	2	0.7	30.95 - 48.60
	4	0.8	25.20 - 47.37
	6	0.9	1.90 - 45.45
-0.50	2	0.7	18.69 - 36.84
	4	0.8	27.49 - 39.18
	6	0.9	10.95 - 39.51

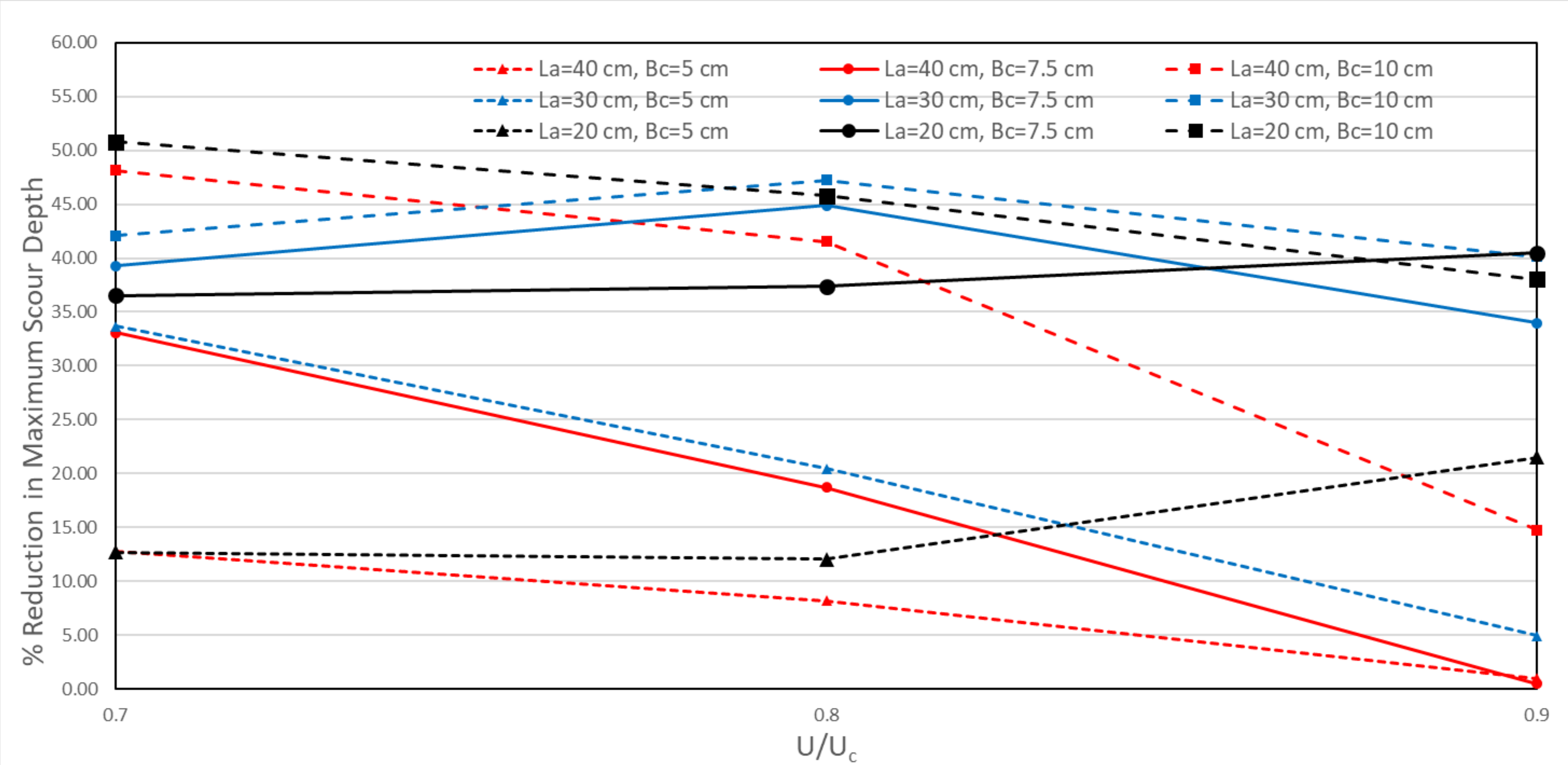

Figure 5.51 Effect of collar size and flow intensity on the maximum scour depth around the rectangular end abutment for $Z_c/y_{0.7}=\pm0.00$

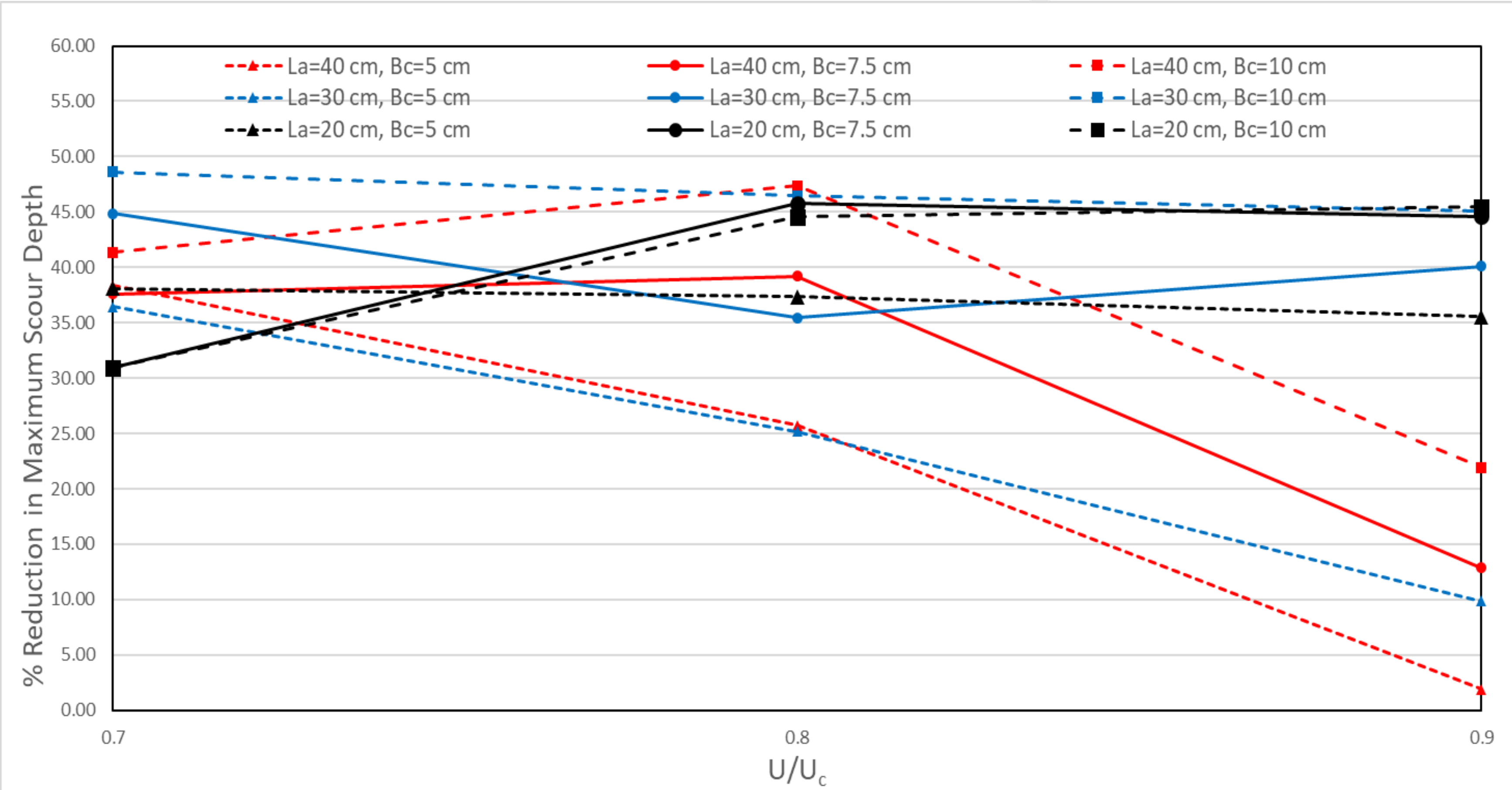

Figure 5.52 Effect of collar size and flow intensity on the maximum scour depth around the rectangular abutments for $Z_c/y_{0.7}$= -0.25

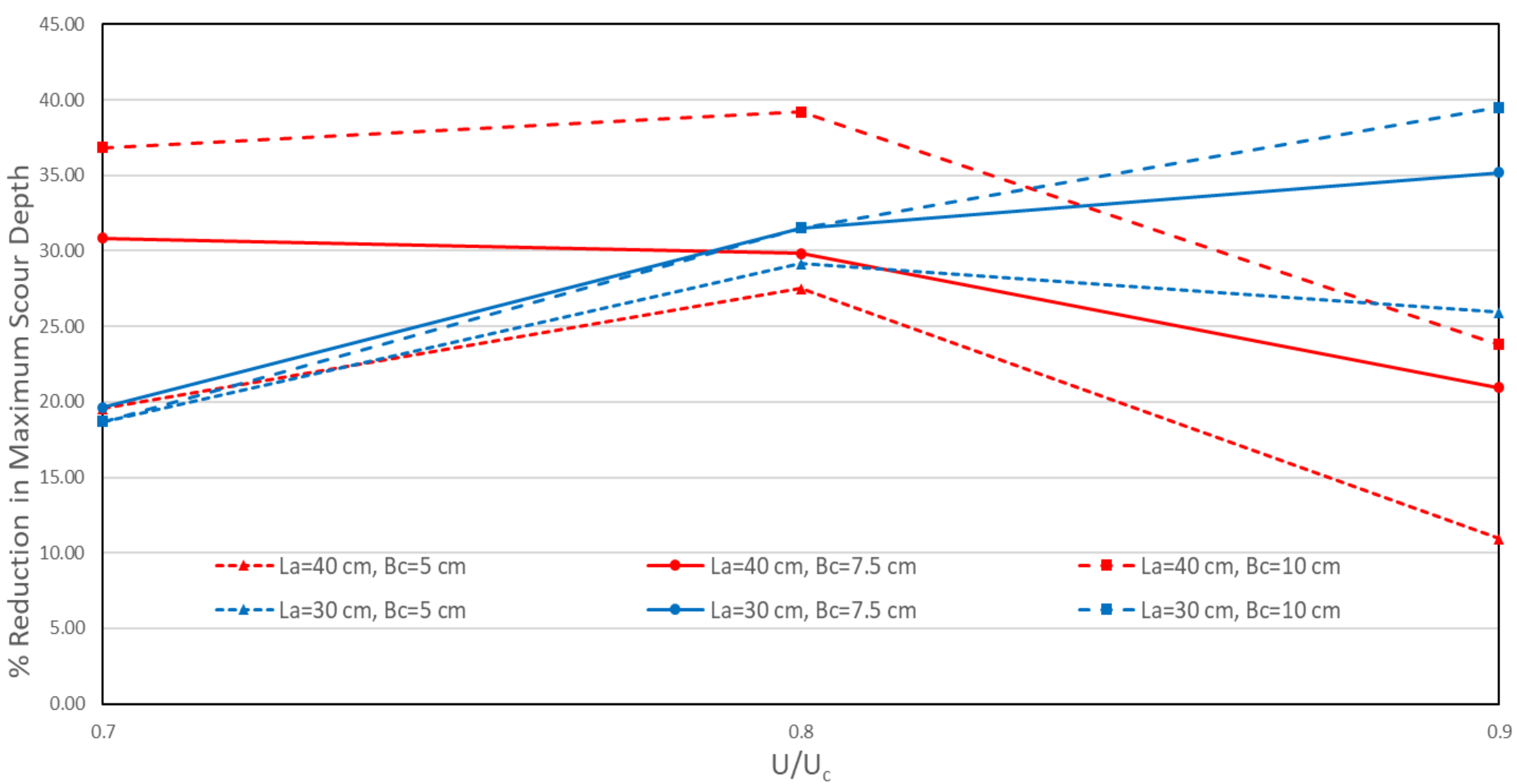

Figure 5.53 Effect of collar size and flow intensity on the maximum scour depth around the rectangular abutments for $Z_c/y_{0.7}$= -0.50

5.6.3 Comparison of the Scour Reduction Performances of the Collars Around the Semi-Circular End and Rectangular Abutments

In this subsection, the scour reduction efficiencies of the rectangular and semi-circular end collars that were attached to the semi-circular end and rectangular abutments respectively are compared to each other. On the figures, the semi-circular end and rectangular abutments are denoted as SC and RC respectively.

5.6.3.1 The Abutment of Length L_a=40 cm

In Figures 5.54-5.56, the comparison of the scour reduction performances of the varying collar sizes and elevations around the semi-circular end and rectangular abutments of length L_a=40 cm are presented. At the end of the first stage of the experiments, at the elevation of $Z_c/y_{0.7}$= ±0.00, the semi-circular end collars were dominantly more effective in reducing the maximum scour depths around the semi-circular end abutments when compared to the rectangular collars around the rectangular abutments for a given collar width. However, when the collars were placed at the elevation of $Z_c/y_{0.7}$= -0.25, the collar efficiency of both abutment shapes started to converge to each other even though the semi-circular end collars were still more effective regardless of the collar width. On the contrary, the rectangular collars became more efficient than the semi-circular end collars at the elevation of $Z_c/y_{0.7}$= -0.50.

At the end of the second stage of the experiments, the semi-circular end collars at the elevation of $Z_c/y_{0.7}$= ±0.00 around the semi-circular end abutments were still more effective in reducing the maximum scour depth than the rectangular collars attached to the rectangular abutments for a given collar width. However, when the collars were placed at the elevation of $Z_c/y_{0.7}$= -0.25, the rectangular collars of B_c=7.5 and 10 cm showed more successful results in reducing the maximum scour depth. At the elevation of $Z_c/y_{0.7}$= -0.50, the maximum scour reduction was observed for the rectangular collar of B_c=10 cm attached to the rectangular abutment.

The efficiencies of the other abutment-collar arrangements were very close to each other.

Finally, at the end of the third stage of the experiments, at all the collar elevations whether at the bed level or below the bed level, the semi-circular end abutments appeared to be more efficient than the rectangular abutments for a given collar width. Nonetheless, it might be stated that the efficiencies of the semi-circular end and rectangular collars converged to each other when the collars were placed deeper into the bed material. In other words, the efficiencies of the rectangular collars started to be more effective below the bed material.

As a final remark it can be concluded that at the end of each stage, semi-circular end collars showed better performances compared to rectangular collars almost at any $Z_c/y_{0.7}$ value tested. The best efficiencies in reducing the maximum scour depth were achieved when the collars were placed on the abutments at the bed level, $Z_c/y_{0.7}$=±0.00.

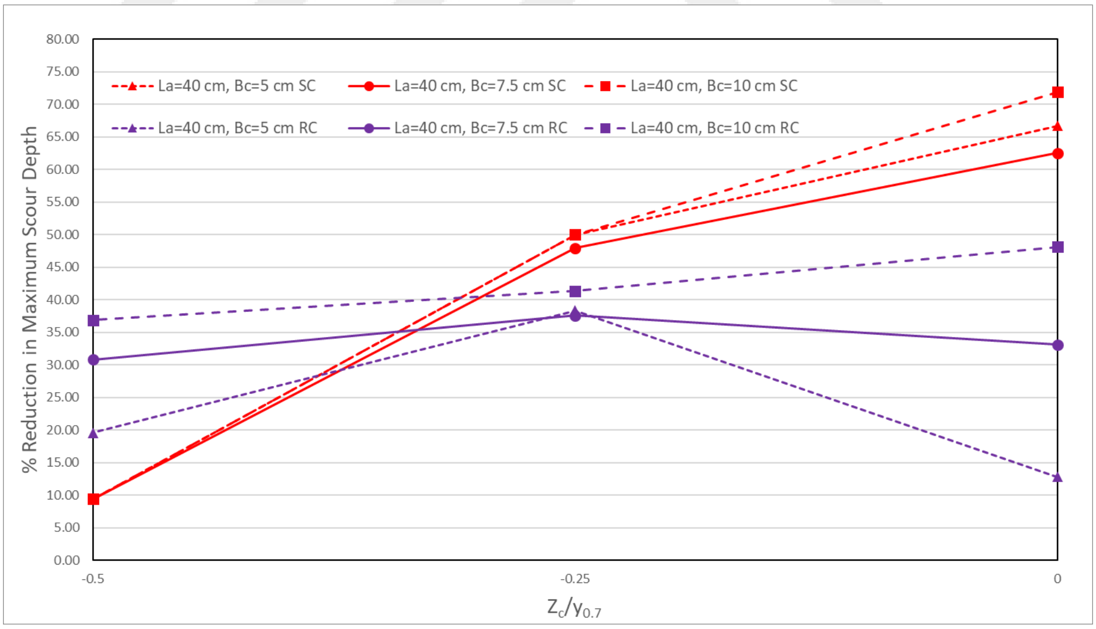

Figure 5.54 Comparison of the effects of collar size and elevation on the maximum scour depth around the semi-circular end and rectangular abutments of length L_a=40 cm (t= 2 hours)

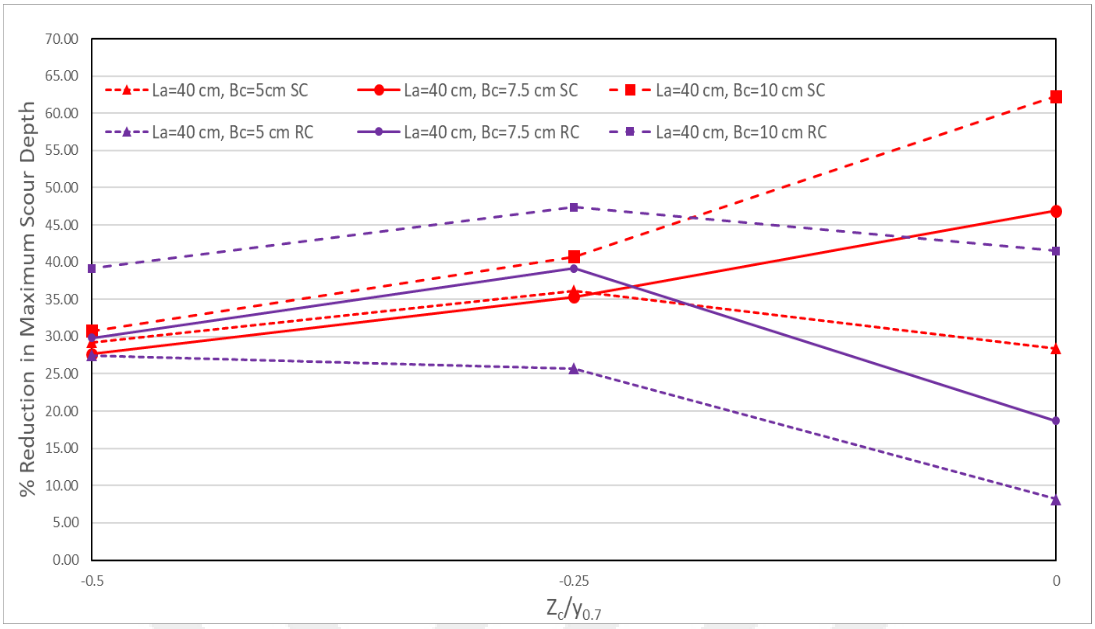

Figure 5.55 Comparison of the effects of collar size and elevation on the maximum scour depth around the semi-circular end and rectangular abutments of length L_a=40 cm (t= 4 hours)

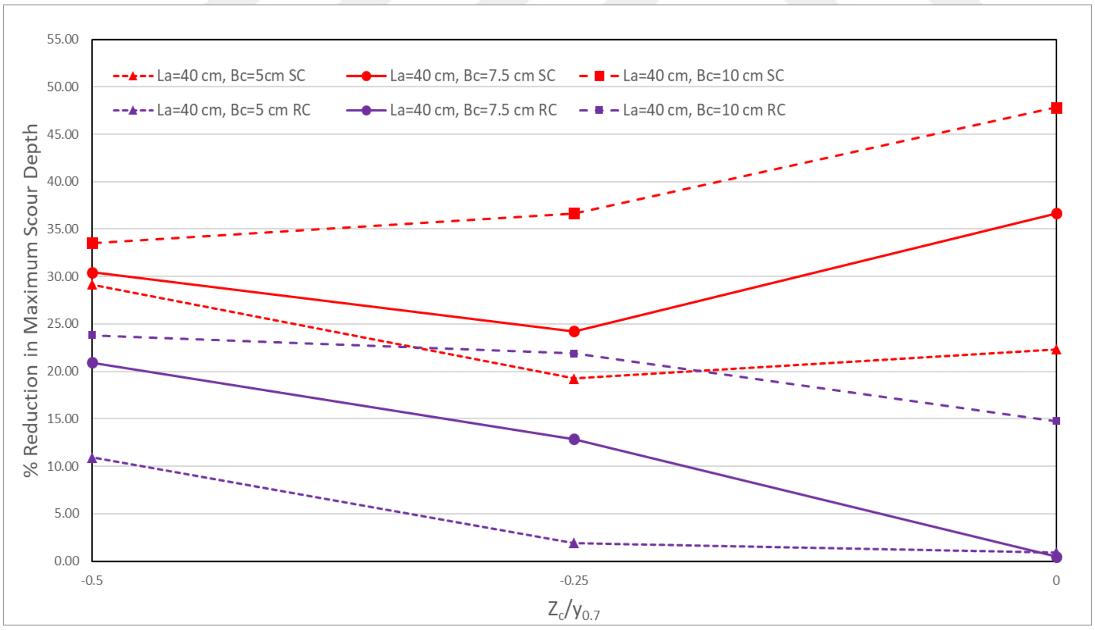

Figure 5.56 Comparison of the effects of collar size and elevation on the maximum scour depth around the semi-circular end and rectangular abutments of length L_a=40 cm (t= 6 hours)

In Figures 5.57-5.59, the comparison of the scour reduction performances of the varying collar sizes and flow intensities around the semi-circular end and rectangular abutments of length L_a=40 cm are presented. When the collars were placed at the elevation of $Z_c/y_{0.7}$= ±0.00, the scour reduction performances of the semi-circular end collars were obtained greater than the rectangular collars at any flow intensity tested, except the case of L_a=40 cm with B_c=10 cm for U/U_c=0.8, for a given collar width. Nonetheless, the efficiencies of both collar shapes around both abutment shapes decreased with increasing flow intensity and time. On the other hand, at the elevation of $Z_c/y_{0.7}$= -0.25, at the initial and final stages of the experiments, the efficiencies of the semi-circular end collars were observed greater than those of the rectangular collars for a given collar width. On the contrary, at the end of the second stage of the experiment with the flow intensity of 0.8, the rectangular collars of B_c=7.5 and 10 cm attached to the rectangular abutments were found to be more effective in reducing the maximum scour depth than the semi-circular end collars. Finally, when the collars were placed at the elevation of $Z_c/y_{0.7}$= -0.50, the efficiencies of the rectangular collars decreased with increasing flow intensity and time; on the contrary, the efficiencies of the semi-circular end collars increased with time. Hence, in this collar elevation, the rectangular collars were found to be more efficient at the 2nd hour with the flow intensity of 0.7 for a given collar width. However, at the end of the 6th hour after applying each flow intensities of 0.7,0.8 and 0.9 for 2 hours, the semi-circular end collars were found to be more efficient in reducing the maximum scour depth than the rectangular collars for a given collar width.

Finally, regarding the effect of abutment and collar shape on the reduction of maximum scour depth it can be stated that the semi-circular end collars are more effective than the rectangular collars at the end of experiment durations of 6 hours with varying flow intensities.

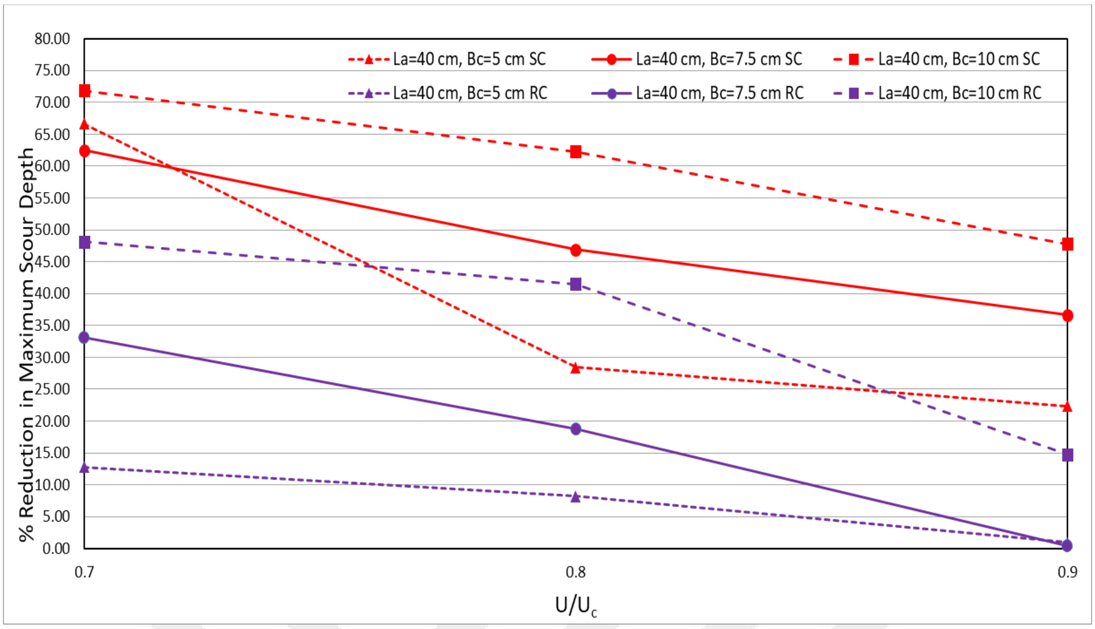

Figure 5.57 Comparison of the effect of collar size and flow intensity on the maximum scour depth around the semi-circular end and rectangular abutments of L_a=40 cm for $Z_c/y_{0.7}$= ±0.00

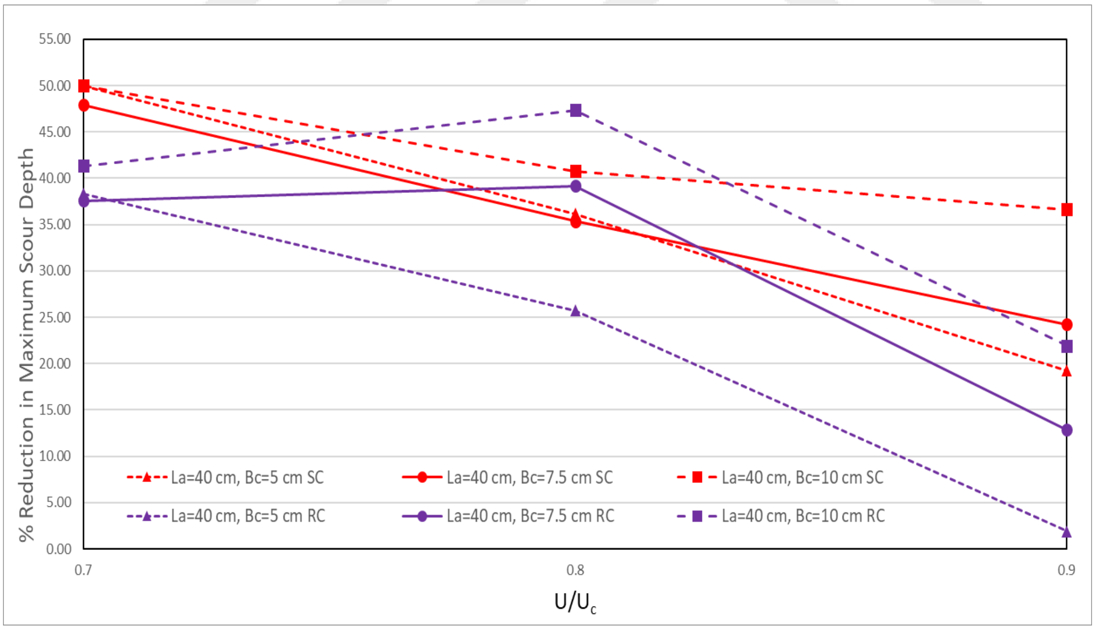

Figure 5.58 Comparison of the effect of collar size and flow intensity on the maximum scour depth around the semi-circular end and rectangular abutments of L_a=40 cm for $Z_c/y_{0.7}$= -0.25

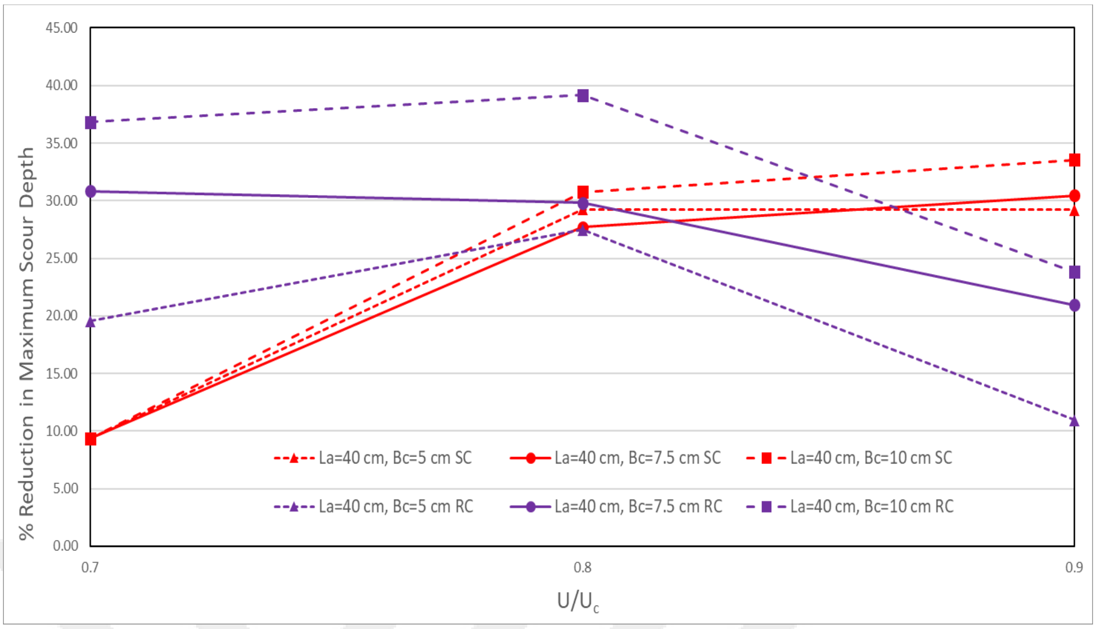

Figure 5.59 Comparison of the effect of collar size and flow intensity on the maximum scour depth around the semi-circular end and rectangular abutments of L_a=40 cm for $Z_c/y_{0.7}$= -0.50

5.6.3.2 The Abutment of Length L_a=30 cm

The comparison of the scour reduction performances of the varying collar sizes and elevations around the semi-circular end and rectangular abutments of length L_a=30 cm are shown in Figures 5.60-5.62. At the end of the first stage of the experiments, when the collars were placed at the elevation of $Z_c/y_{0.7}$= ±0.00, the maximum scour reduction was observed for the semi-circular end collar of B_c=10 cm attached to the semi-circular end abutment. Although the scour reduction efficiencies of the other abutment-collar arrangements were obtained very close to each other, it should be indicated that the efficiencies of the semi-circular end collars were found greater than the rectangular collars for a given collar width. On the other hand, at the elevations of $Z_c/y_{0.7}$= -0.50 and -0.25, the rectangular collars gave more successful results in reducing the maximum scour depth when compared to the semi-circular end collars.

At the end of the second and third stages of the experiments, the performances of the semi-circular end collars regarding the maximum scour reduction were better than those of rectangular collars for a given collar width when the collars were placed at the elevation of $Z_c/y_{0.7}$= ±0.00. Furthermore, the worst scour reduction performance was observed for the rectangular collar of B_c=5 cm around the rectangular abutment. However, when the collars were placed below the bed level, $Z_c/y_{0.7}$= -0.50 and -0.25, the efficiencies of the semi-circular end collars dramatically decreased and at the elevation of $Z_c/y_{0.7}$= -0.50, the rectangular collars started to become more efficient. At the elevation of $Z_c/y_{0.7}$= -0.25, the maximum scour reductions were observed for the rectangular collar of B_c=10 cm. However, the efficiencies of the rectangular collars of B_c=5 and 7.5 cm were found less than those of semi-circular end collars. Furthermore, the minimum scour reduction efficiency at this elevation was observed for the rectangular collar of B_c=5 cm.

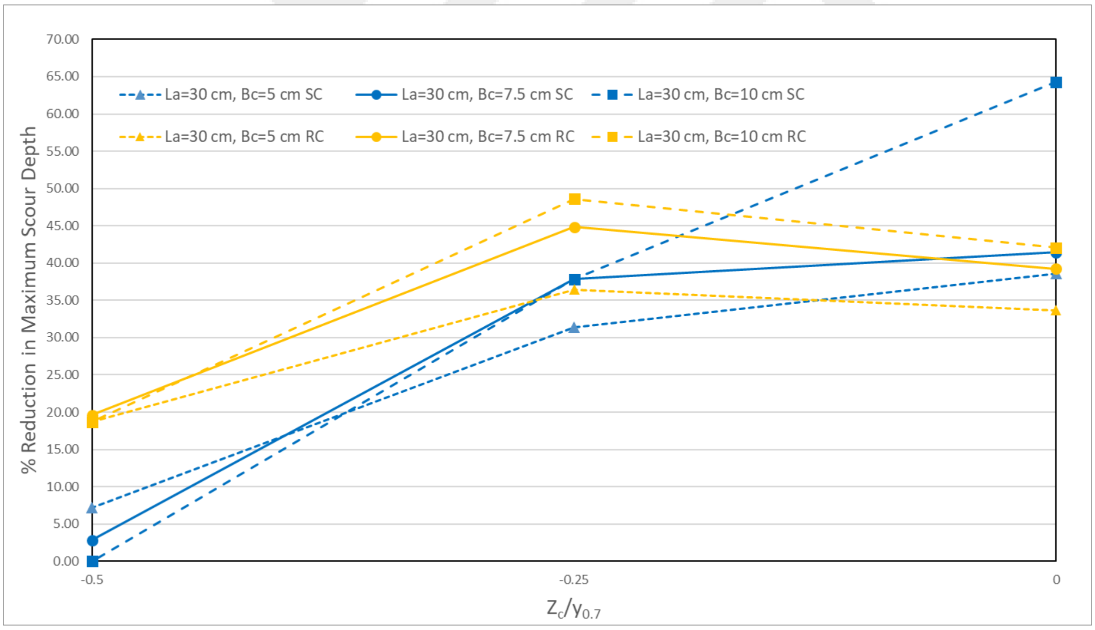

Figure 5.60 Comparison of the effects of collar size and elevation on the maximum scour depth around the semi-circular end and rectangular abutments of length L_a=30 cm (t= 2 hours)

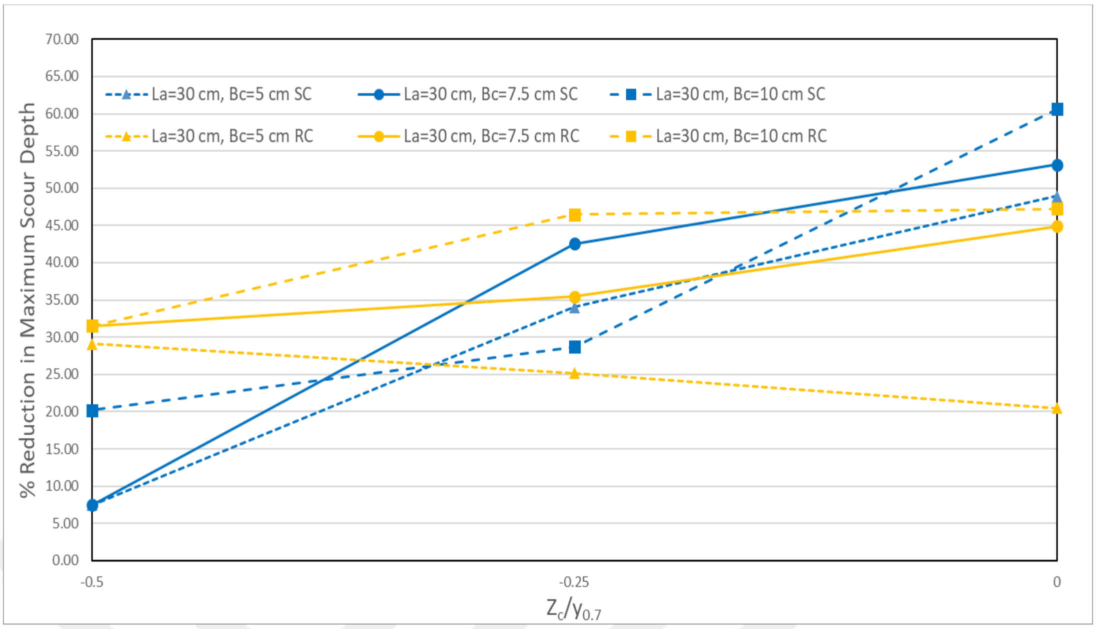

Figure 5.61 Comparison of the effects of collar size and elevation on the maximum scour depth around the semi-circular end and rectangular abutments of length L_a=30 cm (t= 4 hours)

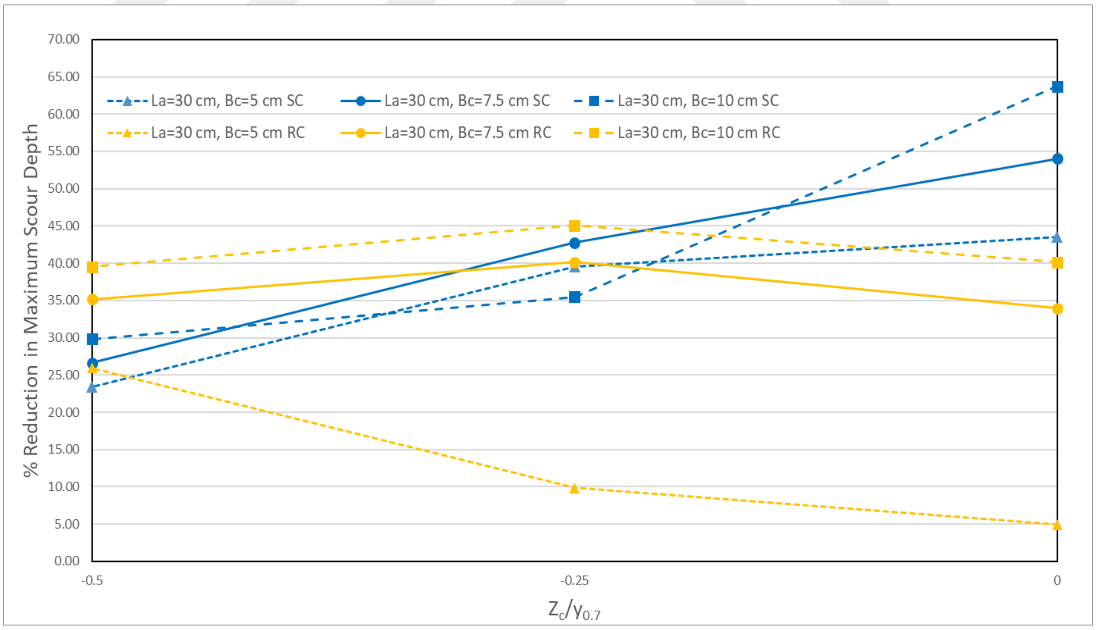

Figure 5.62 Comparison of the effects of collar size and elevation on the maximum scour depth around the semi-circular end and rectangular abutments of length L_a=30 cm (t= 6 hours)

The comparison of the scour reduction performances of the varying collar sizes and flow intensities around the semi-circular end and rectangular abutments of length L_a=30 cm are shown in Figures 5.63-5.65. When the collars were placed at the elevation of $Z_c/y_{0.7}$= ±0.00, the scour reduction performances of the semi-circular end collars were obtained greater than those of the rectangular collars throughout the experiments regardless of the flow intensity and time for a given collar width. On the other hand, at the elevation of $Z_c/y_{0.7}$= -0.25, the maximum scour reductions were observed for the rectangular collar of B_c=10 cm for all the flow intensities tested. During the first stage of the experiments with a flow intensity of 0.7, the rectangular collars were found to be more efficient when compared to the semi-circular end collars for a given collar width. However, rectangular collars started to become less efficient with increasing flow intensity and time. In other words, at the end of the second and third stages of the experiments, at the elevation of $Z_c/y_{0.7}$= -0.25, it was shown that the semi-circular end collars were more effective in reducing the maximum scour depth except for the rectangular collar of B_c=10 cm. Finally, when collars were placed at the elevation of $Z_c/y_{0.7}$= -0.50, the maximum scour reductions were observed with the rectangular collars for a given collar width and flow intensity.

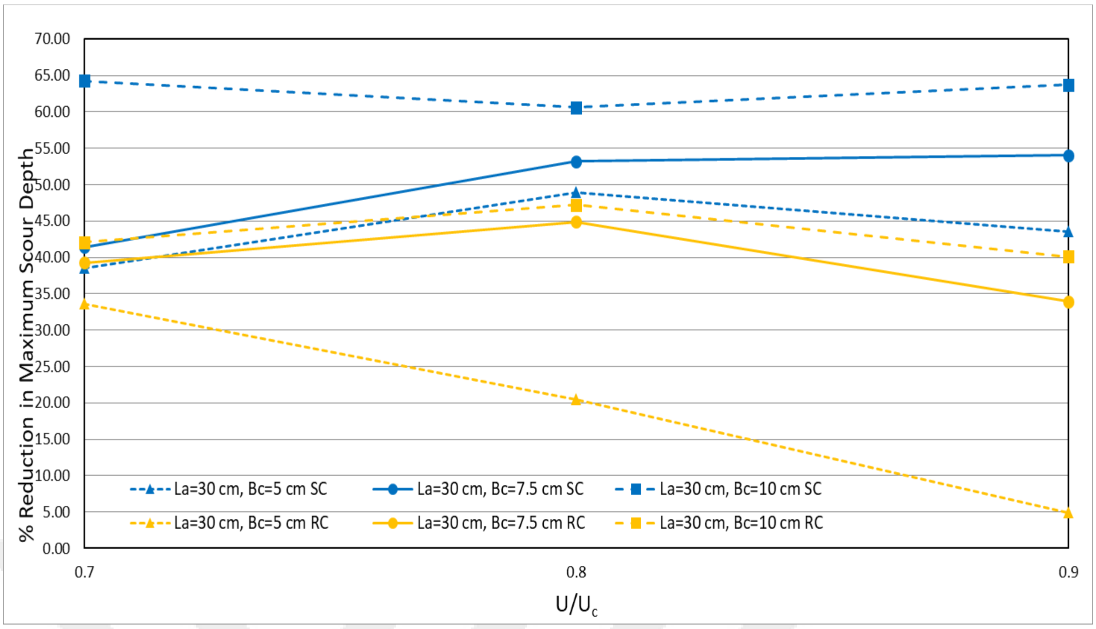

Figure 5.63 Comparison of the effect of collar size and flow intensity on the maximum scour depth around the semi-circular end and rectangular abutments of length L_a=30 cm for $Z_c/y_{0.7}= \pm 0.00$

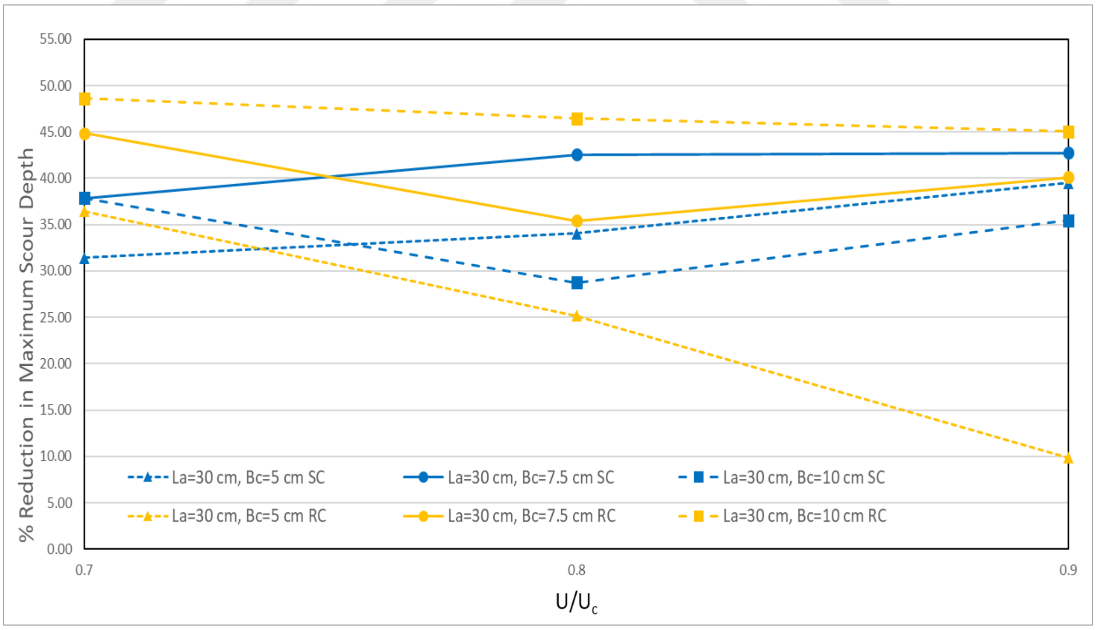

Figure 5.64 Comparison of the effect of collar size and flow intensity on the maximum scour depth around the semi-circular end and rectangular abutments of length L_a=30 cm for $Z_c/y_{0.7}= -0.25$

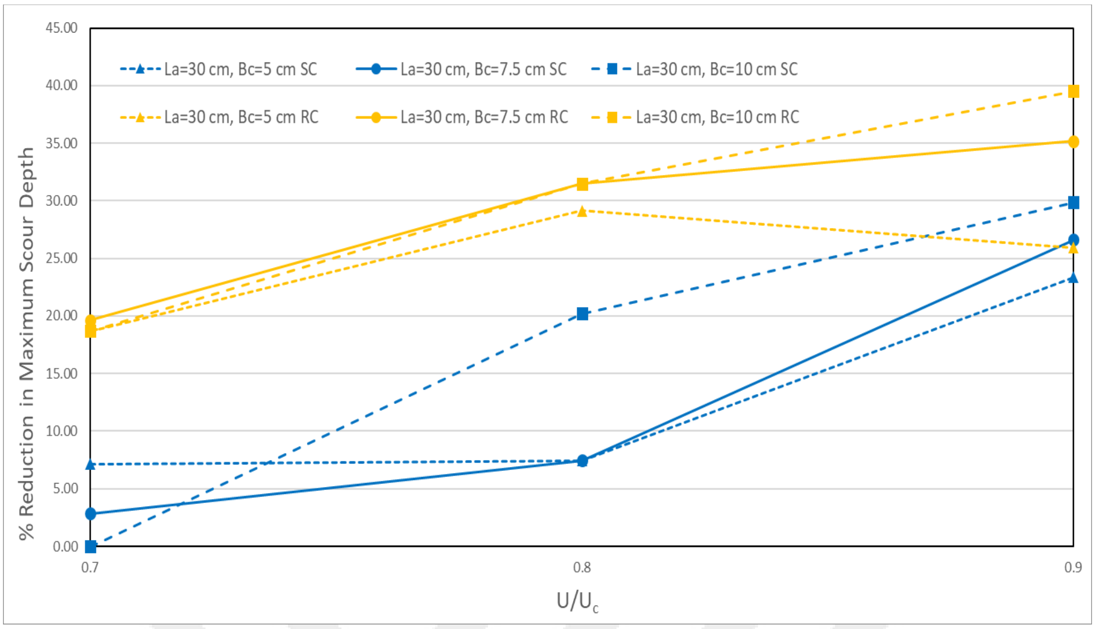

Figure 5.65 Comparison of the effect of collar size and flow intensity on the maximum scour depth around the semi-circular end and rectangular abutments of length L_a=30 cm for $Z_c/y_{0.7}$= -0.50

5.6.3.3 The Abutment of Length L_a=20 cm

In Figures 5.66-5.68, the comparison of the scour reduction performances of the varying collar sizes and elevations around the semi-circular end and rectangular abutments of length L_a=20 cm are presented. At the end of the first stage of the experiments, when the collars were placed at the elevation of $Z_c/y_{0.7}$= ±0.00, the scour reduction performances of the rectangular collars of B_c=7.5 and 10 cm attached to the rectangular abutment were much larger than those of the semi-circular end collars of B_c=7.5 and 10 cm. On the contrary, the semi-circular end collar of B_c=5 cm gave better results than the rectangular collar of B_c=5 cm. At this collar level, the maximum scour reduction was obtained for the rectangular collar of B_c=10 cm around the rectangular abutment. On the other hand, at the elevation of $Z_c/y_{0.7}$= -0.25, the semi-circular end collars had no effect in reducing the maximum scour depth. On the other hand, the rectangular collars around the rectangular abutment had a significant effect in reducing the maximum scour depth around the abutment.

At the end of the second and third stages of the experiments, the semi-circular end collars had more scour reduction efficiencies when compared to the rectangular collars for a given collar width at $Z_c/y_{0.7}= \pm 0.00$. However, when the collars were located lower than the bed level, $Z_c/y_{0.7}= -0.25$, the efficiencies of the rectangular collars increased while the semi-circular end collars decreased. At these stages of the experiments, the maximum scour depths were observed for the semi-circular end collars of B_c=7.5 and 10 cm at the elevation of $Z_c/y_{0.7}= \pm 0.00$ while for the rectangular collars of B_c=7.5 and 10 cm at the elevation of $Z_c/y_{0.7}= -0.25$.

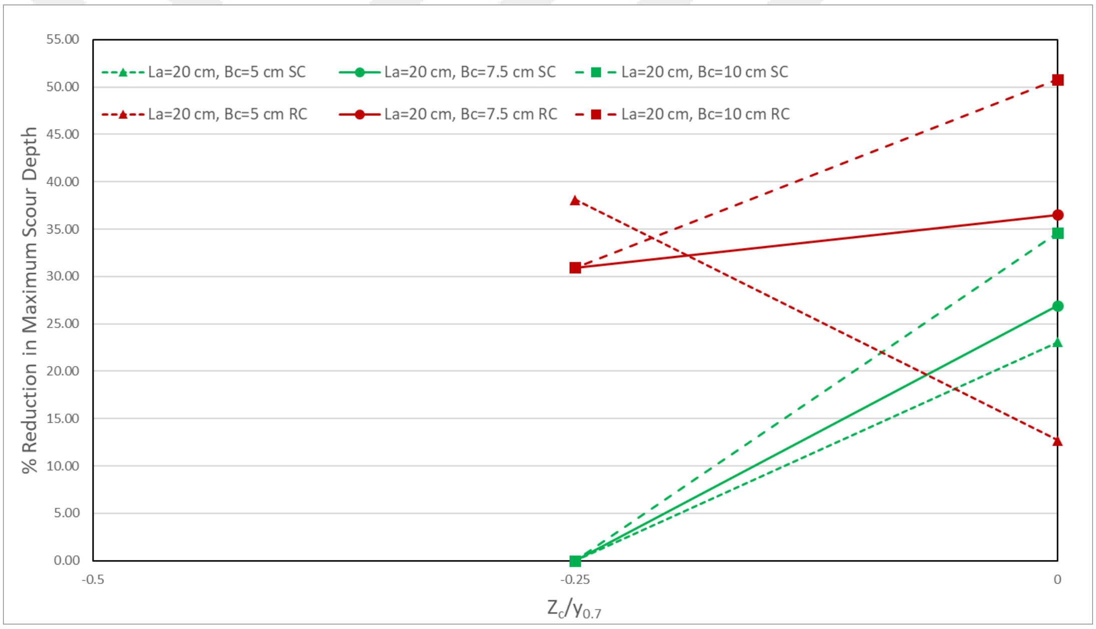

Figure 5.66 Comparison of the effects of collar size and elevation on the maximum scour depth around the semi-circular end and rectangular abutments of length L_a=20 cm (t= 2 hours)

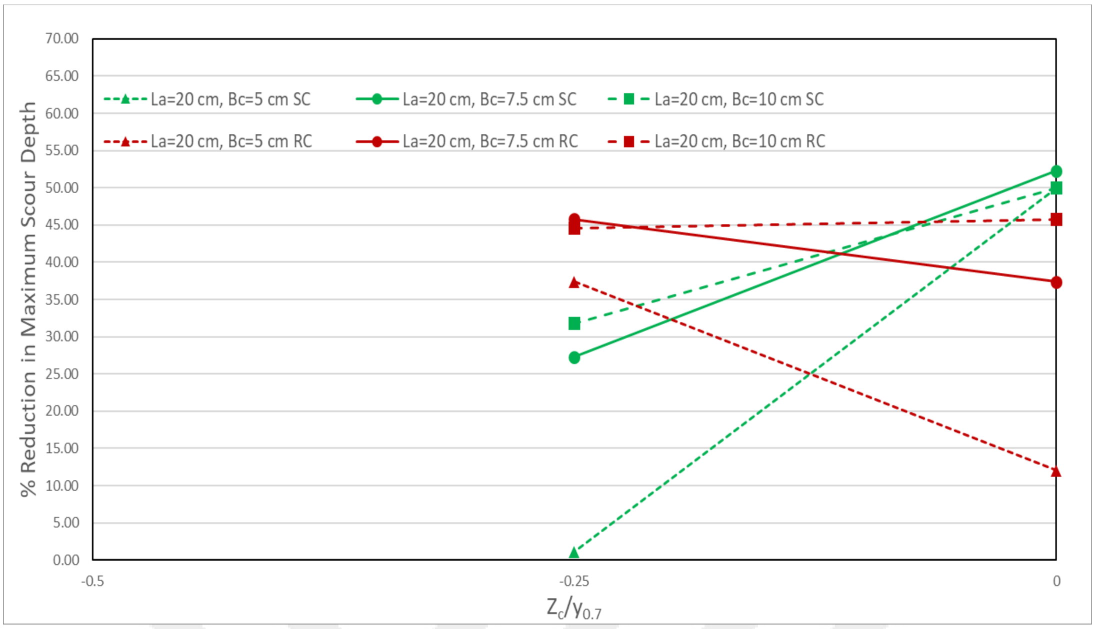

Figure 5.67 Comparison of the effects of collar size and elevation on the maximum scour depth around the semi-circular end and rectangular abutments of length L_a=20 cm (t= 4 hours)

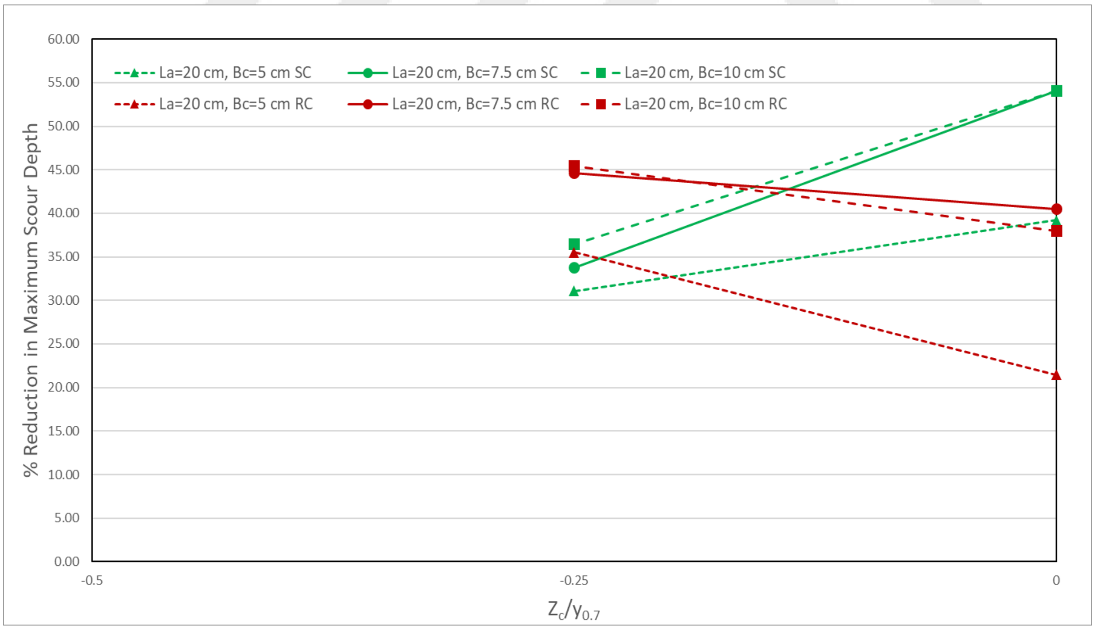

Figure 5.68 Comparison of the effects of collar size and elevation on the maximum scour depth around the semi-circular end and rectangular abutments of length L_a=20 cm (t= 6 hours)

The comparison of the scour reduction performances of the varying collar sizes and flow intensities around the semi-circular end and rectangular abutments of length L_a=20 cm are presented in Figures 5.69 and 5.70. When the collars were placed at the elevation of $Z_c/y_{0.7}$= ±0.00, the scour reduction performances of the rectangular collars of B_c=7.5 and 10 cm were usually obtained greater than those of the semi-circular end collars during the first 2 hours of the experiments having the flow intensity of 0.7. However, as the flow intensity increased, the efficiencies of the semi-circular end collars were obtained better when compared to rectangular collars for a given collar width and flow intensity. On the other hand, at the elevation of $Z_c/y_{0.7}$= -0.25, the rectangular collars showed better performances than the semi-circular end collars at any flow intensity tested.

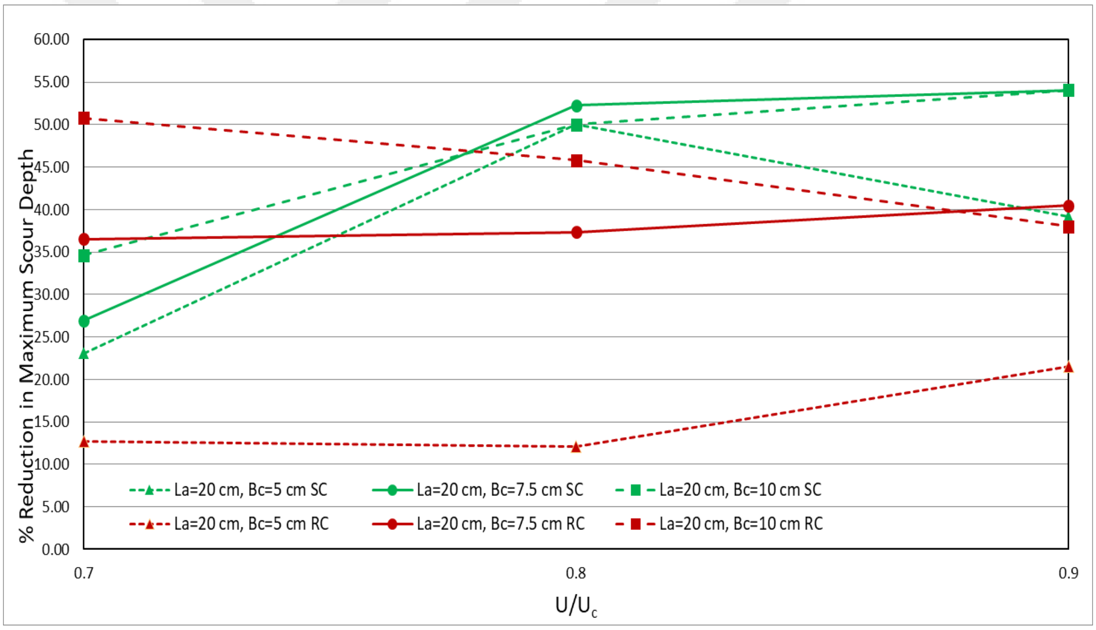

Figure 5.69 Comparison of the effect of collar size and flow intensity on the maximum scour depth around the semi-circular end and rectangular abutments of length L_a=20 cm for $Z_c/y_{0.7}$= ±0.00

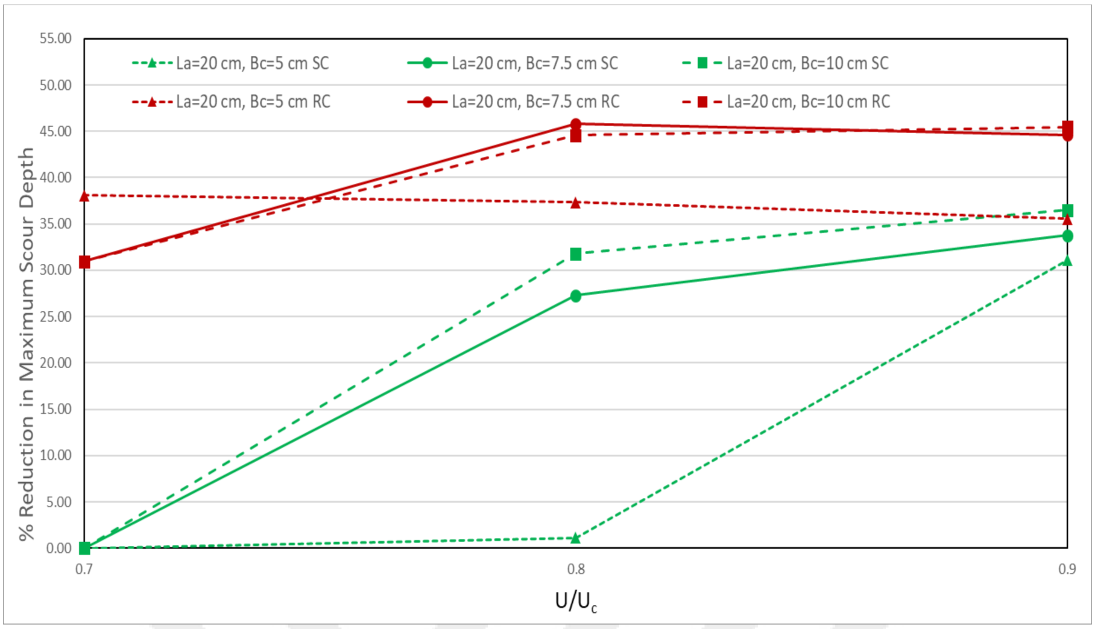

Figure 5.70 Comparison of the effect of collar size and flow intensity on the maximum scour depth around the semi-circular end and rectangular abutments of length L_a=20 cm for $Z_c/y_{0.7}$= -0.25

5.6.3.4 Summary

In summary, the semi-circular end and rectangular collars have a significant impact in reducing the scour depth around the abutments. For the abutment of length L_a=40 cm, the semi-circular end collars around the semi-circular end abutment usually showed more successful results in reducing the maximum scour depth than the rectangular collars around the rectangular abutments. This situation might occur due to the sharp nature of the rectangular collar and abutment that causes stronger vortices and higher bed shear stress that leads to greater scour depths when compared to the semi-circular end ones. However, as the abutment length decreased (i.e., L_a=20 and 30 cm), the rectangular collars showed more successful performances than the semi-circular collars when the collars were placed below the bed level (i.e., $Z_c/y_{0.7}$= -0.50 and -0.25). Especially, the efficiencies of the rectangular collars increased with increasing flow intensity and time. Based on the experimental results, it was obtained that the semi-circular collars provide a reduction in the maximum scour depth by up to 72%; on the other hand, the rectangular collars reduce the maximum scour depth by up to 51%. Table 5.6 presents the ranges of the minimum and maximum reductions in maximum scour depths around the semi-circular end and rectangular abutments as a function of $Z_c/y_{0.7}$ and flow intensity.

Table 5.6 The ranges of minimum and maximum % reductions in maximum scour depths around the semi-circular end and rectangular abutments tested

$2.0 \leq L_a/B_c \leq 8.0$				
$Z_c/y_{0.7}$	t (hour)	U/U_c	The range of % reduction in maximum scour depth	
			Semi-circular end collars	Rectangular collars
±0.00	2	0.7	23.08 - 71.88	12.70 - 50.79
	4	0.8	28.46 - 62.31	8.19 - 47.24
	6	0.9	22.36 - 63.71	0.48 - 40.50
-0.25	2	0.7	0.00 - 50.00	30.95 - 48.60
	4	0.8	1.14 - 42.55	25.20 - 47.37
	6	0.9	19.25 - 42.74	1.90 - 45.45
-0.50	2	0.7	0.00 - 9.38	18.69 - 36.84
	4	0.8	7.45 - 30.77	27.49 - 39.18
	6	0.9	23.39 - 33.54	10.95 - 39.51

5.6.4 Maximum Scour Depths Around the Abutments

As an alternative way to demonstrate the relationship between the dimensionless maximum scour depth and abutment-collar sizes, variation of $[(d_s)_{max,c}/y]$ and $\sqrt{\theta(L_a/B_c)}$ is presented in Figures 5.71 and 5.72 for the semi-circular end and rectangular abutments, respectively. The ϴ parameter represents the ratio of the total area of the abutment with collar to the area of the abutment on the horizontal plane:

$$\Theta = \frac{A_{abutment} + A_{collar}}{A_{abutment}} \tag{5.5}$$

where $A_{abutment}$ and A_{collar} are the areas of the abutment and collar on the plan view, respectively. Θ values are used to indicate the effect of the areal sizes of the abutment models with collars on the reduction of scour around the abutments. The increase in the Θ value, for a given abutment length, means an increase in the collar width.

Figure 5.71 shows that the dimensionless maximum scour depth increases with increasing $\sqrt{\theta(L_a/B_c)}$ for semi-circular end abutments. From the general trend of the data points it can be stated that the dimensionless maximum scour depth increases when the collar was placed deeper into the bed level. However, at the end of the third stage, for the $\sqrt{\theta(L_a/B_c)}$ values greater than 3.80, the collars placed at the elevation of $Z_c/y_{0.7}$= -0.50 led to smaller maximum scour depths when compared to the collars at the elevation of $Z_c/y_{0.7}$= -0.25.

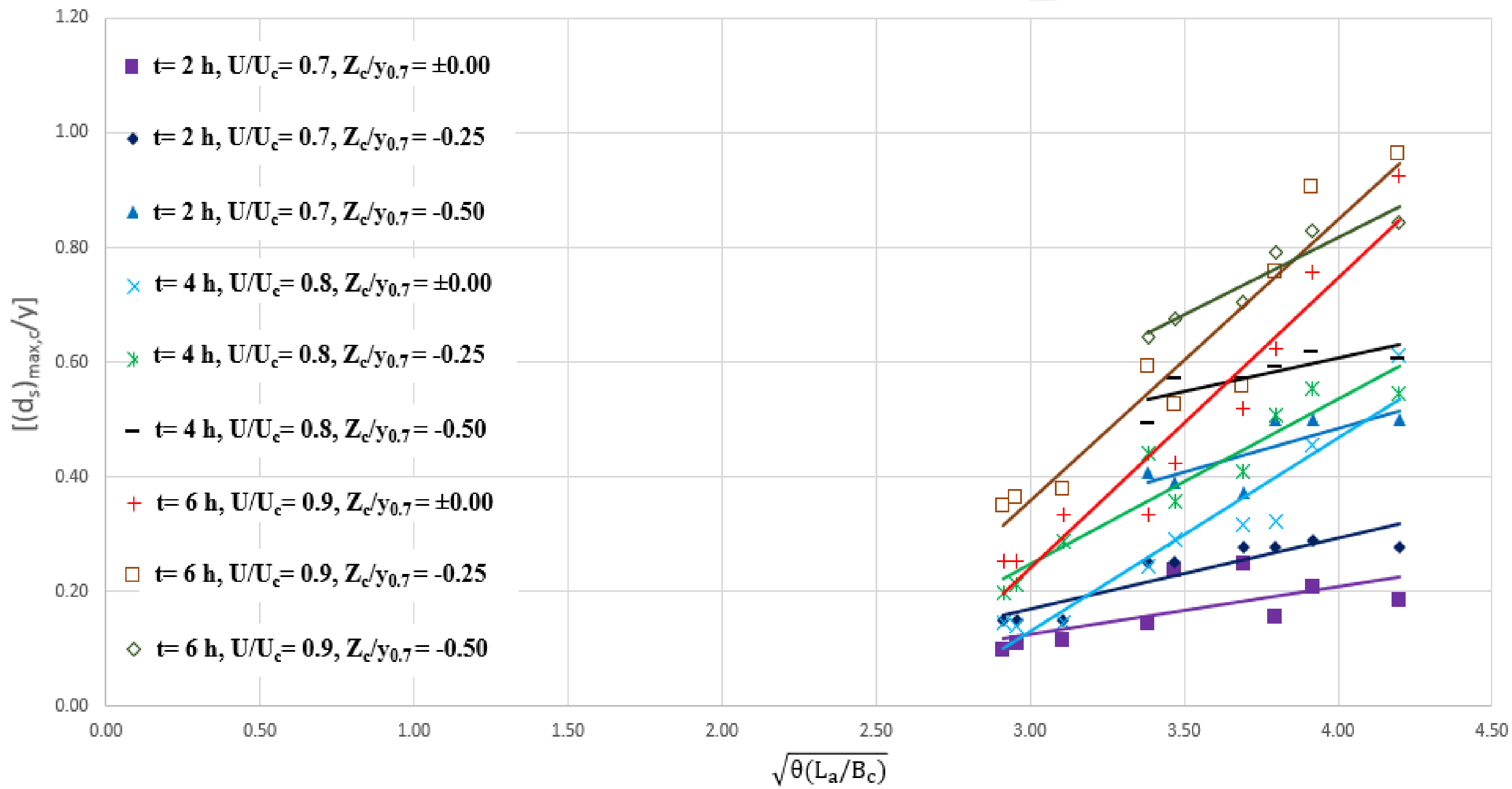

Figure 5.71 Variation of $[(d_s)_{max,c}/y]$ with $\sqrt{\theta(L_a/B_c)}$ for semi-circular end abutments

Similar to the semi-circular end abutments, the dimensionless maximum scour depth around the rectangular abutments increased with increasing $\sqrt{\theta(L_a/B_c)}$. However, Figure 5.72 demonstrates that the dimensionless maximum scour depth around the rectangular abutments generally decreased when the collars were placed below the bed level contrary to the semi-circular end abutments. Only at the end of the first stage of the experiments, the maximum dimensionless scour depths were obtained when the collars were placed at the elevation of $Z_c/y_{0.7}$= -0.50.

From Figures 5.71 and 5.72, for known θ, L_a/B_c and $Z_c/y_{0.7}$ values within the ranges of this study, [$(d_s)_{max,c}/y$] values can be determined for collar applications around the abutments. The linear relationships between the [$(d_s)_{max,c}/y$] and $\sqrt{\theta(L_a/B_c)}$ for various flow intensities, collar elevations and test durations are listed in Tables 5.7 and 5.8.

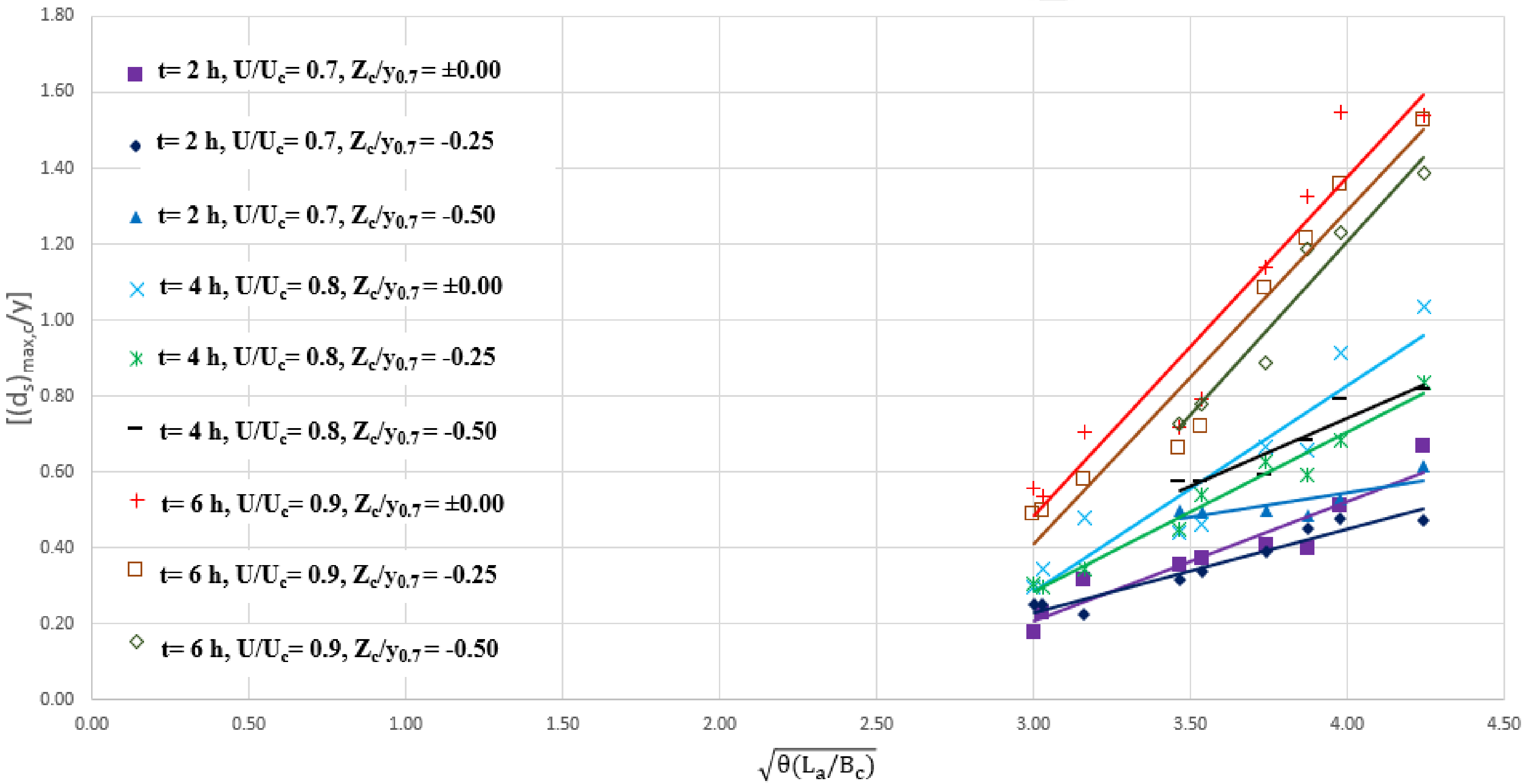

Figure 5.72 Variation of $[(d_s)_{max,c}/y]$ with $\sqrt{\theta(L_a/B_c)}$ for rectangular abutments

Table 5.7 The linear relationships between $[(d_s)_{max,c}/y]$ and $\sqrt{\theta(L_a/B_c)}$ for the semi-circular end abutments with varying flow intensities, collar elevations and test durations

	Equation	R^2
t= 2 h, U/U_c= 0.7, $Z_c/y_{0.7}$ = ±0.00	$[(d_s)_{max,c}/y] = 0.0837\sqrt{\theta\left(\frac{L_a}{B_c}\right)} - 0.1264$	0.4548
t= 2 h, U/U_c= 0.7, $Z_c/y_{0.7}$ = -0.25	$[(d_s)_{max,c}/y] = 0.1243\sqrt{\theta\left(\frac{L_a}{B_c}\right)} - 0.205$	0.8239
t= 2 h, U/U_c= 0.7, $Z_c/y_{0.7}$ = -0.50	$[(d_s)_{max,c}/y] = 0.1553\sqrt{\theta\left(\frac{L_a}{B_c}\right)} - 0.1358$	0.5831
t= 4 h, U/U_c= 0.8, $Z_c/y_{0.7}$ = ±0.00	$[(d_s)_{max,c}/y] = 0.3378\sqrt{\theta\left(\frac{L_a}{B_c}\right)} - 0.8836$	0.9117
t= 4 h, U/U_c= 0.8, $Z_c/y_{0.7}$ = -0.25	$[(d_s)_{max,c}/y] = 0.2895\sqrt{\theta\left(\frac{L_a}{B_c}\right)} - 0.622$	0.8984
t= 4 h, U/U_c= 0.8, $Z_c/y_{0.7}$ = -0.50	$[(d_s)_{max,c}/y] = 0.1175\sqrt{\theta\left(\frac{L_a}{B_c}\right)} + 0.1359$	0.6321
t= 6 h, U/U_c= 0.9, $Z_c/y_{0.7}$ = ±0.00	$[(d_s)_{max,c}/y] = 0.5089\sqrt{\theta\left(\frac{L_a}{B_c}\right)} - 1.2871$	0.9250
t= 6 h, U/U_c= 0.9, $Z_c/y_{0.7}$ = -0.25	$[(d_s)_{max,c}/y] = 0.4925\sqrt{\theta\left(\frac{L_a}{B_c}\right)} - 1.1217$	0.9095
t= 6 h, U/U_c= 0.9, $Z_c/y_{0.7}$ = -0.50	$[(d_s)_{max,c}/y] = 0.2692\sqrt{\theta\left(\frac{L_a}{B_c}\right)} - 0.2593$	0.8969

Table 5.8 The linear relationships between [$(d_s)_{max,c}/y$] and $\sqrt{\theta(L_a/B_c)}$ for the rectangular abutments with varying flow intensities, collar elevations and test durations

	Equation	R^2
t= 2 h, U/U_c= 0.7, $Z_c/y_{0.7}$ = ±0.00	$\left[(d_s)_{max,c}/y\right] = 0.3134\sqrt{\theta\left(\frac{L_a}{B_c}\right)}$ - 0.7334	0.8966
t= 2 h, U/U_c= 0.7, $Z_c/y_{0.7}$ = -0.25	$\left[(d_s)_{max,c}/y\right] = 0.2192\sqrt{\theta\left(\frac{L_a}{B_c}\right)}$ - 0.4281	0.9323
t= 2 h, U/U_c= 0.7, $Z_c/y_{0.7}$ = -0.50	$\left[(d_s)_{max,c}/y\right] = 0.1325\sqrt{\theta\left(\frac{L_a}{B_c}\right)} + 0.0158$	0.6166
t= 4 h, U/U_c= 0.8, $Z_c/y_{0.7}$ = ±0.00	$\left[(d_s)_{max,c}/y\right] = 0.3378\sqrt{\theta\left(\frac{L_a}{B_c}\right)}$ - 0.8836	0.9117
t= 4 h, U/U_c= 0.8, $Z_c/y_{0.7}$ = -0.25	$\left[(d_s)_{max,c}/y\right] = 0.4189\sqrt{\theta\left(\frac{L_a}{B_c}\right)}$ - 0.9722	0.9723
t= 4 h, U/U_c= 0.8, $Z_c/y_{0.7}$ = -0.50	$\left[(d_s)_{max,c}/y\right] = 0.3580\sqrt{\theta\left(\frac{L_a}{B_c}\right)} + 0.6913$	0.8828
t= 6 h, U/U_c= 0.9, $Z_c/y_{0.7}$ = ±0.00	$\left[(d_s)_{max,c}/y\right] = 0.8933\sqrt{\theta\left(\frac{L_a}{B_c}\right)}$ - 2.1943	0.9142
t= 6 h, U/U_c= 0.9, $Z_c/y_{0.7}$ = -0.25	$\left[(d_s)_{max,c}/y\right] = 0.8784\sqrt{\theta\left(\frac{L_a}{B_c}\right)}$ - 2.2236	0.9430
t= 6 h, U/U_c= 0.9, $Z_c/y_{0.7}$ = -0.50	$\left[(d_s)_{max,c}/y\right] = 0.9094\sqrt{\theta\left(\frac{L_a}{B_c}\right)}$ - 2.429	0.9473

Also, to indicate the effect of flow intensity and test duration on the relationship between the dimensionless maximum scour depth and abutment-collar sizes, variation of [$(d_s)_{max,c}/y$] with $\sqrt{\theta(L_a/B_c)}\exp\left(\frac{U}{U_c}\right)\exp\left(\frac{t}{t_p}\right)$ as a function of collar elevations was presented in Figures 5.73 and 5.74 for the semi-circular end and rectangular abutments, respectively. From the figures, it can be stated that the dimensionless maximum scour depths not only increase with increasing abutment and decreasing collar size but also increase with increasing flow intensity and test duration for both semi-circular end and rectangular abutments for a given collar elevation. Furthermore, as $\sqrt{\theta(L_a/B_c)}\exp\left(\frac{U}{U_c}\right)\exp\left(\frac{t}{t_p}\right)$ values increased the efficiencies of the collars located below the bed level increased due to the greater scour depths observed around longer abutment lengths (i.e. L_a=40 cm) and longer test durations with greater flow intensities. For semi-circular end abutments, the maximum dimensionless scour depths generally increased as the collar was located deeper into the bed level as mentioned in previous subsections. However, the maximum dimensionless scour depths were obtained greater when the collar was placed at the elevation of $Z_c/y_{0.7}$= -0.25 when compared to those at the elevation of $Z_c/y_{0.7}$= -0.50 in the case of $\sqrt{\theta(L_a/B_c)}\exp\left(\frac{U}{U_c}\right)\exp\left(\frac{t}{t_p}\right) > 27$. On the other hand, for the rectangular abutments, the greatest and lowest maximum dimensionless scour depths were obtained at the elevations of $Z_c/y_{0.7}$= -0.50 and -0.-25, respectively while $\sqrt{\theta(L_a/B_c)}\exp\left(\frac{U}{U_c}\right)\exp\left(\frac{t}{t_p}\right) < 22$. In addition, in this range, the dimensionless scour depth values of $Z_c/y_{0.7}$= -0.25 and ±0.00 were obtained close to each other. Between the range of $22 < \sqrt{\theta(L_a/B_c)}\exp\left(\frac{U}{U_c}\right)\exp\left(\frac{t}{t_p}\right) < 25$, the greatest and lowest maximum dimensionless scour depths were obtained at the elevation of $Z_c/y_{0.7}$= ±0.00 while the lowest ones were obtained at the elevation of $Z_c/y_{0.7}$= -0.25. Finally, when $\sqrt{\theta(L_a/B_c)}\exp\left(\frac{U}{U_c}\right)\exp\left(\frac{t}{t_p}\right) > 25$, again the greatest maximum dimensionless scour depths were obtained at the elevation of $Z_c/y_{0.7}$= ±0.00 and -0.50, respectively.

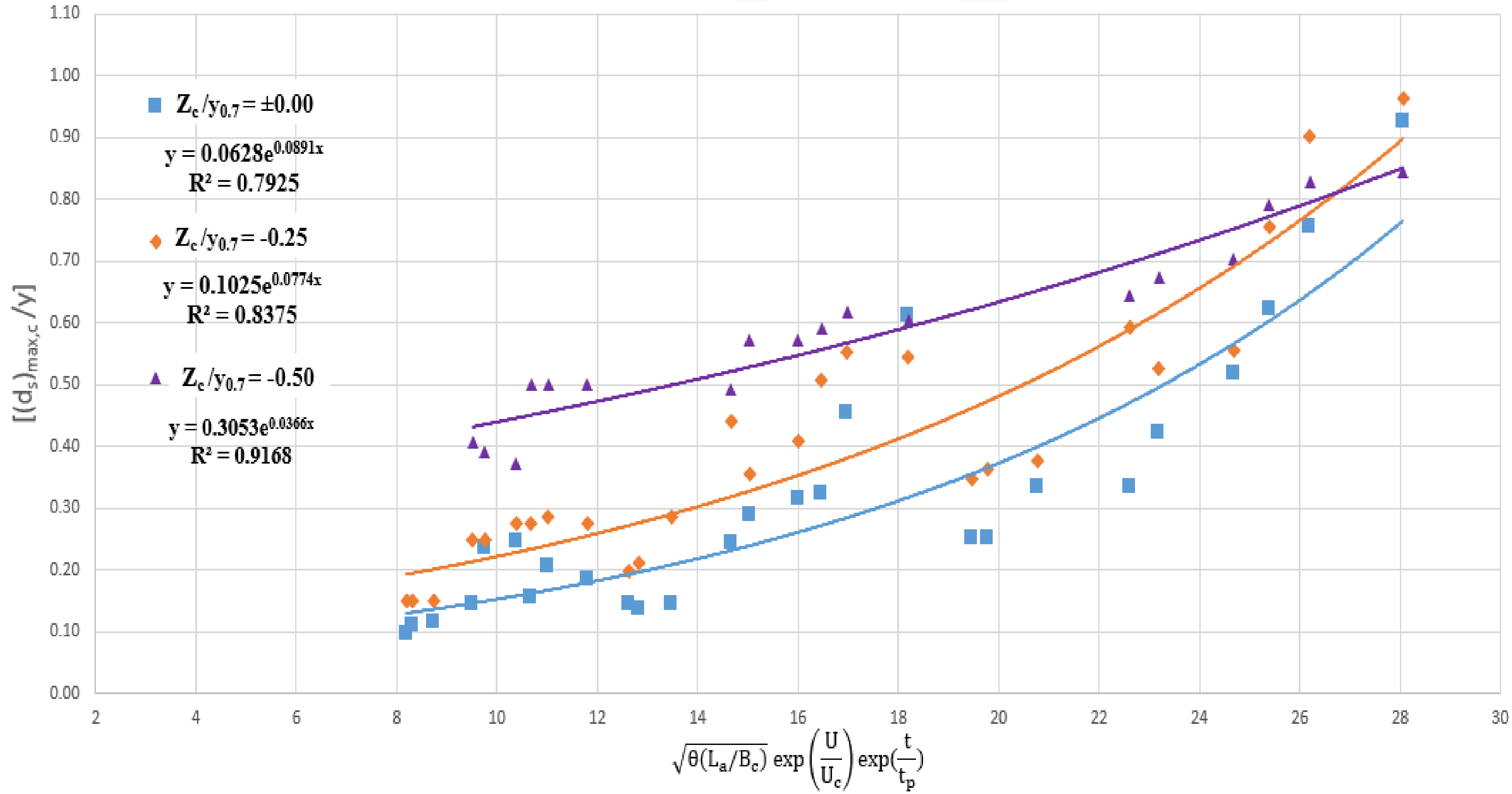

Figure 5.73 Variation of $[(d_s)_{max,c}/y]$ with $\sqrt{\theta(L_a/B_c)}\exp\left(\frac{U}{U_c}\right)\exp\left(\frac{t}{t_p}\right)$ for semi-circular end abutments

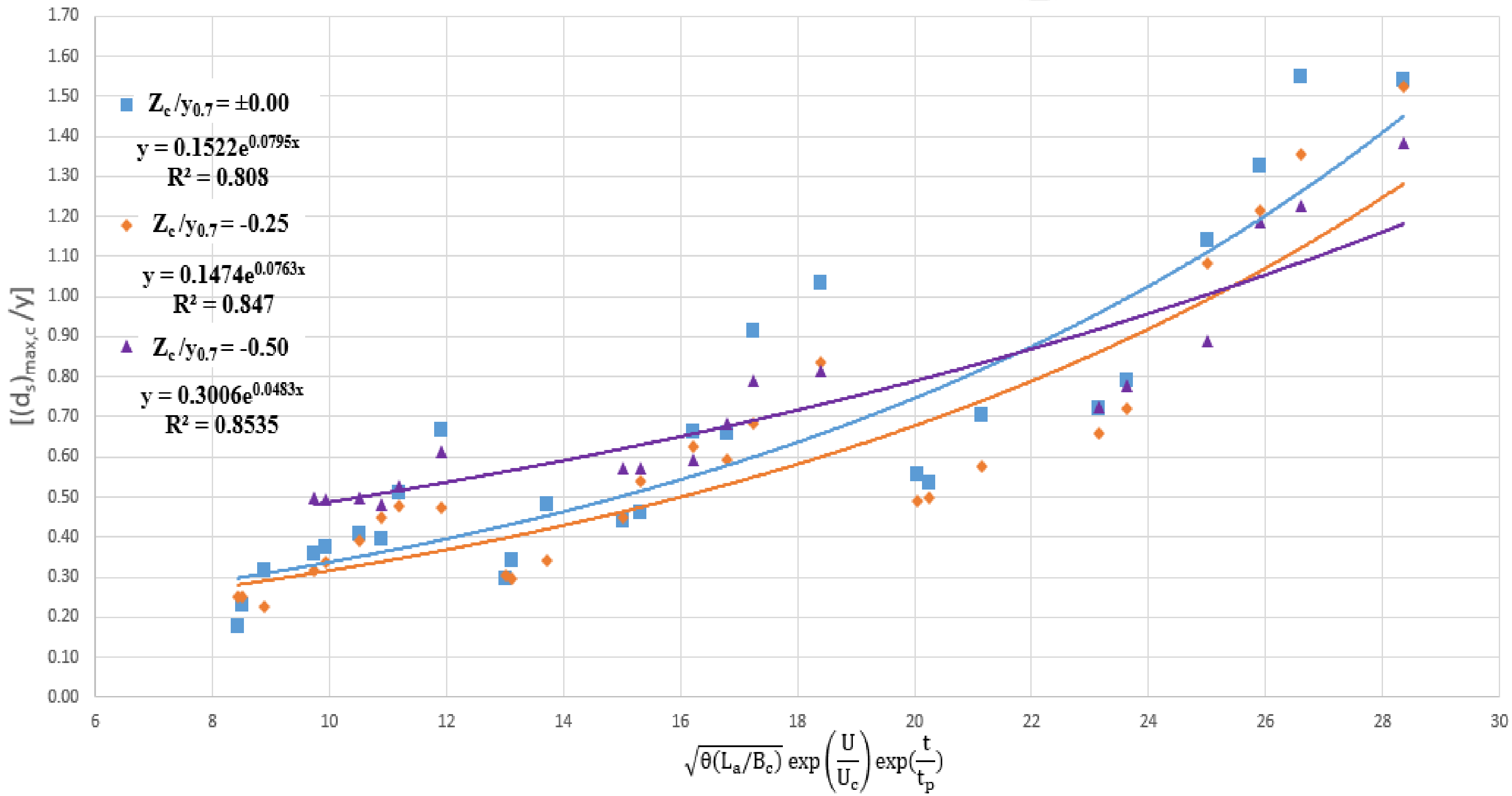

Figure 5.74 Variation of $[(d_s)_{max,c}/y]$ with $\sqrt{\theta(L_a/B_c)}\exp\left(\frac{U}{U_c}\right)\exp\left(\frac{t}{t_p}\right)$ for rectangular abutments

5.6.5 Optimal Design of Abutment-Collar Arrangement

In Tables 5.9 and 5.10, optimal design cases for an abutment-collar arrangement based on collar elevation are given for semi-circular end and rectangular abutments, respectively. $[(d_s)_{max,c}/y]_{opt}$ and $[Z_c/y_{0.7}]_{opt}$ represent the experimental results having the maximum percentage reductions in the maximum scour depths for a given abutment length, collar size, flow intensity and test duration.

Table 5.9 Optimal design parameters of semi-circular end abutments based on tested collar elevations

L_a (cm)	L_a/B	B_c	L_a/B_c	Θ	$(\Theta L_a/B_c)^{0.5}$	y (cm)	t (hour)	U/U_c	Z_c	$[Z_c/y_{0.7}]$	$[(d_s)_{max,c}/y]$	[Reduction%]
40	0.27	5.00	8.00	2.20	4.20	17.40	2	0.7	±0.00	±0.00	0.18	66.67
		7.50	5.33	2.88	3.92	17.40	2	0.7	±0.00	±0.00	0.21	62.50
		10.00	4.00	3.61	3.80	17.40	2	0.7	±0.00	±0.00	0.16	71.88
		5.00	8.00	2.20	4.20	15.20	4	0.8	-4.35	-0.25	0.55	36.15
		7.50	5.33	2.88	3.92	15.20	4	0.8	±0.00	±0.00	0.45	46.92
		10.00	4.00	3.61	3.80	15.20	4	0.8	±0.00	±0.00	0.32	62.31
		5.00	8.00	2.20	4.20	13.50	6	0.9	-8.70	-0.50	0.84	29.19
		7.50	5.33	2.88	3.92	13.50	6	0.9	±0.00	±0.00	0.76	36.65
		10.00	4.00	3.61	3.80	13.50	6	0.9	±0.00	±0.00	0.62	47.83
30	0.20	5.00	6.00	2.27	3.69	17.40	2	0.7	±0.00	±0.00	0.25	38.6
		7.50	4.00	3.01	3.47	17.40	2	0.7	±0.00	±0.00	0.24	41.4
		10.00	3.00	3.81	3.38	17.40	2	0.7	±0.00	±0.00	0.14	64.3
		5.00	6.00	2.27	3.69	15.20	4	0.8	±0.00	±0.00	0.32	48.9
		7.50	4.00	3.01	3.47	15.20	4	0.8	±0.00	±0.00	0.29	53.2
		10.00	3.00	3.81	3.38	15.20	4	0.8	±0.00	±0.00	0.24	60.6
		5.00	6.00	2.27	3.69	13.50	6	0.9	±0.00	±0.00	0.52	43.5
		7.50	4.00	3.01	3.47	13.50	6	0.9	±0.00	±0.00	0.42	54.0
		10.00	3.00	3.81	3.38	13.50	6	0.9	±0.00	±0.00	0.33	63.7
20	0.13	5.00	4.00	2.41	3.11	17.40	2	0.7	±0.00	±0.00	0.11	23.08
		7.50	2.67	3.28	2.96	17.40	2	0.7	±0.00	±0.00	0.11	26.92
		10.00	2.00	4.24	2.91	17.40	2	0.7	±0.00	±0.00	0.10	34.62
		5.00	4.00	2.41	3.11	15.20	4	0.8	±0.00	±0.00	0.14	50.00
		7.50	2.67	3.28	2.96	15.20	4	0.8	±0.00	±0.00	0.14	52.27
		10.00	2.00	4.24	2.91	15.20	4	0.8	±0.00	±0.00	0.14	50.00
		5.00	4.00	2.41	3.11	13.50	6	0.9	±0.00	±0.00	0.33	39.19
		7.50	2.67	3.28	2.96	13.50	6	0.9	±0.00	±0.00	0.25	54.05
		10.00	2.00	4.24	2.91	13.50	6	0.9	±0.00	±0.00	0.25	54.05

Table 5.10 Optimal design parameters of rectangular abutments based on tested collar elevations

L_a (cm)	L_a/B	B_c	L_a/B_c	Θ	$(\Theta L_a/B_c)^{0.5}$	y (cm)	t (hour)	U/U_c	Z_c	$[Z_c/y_{0.7}]$	$[(d_s)_{max,c}/y]$	[Reduction%]
40	0.27	5.00	8.00	2.25	4.24	17.40	2	0.7	-4.35	-0.25	0.47	38.35
		7.50	5.33	2.97	3.98	17.40	2	0.7	-4.35	-0.25	0.48	37.59
		10.00	4.00	3.75	3.87	17.40	2	0.7	±0.00	±0.00	0.40	48.12
		5.00	8.00	2.25	4.24	15.20	4	0.8	-8.70	-0.50	0.82	27.49
		7.50	5.33	2.97	3.98	15.20	4	0.8	-4.35	-0.25	0.68	39.18
		10.00	4.00	3.75	3.87	15.20	4	0.8	-4.35	-0.25	0.59	47.37
		5.00	8.00	2.25	4.24	13.50	6	0.9	-8.70	-0.50	1.39	10.95
		7.50	5.33	2.97	3.98	13.50	6	0.9	-8.70	-0.50	1.23	20.95
		10.00	4.00	3.75	3.87	13.50	6	0.9	-8.70	-0.50	1.19	23.81
30	0.20	5.00	6.00	2.33	3.74	17.40	2	0.7	-4.35	-0.25	0.39	36.45
		7.50	4.00	3.13	3.54	17.40	2	0.7	-4.35	-0.25	0.34	44.86
		10.00	3.00	4.00	3.46	17.40	2	0.7	-4.35	-0.25	0.32	48.60
		5.00	6.00	2.33	3.74	15.20	4	0.8	-4.35	-0.25	0.63	25.20
		7.50	4.00	3.13	3.54	15.20	4	0.8	±0.00	±0.00	0.46	44.88
		10.00	3.00	4.00	3.46	15.20	4	0.8	±0.00	±0.00	0.44	47.24
		5.00	6.00	2.33	3.74	13.50	6	0.9	-8.70	-0.50	0.89	25.93
		7.50	4.00	3.13	3.54	13.50	6	0.9	-4.35	-0.25	0.72	40.12
		10.00	3.00	4.00	3.46	13.50	6	0.9	-4.35	-0.25	0.66	45.06
20	0.13	5.00	4.00	2.50	3.16	17.40	2	0.7	-4.35	-0.25	0.22	38.10
		7.50	2.67	3.44	3.03	17.40	2	0.7	±0.00	±0.00	0.23	36.51
		10.00	2.00	4.50	3.00	17.40	2	0.7	±0.00	±0.00	0.18	50.79
		5.00	4.00	2.50	3.16	15.20	4	0.8	-4.35	-0.25	0.34	37.35
		7.50	2.67	3.44	3.03	15.20	4	0.8	-4.35	-0.25	0.30	45.78
		10.00	2.00	4.50	3.00	15.20	4	0.8	±0.00	±0.00	0.30	45.78
		5.00	4.00	2.50	3.16	13.50	6	0.9	-4.35	-0.25	0.58	35.54
		7.50	2.67	3.44	3.03	13.50	6	0.9	-4.35	-0.25	0.50	44.63
		10.00	2.00	4.50	3.00	13.50	6	0.9	-4.35	-0.25	0.49	45.45

The variation of $[(d_s)_{max,c}/y]_{opt}$ with θ is presented in Figures 5.75 and 5.76. As it was mentioned in the previous subsection, the Θ parameter, which represents the ratio of the total area of the abutment with collar to the area of the abutment on the horizontal plane, was exhibited to emphasize the effect of the collar width on the maximum scour depth. An increase in the Θ parameter, for a given abutment length, means an increase in collar width. Therefore, it can be clearly seen from Figures 5.75 and 5.76, the maximum scour depth usually decreases with increasing θ value for a given abutment length and test duration for both semi-circular end and rectangular abutments. However, for the semi-circular abutment of length L_a=20 cm, alterations on the maximum scour depth with increasing θ value were observed pretty small.

Furthermore, at the end of the 2 and 4 hours of the experiments, almost no change was observed in the maximum scour depth with an increase or decrease in θ value. It can be also stated that the decrease in the maximum scour depth with increasing θ value increases when the greater scour depth potential occurs. In other words, the effect of collar size increased as the abutment length, flow intensity and test duration were increased. In addition, increasing the collar size showed more efficient results in reducing the maximum scour depth for the rectangular abutments when compared to the semi-circular end abutments.

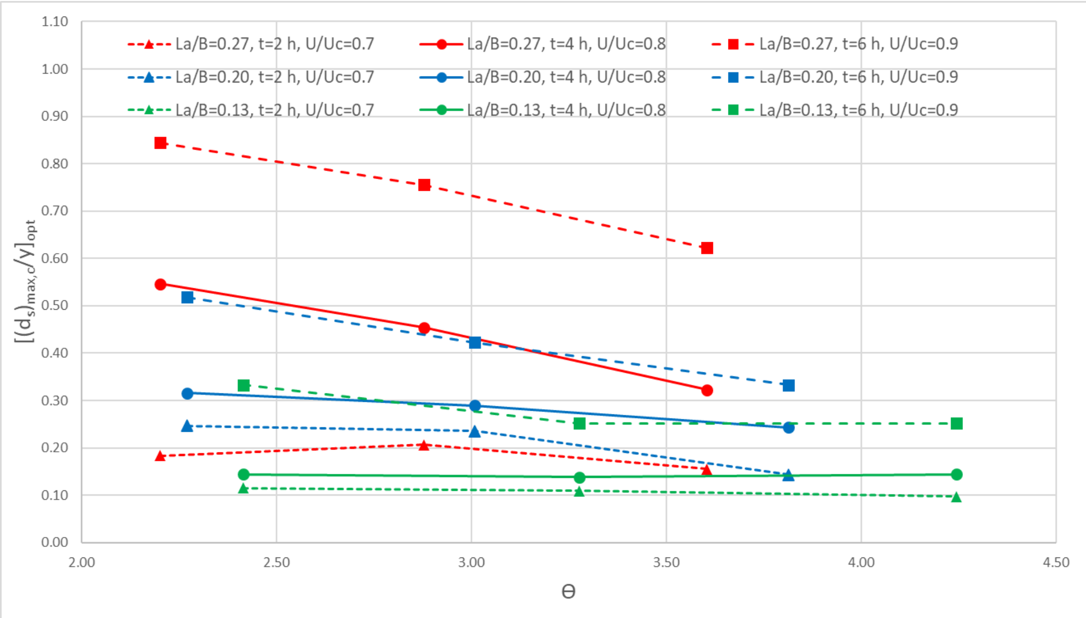

Figure 5.75 Variation of $[(d_s)_{max,c}/y]_{opt}$ with θ for semi-circular end abutments

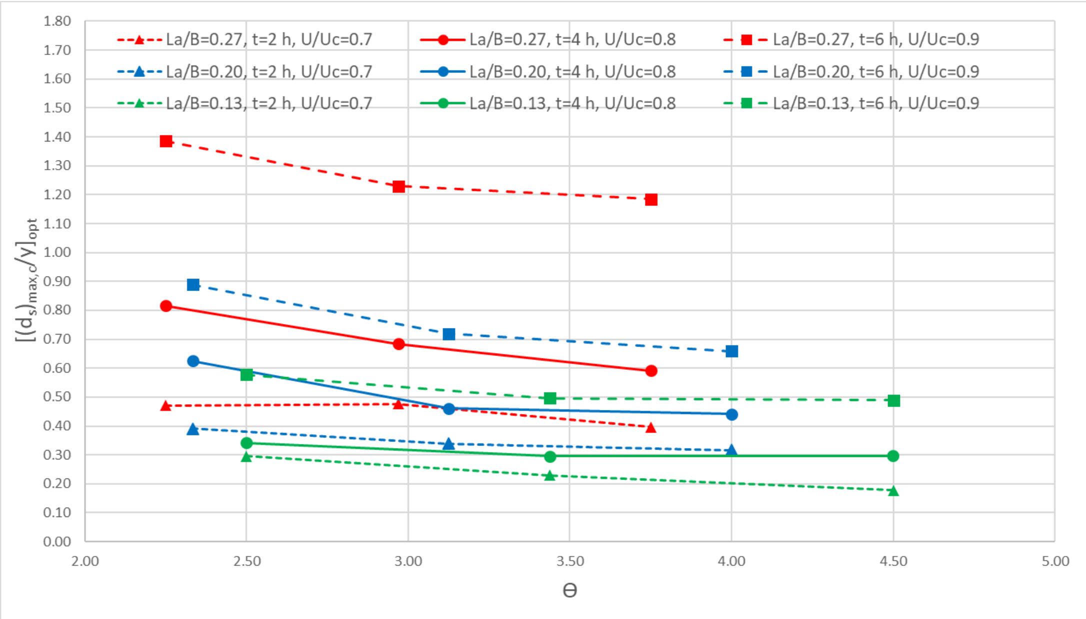

Figure 5.76 Variation of $[(d_s)_{max,c}/y]_{opt}$ with θ for rectangular abutments

Variation of $[(d_s)_{max,c}/y]_{opt}$ with $\sqrt{\theta(L_a)/B_c}$ was plotted in Figure 5.77 as an alternative data presentation for Figures 5.75 and 5.76. In this figure, the trends of the data points showed that the maximum scour depths increase with increasing $\sqrt{\theta(L_a)/B_c}$. Moreover, the greater maximum scour depths were always obtained around the rectangular abutments at the end of the 6th hour of the experiments; on the other hand, the smallest maximum scour depths were obtained around the semi-circular end abutments at the end of the 2nd hour. It was also observed that the trendlines of the data belonging to the semi-circular end abutments at the end of the 4th hour and rectangular abutments at the end of the 2nd hour coincide with each other while the semi-circular end abutments at the end of the 6th hour and rectangular abutments at the end of the 4th hour. In other words, the evolution of the optimal maximum scour depths around the semi-circular end abutments with collars lagged two hours with respect to the rectangular abutments. The linear relationships between the $[(d_s)_{max,c}/y]_{opt}$ and $\sqrt{\theta(L_a/B_c)}$ for various flow intensities and test durations are listed in Table 5.11.

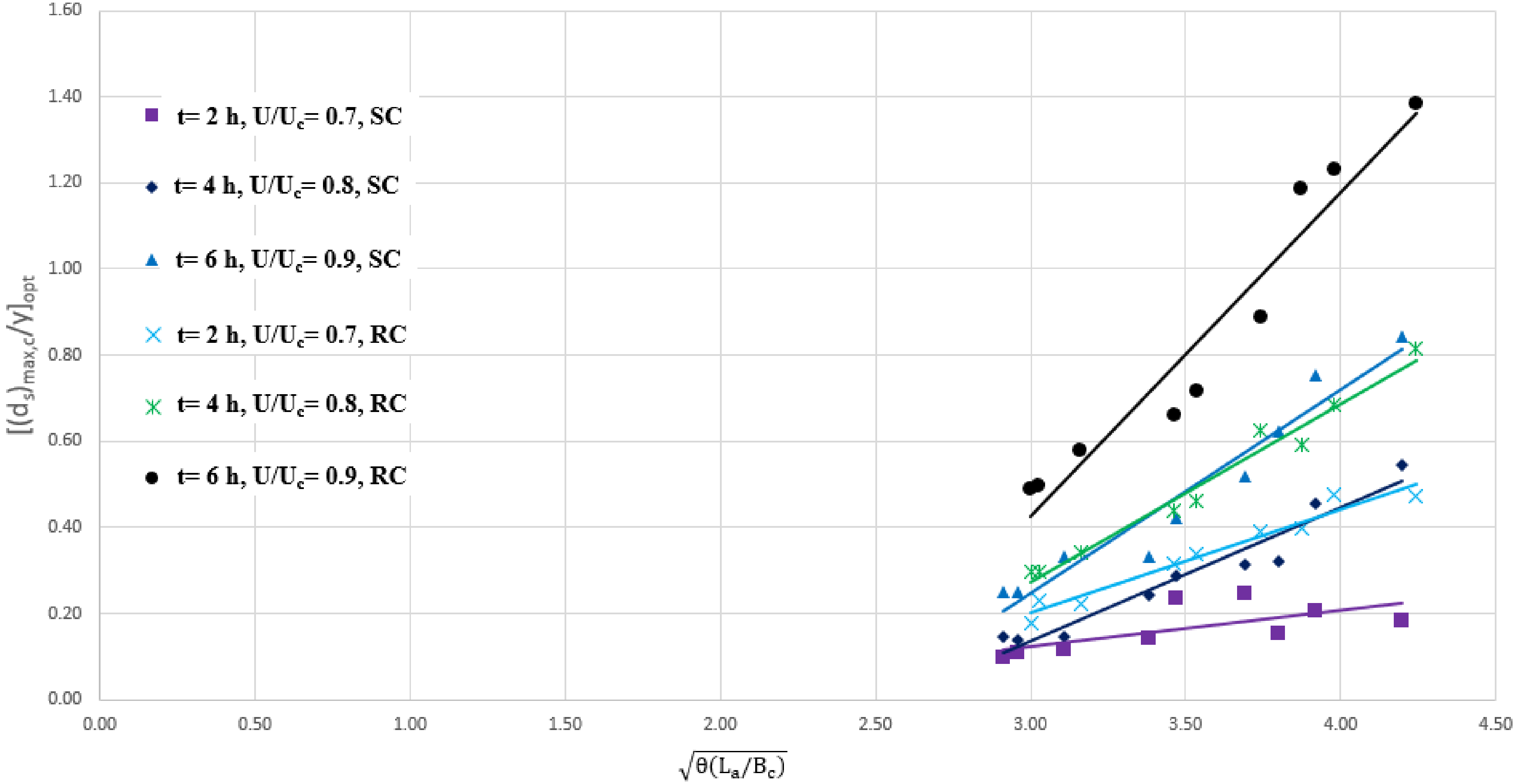

Figure 5.77 Variation of $[(d_s)_{max,c}/y]_{opt}$ with $\sqrt{\theta(L_a/B_c)}$

Table 5.11 The linear relationships between $[(d_s)_{max,c}/y]_{opt}$ and $\sqrt{\theta(L_a/B_c)}$ for varying flow intensities and test durations

	Equation	$\mathbf{R^2}$
t= 2 h, U/U_c= 0.7 SC	$\left[(d_s)_{max,c}/y\right] = 0.0837\sqrt{\theta\left(\frac{L_a}{B_c}\right)}$ - 0.1264	0.4548
t= 2 h, U/U_c= 0.7 RC	$\left[(d_s)_{max,c}/y\right] = 0.2416\sqrt{\theta\left(\frac{L_a}{B_c}\right)}$ - 0.5240	0.9557
t= 4 h, U/U_c= 0.8 SC	$\left[(d_s)_{max,c}/y\right] = 0.3087\sqrt{\theta\left(\frac{L_a}{B_c}\right)}$ - 0.7893	0.9391
t= 4 h, U/U_c= 0.8 RC	$\left[(d_s)_{max,c}/y\right] = 0.4140\sqrt{\theta\left(\frac{L_a}{B_c}\right)}$ - 0.9675	0.9739
t= 6 h, U/U_c= 0.9 SC	$\left[(d_s)_{max,c}/y\right] = 0.4729\sqrt{\theta\left(\frac{L_a}{B_c}\right)}$ – 1.1703	0.9351
t= 6 h, U/U_c= 0.9 RC	$\left[(d_s)_{max,c}/y\right] = 0.7523\sqrt{\theta\left(\frac{L_a}{B_c}\right)}$ – 1.8292	0.9380

The variation of $[\text{Reduction\%}]_{opt}$ with L_a/B_c is presented in Figure 5.78. According to the figure, trendlines of the data indicated that the maximum scour reduction percentages gradually decrease with increasing L_a/B_c for all cases, except for the semi-circular end abutment at the end of the 2nd hour. In this case, it was obtained that the maximum scour reduction percentages increase with increasing L_a/B_c. However, it should not be forgotten that the correlation coefficient, R^2, of that trendline was only measured as 0.1704 that can be accepted as very low. Hence, the relationship between the $[\text{Reduction\%}]_{opt}$ and L_a/B_c for that case could be considered meaningless.

The exponential relationships between the $[\text{Reduction\%}]_{opt}$ and L_a/B_c with their correlation coefficients are presented in Table 5.12.

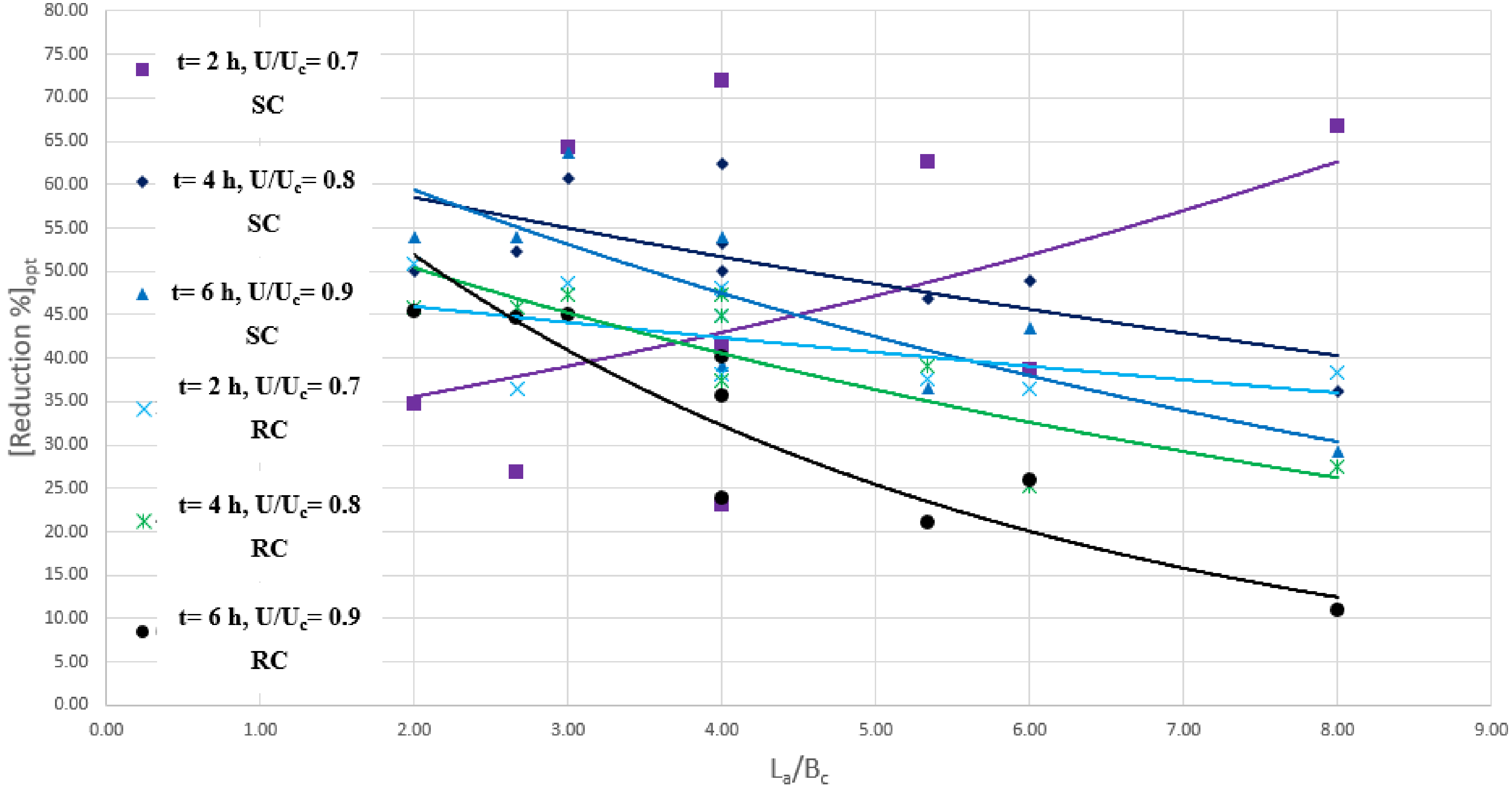

Figure 5.78 Variation of $[\text{Reduction}\%]_{opt}$ with L_a/B_c

Table 5.12 The exponential relationships between the $[\text{Reduction\%}]_{opt}$ and L_a/B_c for the varying flow intensities and test durations

	Equation	R^2
t= 2 h, U/U_c= 0.7 SC	$[\text{Reduction\%}]_{\text{opt}} = 29.457\ e^{0.0943\frac{L_a}{B_c}}$	0.1704
t= 2 h, U/U_c= 0.7 RC	$[\text{Reduction\%}]_{\text{opt}} = 49.849\ e^{-0.0410\frac{L_a}{B_c}}$	0.3238
t= 4 h, U/U_c= 0.8 SC	$[\text{Reduction\%}]_{\text{opt}} = 66.268\ e^{-0.0620\frac{L_a}{B_c}}$	0.4407
t= 4 h, U/U_c= 0.8 RC	$[\text{Reduction\%}]_{\text{opt}} = 62.671\ e^{-0.1090\frac{L_a}{B_c}}$	0.7004
t= 6 h, U/U_c= 0.9 SC	$[\text{Reduction\%}]_{\text{opt}} = 74.246\ e^{-0.1120\frac{L_a}{B_c}}$	0.6726
t= 6 h, U/U_c= 0.9 RC	$[\text{Reduction\%}]_{\text{opt}} = 83.403\ e^{-0.2380\frac{L_a}{B_c}}$	0.8121

5.6.6 Comparison of the Experimental Results with the Previous Studies in the Literature

The results of the present study were also compared with the previous similar studies in the literature such as Kayatürk (2005), Doğan (2008), Daşkın (2011) and Tekin (2012). All of these studies having various abutment shapes and lengths, collar shapes, sizes and elevations, flow characteristics and sediment sizes, were conducted under steady-state clear-water flow conditions in order to investigate the efficiencies of collars in reducing the local scour depth around the abutments. Important parameters of these studies are listed in Table 5.13.

Table 5.13 Abutment, collar, flow and sediment properties of Kayatürk’s (2005), Doğan’s (2008), Daşkın’s (2011) and Tekin’s (2012) studies

Parameter	**Kayatürk (2005)**	**Doğan (2008)**	**Daşkın (2011)**	**Tekin (2012)**
Abutment Shape	Rectangular	Rectangular	Semi-circular end	Semi-circular end
Abutment Length, L_a, (cm)	7.5, 15, 20, 25 and 35	7.5, 15, 20, 25 and 35	15, 20, 25, 30, 35 and 40	15 and 35
Collar width, B_c, (cm)	2.5, 5, 7.5 and 10	2.5, 5, 7.5 and 10	5, 7.5 and 10	5, 7.5 and 10
Collar Shape	Rectangular	Rectangular	Semi-circular end	Semi-circular end
Discharge (m^3/s)	0.050	0.017	0.0678	0.0678
Flow Depth (cm)	10	4.25	13.5	17.4 and 15.2
Sediment diameter, d_{50}, (mm)	1.48	0.90	1.50	1.50
Flow Conditions	Clear-water	Clear-water	Clear-water	Clear-water
U/U_c	-	-	0.9	0.70 and 0.80
U_*/U_{*c}	0.90	0.90	-	-
Test duration (hour)	6	6	3	3

Variation of $[(d_s)_{max,c}/y]_{opt}$ with $\sqrt{\theta(L_a)/B_c}$ for the present study was plotted in Figure 5.79 together with the data of Kayatürk (2005), Doğan (2008), Daşkın (2011) and Tekin (2012). From the figure, it can be seen that all the data show similar trends in terms of the relationship between $[(d_s)_{max,c}/y]_{opt}$ and $\sqrt{\theta(L_a)/B_c}$. The data of Kayatürk (2005) and Doğan (2008) yields larger than the other studies' data, since, these two studies were conducted for longer test durations (6 hours) with vertical-wall abutments. Daşkın's (2011) data fell below the data of Kayatürk's (2005) and Doğan's (2008) data because of the shorter test duration (3 hours) conducted for the semi-circular end abutments. However, it should not be forgotten that if Daşkın's (2011) study were conducted for 6 hours, it might coincide with Kayatürk's (2005) data, since these two studies were performed under similar flow conditions, U/U_c=0.9 and the mean diameters of the bed materials of these two studies were almost the same. Despite Daşkın's (2011) and Tekin's (2012) studies were carried out in the same experimental channel with the same abutment shapes, the mean diameters of the bed materials and the test durations, tested flow intensities, U/U_c=0.7 and 0.8, in Tekin (2012) were smaller than the flow intensity, U/U_c=0.9, tested in Daşkın (2011). Thereby, the data of Tekin (2012) fell below the data of Daşkın (2011) because of the smaller maximum scour depths caused by smaller flow intensities.

It was obtained that the data of the present study for a given test duration and flow intensity generally fall below the previously conducted four studies that were mentioned above. Although the present study had a total test duration of 6 hours which is the same as Kayatürk (2005) and Doğan (2008), and higher than the Daşkın (2011) and Tekin (2012), it was conducted under unsteady-state flow conditions contrary to the four studies which were carried out under steady-state flow conditions. Especially, when the data of the present study belonging to the semi-circular end abutments were compared with the Daşkın (2011) and Tekin (2012) that were carried out at the same experimental setup and the same median size of bed material with the present study, the data of Daşkın (2011) and Tekin (2012) absolutely yielded larger than the data of the present study even though the present study had longer test duration. The present study was conducted by performing a 6-hour step-wised hydrograph, each flow intensity value (U/U_c=0.7, 0.8 and 0.9) was applied for 2 hours, respectively. On the other hand, a single flow intensity value was performed continuously for 3 hours in Daşkın (2011), U/U_c=0.9 and Tekin (2012), U/U_c=0.7 and 0.8. When the dominancy of the flow intensity for the development of the scour depths is taken into account, the greater scour depth values obtained in Daşkın (2011), where the flow intensity of U/U_c=0.9, was applied continuously for 3 hours, for a given $\sqrt{\theta(L_a)/B_c}$ is reasonable. However, Tekin (2012) also yielded larger than the present study despite having smaller flow intensities of U/U_c=0.7 and 0.8. This situation might be explained by the limited strength of the horseshoe vortex which is mainly responsible for the development of local scour, due to the boundary layer thickness developed under unsteady-state flow conditions and also the occurrence of stronger wake turbulences for the steady-state flow conditions than those of unsteady-state, greater scour depths occur for the steady-state flow conditions (Gargari et al., 2021). Nevertheless, the present study's 6 hours data belonging to the rectangular abutment cases nearly converged with the data of Daşkın (2011). Hence, it can be claimed that results at the end of the 6 hours for the under-steady state flow conditions around the rectangular abutments have similar results to the results of the 3 hours under steady-state flow conditions around semi-circular abutments. In addition, the experimental results of Tekin (2012) conducted with a flow intensity of 0.7 for continuously 3 hours showed some compatibility with the data of the present study belonging to the rectangular abutment cases at the end of the 2 hours with the flow intensity value of 0.7. On the other hand, the experimental results of Tekin (2012) conducted with a flow intensity of 0.8 for continuously 3 hours fell a little above the data of the present study belonging to the semi-circular end abutment cases at the end of the 6 hours. However, it should not be forgotten that the optimum collar location was mostly obtained at the bed level for the semi-circular end abutments in the present study. In Daşkın's (2011) and Tekin's (2012) studies optimum collar locations were generally achieved at the locations below the bed level. The linear relationships between the $[(d_s)_{max,c}/y]_{opt}$ and $\sqrt{\theta(L_a/B_c)}$ for these studies are listed in Table 5.14.

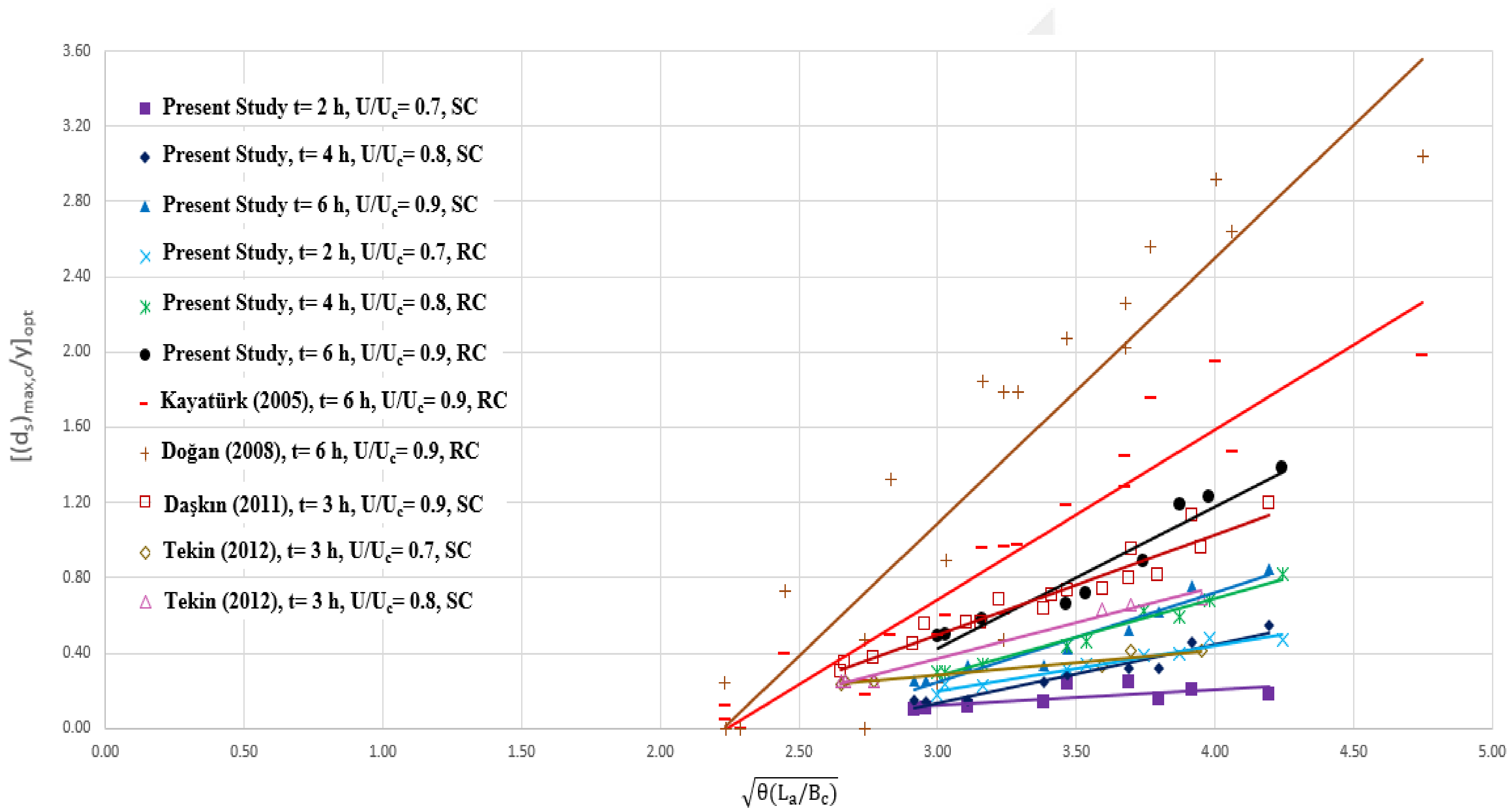

Figure 5.79 Comparison of the variation $[(d_s)_{max,c}/y]_{opt}$ with $\sqrt{\theta(L_a/B_c)}$ obtained from the present study and previous studies in the literature

Table 5.14 The linear relationships between $[(d_s)_{max,c}/y]_{opt}$ and $\sqrt{\theta(L_a/B_c)}$ for the present study and previous studies in the literature

	Equation	R^2
Present Study t= 2 h, U/U_c= 0.7 SC	$[(d_s)_{max,c}/y] = 0.0837\sqrt{\theta\left(\frac{L_a}{B_c}\right)} - 0.1264$	0.4548
Present Study t= 2 h, U/U_c= 0.7 RC	$[(d_s)_{max,c}/y] = 0.2416\sqrt{\theta\left(\frac{L_a}{B_c}\right)} - 0.5240$	0.9557
Present Study t= 4 h, U/U_c= 0.8 SC	$[(d_s)_{max,c}/y] = 0.3087\sqrt{\theta\left(\frac{L_a}{B_c}\right)} - 0.7893$	0.9391
Present Study t= 4 h, U/U_c= 0.8 RC	$[(d_s)_{max,c}/y] = 0.4140\sqrt{\theta\left(\frac{L_a}{B_c}\right)} - 0.9675$	0.9739
Present Study t= 6 h, U/U_c= 0.9 SC	$[(d_s)_{max,c}/y] = 0.4729\sqrt{\theta\left(\frac{L_a}{B_c}\right)} - 1.1703$	0.9351
Present Study t= 6 h, U/U_c= 0.9 RC	$[(d_s)_{max,c}/y] = 0.7523\sqrt{\theta\left(\frac{L_a}{B_c}\right)} - 1.8292$	0.9380
Kayatürk (2005)	$[(d_s)_{max,c}/y] = 0.9037\sqrt{\theta\left(\frac{L_a}{B_c}\right)} - 2.0254$	0.9035
Doğan (2008)	$[(d_s)_{max,c}/y] = 1.4114\sqrt{\theta\left(\frac{L_a}{B_c}\right)} - 3.1434$	0.8105
Daşkın (2011)	$[(d_s)_{max,c}/y] = 0.5308\sqrt{\theta\left(\frac{L_a}{B_c}\right)} - 1.0953$	0.9356
Tekin (2012) U/U_c= 0.7	$[(d_s)_{max,c}/y] = 0.1351\sqrt{\theta\left(\frac{L_a}{B_c}\right)} - 0.1220$	0.9309
Tekin (2012) U/U_c= 0.9	$[(d_s)_{max,c}/y] = 0.3794\sqrt{\theta\left(\frac{L_a}{B_c}\right)} - 0.7676$	0.9812

Variation of [% Reduction] $_{opt}$ with L_a/B_c for the present study was plotted in Figure 5.80 together with the data of Kayatürk (2005), Doğan (2008), Daşkın (2011) and Tekin (2012). The data of the present study at the end of 2nd hour and the data of Tekin (2012) conducted with flow intensity of U/U_c=0.7 were excluded from the graph due to the low correlations of the data. The presented data in the figure showed similar trends as well as in Figure 5.79. As L_a/B_c increases the scour reduction efficiencies of collars decrease for all the data. When L_a/B_c<2, the maximum scour reductions were obtained for Kayatürk (2005) and Doğan (2008) for a given L_a/B_c. However, the trend of these two studies dramatically decreased with increasing L_a/B_c and the scour reduction efficiencies of the other data became greater when L_a/B_c>3. In addition, the maximum scour reductions belonging to the rectangular abutments at the end of the 6th hour showed strong coherency with the data of Kayatürk (2005) and Doğan (2008) for a given L_a/B_c. On the other hand, for L_a/B_c>3, the maximum scour reductions were obtained around the semi-circular end abutments at the end of the 4th hour and then, at the end of the 6th hour. As a final comment, for L_a/B_c>3, it can be noticed that the scour reduction percentages were observed higher for the semi-circular end abutments when compared to the rectangular abutments. Also, the scour reduction percentages decreased with increasing flow intensity and test duration. Indeed, it can be indicated that the scour reduction efficiencies of the collars decreases in such circumstances (e.g., longer abutments, sharp shapes, higher flow intensities and test durations) causing greater scour depths. The exponential relationships between the [Reduction%]$_{opt}$ and L_a/B_c for these four studies are shown in Table 5.15.

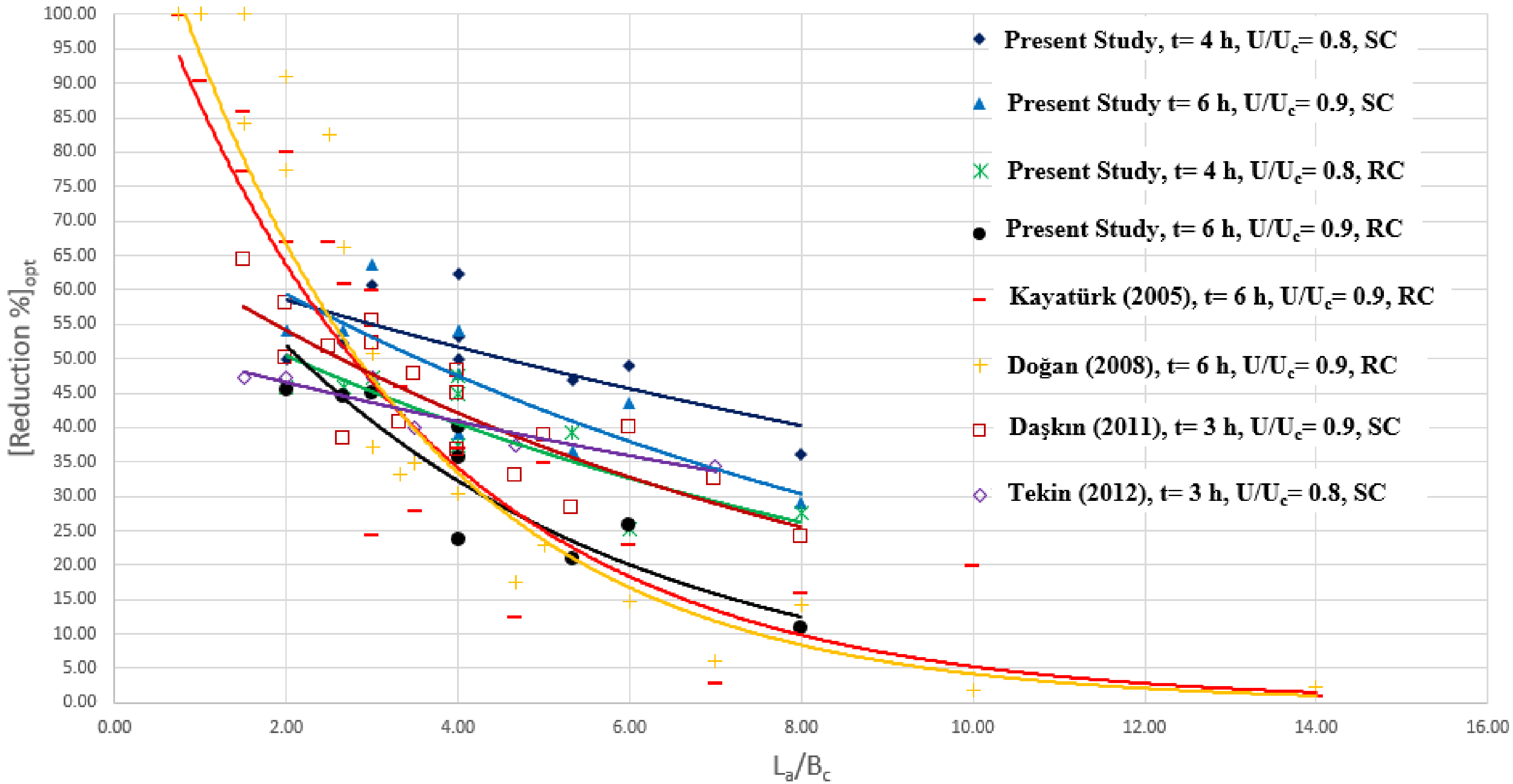

Figure 5.80 Comparison of the variation [% Reduction]$_{opt}$ with L_a/B_c obtained from the present study and previous studies in the literature

Table 5.15 The exponential relationships between the $[\text{Reduction}\%]_{opt}$ and L_a/B_c for the present study and previous studies in the literature

	Equation	**R^2**
t= 4 h, U/U_c= 0.8 SC	$[\text{Reduction}\%]_{\text{opt}} = 66.268\ e^{-0.0620\frac{L_a}{B_c}}$	0.4407
t= 4 h, U/U_c= 0.8 RC	$[\text{Reduction}\%]_{\text{opt}} = 62.671\ e^{-0.1090\frac{L_a}{B_c}}$	0.7004
t= 6 h, U/U_c= 0.9 SC	$[\text{Reduction}\%]_{\text{opt}} = 74.246\ e^{-0.1120\frac{L_a}{B_c}}$	0.6726
t= 6 h, U/U_c= 0.9 RC	$[\text{Reduction}\%]_{\text{opt}} = 83.403\ e^{-0.2380\frac{L_a}{B_c}}$	0.8121
Kayatürk (2005)	$[\text{Reduction}\%]_{\text{opt}} = 118.450\ e^{-0.3110\frac{L_a}{B_c}}$	0.8883
Doğan (2008)	$[\text{Reduction}\%]_{\text{opt}} = 132.820\ e^{-0.3450\frac{L_a}{B_c}}$	0.9228
Daşkın (2011)	$[\text{Reduction}\%]_{\text{opt}} = 69.459\ e^{-0.1250\frac{L_a}{B_c}}$	0.7228
Tekin (2012)	$[\text{Reduction}\%]_{\text{opt}} = 52.996\ e^{-0.0650\frac{L_a}{B_c}}$	0.8637

5.6.7 Effect of Flow Depth on the Maximum Scour Depth at Bridge Abutments

Ninety additional experiments, 6 of them without collars, were carried out for semi-circular end bridge abutments by applying a step-wise hydrograph of 6 hours total duration based on flow intensity and its results are presented in Figure 5.81. However, this time, the flow intensity was increased by increasing the flow discharge and flow depth once every two hours rather than using constant discharge and decreasing the flow depth. Each flow discharge (Q=45, 55 and 65 lt/s) and flow depth (y=11.5, 12.3 and 13 cm) that correspond to U/U_c=0.7, 0.8 and 0.9, respectively, were tested continuously for 2 hours duration. In other words, the experiments mentioned in the previous sections, which can be named first-phase experiments (FPE) were conducted with constant discharge and decreasing flow depth while the experiments mentioned in this subsection, which are named second-phase experiments (SPE) were conducted with increasing discharge and flow depth. The main motivation for performing these experiments was to investigate the effect of flow depth on the maximum scour depth and scour reduction performances of collars. Although the most dominant parameter for scour development is the approach flow velocity or flow intensity, it is known that the approach flow depth has also an effect on the scour depth. In the literature, there is a common opinion that the scour depth increases at a decreasing rate with increasing flow depth (Barbhuiya and Dey, 2004). However, in this study, the flow intensity was increased by decreasing the flow depth, since, the main aim of the study was to examine the effect of flow intensity, abutment length, collar width, collar elevation and test duration on collar performance. Hence, the final scour depth increased with decreasing the flow depth in the previous experiments. For that reason, additional experiments were done for the semi-circular end bridge abutments in order to obtain the direct proportion of the maximum scour depths with collars and flow depth. A sample of the relevant data is provided in Appendix C.

In Figure 5.81, the temporal development of the maximum scour depth without collars is plotted for both the experiments conducted with decreasing and increasing flow depth. From the figure, it can be stated that for a given flow intensity and test duration, the maximum scour depths are always greater for the experiments conducted with higher flow depths. The differences in the maximum scour depths between the FPE and SPE were measured by around 30%, 20% and 4% for the abutments of lengths L_a=20 cm, 30 cm and 40 cm, respectively. According to all the experimental results, the maximum scour depth increases with increasing abutment length. Moreover, it was obvious that the increasing rate of the maximum scour depth increases with decreasing abutment length. Despite Melville (1992) stated that for the short abutments ($L_a/y \leq 1$), the maximum scour depths depend on abutment length rather than flow depth, during the experiments of this study the alterations on the scour depths increased as the abutment length decreased. In other words, as L_a/y decreased for a given flow depth in every flow intensity zone, it seems that the effect of flow depth on the maximum scour depth significantly increases even if L_a/y values converge to 1. However, it should not be forgotten that the L_a/y values within the scope of this study are calculated within the range of 1.15 and 3.48, which indicates that the tested abutments in this study are classified as neither short nor long abutments ($1 \leq L_a/y \leq 25$) based on the classification of Melville (1992). For that reason, the scour depths obtained in this study depend on both abutment length and flow depth for these ranges. Therefore, it is hard to make absolute statements on the combined effect of flow depth and abutment length on the maximum scour depth.

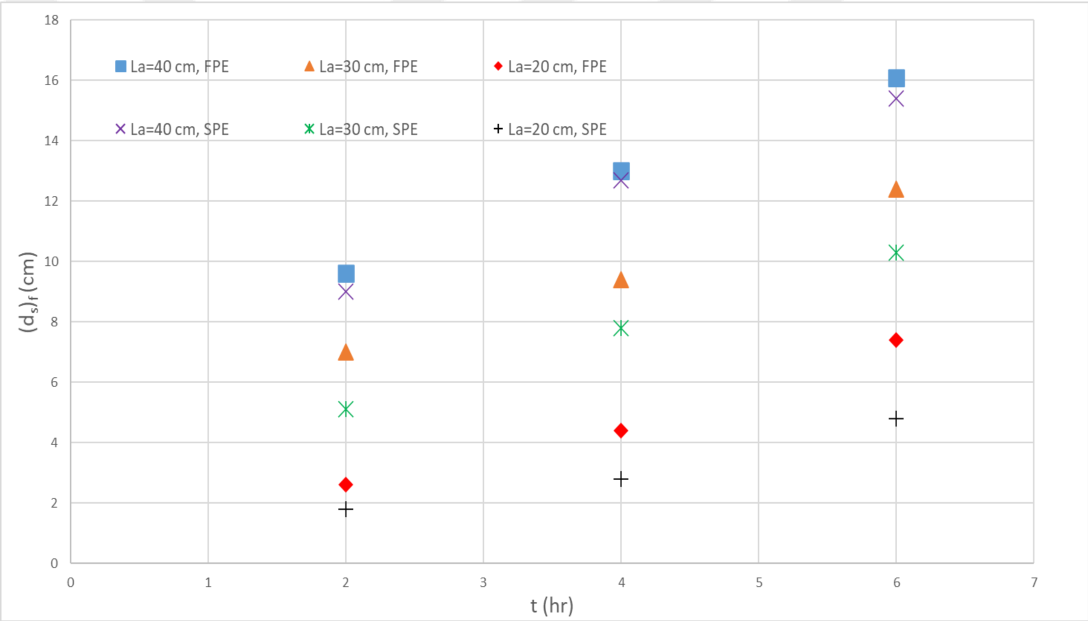

Figure 5.81 Temporal variation of the maximum scour depths without a collar for FPE and SPE

Following the comparison of the maximum scour depths without collars for the FPE and SPE, the comparison of the scour reduction efficiencies of the collars for these two cases is presented in the next subsection. Since the main aim was just to see the effect of flow depth on the performances of the collars, the experimental results of FPE and SPE were plotted together.

5.6.7.1 The Abutment of Length L_a=40 cm

Comparison of the scour reduction efficiencies of the collars based on flow depth for semi-circular end abutment of length L_a=40 cm is demonstrated in Figures 5.82-5.84. From the figures, it can be stated that the scour reduction efficiencies of the collars during FPE and SPE generally showed similar trends at all collar elevations. At the end of the first stage of the experiments with the flow intensity of 0.7, the collar performances were almost obtained the same during FPE and SPE at the elevations of $Z_c/y_{0.7}$= -0.25 and ±0.00. However, at the elevation of $Z_c/y_{0.7}$= -0.25, the collar of B_c=5 cm was more efficient in reducing the maximum scour depth for FPE than SPE. At the elevation of $Z_c/y_{0.7}$= -0.50, the efficiencies of the collars were better for the SPE relative to FPE. The collar locations below (i.e., $Z_c/y_{0.7}$= -0.50 and -0.25, Z_c= -5.75 cm and 2.88 cm) the bed level during SPE was close to bed level because of the smaller flow depths relative to collar locations during FPE (i.e., $Z_c/y_{0.7}$= -0.50 and -0.25, Z_c= -8.70 cm and 4.35 cm). For that reason, this result can be accepted as reasonable. Yet, especially for the smaller scour depths caused by smaller flow intensities and test durations, the collars located near the bed level gave better results in reducing the maximum scour depth. In these circumstances, the collars located deeper into the bed level did not give efficient results, because the scour formation does not reach the collar elevation and thereby, the collar could not manipulate the flow around the abutment. At the end of the second stage of the experiments, the efficiencies of the collars in reducing the maximum scour depth during SPE were almost obtained as the same as FPE. However, at the elevation of $Z_c/y_{0.7}$= -0.25, the efficiency of collar width of B_c=7.5 cm was better during SPE. Finally, at the third stage of the experiments, despite the scour reduction performances of the collars at the elevation of $Z_c/y_{0.7}$= ±0.00 were similar between FPE and SPE, at the elevations of $Z_c/y_{0.7}$= -0.50 and -0.25, the collar efficiencies were better during SPE than FPE, except for the collar of B_c=5 cm. This situation might occur due to the differences in dimensional collar elevations mentioned above.

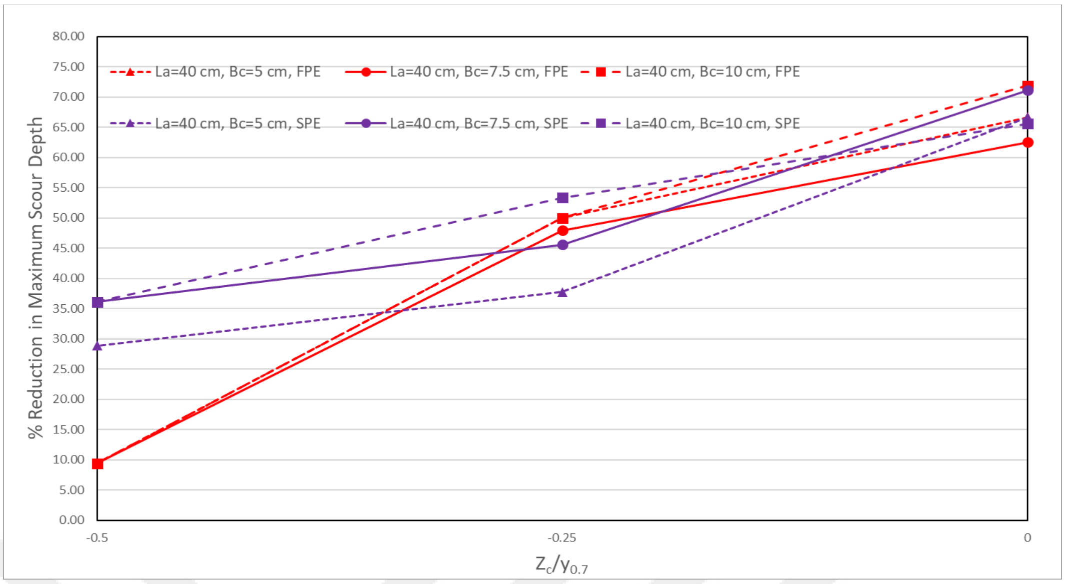

Figure 5.82 Comparison of the effects of collar size and elevation on the maximum scour depth around abutment of length L_a=40 cm for FPE and SPE (t=2 hours)

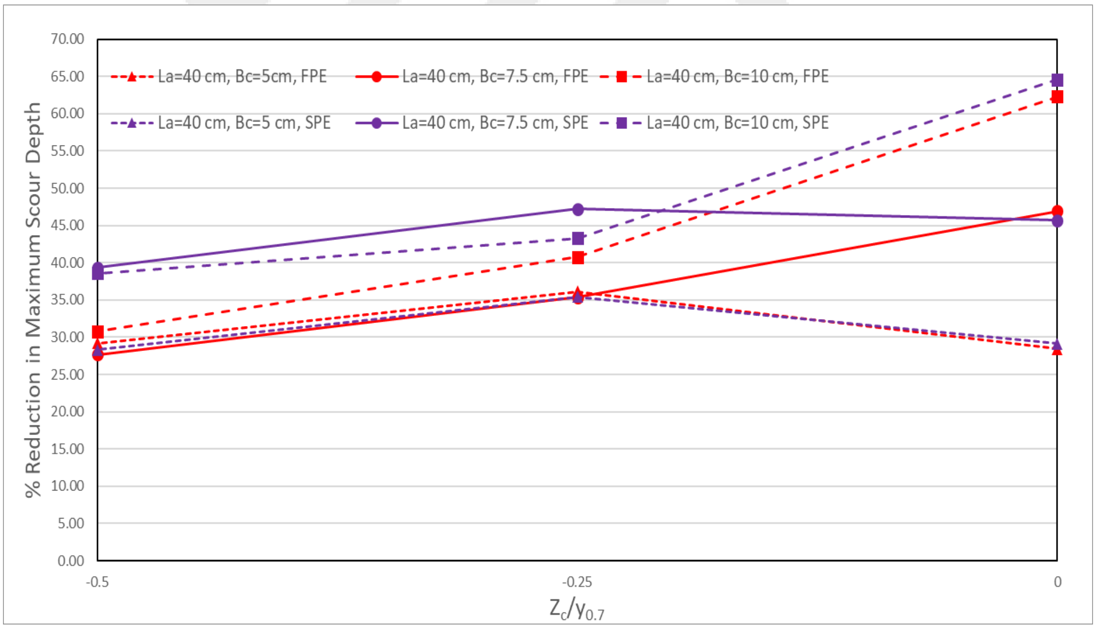

Figure 5.83 Comparison of the effects of collar size and elevation on the maximum scour depth around abutment of length L_a=40 cm for FPE and SPE (t=4 hours)

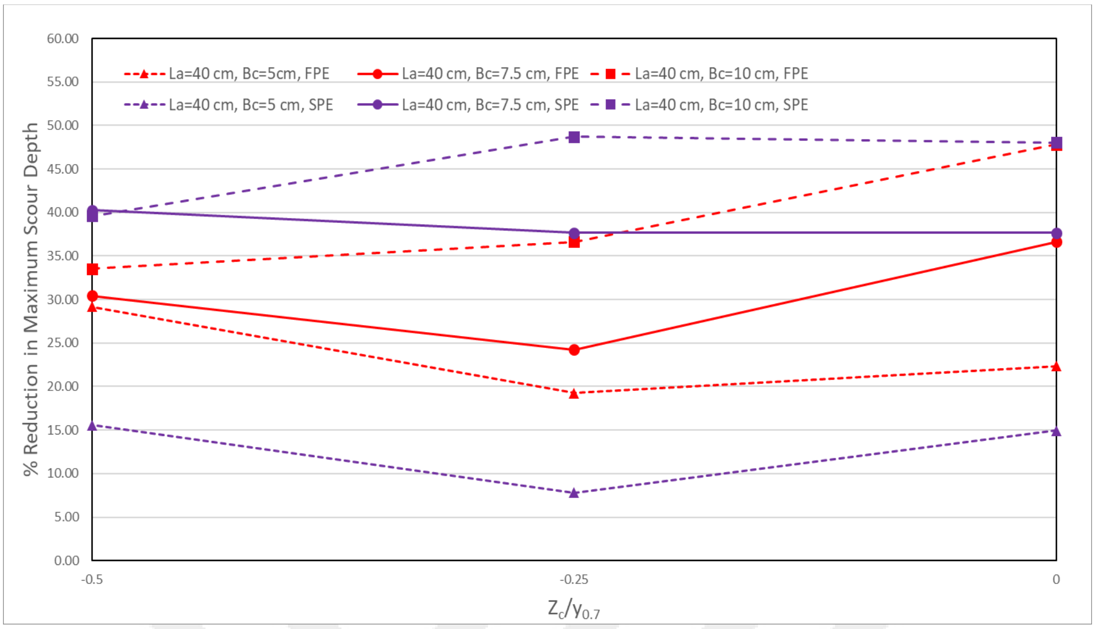

Figure 5.84 Comparison of the effects of collar size and elevation on the maximum scour depth around abutment of length L_a=40 cm for FPE and SPE (t=6 hours)

In Figures 5.85-87, the comparison of the scour reduction performances of the varying collar sizes and flow intensities between FPE and SPE for the abutment of length L_a=40 cm are presented. When the collars were placed at the elevation of $Z_c/y_{0.7}$= ±0.00, the scour reduction performances of the collars were close to each other for the FPE and SPE during each stage of the experiments even the flow intensity and test duration increased. However, at the elevations of $Z_c/y_{0.7}$= -0.25 and -0.50, significant differences were observed between the FPE and SPE in terms of reduction in the maximum scour depth. At the elevation of $Z_c/y_{0.7}$= -0.25, scour reduction efficiencies of the collars at the end of the first and second stages of the experiments were similar for the FPE and SPE. However, at the end of the third stage of the experiments with increased flow intensity and test duration, the collars gave more successful results for SPE in reducing the scour depth, except for the collar of B_c=7.5 cm. At the elevation of $Z_c/y_{0.7}$= -0.50, scour reduction performances of the collars, except the collar of B_c=5 cm, were found to be better for SPE than FPE due to the dimensional collar locations as mentioned above.

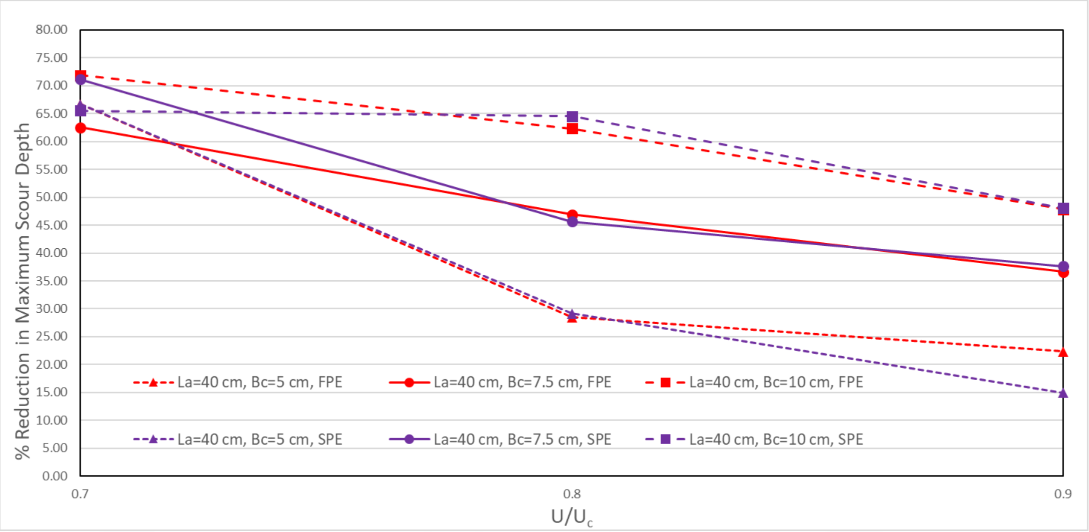

Figure 5.85 Comparison of the effects of collar size and flow intensity on the maximum scour depth around abutment of length L_a=40 cm for FPE and SPE ($Z_c/y_{0.7}$= ±0.00)

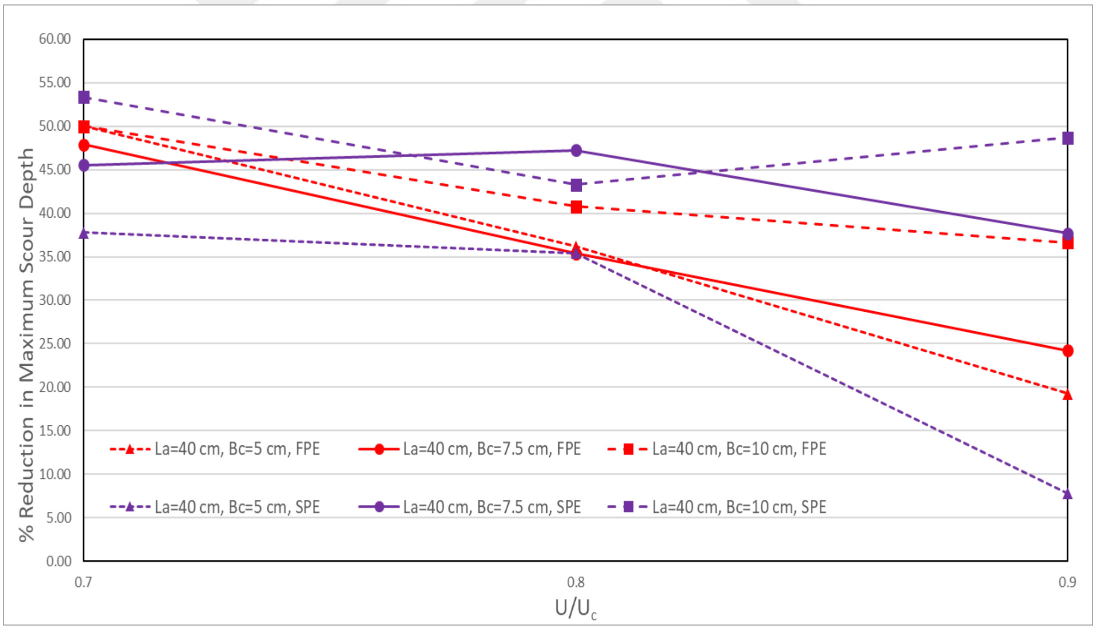

Figure 5.86 Comparison of the effects of collar size and flow intensity on the maximum scour depth around abutment of length L_a=40 cm for FPE and SPE ($Z_c/y_{0.7}$= -0.25)

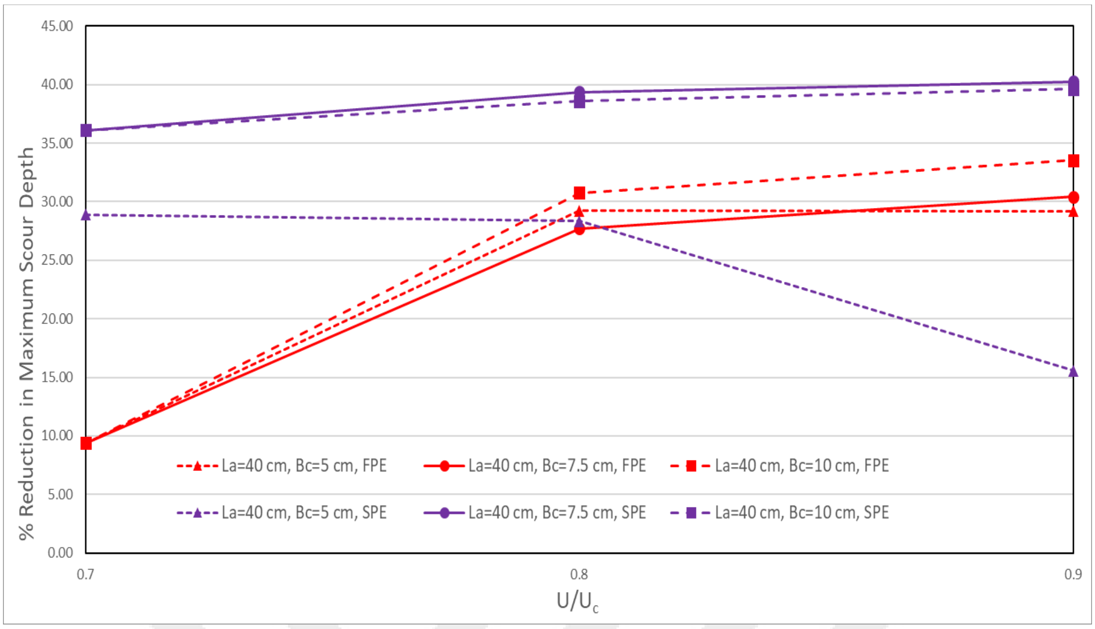

Figure 5.87 Comparison of the effects of collar size and flow intensity on the maximum scour depth around abutment of length L_a=40 cm for FPE and SPE ($Z_c/y_{0.7}$= -0.50)

5.6.7.2 The Abutment of Length L_a=30 cm

Comparison of the scour reduction efficiencies of the collars based on flow depth for semi-circular end abutment of length L_a=30 cm is demonstrated in Figures 5.88-5.90. At the end of the first stage of the experiments, scour reduction performance of the collar of B_c=10 cm during FPE was found to be greater than those during SPE at the elevation of $Z_c/y_{0.7}$= ±0.00. Nevertheless, it should be noticed that the results of each case belonging to the collars of B_c=5 cm and 7.5 cm were found to be close to each other. On the contrary, at the elevation of $Z_c/y_{0.7}$= -0.50, collar efficiency was observed better during SPE despite the efficiencies of the collars for both cases being pretty low. Moreover, at the elevation of $Z_c/y_{0.7}$= -0.50, scour reduction efficiencies during FPE and SPE for a given collar size were close to each other. In this context, it can be stated that as the collars were placed deeper into the bed level, scour reduction efficiencies of the collars increased during SPE while decreasing during

FPE. At the end of the second stage of the experiment, at the elevations of $Z_c/y_{0.7}$=-0.25 and ±0.00, the maximum scour reduction percentages of the collars for a given collar size were similar for both FPE and SPE. However, at the elevation of $Z_c/y_{0.7}$= -0.50 scour reduction efficiencies of the collars were measured better during SPE than FPE like abutment of length L_a=40 cm. Finally, at the end of the third stage of the experiments, the maximum scour reduction efficiencies of the collars for a given collar size was found to be pretty close to each other at all the collar elevations.

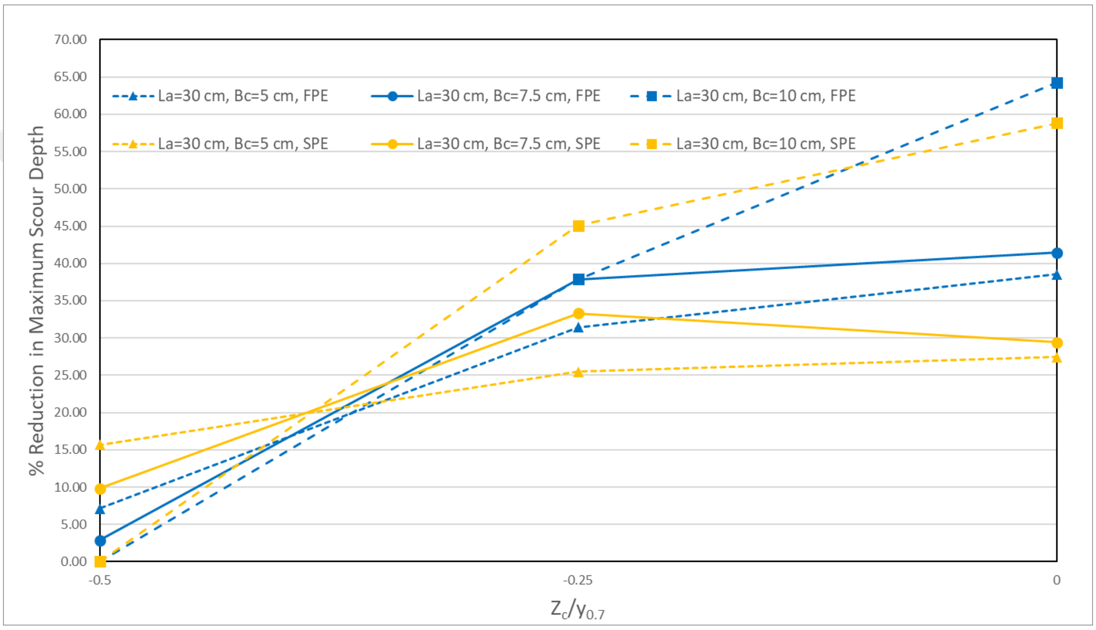

Figure 5.88 Comparison of the effects of collar size and elevation on the maximum scour depth around abutment of length L_a=30 cm for FPE and SPE (t=2 hours)

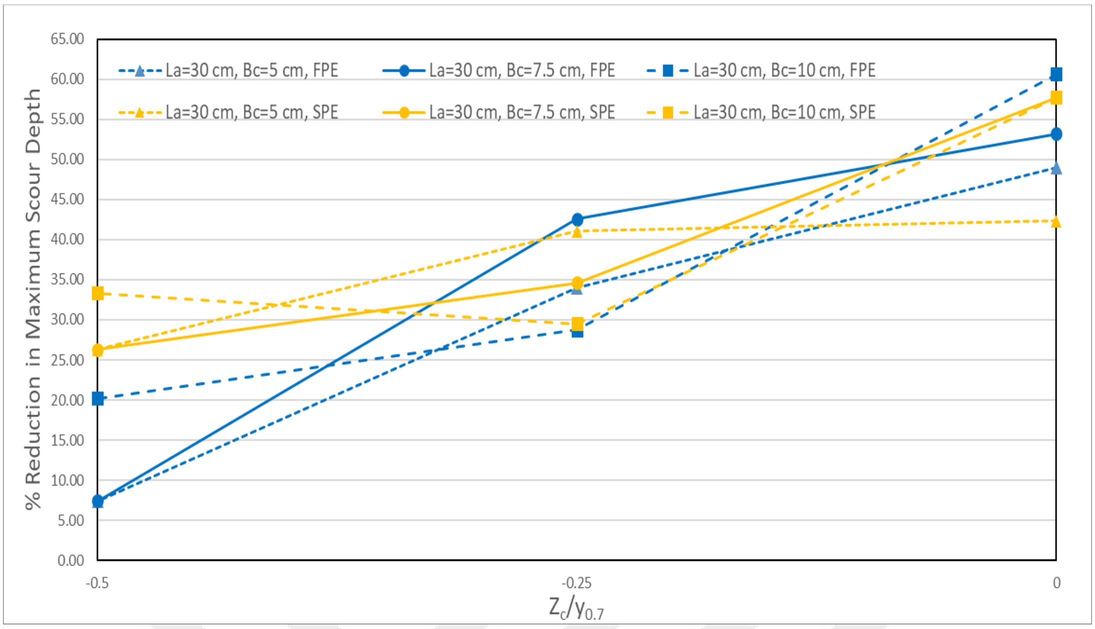

Figure 5.89 Comparison of the effects of collar size and elevation on the maximum scour depth around abutment of length L_a=30 cm for FPE and SPE (t=4 hours)

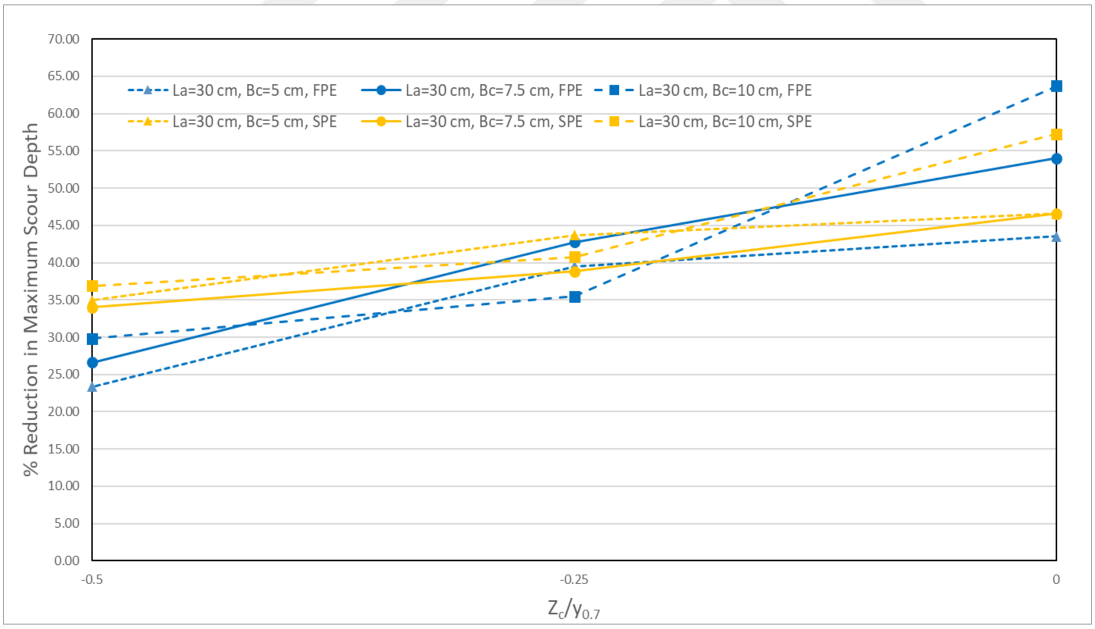

Figure 5.90 Comparison of the effects of collar size and elevation on the maximum scour depth around abutment of length L_a=30 cm for FPE and SPE (t=6 hours)

The comparison of the scour reduction performances of varying collar sizes and flow intensities between FPE and SPE for the abutment of length L_a=30 cm are demonstrated in Figures 5.91-93. At the elevations of $Z_c/y_{0.7}$= -0.25 and ±0.00, the scour reduction performances of the collars during FPE and SPE for a given collar width were close to each other, except for the collar of B_c=10 cm. Furthermore, the efficiencies of the collars of the two cases converged with each other as the flow intensity and test duration increased. At the elevation of $Z_c/y_{0.7}$= -0.50, collars had more efficient in reducing the maximum scour depth during SPE than those of FPE, but as the flow intensity and test duration increased, the efficiency of the collars obtained during two different cases was started to converge each other for a given collar width.

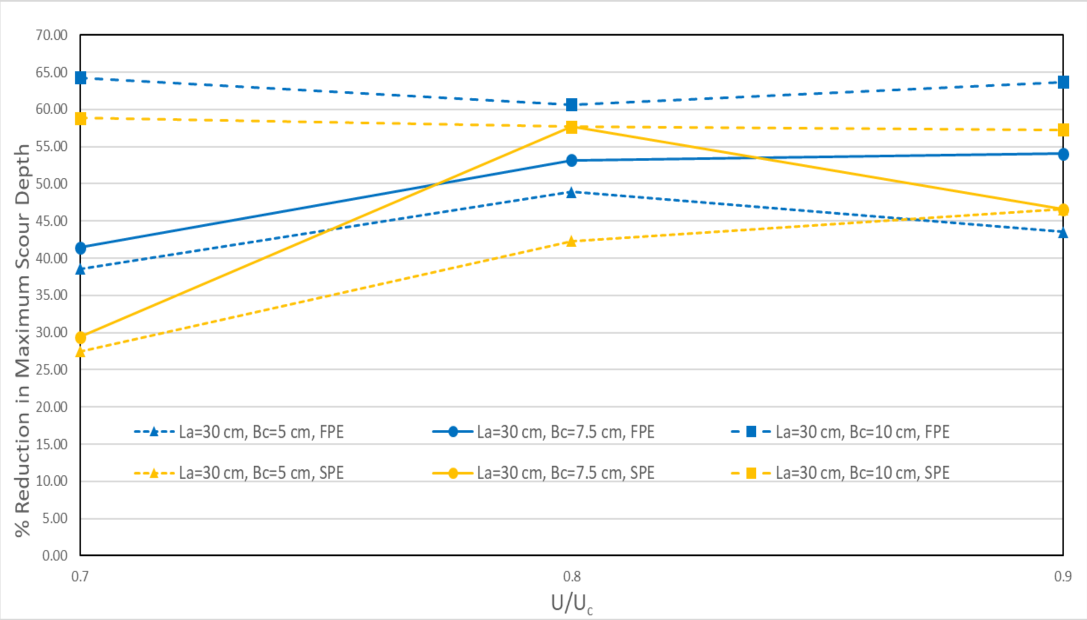

Figure 5.91 Comparison of the effects of collar size and flow intensity on the maximum scour depth around abutment of length L_a=30 cm for FPE and SPE ($Z_c/y_{0.7}$= ±0.00)

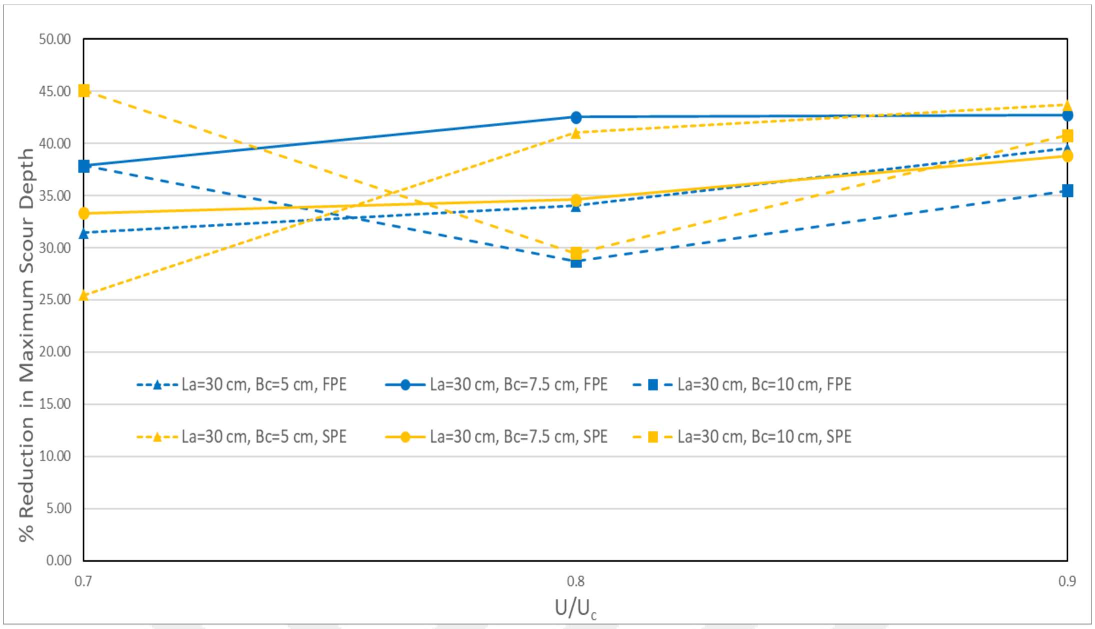

Figure 5.92 Comparison of the effects of collar size and flow intensity on the maximum scour depth around abutment of length L_a=30 cm for FPE and SPE ($Z_c/y_{0.7}$= -0.25)

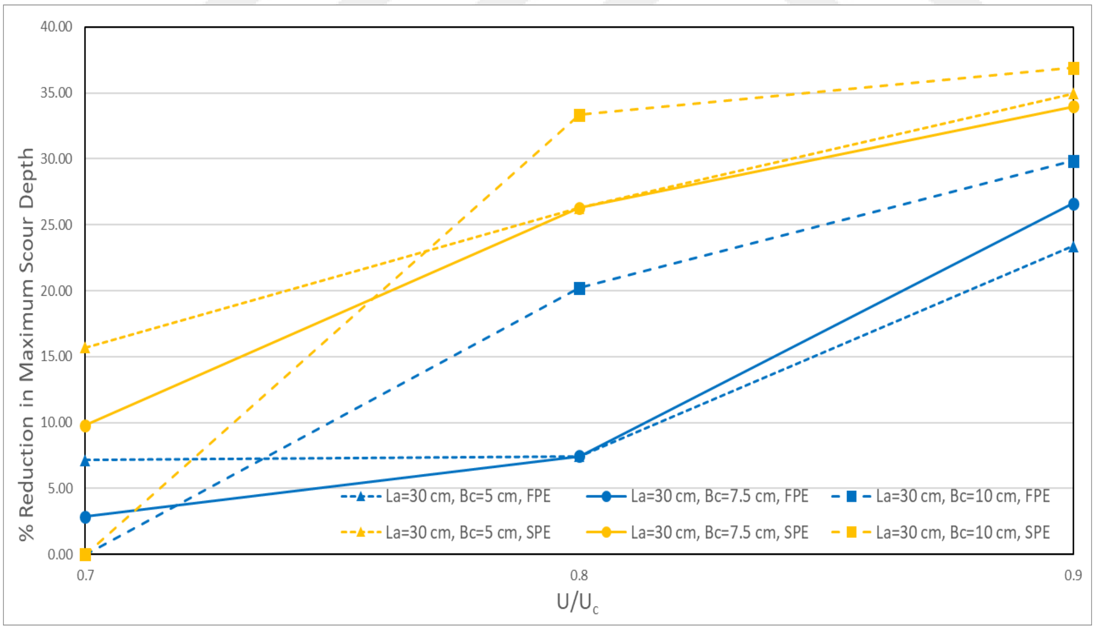

Figure 5.93 Comparison of the effects of collar size and flow intensity on the maximum scour depth around abutment of length L_a=30 cm for FPE and SPE ($Z_c/y_{0.7}$= -0.50)

5.6.7.3 The Abutment of Length L_a=20 cm

The comparison of the scour reduction efficiencies of the collars based on flow depth for semi-circular end abutment of length L_a=20 cm are presented in Figures 5.94-5.96. At the first stage of the experiments, at the elevation of $Z_c/y_{0.7}$= ±0.00, the scour reduction performances of the collars during FPE and SPE were found to be similar to each other. However, as the collars were located below the bed level (i.e, $Z_c/y_{0.7}$= -0.25), the collar efficiency in reducing the maximum scour depth was greater during SPE than FPE like the abutments of lengths L_a=30 cm and 40 cm. Furthermore, the collars did not show any significant effect on maximum scour depth during FPE. At the end of the second and third stages of the experiments, the maximum scour reductions were found to be better during FPE than those in SPE at the elevation of $Z_c/y_{0.7}$= ±0.00. However, at the elevation of $Z_c/y_{0.7}$= -0.25, the maximum scour reductions during FPE and SPE were observed similar to each other.

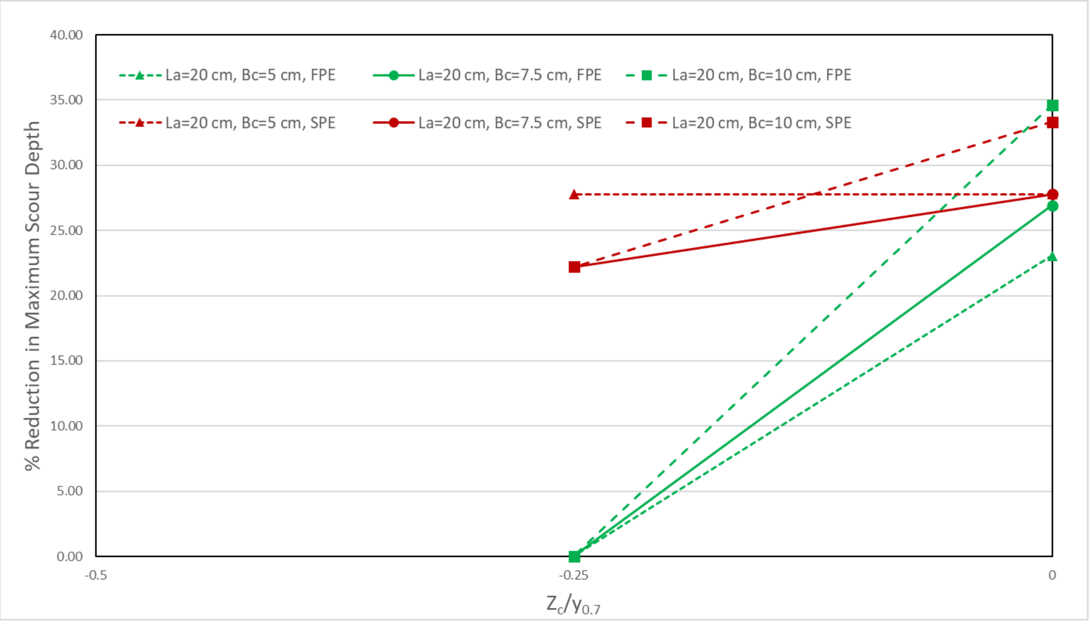

Figure 5.94 Comparison of the effects of collar size and elevation on the maximum scour depth around abutment of length L_a=20 cm for FPE and SPE (t=2 hours)

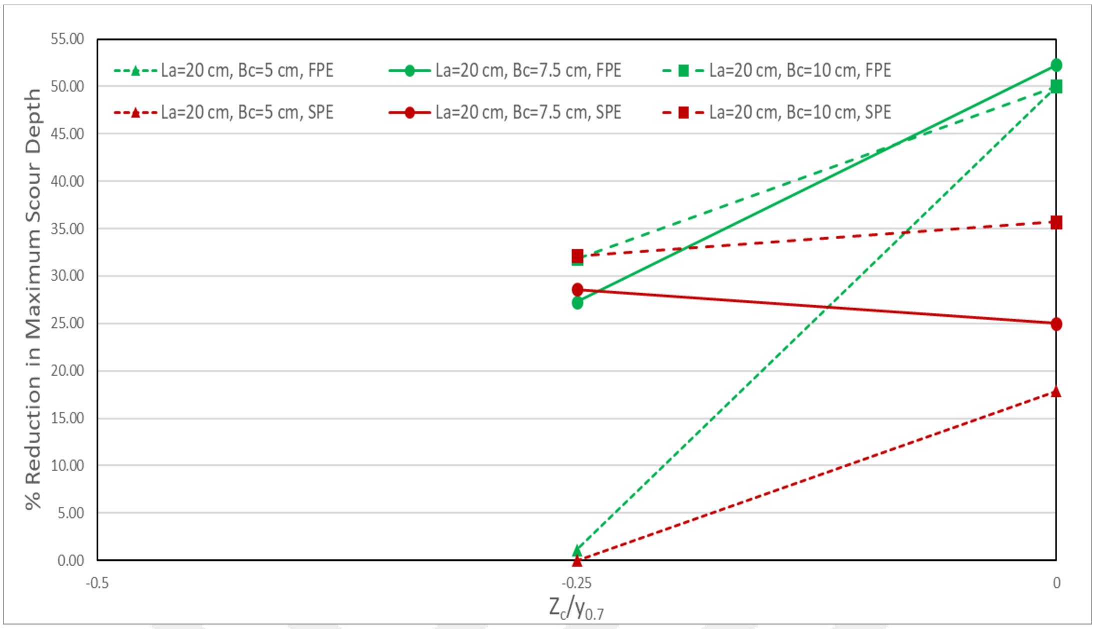

Figure 5.95 Comparison of the effects of collar size and elevation on the maximum scour depth around abutment of length L_a=20 cm for FPE and SPE (t=4 hours)

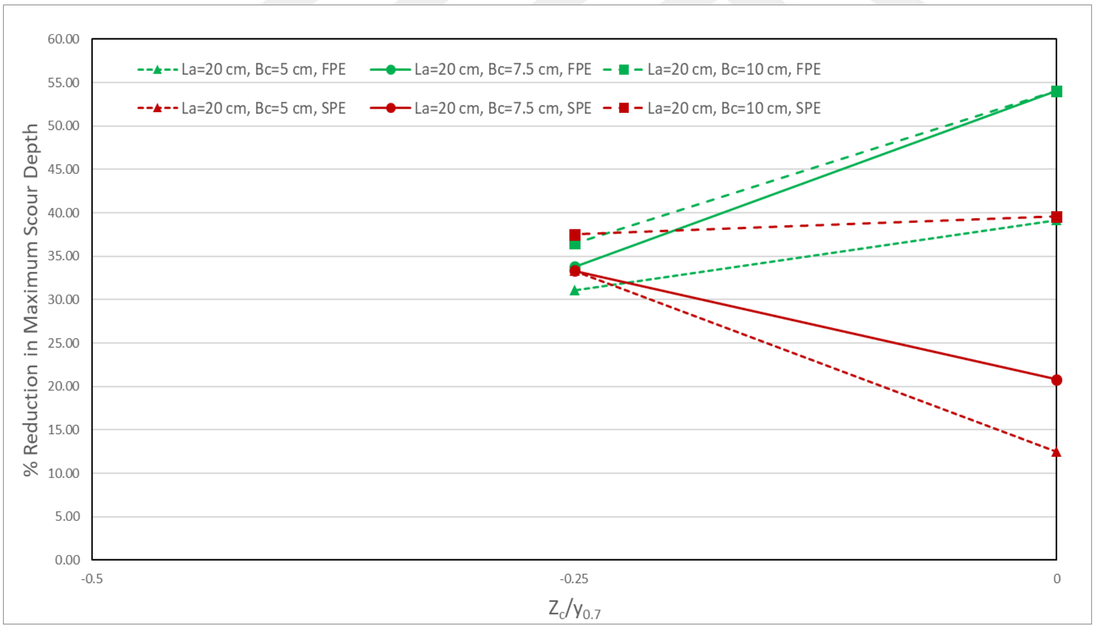

Figure 5.96 Comparison of the effects of collar size and elevation on the maximum scour depth around abutment of length L_a=20 cm for FPE and SPE (t=6 hours)

In Figures 5.97 and 5.98, the comparison of the scour reduction performances of the varying collar sizes and flow intensities between FPE and SPE for the abutment of length L_a=20 cm are presented. Based on the experimental results, at the end of the 2nd hour with the flow intensity of 0.7, the scour reduction percentages due to the collars during FPE and SPE were almost the same with each other at the elevation of $Z_c/y_{0.7}= \pm0.00$. However, as the flow intensity and test duration increased, the scour reduction performances of the collars became better during FPE. At the elevation of $Z_c/y_{0.7}$= -0.25, similar collar performances in reducing the maximum scour depth were obtained at the end of the 4th and 6th hours. Also, it should be underlined that at the end of 2nd hour, the collars did not show any significant effect in reducing the maximum scour depth during FPE. Therefore, for this abutment-collar arrangement, it is hard to make any comments on the effect of flow depth to the efficiencies of the collars.

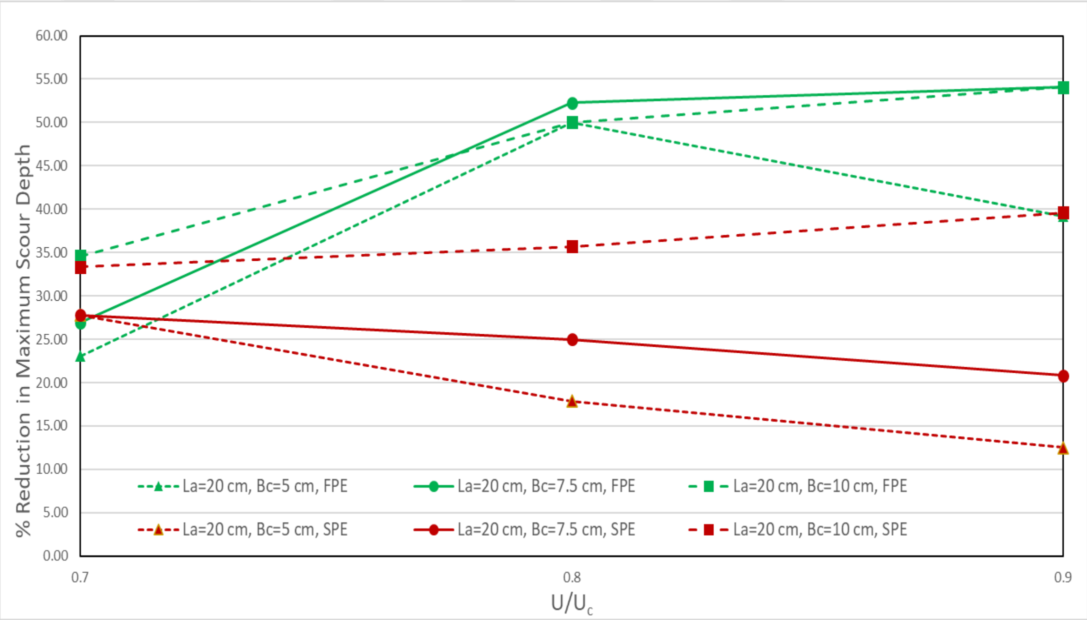

Figure 5.97 Comparison of the effects of collar size and flow intensity on the maximum scour depth around abutment of length L_a=20 cm for FPE and SPE ($Z_c/y_{0.7}= \pm0.00$)

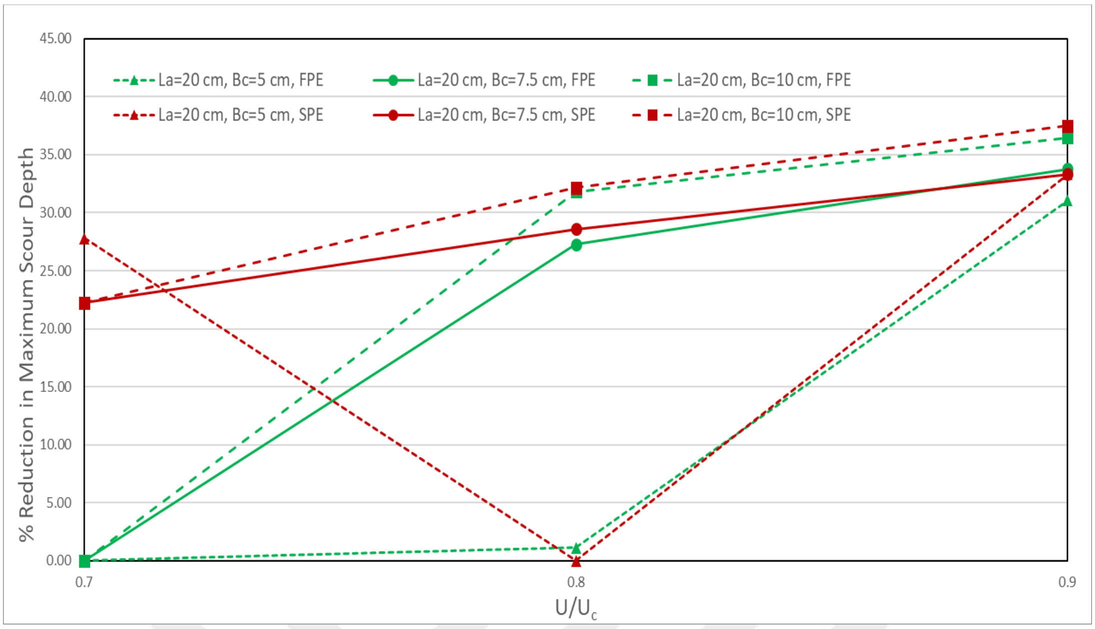

Figure 5.98 Comparison of the effects of collar size and flow intensity on the maximum scour depth around abutment of length L_a=20 cm for FPE and SPE ($Z_c/y_{0.7}$= -0.25)

5.6.7.4 Summary

In summary, the efficiency of the collars at the elevations of $Z_c/y_{0.7}$=-0.25 and ±0.00 around the abutments of lengths L_a=30 cm and 40 cm did not show significant differences in terms of reducing the maximum scour depth during the FPE and SPE. Therefore, it can be stated that the efficiency of the collars mostly depends on abutment length, collar size and elevation, and flow intensity rather than flow depth for this elevation. However, it should be underlined that significant differences were obtained between the FPE and SPE in terms of collar efficiency for the collars at the elevation of $Z_c/y_{0.7}$= -0.25 around the abutment of length L_a=40 cm at the end of the third stage of the experiments. For this case, collar efficiency was found to be better during the SPE. These differences might be caused by the differences in dimensional collar elevation between the FPE and SPE. On the other hand, the collar efficiency was generally obtained better during SPE when the collars were located at the elevation of $Z_c/y_{0.7}$= -0.50 due to the dimensional collar elevations once again. The collars at the elevation of Z_c= -8.70 during FPE was found to be ineffective in reducing the maximum scour depth due to the smaller scour depths can not reach this elevation. On the contrary, the collars at the elevation of Z_c= -5.75 during FPE showed some efficiency in reducing the maximum scour depth because the scour formation reached this elevation and the collar manipulated the flow. On the contrary for the abutments of lengths L_a=30 cm and 40 cm, for the abutment of length L_a=20 cm, flow depth had significant effects to scour reduction performances of the collars. Although, the scour reduction performances of the collars were almost found to be the same during the FPE and SPE when collars were placed to the elevations of $Z_c/y_{0.7}$= -0.25 and ±0.00 at the end of the third and first stages of the experiments, respectively. For the other test durations and abutment-collar arrangements efficiency of the collars during the FPE and SPE differed from each other. At the elevation of $Z_c/y_{0.7}$= ±0.00, the collars were more efficient during FPE while at the elevation of $Z_c/y_{0.7}$= -0.25, the collars gave more successful results during SPE in reducing the maximum scour depth. Increased collar efficiency during SPE at the elevation of $Z_c/y_{0.7}$= -0.25, can be explained by the differences in the dimensional collar elevations which were mentioned in detail above. The ranges of minimum and maximum % reductions in maximum scour depths around the semi-circular end abutments testes during FPE and SPE are listed in Table 5.16.

Table 5.16 The ranges of minimum and maximum % reductions in maximum scour depths around the semi-circular end abutments testes during FPE and SPE

$2.0 \le L_a/B_c \le 8.0$				
$Z_c/y_{0.7}$	t (hour)	U/U_c	The range of % reduction in maximum scour depth	
			FPE (First Phase Experiments)	SPE (Second Phase Experiments)
±0.00	2	0.7	23.08 - 71.88	27.45 - 71.11
	4	0.8	28.46 - 62.31	17.86 - 65.47
	6	0.9	22.36 - 63.71	12.50 - 57.28
-0.25	2	0.7	0.00 - 50.00	22.22 - 53.33
	4	0.8	1.14 - 42.55	0.00 - 47.27
	6	0.9	19.25 - 42.74	7.79 - 48.70
-0.50	2	0.7	0.00 - 9.38	0.00 - 36.11
	4	0.8	7.45 - 30.77	26.28 - 39.37
	6	0.9	23.39 - 33.54	15.58 - 40.26

Variation of $[(d_s)_{max,c}/y]$ and $\sqrt{\theta(L_a/B_c)} * \exp\left(\frac{U}{U_c}\right) * \exp\left(\frac{t}{t_p}\right)$ during FPE and SPE based on the collar elevations plotted together in Figure 5.99 for the semi-circular end abutments. From the figure, it can be seen that similar trends were obtained during the SPE with FPE. Like the FPE, the dimensionless maximum scour depths not only increase with increasing abutment and decreasing collar size but also increase with increasing flow intensity and test duration during the SPE for a given collar elevation. However, for a given $\sqrt{\theta(L_a/B_c)} * \exp\left(\frac{U}{U_c}\right) * \exp\left(\frac{t}{t_p}\right)$, the maximum dimensionless scour depths were found to be less during SPE than FPE because of the smaller flow depths under the same flow conditions lead to smaller scour depths. Also, at the elevation of $Z_c/y_{0.7}$=±0.00, the dimensionless maximum scour depths during the FPE and SPE converged to each other with increasing $\sqrt{\theta(L_a/B_c)} * \exp\left(\frac{U}{U_c}\right) * \exp\left(\frac{t}{t_p}\right)$, on the contrary, the dimensionless maximum scour depths during the FPE and SPE yielded away from each other with increasing $\sqrt{\theta(L_a/B_c)} * \exp\left(\frac{U}{U_c}\right) * \exp\left(\frac{t}{t_p}\right)$ at the elevations of $Z_c/y_{0.7}$=-0.50 and -0.25. The main reason of this situation might be the differences in the dimensional collar elevations which provide an advantage for the collar elevations below the bed level during the SPE.

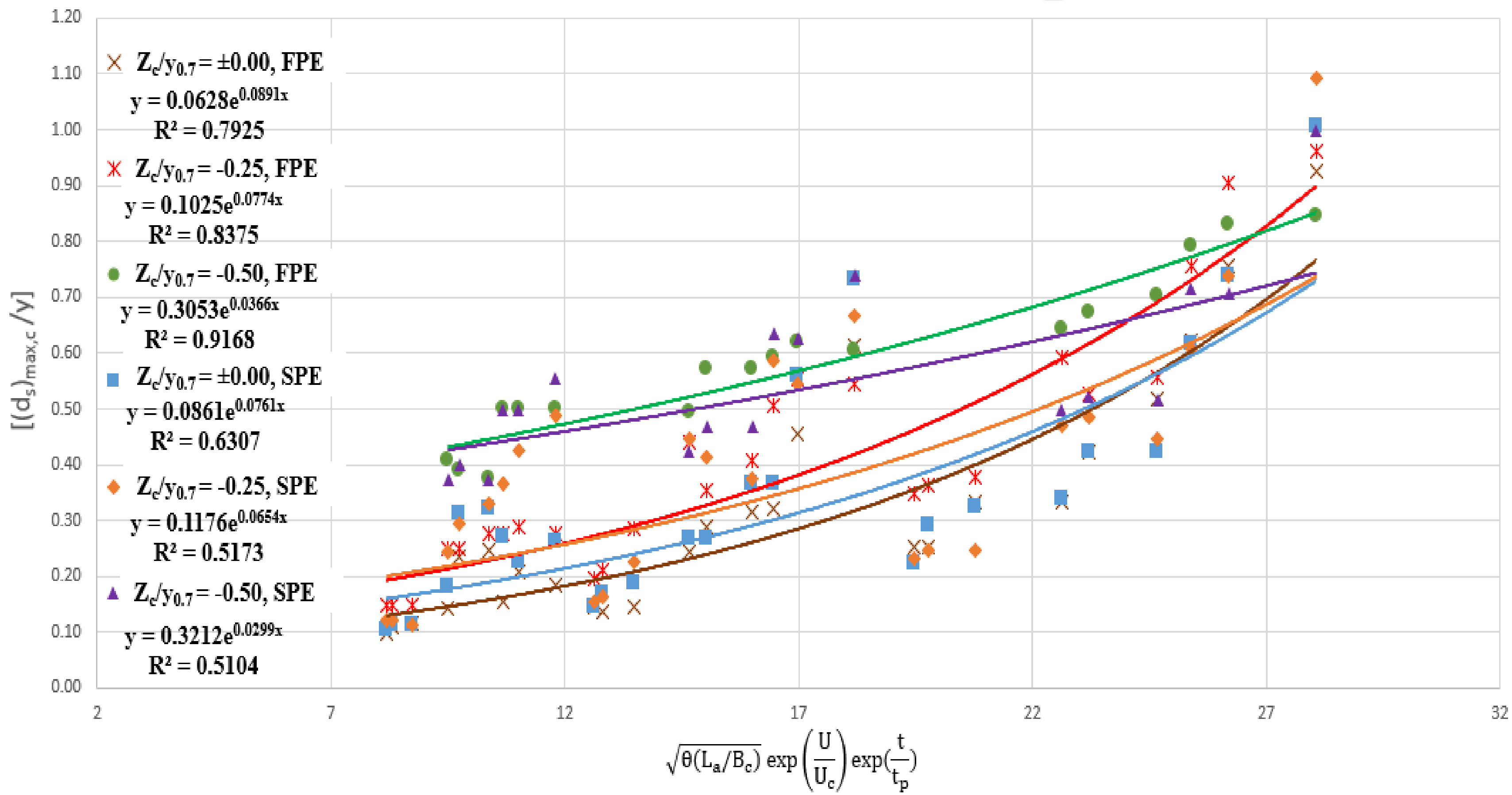

Figure 5.99 Variation of $[(d_s)_{max,c}/y]$ with $\sqrt{\theta(L_a/B_c)}\exp\left(\frac{U}{U_c}\right)\exp\left(\frac{t}{t_p}\right)$ during the FPE and SPE for semi-circular end abutments

CHAPTER 6

CONCLUSIONS

In this study, first of all, a series of experiments were carried out to understand the temporal development of local scour around semi-circular end and rectangular bridge abutments under unsteady-state clear-water flow conditions. A long-duration stepwise hydrograph expressed in terms of flow intensity and composed of three steps each having a time duration of two hours was used in the experiments to represent a flood having a total period of six hours. The effect of flow intensity, abutment length and temporal variation on the development of scour around the abutments were investigated. Furthermore, the maximum scour depths in 15-minute intervals at the upstream, downstream and front sides of the abutments were compared to each other. In addition, the maximum scour depths were theoretically calculated by using the relationship proposed by Oliveto and Hager (2002, 2005a) and compared with the experimental results obtained within the scope of this study. In the second part of the study, the efficiencies of the collars in order to reduce the scour depths around bridge abutments were investigated by applying the same flow and hydrograph properties tested in the first part of the study. Semi-circular end and rectangular collars having various sizes were placed at different elevations with respect to the bed level around semi-circular end and rectangular abutments, respectively, to investigate the effect of abutment length, flow intensity, time, collar size and collar elevation on the scour reduction performances of the collars. Moreover, the experimental results of this study were compared to the previous similar studies found in the literature, which were conducted under steady-state clear-water flow conditions such as Kayatürk (2005), Doğan (2008), Daşkın (2011) and Tekin (2012) to indicate the effect of unsteadiness on the scour reduction performances of the collars. Finally, additional experiments with collars were performed by applying the same flow hydrograph based on flow intensity tested in the previous parts with different flow depths to understand the effect of flow depth on the collar efficiency in reducing the maximum scour depth around the abutments. The following conclusions drawn from this study are listed below:

1. The dimensionless scour depth, d_s/y, at the upstream, downstream and front noses of an abutment increases with increasing dimensionless time, Ut/y, and flow intensity, U/U_c, for semi-circular end and rectangular abutments of the given length.
2. Since the longer abutment lengths cause greater horseshoe vortex and increased bed shear stress zones compared to shorter ones (Koken and Gogus, 2015), as the lengths of the semi-circular end and rectangular abutments increase for a given time and flow intensity, scour depths get deeper around the abutment.
3. For the shorter abutment lengths tested as L_a=15 cm, 20 cm and 25 cm, the occurrence of significant scour depths triggered with the high flow intensity values. Furthermore, around the short abutments, $L_a/y<1$, negligible scour depths are observed for flow intensities less than 0.9.
4. Maximum scour depths always occur at the front nose of the abutment regardless of the abutment length at any flow intensity tested as stated in previous studies such as Ballio and Orsi (2000), Oliveto and Hager (2002) and Kumcu et al. (2014).
5. The rectangular abutments for a given length and test duration tend to create greater scour depths than semi-circular end abutments because of the blunt nature of the rectangular abutments that leads to greater scour depths. In addition, for the abutments of lengths L_a=30, 35 and 40 cm, the maximum scour depths were recorded by around 30% greater for the rectangular abutments than semi-circular end ones. This indication shows strong consistency with Melville's (1992) study that presented the abutment shape factor values for the maximum scour depth around semi-circular and rectangular abutments as 0.75 and 1, respectively. However, for the abutments of lengths L_a=15 cm, 20 cm and 25 cm, the maximum scour depths

around the rectangular abutments were measured much greater than 30% than those of semi-circular ones.

6. The dimensionless scour depths measured at the front side of the abutments, $(d_s)_f/y$ were always greater than those at the upstream side, $(d_s)_u/y$ and downstream, $(d_s)_d/y$ side regardless of the abutment length and shape.
7. The dimensionless scour depths measured at the upstream side of the abutments, $(d_s)_u/y$ were always greater than those at the downstream side, $(d_s)_d/y$ regardless of the abutment length for rectangular abutments. However, the measured scour depths at the downstream side, $(d_s)_d/y$ around the semi-circular end abutments of lengths L_a=15 cm and 20 cm were obtained a little bit larger than those at the upstream side of the abutment. The same situation was also observed for the semi-circular abutments of lengths L_a=25 cm and 30 cm until the end of the 4th hour of the experiments.
8. The experimental results of this study and theoretically calculated results according to the proposed relationship of Oliveto and Hager (2002 and 2005a) showed consistency with each other for the semi-circular end abutments of lengths L_a=30 cm, 35 cm and 40 cm within the ±30% error range. On the contrary, the proposed relationship did not show consistency with the other semi-circular end abutment lengths and all the rectangular abutment lengths.
9. A collar attached around a bridge abutment prevents the direct impact of downflow by deflecting the flow to the sediment. In other words, collars act like a ‘downflow-halting’ device during scour hole development and prevent secondary vortices from evolving around the abutment (Li et al., 2005). Hence, as one of the main outputs of this study, collars are very effective scour countermeasures to reduce or eliminate the scour formation around semi-circular end and rectangular abutments.
10. As the collar size increased, the scour reduction efficiencies of the collars generally increased regardless of the abutment length and shape, because the

larger collars are more successful to prevent the penetration of the vortices into the deeper elevations.

11. As the potential of having greater scour depths due to increased abutment length, blunt abutment shape, higher flow intensity values and increased test duration, the efficiencies of the collars placed below the bed level (i.e., $Z_c/y_{0.7}$=-0.50 and -0.25) increased. However, for the smaller scour depth potential, the collars placed at the bed level, $Z_c/y_{0.7}$=±0.00 gave better results in reducing the maximum scour depths around the abutments. Consequently, for the semi-circular end abutments tested in this study, the most efficient collar performances were generally obtained when the collars were placed at the elevation of $Z_c/y_{0.7}$=±0.00. On the contrary, the collars were placed at the elevations of $Z_c/y_{0.7}$=-0.50 and -0.25 generally gave better results in reducing the maximum scour depth for rectangular abutments.
12. The scour reduction performances of the collars at the elevations of $Z_c/y_{0.7}$=-0.25 and ±0.00 generally decreased with increasing flow intensity and test duration regardless of the abutment shape while at the elevation of $Z_c/y_{0.7}$=-0.50 increased.
13. According to the experimental results, it was obtained that the semi-circular end collars around the semi-circular end abutments reduce the scour depth by around up to 72% while the rectangular collars around the rectangular abutments are around up to 52%. Therefore, the semi-circular collars gave better results in reducing the maximum scour depth than rectangular ones.
14. The dimensionless maximum scour depth with a collar, $[(d_s)_{max,c}/y]$, was found to increase regardless of abutment shape, flow intensity and test duration with increasing $\sqrt{\theta(L_a/B_c)}$ value, where L_a/B_c denotes the abutment length and collar size ratio and θ present the effect of areal sizes of the abutment models with collars on the reduction of maximum scour around the abutments. Also, the linear relationships between $[(d_s)_{max,c}/y]$ and $\sqrt{\theta(L_a/B_c)}$ with varying flow intensities, collar elevations and test durations were listed in Tables 5.7 and 5.8.

15. Variation of $[(d_s)_{max,c}/y]$ and $\sqrt{\theta(L_a/B_c)}\exp\left(\frac{U}{U_c}\right)\exp\left(\frac{t}{t_p}\right)$ shown in Figures 5.73 and 5.74 for the semi-circular end and rectangular abutments showed that the efficiencies of the collars located below the bed level increased as $\sqrt{\theta(L_a/B_c)}\exp\left(\frac{U}{U_c}\right)\exp\left(\frac{t}{t_p}\right)$ values increased.
16. The maximum dimensionless scour depths with collars corresponding to the optimal collar locations, $[(d_s)_{max,c}/y]_{opt}$, decreased for the abutments of lengths L_a=30 cm and 40 cm with increasing θ values for a given abutment length, flow intensity and test duration. On the other hand, $[(d_s)_{max,c}/y]_{opt}$ did not show significant differences with increasing θ values for abutment of length L_a=20 cm.
17. Scour reduction percentages corresponding to the optimal collar locations, $[\text{Reduction\%}]_{opt}$, generally tend to decrease regardless of abutment shape, flow intensity and test duration with increasing L_a/B_c. Also, the exponential relationships between $[\text{Reduction\%}]_{opt}$ and L_a/B_c was presented in Table 5.12.
18. Comparison of the variation of $[(d_s)_{max,c}/y]_{opt}$ and $\sqrt{\theta(L_a/B_c)}$ obtained from this study's data with the studies of Kayatürk (2005), Doğan (2008), Daşkın (2011) and Tekin (2012) conducted under steady-state clear-water flow conditions showed that the maximum scour depths tend to yield greater values under steady-state flow conditions than those under unsteady-state flow conditions for a given $\sqrt{\theta(L_a/B_c)}$ value under similar flow conditions with similar sediment properties.
19. The maximum scour depths increased with increasing flow depth under similar experimental conditions, but flow depth had no significant effects on the magnitude of the scour depths as far as the flow intensity.
20. For the abutments of lengths L_a=30 cm and 40 cm, the scour reduction performances of the collars were generally found to be independent of flow depth. On the contrary, for the abutment of length L_a=20 cm, which was the

shortest abutment length tested within the scope of this study, the flow depth had significant effects on the scour reduction performances of the collars.

For further studies, there are still several interesting subjects to be focused on as a part of abutment scour and its countermeasures techniques. Some of them are listed below as a recommendation for future studies.

1. Different L_a/y, U/U_c and t/t_{max} values not investigated within the scope of this study should be tested to get more general relations for the development of scours and its countermeasures around the abutments of different types as well as semi- circular end and rectangular abutments. In addition, the temporal development of the abutment scour should be investigated by applying different types of hydrographs in terms of peak numbers and shape.
2. Previous studies in the literature and the present study have been focused on clear-water flow conditions. However, experiments on abutment scour and its countermeasures should also be investigated under live-bed conditions to get a better understanding of the abutment scour and the efficiency of its countermeasures.
3. The scour reduction efficiencies of the newly presented shapes of collars such as airfoil and streamlined shapes should be tested and compared with the traditional ones such as semi-circular end and rectangular collars.
4. The scour reduction efficiencies of the different flow-altering countermeasures such as slots and vanes should also be investigated under unsteady-state flow conditions.
5. Since the efficiencies of the flow-altering countermeasures decrease with the temporal development of scour, using a combination of flow-altering countermeasures to decrease or eliminate the scour formation around the bridge element would be helpful (Tafarojnoruz et al., 2012a). Hence, the combined attachment of different flow-altering countermeasures such as the collar, slot and vanes should be tested under steady and unsteady-state flow conditions.

6. Numerical software such as Flow3D, Fluent, OpenFOAM and SSIIM should be used in order to investigate abutment scour and its countermeasures in the computer environment

REFERENCES

Abolfathi, S., Kashefipour, S. M., Fuhrman, D. R. and Bajestan, M. S. (2022). Temporal scouring and backfilling processes around a pile group subject to unsteady hydrographs. Ain Shams Engineering Journal, 13(2), 101565.

Abou-Seida, M. M., Elsaeed, G. H., Mostafa, T. M. S. and Elzahry, E. F. M. (2009). Experimental investigation of abutment scour in sandy soil. Journal of Applied Sciences Research, 5(1), 57-65.

Agrawal, A. K., Khan, M. A., Yi, Z. and Aboobaker, N. (2007). Handbook of scour countermeasures designs (No. FHWA-NJ-2005-027). New Jersey Department of Transportation.

Ahmad, M. (1953). Experiments on design and behavior of spur-dikes. Proceedings of International Hydraulic Convention, 145–159.

Alabi, P. D. (2006). Time Development of Local Scour At A Bridge Pier Fitted With A Collar (Master Thesis), University of Saskatchewan, Canada.

Arneson, L. A., Zevenbergen, L. W., Lagasse, P. F. and Clopper, P. E. (2012). Evaluating scour at bridges (No. FHWA-HIF-12-003). National Highway Institute, United States.

Atarodi, A., Karami, H., Ardeshir, A., Hosseini, K. and Lampert, D. (2021). Experimental investigation of scour reduction around spur dikes by collar using Taguchi method. Iranian Journal of Science and Technology, Transactions of Civil Engineering, 45(2), 971-983.

Ballio, F. and Orsi, E. (2000). Time Evolution of Scour Around Bridge Abutments. Water Engineering Research, 2, 243–259.

Barbhuiya, A. K. and Dey, S. (2004). Local scour at abutments: A review. Sadhana, 29(5), 449-476.

Barkdoll, B. D., Ettema, R. and Melville, B. W. (2007). Countermeasures to protect bridge abutments from scour, 587, Transportation Research Board.

Barkdoll, B. D. (2012). Effects of Climate Change on Bridge Scour, World Environmental and Water Resources Congress 2012: Crossing Boundaries, 2532-2537

Bombar, G. (2020). Scour evolution around bridge piers under hydrographs with high unsteadiness. Iranian Journal of Science and Technology, Transactions of Civil Engineering, 44, 325-337.

Borghei, S. M., Kabiri-Samani, A. and Banihashem, S. A. (2012). Influence of unsteady flow hydrograph shape on local scouring around bridge pier. In Proceedings of the Institution of Civil Engineers-Water Management, 165(9), 473-480.

Breusers, H. N. C. (1967). Time scale of two dimensional local scour. Proceedings of 12th Congress IAHR, 3(C32).

Breusers, H. N. C., Nicollet, G. and Shen, H. W. (1977). Local scour around cylindrical piers. Journal of Hydraulic Research, 15(3), 211- 252.

Breusers, H. N. C. and Raudkivi, A. J. (1991). Scouring. IAHR Hydraulic Structures Design Manual 2, AA Balkema, Rotterdam, The Netherlands.

Cao, X. M., and Gu, Z. H. (2015). Three classification criteria and their comparison impact scale between double non-submerged spur dikes. Journal of ZheJiang University (Engineering Science), 49(2), 200-207.

Cardoso, A. H. and Bettess, R. (1999). Effects of time and channel geometry on scour at bridge abutments. ASCE Journal of Hydraulic Engineering, 125, 388–399.

Chabert, J. and Engeldinger, P. (1956). Etude des affouillements autour des piles de points (Study of scour at bridge piers). Bureau Central d.Etudes les Equipment d.Outre-Mer, Laboratoire National d.Hydraulique, France.

Chang, W. Y., Lai, J. S. and Yen, C. L. (2004). Evolution of scour depth at circular bridge piers. Journal of Hydraulic Engineering, 130(9), 905-913.

Chiew, Y. M. (1984). Local scour at bridge piers (Doctoral Thesis), The University of Auckland, New Zealand.

Chiew, Y. M. (1992). Scour protection at bridge piers. Journal of Hydraulic Engineering, 118(9), 1260-1269.

Coleman, S. E., Lauchlan, C. S. and Melville, B.W. (2003). Clear-water scour development at bridge abutments. Journal Hydraulic Research. 41, 521–531.

Cunha, L. V. (1975). Time evolution of local scour. Proceedings of 16th Conference of International Association of Hydraulic Research (Delft: IAHR), 285–299.

Dargahi, B. (1990). Controlling mechanism of local scouring. ASCE Journal of Hydraulic Engineering, 116, 1197–1214.

Daşkın, S. (2011). Effects of collars on local scour around semi-circular end bridge abutments (Master thesis), Middle East Technical University, Ankara, Turkey.

Dey, S. and Barbhuiya, A. K. (2005a). Turbulent flow field in a scour hole at a semicircular abutment. Canadian Journal of Civil Engineering, 32(1), 213-232.

Dey, S. and Barbhuiya, A. K. (2005b). Time variation of scour at abutments. Journal of Hydraulic Engineering, 131(1), 11-23.

Dey, S. and Barbhuiya, A. K. (2006). Velocity and turbulence in a scour hole at a rectangular abutment. Flow Measurement and Instrumentation, 17(1), 13-21.

Doğan, A. E. (2008). Effects of collars on scour reduction at bridge abutments (Master thesis), Middle East Technical University, Ankara, Turkey.

Dongol, D. M. S. (1994). Local scour at bridge abutments. Rep. No. 544, School of Engineering, University of Auckland, Auckland, New Zealand.

Ettema, R. (1980). Scour at bridge piers. Rep. No. 216, School of Engineering, University of Auckland, Auckland, New Zealand.

Farshad, R., Kashefipour, S. M., Ghomeshi, M. and Oliveto, G. (2022). Temporal Scour Variations at Permeable and Angled Spur Dikes under Steady and Unsteady Flows. Water, 14(20), 3310.

Federal Highway Administration, (2001). Evaluating Scour At Bridges. National Highway Institute, Publication No. FHWA NHI 01-001, HEC No. 18, United States.

Francesco, B. and Enrico, O. (2001). Time evolution of scour around bridge abutments. Water Engineering Research, 2(4), 243-259.

Franzetti, S., Larcan, E. and Mignosa, P. (1982). Influence of test duration on the evaluation of ultimate scour around circular piers. Proceedings of International Conference of Hydraulics and Modelling of Civil Structures, Coventry, England, 381–396.

Froehlich, D. C. (1989). Local scour at bridge abutments. ASCE Journal of Hydraulic Engineering, 13-18.

Garde, R. J., Subramanya, K. and Nambudripad, K. D. (1961). Study of scour around spur dikes. ASCE Journal of the Hydraulics Division, 87(HY6), 23-37.

Gargari, M. K., Kirca, V. O. and Yagci, O. (2021). Experimental investigation of gradually-varied unsteady flow passed a circular pile. Coastal Engineering, 168, 103926.

Gaudio, R., Tafarojnoruz, A. and Calomino, F. (2012). Combined flow-altering countermeasures against bridge pier scour. Journal of Hydraulic Research, 50(1), 35-43.

Gill, M. A. (1972). Erosion of sand beds around spur-dikes ASCE Journal of Hydraulic Engineering, 98, 1587–1602.

Gjunsburgs, B., Radzevičius, A., Šadzevičius, R. and Skominas, R. (2021). Scours evolution at bridge abutments under unsteady flow events. Iranian Journal of Science and Technology, Transactions of Civil Engineering, 45(3), 1951-1957.

Gogus, M., and Dogan, A. E. (2010). Effects of collars on scour reduction at bridge abutments. Proceedings 5th International Conference on Scour and Erosion (ICSE-5), November 7-10, 2010, San Francisco, USA, 997-1007.

Gogus, M., Daskin, S. and Gokmener, S. (2023). Effects of collars on local scour around semi-circular end bridge abutments. In Proceedings of the Institution of Civil Engineers-Water Management , 1-11.

Gokmener, S. and Gogus, M. (2022). Local scour evolution around semi-circular end bridge abutment in quasi-unsteady condition. In Proceedings of the Institution of Civil Engineers-Water Management, 175(4), 163-177.

Gu, Z., Cao, X., Gu, Q. and Lu, W. Z. (2020). Exploring proper spacing threshold of non-submerged spur dikes with ipsilateral layout. Water, 12(1), 172.

Gumgum, F. and Guney, M. S. (2020). Time Dependent Live-bed Scour Around Circular Piers under Flood Waves. Periodica Polytechnica Civil Engineering, 64(1), 65-72.

Hager, W. H. and Unger, J. (2010). Bridge pier scour under flood waves. Journal of Hydraulic Engineering, 136(10), 842-847.

Hasegawa, Y., Nakagawa, H., Takebayashi, H. and Kawaike, K. (2020). Three-dimensional flow characteristics in slit-type permeable spur dike fields: efficiency in riverbank protection. Water, 12(4), 964.

Hoffmans, G. J. C. M. and Verheij, H. J. (1997). Scour Manual, Balkema.

Hoffmans, G., Buschman, F. and Van der Wal, M. (2022). Turbulence approach for predicting scour at abutments. Journal of Hydraulic Research, 60(4), 588-605.

Hosseinjanzadeh, H., Khozani, Z. S., Ardeshir, A. and Singh, V. P. (2021). Experimental investigation into the use of collar for reducing scouring around short abutments. ISH Journal of Hydraulic Engineering, 27(1), 616-632.

Imhof, D.(2004). Risk Assessment of Existing Bridge Structures (Doctoral Thesis), University of Cambridge, UK.

Izzard, C. F. and Bradley, J. N. (1958). Field verification of model tests on flow through highway bridges and culverts. Proceedings of the 7th Hydraulics Conference arranged by the Iowa Institute of Hydraulic Research, State University of Iowa , 225-241.

Johnson, P. A., Hey, R. D., Tessier, M. and Rosgen, D. L. (2001). Use of vanes for control of scour at vertical wall abutments. Journal of Hydraulic Engineering, 127(9), 772-778.

Kandasamy, J. K. (1985). Local scour at skewed abutments. Rep. No. 375, School of Engineering, University of Auckland, Auckland, New Zealand.

Kandasamy, J. K. (1989). Abutment scour. Rep. No. 458, School of Engineering, University of Auckland, Auckland, New Zealand.

Kandasamy, J. K. and Melville, B. W. (1998). Maximum Local Scour Depth at Bridge Piers and Abutments. Journal of Hydraulic Engineering, 36(2), 183-198.

Karami, H., Hosseinjanzadeh, H., Hosseini, K. and Ardeshir, A. (2018). Scour and three-dimensional flow field measurement around short rectangular abutment protected by collar. KSCE Journal of Civil Engineering, 22(1), 141-152.

Kayatürk, Ş. Y. (2005). Scour and Scour Protection at Bridge Abutments (Doctoral Thesis), Middle East Technical University, Ankara, Turkey.

Khajavi, M., Kashefipour, S. M. and Bejestan, M. S. (2022). Bridge Abutment Protection against Scouring for Unsteady Flow Conditions. Periodica Polytechnica Civil Engineering, 66(1), 310-322.

Khosravinia, P., Malekpour, A., Hosseinzadehdalir, A. and Farsadizadeh, D. (2018). Effect of trapezoidal collars as a scour countermeasure around wing-wall abutments. Water Science and Engineering, 11(1), 53-60.

Kohli, A. and Hager, W. H. (2001). Building scour in floodplains. Water Maritime Engineering, Procedings of Institution of Civil Engineers, 148, 61–80.

Koken, M. (2011). Coherent structures around isolated spur dikes at various approach flow angles. Journal of Hydraulic Research, 49(6), 736-743.

Koken, M. and Gogus, M. (2015). Effect of spur dike length on the horseshoe vortex system and the bed shear stress distribution. Journal of Hydraulic Research, 53(2), 196-206.

Kothyari, U. C., Garde, R. C. J. and Ranga Raju, K. G. (1992). Temporal variation of scour around circular bridge piers. Journal of Hydraulic Engineering, 118(8), 1091-1106.

Kothyari, U. C., & Ranga Raju, K. G. (2001). Scour around spur dikes and bridge abutments. Journal of hydraulic research, 39(4), 367-374.

Kumar, V., Raju, K. G. R. and Vittal, N. (1999). Reduction of local scour around bridge piers using slots and collars. Journal of Hydraulic Engineering, 125(12), 1302-1305.

Kumcu, Ş. Y., Gögüş, M. and Kökpinar, M. A. (2007). Temporal scour development at bridge abutments with a collar. Canadian Journal of Civil Engineering, 34(4), 549-556.

Kumcu, S. Y., Kokpinar, M. A. and Gogus, M. (2014). Scour protection around rectangular bridge abutments with collars. KSCE Journal of Civil Engineering, 18(6), 1884-1895.

Kumcu, S. Y., Kokpinar, M. A. and Gogus, M. (2022). Effect of collars on the downstream movement of the maximum scour depth location around bridge abutments and piers. Iranian Journal of Science and Technology, Transactions of Civil Engineering, 46(2), 1421-1432.

Kwan, F. (1984). Study of abutment scour. Report No. 328, University of Auckland, School of T. Engineering Department.

Kwan, F. (1988). Study of Abutment Scour. Report No. 451, University of Auckland, School of T. Engineering, Department of Civil Engineering Private Bag, Auckland, New Zealand.

Kwan, T. F. and Melville, B. W. (1994). Local scour and flow measurements at bridge abutments. Journal of Hydraulic Research, 32, 661–673

Lai, J. S., Chang, W. Y. and Yen, C. L. (2009). Maximum local scour depth at bridge piers under unsteady flow. Journal of Hydraulic Engineering, 135(7), 609-614.

Lagasse, P. F., Zevenbergen, L. W., Schall, J. D. and Clopper, P. E. (2001). Bridge scour and stream instability countermeasures. experience, selection, and design guidance (No. FHWA/NHI-01-003). United States. Federal Highway Administration. Office of Bridge Technology.

Laursen E. M. and Toch A. (1956). Scour around bridge piers and abutments. Bull. No. 4, Iowa Highways Research Board, Ames, Iowa.

Laursen, E.M. (1958). Scour at bridge crossings. Bull. No. 8, Iowa Highways Research Board, Ames, Iowa.

Laursen, E. M. (1960). Scour at bridge crossings. Journal of the Hydraulics Division, 86(2), 39-54.

Laursen, E. M. (1963). An analysis of relief bridge scour. Journal of the Hydraulics Division, 89(3), 93-118.

Li, H. (2005). Countermeasures against scour at bridge abutments (Doctoral Thesis), Michigan Technological University, Michigan, United States.

Li, H., Barkdoll, B. and Kuhnle, R. (2005). Bridge abutment collar as a scour countermeasure. In Impacts of Global Climate Change, 1-12.

Li, H., Kuhnle, R. A. and Barkdoll, B. D. (2006). Countermeasures Against Scour At Abutments. National Sedimentation Laboratory, Research Report No. 49, U.S.

Link, O., Castillo, C., Pizarro, A., Rojas, A., Ettmer, B., Escauriaza, C. and Manfreda, S. (2017). A model of bridge pier scour during flood waves. Journal of Hydraulic Research, 55(3), 310-323.

Liu, H. K., Chang, F. M. and Skinner, M. M. (1961). Effect of bridge constriction on scour and backwater (Doctoral dissertation, Colorado State University. Libraries).

Lu, J. Y., Shi, Z. Z., Hong, J. H., Lee, J. J. and Raikar, R. V. (2011). Temporal variation of scour depth at nonuniform cylindrical piers. Journal of Hydraulic Engineering, 137(1), 45-56.

Melville, B.W. (1992). Local Scour at Bridge Abutments. ASCE Journal of Hydraulic Engineering, 118, 615- 631.

Melville, B. W. (1997). Pier and abutment scour: integrated approach. Journal of Hydraulic Engineering, 123(2), 125-136.

Melville, B. W. and Chiew, Y. M. (1999). Time Scale for Local Scour at Bridge Piers. Journal of Hydraulic Engineering, 125(1), 59-65.

Melville, B. W. and Coleman, S. E. (2000). Bridge Scour, Water Resources Publications, LLC, Colorado, USA.

Moncada, M. A. T., Aguirre-Pe, J., Bolivar, J. C. And Flores, E. J. (2009). Scour protection of circular bridge piers with collars and slots. Journal of Hydraulic Research, 47(1), 119-126.

Nasr, A., Kjellström, E., Björnsson, I., Honfi, D., Ivanov, O. L. and Johansson, J. (2020). Bridges in a Changing Climate: A Study of the Potential Impacts of Climate Change on Bridges and Their Possible Adaptations. Structure and Infrastructure Engineering, 16(4), 738-749.

Neill, C. R. (1973). Guide to bridge hydraulics.Toronto: University of Toronto Press.

Oliveto, G. and Hager, W. H. (2002). Temporal evolution of clear-water pier and abutment scour. ASCE Journal of Hydraulic Engineering, 128, 811- 820.

Oliveto, G. and Hager, W.H. (2005a). Further Results to time-dependent local scour at bridge elements. Journal of Hydraulic Engineering, ASCE, 131(2), pp. 97-105.

Oliveto, G. and Hager, W. H. (2005b). Closure to “Further results to time-dependent local scour at bridge elements”. Journal of Hydraulic Engineering 132(9), 997-998

Osroush, M., Hosseini, S. A. and Kamanbedast, A. A. (2021). Countermeasures against local scouring around bridge abutments: combined system of collar and slot. Iranian Journal of Science and Technology, Transactions of Civil Engineering, 45(1), 11-25.

Pandey, M., Azamathulla, H. M., Chaudhuri, S., Pu, J. H., & Pourshahbaz, H. (2020). Reduction of time-dependent scour around piers using collars. Ocean Engineering, 213, 107692.

Papanicolaou, A. N. and Hilldale, R. (2002). Turbulence characteristic in a gradual channel transition. Journal of Engineering, ASCE, 128(9), 948- 961.

Papanicolaou, A., Kjos, L. J. and Fox, J. F. (2004). Investigation of flow and local scour characteristics around a partially submerged permeable, WSDOT (No. WA-RD 581.1), Washington State Department of Transportation.

Pizarro, A., Ettmer, B., Manfreda, S., Rojas, A. and Link, O. (2017). Dimensionless effective flow work for estimation of pier scour caused by flood waves. Journal of Hydraulic Engineering, 143(7), 06017006.

Raikar, R. V., Hong, J. H., Deshmukh, A. R. and Guo, W. D. (2022). Parametric Study on Abutment Scour under Unsteady Flow. Water, 14(11), 1820.

Rajaratnam, N. and Nwachukwu, B. A. (1983). Flow near groin-like structures. ASCE Journal of Hydraulic Engineering, 109, 463–480

Raudkivi, A. J. and Ettema, R. (1983). Clear-water scour at cylindrical piers. ASCE Journal of Hydraulic Engineering, 109, 338–350.

Richardson, E. V. and Davis, S. R. (2001). Evaluating scour at bridges (No. FHWA-NHI-01-001). United States. Federal Highway Administration. Office of Bridge Technology.

Richardson, J.R. and Richardson, E.V. (1993). Discussion of "Local Scour at Bridge Abutments", by B.W. Melville. Journal of Hydraulic Engineering, ASCE, 119(9), pp. 1069-1071.

Rouse, H. (1965). Engineering hydraulics: sediment transportation. New York: John Wiley and Sons.

Salamatian, S. A., Karimaee,Tabarestani, M. and Zarrati, A. R. (2014). Local scour at a cylindrical bridge pier under a flood hydrograph. River Flow, 1387-1391.

Sastry, C. L. N. (1962). Effect of spur-dike inclination on scour characteristics (Master Thesis), University of Roorkee, Roorkee, India.

Solati, S., Vaghefi, M. and Behroozi, A. M. (2021). Effect of duration and pattern of hydrographs on scour around pier in sharp bend under incipient motion and live bed conditions. International Journal of Civil Engineering, 19(1), 51-65.

Tabarestani, M. K. and Zarrati, A. R. (2017). Local scour calculation around bridge pier during flood event. KSCE Journal of Civil Engineering, 21(4), 1462-1472.

Tabarestani, M.K. and Zarrati, A. R. (2019). Local scour depth at a bridge pier protected by a collar in steady and unsteady flow. In Proceedings of the Institution of Civil Engineers-Water Management 172(6), 301-311.

Tafarojnoruz, A., Gaudio, R. and Calomino, F. (2012a). Evaluation of flow-altering countermeasures against bridge pier scour. Journal of Hydraulic Engineering, 138(3), 297-305.

Tafarojnoruz, A., Gaudio, R. and Calomino, F. (2012b). Bridge pier scour mitigation under steady and unsteady flow conditions. Acta Geophysica, 60(4), 1076-1097.

Tekin, F. (2012). Local scour characteristics around semi-circular end bridge abutments with and without collars (Master thesis), Middle East Technical University, Ankara, Turkey.

Tey, C. B. (1984). Local scour at bridge abutments. Rep. No. 329, School of Engineering, University of Auckland, Auckland, New Zealand

Valela, C., Nistor, I., Rennie, C. D., Lara, J. L. and Maza, M. (2021). Hybrid modeling for design of a novel bridge pier collar for reducing scour. Journal of Hydraulic Engineering, 147(5), 04021012.

Valela, C., Rennie, C. D. and Nistor, I. (2022). Improved bridge pier collar for reducing scour. International Journal of Sediment Research, 37(1), 37-46.

Wardhana, K. and Hadipriono, F. C. (2003). Analysis of recent bridge failures in the United States. Journal of Performance of Constructed Facilities, 17(3), 144-150.

Whitehouse, R. J. S. (1997). Scour at marine structures: a manual for engineers and scientists. Res. Rep. SR417, HR Wallingford Limited, Wallingford, UK.

Wong, W. H. (1982). Scour at bridge abutments. Rep. No. 275, School of Engineering, University of Auckland, Auckland, New Zealand.

Yanmaz, A. M. and Altinbilek, H. D. (1991). Study of time-dependent local scour around bridge piers. Journal of Hydraulic Engineering, 117(10), 1247-1268.

Yılmaz, K. (2014). Application of collars as a scour countermeasure for spill-through abutments (Master's thesis), Middle East Technical University, Ankara, Turkey.

Zaghloul, N. A. and McCorquodale, J. A. (1975). A stable numerical model for local scour. Journal of Hydraulic Research, 13(4), 425-444.

Zaghloul, N. A. (1983). Local scour around spur-dikes. Journal of Hydrology, 60, 123– 140.

Zarrati, A. R., Gholami, H. and Mashahir, M. B. (2004). Application of collar to control scouring around rectangular bridge piers. Journal of Hydraulic Research, 42(1), 97-103.

APPENDICES

A. Experimental Results of the Temporal Development of Local Scour Around Bridge Abutments

In this part, a sample of the experimental results of the temporal development of local scour around the semi-circular end and rectangular bridge abutments are given in Tables A.1 and A.2. Measurements were taken from Inducer 5, Inducer 12, and Inducer 17 for the upstream, front and downstream sides of the abutments, respectively. The positive sign data denotes the scouring, on the other hand, the negative sign data denotes sedimentation.

Table A.1 Experimental results of the temporal development of the local scour depth around semi-circular end abutments of lengths L_a= 35 and 40 cm

		Experiment No					
		SC1			SC2		
t (min)	U/U_c	$(d_s)_d$ (cm)	$(d_s)_u$ (cm)	$(d_s)_f$ (cm)	$(d_s)_d$ (cm)	$(d_s)_u$ (cm)	$(d_s)_f$ (cm)
15	0.7	3.51	4.14	6.81	3.11	2.01	5.25
30	0.7	4.23	4.57	7.71	3.62	2.62	5.89
45	0.7	4.96	5.12	8.2	3.73	3.09	6.1
60	0.7	5.65	5.43	8.38	3.94	3.46	6.47
75	0.7	5.91	5.85	8.63	4.1	3.7	6.69
90	0.7	6.14	6.1	8.88	4.41	3.8	6.81
105	0.7	6.5	6.53	9.2	4.48	4.01	6.87
120	0.7	6.78	6.69	9.6	4.96	4.14	7.17
135	0.8	8.02	7.65	10.92	6.06	5.42	8.14
150	0.8	8.76	8.25	11.17	6.71	5.96	8.83
165	0.8	8.89	8.8	11.66	6.96	6.31	9.07
180	0.8	9.37	9.17	12.12	7.07	6.64	9.69
195	0.8	9.77	9.5	12.42	7.72	6.86	9.93
210	0.8	10.08	9.85	12.52	8.09	7.2	10.17
225	0.8	10.25	10.08	12.85	8.54	7.35	10.49
240	0.8	10.33	10.25	13	8.58	7.59	10.73
255	0.9	10.35	10.55	13.52	8.64	9.29	11.75
270	0.9	10.58	11.05	13.94	9.36	10.03	12.09
285	0.9	11.55	11.75	14.61	9.69	10.68	12.52
300	0.9	11.92	12.22	14.83	10.27	11.26	12.81
315	0.9	12.47	12.46	15.38	10.38	11.67	13.38
330	0.9	12.68	12.92	15.5	10.74	12	13.54
345	0.9	12.93	13.27	15.75	11.07	12.28	14.15
360	0.9	13.11	13.47	16.09	11.57	12.62	14.41

Table A.2 Experimental results of the temporal development of the local scour depth around rectangular abutments of lengths L_a= 35 and 40 cm

		Experiment No					
		RC1			RC2		
t (min)	U/U_c	$(d_s)_d$ (cm)	$(d_s)_u$ (cm)	$(d_s)_f$ (cm)	$(d_s)_d$ (cm)	$(d_s)_u$ (cm)	$(d_s)_f$ (cm)
15	0.7	3.41	6.36	8.64	2.36	5.74	7.58
30	0.7	4.58	7.21	9.74	3.46	6.52	8.30
45	0.7	4.88	7.78	11.49	3.96	7.29	8.98
60	0.7	5.80	8.44	12.01	4.24	7.97	9.51
75	0.7	7.05	8.67	12.04	5.00	8.05	9.98
90	0.7	7.51	9.20	12.57	5.58	8.20	10.52
105	0.7	7.92	9.37	12.88	5.69	8.73	11.88
120	0.7	8.11	9.67	13.31	5.95	8.96	12.03
135	0.8	10.21	11.59	14.97	8.09	10.60	12.06
150	0.8	10.37	12.32	16.13	8.74	10.88	12.51
165	0.8	10.90	13.04	16.31	9.33	11.46	12.60
180	0.8	11.17	13.51	16.31	9.80	11.73	13.88
195	0.8	11.63	13.66	16.30	10.25	12.01	14.43
210	0.8	12.21	14.00	16.53	10.33	12.58	14.49
225	0.8	12.48	14.38	16.63	10.88	12.68	14.65
240	0.8	12.32	14.54	17.08	10.99	12.99	14.69
255	0.9	13.01	15.08	18.25	9.92	12.86	15.31
270	0.9	13.23	15.50	18.87	10.58	13.09	15.87
285	0.9	14.09	16.30	19.16	10.62	13.83	16.34
300	0.9	14.63	16.56	19.41	11.41	14.04	16.60
315	0.9	14.97	16.84	19.78	11.43	14.45	16.63
330	0.9	15.16	17.24	20.07	11.70	14.72	16.94
345	0.9	15.44	17.79	20.21	11.97	14.97	17.06
360	0.9	15.94	17.81	20.30	12.21	15.39	17.44

B. Experimental Results of the Application of Collars As a Scour Countermeasure Around Bridge Abutments

In this part, a sample of experimental results of the application of collar as a scour countermeasure around the semi-circular end and rectangular bridge abutments are given in Tables B.1 and B.2 Measurements were done with a point gauge with an accuracy of ±1 mm after the experiments were completed.

Table B.1 Experimental results of the application of collars as a scour countermeasure around semi-circular end abutment of length L_a= 40 cm

L_a (cm)	L_a/B	B_c (cm)	L_a/B_c	Θ	$(Θ*L_a/B_c)^{0.5}$	y (cm)	t (hour)	U/U_c	Z_c (cm)	$[Z_c/y_{0.7}]$	$[(d_s)_{max,c}/y]$	[%Reduction]
40	0.27	5	8.00	2.20	4.20	17.4	2	0.7	±0.00	±0.00	0.18	66.67
		5	8.00	2.20	4.20	15.2	4	0.8	±0.00	±0.00	0.61	28.46
		5	8.00	2.20	4.20	13.5	6	0.9	±0.00	±0.00	0.93	22.36
		5	8.00	2.20	4.20	17.4	2	0.7	-4.35	-0.25	0.28	50.00
		5	8.00	2.20	4.20	15.2	4	0.8	-4.35	-0.25	0.55	36.15
		5	8.00	2.20	4.20	13.5	6	0.9	-4.35	-0.25	0.96	19.25
		5	8.00	2.20	4.20	17.4	2	0.7	-8.70	-0.50	0.50	9.38
		5	8.00	2.20	4.20	15.2	4	0.8	-8.70	-0.50	0.61	29.23
		5	8.00	2.20	4.20	13.5	6	0.9	-8.70	-0.50	0.84	29.19
		7.5	5.33	2.88	3.92	17.4	2	0.7	±0.00	±0.00	0.21	62.50
		7.5	5.33	2.88	3.92	15.2	4	0.8	±0.00	±0.00	0.45	46.92
		7.5	5.33	2.88	3.92	13.5	6	0.9	±0.00	±0.00	0.76	36.65
		7.5	5.33	2.88	3.92	17.4	2	0.7	-4.35	-0.25	0.29	47.92
		7.5	5.33	2.88	3.92	15.2	4	0.8	-4.35	-0.25	0.55	35.38
		7.5	5.33	2.88	3.92	13.5	6	0.9	-4.35	-0.25	0.90	24.22
		7.5	5.33	2.88	3.92	17.4	2	0.7	-8.70	-0.50	0.50	9.38
		7.5	5.33	2.88	3.92	15.2	4	0.8	-8.70	-0.50	0.62	27.69
		7.5	5.33	2.88	3.92	13.5	6	0.9	-8.70	-0.50	0.83	30.43
		10	4.00	3.61	3.80	17.4	2	0.7	±0.00	±0.00	0.16	71.88
		10	4.00	3.61	3.80	15.2	4	0.8	±0.00	±0.00	0.32	62.31
		10	4.00	3.61	3.80	13.5	6	0.9	±0.00	±0.00	0.62	47.83
		10	4.00	3.61	3.80	17.4	2	0.7	-4.35	-0.25	0.28	50.00
		10	4.00	3.61	3.80	15.2	4	0.8	-4.35	-0.25	0.51	40.77
		10	4.00	3.61	3.80	13.5	6	0.9	-4.35	-0.25	0.76	36.65
		10	4.00	3.61	3.80	17.4	2	0.7	-8.70	-0.50	0.50	9.38
		10	4.00	3.61	3.80	15.2	4	0.8	-8.70	-0.50	0.59	30.77
		10	4.00	3.61	3.80	13.5	6	0.9	-8.70	-0.50	0.79	33.54

Table B.2 Experimental results of the application of collars as a scour countermeasure around rectangular abutment of length L_a= 40 cm

L_a (cm)	L_a/B	B_c (cm)	L_a/B_c	Θ	$(Θ*L_a/B_c)^{0.5}$	y (cm)	t (hour)	U/U_c	Z_c (cm)	$[Z_c/y_{0.7}]$	$[(d_s)_{max,c}/y]$	[%Reduction]
40	0.27	5	8.00	2.25	4.24	17.4	2	0.7	±0.00	±0.00	0.67	12.78
		5	8.00	2.25	4.24	15.2	4	0.8	±0.00	±0.00	1.03	8.19
		5	8.00	2.25	4.24	13.5	6	0.9	±0.00	±0.00	1.54	0.95
		5	8.00	2.25	4.24	17.4	2	0.7	-4.35	-0.25	0.47	38.35
		5	8.00	2.25	4.24	15.2	4	0.8	-4.35	-0.25	0.84	25.73
		5	8.00	2.25	4.24	13.5	6	0.9	-4.35	-0.25	1.53	1.90
		5	8.00	2.25	4.24	17.4	2	0.7	-8.70	-0.50	0.61	19.55
		5	8.00	2.25	4.24	15.2	4	0.8	-8.70	-0.50	0.82	27.49
		5	8.00	2.25	4.24	13.5	6	0.9	-8.70	-0.50	1.39	10.95
		7.5	5.33	2.97	3.98	17.4	2	0.7	±0.00	±0.00	0.51	33.08
		7.5	5.33	2.97	3.98	15.2	4	0.8	±0.00	±0.00	0.91	18.71
		7.5	5.33	2.97	3.98	13.5	6	0.9	±0.00	±0.00	1.55	0.48
		7.5	5.33	2.97	3.98	17.4	2	0.7	-4.35	-0.25	0.48	37.59
		7.5	5.33	2.97	3.98	15.2	4	0.8	-4.35	-0.25	0.68	39.18
		7.5	5.33	2.97	3.98	13.5	6	0.9	-4.35	-0.25	1.36	12.86
		7.5	5.33	2.97	3.98	17.4	2	0.7	-8.70	-0.50	0.53	30.83
		7.5	5.33	2.97	3.98	15.2	4	0.8	-8.70	-0.50	0.79	29.82
		7.5	5.33	2.97	3.98	13.5	6	0.9	-8.70	-0.50	1.23	20.95
		10	4.00	3.75	3.87	17.4	2	0.7	±0.00	±0.00	0.40	48.12
		10	4.00	3.75	3.87	15.2	4	0.8	±0.00	±0.00	0.66	41.52
		10	4.00	3.75	3.87	13.5	6	0.9	±0.00	±0.00	1.33	14.76
		10	4.00	3.75	3.87	17.4	2	0.7	-4.35	-0.25	0.45	41.35
		10	4.00	3.75	3.87	15.2	4	0.8	-4.35	-0.25	0.59	47.37
		10	4.00	3.75	3.87	13.5	6	0.9	-4.35	-0.25	1.21	21.90
		10	4.00	3.75	3.87	17.4	2	0.7	-8.70	-0.50	0.48	36.84
		10	4.00	3.75	3.87	15.2	4	0.8	-8.70	-0.50	0.68	39.18
		10	4.00	3.75	3.87	13.5	6	0.9	-8.70	-0.50	1.19	23.81

C. Experimental Results of the Effect of Flow Depth on Scour Depths and Efficiencies of the Collars As a Scour Countermeasure Around Bridge Abutments

In this part, a sample of experimental results of the effect of flow depth on scour depths and efficiencies of the collars around the semi-circular bridge abutments is given in Table C.1. Measurements were done with a point gauge with an accuracy of ±1 mm after the experiments were completed.

Table C.1 Experimental results of the effect of flow depth on efficiencies of the collars as a scour countermeasure around semi-circular end abutment of length L_a= 40 cm

L_a (cm)	L_a/B	B_c (cm)	L_a/B_c	Θ	$(Θ*L_a/B_c)^{0.5}$	y (cm)	t (hour)	U/U_c	Z_c (cm)	$[Z_c/y_{0.7}]$	$[(d_s)_{max,c}/y]$	[%Reduction]
40	0.27	5	8.00	2.25	4.24	11.5	2	0.7	±0.00	±0.00	0.26	66.67
		5	8.00	2.25	4.24	12.3	4	0.8	±0.00	±0.00	0.73	29.13
		5	8.00	2.25	4.24	13	6	0.9	±0.00	±0.00	1.01	14.94
		5	8.00	2.25	4.24	11.5	2	0.7	-4.35	-0.25	0.49	37.78
		5	8.00	2.25	4.24	12.3	4	0.8	-4.35	-0.25	0.67	35.43
		5	8.00	2.25	4.24	13	6	0.9	-4.35	-0.25	1.09	7.79
		5	8.00	2.25	4.24	11.5	2	0.7	-8.70	-0.50	0.56	28.89
		5	8.00	2.25	4.24	12.3	4	0.8	-8.70	-0.50	0.74	28.35
		5	8.00	2.25	4.24	13	6	0.9	-8.70	-0.50	1.00	15.58
		7.5	5.33	2.97	3.98	11.5	2	0.7	±0.00	±0.00	0.23	71.11
		7.5	5.33	2.97	3.98	12.3	4	0.8	±0.00	±0.00	0.56	45.67
		7.5	5.33	2.97	3.98	13	6	0.9	±0.00	±0.00	0.74	37.66
		7.5	5.33	2.97	3.98	11.5	2	0.7	-4.35	-0.25	0.43	45.56
		7.5	5.33	2.97	3.98	12.3	4	0.8	-4.35	-0.25	0.54	47.24
		7.5	5.33	2.97	3.98	13	6	0.9	-4.35	-0.25	0.74	37.66
		7.5	5.33	2.97	3.98	11.5	2	0.7	-8.70	-0.50	0.50	36.11
		7.5	5.33	2.97	3.98	12.3	4	0.8	-8.70	-0.50	0.63	39.37
		7.5	5.33	2.97	3.98	13	6	0.9	-8.70	-0.50	0.71	40.26
		10	4.00	3.75	3.87	11.5	2	0.7	±0.00	±0.00	0.27	65.56
		10	4.00	3.75	3.87	12.3	4	0.8	±0.00	±0.00	0.37	64.57
		10	4.00	3.75	3.87	13	6	0.9	±0.00	±0.00	0.62	48.05
		10	4.00	3.75	3.87	11.5	2	0.7	-4.35	-0.25	0.37	53.33
		10	4.00	3.75	3.87	12.3	4	0.8	-4.35	-0.25	0.59	43.31
		10	4.00	3.75	3.87	13	6	0.9	-4.35	-0.25	0.61	48.70
		10	4.00	3.75	3.87	11.5	2	0.7	-8.70	-0.50	0.50	36.11
		10	4.00	3.75	3.87	12.3	4	0.8	-8.70	-0.50	0.63	38.58
		10	4.00	3.75	3.87	13	6	0.9	-8.70	-0.50	0.72	39.61

CURRICULUM VITAE

Surname, Name: Gökmener, Serkan

EDUCATION

Degree	Institution	Year of Graduation
MS	METU Civil Engineering	2016
BS	METU Civil Engineering	2012
High School	Bilfen High School, İstanbul	2006

FOREIGN LANGUAGES

Advanced English, Elementary German

PUBLICATIONS

1. Gogus, M. and Gokmener, S. “Critical Submergence for Single and Multiple Horizontal Intake Structures”, Arabian Journal for Science and Engineering, (pp. 1-25) (2023)

2. Gogus, M., Daskin, S. and Gokmener, S. “Effects of Collars on Local Scour Around Semi-Circular End Bridge Abutments”, Proceedings of the Institution of Civil Engineers-Water Management, (pp. 1-11) (2023)

3. Gokmener, S. and Gogus, M. “Local Scour Evolution Around Semi-circular End Bridge Abutment in Quasi-Unsteady Condition”, Proceedings of the Institution of Civil Engineers-Water Management, 175(4), 163-177 (2022)

4. Yavuz, C., Gokmener, S. And Yilmaz, K. “Trajectory Length Determination for Bottom Outlet of Inoren Regulator and HEPP”, 13th International Congress on Advanced Civil Engineering, (2018)

Basketball, Cycling, Literature, History, Movies, Photography